LEGIBILITY NOTICE

A major purpose of the Technical Information Center is to provide the broadest dissemination possible of information contained in DOE's Research and Development Reports to business, industry, the academic community, and federal, state and local governments.

Although a small portion of this report is not reproducible, it is being made available to expedite the availability of information on the research discussed herein.

1

108
1-31-83

(2)

I-8941

Dr. 1344

ORNL/FEDC-82/2

FED BASELINE ENGINEERING STUDIES REPORT

P.H. SAGER, et al.

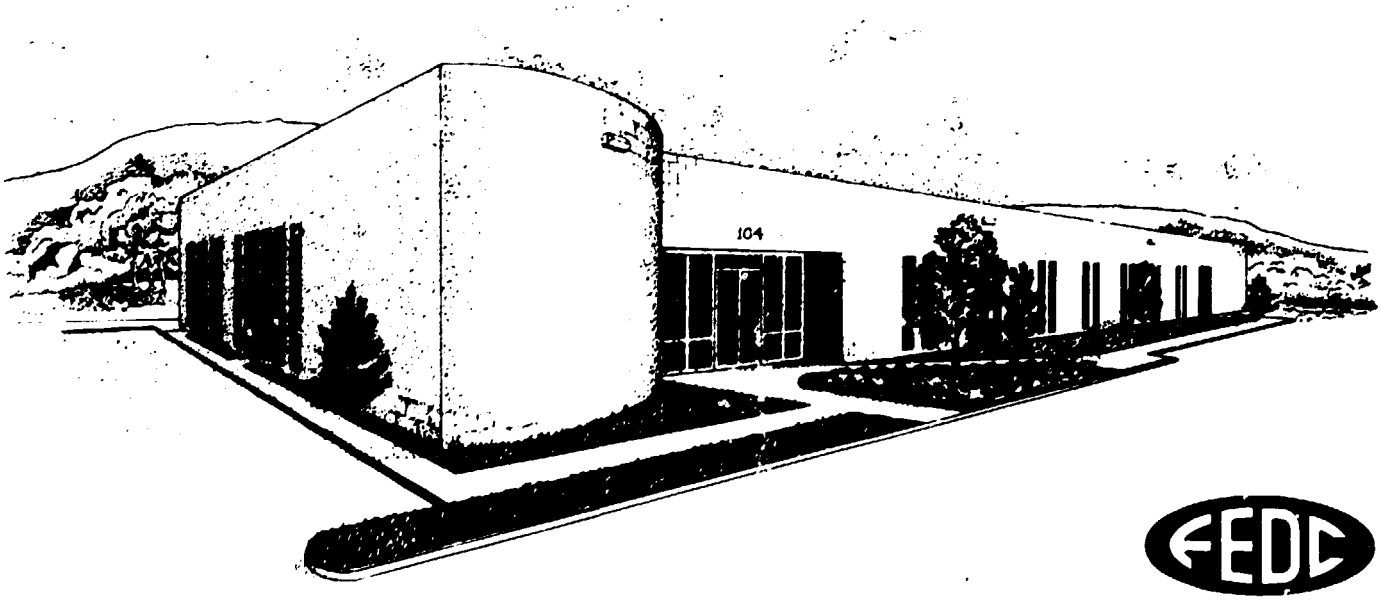

FEDC

FUSION ENGINEERING DESIGN CENTER

Oak Ridge National Laboratory * Oak Ridge, Tennessee

MASTER

DISTRIBUTION OF THIS DOCUMENT IS UNLIMITED

ORNL/FEDC--82/2

DE83 010328

ORNL/FEDC-82/2
Dist. Category UC-20

Contract No. W-7405-eng-26

FED BASELINE ENGINEERING STUDIES REPORT

P. H. Sager, et al.

Date Published: April 1983

DISCLAIMER

This report was prepared as an account of work sponsored by an agency of the United States Government. Neither the United States Government nor any agency thereof, nor any of their employees, makes any warranty, express or implied, or assumes any legal liability or responsibility for the accuracy, completeness, or usefulness of any information, apparatus, product, or process disclosed, or represents that its use would not infringe privately owned rights. Reference herein to any specific commercial product, process, or service by trade name, trademark, manufacturer, or otherwise does not necessarily constitute or imply its endorsement, recommendation, or favoring by the United States Government or any agency thereof. The views and opinions of authors expressed herein do not necessarily state or reflect those of the United States Government or any agency thereof.

Prepared by the
OAK RIDGE NATIONAL LABORATORY
Oak Ridge, Tennessee 37830
operated by
UNION CARBIDE CORPORATION
for the
DEPARTMENT OF ENERGY

NOTICE
PORTIONS OF THIS REPORT ARE ILLEGIBLE.
It has been reproduced from the best available copy to permit the broadest possible availability.

PREFACE

This document is one of four describing studies performed in FY 1982 within the context of the Fusion Engineering Device (FED) Program for the Office of Fusion Energy, Department of Energy. The documents are:

1. FED Baseline Engineering Studies,
2. Considerations of an Advanced Performance Fusion Engineering Device — FED-A,
3. FED-R, A Fusion Engineering Device Utilizing Resistive Magnets, and
4. Technology Demonstration Facility — TDF.

These studies were designed to extend the studies on the FED Baseline and to develop innovative and alternative concepts for the FED.

This report describes the FED Baseline Engineering Studies. These studies have been a continuation of the FED Baseline concept developed in FY 81. The objectives of these studies have been to focus on means to improve design definition, resolve design issues of feasibility, and identify ways to reduce the overall cost. These studies were performed by the Design Center staff with support from other fusion institutions. P. H. Sager of the FEDC served as Project Manager.

TABLE OF CONTENTS

PREFACE iii

LIST OF FIGURES xi

LIST OF TABLES xv

LIST OF CONTRIBUTORS xix

ACKNOWLEDGMENTS xxi

ABSTRACT xxiii

1. INTRODUCTION 1-1

REFERENCES 1-6

2. SUMMARY 2-1

2.1 REACTOR DESIGN OPTIONS 2-2

2.1.1 Basic Configuration Options 2-2
2.1.2 Lower Outboard EF Coil 2-6

2.2 TORUS DESIGN STUDIES 2-6

2.2.1 Inboard Gap Shielding 2-6
2.2.2 Torus Current Path 2-8
2.2.3 Torus Spool 2-8
2.2.4 Test Module Shielding 2-10
2.2.5 Seismic Response 2-10
2.2.6 Poloidal Geometry Effects on the Thermal Characteristics of the First Wall 2-10

2.3 MAGNET SYSTEM STUDIES 2-11

2.4 ELECTROMAGNETIC STUDIES 2-14

2.5 MAINTENANCE STUDIES 2-15

2.6 FACILITY DESIGN STUDIES 2-19

2.7 RAM REQUIREMENTS 2-19

2.8 SAFETY 2-19

2.9 COST PROJECTIONS 2-23

3. REACTOR DESIGN CONFIGURATIONS 3-1

3.1 INTRODUCTION 3-1

3.2 REACTOR DESIGN DEFINITIONS 3-2

3.3 VACUUM BOUNDARY EVALUATION 3-11

3.3.1 Major Features 3-11
3.3.2 Evaluation Criteria 3-16
3.3.3 Approach to Evaluation 3-17
3.3.4 Evaluation Rationale 3-17
3.3.5 Summary of Scoring 3-21

3.4 COMBINED VACUUM BOUNDARY (FED 400) STRUCTURAL ANALYSIS 3-21

3.4.1 Structural Description 3-23
3.4.2 Load Conditions 3-26
3.4.3 Atmospheric Pressure Loads 3-26
3.4.4 250°C Bakeout Condition 3-28

3.5 PF SYSTEM CONFIGURATION OPTIONS 3-30

3.6 TF SYSTEM CONFIGURATION STUDY 3-40

3.6.1 Sizing of Case 3-40
3.6.2 Sizing of Intercoil Support Structure (ISS) 3-41
3.6.3 Costing 3-41

3.7 RAM ASSESSMENT 3-44

3.8 R&D ASSESSMENT 3-47

3.9 REACTOR COST STUDY 3-48

3.10 OVERALL EVALUATION 3-55

3.11 POLOIDAL DIVERTOR REACTOR DESIGN OPTION 3-57

REFERENCES 3-59

4. TORUS DESIGN STUDIES 4-1

4.1 INTRODUCTION 4-1

4.2 INBOARD GAP SHIELDING 4-4

4.2.1 Inboard Gap Configuration 4-4
4.2.2 Shielding Requirements 4-4
4.2.3 Shield Materials and Material Distribution 4-8
4.2.4 Shield Configuration 4-8
4.2.5 Attachment/Assembly 4-11

4.3 TORUS CURRENT PATH 4-13

4.3.1 Torus Current Path Requirements 4-15
4.3.2 Candidate Electrical Conductor Concepts 4-16
4.3.3 Electrical Conductor Design 4-20
4.3.4 Arcing Design 4-29
4.3.5 Eddy Current Design 4-31

4.4 TORUS SPOOL 4-35

4.4.1 Torus Current Path Requirements 4-38
4.4.2 Spool Configuration 4-39
4.4.3 Candidate Concepts 4-41
4.4.4 Evaluation of Concepts 4-57

4.5 TEST MODULE SHIELDING 4-61

4.5.1 Test Module Configuration 4-66
4.5.2 Test Module Shielding Effectiveness 4-66

4.5.3 Service Connections 4-67
4.5.4 External Shield Assembly Concept 4-67

4.6 SEISMIC RESPONSE 4-68

4.7 TEMPERATURE VARIATIONS OF THE FIRST WALL 4-72

4.7.1 Approach 4-74
4.7.2 Results 4-74
4.7.3 Conclusions 4-77

REFERENCES 4-80

5. MAGNET SYSTEMS 5-1

5.1 INTRODUCTION 5-1

5.2 TOROIDAL FIELD COILS 5-2

5.2.1 Superfluid Helium Cooled Coil Design 5-2
5.2.2 Redesign of Coil Case 5-10
5.2.3 Redesign of Intercoil Support Structure 5-12
5.2.4 Fracture Mechanics Methodology 5-17
5.2.5 Permissible Radiation Dose for Candidate Insulators 5-18
5.2.6 Thermal Analysis of Internally Cooled Conductors 5-24

5.3 POLOIDAL FIELD COILS 5-28

5.3.1 8-T Solenoid Design Using-Boiling-Cooled Conductor (PBCC) 5-31
5.3.2 Ring Coil Design Using Pool-Boiling-Cooled Conductor (PBCC) 5-44
5.3.3 8-T Central Solenoid and Ring Coil Design Using Forced Cooled Conductors 5-54
5.3.4 Structural Evaluation of Internally Cooled Cable Superconductor (ICCS) for PF Central Solenoid and Ring Coils 5-72
5.3.5 Impact of Poloidal Field Coil Faults on Coil Design and Operations 5-85
5.3.6 50-kA Vapo Cooled PF Coil Current Leads 5-95

5.4 CRYOSTAT DESIGN WITHOUT LIQUID NITROGEN SHIELD 5-101

REFERENCES 5-105

6. ELECTROMAGNETIC STUDIES 6-1

6.1 INTRODUCTION 6-1

6.2 DISRUPTIONS 6-2

6.3 STARTUP VOLTAGE AND ENERGY 6-4

6.4 CONTROL 6-7

REFERENCES 6-9

7. MAINTENANCE STUDIES 7-1

7.1 INTRODUCTION 7-1

7.2 SECTOR REPLACEMENT 7-2

7.2.1 Sector Removal 7-2
7.2.2 Sector Replacement 7-6

7.3 EQUIPMENT SPECIFICATIONS 7-7

7.3.1 General Requirements for Equipment Design 7-9
7.3.2 Movable Manipulator System Requirements 7-10
7.3.3 Sector Handling Machine Requirements 7-10
7.3.4 In-Vessel Manipulator Systems Requirements 7-11

7.4 TORUS SECTOR MAINTENANCE EQUIPMENT STUDIES 7-12

7.4.1 Sector Handling Machine 7-12
7.4.2 Movable Manipulator System 7-20
7.4.3 Sub-Component Handling Machine 7-29
7.4.4 Limiter Blade Handling Machine 7-33
7.4.5 Equipment Costs 7-36

7.5 IN-VESSEL MANIPULATOR SYSTEM 7-36

7.5.1 In-Vessel Maintenance Operations 7-36
7.5.2 In-Vessel Manipulator System 7-48
7.5.3 IVMS Cost 7-54
7.5.4 Supporting Equipment for In-Vessel Operations 7-54

7.6 TF COIL REPLACEMENT 7-63

7.6.1 Objective 7-63
7.6.2 Approach 7-63
7.6.3 Stepwise Removal 7-65
7.6.4 Major Problem Areas 7-65
7.6.5 Cutting and Welding 7-79
7.6.6 Key Issues for Baseline Revisions 7-80

REFERENCES 7-84

8. FACILITY DESIGN STUDIES 8-1

8.1 INTRODUCTION 8-1

8.2 HOT CELL FACILITY 8-1

8.2.1 Hot Cell Requirements 8-2
8.2.2 Hot Cell Design Issues and Options 8-2
8.2.3 Hot Cell Investigations and Studies 8-6
8.2.4 Hot Cell Design Description 8-8

8.3 REACTOR BUILDING 8-12

8.3.1 Reactor Building Issues and Options 8-13
8.3.2 Reactor Building Design 8-13

8.4 FACILITY PLOT PLAN 8-16

REFERENCE 8-18

9. RAM REQUIREMENTS 9-1

9.1 INTRODUCTION 9-1

9.2 OVERALL DEVICE REQUIREMENTS 9-1

9.3 DEVELOPING SYSTEM AND COMPONENT REQUIREMENTS 9-4

9.4 SYSTEM REQUIREMENTS 9-7

9.5 SELECT COMPONENT REQUIREMENTS 9-7

10. SAFETY STUDIES 10-1

10.1 INTRODUCTION 10-1

10.2 ACTIVATION OF BUILDING WALLS AND STRUCTURES 10-1

10.3 CONTAMINATION IN THE REACTOR BUILDING 10-2

10.3.1 Stainless Steel Debris 10-3
10.3.2 Carbon Debris 10-4
10.3.3 Cleanup and Control of Radioactive Debris 10-4
10.3.4 Conclusions 10-6

10.4 TRITIUM ISSUES 10-7

10.4.1 Liners and Coatings 10-7
10.4.2 Tritium Leakage Sources 10-7

10.5 CRYOGENIC BLOWDOWN 10-8

10.6 CARBON-14 PRODUCTION 10-8

10.7 CONCLUSIONS 10-9

REFERENCE 10-10

11. COST PROJECTIONS 11-1

11.1 INTRODUCTION 11-1

11.2 COSTING METHODOLOGY 11-2

11.2.1 Costing Assumptions 11-2
11.2.2 Direct Capital Cost 11-3
11.2.3 Indirect Capital Cost 11-3

11.3 ESCALATED BASELINE COST PROJECTION 11-3

11.4 POTENTIAL COST IMPACT OF BASELINE ENGINEERING STUDIES 11-5

11.4.1 Modified Reactor Configurations 11-5
11.4.2 ISS Design for Reduced AC Losses 11-6
11.4.3 Facility Costing Studies 11-6
11.4.4 Maintenance Equipment Design and Costing Study 11-11
11.4.5 TF Coil Case Construction 11-12

11.4.6 Elimination of FED Cold Shields 11-14
11.4.7 Tritium Breeding Economics 11-15
11.4.8 Impact of an 8-T Forced Flow Solenoid 11-19
11.4.9 Torus Support Spool Candidate Concepts 11-20

11.5 OVERALL COST IMPACT 11-21

REFERENCES 11-23

LIST OF FIGURES

1-1	FED reference configuration, elevation view	1-3
1-2	FED reference configuration, plan view	1-4
2-1	Configuration options	2-3
2-2	FED-400 elevation view	2-7
2-3	Multiple shield rings	2-9
2-4	TF coil case concepts	2-12
2-5	Intercoil support structure concept	2-13
2-6	Movable manipulator system	2-16
2-7	Sector handling device	2-17
2-8	In-vessel manipulator system (IVMS)	2-18
2-9	Hot cell facility	2-20
3-1	Reactor design diagram	3-3
3-2	FED reference configuration (FED 300) elevation view	3-4
3-3	Cryostat configuration	3-5
3-4	Torus reactor system	3-6
3-5	Semicombined vacuum boundary configuration	3-7
3-6	FED 301 cryostat configuration	3-8
3-7	USA cryostat configuration, Phase II	3-9
3-8	Vacuum duct and lower outboard PF coil locations for FED 300 and FED 400	3-10
3-9	Alternative No. 1 — FED-baseline	3-12
3-10	Alternative No. 2 — partially integrated vacuum boundary	3-13
3-11	Alternative No. 3 — fully integrated	3-14
3-12	(a) Combined vacuum boundary structure, (b) finite element model (plate elements)	3-22
3-13	Combined vacuum vessel finite element model plate gauges	3-24
3-14	Bar element representation of structural rings and stiffeners	3-25
3-15	Deflected shapes for the pressure load condition	3-27
3-16	Bakeout temperatures	3-29
3-17	Effects of breather on stresses	3-31
3-18	Deflected shape for 250°C bakeout condition	3-32
3-19	PF coil locations	3-33
3-20	Design concept for supporting a repositioned lower outboard EF coil	3-34
3-21	FED baseline (FED 300) and FED 300/S-C PF coil configuration options	3-36
3-22	PF configuration options for the reduced size TF concept (FED 301)	3-37
3-23	PF configuration for the minimum size TF coil concept (FED 400)	3-38
3-24	Intercoil support structure concept	3-42
4-1	Torus regions addressed in FY 82 studies	4-3
4-2	FED elevation showing region modeled by MCNP	4-5
4-3	FED-baseline radial build	4-6
4-4	Multiple shield rings — final version	4-7

4-5 Interrupted cryostat concept 4-10
4-6 Gap shield configuration 4-12
4-7 FED baseline sector gap configuration 4-14
4-8 Electrical conductor options 4-17
4-9 Inboard electrical strap concept 4-23
4-10 Outboard electrical strap concept 4-24
4-11 Copper strap length and thickness for given stress and operating temperature 4-25
4-12 Bellows contact concept 4-27
4-13 Electrical contact configuration 4-28
4-14 Figure configuration for arcing contact 4-30
4-15 Eddy current paths in shield sector during disruption 4-32
4-16 Forces resulting from eddy currents in sectors 4-33
4-17 Sector force balance 4-36
4-18 Sector attach fittings and bolts 4-37
4-19 Torus spool 4-40
4-20 Spool finite element model 4-42
4-21 Spool structural concept 4-44
4-22 Inboard cylinder thicknesses 4-45
4-23 Effect of door vacuum seal thickness on toroidal electrical resistance 4-47
4-24 Comparison of spool electrical resistance with and without electrical breaks 4-48
4-25 Dielectric break design option: dielectric gasket and vacuum seal 4-51
4-26 Dielectric break design option: high resistance metal bellows 4-52
4-27 Dielectric break design option: high resistance thin metal sheet 4-53
4-28 Baseline dielectric break/vacuum seal design multilayer thin sheets used for vacuum seal 4-54
4-29 Dielectric break design option: electrically insulated omega seal 4-55
4-30 Test module installation in outboard shield 4-62
4-31 Two types of test module installation 4-63
4-32 Concept for external test module shield installation 4-64
4-33 Detail views of test modules and external shield 4-65
4-34 Components for seismic analysis 4-69
4-35 Components and elements used in FED seismic analysis 4-70
4-36 Representative mode shapes under seismic load 4-73
4-37 Maximum surface temperatures 4-76
5-1 Configurations and dimensions for 10 T grade conductor 5-4
5-2 Critical current I_c as a function of field and temperature 5-6
5-3 TF winding cross section (inboard region) for superfluid shown with modified conductor (U channel) 5-8

5-4 Comparison of TF coil case concepts 5-11
5-5 TF coil rib dimensions 5-13
5-6 Intercoil support structure concept 5-15
5-7 Attachment of ISS beams to TF coil case 5-16
5-8 Allowable stress vs number of cycles for selected initial flaw sizes (316 LN material) 5-20
5-9 Pressure and temperature variation in first 0.2 second 5-29
5-10 Pressure and temperature variation in first 1.8 seconds ($Nu \sim Re^{4/15}$) 5-30
5-11 50 kA PF coil conductor 5-33
5-12 Typical solenoid double pancake 5-34
5-13 Runaway temperature as a function of the fraction of geometrical perimeter available for cooling 5-41
5-14 Thermal response of 50 kA conductor in a pool bath cooled system to a 6 s total current reversal with 7 T maximum field 5-43
5-15 Coils EF2 and EF3 winding pack layout 5-48
5-16 Top structural support block for coils EF2 and EF3 to provide deentrainment and vapor removal channels 5-49
5-17 FED 8 T/10 T magnetic system with forced cooled PF coils 5-55
5-18 Schematic of central solenoid cross section with ICCS 5-58
5-19 Central solenoid, layout, splices, and mainfolding details 5-59
5-20 EF_2 winding and coil case schematic with ICCS 5-62
5-21 EF_3 winding schematic with ICCS 5-63
5-22 ICCS conductor dimensions and configuration for use in the central solenoid and PF coils of FED 5-65
5-23 Critical current I_c and load lines for central solenoid, EF_2 and EF_3 5-67
5-24 Cross section of conduit and superconductor in the ICCS 5-76
5-25 ICCS conductor configuration 5-76
5-26 General free body diagram of support channel 5-77
5-27 Idealized free body diagram of a channel located on the top (or bottom) of a coil design model 1 5-77
5-28 ADINA finite element structural model of a coil cross section 5-79
5-29 Forced flow, ICCS 10 kV discharge voltage with no coil shorted 5-89
5-30 Forced flow, ICCS 10 kV discharge voltage with coil EF5 shorted 5-90
5-31 Bath cooled, PBCC 3 kV discharge voltage with no coil shorted 5-91
5-32 Bath cooled, PBCC 3 kV discharge voltage with coil EF5 shorted 5-92
5-33 50 kA vapor cooled lead 5-96
5-34 Cryostat concept 5-102

6-1	Plasma current decay	6-5
7-1	FED sector replacement	7-3
7-2	Floor assembly of the sector handling machine	7-14
7-3	Push/pull chain system for sector movement	7-15
7-4	Detachable lifting fixture	7-16
7-5	Containment box and seal configuration	7-17
7-6	Movable manipulator system	7-21
7-7	Undercarriage for the MMS	7-23
7-8	MMS tip end	7-25
7-9	MMS tip end	7-26
7-10	MMS control console arrangement	7-28
7-11	Sub-component handling machine	7-31
7-12	Limiter blade handling machine	7-34
7-13	MMS entry ports	7-39
7-14	Task logic for the in-vessel replacement of F/W armor tiles	7-43
7-15	Downtime cost vs occurrence	7-47
7-16	In-vessel manipulation system — assembly	7-49
7-17	In-vessel manipulation system — elevation	7-50
7-18	In-vessel manipulation system — plan	7-51
7-19	Movable manipulator system	7-55
7-20	Equipment setup for removal of the ICRH shield module plug	7-58
7-21	Removal of torus shield plug	7-59
7-22	Support platform for IVMS	7-62
7-23	IVMS installation	7-64
7-24	FED magnetic system arrangement	7-67
7-25	Resistive coil joint design	7-68
7-26	Cryostat structure	7-70
7-27	FED TF coil and surrounding support structure	7-71
7-28	Cutaway view of TF coil and its support structure	7-72
7-29	Plan view of TF intercoil structure	7-73
7-30	Complex disassembly of EF coil #4	7-77
7-31	The spool arrangement and the torus sector	7-81
7-32	Torus spool	7-82
8-1	Hot cell facility layout	8-9
8-2	Reactor building layout	8-14
8-3	Facility plot plan	8-17
9-1	Acceptable combinationations of λ and MTTR	9-6
10-1	Access for the removal of eroded particulate matter	10-5
11-1	Unit cost vs building volume	11-9

LIST OF TABLES

1-1	Key parameters for the FED baseline	1-2
2-1	Features of reactor design options	2-4
2-3	FED system failure rate and downtime ratio requirements	2-21
2-4	Potential changes to FED Baseline costs	2-24
3-1	Comparison of vacuum boundary options	3-18
3-2	Assessment and scoring of vacuum boundary configurations	3-20
3-3	Summary of PF configuration study	3-39
3-4	Summary of weight and cost for TF coil cases and intercoil support structure	3-43
3-5	RAM impact of proposed design options assuming space ring coils not available	3-45
3-6	R&D requirements for R&D baseline options	3-49
3-7	FED Baseline parametric variation as a function of TF coil shape, PF coil configuration, and vacuum boundary design for constant values of burn time and wall loading	3-53
3-8	Cost breakdown for parameter variation shown in Table 3-7	3-54
3-9	Summary of reactor design concepts	3-56
4-1	Performance for a number of shield compositions	4-9
4-2	Assessment of candidate electrical contact concepts	4-19
4-3	Conductor evaluation scoring	4-21
4-4	Material properties	4-43
4-5	Spool required resistances	4-49
4-6	Design consideration results for the high-resistive break	4-56
4-7	Cost of Inconel torus spool with no breaks	4-59
4-8	Cost of stainless steel torus spool with high-resistance breaks	4-60
4-9	Impact of lateral support on lateral response	4-71
4-10	Key assumptions and analysis conditions	4-75
4-11	Results of first wall temperature sensitivity analysis	4-78
5-1	Parameters of conductors for superfluid option	5-5
5-2	FED TF coil design parameters for superfluid option	5-9
5-3	Parameters of stability study of ICC for FED TF coil	5-26
5-4	Computed steady-state parameters	5-27
5-5	8-T central solenoid and 50-kA PBCC dimensions	5-32
5-6	FED 8-T central solenoid OH1-OH2-EF5 losses	5-36
5-7	FED 8-T central solenoid OH1-OH2-EF5 losses	5-37
5-8	Heat transfer coefficients	5-40
5-9	50-kA PBCC recovery time for initial temperatures	5-40
5-10	Thin metal liner composite dewar eddy current losses	5-45

5-11 50-kA cable for poloidal field coils based on 20-MJ coil conductor 5-46
5-12 Poloidal field ring coils and 50-kA conductor dimensions 5-47
5-13 FED PF ring coil losses and vapor dynamics data for entire winding 5-51
5-14 FED PF coil loss study and vapor dynamics data for high field region during starting period 5-52
5-15 Design parameters of central solenoidal modules OH_1, OH_2, and OH_5 5-57
5-16 Design parameters of ring coils 5-61
5-17 Parameters of ICCS conductor of PF coils 5-64
5-18 Summary of AC losses in central solenoid, EF_2, and EF_3 coils with ICCS conductor 5-68
5-19 Peak heat loads and winding stability data for central solenoid, EF_2, and EF_3 coils 5-71
5-20 Allowable design stresses for structural components 5-74
5-21 Summary of ICCS support channel design 5-80
5-22 Comparison of forced-flow and bath-cooled ring coil designs 5-82
5-23 Construction forces calculated for winding OH1 5-84
5-24 Parameters of ICCS poloidal field coils 5-93
5-25 Maximum current and turns for the PBCC coils 5-94
5-26 Current change in shorted superconducting coils as a result of an emergency discharge 5-94
5-27 50-kA vapor-cooled lead characteristics 5-99
5-28 Circulating current loss in copper blocks 5-100
7-1 Sector removal procedures and equipment 7-4
7-2 Sector replacement procedures and equipment 7-5
7-3 Maintenance equipment for the removal and replacement of one sector 7-8
7-4 Summary of equipment costs 7-37
7-5 Time and motion evaluation to reach F/W armor tiles in situ 7-44
7-6 Component weights to be handled for in-vessel maintenance operations 7-56
7-7 The volume of the counterweight is significantly impacted by the choice of material 7-61
7-8 FED TF coil maintenance: major tasks 7-66
7-9 Characteristics of control coil removal 7-74
7-10 Characteristics of EF coil removal 7-76
8-1 Summary of hot cell facility tours and discussions 8-7
8-2 Hot cell facility characteristics 8-10
8-3 Tokamak building characteristics 8-15
9-1 Proposed FED operation plan 9-2
9-2 FED system failure rate (λ) and downtime ratio (ρ) requirements 9-8
9-3 Failure rate (λ) and downtime ratio (ρ) requirements for select FED components 9-9
11-1 Cost escalation summary 11-4
11-2 Recommended structures and site cost estimates 11-10

11-3 Major maintenance equipment cos update 11-13
11-4 Partial tritium breeding cost evaluation 11-16
11-5 Full tritium breeding cost evaluation 11-18
11-6 Summary of potential cost reductions/increases — FED Baseline 11-22

ENGINEERING STUDIES FOR FED BASELINE

LIST OF MAJOR CONTRIBUTORS

CHAPTER 1

P. Sager (FEDC/GA)

CHAPTER 2

P. Sager (FEDC/GA)
R. Barrett (FEDC/B&R)
T. Brown (FEDC/Grumman)
G. Fuller (FEDC/MDAC)
S. Kalsi (FEDC/GE)
J. Murray (FEDC/PPPL)
W. Reiersen (FEDC/Grumman)
G. Smith (Grumman)

CHAPTER 3

T. Brown (FEDC/Grumman)
B. Cramer (FEDC/MDAC)
R. Hooper (FEDC/GE)
W. Reiersen (FEDC/Grumman)
L. Reid (FEDC/UCC-ND Engr.)
G. Smith (Grumman)
V. Srivastava (FEDC/GE)
F. Wu (FEDC/ORNL)

CHAPTER 4

G. Fuller (FEDC/MDAC)
J. Davisson (MDAC)
B. Engholm (FEDC/GA)
M. Griffin (MDAC)
J. Haines (FEDC/MDAC)
J. Kirchner (FEDC/MDAC)
D. Lee (FEDC/MDAC)
C. Lilly (MDAC)
J. Murray (FEDC/PPPL)
P. Sager (FEDC/GA)

CHAPTER 5

S. Kalsi (FEDC/GE)
R. Hooper (FEDC/GE)
B. Hunter (FEDC/GE)
J. Rogers (LANL)
V. Srivastava (FEDC/GE)
L. Turner (ANL)
F. W. Wiffen (FEDC/ORNL)

CHAPTER 6

J. Murray (FEDC/PPPL)
S. Borowski (FEDC/ORNL)
G. Bronner (PPPL)
D. Strickler (FEDC/ORNL)

CHAPTER 7

P. Spampinato (FEDC/Grumman)
L. Dietz (Grumman)
N. Grant (ORNL)
D. Kuban (UCC-ND Engr.)
L. Masson (EG&G/INEL)
K. Watts (EG&G/INEL)

CHAPTER 8

R. Barrett (FEDC/B&R)
S. Ghosc (Bechtel)
L. Masson (EG&G/INEL)

CHAPTER 9

W. Reiersen (FEDC/Grumman)

CHAPTER 10

R. Barrett (FEDC/B&R)
B. Engholm (FEDC/GA)
G. Fuller (FEDC/MDAC)
J. Haines (FEDC/MDAC)
S. Herring (EG&G/INEL)
P. Spampinato (FEDC/Grumman)

CHAPTER 11

G. Smith (Grumman)
R. Barrett (FEDC/B&R)
B. Cramer (FEDC/MDAC)
R. Hooper (FEDC/GE)
W. Reiersen (FEDC/Grumman)
L. Reid (FEDC/UCC-ND Engr.)
P. Sager (FEDC/GA)
P. Spampinato (FEDC/Grumman)
F. Wu (FEDC/ORNL)

ACKNOWLEDGMENTS

These studies were carried out and supported by a large segment of the Fusion community, both at the Fusion Engineering Design Center and other institutions (as indicated by the List of Major Contributors), in addition to technical information and support by other contributors too numerous to track. Special recognition is due to T. E. Shannon and C. A. Flanagan, who reviewed the major technical results of the studies.

The production of this report reflects the contribution of numerous individuals at the Design Center and the FED Publications Office. P. J. Fogarty and M. H. Kunselman did the design layout drawings included in the report. Nancy Irby accomplished the major task of typing the entire draft. The FED Publications Office was responsible for the artwork, final layout and typing, proofing, and publication of the document. To all these great people: many thanks.

P. H. Sager
Technical Editor

ABSTRACT

Studies were carried out on the FED Baseline to improve design definition, establish feasibility, and reduce cost. Emphasis was placed on cost reduction, but significant feasibility concerns existed in several areas, and better design definition was required to establish feasibility and provide a better basis for cost estimates.

A comparison of basic configurations indicated that a design with a fully combined plasma chamber vacuum boundary and TF coil cryostat with all-external EF coils results in a capital cost savings of approximately $182 M. Other potential savings were obtained through design changes or better design definition of the intercoil support structure, remote maintenance equipment, TF coil case construction, and torus support spool, through an increase in the OH/EF solenoid field to 8 T and through elimination of the cryostat coil shields. The savings for these improvements totaled $45 M, or about 4%. The estimate of the facility cost had to be revised upward by about the same time amount, however, due to better design definition and revision of the unit costs. The overall capital cost savings, therefore, totaled about $182 M, or 17%.

Design definition and feasibility studies included the development of a labyrinth shield ring concept to prevent radiation streaming between the torus spool and the TF coil cryostat. The labyrinth shield concept which was developed reduced radiation streaming sufficiently to permit contact maintenance of the inboard EF coils. This potential problem would also be overcome by the adoption of the combined vacuum boundary concept which embodies relocation of the inboard EF coils to outside the TF coil bore.

Various concepts of preventing arcing between adjacent shield sectors were also explored. It was concluded that installation of copper straps with molybdenum thermal radiation shields would provide the most reliable means of preventing arcing.

Other design studies included torus spool electrical/structural concepts, test module shielding, torus seismic response, poloidal

conditions in the magnets, disruption characteristics, and eddy current effects. These additional studies had no significant impact on cost but did confirm the feasibility of the basic FED Baseline concept.

1. INTRODUCTION

A baseline design was developed for the Fusion Engineering Device (FED) in 1981.[1] This reactor was designed to:[2]

1. achieve the sustained production of fusion power in order to extract power from a blanket module under conditions that extrapolate to net power production in a fusion demonstration plant,
2. demonstrate a full fuel cycle operation to assure fuel self-sufficiency for a fusion demonstration plant, and
3. demonstrate the construction, safe operation, and maintainability of a device which integrated technologies representative of a fusion demonstration plant.

In order to accomplish this mission, a driven plasma burn mode with a fusion power multiplication factor (Q) of at least 5, a neutron wall loading of approximately 0.5 MW/m^2, and a burn time of about 100 s were adopted. Limited extended capability (2.5×10^4 pulses) was also provided with the potential of reaching ignition. This resulted in a maximum toroidal field (for the limited number of pulses) of 10 T, a machine major radius to 5.0 m and a plasma minor radius of 1.3 m (Table 1-1). At this rating, the plasma fusion power is 450 MW, and the wall loading is 1.0 MW/m^2. For this mode of operation, the burn time was estimated to be 50 s. For the Q = 5 rating, at which most of the engineering testing would be accomplished (2.5×10^5 pulses), the plasma fusion power is 180 MW. RF was adopted for startup assist (ECRH/ICRH) and bulk heating (ICRH) with neutral beam injection as an alternate for bulk heating. A pumped limiter was adopted for ash removal and impurity control with a poloidal divertor as an alternate.

The overall reactor design resulting from the 1981 study is illustrated in Figs. 1-1 and 1-2. The machine has 10 NbTi toroidal field (TF) coils enclosed in a cryostat which has access apertures between the outboard legs of adjacent TF coils. A spool structure, which supports the bulk shield and forms a vacuum boundary for the plasma chamber, is located in the toroidal bore of the TF coils. The bulk shield is segmented into ten sectors which are inserted through the access apertures

Table 1-1. Key parameters for the FED baseline

	8 T	10 T
Major radius (m)	5.0	
Plasma radius (m)	1.3	
Plasma elongation	1.6	
Fusion power (MW)	180	450
Neutron wall loading (MW/m^2)	0.4	1.0
Heating power (MW)		
Initial	50	
Burn	36	0
Q	5	Ignited
Burn time (s)	$\geq$100	~50
Duty factor	0.65	0.5
Average D-T density (m^{-3})	0.8×10^{20}	1.2×10^{20}
Average total beta (%)	5.2	
Plasma current (MA)	5.4	6.5
TF coil clear bore, width × height (m)	7.4 × 10.9	
Field on axis (T)	3.6	4.6
Number of full field pulses	2.5×10^5	2.5×10^4
Availability (%)[a]	10-20	10-20

[a]Defined as ratio of operating time to operating time plus downtime.

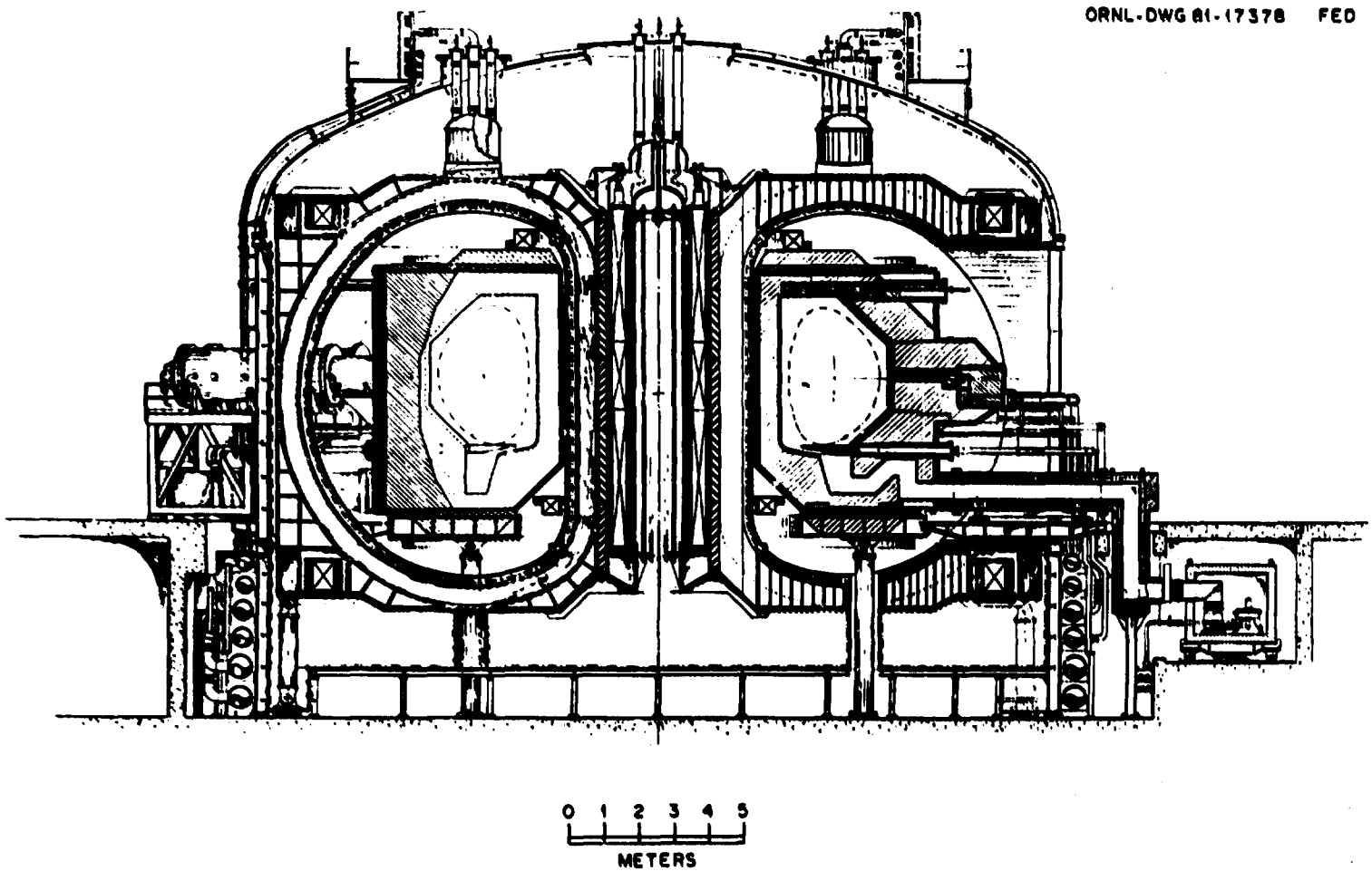

Fig. 1-1. FED reference configuration, elevation view.

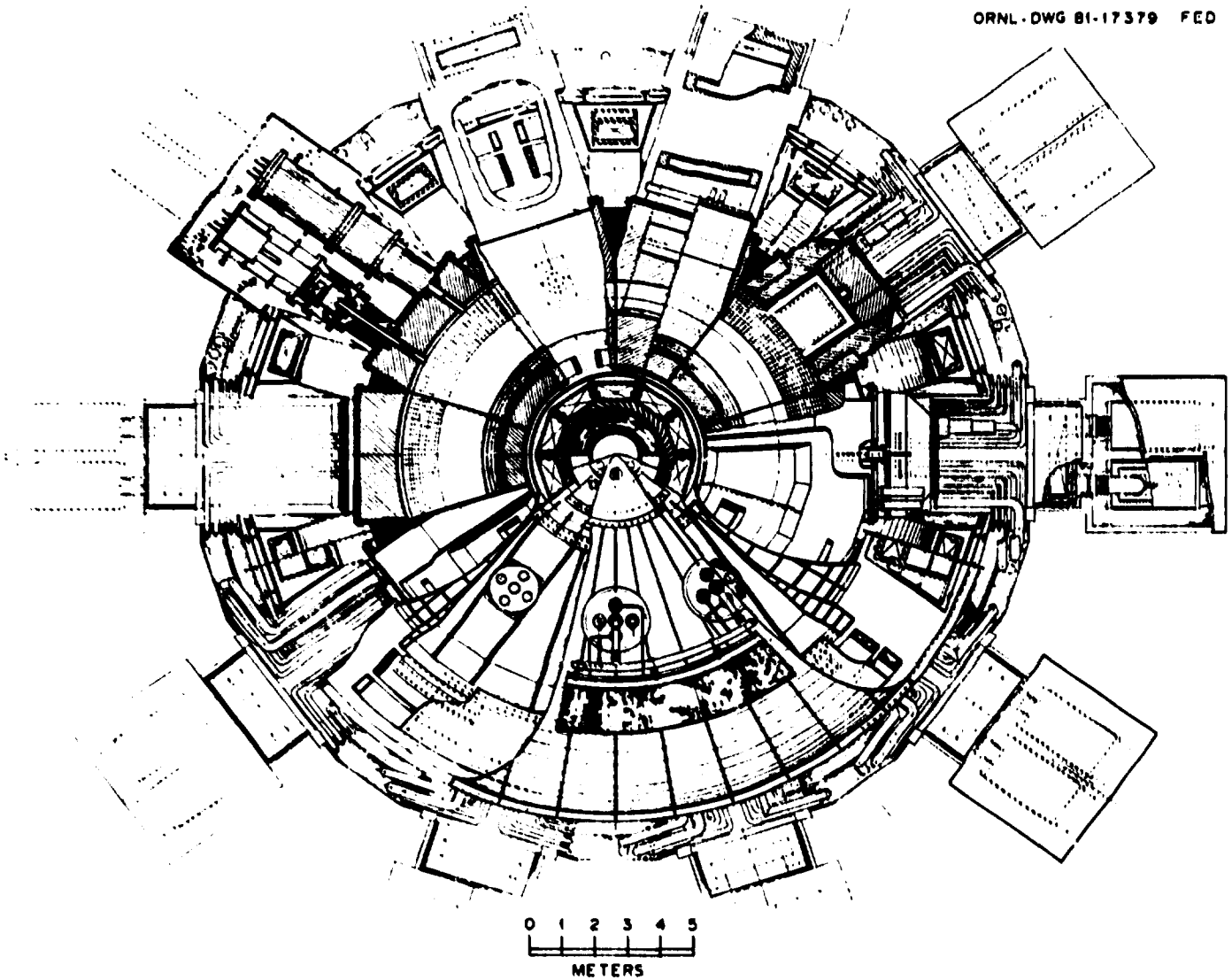

Fig. 1-2. FED reference configuration, plan view.

into the spool structure with the sectors seal-welded to the outboard perimeter of the spool structure to complete the plasma chamber vacuum boundary. The poloidal field coil system includes a central solenoid, two superconducting equilibrium field (EF) coils located outside the TF coils and outboard of the plasma, and two normal conducting EF coils located inside the TF coil bore inboard of the plasma, along with four control coils inside the TF coil bore. The pumped limiter blades are installed in penetrations in the shield sectors to provide ready removal and replacement.

The FED Baseline total capital cost was projected to be approximately $2,200 million (in 1981 dollars).[1] This was perceived to be higher than desired. Accordingly, in the beginning of FY 1982 a survey was made of potential cost savings which might be made. On the basis of this survey, it was concluded that a total net savings of approximately 20% might be realized. Studies were, therefore, undertaken to further explore the design changes which might result in substantial cost savings ($\gtrsim$\$10 million). Some of the potential savings were identified with straightforward design modifications, such as the use of epoxy-fiberglass panels in the intercoil support structure to reduce eddy current losses and refrigeration system cost. More radical design changes which involved combining the plasma chamber vacuum boundary with the TF coil cryostat and placing all the EF coils outside the TF coils, however, accounted for the bulk of the potential cost savings.

It was also recognized that the design of some of the components of the FED Baseline were inadequately defined to establish feasibility and provide a basis for a reliable cost estimate. Studies of the remote maintenance equipment, for example, were initiated to develop design concepts and initial cost estimates.

A systematic study was also carried out to establish an apportionment of the reliability and maintainability requirements of the major components and subsystems. This was judged to be necessary for future design efforts on the FED Baseline.

Finally, the cost projections for the FED Baseline were updated to reflect 1982 costs and the cost impact of proposed design changes.

REFERENCES

1. Flanagan, C. A., et al., "Fusion Engineering Device Design Description," ORNL/TM-7948, December 1981.
2. "The Fusion Engineering Device," DOE/TIC-11600, October 1981.

2. SUMMARY

The design studies performed in FY 1982 for the FED Baseline can be divided into three categories: (1) those concerned with the basic configuration of the reactor, (2) those concerned with better definition of or improvement in the design of the components and subsystems, and (3) those concerned with defining the overall system considerations, such as availability and maintainability, safety, and cost. In the studies of the basic configuration, the performance requirements were assumed to be fixed, and emphasis was placed on arrangements which would result in major cost reductions. In the component and subsystem design studies and in the system studies, however, the basic configuration was assumed to be fixed as derived in the previous FED studies (Figs. 1-1 and 1-2); and emphasis was placed on design definition and feasibility.

The studies show that substantial capital cost savings can be achieved and that the basic design concept is feasible. The major conclusions are:

- A capital cost savings of approximately 17% can be realized by combining the plasma chamber vacuum boundary with the TF coil cryostat, increasing the number of TF coils from 10 to 12, and decreasing the size of the TF coils.
- The radiation streaming in the gap between the torus spool structure and TF coil cryostat of the FED Baseline can be controlled with the installation of labyrinth shield rings.
- Arcing between adjacent shield sectors can be prevented with the installation of copper straps which are protected with molybdenum thermal shields.
- The required torus spool electrical characteristics can be obtained with the use of 316 stainless steel structural material and dielectric breaks.
- Lateral deflections of the torus can be controlled in the event of a seismic disturbance with the installation of lateral restraints at the base of the spool structure.

- A capital savings of approximately $9 M can be realized by the use of epoxy-fiberglass box structure shells in the TF coil intercoil support structure.
- An additional $9 M in capital cost savings can be realized by increasing the ohmic heating solenoid from 7 to 8 T.
- The facility costs are expected to increase by approximately $45 M, due mainly to a reassessment of the unit cost of the reactor building and hot cell facility.
- The overall capital cost of the FED Baseline is expected to decrease by $182 M, or 17%, if all the design changes and cost adjustments identified are adopted.

2.1 REACTOR DESIGN OPTIONS

A number of configuration options were investigated as reflected in Fig. 2-1; their dominant features are summarized in Table 2-1. The changes which potentially result in major cost savings include a combined TF coil and plasma chamber vacuum boundary, a revised TF coil shape with a reduced vertical bore, all external superconducting PF coils, and combinations of these systems. An independently supported lower outboard PF coil offers the possibility of an improvement in maintainability.

2.1.1 Basic Configuration Options

It was recognized that the combination of the TF coil cryostat, the torus spool inboard wall structure, and the clearance provided between these two structures result in a substantial displacement of the plasma from the TF coil pack with little shielding effect. Since the field at the coil pack is limited by technology considerations, the field at plasma axis (and, therefore, the performance of the reactor) is directly affected by the radial build, which includes the two vacuum vessels and the clearance between them.

The possibility of combining the vacuum boundary in the inboard region alone (Fig. 2-1) was explored. For this case, the basic

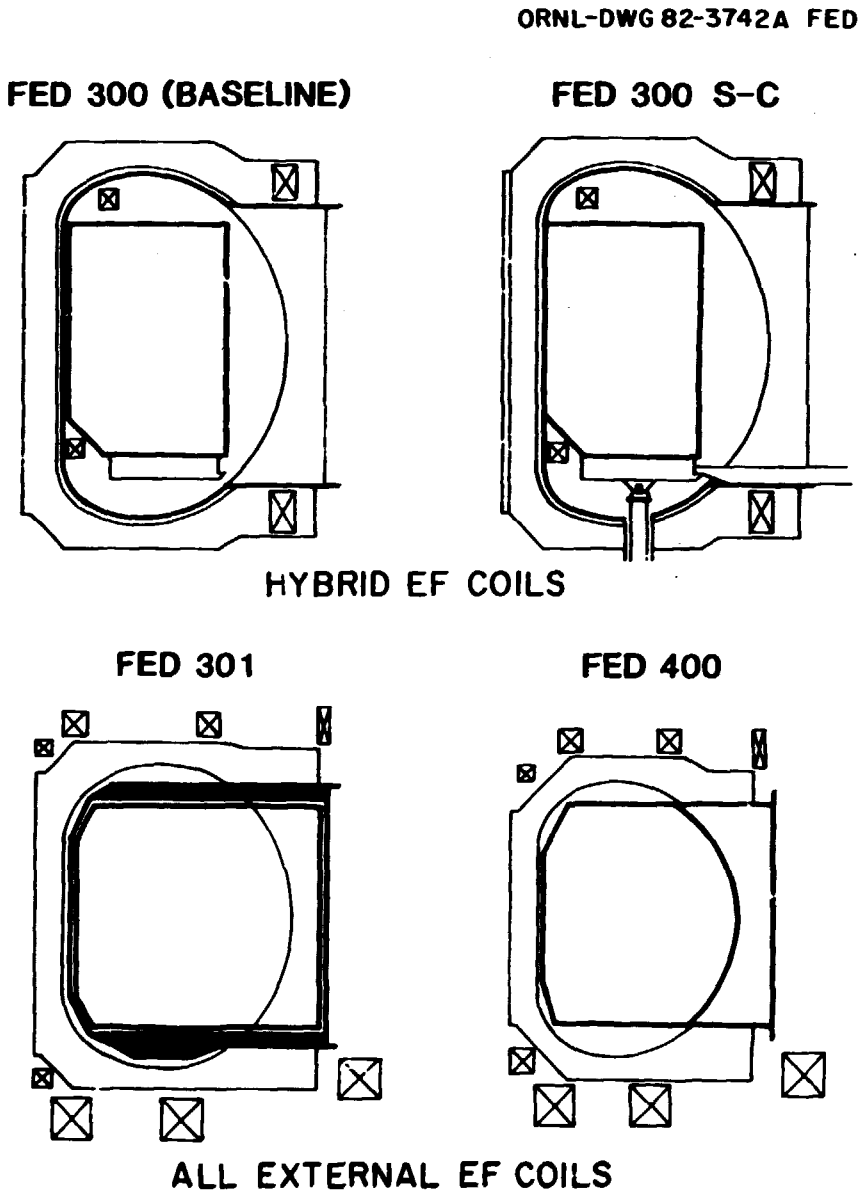

Fig. 2-1. Configuration options.

Table 2-1. Features of reactor design options

	FED 300 (Baseline)	FED 300 S-C	FED 301	FED 400
No. TF coils	10	10	10	12
No. torus sectors	10	10	10	12
Plasma edge ripple,%	0.8	1.2	1.2	1.2
TF coil bore, m	7.8 × 11.25	7.8 × 11.25	7.65 × 9.5	6.5 × 8.6
Coil configuration	Constant tension	Constant tension	Arbitrary	Arbitrary
EF coil placement	External/internal	External/ internal	External	External
Vacuum boundary	Separate	Semi-combined	Fully combined	Fully combined

configuration of the TF coils is retained, and the normal conducting PF coils in the toroidal bore of the TF coils are left unchanged. The major radius can be reduced by 35 cm while maintaining the neutron wall loading at 0.4 MW/m^2 (8 T at TF coil pack) and burn time at 100 s. The potential cost savings for this case was estimated to be $70 million in direct capital cost.

A second option explored involves the use of reduced-size TF coils (with a corresponding increase in toroidal field ripple from 0.8% to 1.2% at plasma edge) and relocation of the inboard EF coils to outside of the TF coil bore where they are changed to superconducting coils. This arrangement does not involve a change in the radial build, but it results in an overall cost savings of $25 million. This cost savings is due primarily to a change in the mechanical arrangement of the torus which permits an increase in the ripple to 1.2%.

The third option incorporates both the combined vacuum boundary and the all-external EF coil arrangement. In addition, the TF coil configuration is changed to reduce the coil bore height-to-width ratio, and the number of TF coils is increased from 10 to 12. Both of these changes permit the use of a minimum-size TF coil consistent with ripple and access constraints and minimize the cost of both the TF coil and PF coil systems, as well as the cost of overall reactor plant due to decreased major radius. The total cost savings of this option as compared to the baseline is approximately $150 million.

These three options were compared with the baseline in terms of R&D requirements, maintainability and availability, and other qualitative factors, as well as cost. There appeared to be no differences in the other factors as significant as the differences in cost. The R&D requirements appeared to be about equal. The specific design developed for the combined vacuum boundary appeared to provide for a somewhat simpler procedure for the very difficult process of a TF coil replacement. Flexibility to accommodate and provide access to the torus, however, might be somewhat compromised where the common vacuum boundary is adopted at the top and bottom of the plasma chamber.

It appears clear that the common vacuum boundary should be adopted, at least in the inboard region between the torus and the inboard leg of

the TF coil. Also, if a 1.2% ripple is acceptable, the fully integrated vacuum boundary with the all-external EF coils and the modified TF coil configuration (Fig. 2-2) should be adopted in any future tokamak designs similar to the FED Baseline.

2.1.2 Lower Outboard EF Coil

An area of major concern with the 1981 FED Baseline design was the replacement of the lower outboard EF coil in the event of a failure of this component. It appeared that it would be necessary to remove and replace this coil by progressively installing and removing reactor supports while shifting the EF coil laterally. Since the reactor weighs on the order of 10,000 tons, this would be an extremely difficult and time-consuming process.

As an alternative, the possibility of using a somewhat larger outboard EF coil (Fig. 2-2) which would be separately supported and could be removed by hoisting it around the rest of the reactor was explored. This appears to offer a major benefit in terms of maintainability of the reactor without a serious cost penalty. Accordingly, it is recommended that this design concept be adopted in future studies of FED-type reactors.

2.2 TORUS DESIGN STUDIES

In the torus design studies, emphasis was placed on design definition in order to establish feasibility in critical areas.

2.2.1 Inboard Gap Shielding

Early in the FED design activities it was recognized that the gap between the spool structure and the magnet system cryostat at the inboard leg of the TF coil was a source of neutron streaming. The streaming would result in activation of regions above and below the torus where contact maintenance activities are desired. Several configurations of local shielding were examined from a neutronics performance

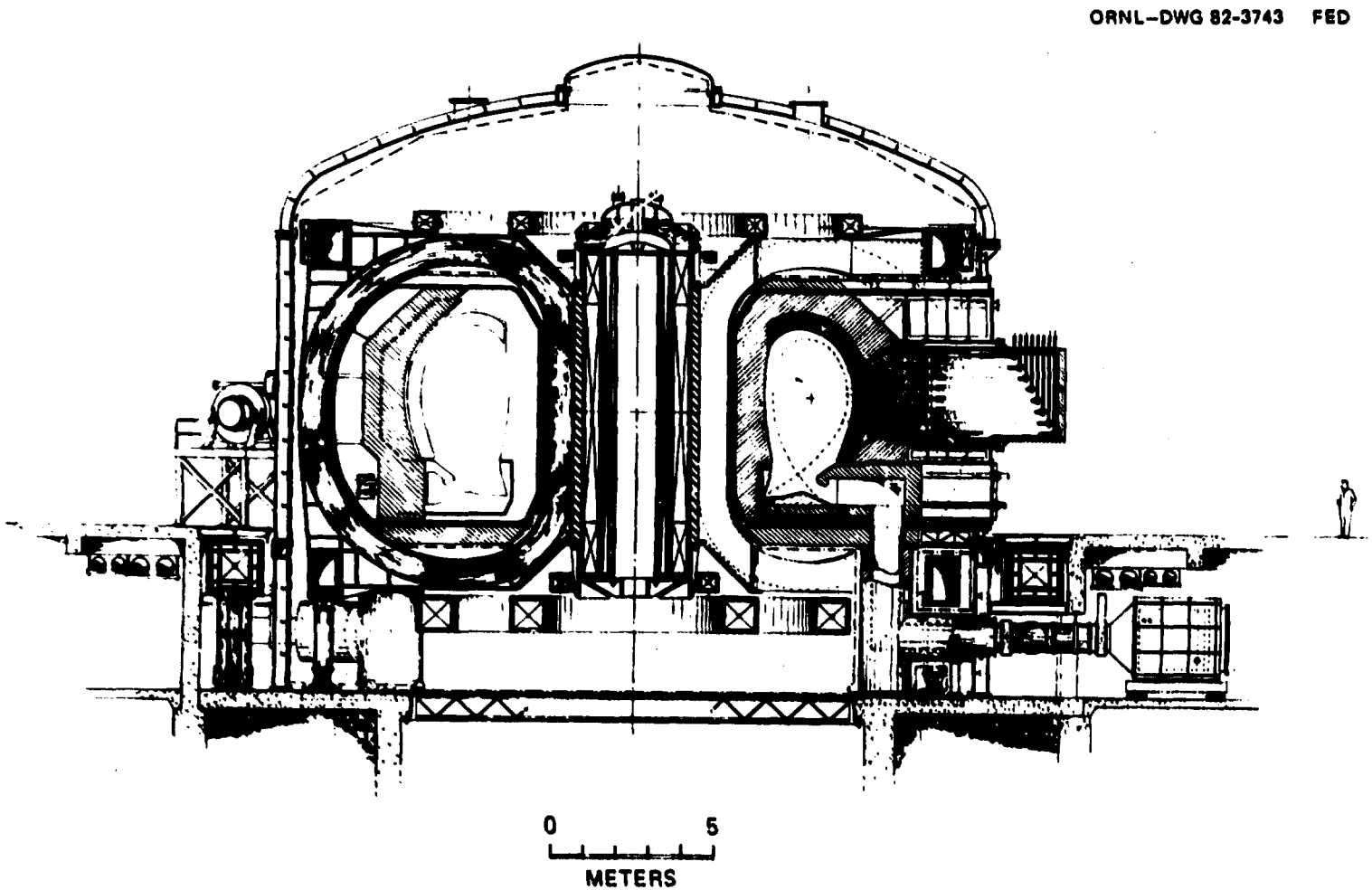

Fig. 2-2. FED-400 elevation view.

standpoint. A labyrinth configuration was chosen. The design (Fig. 2-3) consists of two sets of shield rings, one set installed between the TF coil cases and the TF coil cryostat and the other between the cryostat and the spool inboard wall. The shield rings are fabricated from stainless steel and boron carbide. While this design results in some very localized regions of high activity, the general level of activity is acceptable.

2.2.2 Torus Current Path

A major concern in the design of the torus is the ability to accept major disruptions without significant uncontrolled arcing between the shield sectors and other components located near the inner surface of the shield. Damage predictions for uncontrolled arcing conditions indicate a severe loss of surface material, with serious maintenance consequences.

A design approach to prevent arcing is to bridge the gaps between the shield sectors and between adjacent first wall panels with a toroidal conductor. A number of design configurations were defined and evaluated to establish the preferred approach.

A simple copper strap passively cooled and protected by a thin molybdenum thermal shield was selected because of the inherent reliability of the passive features and a large capacity for handling induced currents.

2.2.3 Torus Spool

The torus spool located at the outside of the bulk shield must be designed (1) with electrical properties consistent with good startup and control characteristics for the system and (2) to aid in achieving the disruption control. These requirements dictate that the electrical resistance of the torus spool should be approximately ten times the electrical resistance (toroidal) of the shield inner surface.

For the design approach where copper straps are employed at the shield inner surface, a resistance of about 400 $\mu\Omega$ is required at the

ORNL-DWG 82-3744 FED

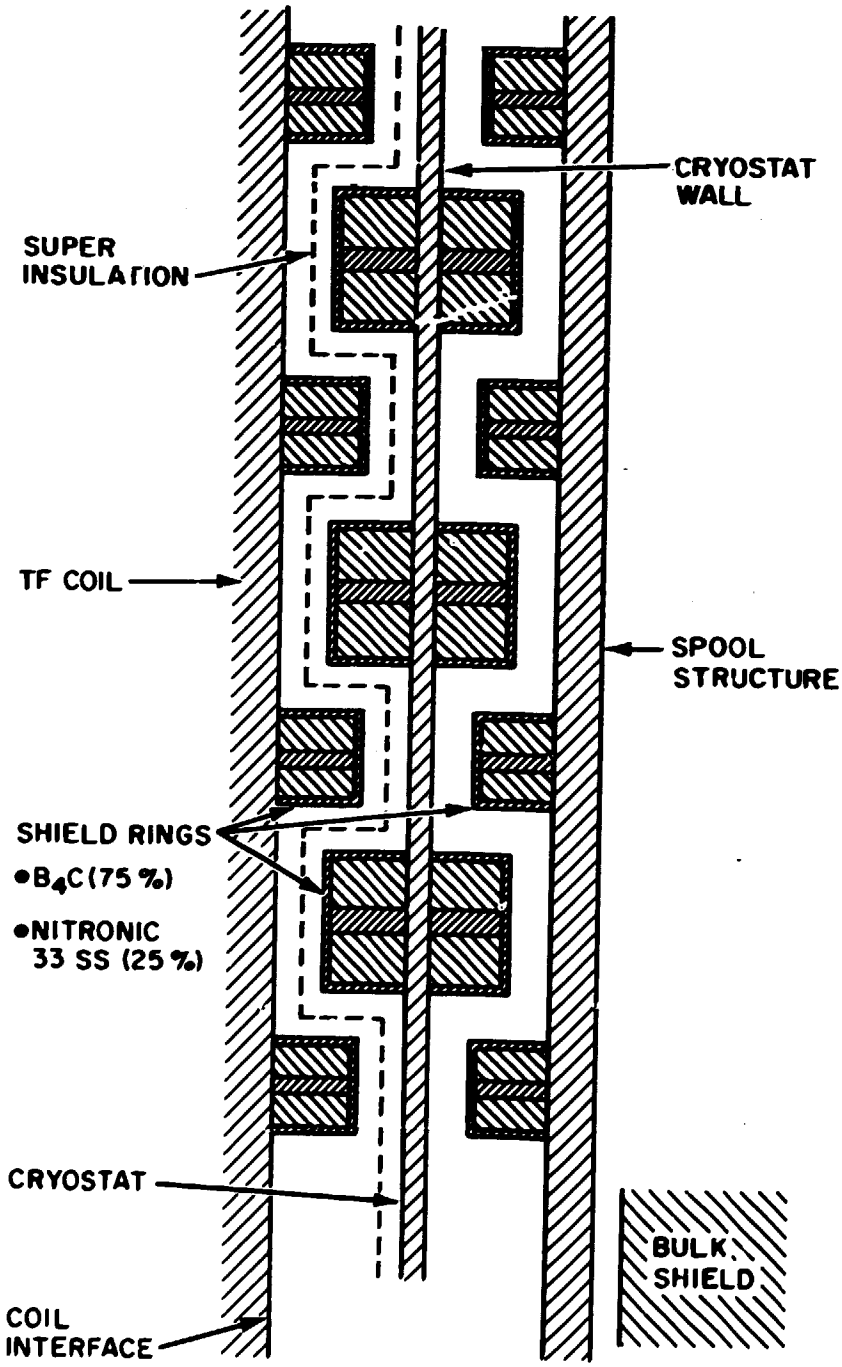

Fig. 2-3. Multiple shield rings.

spool. The incorporation of Inconel in the total spool structure comes marginally close to meeting this objective, with only the basic structure providing the resistance. The use of 316 SS with high-resistance breaks in at least two of the radial frame members, which results in a lower cost and significantly more margin in electrical resistance, was selected as the preferred approach.

2.2.4 Test Module Shielding

A significant fraction of the volume occupied by a test module is unavailable for neutron shielding. This must be replaced at the outer perimeter of the FED torus for those two sectors dedicated to support of the test modules. A conceptual design of a portable shield was accomplished which gives access to the modules individually such that module replacement does not interfere with other auxiliary subsystems located in the vicinity. This portable shield, fabricated of Neutronic 33, water and lead, has a total thickness of 35 cm.

2.2.5 Seismic Response

A simplified NASA structural analysis (NASTRAN) finite element model of the FED Baseline was developed and used in modal and response analyses. Mode shapes and resonant frequencies were calculated, and deflections and activations due to a seismic input were predicted. The results indicate that the maximum lateral deflection of the center of gravity of a shield sector is 0.86 cm, with a lateral constraint of a torus support ring incorporated at the bottom of the spool. Without this constraint, the deflections would be about six times larger.

2.2.6 Poloidal Geometry Effects on the Thermal Characteristics of the First Wall

Including poloidal variations in the geometry of the first wall resulted in ranges in temperatures for the armor tiles on the inboard wall having a lower bound of 1100°C and an upper bound of 1500°C. These analyses were conducted for the 10-T operating scenario and for worst

case wall thermal loads, i.e., plasma edge conditions. These temperatures are above the methane temperature window but in a region where recent experiments have shown high erosion.

Sensitivity studies showed that the tile temperatures are strongly dependent on plasma edge conditions, magnetic field, stainless steel emittance, and contact conductance between the mechanically attached graphite tile and the shield surfaces.

The design for the outboard first wall panels and their coolant systems performs adequately with material temperatures less than 340°C for all conditions examined.

2.3 MAGNET SYSTEM STUDIES

In the magnet system studies, emphasis was placed on design modifications which might result in significant cost reductions. An examination of the TF coil structure reflected that approximately $8 M could be saved by adopting a built-up structure in place of the heavy wall coil case (Fig. 2-4) reflected in the baseline design.

In the FED Baseline, the stainless steel intercoil structure resulted in high eddy current losses and, therefore, high cryogenic refrigeration system costs. Using epoxy-fiberglass box structure shells and insulated joints to structurally tie the stainless steel load-carrying webs (Fig. 2-5), the eddy currents can be dramatically reduced. This results in a potential net savings of $9 M, most of which is in the reduction of the cryogenic refrigeration system capacity.

A third area of potential cost savings examined was that of the adoption of an 8-T ohmic heating solenoid. With the comparatively slow startup for the FED Baseline (6 s), the maximum field in the ohmic heating solenoid can be increased from 7 to 8 T. For a specified burn time and wall loading, this makes it possible to reduce the bore of the ohmic heating solenoid and, thereby, reduce the major radius. The resulting overall cost savings is about $9 M.

Another potential capital cost savings explored was the elimination of the cryostat cold shield. While the heat load to the liquid helium

ORNL-DWG 82-3745 FED

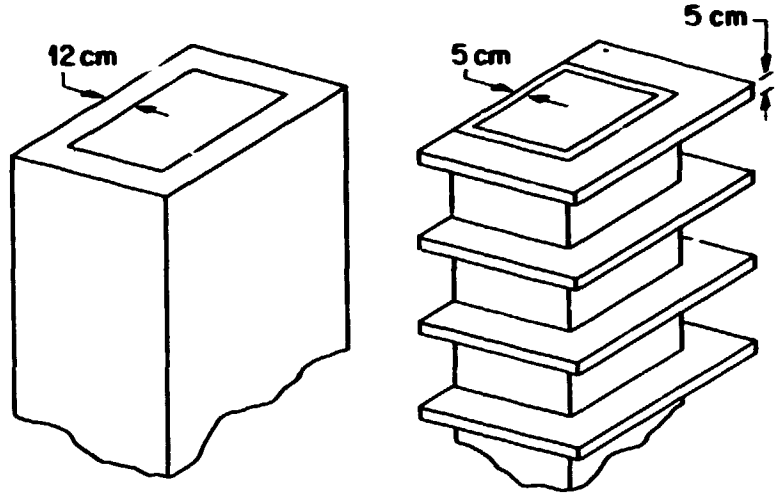

(*a*) THICK-WALL DESIGN (*b*) BUILD-UP DESIGN

Fig. 2-4. TF coil case concepts.

ORNL-DWG 82-3746 FED

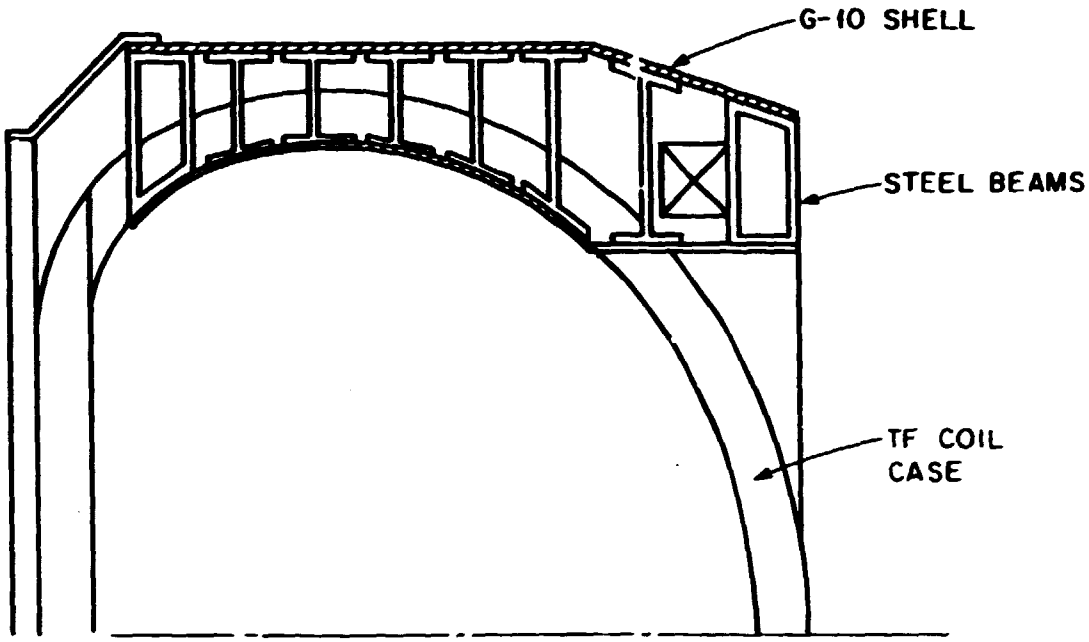

Fig. 2-5. Intercoil support structure concept.

refrigeration system and the cost of that system are increased somewhat, the study indicated a net savings of about $5 M. There would be an even greater savings due to the possible decrease in radial build, but in the study to reduce the radiation streaming in the inboard gaps between the torus spool and the TF coils, it was found that the space reserved for the cold shield had to be used for installation of shield rings.

Several other studies were performed to validate the FED Baseline design and to further our capability to continue the evolution of the design development. An analysis was carried out to verify that no helium entrainment occurs in the ohmic heating solenoid and ring coils during pulsed operation. Several fault conditions were examined; all coils were found to be trouble-free, except for a potential overcurrent problem in the central section of the ohmic heating solenoid in the event of an unintentional shutdown. This can be alleviated by discharging the coil over a time period much longer than the normal shutdown time of 10 s.

2.4 ELECTROMAGNETIC STUDIES

Electromagnetic studies were further pursued to better define disruption characteristics, to consider the startup coil requirements, and to develop analytical tools for obtaining solutions for induced eddy currents.

It was recognized that the requirements on disruption developed for ETF and used for FED needed updating. The disruption time and inductive energy specified for the current decay phase of disruption are not constraints as given but really depend on the electromagnetic characteristics of the torus near the plasma. The disruption time can be increased, and the energy dissipated on the small surface area of the inner wall can be decreased by providing a good conducting shell near the plasma.

A study of the current decay phase of disruption was completed. This study shows that the FED design disruption time is 25 ms rather than the earlier estimated 10 ms. The energy producing the possible melt area on the first wall is 3 megajoules rather than the 30 megajoules

estimated earlier. This could permit elimination of the inboard wall armor in future designs.

A review of the rf-assisted startup indicated that the required plasma startup voltage can be reduced from 250 volts to about 10 volts. This makes it possible to use a reasonable size startup coil. Since this coil requirement is considered to be a modest one, design of this component has been deferred pending further effort on components with greater impact.

The analytical tools for obtaining solutions for eddy currents and their effects were reviewed, and improvements were made in the procedures for determining the energy losses, voltseconds, and startup coil sizes required for any tokamak. These tools will be available for the future work on this subject.

2.5 MAINTENANCE STUDIES

Maintenance studies were carried out in order to gain a better understanding of key disassembly scenarios and to develop more reliable cost estimates for maintenance equipment. The replacement scenario for a torus sector was further developed over earlier work and was used to identify the major equipment needed, as well as specifications for that equipment. Three major equipment concepts resulted; they are: the "Movable" Manipulator System (Fig. 2-6), the Sector Handling Device (Fig. 2-7), and the In-Vessel Manipulator System (Fig. 2-8). Cost estimates were also developed for these designs. Test module handling equipment and limiter module handling equipment, which are also needed for operations on the torus, were investigated in less detail.

An in-depth development of the replacement of a TF coil was also developed to assess the maintainability of the basic FED configuration. Several modifications to the design were identified to ease the problems of handling and the impact to downtime resulting from this major replacement operation.

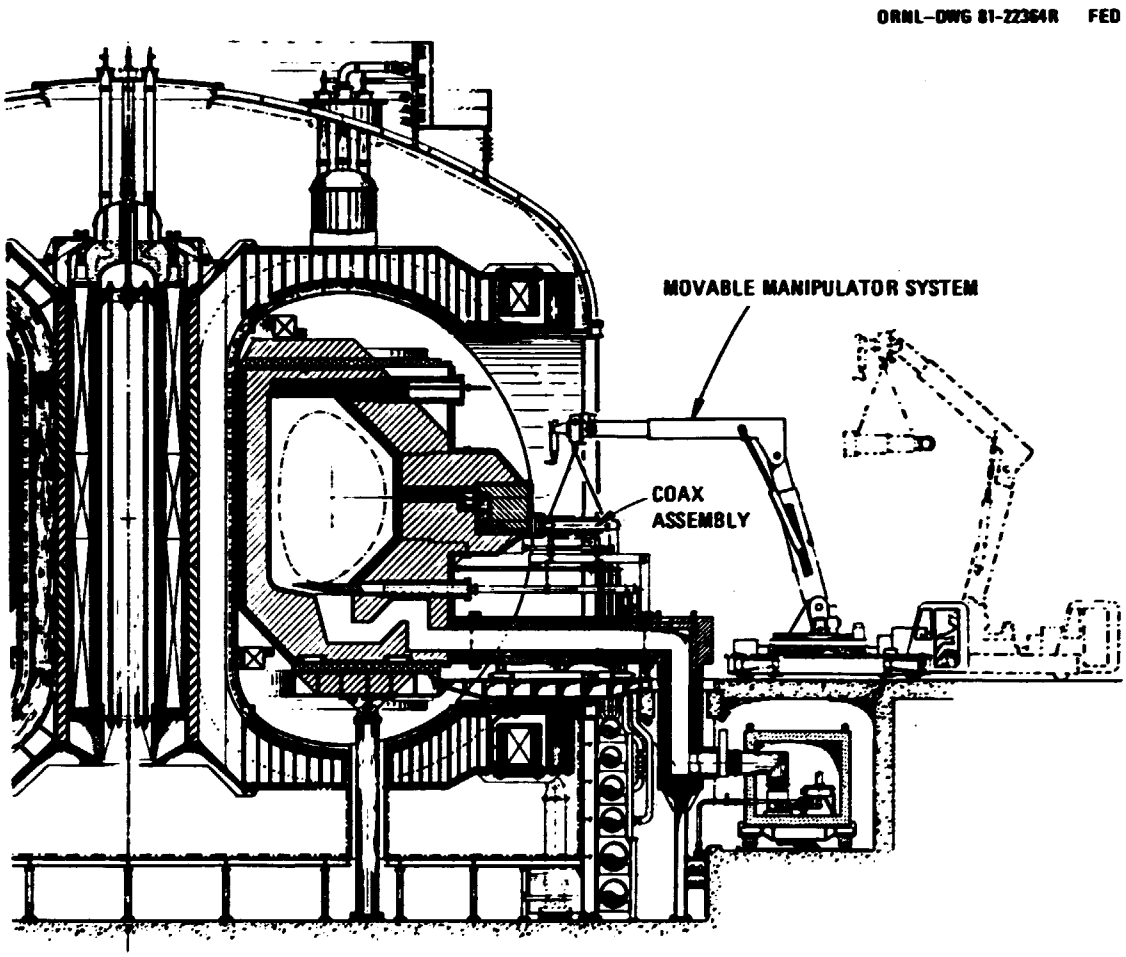

Fig. 2-6. Movable manipulator system.

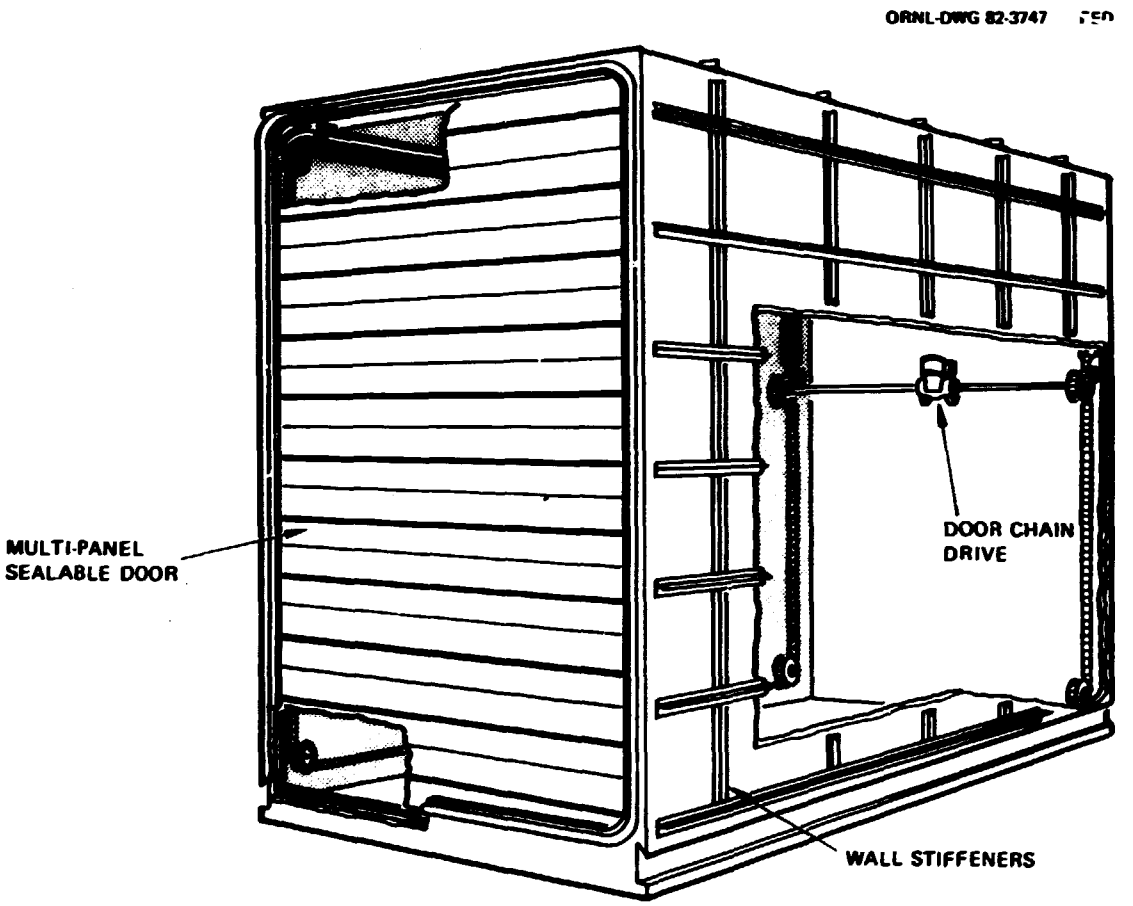

Fig. 2-7. Sector handling device.

ORNL-DWG R1-22367 FED

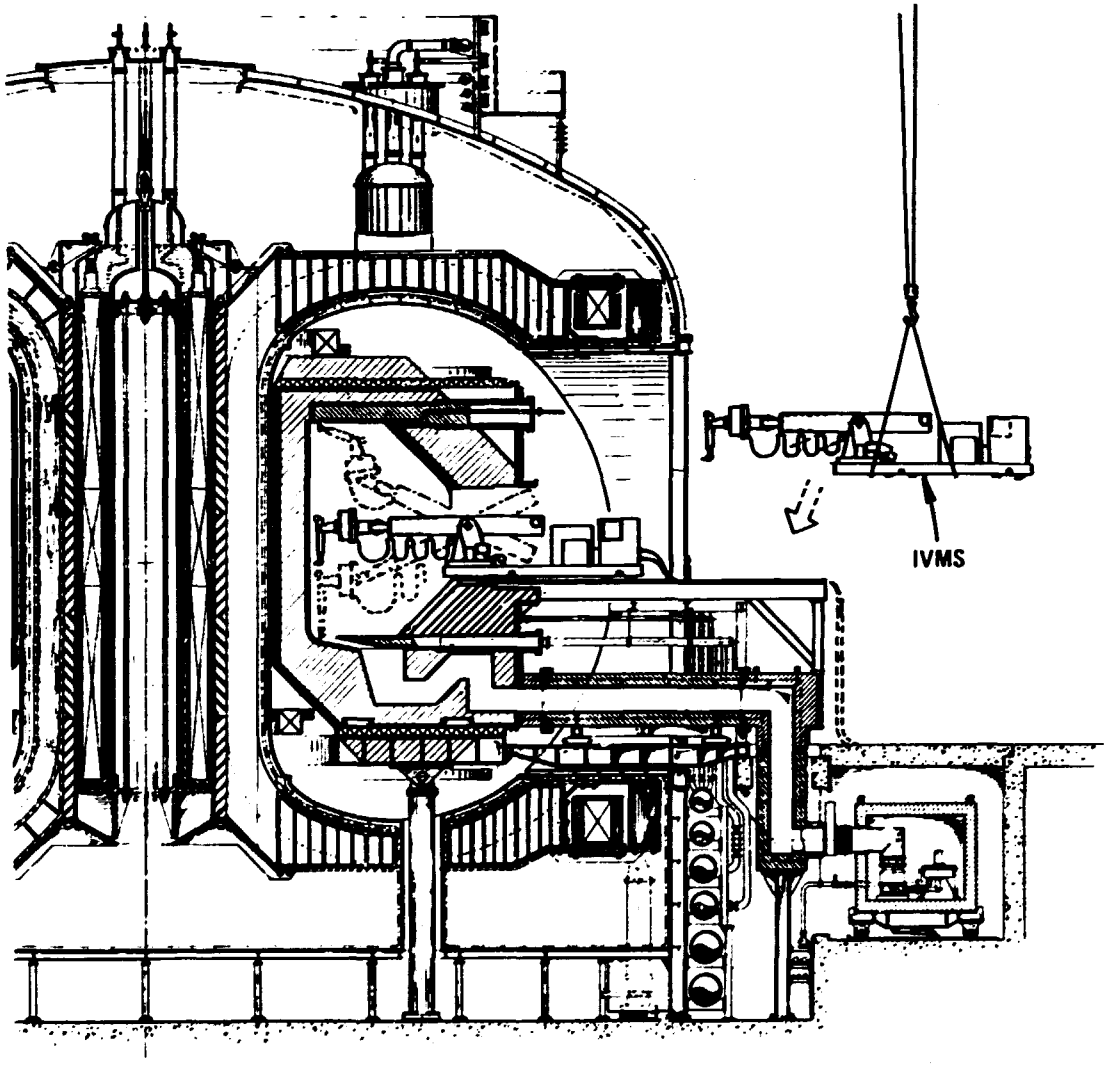

Fig. 2-8. In-vessel manipulator system (IVMS).

2.6 FACILITY DESIGN STUDIES

Design options for the hot cell facility were investigated. This investigation was based on information gathered from interviewing designers and operating personnel of several hot cell facilities at three national laboratories. The study also included a review of hot cell facility requirements. As a result of the study, the FED Baseline hot cell facility design was completely revised (Fig. 2-9).

The revision of the hot cell building led to a different approach for removing the PF coil from the reactor building. The reactor building design was revised to reflect this modified approach, and the suggested site plan was revised to reflect the changes in the hot cell facility and reactor building.

2.7 RAM REQUIREMENTS

An analysis was done to determine RAM (reliability, availability, and maintainability) requirements for FED. The 8-T D-T engineering testing phase of operation involves approximately 200,000 pulses in a five year period. Assuming a pulse length of 152 s, FED would have to achieve an availability greater than 19% in order to complete the indicated operations in the time allotted. Furthermore, due to the nature of the tests conducted during that phase of operation, long periods ($>10^3$ cycles) of continuous operation are required. Thus, an MTBF (mean time between failures) requirement of 72 hours was established. A top-level breakdown of system requirements, consistent with this overall requirement, is shown in Table 2-3.

2.8 SAFETY

Several applications of the safety standards and criteria to FED design situations were identified and studied.

Activation of reactor building walls and structures was identified as producing higher than expected dose rates within the reactor building; this has a significant impact on maintenance operations. The magnitude

ORNL-DWG 82-3748 FED

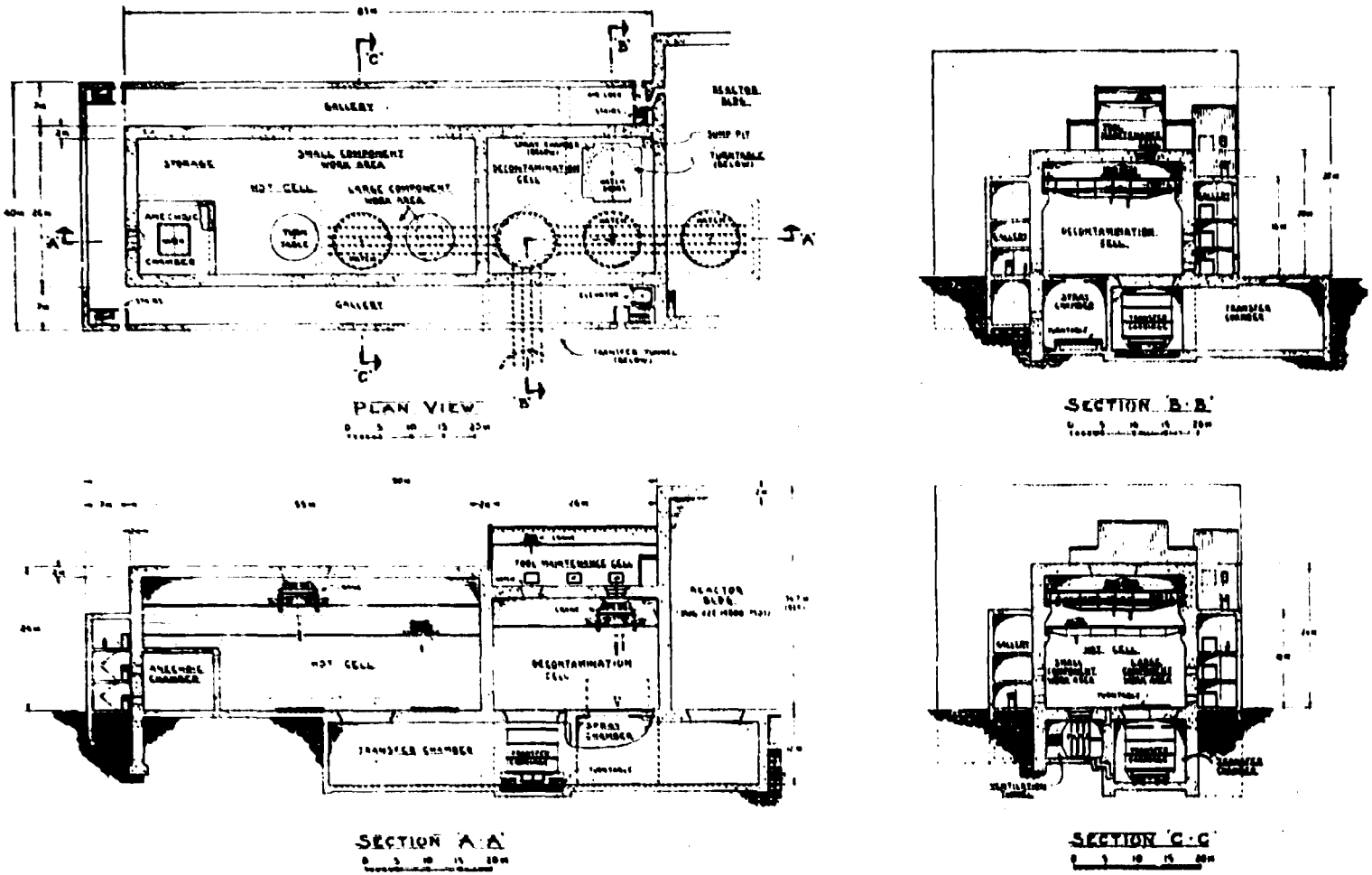

Fig. 2-9. Hot cell facility.

Table 2-3. FED system failure rate and downtime ratio requirements

System	Failure rate λ_{MAX}	Downtime ratio ρ_{MAX}[a]
Coil systems	1.5-3[b]	5.0-1
Torus systems	1.8-3	4.5-1
RF systems	1.3-3	1.1-1
Fuel systems	7.4-4	2.5-2
Diagnostics	5.1-4	8.6-2
Experimental systems	3.0-4	7.0-2
Info. & control systems	6.0-3	1.2-2
Heat transport systems	1.4-4	8.1-2
AC power systems	1.5-4	9.0-3
Facilities systems	2.0-4	6.4-3

[a] $\rho = \lambda * MTTR$

[b] Read as 1.5×10^{-3}

of the potential activation was estimated to be between 1 and 20 mR/hr. A possible design option, to reduce this activation, is to add boron to the structural concrete. However, this option is expensive. Another possible solution is to specifically tailor the concrete aggregate to this application. While this would be less expensive than boron additions, the actual costs would be highly site-dependent and cannot be estimated until a site is selected.

Radioactive contamination within the reactor building may also significantly affect maintenance operations. Potential sources of contamination from within the plasma chamber were identified and assessed. The results indicate that special attention will be necessary in both design and operation to control the contamination within the reactor building. Initial efforts to accommodate these expected contamination sources were to incorporate enclosures around shield sector handling machines, to plan for decontamination operations within the plasma chamber before sector removal, and to provide special transport techniques to transfer components to and from the reactor building. Additional techniques for contamination control need to be investigated.

Tritium safety issues continue to be studied to improve the protection of both the general public and the operating staff. Scoping studies indicated the tritium absorption by bare concrete and later release to the reactor building atmosphere could pose significant difficulties for maintenance operations. Coatings and liners for the concrete are being studied to determine suitable materials for this function. Epoxy paint is suggested as the most cost-effective technique for coating the concrete, but additional confirmatory material testing is required to verify this application.

Potential tritium leakage sources within the reactor building during normal operation are being identified, and the magnitude of the leakages are being scoped. Initial studies show that tritium leakage from the plasma vacuum chamber should be very small. The major sources of tritium leakage are now expected to be the leakage of tritiated water from the first wall and limiter coolant systems.

Identification and investigation of cryogenic blowdown scenarios have been continued in an effort to scope the potential impact on

reactor building and ventilation systems design. Cryogenic blowdown was identified as the major potential mechanism for causing tritium to be released from the reactor building. Current studies show that blowdown would take several minutes and would be easier to control than originally anticipated.

Carbon-14 was identified as a possible radioactive material that may require special control. Early estimates of C-14 production were based on activation of the reactor building air and showed very small hazard potential. However, activation of the liquid nitrogen for cold shields in the cryogenic systems could lead to significantly more C-14 production. Initial scoping calculations indicate that the C-14 production will be small but still may be significant enough to force the design and operation of the liquid nitrogen system as a radioactive system and to suggest that systems be designed for recovery of C-14 for burial as solid waste instead of venting it to the atmosphere.

2.9 COST PROJECTIONS

The FED Baseline configuration costs (Ref. 1) comprised a total direct cost of $1044.7 M and an overall total (direct plus indirect) of $2172.0 M in FY 1981 dollars. Applying an escalation factor of 10%, the corresponding total direct and overall costs in 1982 dollars become $1149 M and $2389 M, respectively.

The cost impacts stemming from the cost-related trade studies and investigations are summarized in Table 2-4. Adoption of a minimum-size, 12-TF coil configuration (FED 400) would result in a savings of about 17% in direct capital cost. Since the other proposed cost savings are offset by increases in the facility cost, the overall net savings also is approximately 17%.

The study of tritium breeding economics revealed that the operational cost savings afforded by breeding tritium for FED is far outweighed by the capital cost increase required to provide breeding capability. Incorporation of a partial blanket coverage breeding capability would result in a net cost increase of $33 M in life cycle cost of the

Table 2-4. Potential changes to FED Baseline costs

Cost element	Capital cost (M)[1]	Operational cost ($M)
1. Modified reactor configuration	-182	--
2. Intercoil supp't. struct. redesign	-9	-23
3. Facility changes (design & unit cost)	+45	--
4. Maintenance equipt. design changes	-2	--
5. TF coil case construction	-8	-21
6. Elimination of cryostat cold shields	-5	+4
7. 8-T forced flow solenoid	-9	--
8. Torus supp't. spool	-11	--
TOTAL	-182	

[1]"+" reflects cost increase; "-" reflects cost decrease.

machine. Incorporation of a full breeding blanket would result in a net cycle cost increase of about $129 M. If the operational requirements for the FED are substantialy increased, however, futher analysis may reflect an economic benefit is providing at least a partial tritium breeding blanket.

3. REACTOR DESIGN CONFIGURATIONS

3.1 INTRODUCTION

Reactor cost studies carried out on FED have highlighted the large cost sensitivities associated with the size of the TF coil, the PF system, and the plasma-to-TF coil radial build dimension. Maintenance of a fusion device always commands a high priority, since the operational feasibility of a reactor is largely dependent on the degree of difficulty associated with replacing component parts. Further special studies have been conducted since the FED Baseline design was completed; therefore, the FED Baseline design was reevaluated to determine if there were any configuration options available that would reduce its cost and/or improve the maintenance characteristics of the device.

A reactor design evolved from this study (defined as FED 400) which incorporates the following design features:

1. twelve reduced-size TF coils,
2. combined vacuum boundary between the superconducting (S/C) magnetic system and torus plasma chamber,
3. a lower outboard EF coil located in a separate vacuum boundary,
4. the same number of torus segments as TF coils,
5. vacuum pumping ducts relocated to pass down through the TF inter-coil structure and provide the gravity support for the torus, and
6. all exterior PF coils.

In order to evaluate the incremental cost or maintenance impact of each major change, three additional reactor design options were defined, which provided a transition from the reference FED configuration to this reduced-size reactor concept (FED 400). Studies covering cost, R&D, TF coil structure, maintenance, and availability were performed to evaluate the implications associated with each change in the design.

The design definition and discrete studies of the reactor options plus an overall evaluation of the designs considered are detailed in this section of the report.

3.2 REACTOR DESIGN DEFINITIONS

The designations and key features for the four reactor design options discussed in this section of the report are listed below:

FED 300 (Baseline Design)

- Separate vacuum boundaries between the torus plasma chamber and TF coils
- Hybrid PF system (interior copper coils and exterior superconducting coils)
- Ten constant-tension TF coils

FED 300/S-C

- A semi-combined vacuum boundary
- Hybrid PF system
- Ten constant-tension TF coils

FED 301

- Separate vacuum boundaries
- All-exterior PF coils
- Ten arbitrary-shaped TF coils (non-constant-tension)

FED 400

- Combined vacuum boundary
- All-exterior PF coils
- Twelve arbitrary-shaped TF coils
- Vacuum duct passes through bottom of vacuum boundary, thus allowing more optimum lower outboard PF coil location

Figure 3-1 illustrates pictorially the four reactor designs that represent the incremental steps from the FED Baseline design (FED 300) to a minimum-size TF coil concept of FED 400. Selected views of the four design steps are shown in Figs. 3-2 through 3-8. The FED 300 baseline is shown in Figs. 3-2 and features a separate vacuum boundary. The TF magnet cryostat is shown in Fig. 3-3, and the torus vacuum boundary spool is shown in Fig. 3-4. The FED 300/S-C configuration (Fig. 3-5) is identical to the baseline design, except it has a combined vacuum boundary along the cylindrical section between the TF coil

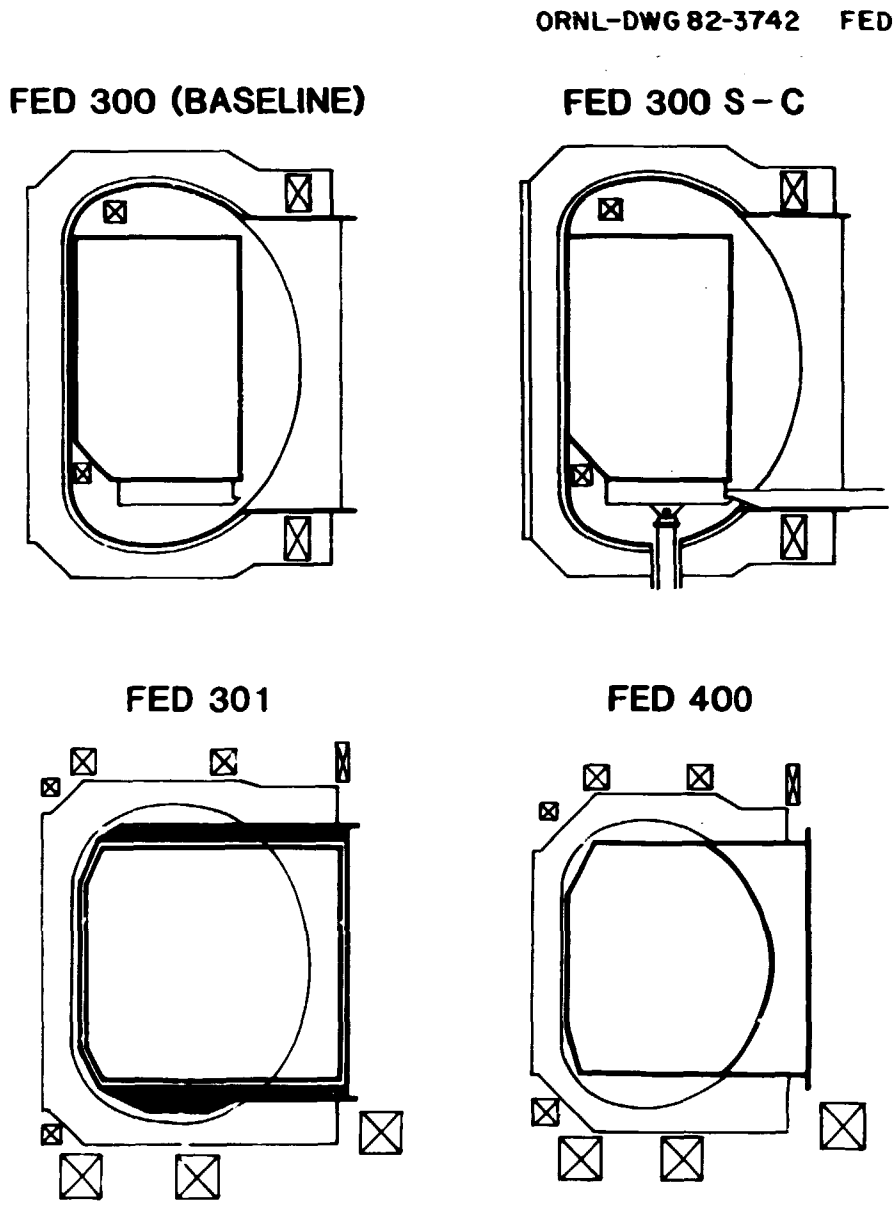

Fig. 3-1. Reactor design diagram.

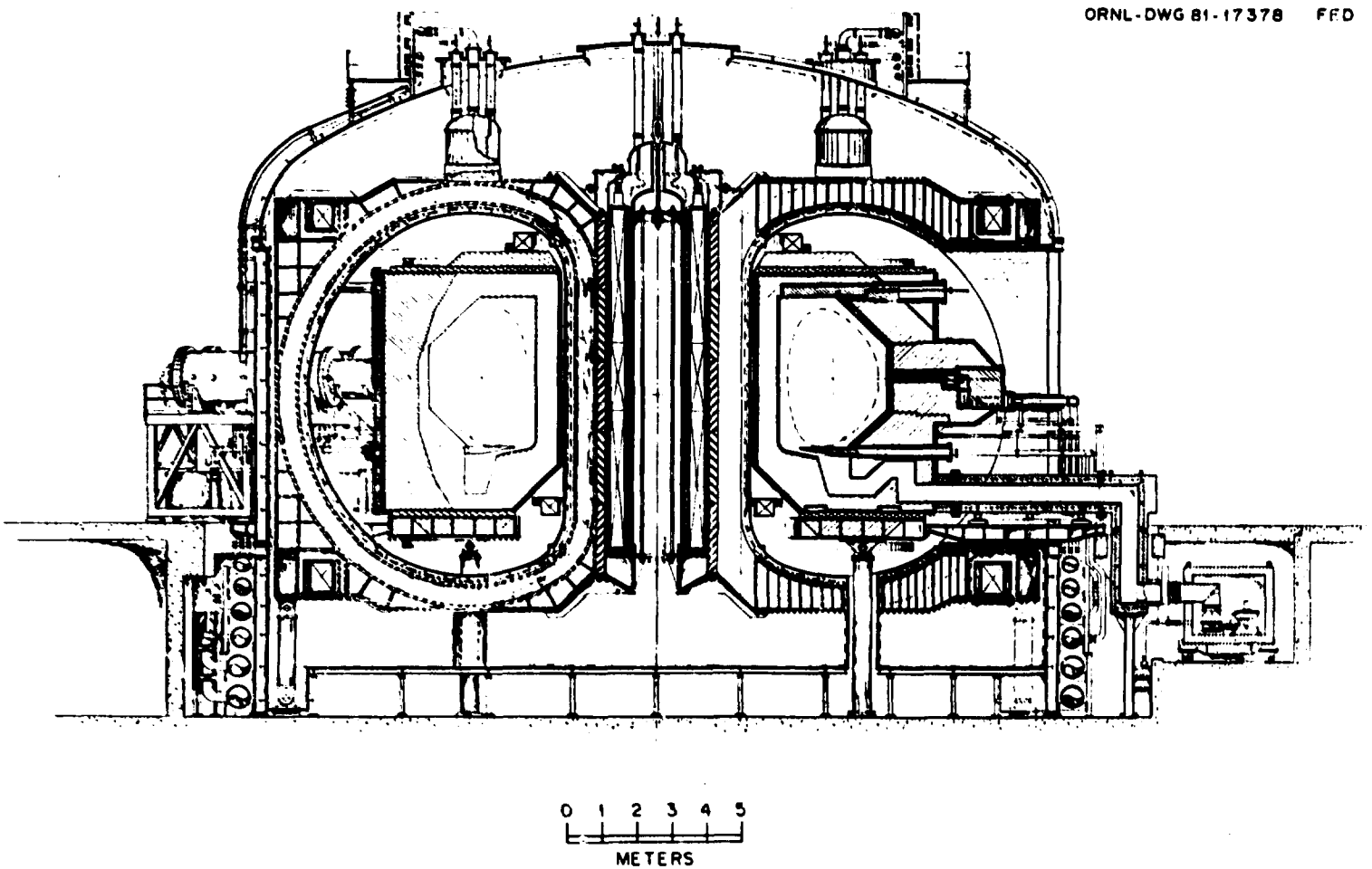

Fig. 3-2. FED reference configuration (FED 300) elevation view.

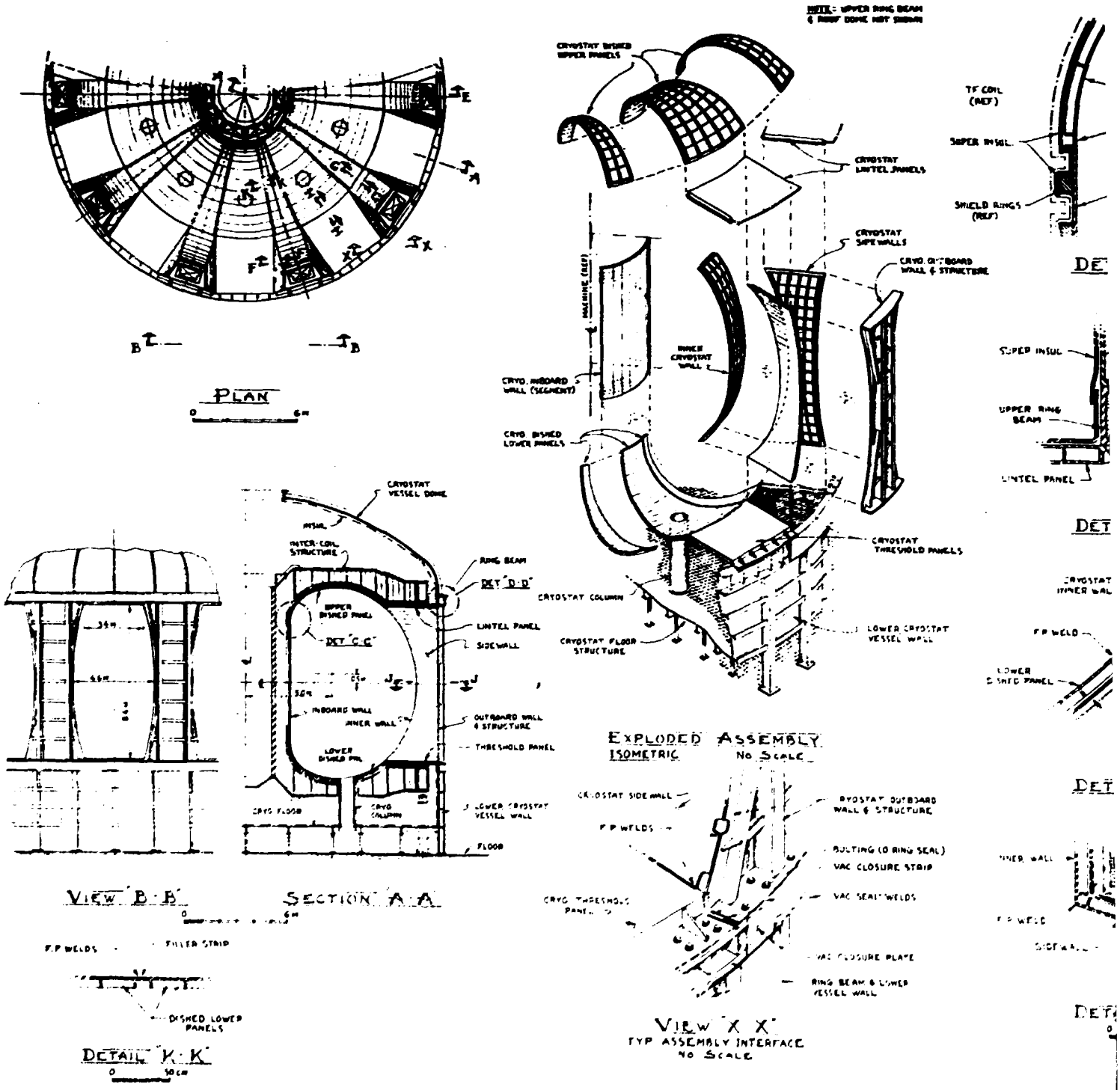

Fig. 3-3. Cryostat configuration.

ORNL-DWG 82-3749 FED

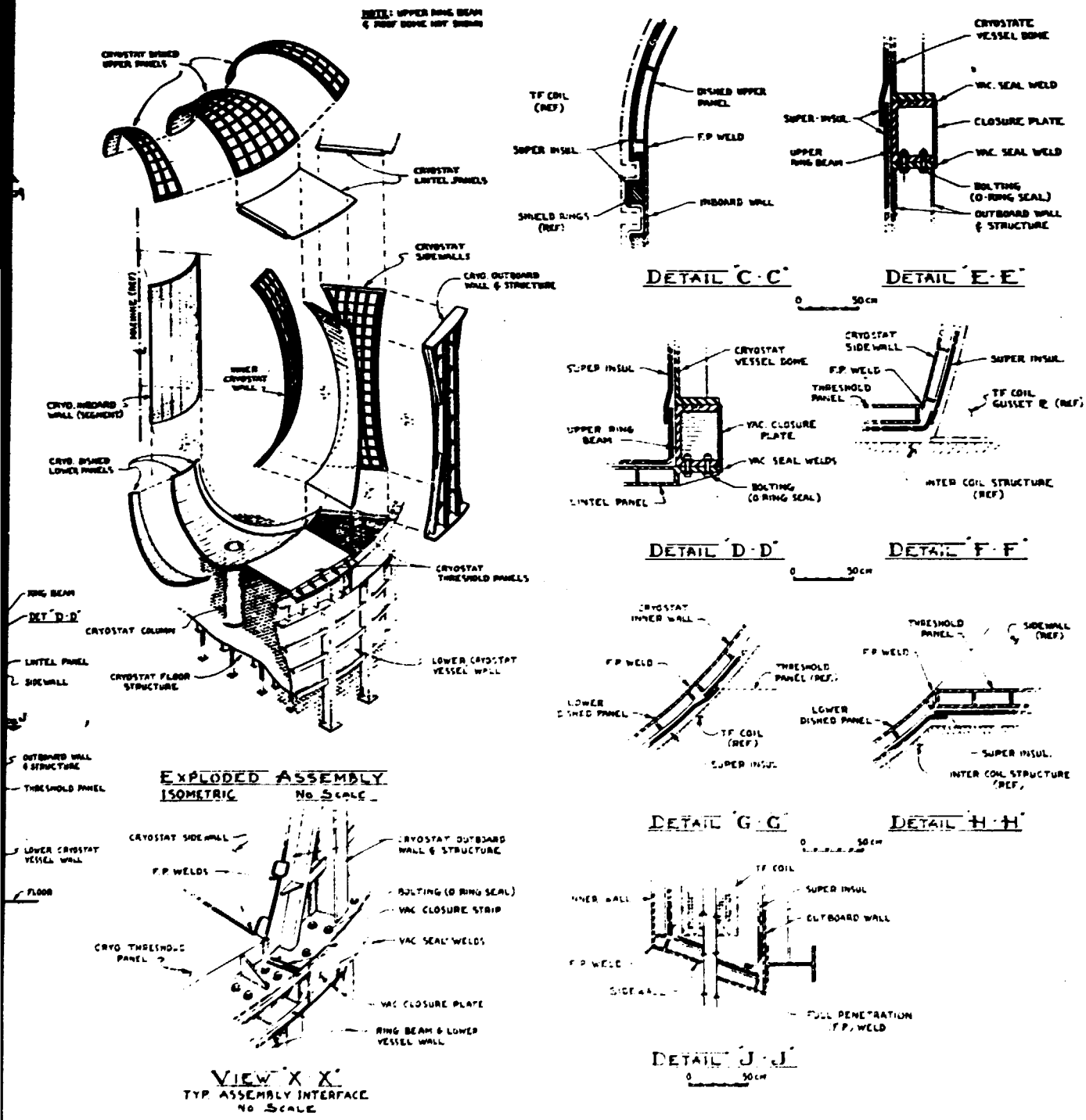

Fig. 3-3. Cryostat configuration.

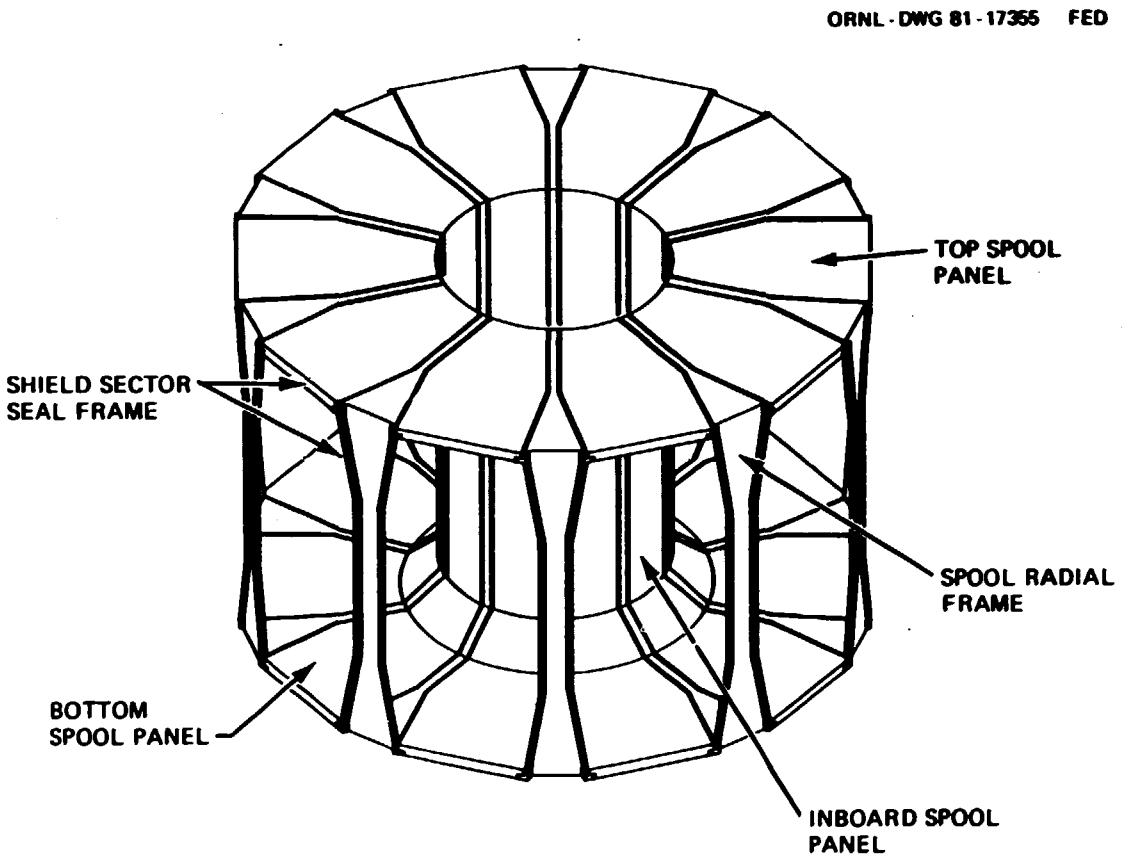

Fig. 3-4. Torus reactor system.

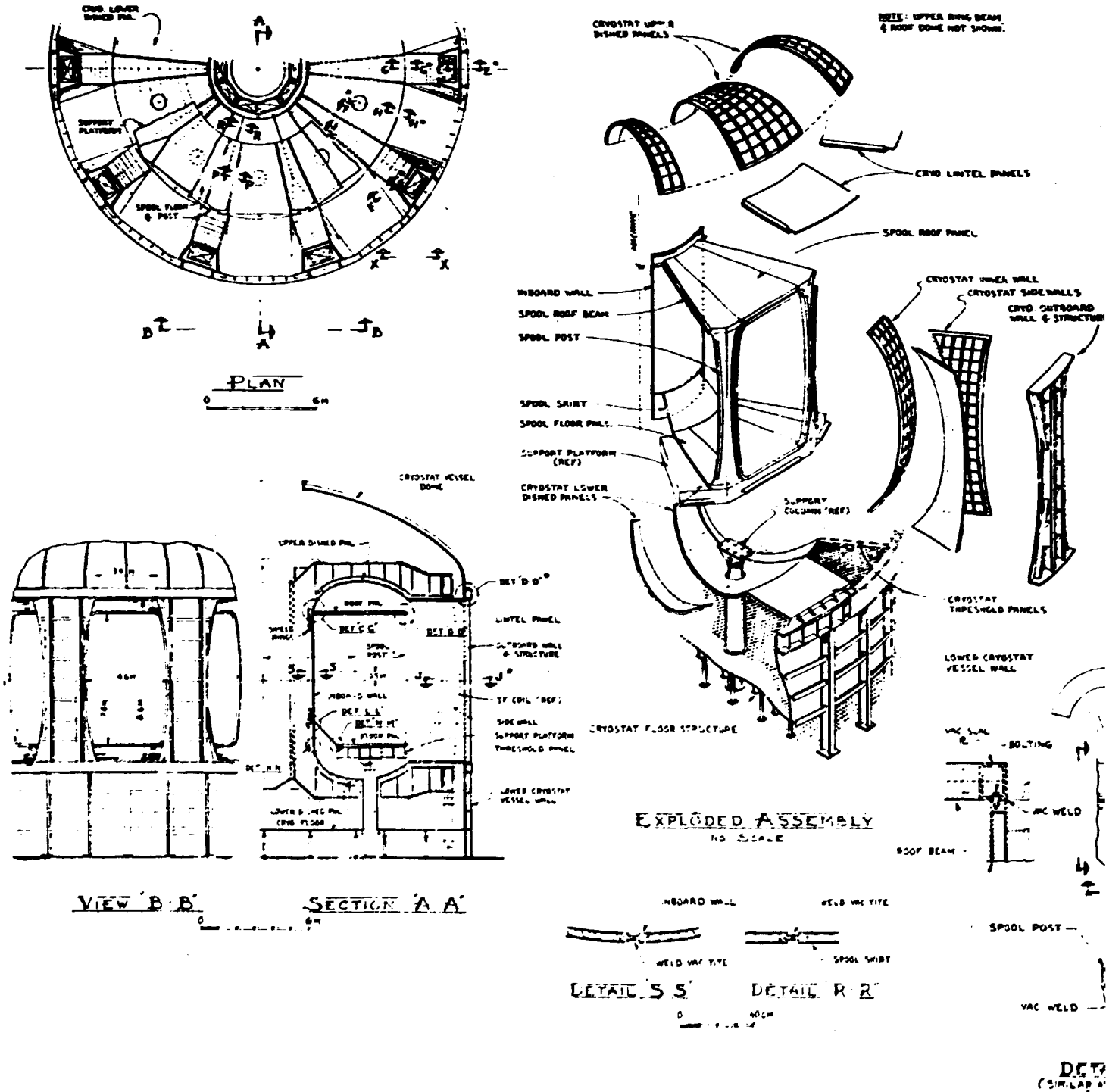

Fig. 3-5. Semicombined vacuum boundary configuration.

ORNL-DWG 82-3750 FED

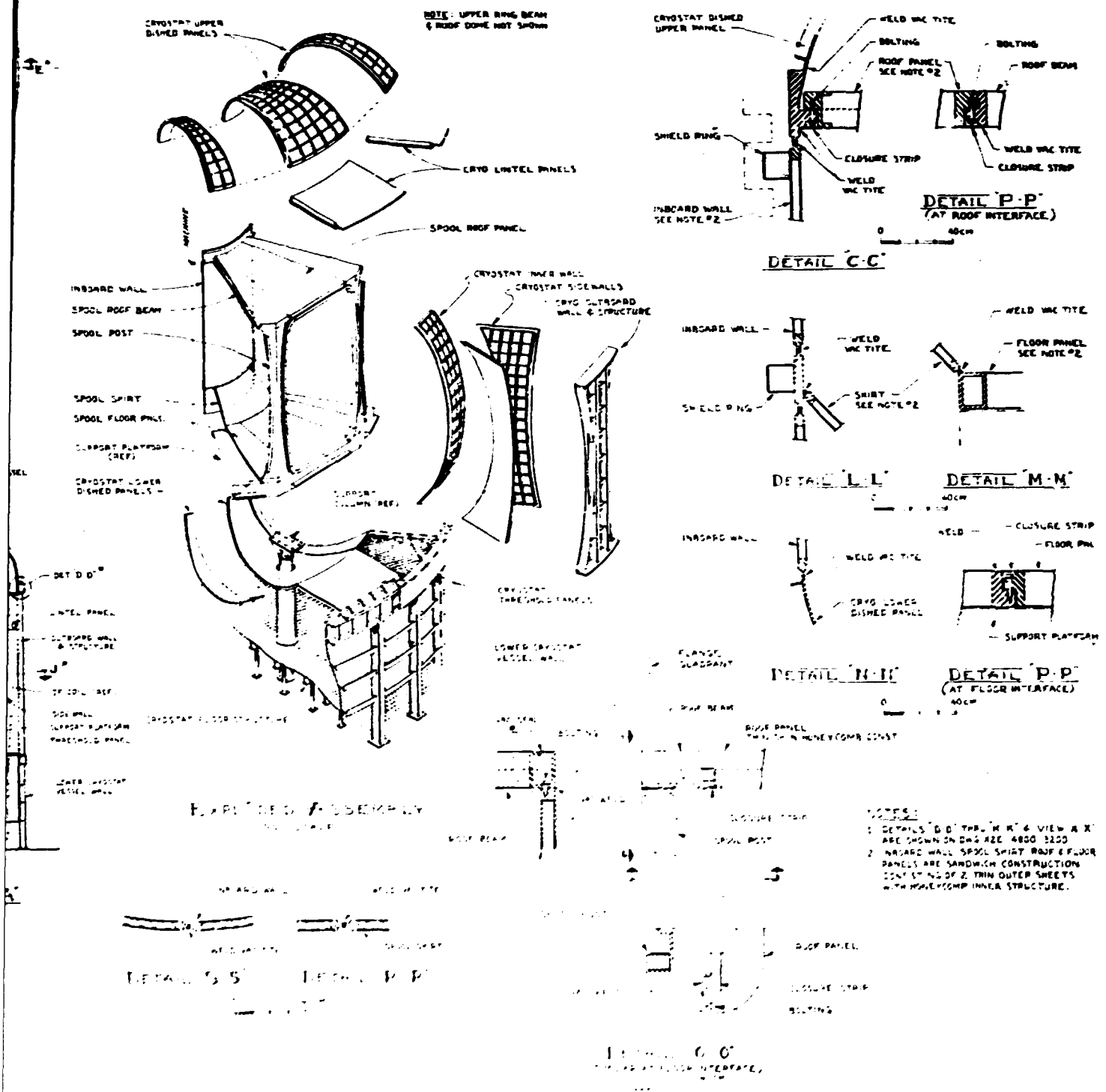

Fig. 3-5. Semicombined vacuum boundary configuration.

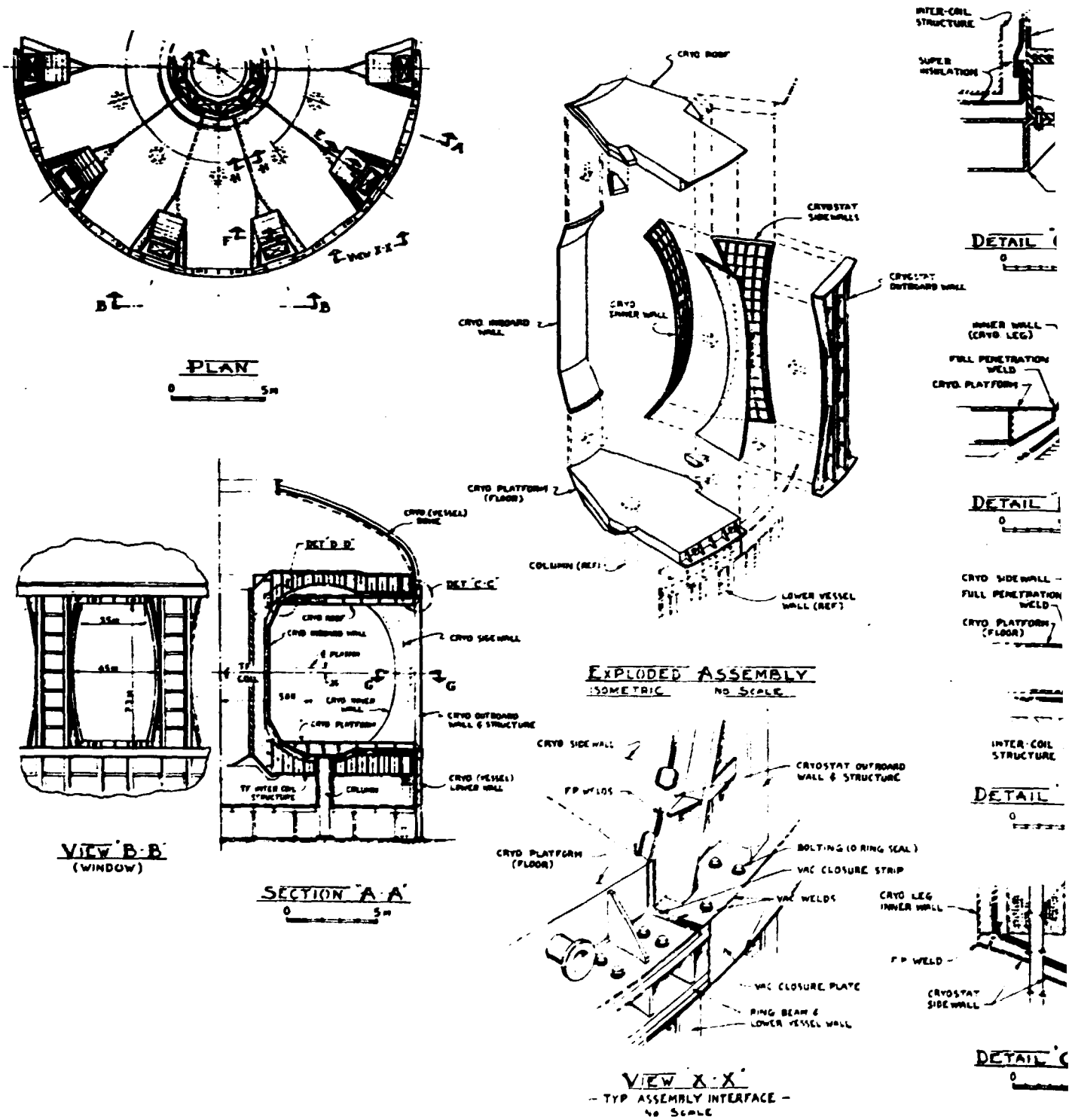

Fig. 3-6. FED 301 cryostat configuration.

ORNL-DWG 82-3751 FED

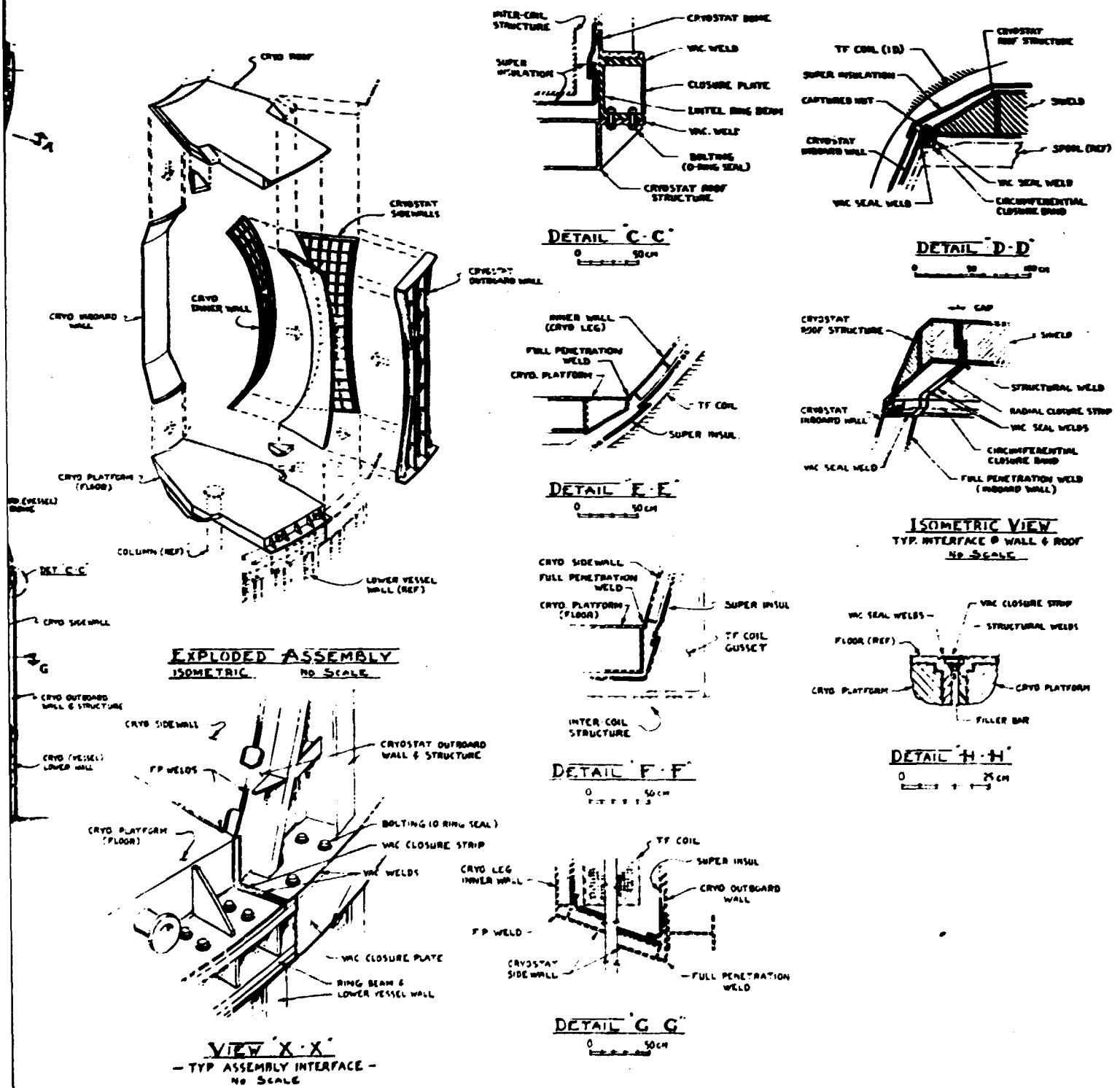

Fig. 3-6. FED 301 cryostat configuration.

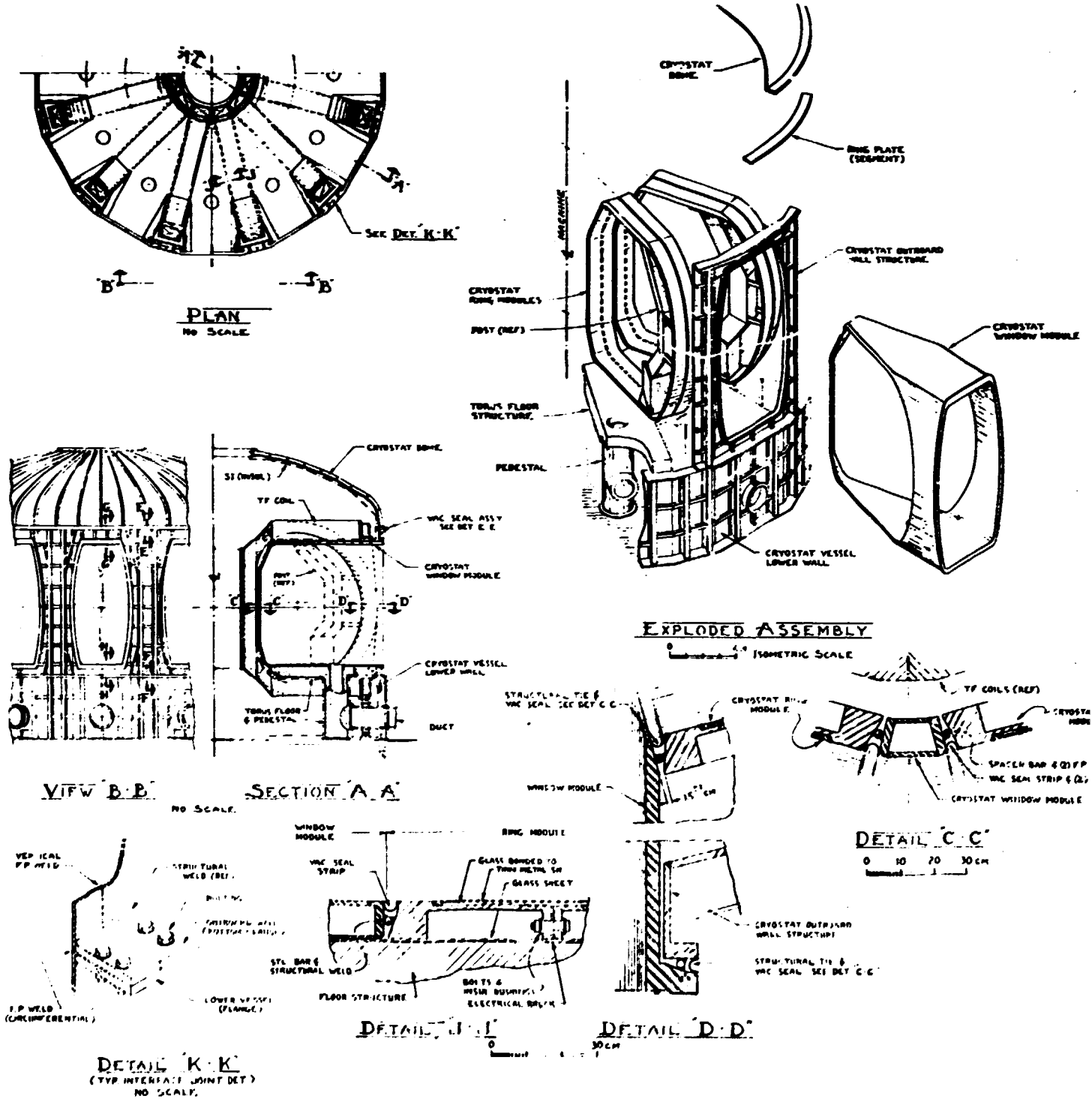

Fig. 3-7. USA cryostat configuration, Phase II.

ORNL-DWG 82-3752 FED

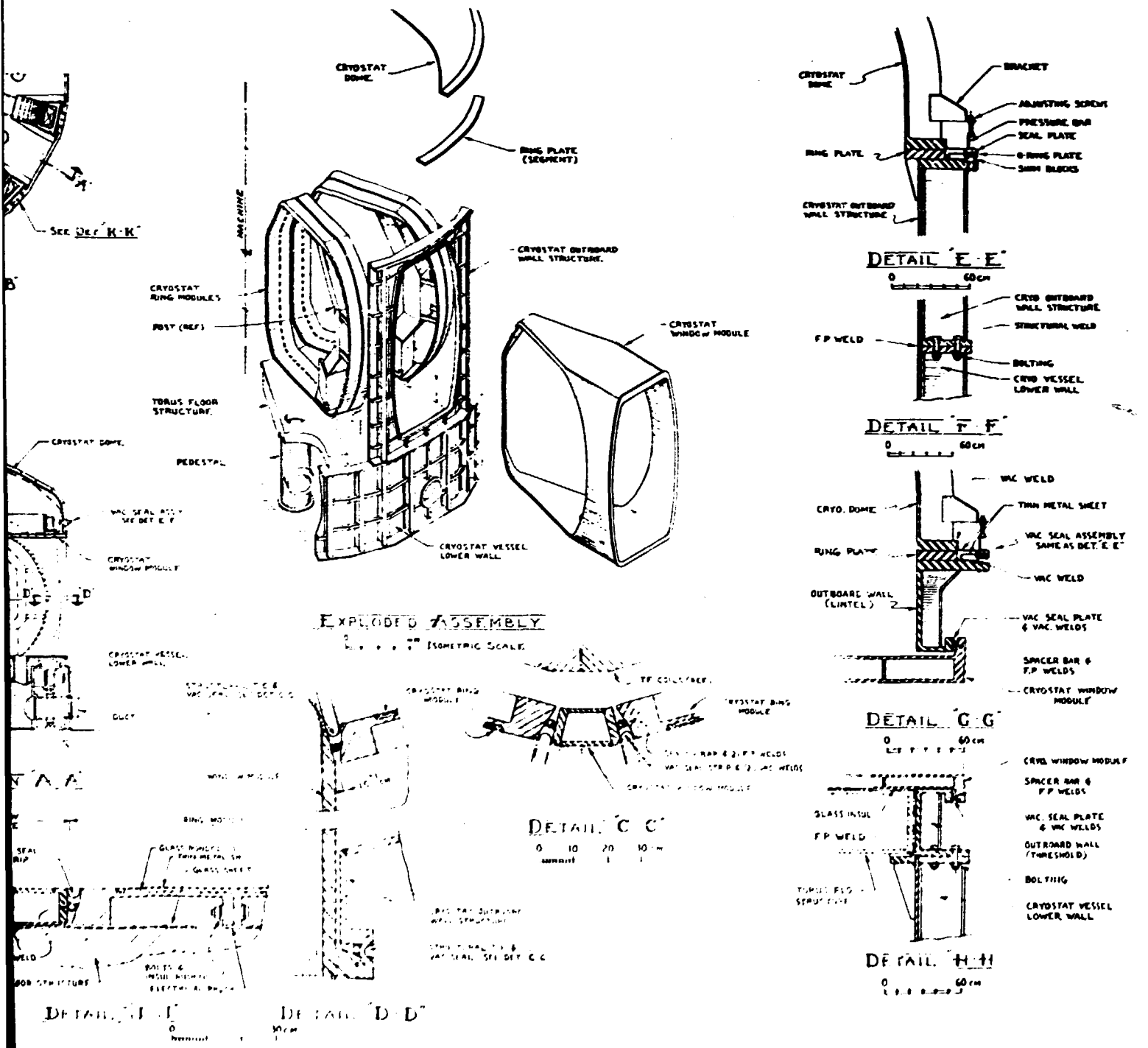

Fig. 3-7. USA cryostat configuration, Phase II.

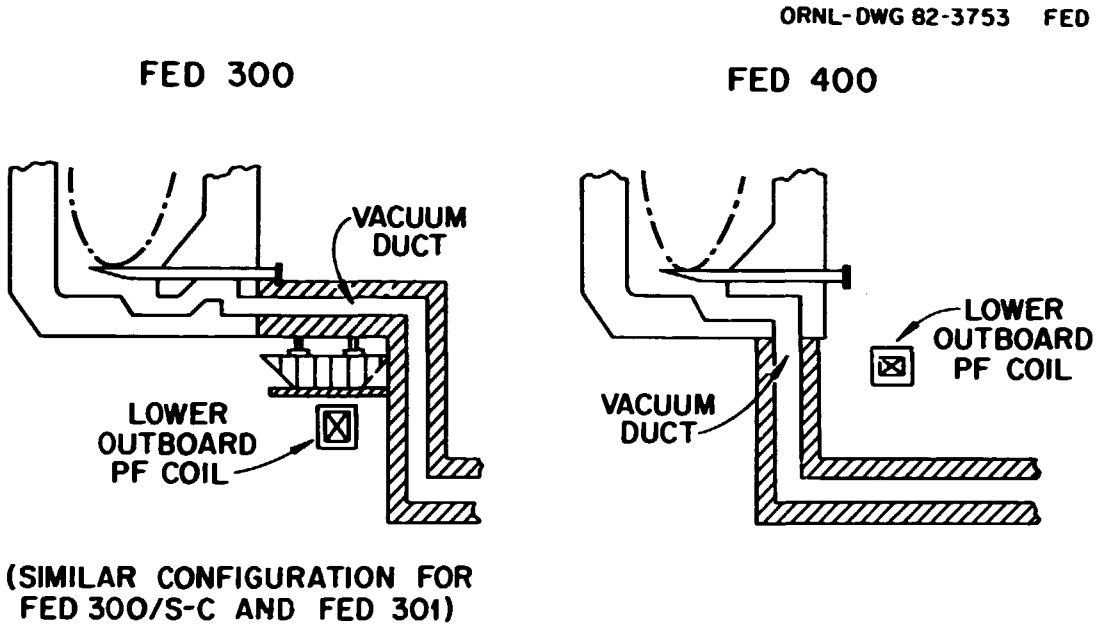

Fig. 3-8. Vacuum duct and lower outboard PF coil locations for FED 300 and FED 400.

inboard legs and the torus. The FED 301 configuration (Fig. 3-6) provides a 1.2% ripple, reduced-size, 10-TF coil system with a separate vacuum boundary, as in the baseline, yet still allows equal torus sectors (ten) to pass between adjacent TF coils. In addition to reducing the size of the TF coil, an all-exterior PF coil system was incorporated. All other features are the same as the baseline. The FED 400 configuration, Fig. 3-7, provides a 12-TF coil, 1.2% ripple system, a combined vacuum boundary, equal torus sectors, and all-exterior PF coils. With this design, a full shield module is extracted in a straight line motion between the reduced-size TF coils, as in the baseline design; however, a small shield post remains under each TF coil, which requires an in-situ maintenance approach.

The location of the vacuum pumping duct in FED 400 is also different than in any of the other configurations. As illustrated in Fig. 3-8, the pump duct in FED 400 passes through the bottom of the combined torus plasma and magnet vacuum boundary, whereas the vacuum duct in the other configurations passes through the outboard vacuum boundary surface. Because of the obstruction caused by the vacuum duct, the lower outboard PF coil in FED 300 (as well as FED 300/S-C and FED 301) is forced to be lower than this coil in FED 400 and, thus, it is at a less optimum location relative to the plasma. This results in a significant PF system cost savings for FED 400.

3.3 VACUUM BOUNDARY EVALUATION

Three generic vacuum boundary options, including the FED Baseline (FED 300) configuration, were separately evaluated to provide future guidance of the design approach for FED. The alternatives are illustrated schematically in Figs. 3-9, 3-10, and 3-11.

3.3.1 Major Features

Figure 3-9 is representative of the FED Baseline (FED 300), as well as FED 301. The TF magnet system and the torus plasma chamber have separate vacuum boundaries with the volume between the boundaries occupied

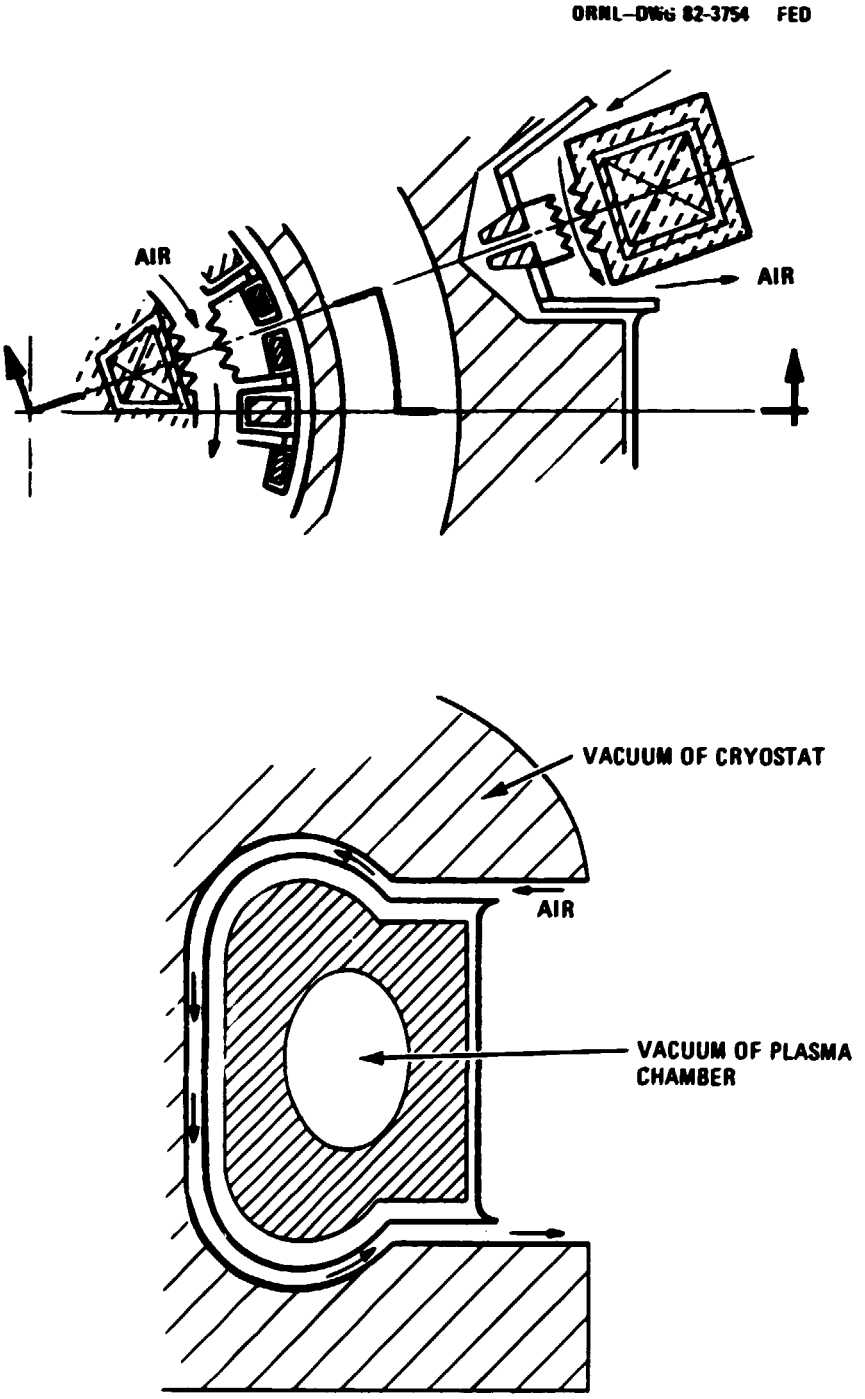

Fig. 3-9. Alternative No. 1 — FED-baseline.

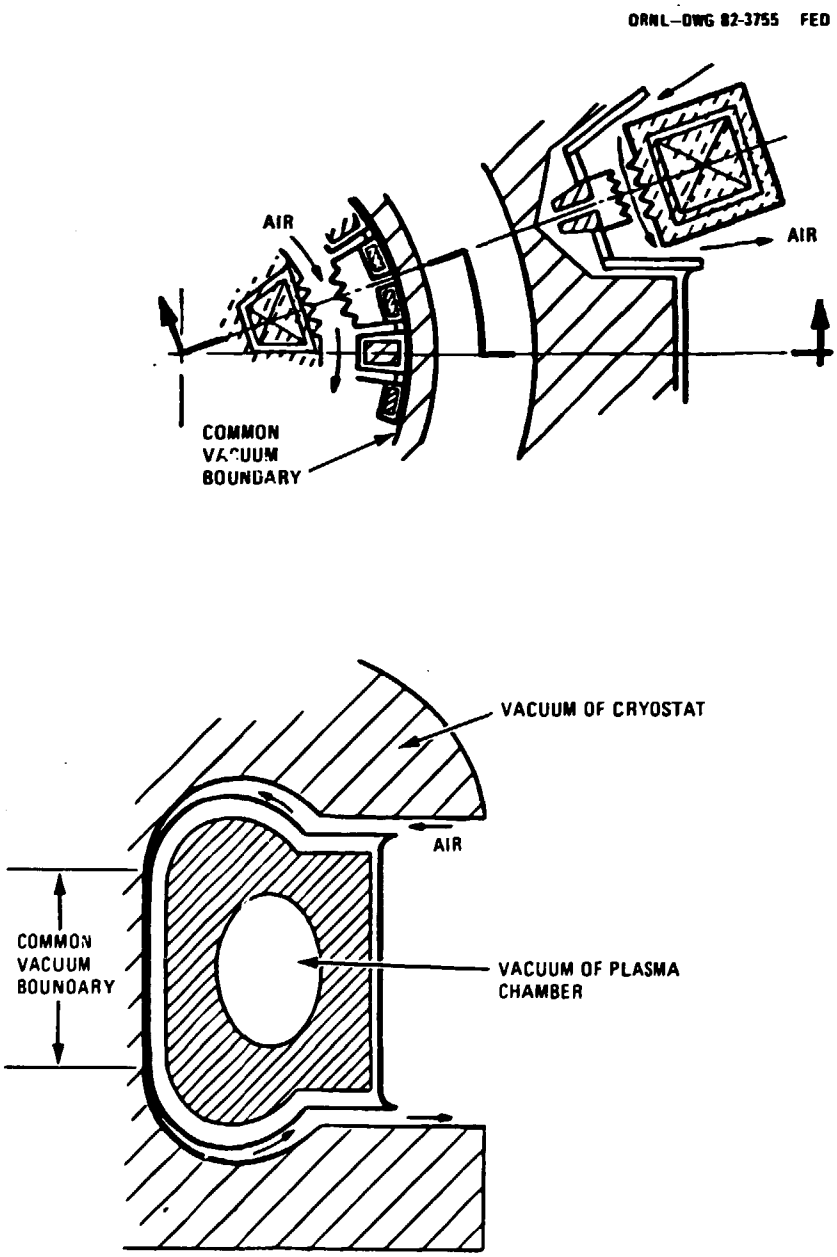

Fig. 3-10. Alternative No. 2 — partially integrated vacuum boundary.

ORNL-DWG 82-3756 FED

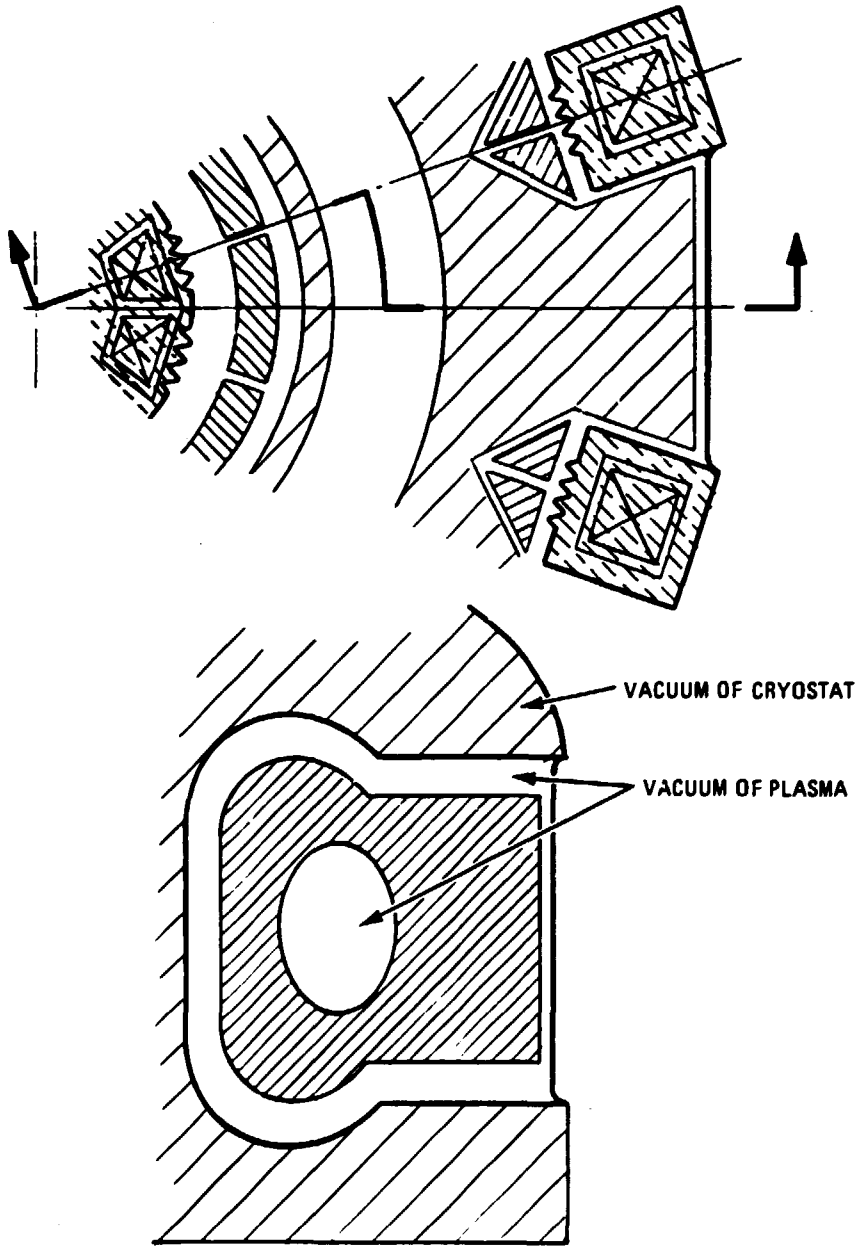

Fig. 3-11. Alternative No. 3 — fully integrated.

by air at normal atmospheric pressure. The walls defining each of the vacuum boundaries are single walls, i.e., walls that do not contain a pumped volume.

Figure 3-10 is an option whereby the vacuum boundaries of both the magnet system and the plasma chamber are integrated at the inboard vertical wall. This configuration represents the FED 300/S-C design option. As in the case of the baseline, the walls are single walls.

A fully integrated vacuum boundary concept, which represents FED 400, is illustrated in Fig. 3-11. This employs single-walled vacuum boundaries, as in the other options discussed above.

Double-walled concepts are viable alternatives for each of the concepts presented above. However, it was decided to review the merits of the three vacuum boundary configuration options first, using the single-wall approach and then assessing the benefit of adding the dual-wall feature.

Major differences between the three options are in the cost and complexity (maintainability and reliability). The integrated vacuum boundary concepts allow for a smaller radial build and, hence, a smaller reactor cost. This design approach also will permit a somewhat simpler design, resulting in fewer cutting and welding operations. In the case of seismic response, the separated vacuum boundaries allow a decoupled response, and there may be some advantage resulting.

All of the concepts are assumed to use a non-replaceable vacuum boundary floor under the reactor and a lower outer vacuum wall (vertical ring outside of the TF coils below the floor level). These are assumed to require hands-on maintenance for replacement. The overhead dome, floor, and lower outer wall do not vary between concepts and, therefore, were not included in the evaluation. The dome utilizes a planar elastomer seal and normally would be removed using contact procedures. However, it could also be removed using remote methods.

3.3.2 Evaluation Criteria

The criteria which were employed in the evaluation are:

1. Maintainability/Assembly/Availability. These criteria can best be applied by evaluating the number of replaceable parts in the vacuum boundary. This is a good indicator of the time required for replacement, since replacement time is more dependent on the number of steps required than size. The fault isolation capability is also a good indication of the time-to-replace, since it will have a direct bearing on the time required to determine the location of a leak. The complexity of TF coil replacement is a good measure of the maintainability of the machine. The seal joint design is a good indicator of reliability, replacement time, and maintainability.
2. Cost. This can best be quantified by radial build, building height requirements, and the number of pieces of maintenance equipment. Radial build is estimated to cost $5 M/cm; building height is estimated to cost $1 M/m. Each major piece of maintenance equipment is assumed to cost $3 M.
3. Penetrations and Access. Difference in the design, such as use of dual doors, affects the reactor complexity and is measured by this factor.
4. Plasma Control. Differences highlighted by this factor are the location of the control coils inside the reactor vacuum or locating them in air, and the ability to provide the necessary toroidal resistance for startup and disruption control.
5. Safety and Tritium Containment. The ability to contain tritium without excessive permeation or release of tritium is assessed by this factor. For purposes of this evaluation, it is assumed that air purge and intermediate vacuum pumping provide a similar capability.
6. Reactor Relevance. This factor is measured based on the concept application to the DEMO reactor, Ref. 1.

7. Performance. The performance is related to the capability of a design to be baked out and the effect of neutron streaming. Assigning numerical values to the above factors provides a basis for identifying a single preferred concept.

3.3.3 Approach to Evaluation

The details of the baseline are shown in Fig. 3-3. Similar details for 300/s-c are shown in Fig. 3-5. This arrangement provides a common vacuum boundary along the vertical weld. The details of FED 400, which has the completely integrated vacuum boundary, are shown in Fig. 3-7. The drawings constructed to support the details (shown in Figs. 3-3, 3-5, and 3-7) were used to determine the length of the weld seal, the number of pieces, etc.

Table 3-1 provides the resulting assessment of each of the criteria. This assessment was then quantified, and the results are presented in Table 3-2.

3.3.4 Evaluation Rationale

The values or scores in Table 3-2 were obtained in the following way: Eight scoring criteria were established as described earlier and shown in the left-hand column. Each configuration option was scored on a scale of from 0 to 5, with the highest number assigned to the most preferred characteristic. Then, each score was weighted according to the importance of each criterion. For instance, maintainability/assembly/availability, cost, plasma control, and performance were given a weighting factor of 5. Safety was also given a factor of 5. Reactor relevance, R&D requirements, and penetrations and access were given weighting factors somewhat lower, depending on the ease of attaining prescribed levels.

Maintainability/Assembly/Availability. All configurations were judged as essentially equal (see Section 3.7).

Cost. FED 400 received the highest score because of smaller radial build and a lower number of major maintenance equipment items.

Table 3-1. Comparison of vacuum boundary options

	Separate vacuum boundaries FED baseline (FED 300 and 301)	Semi-combined vacuum boundaries FED 300/S-C
1. Maintainability/ Assembly/Availability (2)(3)(4)(5)(7)		
No. of replaceable parts (MTTR, WTBF) of vacuum boundary	156 for TF coil 24 for spool	Not determined; less tha FED 300, more than FED 4
Fault isolation capability		
Leak detection	No provisions	No provisions
Worker radiation expos.	Hands-on only	Hands-on only
TF coil replacement	Remove 15 panels ∿230 meters of weld	Similar to baseline
Seal joints	Spool & wall	Not determined
Number	156+	
Length	1400 m 264 triple point	
Type	Butt weld structural	Butt weld structural
Complexity (planar, triple point)	Triple point	Triple point
Compatibility of design with remote techniques	Difficult	Similar to baseline
2. Cost (6)		
Radial build	2 walls	Eliminates 1 wall; -15 c
Maintenance equip/fixtures	15 major pieces	Not determined
Building height	----	-----
3. Penetrations & access (8)	Same	Similar to baseline
4. Plasma control (9)	Could add dielectric ring to plasma chamber	Similar to FED 400
Electrical resistance control coil	In air	In air

ble 3-1. Comparison of vacuum boundary options

vacuum boundaries ED baseline 300 and 301)	Semi-combined vacuum boundaries FED 300/S-C	Combined vacuum boundary FED 400
TF coil pool	Not determined; less than FED 300, more than FED 400	36
sions only	No provisions Hands-on only	No provisions Hands-on, remote may be possible on window and ring modules
5 panels ers of weld wall	Similar to baseline Not determined	Break 6 seals All planar Spool 36 900 m
le point		Wall (not to be removed) 12+ 200 m
d structural oint	Butt weld structural Triple point	Butt weld Planar/triple point
t	Similar to baseline	Good - for planar seals; Hands-on at door
pieces	Eliminates 1 wall; -15 cm Not determined -----	Eliminates 1 wall; -15 cm ∿10 major pieces +10 m
	Similar to baseline	Separate door complicates parts
d dielectric ring to hamber	Similar to FED 400 In air	May require multiple dielectric rings In vacuum

Table 3-1. Comparison of vacuum boundary options (cont'd.)

	Separate vacuum boundaries FED baseline (FED 300 and 301)	Semi-combi vacuum bound FED 300/S
5. Safety (tritium leakage/ control) (1)	Single boundary and air purge	Single bound air purge
R&D requirements	Remote welders/cutters/fixtures triple point welds	Remote welde fixtures triple point
6. Reactor relevance	Not similar to demo	Not similar
7. Performance		
Same area	Same	Same
Virtual leaks	Surface welds	Surface weld
Bakeable	Yes--differential motion permitted	Yes--creates
Neutron streaming	3 paths	2 paths

mparison of vacuum boundary options (cont'd.)

boundaries line d 301)	Semi-combined vacuum boundaries FED 300/S-C	Combined vacuum boundary FED 400
and air purge	Single boundary and air purge	Single boundary
cutters/fixtures lds	Remote welders/cutters/ fixtures triple point welds	Remote welders/cutters/fixtures
demo	Not similar to demo	Similar to demo
	Same	Same
	Surface welds	Weld structure, etc., will have vents
al motion permitted	Yes--creates stresses	Yes--requires special design features to allow differential motion
	2 paths	2 paths

Table 3-2. Assessment and scoring of vacuum boundary configurations

	Weight factor	Separate vacuum boundaries FED baseline (FED 300 and 301)		Semicombined vacuum boundaries (FED 300/S-C)		Combined vacuum boundaries (FED 400)	
		Value	Total	Value	Total	Value	Total
Maintainability/assembly/ availability	5	3	15	3	15	3	15
Cost	5	2	10	4	20	5	25
Penetrations and access	2	3	6	3	6	3	6
Plasma control	5	3	15	2	10	2	10
Safety	5	3	15	2	10	2	10
Reactor relevance	3	1	3	1	3	4	12
Performance	5	5	25	4	20	4	20
R&D requirements	3	3	9	3	9	3	9
TOTAL: overall ranking			98		93		107

Penetrations and Access. All options received the same score.

Plasma Control. The FED Baseline (FED 300) received the highest score, based on the easier task of installing high-resistance breaks for passively controlling the eddy current fields.

Safety. The FED Baseline received the highest score because of separate boundaries (tritium containment).

Reactor Relevance. FED 400 received the highest score because of common vacuum boundaries similar to the perceived most desirable DEMO features (Ref. 1).

Performance. FED 300 received the highest score because of better response to bakeout temperatures.

R&D Requirements. All configurations were judged to be essentially the same.

3.3.5 Summary of Scoring

Based on the total number of weighted points, the FED 400 vacuum boundary configuration ranks as the most desirable, having the highest score. Features that dominate in the preferred configuration are a common vacuum boundary, smaller device size, all-external PF coils, and lower cost.

3.4 COMBINED VACUUM BOUNDARY (FED 400) STRUCTURAL ANALYSIS

In the evaluation of the FED 400 combined vacuum boundary design concept, it was perceived that a feasibility issue was the structural response to combined pressure and thermal loadings due to bakeout. Hence, the following analysis was conducted to determine what additional structural features may be required to provide an adequate response to these loadings.

A NASTRAN (NASA Structural Analysis) finite element model was developed which consisted of approximately 175 plate elements and 50 bar elements, as shown in Fig. 3-12. The plate elements represent the vacuum wall from the chamber floor to the top of the cryostat dome. Bar elements were used to represent toroidal rings near the top and bottom

ORNL-DWG 82-3783 FED

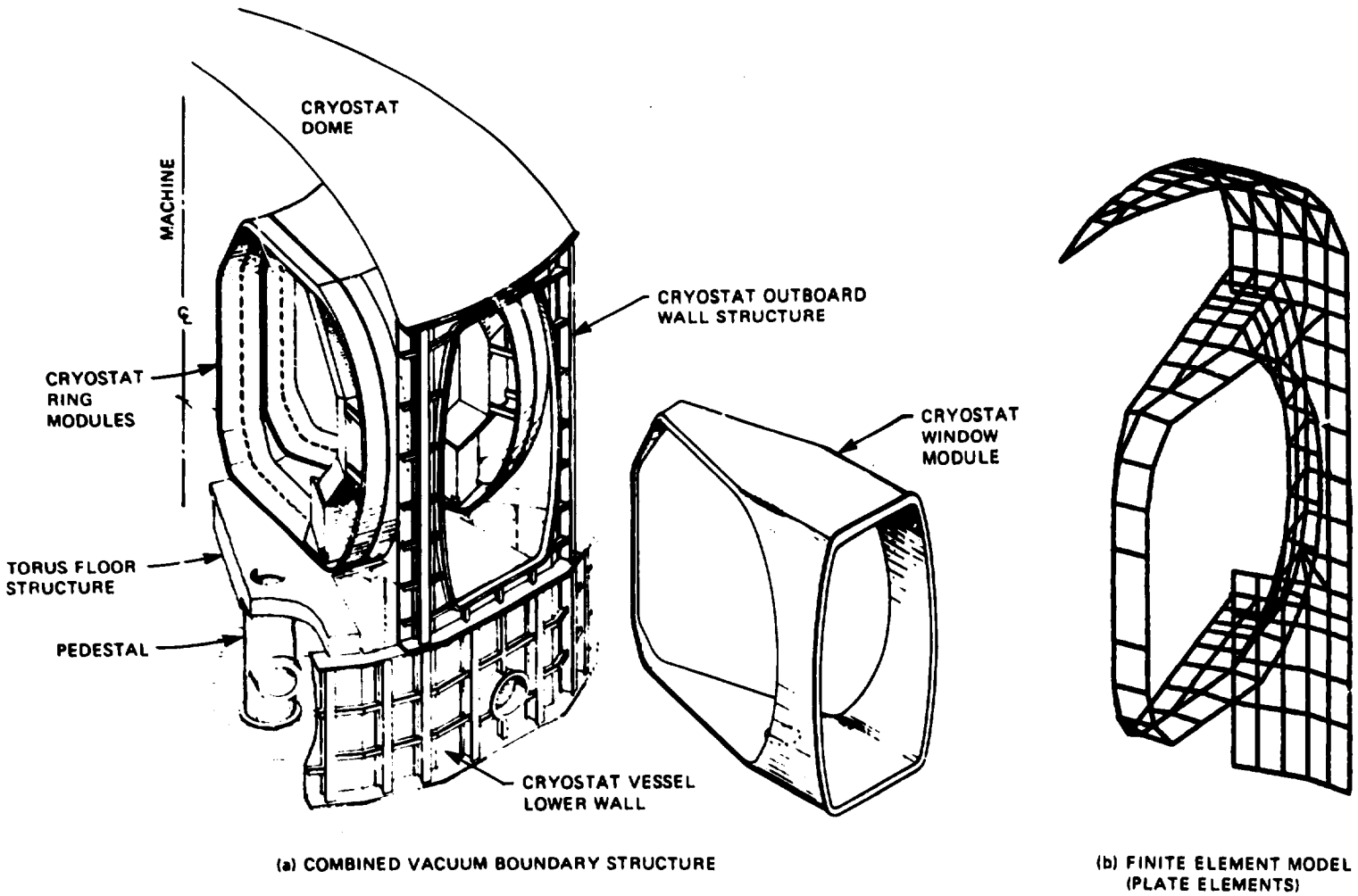

Fig. 3-12. (a) Combined vacuum boundary structure, (b) finite element model (plate elements).

of the window module, the flange around the edge of the door, and the vertical beam between doors. Only a 15° segment of the structure is modeled due to symmetry. (The door, while not shown in Fig. 3-12, was included in the model.)

3.4.1 Structural Description

Plate thickness and bending stiffness requirements were calculated for the one atmosphere differential pressure load. A double-wall sandwich configuration was used for the cryostat window module and the outboard cryostat wall. This wall configuration allows adequate bending stiffness by providing sufficient section depth and allows space for any required cooling. Two different wall depths were used in the model and are shown in Fig. 3-13. The top and bottom of the cryostat window module were analyzed as a 5-m x 2.0-m flat plate with fixed edges. The maximum bending moment in this plate is 55,000 N·m/m (12,400 in-lb/in.). This results in the 7.9-cm-deep cross section with a wall thickness of 0.64 cm. The remainder of the cryostat window module and the outboard cryostat wall bending stiffness was based on an evaluation of the side walls of the cryostat window module. This portion of the shell was analyzed as a 2 m x 7 m rectangular plate. The maximum bending moment in this plate is 36,000 N·m/m (8,000 in-lb/in.). This results in the 5.8 cm wall depth shown with a 0.64 cm wall thickness. The rib spacing was set at a distance of 10 cm. This spacing results in local bending stresses of 140 MPa (≈20 ksi) for an internal coolant pressure of 1 MPa (150 psi). The cryostat dome was assumed to be a solid plate with a thickness of 7.0 cm. This was based on previous analyses of cryostat thickness requirements, Ref. 2. Thermal loads were not considered in these preliminary analyses used to develop inputs for the structural model.

Bar elements represent the toroidal rings in the outboard cryostat wall above and below the window module as shown Fig. 3-14. Bar elements were also used to represent the vertical stiffeners in the outboard cryostat wall between the window modules. These stiffeners were sized

ORNL-DWG 82-3764 FED

REGION OF SHELL	SHELL GEOMETRY
TOP AND BOTTOM OF CRYOSTAT WINDOW MODULE	DOUBLE WALL SANDWICH 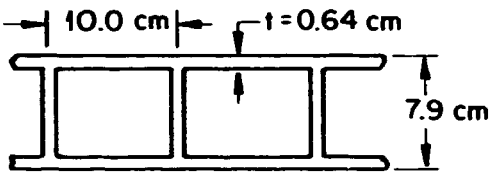
ALL OTHER REGIONS	DOUBLE WALL SANDWICH 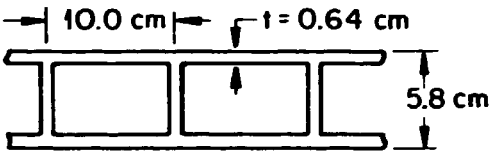

Fig. 3-13. Combined vacuum vessel finite element model plate gauges.

ORNL DWG 82-3765 FED

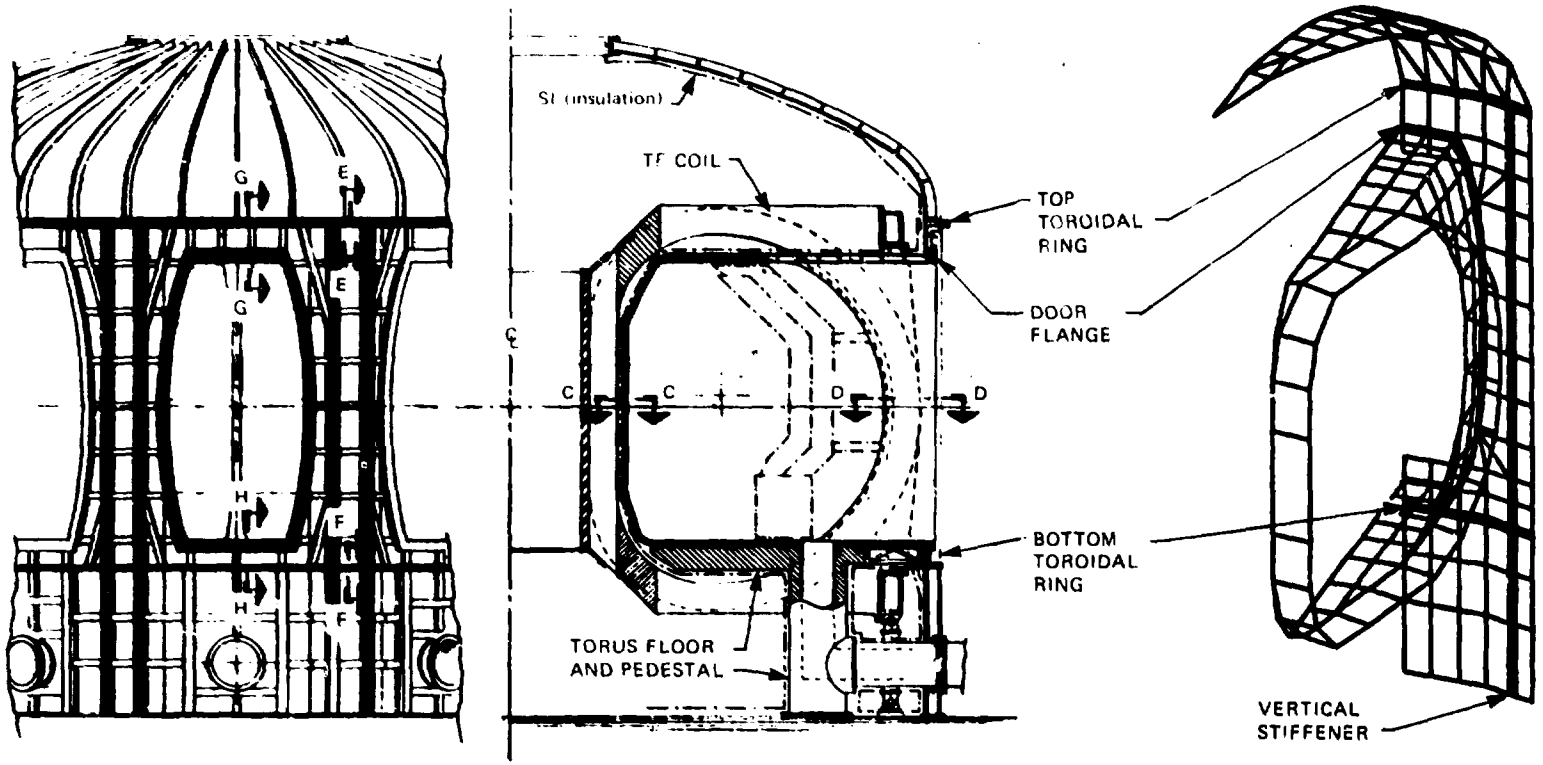

Fig. 3-14. Bar element representation of structural rings and stiffeners.

to transfer the atmospheric pressure load from the cryostat dome to the building floor. The load in those stiffeners was calculated to be 360,000 N (80,000 lbs), resulting in an I-beam cross-section column with a depth of 25 cm and a flange thickness of 2.5 cm. The flange around the edge of the window module was also modeled with bar elements based on drawing dimensions.

3.4.2 Load Conditions

Two conditions were evaluated. The first was an atmospheric pressure load on the plasma chamber side of the vacuum wall. This was evaluated without the door. This condition will exist when the doors are removed but a vacuum is maintained on the magnet side of the vacuum wall. The second condition evaluated was bakeout at 250°C. The door was added to the model for this analysis.

3.4.3 Atmospheric Pressure Loads

Several load conditions are possible since the vacuum can be in either the magnet chamber, the plasma chamber, or both. For initial purposes of evaluation, the condition with the vacuum only in the magnet chamber was analyzed. This provides the differential pressure over the regions used in determining the plate thicknesses. The door was not included in the model for this evaluation.

Shown in Fig. 3-15 is the deflected shape superimposed on the model. The largest deflections are approximately 1.8 cm. This deflection occurs near the middle of the top and bottom panels of the cryostat window module. The deadweight of the shield was not included in the analysis. Thus, the bottom of the cryostat window module may be attached to a support ring or may be loaded by the shield deadweight, in which case its deflection from differential pressure loads is limited.

Two other locations on the shell where significant deflections occur are at the top of the cryostat dome and at the outboard cryostat wall over the center of the TF coil. These deflections are 0.73 cm and 0.94 cm, respectively. No deflection criteria have been defined for the

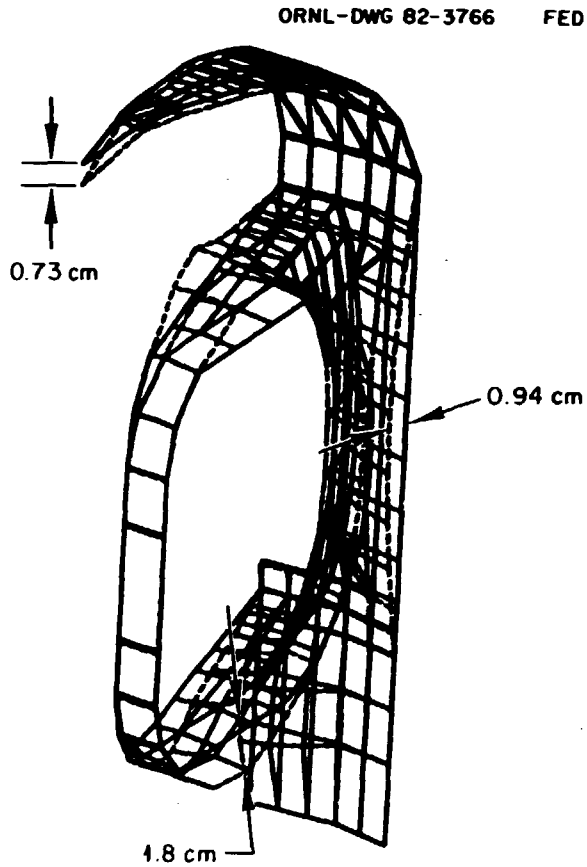

Fig. 3-15. Deflected shapes for the pressure load condition.

vacuum vessel at this time. However, additional stiffness can easily be provided if required by increasing the plate depths.

The axial load in the top toroidal ring is approximately 800,000 N (180,000 lbs) tension. This results in a tendency for the cryostat dome to push outward on the outboard cryostat wall. The load in the bottom toroidal ring is approximately 2×10^6 N (450,000 lbs) compression. Hence, the ring takes approximately 50% of the total hoop compression load in the portion of the outboard cryostat wall below the door. The vertical load caused by pressure on the dome is shared primarily by the vertical stiffeners and the door flange. At the vertical centerline of the door, approximately 70% (760,000 N) of this load is on the vertical stiffener.

3.4.4 250°C Bakeout Condition

The bakeout condition was evaluated by providing the appropriate structural temperatures. Temperatures calculated for use in the analysis are shown in Fig. 3-16. Plate elements representing a door structure were added to the model for bakeout analysis. The door has a linear temperature gradient from 250°C on the inside to 222°C on the outside. The outboard cryostat wall and the cryostat dome are insulated from the cold magnets and are exposed to ambient temperature. The temperatures, therefore, drop off rapidly with distance from the door flange.

The inner portion of the structure, at 250°C, tries to grow radially outward relative to the cooler outboard cryostat wall. This causes large stresses in the structure near the joint between the hot and cool surfaces. Two structural configurations were evaluated: first was the continuous structure, as defined earlier. Second, a "breather" joint was included in the model to allow free radial expansion of the window module. This consisted of eliminating the connection between the cryostat window module and the outboard cryostat wall at the door flange.

Without the breather joint, the window module and ring module inner structure (@250°C) push the adjacent outboard cryostat wall radially outward. This results in large bending stresses in the cryostat wall.

ORNL-DWG 82-3767 FED

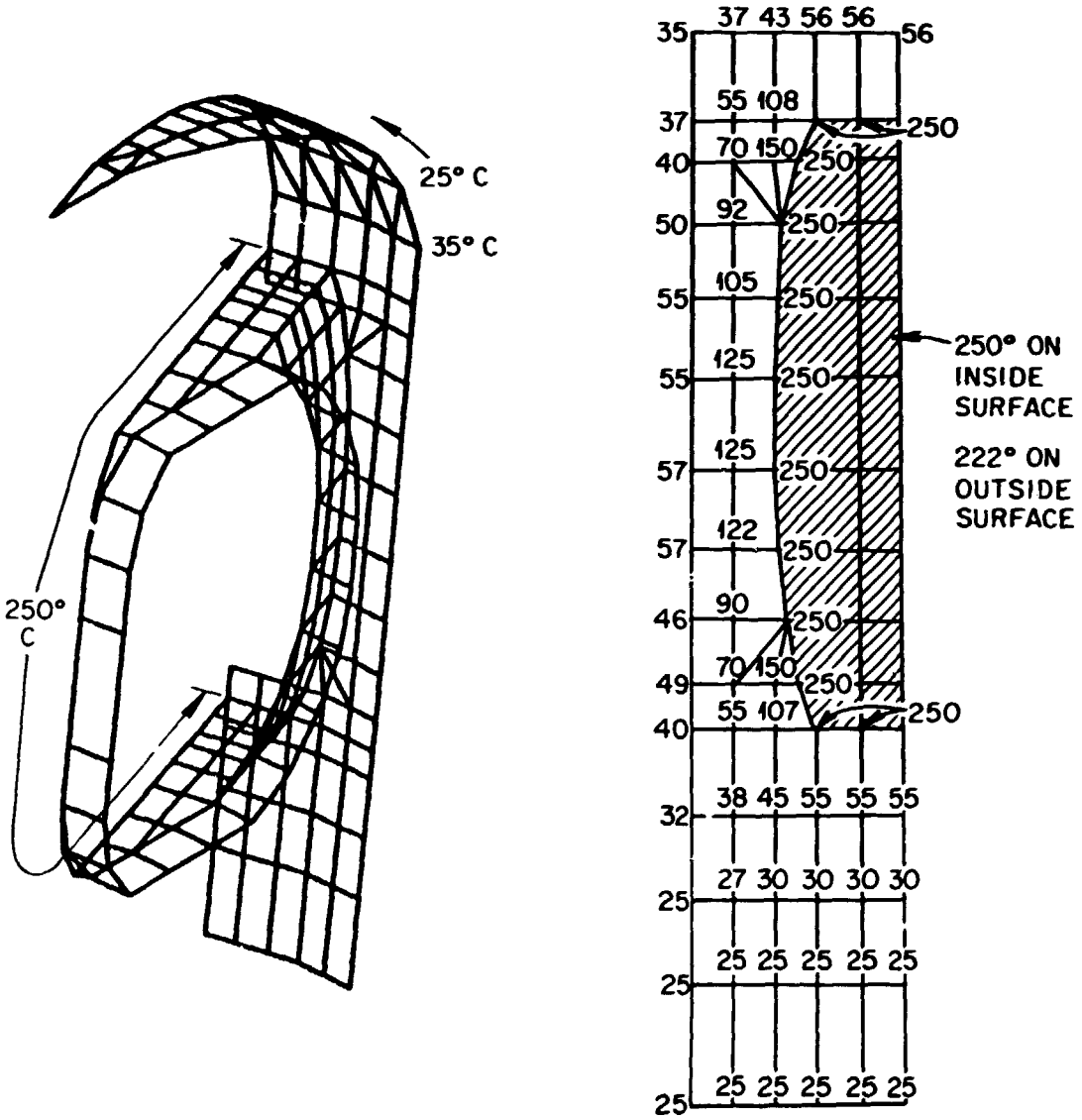

Fig. 3-16. Bakeout temperatures.

Shown in Fig. 3-17 is a comparison of outer fiber stresses in the outboard cryostat wall and in the bottom of the cryostat window module both with and without the breather joint. The comparison shows that the bending stresses in the shell essentially disappear with the addition of the breather joint. Relatively high in-plane toroidal stresses remain in the outboard cryostat wall, however, and are due to the gradient from 250°C to room temperature that exists in the wall.

Maximum outer fiber stresses (calculated elastically) in the outboard cryostat wall without the breather joint are approximately 1070 MPa (155 ksi). These stresses occur near the bottom corners of the door and are reduced significantly by the addition of the breather joint. However, stresses of approximately 400 MPa (60 ksi) along the edge of the door tend to remain even with the breather joint. Thermal insulation or cooling of these local regions during bakeout may be appropriate to reduce these stresses.

The resulting deflected shape for the bakeout condition is shown as an overlay on the model in Fig. 3-18. These deflections are a maximum of approximately 2 cm vertically at the top of the dome and 4 cm radially outward at points along the outer cylinder. Addition of the breather joint does not significantly affect deflections during bakeout.

3.5 PF SYSTEM CONFIGURATION OPTIONS

The PF system and the location of PF coils has a major cost and maintenance impact on a tokamak device. Figure 3-19 illustrates possible coil locations that have been identified for each of the four reactor configuration options under investigation. A departure from the FED Baseline PF coil arrangement is evident in two areas: (1) all-exterior PF coils are considered for FED 301 and FED 400 and (2) consideration is given to locating the outboard EF coils in a separate vacuum cryostat, independent of the TF coil cryostat. Figure 3-20 shows the design concepts that are under investigation for supporting a repositioned lower outboard EF coil.

In order to determine the impact of the PF magnetic system, in terms of magnetic fields, forces, and power supply requirements, on the

ORNL-DWG 82-3768 FED

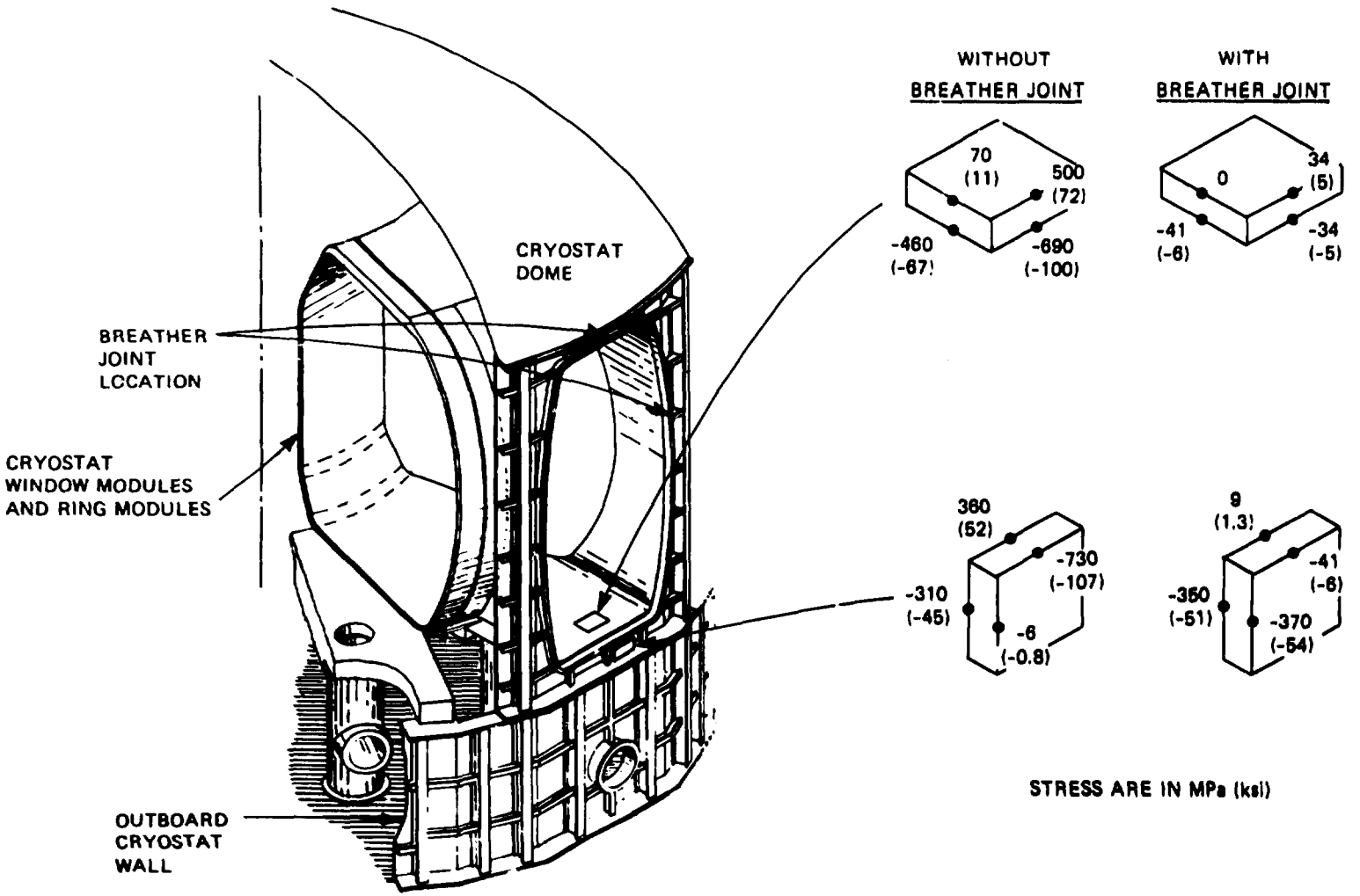

Fig. 3-17. Effects of breather on stresses.

ORNL—DWG 82-3769 FED

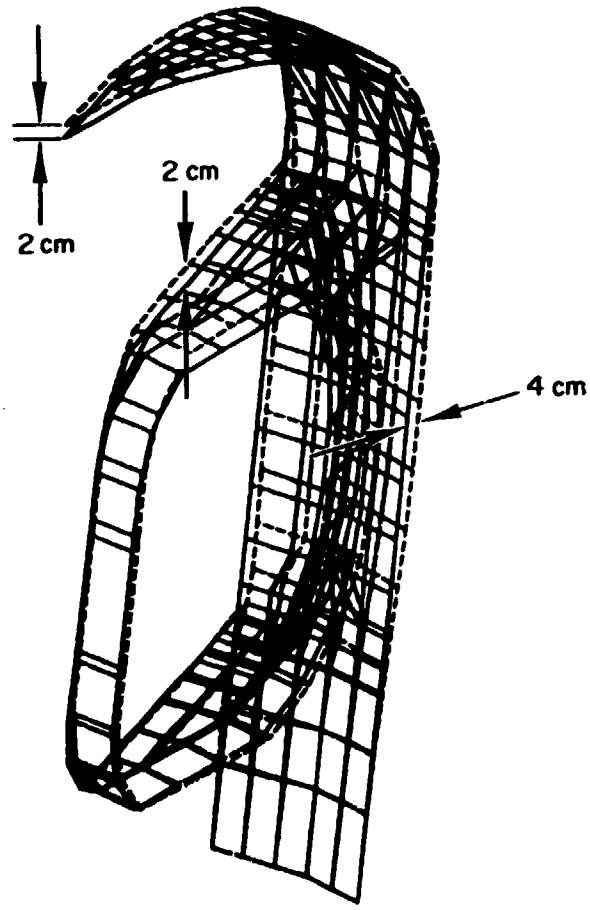

Fig. 3-18. Deflected shape for 250°C bakeout condition.

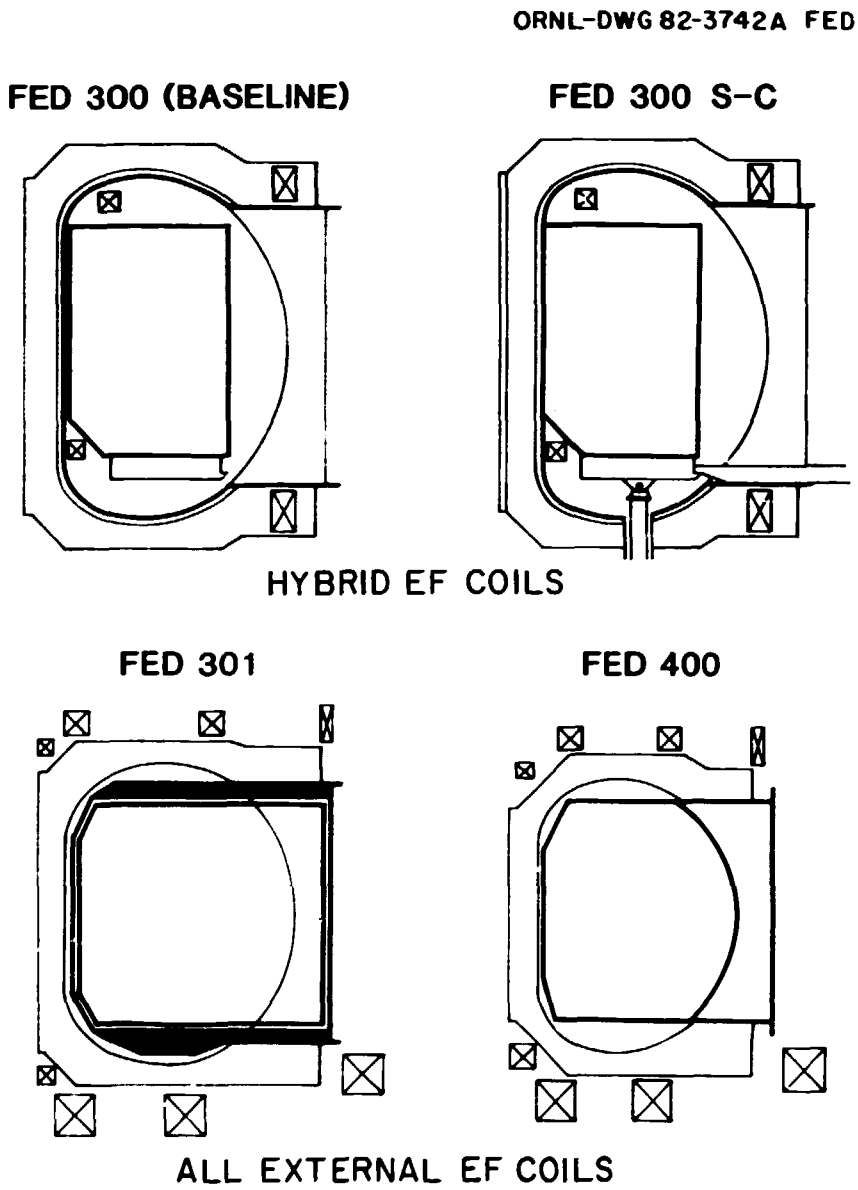

Fig. 3-19. PF coil locations.

ORNL-DWG 82-3770 FEO

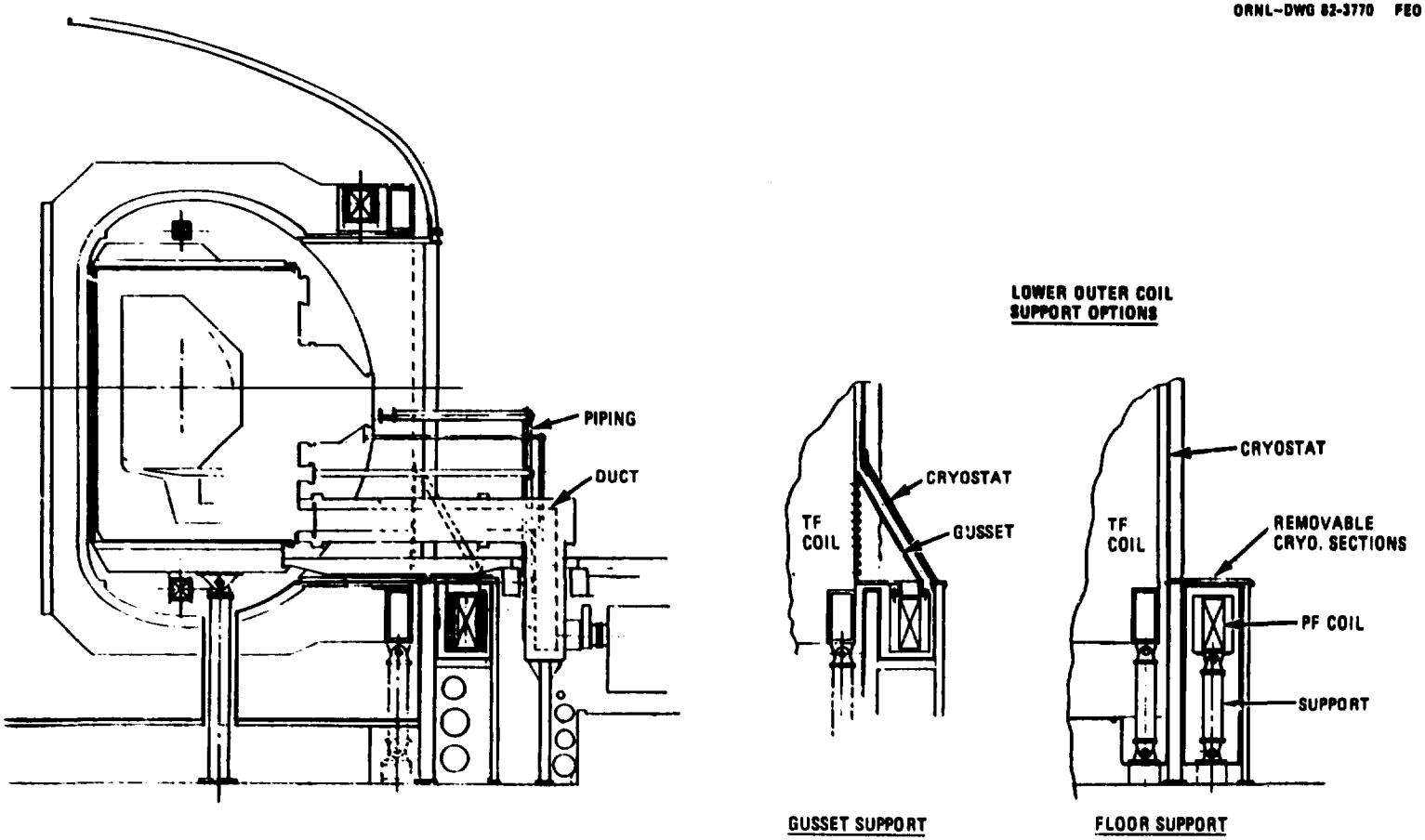

Fig. 3-20. Design concept for supporting a repositioned lower outboard EF coil.

different reactor designs, PF currents were defined for both a pumped limiter and poloidal divertor shaped plasma for various PF coil locations. (While the poloidal divertor was not used in the basic reactor design concepts studied in the present effort, the PF coil requirements were established to provide data for possible future studies.) The plasma requirements (Sect. 1, Ref. 1) that were held roughly constant for the four configuration options are:

- 5.0-m major radius,
- 6.5-MA plasma current,
- 1.6 elongation,
- 0.2 triangularity, and
- continuous scrapeoff for a pumped limiter or null coincident with the defined plasma edge for the divertor case.

The EF currents are for a high beta plasma at the end of burn.

Figures 3-21 through 3-23 show pictorially the range of coil locations considered and the required EF currents to shape the plasma. The perimeter (P) of the TF coil mid-surface is indicated in each of these figures. The divertor condition on both the FED 301 and FED 400 configuration required a reduction in the solenoid current, plus the addition of an upper EF coil in order to establish a divertor plasma shape with a 1.6 elongation.

The impact of the PF system on the TF coils, discussed in the following subsection, was evaluated in terms of the out-of-plane forces and fields imposed on the TF coil. These forces and fields as well as the PF coil currents are listed in Table 3-3. PF coil configuration options (B) and (C) for FED 300, FED 300/S-C, and FED 301 result in lower EF coil currents, TF coil loads, and TF peak pulsed fields compared to option (A). However, option (A) was selected for the cost studies documented in subsection 3.9 because it has a slightly lower overall reactor cost.

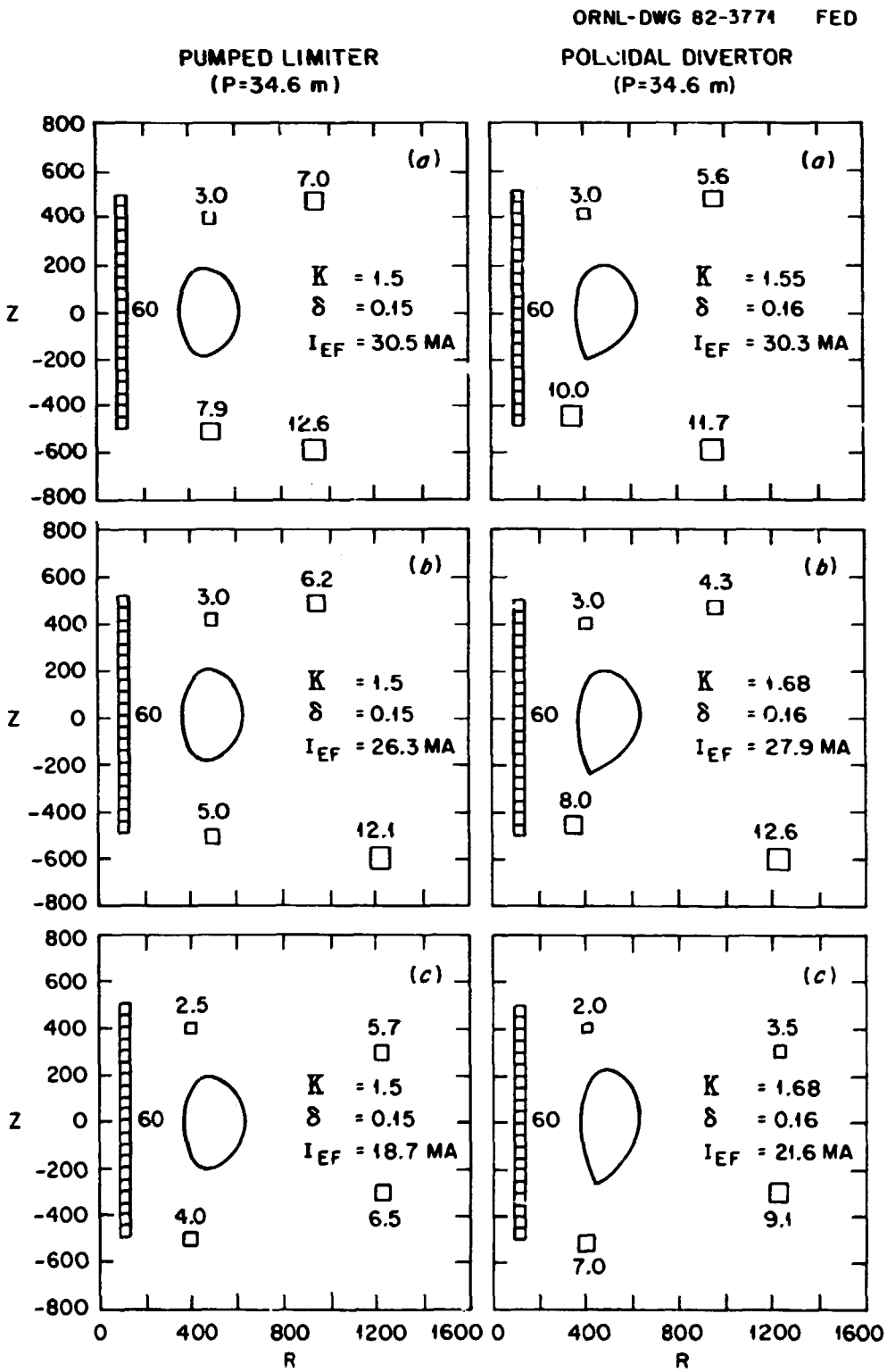

Fig. 3-21. FED baseline (FED 300) and FED 300/S-C PF coil configuration options.

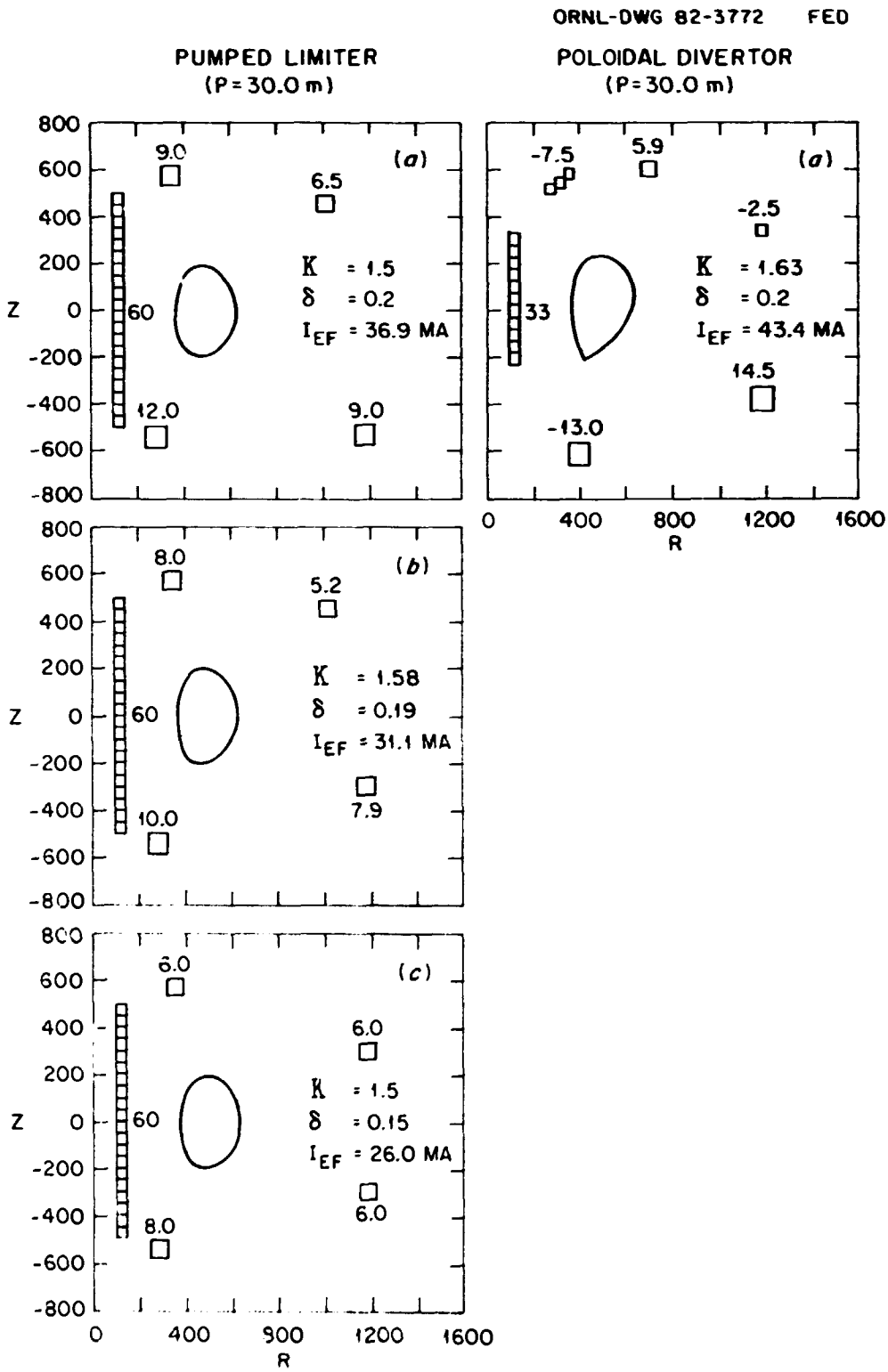

Fig. 3-22. PF configuration options for the reduced size TF concept (FED 301).

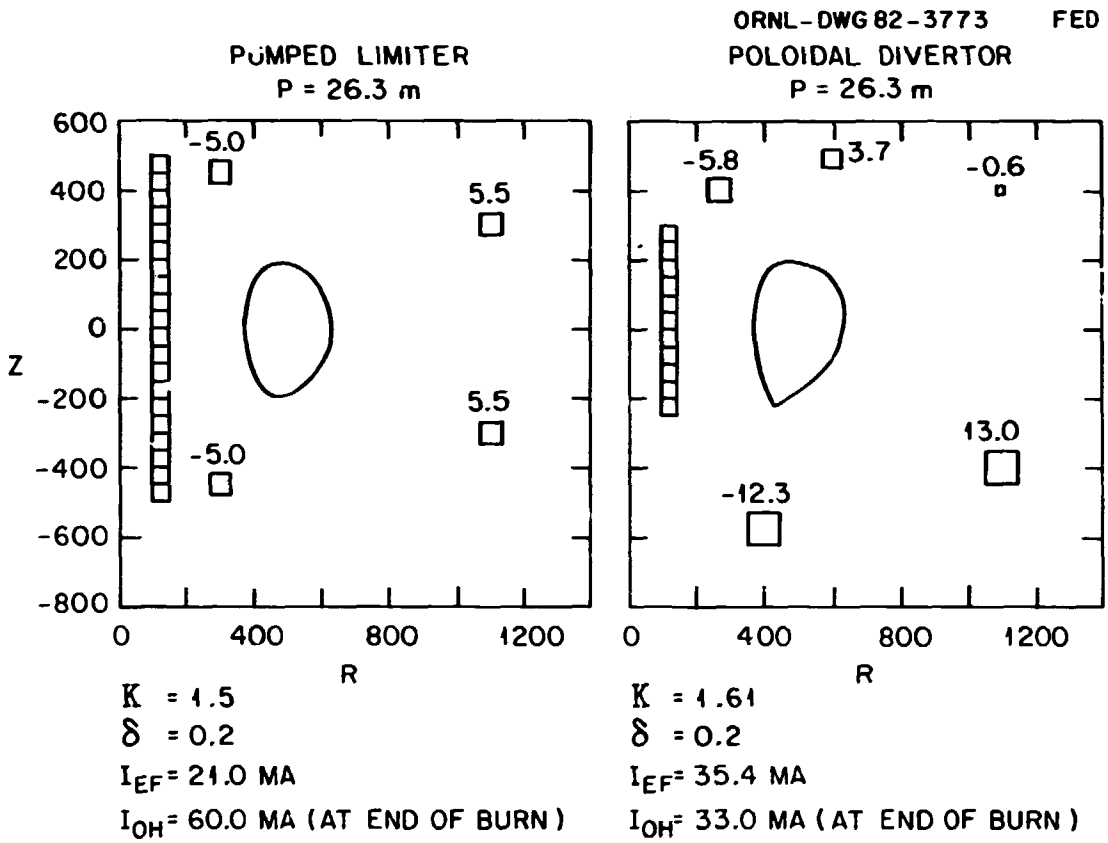

Fig. 3-23. PF configuration for the minimum size TF coil concept (FED 400).

Table 3-3. Summary of PF configuration study

Configuration	Impurity control method	Total PF curnt (MA) OH/EF	TF OT moment (MN-m)	TF peak running load (MN/m)	TF peak pulsed field (T) B PERP	B TANG
FED Baseline	Pumped Limiter					
FED 300	(A)	60/30.5	432	20.8		
	(B)	60/26.3	377	12.2		
	(C)	60/18.7	290	6.8	.8	1.0
	Poloidal Divertor					
	(A)	60/30.3	445	18.4	1.6	2.3
	(B)	60/27.9	380	9.9	.9	1.7
FED 301	Pumped Limiter					
	(A)	60/36.9	226	21.3	1.9	2.3
	(B)	60/31.1	205	18.7	1.7	1.8
	(C)	60/26.0	212	15.6	1.4	1.5
	Poloidal Divertor					
	(A)	33/43.4	230	16.1	1.5	2.3
FED 400	Pumped Limiter					
	(A)	60/21.0	126	15.9	1.9	2.3
	Poloidal Divertor					
		33/35.4				

NOTE: (1) All cases run at the end of burn (high β) with plasma.
(2) FED 300 and FED 301 configurations have 10-TF coils at 10 T; FED 400 configuration has 12-TF coils at 9.3 T.
(3) All configurations are at SM major radii.

3.6 TF SYSTEM CONFIGURATION STUDY

One of the factors which can influence the choice of a TF coil shape and a PF coil configuration is the cost of the support structure required for a candidate configuration. The weight and cost of TF coil cases and TF coil intercoil support structure (ISS) were computed for TF coil sizes and PF coil configurations, representing those required for the four reactor configuration options. The coil configurations surveyed are shown in Fig. 3-21 through 3-23; the perimeter P is used as an indication of the size of the TF coil.

3.6.1 Sizing of Case

For purposes of sizing the case thickness, the coil perimeter was divided into three regions: inboard (the region where adjacent coil cases wedge together), outboard (the open window region between adjacent TF coils), and the ISS region (the portion of the coil case not included in either of the first two categories). The case thickness in each region was sized to accommodate the maximum out-of-plane running load in that region. In the ISS region, a 5-cm-thick case was used in conjunction with 5-cm-thick stiffening ribs at intervals. The spacing and depth of the ribs was determined by considering the bending stresses in the ribs and in the case sidewall due to out-of-plane loads. The weight of the ribs was included in the weight of the case. In the present comparative study, it was assumed for simplicity that in the outboard region a uniform thickness case is used, since in at least part of this region, stiffening ribs on the sidewall would encroach upon the space between TF coils which is needed for sector removal. More detailed design analysis on an individual basis could perhaps justify use of ribs in at least part of the outboard region as in the ISS region; this would lead to some reduction in case weight.

3.6.2 Sizing of Intercoil Support Structure (ISS)

The ISS, shown schematically in Fig. 3-24, consists of an exoskeletal array of box-beams and I-beams with an inner and outer shell of G-10. The radially innermost and outermost beams are box-beams, while the remaining beams are I-beams. The beams are fabricated from 5-cm-thick plate material and are spaced about 1 m apart. The box-beam width and I-beam flange width is 0.5 m. The beam depth was sized to accommodate the net overturning moment on the TF coil without sustaining bending stresses in excess of the allowable.

3.6.3 Costing

Consistent with past practice, the cost of the TF coil cases and the intercoil support structure was estimated as $26 per kg ($12 per lb) of fabricated structure. For the TF coil case, a previous study showed that the cost per unit weight of the case is about the same whether the built-up ribbed case or the heavier uniform thickness case is used. The cost benefit associated with the built-up ribbed concept is reflected in the reduced weight.

The results of the comparison are shown in Table 3-4. The results show that there is no substantial variation in TF coil case weight from one configuration to the next. The ISS weights associated with the reduced-size TF coil (FED 400 and FED 301) are significantly lower than those corresponding to the present baseline (FED 300) TF coil shape for two reasons: (a) the configurations using the smaller TF coil have lower overturning moments and can use smaller cross-section ISS beams and (b) because of the smaller TF coils, the average circumferential length (and, therefore, weight) of the ISS beams is less. While the ISS weights for the reduced-size TF coil shape (FED 400 and FED 301) are in general a substantial reduction from those associated with the present baseline (FED 300) TF coil, there is no significant variation among choices (A), (B), and (C) within either group. The smaller TF coils afford a potential savings in ISS cost up to about $10 M.

ORNL-DWG 82-3746A FED

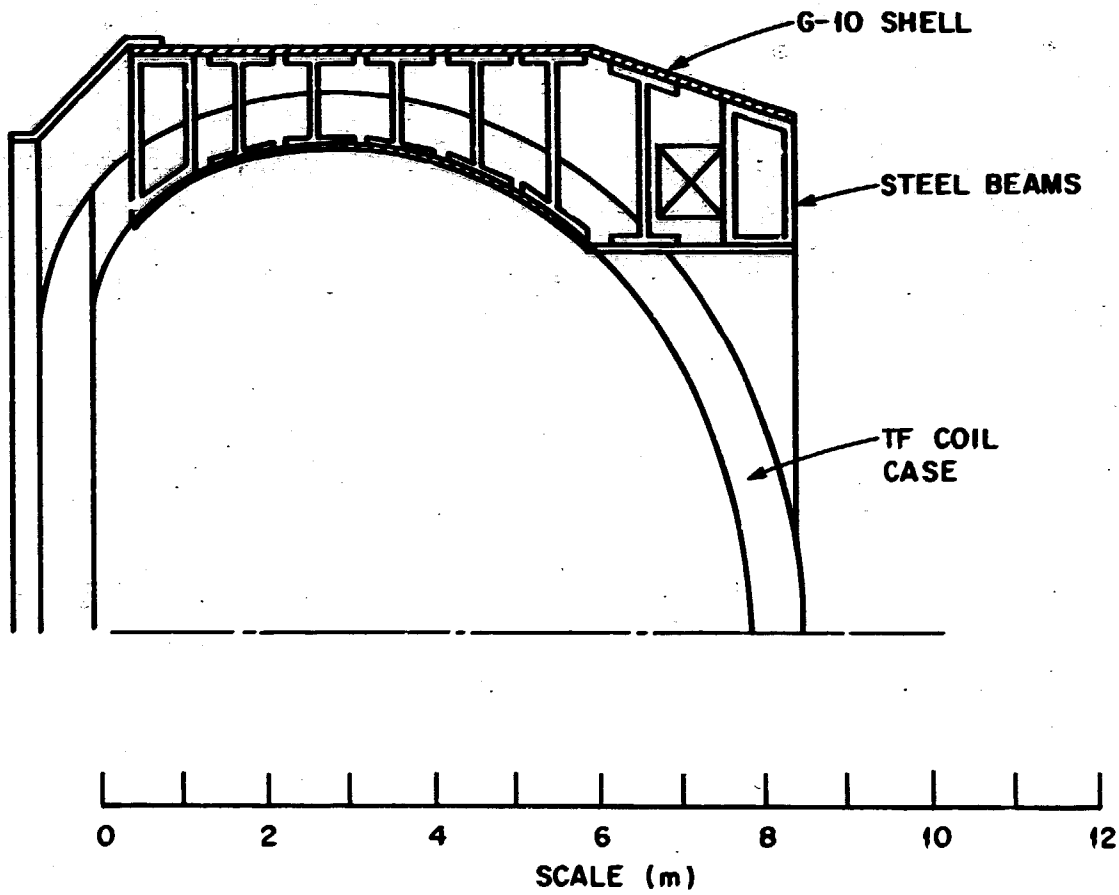

Fig. 3-24. Intercoil support structure concept.

Table 3-4. Summary of weight and cost for TF coil cases and intercoil support structure

		TF coil cases			ISS			
		Number of coils	Weight (10^3 kg) (Total all coils)	Cost ($M) (Total all coils)	M_x (MN-m)	Weight (10^3 kg)	Cost ($M)	TF coil case & ISS cost
FED 300 (or FED 300 S-C)	(A)	10	779	20.3	432	674	17.5	37.8
(P = 34.6 m)	(B)	10	683	17.8	377	634	16.5	34.3
	(C)	10	651	16.9	291	566	14.7	31.6
FED 301	(A)	10	737	19.2	226	436	11.3	30.5
(P = 30.0 m)	(B)	10	710	18.5	205	417	10.8	29.3
	(C)	10	679	17.7	212	424	11.0	28.7
FED 400		12	660	17.2	126	279	7.2	24.4
(P = 26.3 m)								

3.7 RAM ASSESSMENT

An analysis was performed to assess the reliability, availability, and maintainability (RAM) impacts of the proposed four FED design options.

In order to perform the analysis, it was necessary to establish for each configuration

- global maintenance constraints, e.g., radiation cooldown time
- an operating scenario which would accommodate scheduled maintenance requirements, and
- failure rate and downtime ratios (unscheduled maintenance parameters) for systems and components.

In Sect. 9 of this report, global maintenance constraints for the baseline design are detailed. These constraints were assumed common to all configurations under study.

An operating scenario is proposed in Section 9 which accommodates anticipated scheduled maintenance requirements for the baseline design. Study of the proposed configuration options did not reveal any scheduled maintenance requirements which were significantly different from those of the baseline design. Thus, it was appropriate to adopt that operating scenario for proposed configuration options.

Section 9 specifies failure rate, λ, and downtime ratio, ρ (defined as the product of the failure rate and mean time to repair), requirements for the baseline systems and components. For this analysis, the requirements specified in Sect. 9 were taken to be representative of the failure rates and downtime ratios of the baseline systems and components. For each of the proposed configuration options, those systems/components which would be expected to have significantly different failure rates or downtime ratios were identified and new values generated. Table 3-5 lists those systems and components which were identified as having a potential impact on unscheduled maintenance. It may be noted that FED 300/S-C is shown in the same column as FED 300. This is because its unscheduled maintenance parameters should be virtually indistinguishable from those of the baseline (FED 300) design.

Table 3-5. RAM impact of proposed design options assuming space ring coils not available

	FED 300 and FED 300/S-C			FED 301			FED 400		
	λ[b]	MTTR[c]	ρ[d]	λ	MTTR	ρ	λ	MTTR	ρ
TF windings	2.1-5[a]	5,840	0.123	1.9-5	5840	0.111	1.7-5	4380	0.074
TF leads	4.0-5	1,176	0.047	4.0-5	1176	0.047	4.8-5	1176	0.056
TF other	3.1-4	80	0.025	3.1-4	80	0.025	3.1-4	80	0.025
EF1 winding	2.0-6	1,176	0.002	5.0-6	4015	0.020	2.9-6	3285	0.010
EF1 leads	4.0-6	48	0.000	8.0-6	1176	0.009	4.0-6	1176	0.005
EF1 other	1.0-4	9	0.001	1.0-4	20	0.002	1.0-4	20	0.002
EF4 winding	3.5-6	1,344	0.005	5.5-6	4015	0.022	2.9-6	3285	0.010
EF4 leads	8.0-6	48	0.000	1.2-5	1176	0.014	4.0-6	1176	0.005
EF4 other	1.1-4	11	0.001	1.0-4	20	0.002	1.0-4	20	0.002
EF2 winding	9.4-6	5,840	0.055	9.2-6	5840	0.054	8.6-6	5475	0.047
EF2 leads	8.0-6	1,176	0.009	8.0-6	1176	0.009	4.0-6	1176	0.005
EF2 other	1.0-4	20	0.002	1.0-4	20	0.002	1.0-4	20	0.002
EF3 winding	1.6-5	10,220	0.164	1.3-5	7300	0.095	8.6-6	5840	0.050
EF3 leads	1.2-5	1,176	0.014	8.0-6	1176	0.009	4.0-6	1176	0.005
EF3 other	2.0-4	15	0.003	2.0-4	15	0.003	1.0-4	20	0.002
Sector modules	7.2-5	420	0.030	7.2-5	420	0.030	7.2-5	420	0.030
Shield posts	3.6-6	504	0.002	3.6-6	504	0.002	4.5-6	504	0.002
Sector modules/shield posts other	1.5-4	34	0.005	1.5-4	34	0.005	1.8-4	32	0.006
Spool structure	5.1-6	672	0.003	5.1-6	672	0.003	---	---	---
Bellows contacts	2.2-5	420	0.009	2.2-5	420	0.009	1.3-5	420	0.005
Balance of plant	1.3-2	65	0.844	1.3-2	65	0.844	1.3-2	65	0.844
TOTAL	1.4-2	96	1.344	1.4-2	94	1.317	1.4-2	85	1.187
OT/SOT[e]		0.630			0.636			0.665	
Availability		0.227			0.229			0.239	

[a]Read as 2.1×10^{-5}.

[b]λ ∿ failures/operating hour.

[c]MTTR (mean time to repair) ∿ hours.

[d]ρ ∿ (dimensionless) = λ × MTTR.

[e]Operating time/scheduled operating time.

By summing the failure rates and downtime ratio of the components and systems listed in Table 3-5, the RAM impacts of the proposed alternate configurations can be assessed. The overall reliability of each configuration is driven by those systems and components common to all the configurations, denoted in Table 3-5 as "Balance of Plant." Thus, the reliability impact of the proposed alternate configurations is imperceptible.

The maintainability of a device can be measured by its mean time to repair, MTTR. The MTTR varies from 96 h for the FED 300 class devices to 85 h for FED 400. This results in approximately a 5% improvement in availability, from 23% to 24%.

In developing the above assessment, it was assumed that spare ring coils would not be available in the event of a failure. Based on previous work done on the cost effectiveness of providing spares, this appears to be a reasonable assumption. However, if spare ring coils are assumed to be provided, the relative configurations were found to remain essentially equivalent.

A fully combined vacuum boundary (FED 400) offers some potential RAM advantages. TF coil removal and replacement should be simpler with a fully combined vacuum boundary for the following reasons:

- There is no spool structure blocking TF coil removal.
- The "C" section of the main vacuum vessel can be built from modules which are poloidally continuous. Thus, the need to assemble individual panels into a shell remotely is eliminated. All welds are planar, which is a very desirable feature for remote maintenance. Also, triple point welds are absent from "C" section construction.
- The outer wall of the main vacuum vessel remains intact during TF coil removal and replacement.

Elimination of the spool structure (a consequence of a fully combined vacuum boundary) eliminates the potential for troublesome vacuum leaks through the spool into the plasma vacuum chamber. However, leaks through the "C" section of the main vacuum vessel may be a serious problem in all of the proposed configurations.

Two of the candidate configurations, FED 301 and FED 400, feature superconducting inboard PF coils (EF1 and EF4) located outside the TF coil bore. The other configurations feature resistive EF1 and EF4 coils located inside the TF coil bore. External superconducting coils have the advantage of being more maintainable. Internal resistive coils, particularly EF4, will have limited access, and the radiation environment might restrict manned access to the coils. Also, internal resistive coils must be assembled in place, whereas external superconducting coils can be installed as a single pretested module. However, there are disadvantages to external superconducting coils as well. Associated with superconducting coil maintenance may be a long (approximately six weeks) thermal cycling time which would offset the inherent maintainability advantage. Furthermore, if spares are not provided for EF1 and EF4 (a likely prospect), the time awaiting coil repair or replacement would probably be substantially longer for a superconducting coil than for its resistive counterpart.

Another distinction between the configurations is the number of TF coils. In featuring a minimum-size TF coil, it is necessary on the FED 400 configuration to go from 10 to 12 TF coils to meet the ripple requirement. In doing so, there is up to a 20% increase in the number of certain components required for reactor operation, e.g., TF coil power leads. This was considered to have minor negative impacts.

In conclusion, the differences in RAM impacts associated with the four design options represent small perturbations on the overall RAM characteristics of the device. However, specific features, included in the FED 400 configuration, such as locating EF3 in a separate vacuum vessel and adopting a fully combined vacuum boundary appear desirable from the standpoint of RAM impact and should be considered for inclusion in future design iterations.

3.8 R&D ASSESSMENT

The objective of this study was to compare the R&D requirements of the four FED design options. The basic approach taken in implementing the study was to first list all the elements of the R&D program

identified for the FED Baseline (FED 300) in Refs. 1 and 2 and then to determine the applicability of each baseline R&D program element to the other three configuration options. Two questions were considered in conducting the applicability review. Are there any R&D program elements which are not applicable to one or more of the variants to the baseline? Are there any additional R&D programs required beyond those specified for the baseline?

The engineering or physics issues falling within each of the major R&D categories listed above are shown in Table 3-6. Cognizant FEDC personnel were called upon to review the possible applicability of those engineering/physics issues falling within their areas of expertise.

Upon completion of the R&D applicability assessment by the cognizant FEDC personnel, it was concluded that the basic FED engineering and physics R&D programs identified in the referenced documents apply equally to all four of the FED options considered. No additions or deletions were identified.

3.9 REACTOR COST STUDY

A parametric study was carried out on the four design options defined in Sect. 3.2 to evaluate merits of the different design features involving TF coil size, PF coil placement, and vacuum boundary design. To generate a consistent set of device performance and cost estimates for the four configuration options, the FEDC systems code was employed. The impact of maintaining both constant wall loading (1.05 MW/m^2) and constant burn time (50 s at a maximum toroidal field of 10 T) on the performance and cost of the four configuration options is disclosed in Tables 3-7 and 3-8. With comparable machine performance, namely, the same burn time and neutron wall loading, it is seen from Tables 3-7 and 3-8 that:

1. For constant tension TF coil cases, utilizing a semicombined vacuum boundary, FED 300/S-C, which saves 15 cm between the TF coil and shield, results in a cost savings of 6% (Cases 1 and 4).

Table 3-6. R&D requirements for R&D baseline options

Area	Specific item	Engineering/physics issue
1. Nuclear systems	1. First wall and limiter	1. Better characterization of graphite armor and better understanding of sputtering 2. Better understanding of stainless steel wall under melted conditions 3. Compatibility of limiter substrate with graphite surface material (bonding, etc.)
	2. Torus spool	1. Practicability of dielectric breaks or high-resistance structural techniques
	3. Shield sectors	1. Means of insuring high current toroidal path near plasma side of shield 2. Behavior of dielectric coating on shield laminations 3. Investigation of accelerated corrosion of stainless steel in water in magnetic field
	4. Vacuum pumping	1. Generic research on implantation and permeation of tritium in stainless steel 2. Demonstrate performance and safety of overall tritium system 3. Data on tritium adsorption/desorption for different surface materials and temperatures 4. Research in development of tritium permeation barriers
	5. Nuclear analysis	1. More advanced analysis techniques and expanded nuclear database
2. Auxiliary heating	1. ECRH	1. High-frequency gyrotron tubes (80-100 GHz) 2. Development of transmission system components (arc detectors, etc.) 3. Launcher concept w/high mode purity

Table 3-6 (continued)

Area	Specific item	Engineering/physics issue
	2. ICRH	1. Reactor relevant launcher, cooled transmission lines, directional couplers, etc.
	3. NBI	1. High current (40 A), high voltage (150 keV), long pulse (∿100 s) source that will work in nuclear environment 2. Prototype beam line w/radiation hardening and tritium containment features 3. Direct recovery technology should be developed for High-energy, 150 keV, long pulse (∿100 s) systems
3. Magnetic systems	1. TF and PF coils	1. Large coils at 10 T 2. Development work on high current coils 3. Behavior on high-strength stainless steel cryogenic temperatures 4. Impact of nuclear radiation on voltage breakdown in liquid helium 5. Alternates to polymeric insulators 6. Investigation of fretting and wear in magnets subject to pulsed 1 ds 7. Concept for minimizing eddy current losses in S/C PF coils
4. Remote maintenance		1. Efficient remote maintenance techniques for handling activated components up to 400 tons
5. Fueling	1. Fuel pellet injectors	1. Completion of experimental work on pneumatic and centrical fuelers 2. Development of a tritium-tight injector 3. Test facility to verify homogeneity and reproducibility of tritium pellets 4. Pellet integrity at high velocities

Table 3-6 (continued)

Area	Specific item	Engineering/physics issue
6. Diagnostics, instrumentation, and control		1. Proper functioning of diagnostics in radiation flux and required fluence levels 2. Human factors and man-machine interface 3. Control of the plasma — will need a control simulator
7. Safety and environment		1. Potential environmental concerns, including radiation exposure and high magnetic fields 2. Planning for avoidance of potential hazards including cryogens, high voltage, high currents, massive shielding, and radioactivity
8. Physics R&D requirements	1. Plasma performance	1. Size scaling of energy confinement 2. Temperature scaling of energy confinement 3. Beta limits and beta scaling of confinement 4. Cross section shaping 5. Achievement of low q with minimal disruptivity 6. Disruption characterization 7. Ion thermal transport 8. Ripple effects 9. Particle confinement and pellet injection
	2. Plasma heating	1. Physics of high-power ion cyclotron heating (must choose ICRH vs NBI) before starting reactor building design 2. Current drive by ion cyclotron waves 3. Physics of high-power neutral beam heating 4. Current drive by neutral beam injection 5. RF assisted current initiation

Table 3-6 (continued)

Area	Specific item	Engineering/physics issue
	3. Impurity control	1. Pumped limiter operation 2. Poloidal divertor operation 3. Impurity transport and edge physics 4. Neutral beam and RF driven impurity flow reversal

Table 3-7. FED Baseline parametric variation as a function of TF coil shape, PF coil configuration, and vacuum boundary design for constant values of burn time and wall loading

$L_w \sim 1.05\ MW/m^2$

T_B = constant (50 s)

	FED 300	FED 300/S-C	FED 301	FED 400
TF coils	Constant tension	Constant tension	Arbitrary shape	Arbitrary shape
PF system	Hybrid	Hybrid	Exterior	Exterior
Vacuum	Separate	Combined	Separate	Combined
a, m	1.3	1.2	1.3	1.17
R_o, m	4.836	4.560	4.952	4.606
I_p, mA	6.553	6.168	6.521	5.992
L_w, MW/m^2	1.01	1.05	1.04	1.08
P_{fusion}, MW	417.1	378.0	439.3	381.5
B_{max}, T	10.0	10.0	10.0	10.0
T_{burn}, s[a]	-45.3	-48.1	-45.9	-57.5
$ (M)	827.0	779.4	794.0	682.9
Rel. cost	1.00	0.942	0.960	0.826

[a]Burn time of 50 s achieved for 10-tesla peak field; burn time is 100 s at 8 tesla.

Table 3-8. Cost breakdown for parameter variation shown in Table 3-7

Constant burn time and wall load	FED 300	FED 300	FED 300	FED 300/S-C	FED 301	FED 400
TF coils	Constant tension	Constant tension	Constant tension	Constant tension	Arbitrary shape	Arbitrary shape
PF system	Hybrid (A)	Hybrid (B)	Hybrid (C)	Hybrid (A)	Exterior (D)	Exterior (F
Vacuum	Separate	Separate	Separate	Combined	Separate	Combined
Cost: $M						
Shield	77.3	78.5	81.6	69.4	79.1	69.0
TF	128.9	134.6	149.3	116.1	109.5	97.9
PF	85.5	90.3	73.1	78.6	96.8	58.0
Heating	72	72.9	74.9	69	73	68.4
Elec.	100.6	103.2	80.6	87.4	82.6	55.0
Facility	151.8	159.3	159.1	153.9	154.6	145.8
Others	210.9	210.2	210.9	205	198.3	188.8
Total	827.0	849.0	829.5	779.4	794.0	682.9
Rel. cost	1.000	1.027	1.003	0.942	0.960	0.826

2. A reduced-size TF coil (i.e., arbitrary shape as opposed to constant tension) coupled with an all-exterior PF system, FED 301, results in a cost decrease of 4% (Cases 1 and 3).
3. The FED 400 design, combined vacuum boundary 12 non-constant-tension TF coils, all-exterior PF system, shows a potential cost savings of approximately 17% (Cases 1 and 4).

The cost reductions for the FED 300/S-C and FED 301 configurations are 6% and 4%, respectively, compared to the baseline FED 300 configuration. FED 400 combines the key features of FED 300/S-C (combined vacuum boundary) and FED 301 (reduced TF coil size and external PF coils), along with a rerouting of the vacuum pumping duct. This pumping duct change allows the PF coil in FED 400 to be located closer to the plasma and, therefore, lowers the PF system cost. If this change were made to the FED 300 configuration, the cost savings are estimated to be 5%. Adding these three incremental cost savings (6% + 4% + 5%), a total cost savings of 15% is expected in going from the FED 300 to FED 400 configuration. This is consistent with the systems code result of a 17% cost savings.

3.10 OVERALL EVALUATION

Table 3-9 summarizes the outcome of the studies of the overall reactor design concepts. The only two areas which showed a significant difference between the configuration concepts proposed were cost and maintenance. Incorporating the design aspects of FED 400 reduces the size of the device; therefore, a 17%+ cost savings can be realized over the Baseline FED 300 design. At the same time, the maintenance aspects of the PF and TF coils and vacuum boundary are improved, while the maintenance characteristics of the torus shield modules are retained. The plasma chamber bakeout condition requires that thermal growth capability be designed into the combined vacuum boundary structure in order to reduce the thermal loads to an acceptable level. This design requirement imposed on the FED 400 concept is not envisioned to be a feasibility problem that would prohibit adopting the combined vacuum vessel concept. Startup coils pose problems of one form or another on

Table 3-9. Summary of reactor design concepts

	FED 300	FED 300/S-C	FED 301	FED 400
Cost	1.0	0.94	0.96	0.83
R&D requirements	Same	Same	Same	Same
Maintenance				
PF coil replacement	Difficult to replace interior copper coils and lower outboard EF coil	Difficult to replace interior copper coils and lower outboard EF coil	Coil replacement is feasible	Coil replacement is feasible
TF coil replacement	Very difficult	Very difficult	Very difficult	Most feasible approach
Startup coils	Space available but difficult access	Space available but difficult access	Require exterior coils	Require exterior coils or interior coils in a vacuum
Vacuum boundary	Complicated, yet more amenable to bakeout	Complicated, yet more amenable to bakeout	Complicated, yet more amenable to bakeout	Less complicated but bakeout sensitive
Torus shield	Same	Same	Same	Same
Penetrations and access	Access available at top of torus, vacuum duct complicates access	Same as FED 300	Torus access through face of torus, vacuum duct complicates access	Torus access top through face of torus and/or down through S/C dome
Availability	Same	Same	Same	Slightly favored
Safety	Same	Same	Same	Same
Power reactor relevance	Some component maintenance is still in question	Some component maintenance is still in question	Some component maintenance is still in question	Yes
Design flexibility	Large TF coils will allow more space to reconfigure a larger internal torus arrangement	Same as FED 300	Reduced-size TF coils will offer less flexibility to alter the internal component arrangement once the design is set	Same as FED 301

all configuration options. For example, on the baseline configuration (FED 300), startup coils can be located close to the plasma, reducing their current requirements; however, internal coils inherently cause maintenance problems. In the cases of FED 301 and FED 400 configurations, the startup coils are located exterior to the TF coil, thereby simplifying their maintenance; however, they require higher currents because they are farther from the plasma. From the standpoint of design flexibility, the Baseline FED 300 configuration is deemed to be more flexible than that of the reduced-size TF concepts of FED 301 and FED 400 in terms of offering more internal space inside the TF coil bore to add or alter coil components or possibly reconfigure a larger torus arrangement.

The conclusion drawn from these evaluations is that a cost and maintenance advantage can be gained by departing from the Baseline FED 300 configuration and incorporating the FED 400 concept in the Baseline FED reactor design.

It is not yet clear what arrangement will be adopted for future power reactors. The most recent tokamak power reactor study (Ref. 3), however, featured an arrangement not unlike FED 400. It can, therefore, be concluded that the FED 400 concept is at least as likely as the other concepts to be power reactor relevant. Since the cost and maintenance advantages far outweigh any potential problem with startup coils' current requirements and design feasibility, a configuration change to adopt the FED 400 design is recommended.

3.11 POLOIDAL DIVERTOR REACTOR DESIGN OPTION

Because of the present uncertainties involved in the choice of impurity control methods, the possibility of designing the FED to accommodate either a pumped limiter or a poloidal divertor was examined. It was concluded that the FED configuration can be designed with sufficient flexibility to accommodate both a pumped limiter and poloidal divertor impurity control system. This implies that the torus support spool be modified to provide the flexibility of encompassing either a divertor or limiter-shaped plasma plus allow the limiter and divertor modules to be extracted from the same location. It also may be necessary

to make the TF coils somewhat larger to accommodate the additional space requirements of the poloidal divertor. This, in turn, could result in larger PF coils and higher capacity power supplies.

The FED 400 configuration was developed initially for the operating condition of a divertor impurity control system. For this reason, the vacuum pumping duct was configured to pass down between the TF coil intercoil structure and provide the structural support for the torus gravity loads. This arrangement allowed a divertor module to be extracted without requiring the removal of the vacuum duct, as would be the case in the reference FED design. A pumped limiter module could then be located in the envelope space allotted for the divertor module.

REFERENCES

1. FED: Technology R&D Requirements for Construction, DOE/TIC-11600, October 1981.
2. FED: Physics Basis & Physics R&D Requirements, DOE/TIC-11600, October 1981.
3. STARFIRE — A Commercial Tokamak Fusion Power Plant Study, Argonne National Laboratory, ANL/FPP-80-1, Vol. II, 1980.

4. TORUS DESIGN STUDIES

This section discusses six discrete design problems associated with the torus. These are:

- Limiting the neutron and gamma streaming from the space between the inboard TF coil leg, vertical inboard wall of the magnet cryostat and the torus spool
- Achieving the desired electrical resistance properties of the torus spool
- Defining a design approach to obtaining a satisfactory electrical resistance at the inner surface of the shield
- Providing adequate shielding for test modules
- Defining the overall response of the torus to seismic loadings
- Assessing the first wall thermal response to an improved definition of the poloidal distribution of heat loads

4.1 INTRODUCTION

The design activities discussed in this section address three important objectives for the FED. These are:

- Achieving contact maintenance conditions at the outside of the reactor
- Achieving satisfactory electrical properties for the torus to properly support startup and prevent damage from disruptions
- Achieving satisfactory structural and thermal response from torus components

The achievement of contact maintenance conditions requires that contamination in the reactor room be kept at acceptable levels and that a shutdown dose rate be limited to 2.5 mrem/h 24 h after shutdown. Achieving the shutdown dose rate requires a certain bulk shield performance (neutron flux at the outer surface) for the outboard portions and control over neutron and gamma streaming in gaps and penetrations. It is this latter factor which is the subject of Sections 4.2 and 4.5. The neutron flux at the outer surface of the inboard shield is determined by

TF coil protection requirements. This flux is higher than permissible for shutdown dose rates. Furthermore, the neutrons emerging from the outer surface of the inboard shield may stream down the gap between the TF coil, TF coil cryostat and the torus spool. The regions above and below the spool contain PF coils which are maintained with contact techniques. These techniques dictate a dose rate limitation of 2.5 mrem/h. Hence, the neutron streaming intensity must be limited to the flux required of the outboard shield (10^6 neutrons/cm^2 s).

The test modules, located in two dedicated shield sectors, present another type of shielding problem. Each module contains a test volume which must be assumed to be essentially a void in terms of shielding effectiveness. The problem is then to provide additional shielding at the outer surface without limiting access to the individual modules.

Achieving the desired electrical properties in the torus is essentially that of designing for a level of electrical resistance in the inner surface of the shield sector (next to the plasma) and at the outer surface of the torus (spool). The design of the inner surface toroidal current path is discussed in Sect. 4.3 and is the problem of bridging the gaps that exist between shield sectors with enough conductor to adequately handle the induced currents resulting from plasma disruptions. The design of the outer surface is one of preventing currents during startup and of inducing the required current to flow in the plasma. This design, involving both high-resistance load-carrying structure and high-resistance breaks, is discussed in Sect. 4.4.

The torus of the FED Baseline is shown in Fig. 4-1 in elevation. Illustrated in this view are the following regions:

1. Inboard wall region where neutron streaming must be limited
2. Shield inner surface where toroidal electrical flow path must be provided
3. Outer torus surface (spool) where toroidal electrical resistances must be significantly higher than at region (2)
4. Test module installation where shield volume must be replaced at outer surface
5. Torus and support structure which must respond adequately to seismic loadings

ORNL-DWG 82-3795 FED

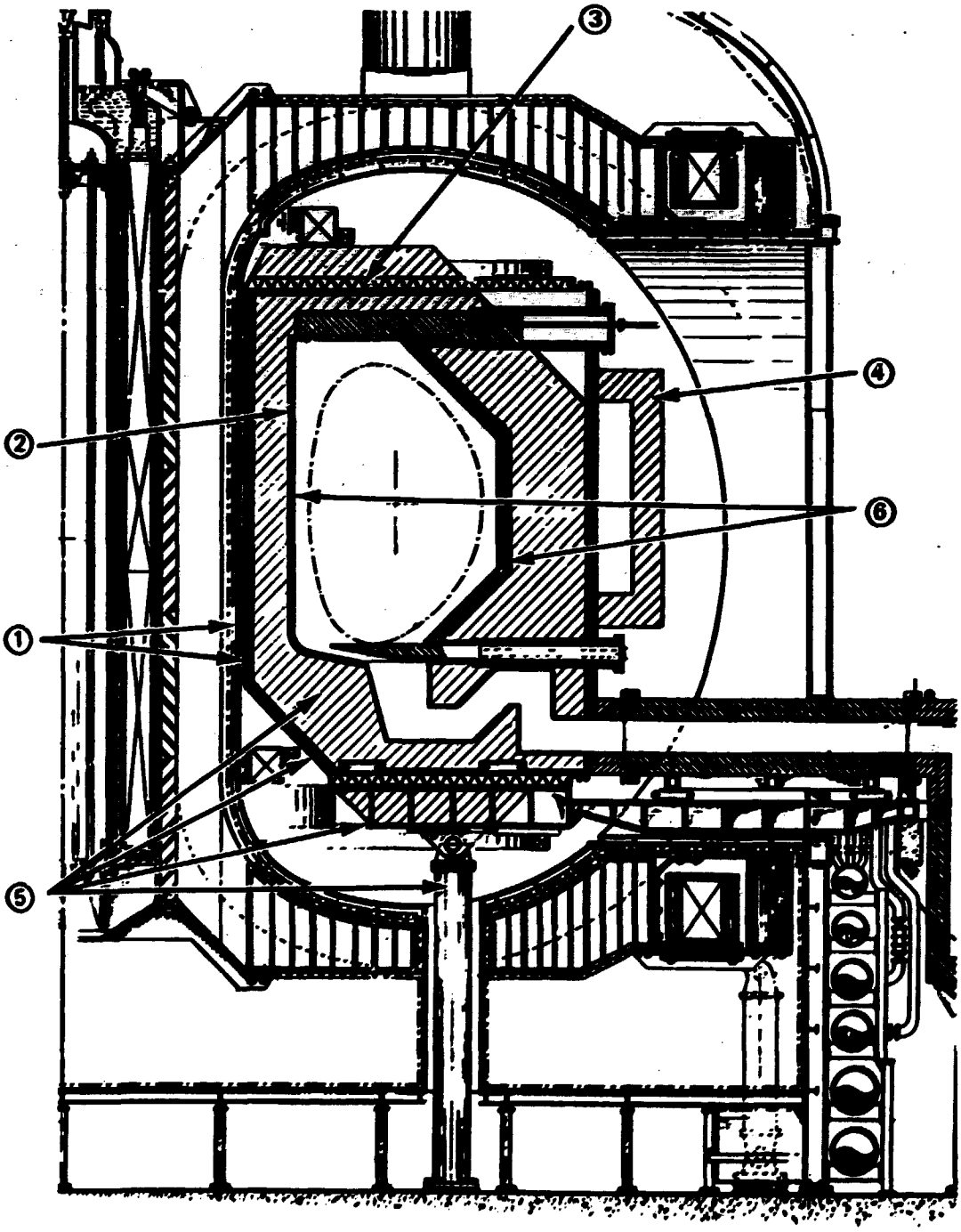

Fig. 4-1. Torus regions addressed in FY 82 studies.

6. First wall surfaces which must provide adequate thermal response to poloidally distributed heat loads

4.2 INBOARD GAP SHIELDING

Controlling neutron and gamma streaming through gaps and penetrations is a challenge deserving attention throughout the design process. The problem is compounded by the fact that the inboard shield is designed to limit the neutron flux to the level at which activation would permit contact maintenance (2.5 mrem/h 24 h after shutdown). The question then is how to keep this neutron flux from activating the materials in regions where contact maintenance activities are planned.

The region of interest is shown in Fig. 4-2. A radial build for the FED baseline is shown in Fig. 4-3.

4.2.1 Inboard Gap Configuration

The recommended solution to the inboard gap streaming problem is illustrated in Fig. 4-4. Two shield ring systems are installed, one at the top and one at the bottom of the spool structure. The shield extends over a vertical span of some 1.15 m and consists of 14 overlapping shield rings. Four rings are attached to the torus spool and four to the TF coil magnets. The remaining six rings are attached to the magnet system cryostat.

The shield materials consist of Nitronic 33 stainless steel (25%) and boron carbide (75%).

There is a radial gap between the cryostat mounted shield rings and the spool of 4.40 cm to allow for seismic motion. A gap of 5.35 cm is provided on the cryostat side.

4.2.2 Shielding Requirements

The objective of the shielding of the gap between the spool and the TF coil cryostat and between the cryostat and the TF coil magnet cases is to achieve the shutdown dose rate of 2.5 mrem/h outside the reactor 24 h after shutdown. In order to achieve this level, a neutron flux

ORNL-DWG 82-3796 FED

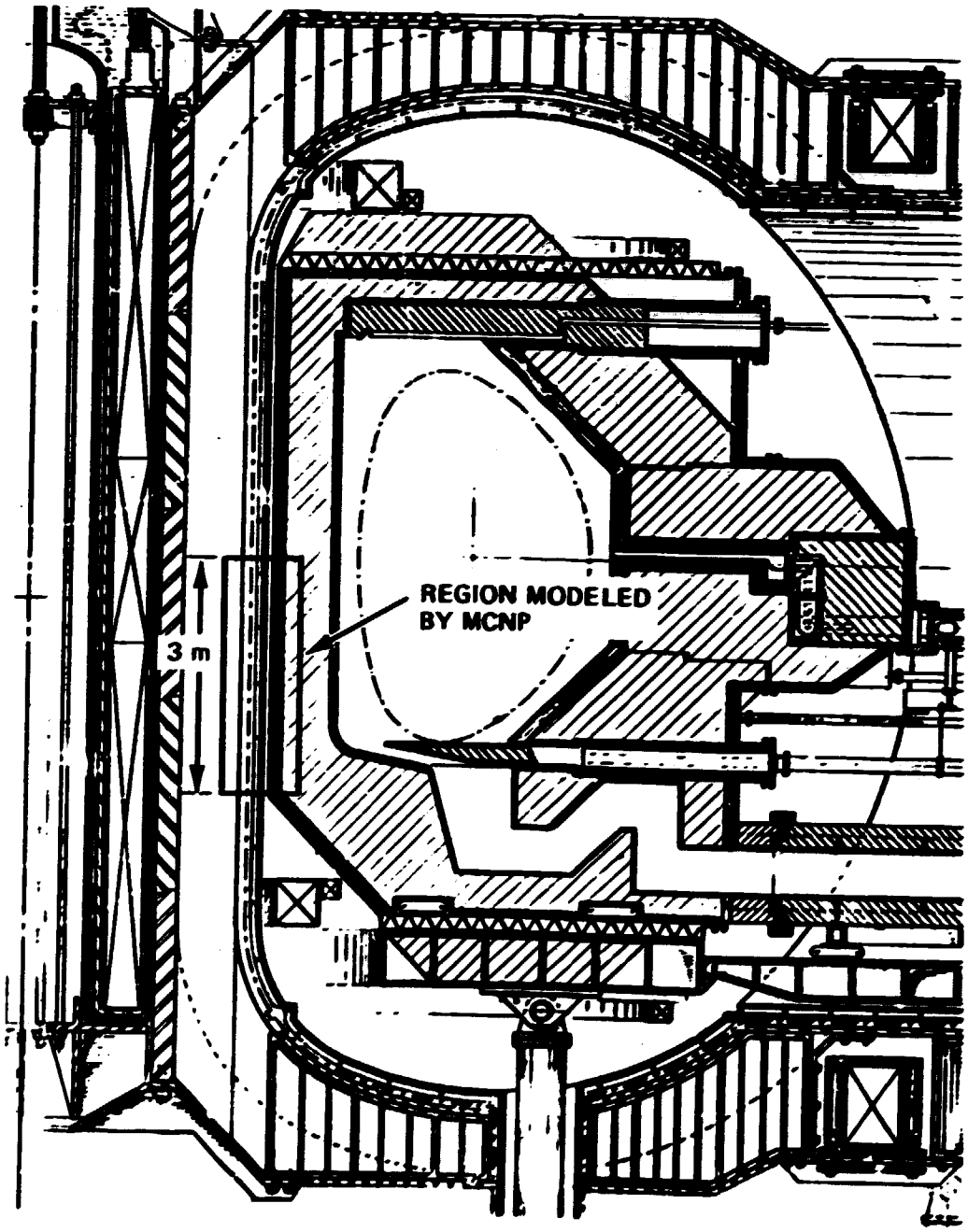

Fig. 4-2. FED elevation showing region modeled by MCNP.

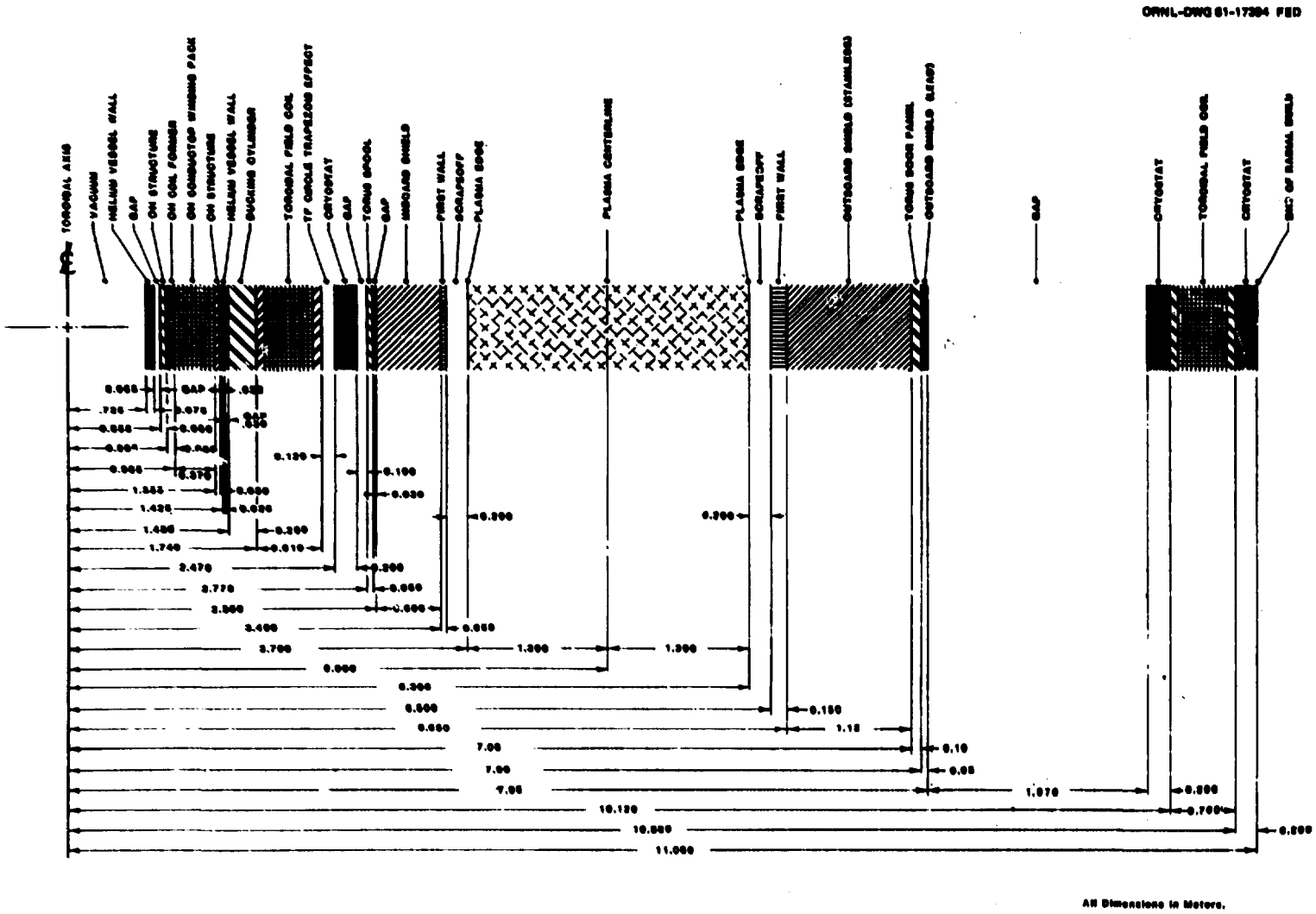

Fig. 4-3. FED-baseline radial build.

ORNL-DWG 82-3744A FED

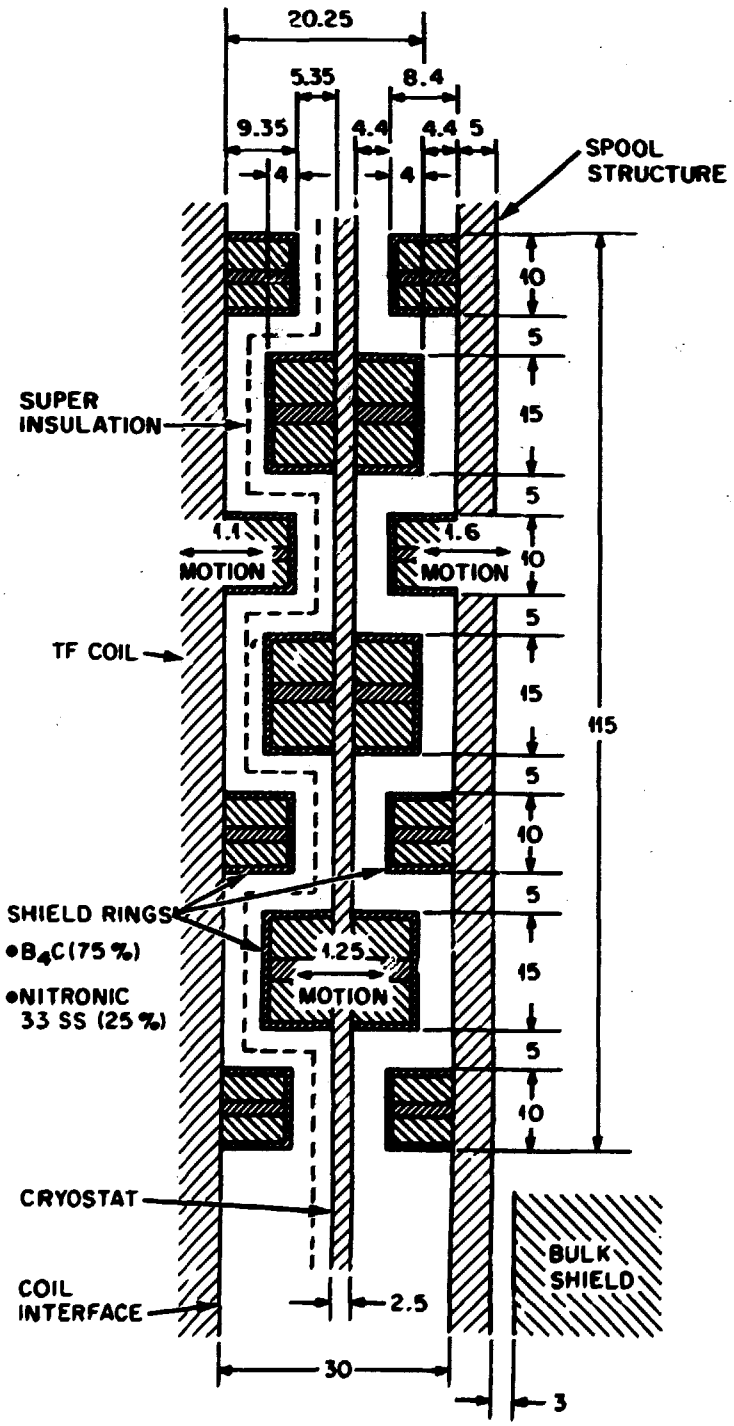

ALL DIMENSIONS IN cm

Fig. 4-4. Multiple shield rings – final version.

of between 1×10^6 and 2×10^6 neutrons/cm^2-s is acceptable. It is estimated (Ref. 1) that a shutdown dose rate of several rem/hr exists in the gap 24 h after shutdown if no shielding is provided. A solid shield of 0.35 m would be required to reduce this dose rate to 2.5 mrem/h if no interleaving were incorporated.

4.2.3 Shield Materials and Material Distribution

A number of materials and material distributions were analyzed and summarized in Table 4-1. These analyses were based on a single solid shield with no streaming paths.

In examining the results shown in Table 4-1, several conclusions were made:

1. There is only a small advantage in a graded shield material distribution over a simple two-component material.
2. In view of the complexity of incorporating water as a material, boron carbide is recommended as a substitute for only a small penalty in neutron flux (25% steel, 75% B_4C).

4.2.4 Shield Configuration

Since a solid shield block is impractical to install, several labyrinth configurations were developed and analyzed with a Monte Carlo analysis using the Los Alamos MCNP code for the combination of neutron streaming and neutron attenuation. The labyrinth configurations require space for seismic motion and for thermal expansions. Hence, in some cases, a net increase in radial build of the machine is required to incorporate them.

In an effort to minimize the impact on radial build, the interrupted cryostat configuration shown in Fig. 4-5 was developed. In this concept, provision is made for allowing the shield block on the TF coil to pass across the principal surface of the cryostat. This is accomplished by jogging the cryostat surface.

For the cases of average source energies of $\bar{E} = 3$ MeV and $\bar{E} = 1.6$ MeV, the flux is 7.1×10^6 for the lower energy spectrum, or about a factor of

Table 4-1. Performance for a number of shield compositions

Material	Total thickness (cm)	Total gap width (cm)	Energy spectrum (MeV)	Neutron flux neutrons (cm^2-s)
No shield	--	30	3.0	7.2×10^8 ($\pm$9%)
316 SS (100%)	30	30	3.0	3.3×10^7 ($\pm$12%)
50% 316 SS/ 50% water	30	30	3.0	3.2×10^6 ($\pm$30%)
50% 316 SS/ 50% water	30	38	3.0	6.2×10^6 ($\pm$17%)
Graded*	30	38	3.0	4.6×10^6 ($\pm$13%)
50% 316 SS/ 50% water	40	38	3.0	2.5×10^6 ($\pm$24%)
25% 316 SS/ 75% water	40	38	3.0	2.6×10^6 ($\pm$25%)
Graded*	40	38	3.0	1.5×10^6 ($\pm$22%)
50% 316 SS/ 50% water	40	38	1.6	0.93×10^6
25% 316 SS/ 75% B_4C	40	38	1.6	1.06×10^6
50% 316 SS/ 50% B_4C	40	38	1.6	1.47×10^6

*Graded
- Top layer 100% steel
- Second layer 75% steel, 25% water
- Third layer 50% steel, 50% water

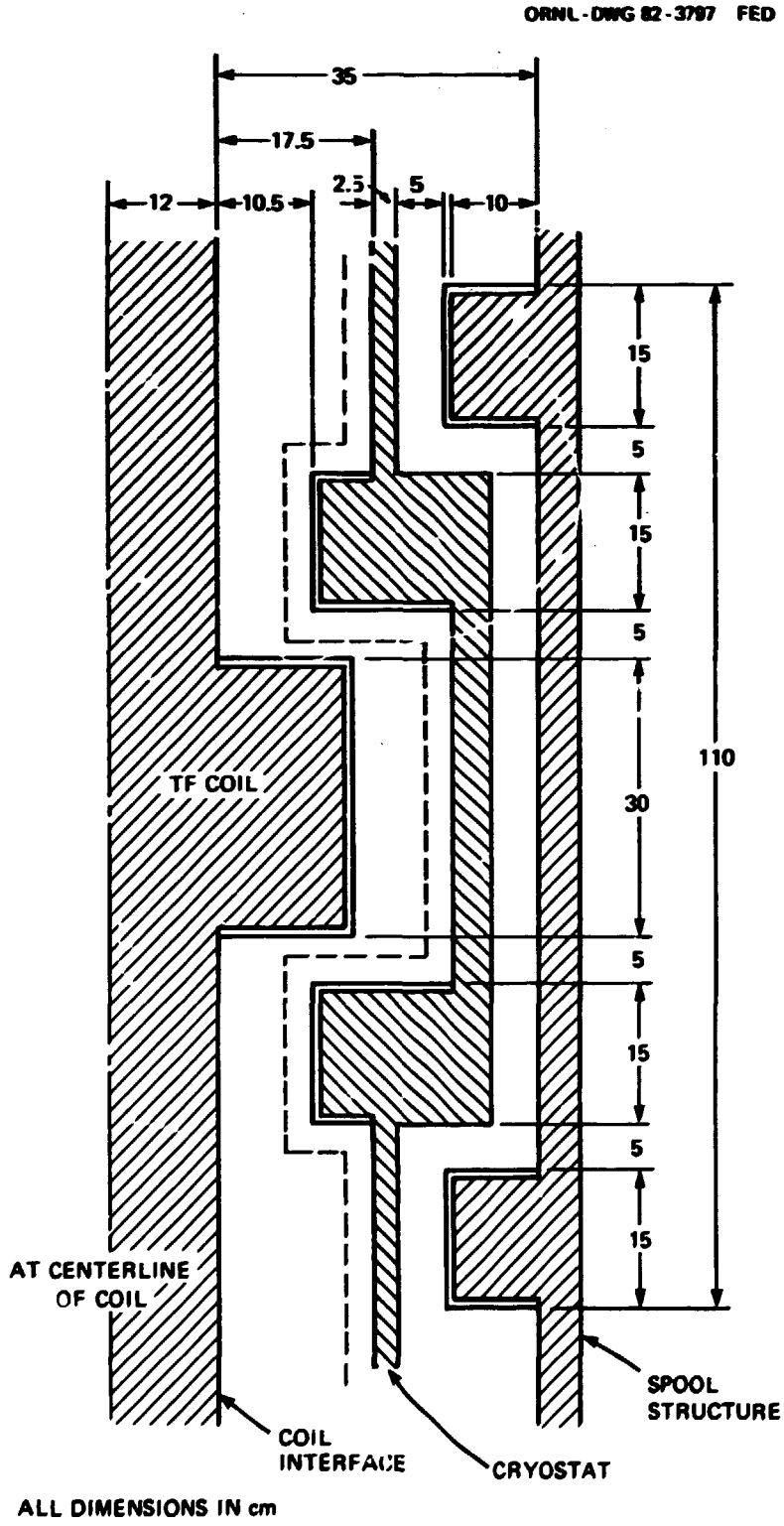

Fig. 4-5. Interrupted cryostat concept.

10 too high. There is, however, some savings in radial build. Another cost factor is the additional complexity in the cryostat design and fabrication.

A final arrangement of shield material as modelled in the MCNP program is illustrated in Fig. 4-6. In this example, there is a 3-cm gap between the spool vertical wall and the shield sector. The actual design provides for this gap to permit thermal expansion of the sector. The spool panel is actually a single surface with external vertical rib stiffeners. The shield blocks may be fitted in between the ribs. Hence, the model depicted in Fig. 4-6 shows shield material extending radially to within 3 cm of the shield. The neutron flux is high in this region (at the bottom of the gap), about 8.8×10^7 neutrons per cm^2-s. When the FED device is operating, the operating temperatures will result in a gap of only 0.7 cm. In this case, the flux drops to 2×10^7 neutrons/cm^2-s over a very small region.

4.2.5 Attachment/Assembly

The addition of the gap streaming shield rings (Fig. 4-4) requires a specific assembly sequence. The shield rings attached to the TF coil casing are installed after the TF coils. The ring consists of a number of segments equal to the number of TF coils. The adjacent ring segments overlap each other in the toroidal direction but are not load-carrying members.

The shielding ring on the vacuum side of the magnet vacuum vessel is attached prior to assembly of the vacuum vessel. At each edge of the ring segment a relief notch is provided, through which the weld inspection X-ray film is passed. The magnet vacuum vessel external ring segments are installed after completion of the vacuum vessel. Each adjacent ring segment provides an overlap to protect against streaming.

Each shield ring on the torus spool has twice the number of segments as the number of TF coils. Half are installed on the radial frames and half on the spool inboard panel surface. The segments attached to the spool radial frame are of different arc lengths, thus preventing vertical

ORNL-DWG 82-3798 FED

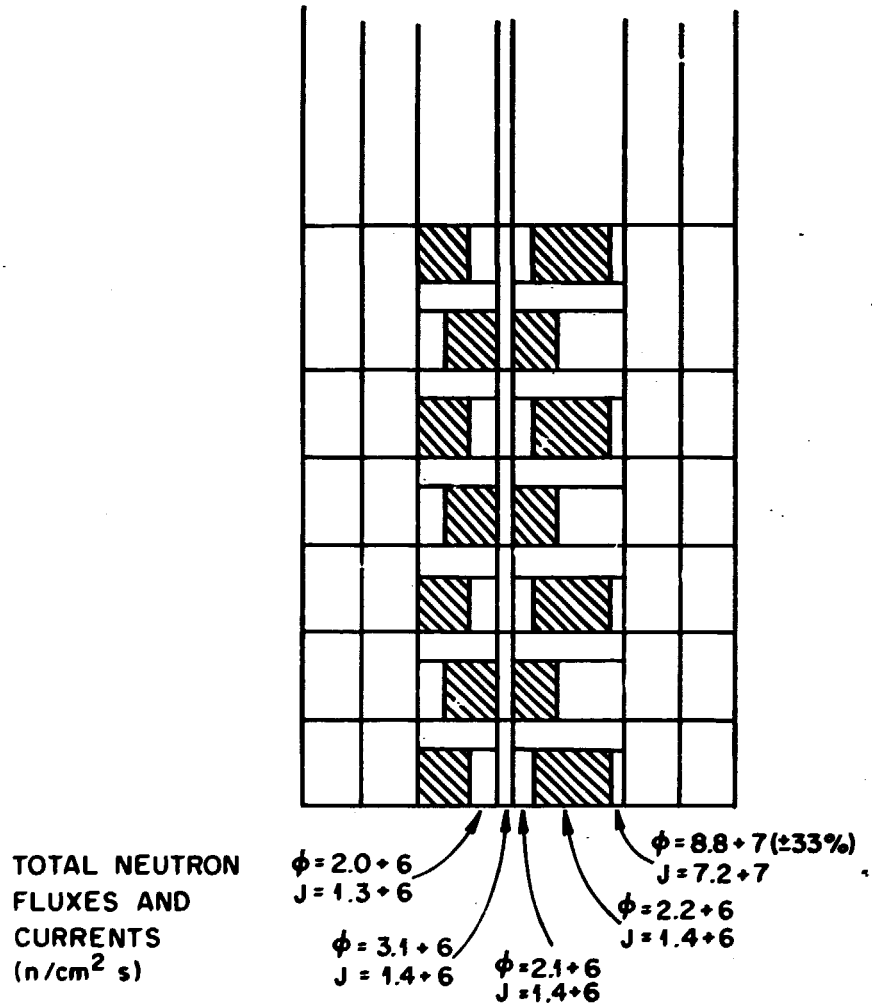

Fig. 4-6. Gap shield configuration.

streaming between the shield rings due to staggering of the gaps between adjacent segments.

4.3 TORUS CURRENT PATH

The FED Baseline bulk shield is composed of ten 36° shield sectors separated by small (≈1-2 cm) gaps (Fig. 4-7). When a major disruption occurs, large currents are induced in the inner surfaces of the shield sectors caused by the collapsing plasma current in the latter period of the disruption. The design objective is to accommodate these currents without damage to the torus components or to the magnet system. There are three ways in which these currents might be accommodated:

1. Continuous toroidal flow (based on the existence of conductors which bridge the gaps between sectors)
2. Arcing between sectors
3. Fully developed eddy currents in each of the ten sectors

If a low-resistance, high-current capacity path is established between sectors at the inner surface location, then the disruption induced currents are harmlessly dissipated. Since gaps are provided between shield sectors, to facilitate their removal and replacement and for thermal expansion, it is necessary to provide electrical conductor(s) to span the gaps. The conductor designs are discussed in Sect. 4.3.2 and 4.3.3.

If the voltage drop between sectors is sufficiently high during a disruption and if gaps exist between the sectors, then arcing will occur. From the design standpoint, the question must then be addressed, "Can we design the sector-to-sector interfaces in such a way that we can accommodate the arcing without significant material damage?". Section 4.3.4 discusses the possible design approaches for the arcing problem.

The condition for fully developed eddy currents to exist is that the return current path voltage drop internal in the sector is sufficiently low to prevent arcing between the sectors. If this condition is satisfied, then the eddy currents will result in overturning moments on

ORNL-DWG 81-17385R FED

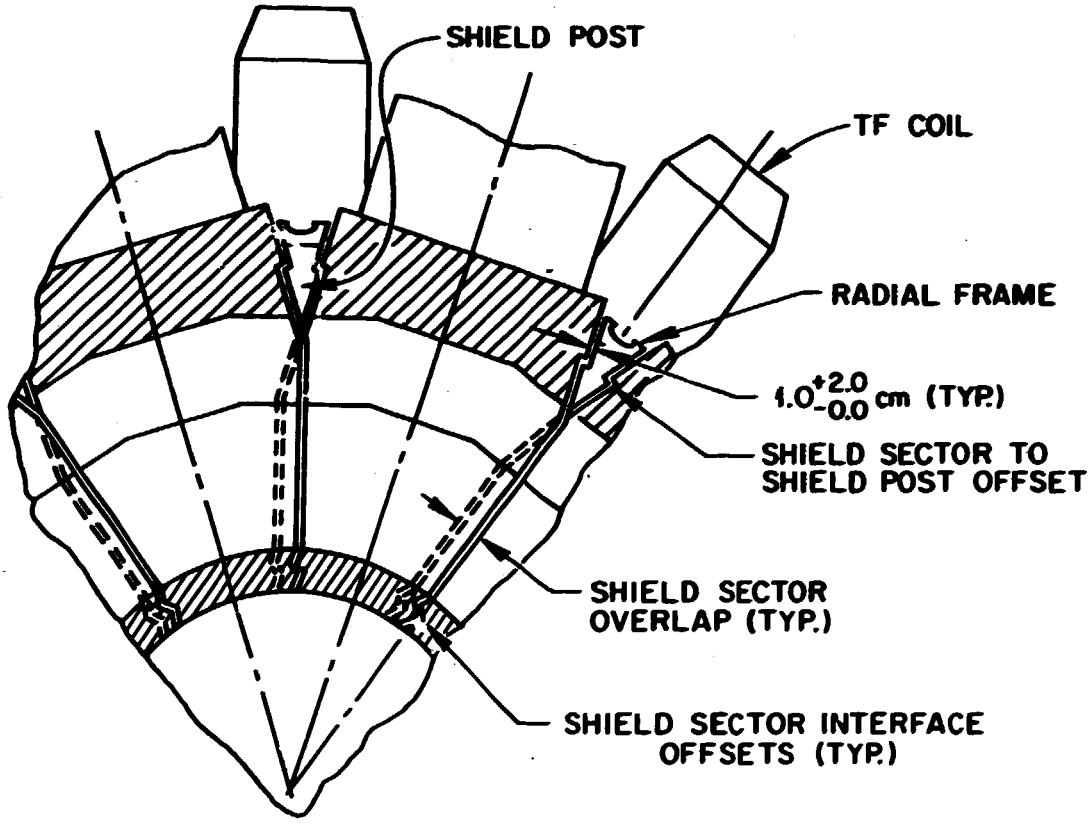

Fig. 4-7. FED baseline sector gap configuration.

the sectors that must be reacted if sufficiently large. This condition is analyzed in Sect. 4.3.5.

Electrical conductors for providing a toroidal current path in the event that a disruption occurs were chosen as the preferred design approach for accommodating these currents. This decision was made based on the following observations regarding the other two options:

1. Arcing locations are and probably will not be known with sufficient confidence to justify a design.
2. Design of the sector internal configuration to establish low-resistance eddy current flow paths presents a complex problem that probably will result in a high cost for manufacturing the torus.

4.3.1 Torus Current Path Requirements

Since the torus is inside both the TF and PF fields, any induced currents in the structure will result in forces on the structure. In addition, the current decay times of disruption can be controlled by eddy currents. Large eddy currents induced on the inner walls of the torus retard the plasma movement. This allows the plasma magnetic stored energy to be dissipated in the torus as I^2R heating instead of thermal heating of the surface in contact with the plasma.

The requirements for torus current paths have three basic features: (1) design eddy currents paths in parallel to the high TF fields to minimize mechanical forces and overturning moments, (2) provide a good toroidal current path near the plasma to control the disruption damage, and (3) provide high-resistance toroidal current paths in all structures, including the vacuum boundaries, located beyond the highly conducting first wall.

In the FED Baseline, the replaceable first wall coolant panels are designed to conduct eddy currents toroidally and are electrically connected to the torus wall. The torus walls between segments are connected electrically at the surfaces near the plasma. The internal shell of FED, therefore, has a toroidal path equivalent to 3 to 4 cm of stainless steel.

4.3.2 Candidate Electrical Conductor Concepts

A large number of concepts for electrical conductors were reviewed and assessed. The six concepts finally evaluated are shown in Fig. 4-8.

Candidate 1 is a sector-to-sector or first wall panel to first wall panel strap. It has a V-cross-section to accommodate toroidal displacement resulting from thermal expansion and to allow some flexibility in installation to adapt the strap to various gap conditions. It is sized to permit passive cooling. In the inboard regions, it is attached below the armor tile. In the outboard region, it is attached to the actively cooled stainless steel first wall panels.

Candidate 2 is a hydraulically operated bellows. The bellows contains a nested set of springs which function principally as the electrical conductor. The bellows uses water as the pressurant which is the active cooling medium. Upon pressurization of the bellows with water, the electrical contact is closed across the sector-to-sector gap. Evacuation of the pressurant retracts the bellows and breaks the contact.

Candidate 3 is a poloidal continuous strap inserted from the outside of the shield sectors and clamped in place to bridge the sector-to-sector gap. The strap consists of a segmented copper conductor, continuous stainless steel strap for carrying the hoop tension loads, and hat section segments for providing toroidal strength.

Candidate 4 is an approach for establishing sector-to-sector contact through crushable or deformable inserts. These inserts take advantage of the wedging action inherent in the geometry of the FED Baseline segmentation concept. The crushable element consists of a tube made of a high-conductivity metal.

Candidate 5 is a rotatable bar connector that is positioned from the inside of the plasma chamber by torquing the bar into place with a special wrench. Part of the torquing action rotates the bar, and the final torquing clamps the bar down on the adjacent sector contact pad. Current flows from the sector structure, through a partial sleeve, through a bushing on one end of the bar, and through the bar itself and into a pad on the adjacent sector.

ORNL-DWG 82-3799 FED

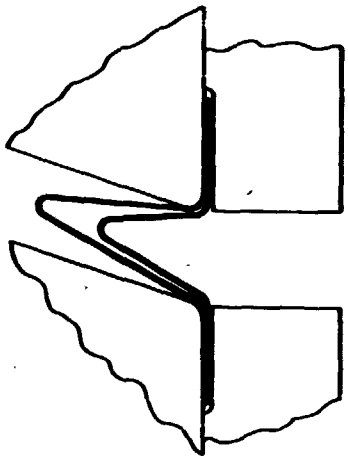

SECTOR–TO–SECTOR STRAP

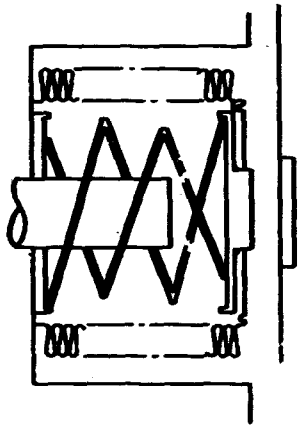

HYDRAULICALLY OPERATED BELLOWS

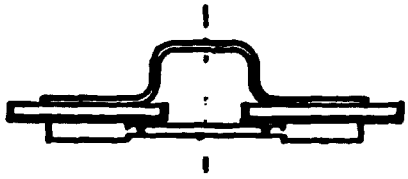

POLOIDAL STRAP

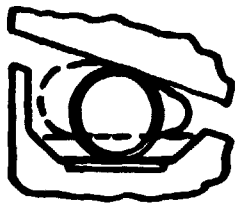

CRUSHABLE INSERTS

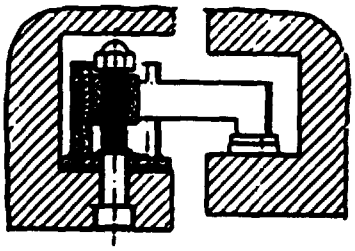

BAR CONNECTOR
(MECHANICALLY POSITIONED
FROM INSIDE TORUS)

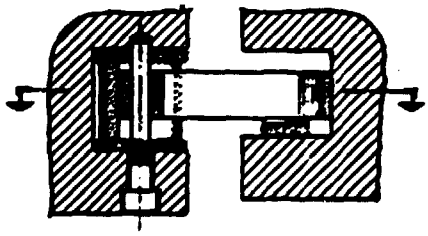

BAR CONNECTOR
(TF FIELD ACTIVATED)

Fig. 4-8. Electrical conductor options.

Candidate 6 is similar to 5, except that the torque is developed by the interaction of the toroidal magnetic field. Contact pressure is through the torque reaction at the adjacent sector pad.

The seven candidates were evaluated, and the qualitative assessments are indicated in Table 4-2. The seven candidates are listed down the left-hand column. The criteria for the evaluation are listed across the remaining columns. The interpretation of these criteria is as follows:

a. Effectiveness for carrying current. Some of the contacts are discrete, and their installation occupies a large volume relative to the conductor size. These are rated lower than the strap type, which is more like a continuous bus-bar.

b. Requirement for remote handling. This is related to the ease of replacement in-situ. Some concepts require pulling a sector and taking it to the hot cell. Other concepts can be replaced in-situ but require very sophisticated remote handling equipment. The more the in-vessel remote handling, the lower the score.

c. Tolerance to misalignment of sectors. Low tolerance received low scores. It is assumed that misalignment will exist.

d. Provisions for controlling contact pressure. This is somewhat related to the previous criteria. In addition, however, a positive bolt or screw attachment is given a higher rating than one that is dependent upon magnetic field forces.

e. Reliability. This depends on whether or not it is active or passive and the general complexity of the component. How stringent must the quality control procedures be?

f. Impact of a failure. Rating depends on answers to the following questions:

   1. Will a failure result in a hazardous situation?
   2. Will a failure shut down the device?
   3. Can the device continue to operate safely with one failure? Two failures? Three failures?

g. Impact on shield effectiveness. The rating depends on how much shield volume is used up by the contact installation. The more the volume, the lower the rating.

Table 4-2. Assessment of candidate electrical contact co

Weighting factor	15	25	40	35	20
			Criteria		
	A	B	C	D	E
Configuration	Effectiveness for carrying current	Requirement for remote handling	Tolerance to misalignment of sectors	Provisions for controlling contact pressure	Reliability
Sector-to-sector strap	High	Severe	Will be a headache	Through attachment technique -good-	Good
Hydraulically operated bellows contact	Feasible but may have little margin	None	Good	Good	Will require major test program
Poloidal strap	Fair	None (installation of remote equipment to remove after arc welding from outside)	Major problem	Limited	Fair--probably affected adversely by thermal expansion
Crushable inserts	Dependent on contact extent & pressure	Probably none Will need in-situ	Major problem	No control	Adversely affected by radiation creep
Bar connector (mechanically positioned)	Good	Requires activation from inside walls	Good	Good	Good
Bar connector (TF field activated)	Dependent on contact pressure	None unless toroidal field is off	Fair	Limited	Uncertain, probably fair

ssessment of candidate electrical contact concepts

	40	35	20	30	5	10
	Criteria					
	C	D	E	F	G	H
	Tolerance to misalignment of sectors	Provisions for controlling contact pressure	Reliability	Impact of a failure	Impact on shield effectiveness	Cost
	Will be a headache	Through attachment technique -good-	Good	Probably small	Negligible	Small for strap; significant for remote equipment
	Good	Good	Will require major test program	Reactor shutdown	Volume occupied by bellows must be replaced	Moderate
o r arc m	Major problem	Limited	Fair--probably affected adversely by thermal expansion	Probably small	Negligible	Small
ne n-	Major problem	No control	Adversely affected by radiation creep	Probably small	Negligible	Moderate
	Good	Good	Good	Small	Some shield volume lost	Moderate
f	Fair	Limited	Uncertain, probably fair	Small single failure	Some shield volume lost	Moderate

h. Cost. This has two parts. One is the cost to develop and manufacture the contact. The second is the relative cost of the remote handling equipment.

Shown in Table 4-2 are the results of the quantified evaluation. Across the top of the table are the criteria used in the evaluation abbreviated as A, B, C, etc. These letters are also designated with the appropriate descriptive titles in Table 4-3 for reference. Each of the concepts is listed down the left-hand column. The scores, shown in Table 4-2, are based on a 1-5 rating, with the higher score equivalent to the most desirable quality. The score is the numerator (X/) in the evaluation. Each criterion is given a weighting factor according to its perceived importance. The weighting factors are from 5 to 40 in multiples of five. We have precluded the possibility of two criteria having the same weighting factor. The criteria which were assigned the highest weighting factors were those where any attempt to improve that feature of the design would have a major impact on the design either as cost, technical risk, or simply as a rippling factor through other components. The weighting factors are shown at the top of each criteria column. The product of each score and the appropriate weighting factor is the weighted score and is shown as the denominator (/XX). The summation of the weighted scores is shown in the right-hand column.

The result of the above scoring is that the copper sector-to-sector strap received the highest score. This high score resulted primarily from a high rating on the following criteria:

1. Effectiveness in carrying high currents
2. Provisions for controlling contact pressure
3. Reliability
4. Impact of a failure

4.3.3 Electrical Conductor Design

Strap design

The concept discussed in this section is a copper strap design which spans the gaps between sectors. The strap concept for the inboard,

Table 4-3. Conductor evaluation scoring

Concept (Weighting factor)	Criteria A (15)	B (25)	C (40)	D (35)	E (20)	F (30)	G (5)	H (10)	Total	Rank
Sector-to-sector strap	5/75	2/50	3/120	5/127	5/100	5/150	5/25	3/30	725	1
Hydraulically operated bellows contact	3/45	5/125	4/200	5/175	2/40	2/60	4/20	4/20	705	3
Poloidal strap	4/60	3/75	3/120	3/105	3/60	4/120	2/10	3/30	580	6
Crushable inserts	4/60	2/100	4/160	2/70	4/80	5/150	5/25	4/40	685	4
Bar connector (mechanically positioned)	3/45	2/50	4/160	5/175	4/80	5/150	4/20	3/30	715	2
Bar connector (magnetically positioned)	3/45	4/100	3/120	2/70	3/60	5/150	4/20	4/40	605	5

top, and bottom is shown in Fig. 4-9 and for the outboard regions is shown in Fig. 4-10. Concept consists of copper straps bolted to the first wall panels on the outboard and the shield on the inboard, top, and bottom. For thermal protection, a titanium zirconium molybdenum (TZM) strap is placed in front of the copper strap.

With good thermal contact between the copper strap and shield, the maximum temperature for a 0.1-cm-thick and 17-cm-long copper strap is 400°C for normal operating conditions with a magnetic field of 10 T. During plasma disruptions, the copper temperatures will rise to 600°C.

Limiting the TZM strap temperature to <1200°C with a maximum stress of 345 MPa (50 ksi) and length of 12 cm results in a thickness of 0.3 cm.

Figure 4-11 shows the copper strap length vs thickness relationship for three allowable stress values (100, 210, and 310 MPa) and maximum operating temperatures of 300°C, 400°C, and 500°C, respectively. Since a maximum operating temperature of 400°C was selected, the range of material thickness (at 200 MPa stress level) is between 0.075 and 0.125 cm. The thickness of 0.1 cm was selected, since it is a standard commercial thickness.

The electrical requirements established for disruption conditions are as follows:

1.	Current on the inboard, top, and bottom surfaces, A	3.4×10^6
2.	Current in outboard surfaces, A	1.6×10^6
3.	Voltage drop across strap, V	<10

The calculated voltage drops across the inboard and outboard straps are 3 V and 2 V, respectively. These calculations assume that the disruption currents are uniformly distributed and that no current flows through the TZM thermal shield.

To remove the inboard, top, or bottom electrical strap requires the removal of a row of graphite tiles on each adjacent shield sector and the strap. The outboard strap removal requires the removal of attachment fasteners. An alternate approach is to remove the straps by either sawing, grinding, or torch cutting and removing the pieces after the sector has been extracted. The alternative methods require significantly

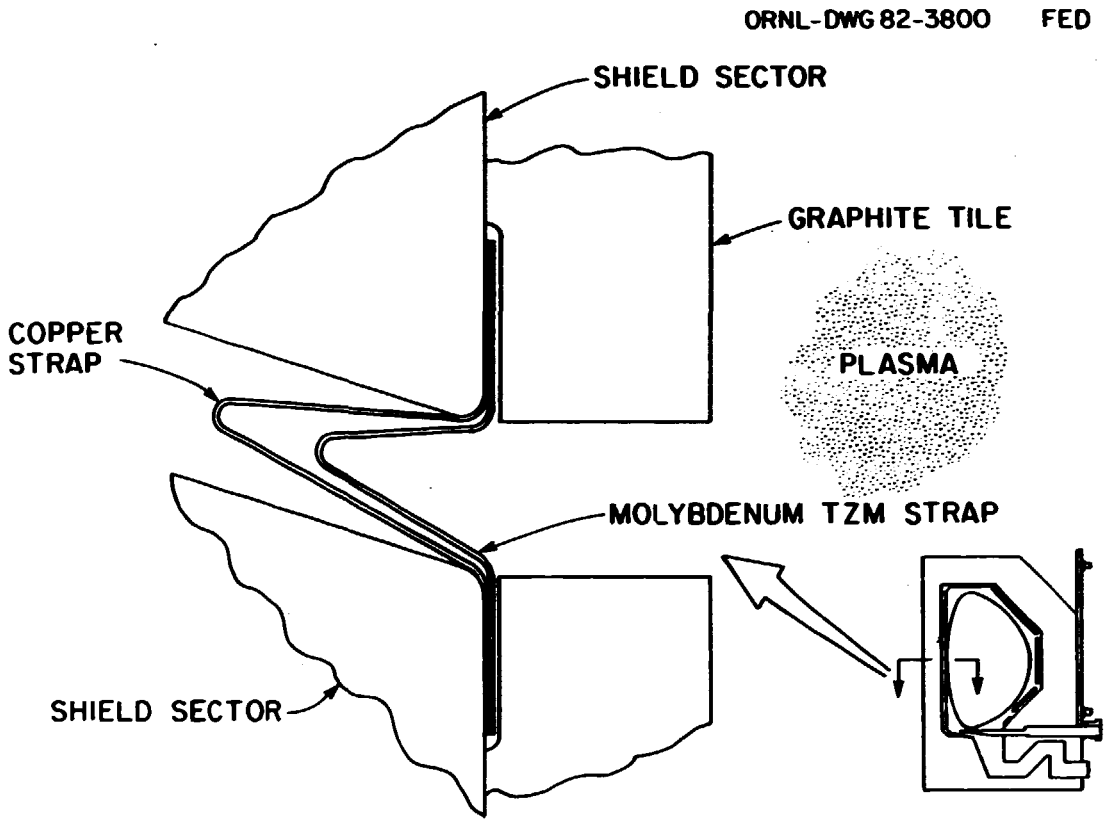

Fig. 4-9. Inboard electrical strap concept.

ORNL-DWG 82-3801 FED

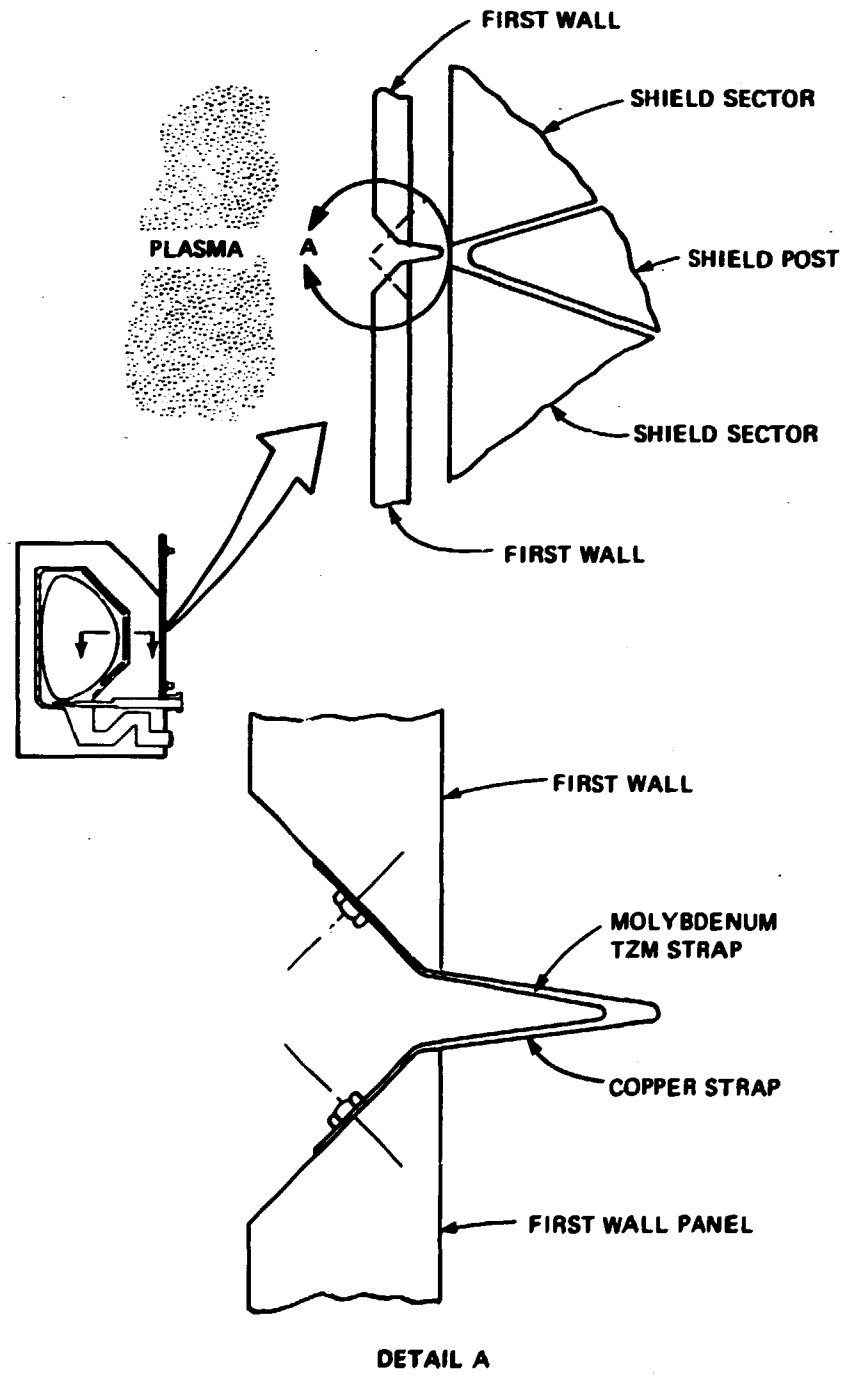

Fig. 4-10. Outboard electrical strap concept.

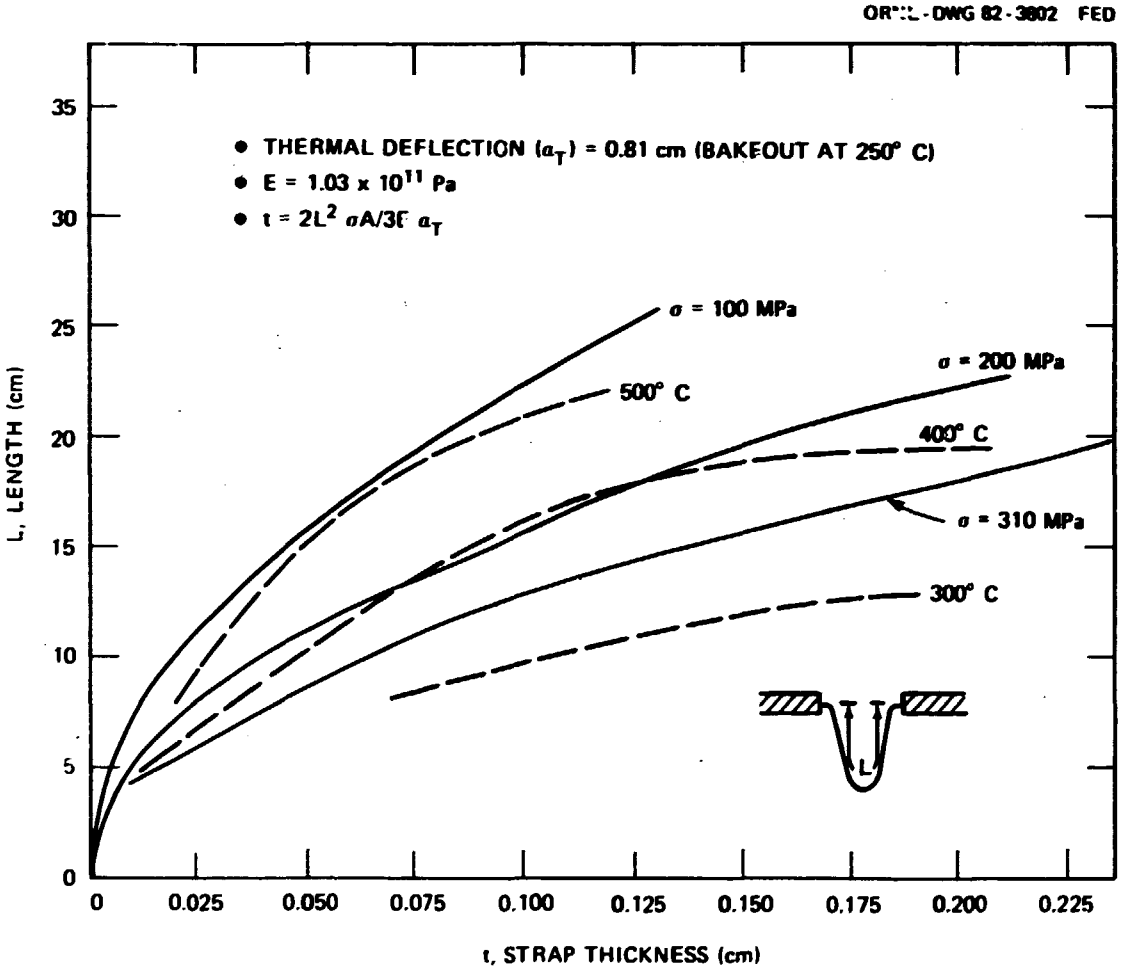

Fig. 4-11. Copper strap length and thickness for given stress and operating temperature.

less time for removal activities. Reinstallation can only be accomplished with internal remotely operated manipulator systems.

Bellows design

The bellows conductor contact concept provides a high-conductivity electrical path and is readily maintainable. The bellows contact system is designed so that it can be operated and controlled externally. The advantages of the bellows system are as follows: (1) has high tolerance to sector misalignment, (2) permits sector removal without internal operations, (3) permits sector removal without damage to components, (4) is easily installed, and (5) accommodates sector thermal expansion. The disadvantage of the bellows is the number required and the potential of water leakage.

The bellows contact concept is shown in Fig. 4-12. This concept consists of a convoluted Inconel 625 bellows assembly which contains 60 copper conductor filaments (springs) in six concentric layers. Each layer consists of ten springs. All ten springs per layer are wound in the same direction, with the layers wound in alternate directions.

Each of the bellows assemblies was electrically sized to carry a current of 200 KA, with a voltage drop $\lesssim$10 V. Most of the current flows through the copper conductor, with only a small portion flowing through the Inconel 625 bellows (copper resistance of $\sim 4.3 \times 10^{-6}$ Ω-cm, compared to the Inconel 625 resistance of $\sim 110 \times 10^{-6}$ Ω-cm).

Figure 4-13 is a scale layout and shows the electrical conductor configuration. This configuration provides for a coolant water inlet to the copper base and a flow path into the bellows past the copper conductors. The coolant outlet is an annulus around the copper conductor support and connects to the outlet port.

For each sector, the inboard and outboard bellows are connected in separate coolant loops. The inboard water coolant flows in series through each of the inboard bellows assemblies, and the outboard coolant flows in series through each of the 8 outboard bellows assemblies. The coolant pressure drops are about 0.28 MPa (40 psi) in the inboard system and 0.14 MPa (20 psi) in the outboard system. The maximum temperatures

ORNL-DWG 82-3803 FED

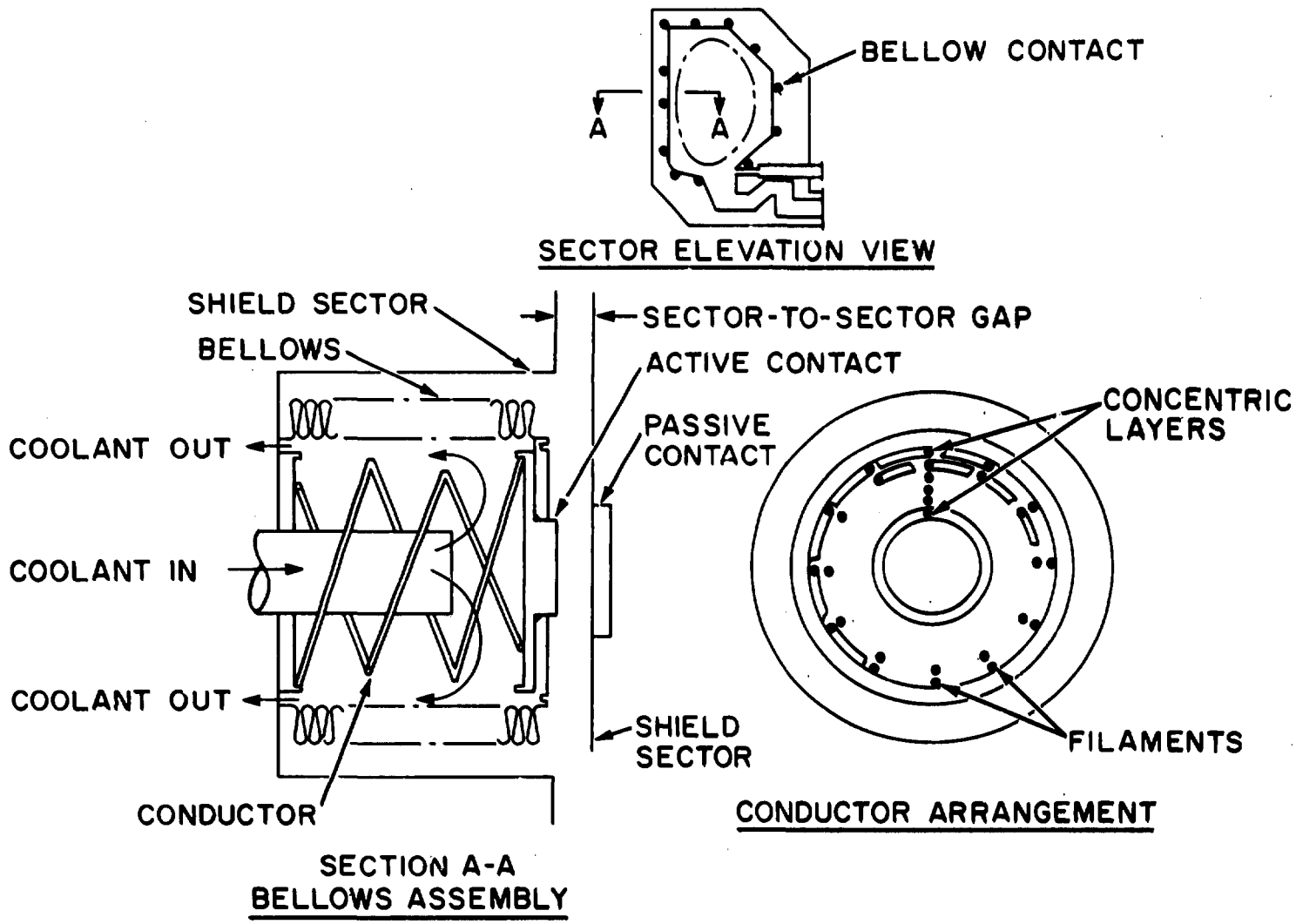

Fig. 4-12. Bellows contact concept.

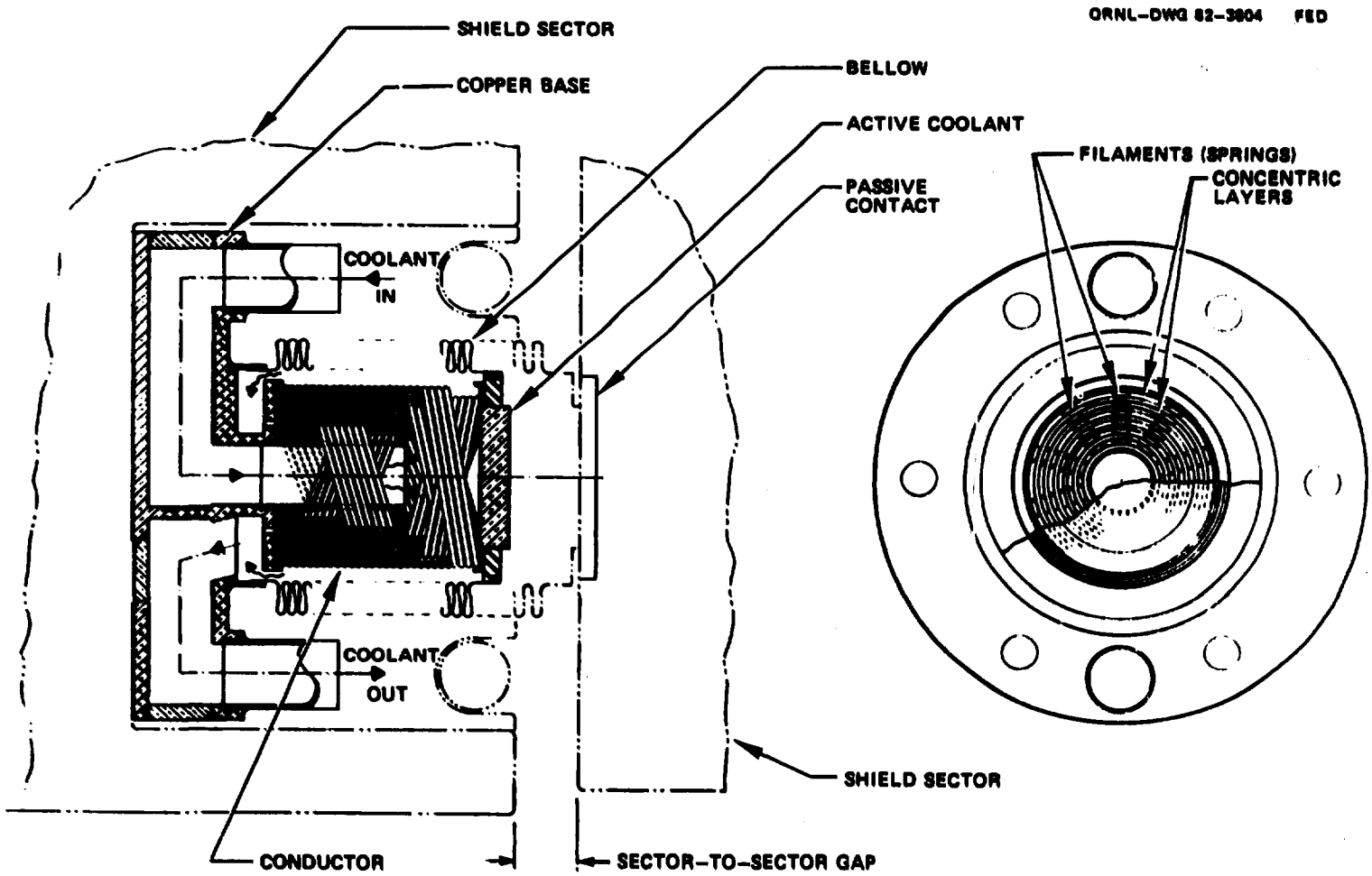

Fig. 4-13. Electrical contact configuration.

of the water, bellows walls, and copper wires are below 100°C during normal operation.

The electrical contact area per bellows assembly is sized for a current density of 6700 A/cm^2. Thus, a contact area of 30 cm^2 is provided for a current of 200 kA per bellows assembly. The final selection of contact material has not been made. The passive contact on the adjacent shield sector is larger than the active contact, to allow for sector misalignment.

4.3.4 Arcing Design

The arcing design concept provides another method of dissipating electrical energy from disruptions at the inner surface of the torus. It is based on providing a sacrificial surface for arcing and assumes that the arcing location may be controlled. The arcing contact surface materials considered are graphite, copper, aluminum, stainless, molybdenum, tantalum, and tungsten. These contacts would be located along the internal periphery of the shield sector. The sacrificial contacts must provide an area of least electrical potential. The contacts can be located in discrete points or as a continuous strip. The continuous strip concept is least sensitive to misalignment, radial or vertical. A typical cross section of a continuous arcing contact is shown in Fig. 4-14.

The selection of a sacrificial surface contact material must consider such factors as erosion, resistance, thermal conductivity, and plasma contamination. From Ref. 2, materials with low erosion, in decreasing order, are tungsten, carbon, molybdenum, titanium, and copper. Since this erosion occurs during a plasma disruption, it can be assumed that the eroded particles will not adversely affect the plasma. Due to the low vapor pressure of the high "Z" materials (tungsten and molybdenum), the eroded particles will redeposit in the area of the arcing pads. Therefore, the "Z" of the arcing pad material need not be considered. Then, the primary parameters for the material selection are (1) thermal stability, (2) electrical resistivity, (3) volumetric erosion, and (4) producibility. Tungsten and molybdenum both have similar characteristics in meeting the first three parameters. The

ORNL-DWG 6:-'9243A FED

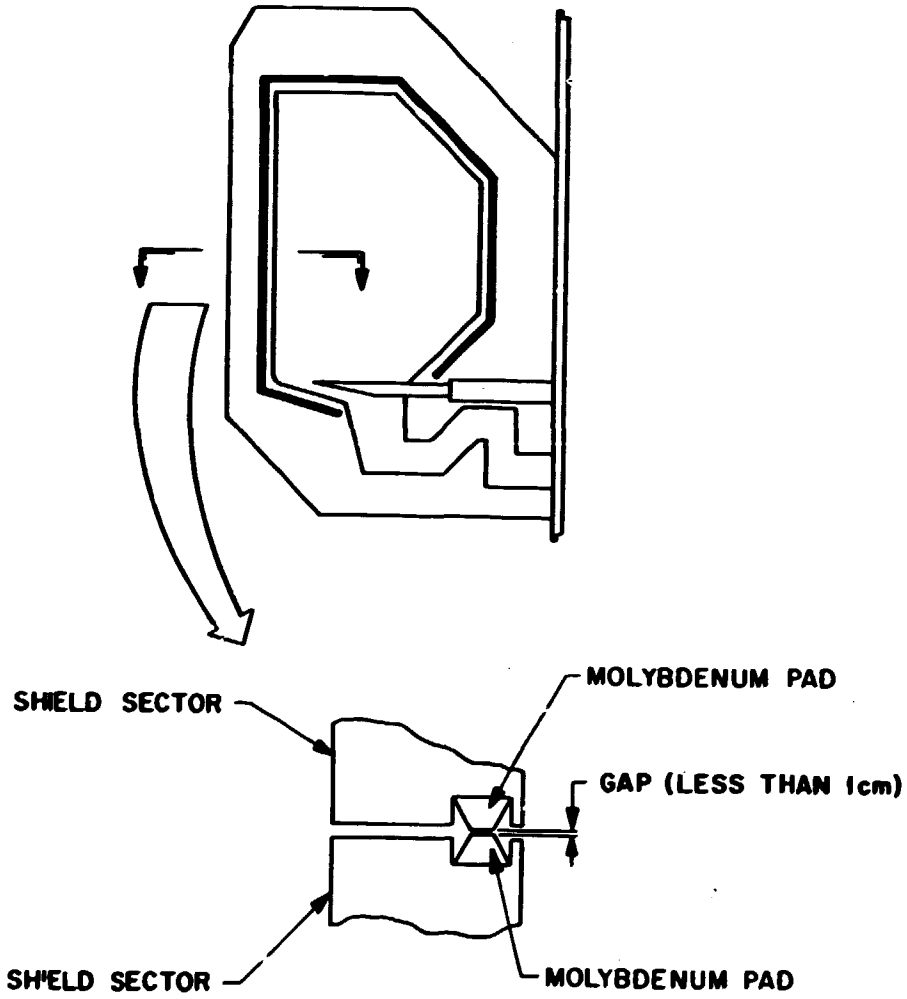

Fig. 4-14. Figure configuration for arcing contact.

working properties of molybdenum (which can be worked at room temperature) make it the arcing pad material choice. Tungsten is brittle at room temperature and must be worked hot, between 400°C and 1650°C (Ref. 3).

4.3.5 Eddy Current Design

During the current quench phase of a disruption, the field around the plasma generated by the current in the plasma collapses, causing a current to be induced in the shield sectors. If the sectors are electrically connected near the inner surface or if conditions are such that arcing can occur, the currents will flow toroidally in the inner surface. However, if the sectors are not electrically connected and the voltage drop in the eddy current circuit is small relative to the arcing potential, then the eddy currents will propagate in paths normal to the radial planes of the torus sectors; and there will be forces induced on the sectors.

This section discusses the magnitude of the induced forces and their impact on the torus structure. The following assumptions were made:

1. There is full eddy current development in the shield sector during disruption (no electrical contact between sectors and no arcing).
2. Current induced in sectors is as follows:

Current in the inboard, top, and bottom surfaces, A	3.4×10^6
Current in the outboard surfaces, A	1.6×10^6

3. The induced forces in the 45° facets and in the limiter may be ignored for the purpose of the overall sector evaluation.
4. Forces are assumed static (no accounting for dynamic effects).

Forces generated by eddy currents

Forces are generated in the sector side walls as a result of the eddy current flow, Fig. 4-15. Figure 4-16 shows the resulting forces generated by the eddy current interaction with the magnetic fields in a

ORNL-DWG 82-3806 FED

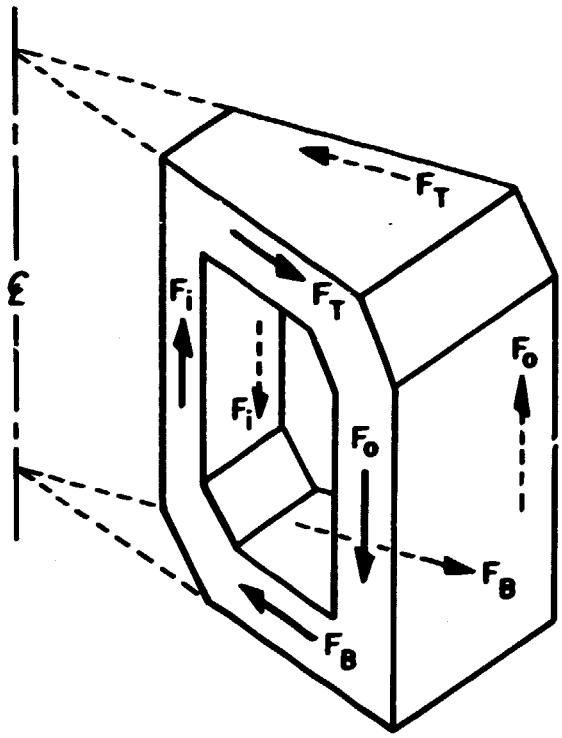

Fig. 4-15. Eddy current paths in shield sector during disruption.

ORNL-DWG 82-3805 FED

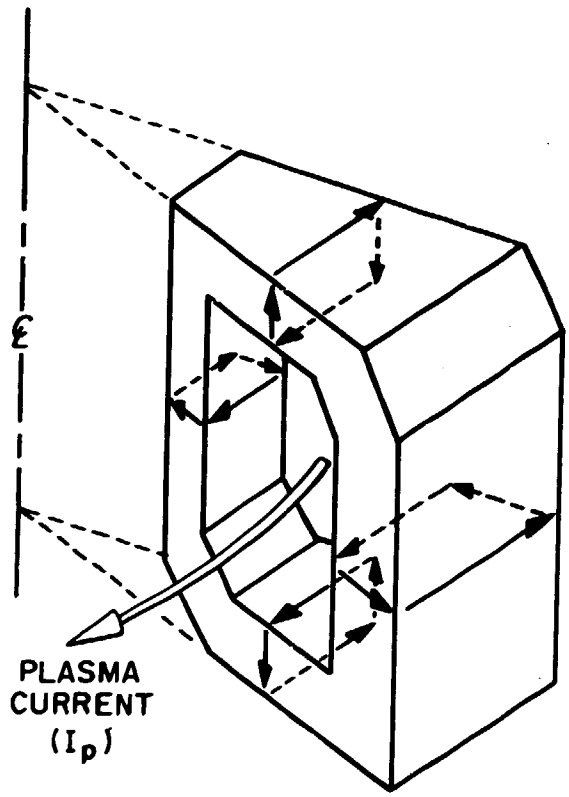

Fig. 4-16. Forces resulting from eddy currents in sectors.

shield sector. Also, the identified external forces are labeled. $F_o\uparrow$ and $F_o\downarrow$ are forces in the outboard side walls. $F_i\uparrow$ and $F_i\downarrow$ are forces in the inboard side walls. These forces are calculated as follows:

$$F_o = B\ell I \text{ (Newtons)}$$

where

$B = 3$ Tesla ($3 \times 10{,}000$ gauss)
$\ell = 1.0$ m
$I = 1.6 \times 10^6$ amps, $1.6 \times 10^6/10$ abamps
$F_o = 4.71 \times 10^6$ Newtons, (1.06×10^6 lbs)

and

$$F_i = B\ell I \text{ (Newtons)}$$

where

$B = 10$ Tesla
$\ell = 0.60$ m
$I = 3.4 \times 10^6$ amp
$F_i = 2.04 \times 10^7$ Newtons (4.59×10^6 lbs)

$F_T\rightarrow$ and $F_T\leftarrow$ are in the top side walls. $F_B\rightarrow$ and $F_B\leftarrow$ are in the bottom side walls. Couples resulting from forces $\vec{F}_B$, $\overleftarrow{F}_B$ and $\vec{F}_T$, $\overleftarrow{F}_T$ are about equal in magnitude and opposite in direction. They result in a net zero twisting moment about the vertical axis.

Reacting eddy current forces

Overturning moments are produced on the sector by $F_o\uparrow$, $F_o\downarrow$ and $F_i\uparrow$, $F_i\downarrow$. These overturning moments are resisted by the weight of the sector F_w, reactions between the sector front faces and spool structure radial frame, and bearing loads along the tipping edge.

The forces can be balanced by loads of 450,000 lbs between shield sector and adjacent radial frames and a distributed upward load along the side edges. The force balance for the sector is shown in Fig. 4-17.

The load between sectors and the adjacent radial frame can be carried, as shown in Fig. 4-18, by two plates, each bolted with eight 1-1/2-in. dia. bolts on each sector. To accommodate the bolts, each plate must be approximately 1.25 m (50 in.) long. The resulting bolt shear stress is 124 MPa (18,000 psi). The required thickness of the attach plates is approximately 1.5 cm (0.6 in.)

4.4 TORUS SPOOL

The torus spool is a continuous toroidal structure at the outer boundary of the shield. In order to facilitate the startup of the plasma, it is important that the structure surrounding the plasma does not unduly absorb the induced currents from the transformer primary windings. Normally, this is achieved by designing the structure with high electrical resistance.

The spool consists, for the most part, of built-up structure. Hence, it is possible to maximize the electrical resistance by designing for minimum gage components and by choosing materials with high electrical resistivity. Because a certain structural response must be achieved, there are definite limits on the maximum electrical resistance which can be realized in the design. This approach is described in Sect. 4.4.3.

The electrical resistance of the basic structure can be increased by introducing high-resistance electrical breaks. There are techniques whereby the major structural loads are carried across an electrically insulated break. A high-resistance path such as a thin metal bellows is provided to seal the break region for vacuum integrity. This approach is also described in Sect. 4.4.3.

ORNL-DWG 82-3807 FED

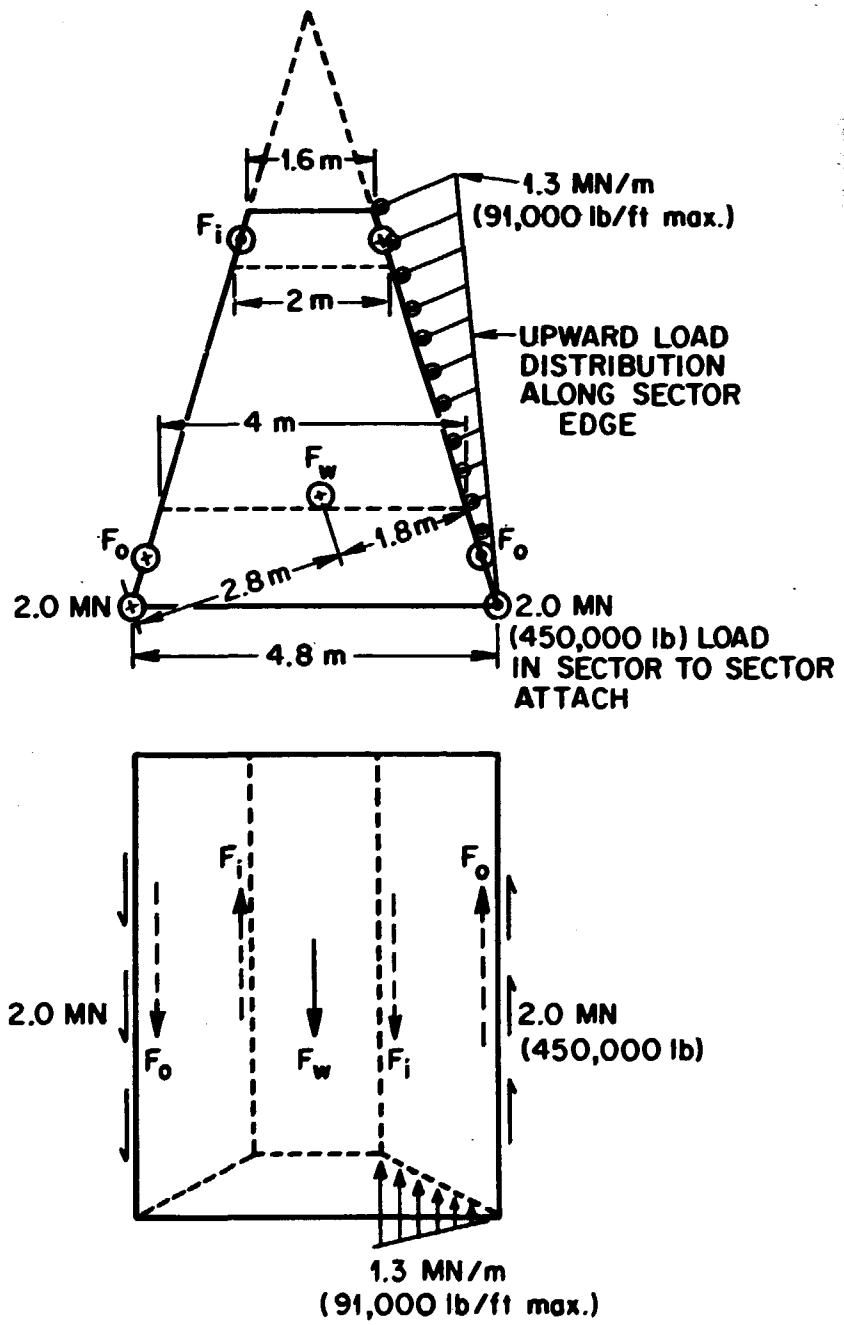

Fig. 4-17. Sector force balance.

ORNL-DWG 82-3806 FED

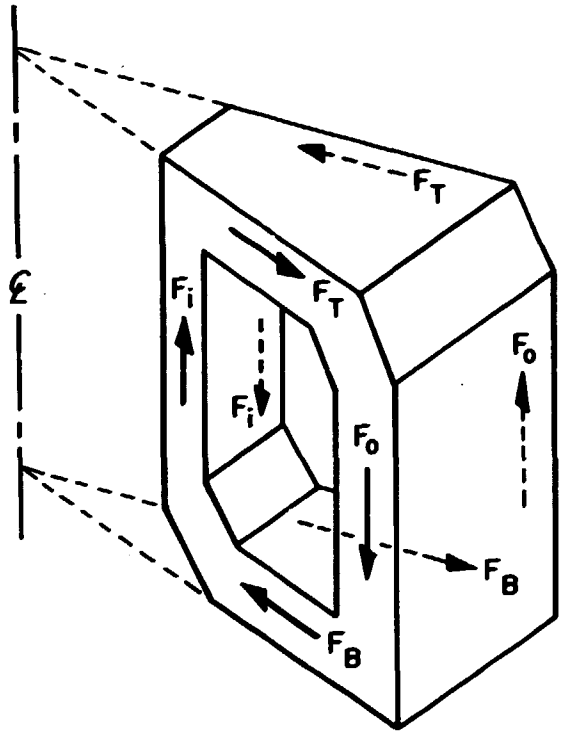

Fig. 4-18. Sector attach fittings and bolts.

4.4.1 Torus Current Path Requirements

Since the torus is subject to both the toroidal and poloidal fields, any induced currents in the structure will result in forces on the structure. In addition, the current decay times of disruption can be controlled by eddy currents. Large eddy currents induced on the inner walls of the torus retard the plasma movement. This allows the plasma magnetic stored energy to be dissipated in the torus as I^2R heating instead of thermal heating of the surface in contact with the plasma.

The requirements for torus current paths have three basic features: (1) design eddy currents paths parallel to the high toroidal fields to minimize the mechanical forces and overturning moments, (2) provide a good toroidal current path near the plasma to control the disruption damage, and (3) provide high-resistance external toroidal current paths.

In the FED Baseline, the replaceable first wall coolant panels are designed to conduct eddy currents toroidally and are electrically connected to the torus wall. The torus walls between segments are connected electrically at the surfaces near the plasma. The internal shell of FED, therefore, has a toroidal path equivalent to 3 to 4 cm of stainless steel.

The torus spool is basically a vacuum enclosure and should be designed to conduct the minimum induced eddy-currents. It does not provide any useful self-stabilization of the plasma, because it is located about a meter away from the edge of the plasma. The induced currents resulting from startup or control fields retard the desired field penetrations and produce energy losses. Its resistance should, therefore, be as high as possible. The requirement on the toroidal resistance is that the total time constant of all structures external to the enclosure next to the plasma be 1/5 of the internal shell time constant. This results in a torus spool resistance of $\sim$10 times the internal shell resistance.

4.4.2 Spool Configuration

The spool structure (Fig. 4-19) provides a vacuum boundary over the inner, top, and bottom surfaces of the torus. Together with the shield sector front panel, it completes the vacuum boundary on the outer surface of the torus. In addition to the vacuum containment function, the spool must provide a "high" electrical resistance relative to the inner surfaces of the shield sectors. The design approach to achieve the relatively high resistance is to employ thin gage panels. The approach is similar to that used to achieve "minimum weight design." The spool structure consists of ten radial frames, equally spaced, located beneath each of the TF coils, and interconnected by ten panel assemblies. The assembly of two radial frames and the connecting panels forms a bay into which the shield sector is inserted. A seal frame is welded to the outer periphery of this subassembly.

The radial frames serve the functions of (1) providing a structural tie between spool panels, (2) acting as part of the vacuum boundary. The radial frame components are machined of stainless steel plate stock. Built-up structure could also be considered, depending on material availability and cost.

The spool panel assembly consists of three panels (top, inboard, and bottom). The top panel consists of thin outer and inner skins which are stiffened by radial beams, peripheral frames, and thin corrugated toroidal stiffeners. The inboard panel consists of a thin inner skin with external vertical stiffeners and a machined edge frame. The bottom panel is a thin, double-skin sandwich construction with beams located to carry the shield sector dead weight and rolling loads (during sector installation/removal).

Further design and analysis will be needed to fully define the requirements for the spool structure. For example, additional stiffeners (not shown) will be required for the thin skins. However, since it has been assumed that toroidal stiffeners can be provided with electrical breaks, design of these elements has not been emphasized because they do not affect the overall electrical resistance calculations.

ORNL-DWG 81-17355 FED

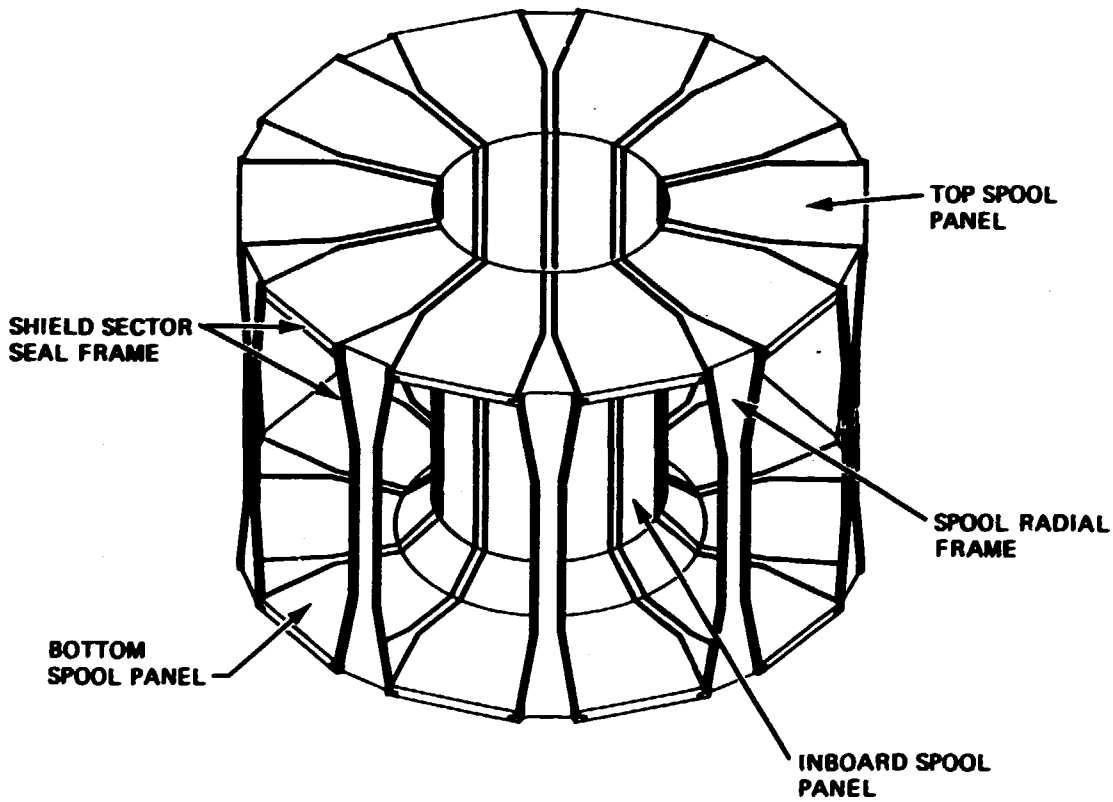

Fig. 4-19. Torus spool.

For eddy current control and electrical isolation of the bulk shield from the spool structure, key surfaces of the spool are coated with a dielectric material. The FED Baseline coating is Al_2O_3 and is applied to the inboard and outboard surfaces of the bottom spool flange, outboard surface of the top spool flange, and inboard surface of the outboard leg of the radial frame. The spool structure is considered to be semipermanent (good for the life of the reactor) and requires a minimum of active cooling. Cooling is provided only in the spool structure bottom flange, which due to the vacuum duct design is protected by a bottom shield thickness of 0.3 m in the area with direct plasma view.

4.4.3 Candidate Concepts

High-resistance spool structure

In the development of the FED Baseline (Ref. 1), atmospheric pressure, top shield slab weight, and plasma disruption electromagnetic loads were used to establish the spool structure design. Subsequently, a finite element analysis was conducted with the goal of providing a better definition of spool deflections and internal loads. At the same time, EF magnet loads were identified as requiring support by the spool and plasma disruption electromagnetic loads were reduced significantly, from 0.2 MPa to 0.01 MPa (1.5 psi). The finite element model is shown in Fig. 4-20. Three materials were considered: Inconel 625, 6Aℓ-4V titanium, and annealed 316 stainless steel. Room temperature properties are shown in Table 4-4. Allowable stresses used were S_m for membrane stresses and 1.5 S_m for bending stresses.

Resulting internal spool loads provided a basis for developing the structural concept depicted in Fig. 4-21. Main features of this spool structure are the inboard cylinder, top and bottom plates, radial beams, toroidal stiffeners, and toroidal rings. The inboard cylinder is a single-skin construction with vertical stiffeners. The skin takes the hoop tension load. Stiffeners are provided to preclude buckling under axial compression loads. Dimensions are shown in Fig. 4-22.

ORNL-DWG 81-19398 FED

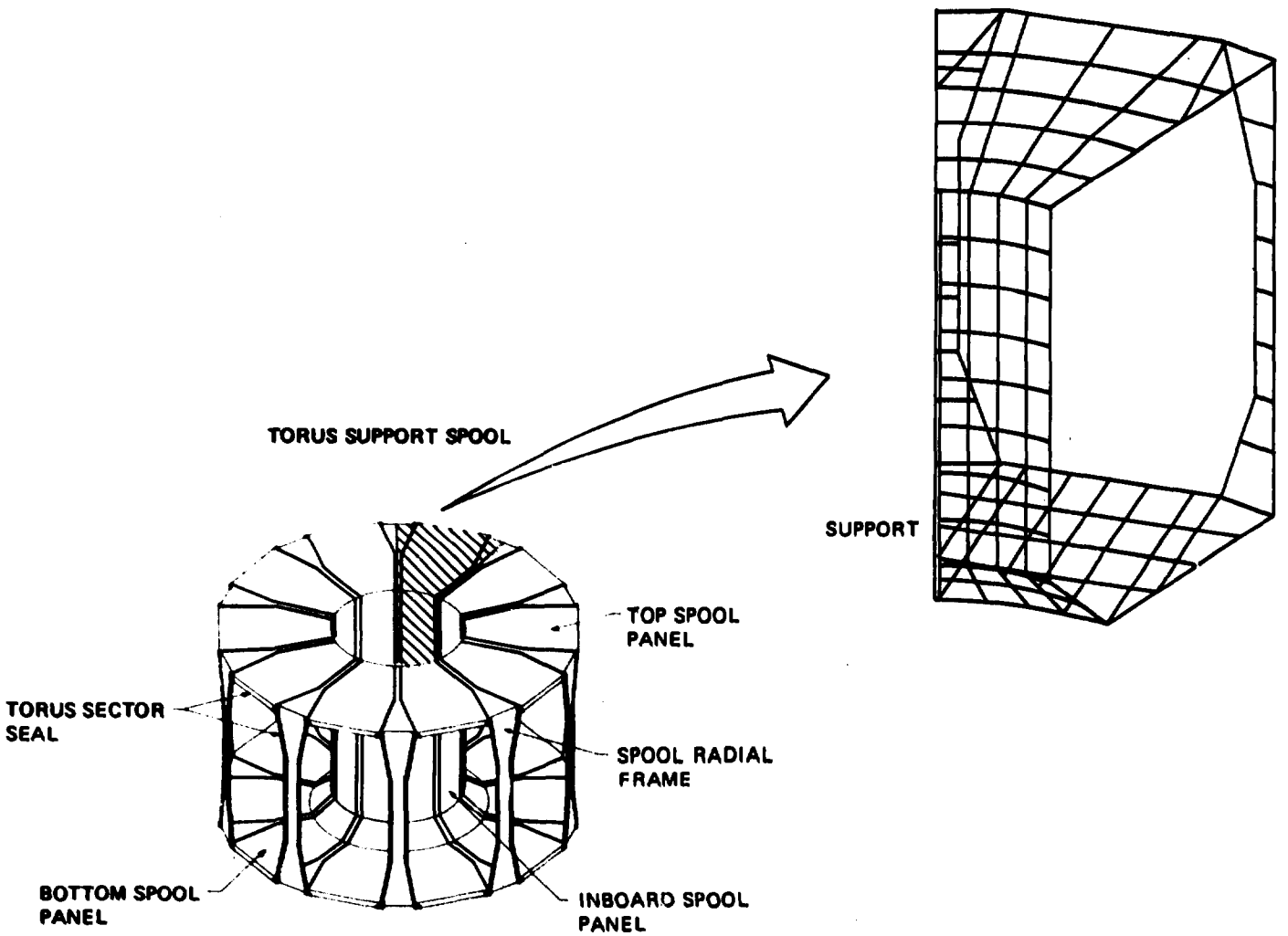

Fig. 4-20. Spool finite element model.

Table 4-4. Material properties

Material	Yield strength, MPa (ksi)	Allowable stress intensity S_m, MPa (ksi)	Elastic modulus GPa (psi)
Inconel 625	370 (54)	250 (36)	207 (30×10^6)
6Al-4V-Ti	900 (130)	325 (47)	110 (16×10^6)
316 SS	250 (36)	165 (24)	207 (30×10^6)

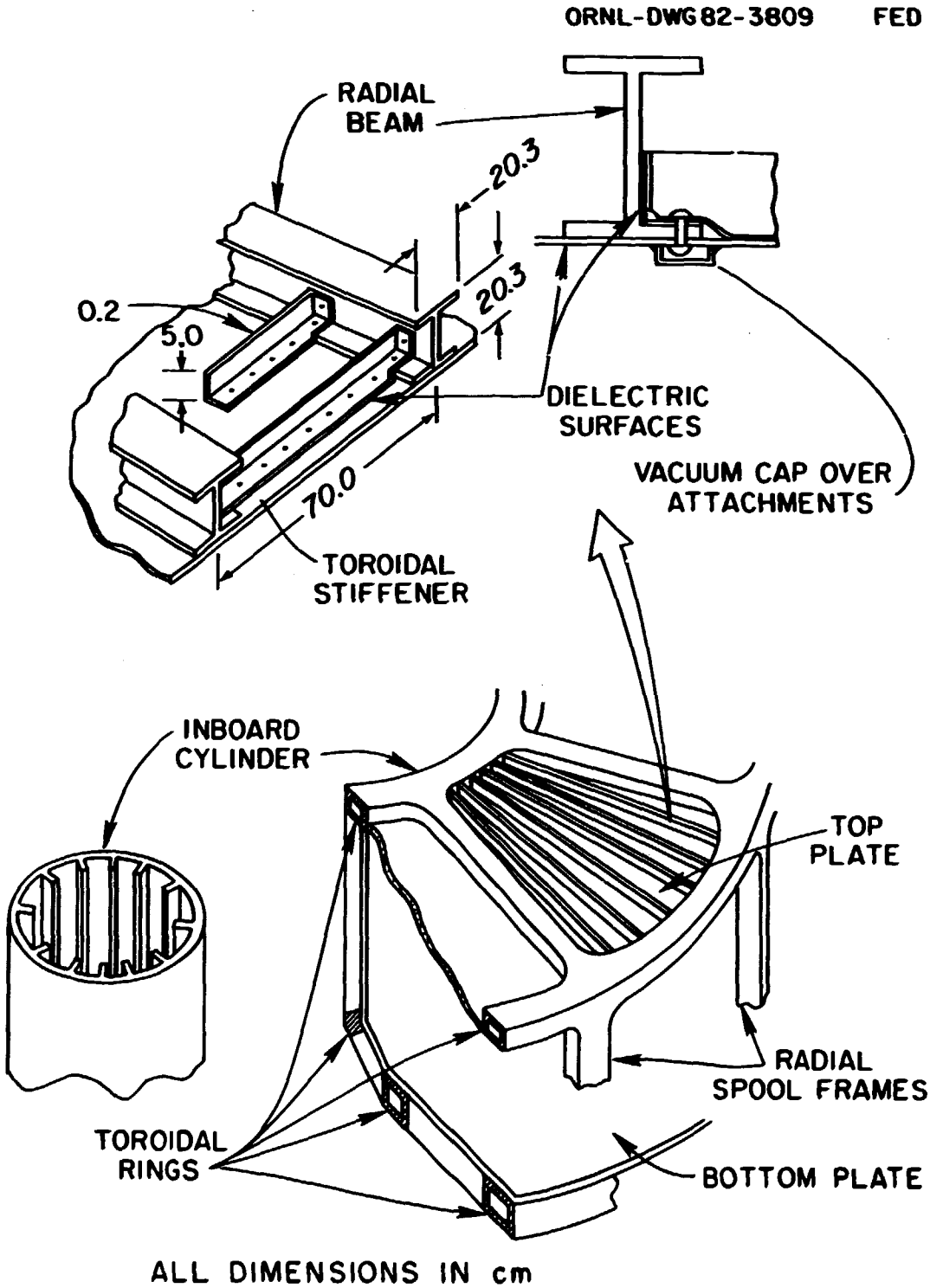

Fig. 4-21. Spool structural concept.

ORNL–DWG 82-3810 FED

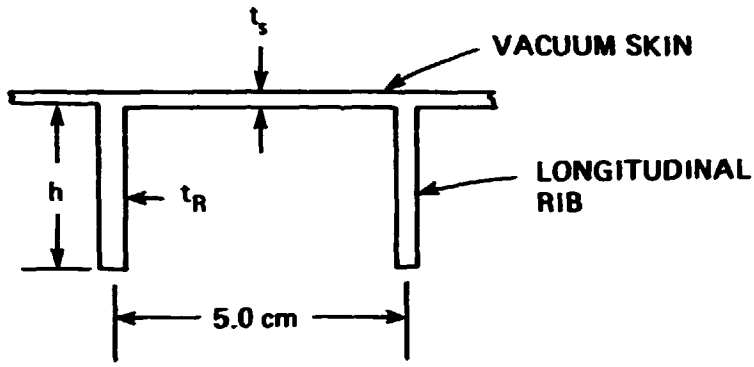

MATERIAL	t_s (cm)	h′(cm)	t_R (cm)	CRITICAL FOR
316 ss	0.25	4.1	0.32	BENDING AND MEMBRANE
6Al-4V Ti	0.16	4.1	0.64	BUCKLING
INCONEL 625	0.19	4.1	0.32	BENDING AND MEMBRANE

Fig. 4-22. Inboard cylinder thicknesses.

The loads on the top and bottom of the spool are transmitted to radial beams by the skin and toroidal stiffeners. The radial beams transfer loads to toroidal rings which distribute the loads to the inboard cylinder and the outboard legs of the radial frames. The five toroidal rings take combined axial, bending, and torsion loads.

To electrically isolate the toroidal skin stiffeners, coated or oxidized surfaces were provided between the stiffeners and skin and dielectric bushings and pads were provided around fasteners (Fig. 4-21).

The main components in the spool electrical resistance are the skin and the toroidal rings. The calculated spool resistances for the three materials are 140 μΩ for stainless steel, 400 μΩ for Inconel, and 710 μΩ for titanium.

The shield sector doors were considered to be short circuits. However, the bellows seals joining the doors to the spools were considered in the resistance calculations. The effect of the thickness of the door seals on spool resistance is shown in Fig. 4-23.

High-resistance breaks

Shown in Fig. 4-24 is the comparison of electrical resistance of the stainless steel spool without breaks and with two high-resistance breaks. The requirement for electrical resistance of the torus spool is a function of the resistance of the shield inner surface and the method for connecting the shield sectors. Two methods described in Sect. 4.3.3 were bellows and copper straps. The resistances of the shield inner surface using these methods, the required spool resistance (approximately ten times shield inner surface resistance) and the resistance of spool configurations are shown in Table 4-5. Comparison of these shows that electrical breaks (possibly more than two) will be needed to accomplish the resistance requirements for structural materials such as stainless steel and Inconel.

To provide an electrical resistance in the spool structure of ∿10 times the resistance of the surface nearest the plasma (including the electrical contacts), dielectric breaks can be installed in the spool radial frames. The dielectric break joints must serve two functions:

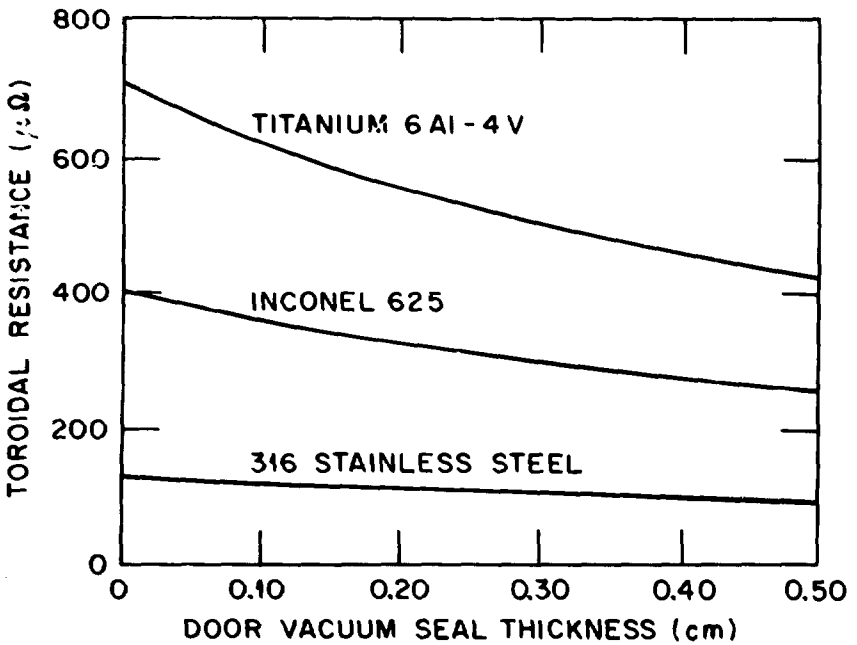

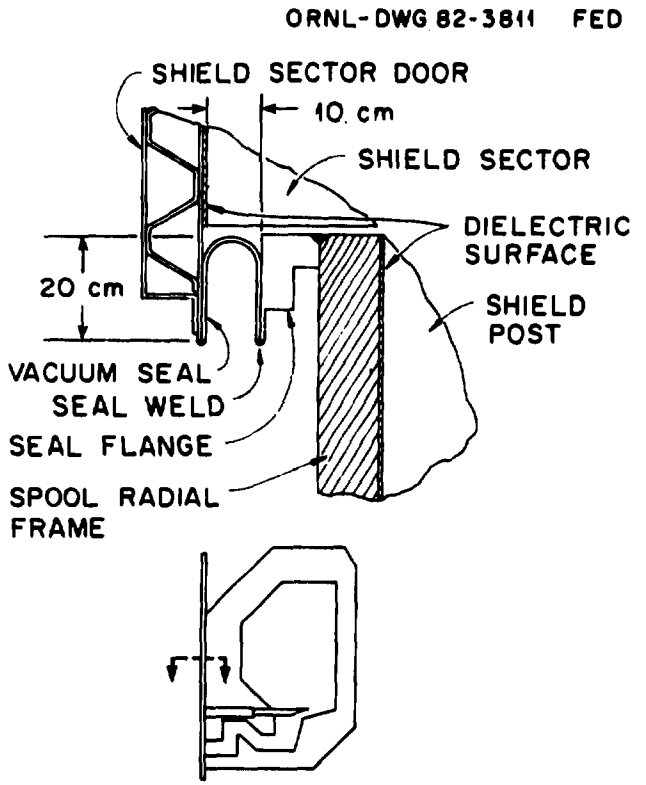

Fig. 4-23. Effect of door vacuum seal thickness on toroidal electrical resistance.

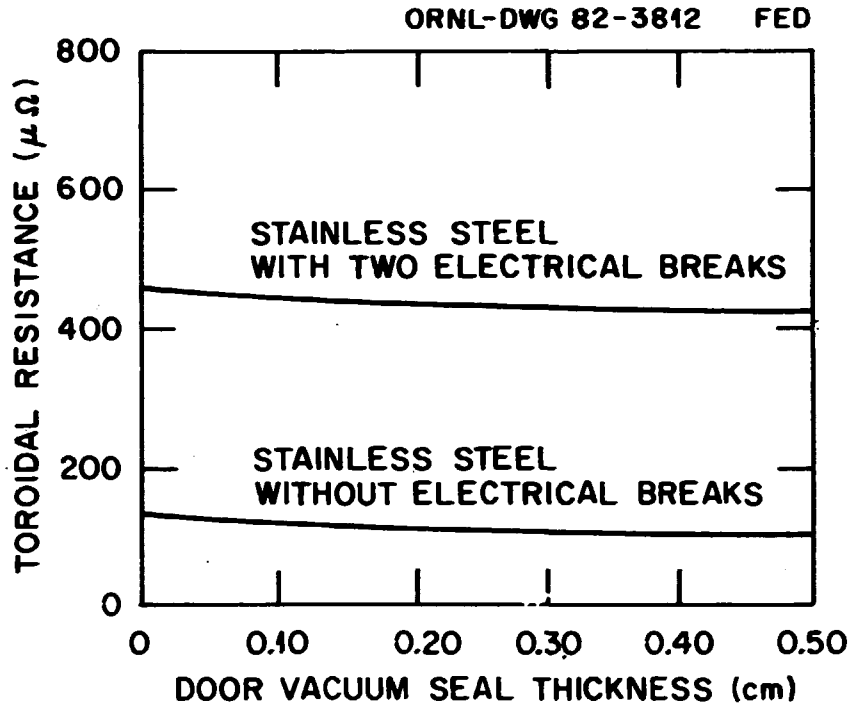

Fig. 4-24. Comparison of spool electrical resistance with and without electrical breaks.

Table 4-5. Spool required resistances

	Material/concept (seal t = 0.20 cm)			
	Stainless steel w/out breaks	Stainless steel w/breaks	Inconel w/out breaks	Titanium w/out breaks
Toroidal electrical resistance - μΩ	120	430	320	530
Resistance of shield inner surface using bellows connections		80		
Required spool resistance		800		
Resistance of shield inner surface using strap connections		40		
Required spool resistance		400		

(1) must be an electric insulator and (2) must provide a positive vacuum seal to maintain the plasma chamber vacuum integrity.

Several options for the high-resistance break design were investigated and are shown in Figs. 4-25 through 4-29:

Fig. 4-25 — A dielectric gasket which would also serve as the vacuum seal

Fig. 4-26 — Same as Fig. 4-25, except incorporates a high-resistance metal bellows with radial convolutions for the vacuum seal

Fig. 4-27 — Same as Fig. 4-25, except incorporates a high-resistance thin metal sheet for the vacuum seal

Fig. 4-28 — Same as Fig. 4-27, except a multilayer, folded thin sheet is used for vacuum seal

Fig. 4-29 — Same as Fig. 4-25, except incorporates an electrically insulated omega seal for the vacuum seal

The design considerations for each option were evaluated; the results are discussed in Table 4-6. The design shown in Fig. 4-28, which incorporates a high-resistance multilayer, folded sheet configuration for the vacuum seal, was selected based on the following advantages over the other options:

1. Offers relatively unlimited margin for increasing electrical resistance for a given toroidal span
2. Has small effect on radial build
3. Has small impact on shielding
4. Provides a reliable vacuum seal
5. Fabrication requirements seem relatively simple

The design configuration selected offers a feasible approach for incorporating high-resistance breaks into the vacuum vessel and torus spool. Further analysis is required to develop the design in more detail and to describe a reasonable fabrication procedure. The number of breaks required in the device will be determined by the overall electrical resistance requirements and high-resistance vacuum seal detail design.

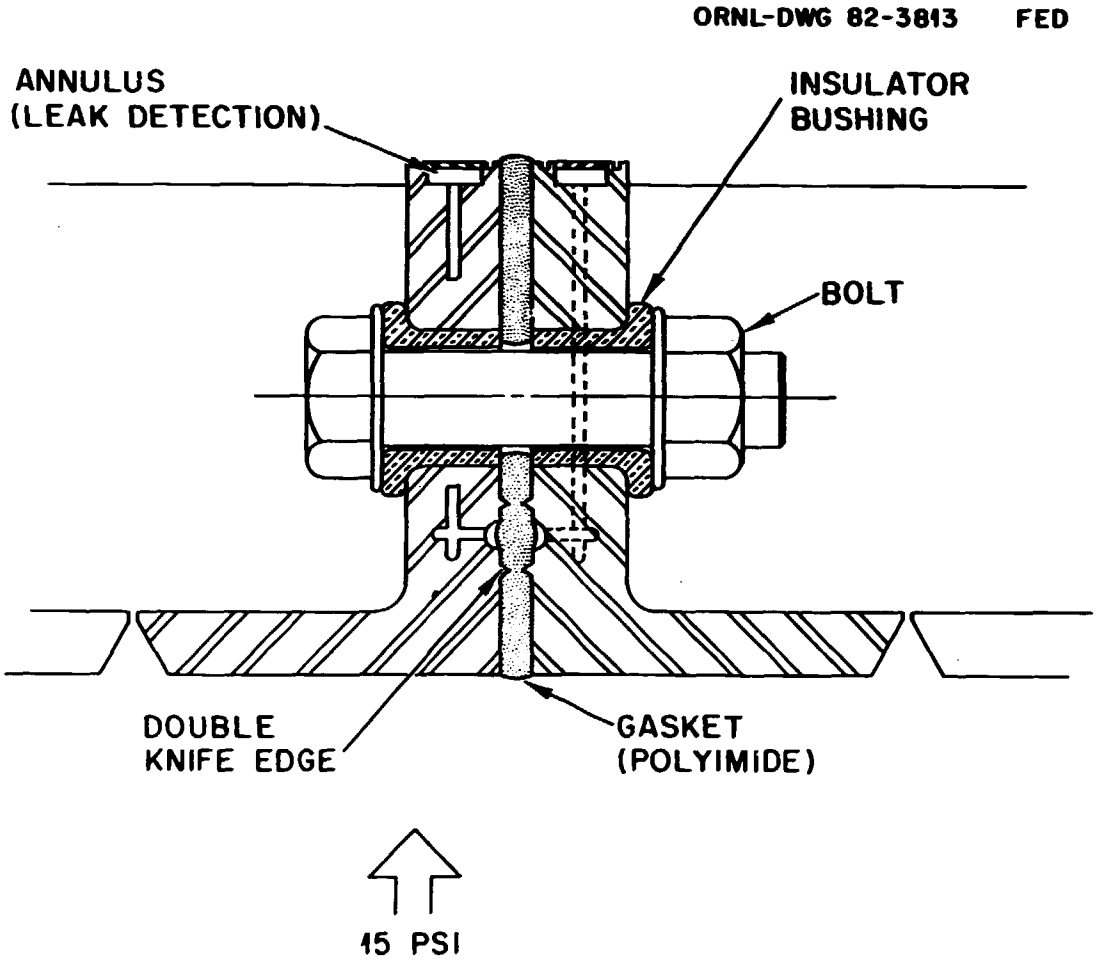

Fig. 4-25. Dielectric break design option: dielectric gasket and vacuum seal.

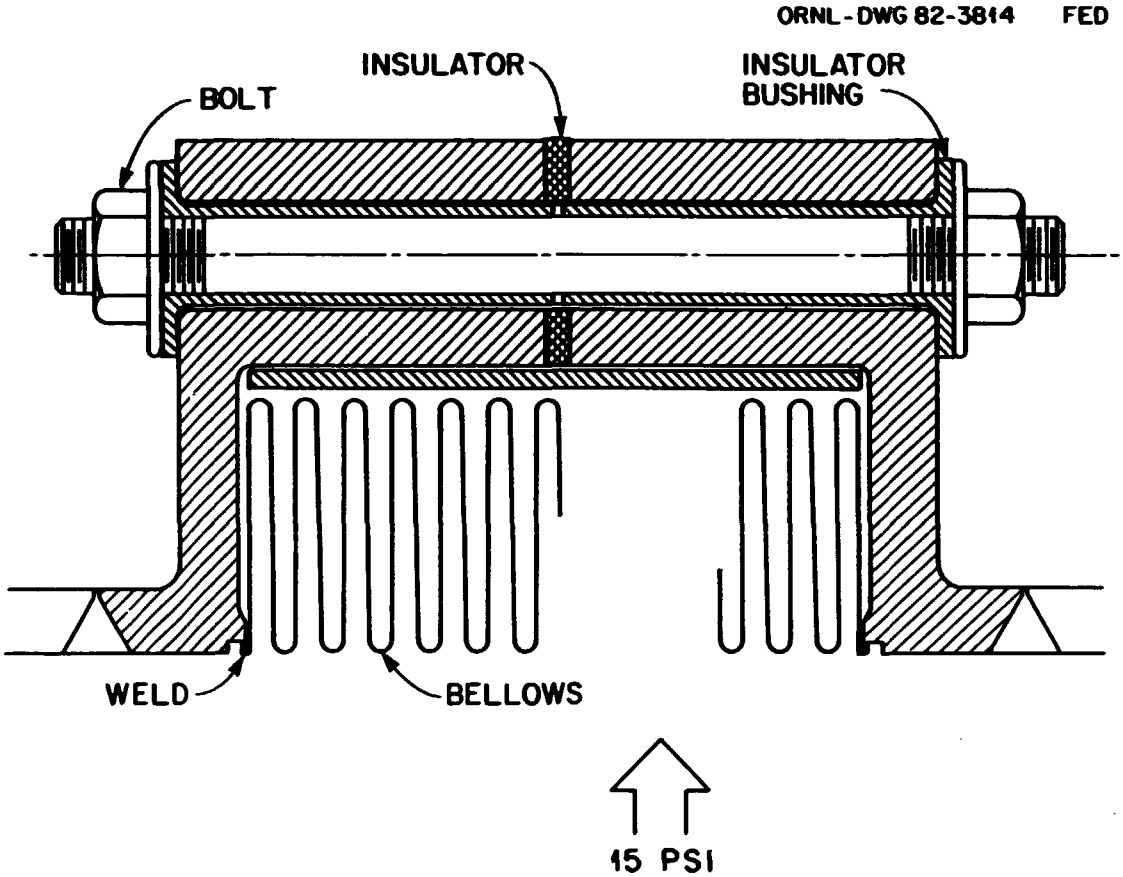

Fig. 4-26. Dielectric break design option: high resistance metal bellows.

ORNL-DWG 82-3815 FED

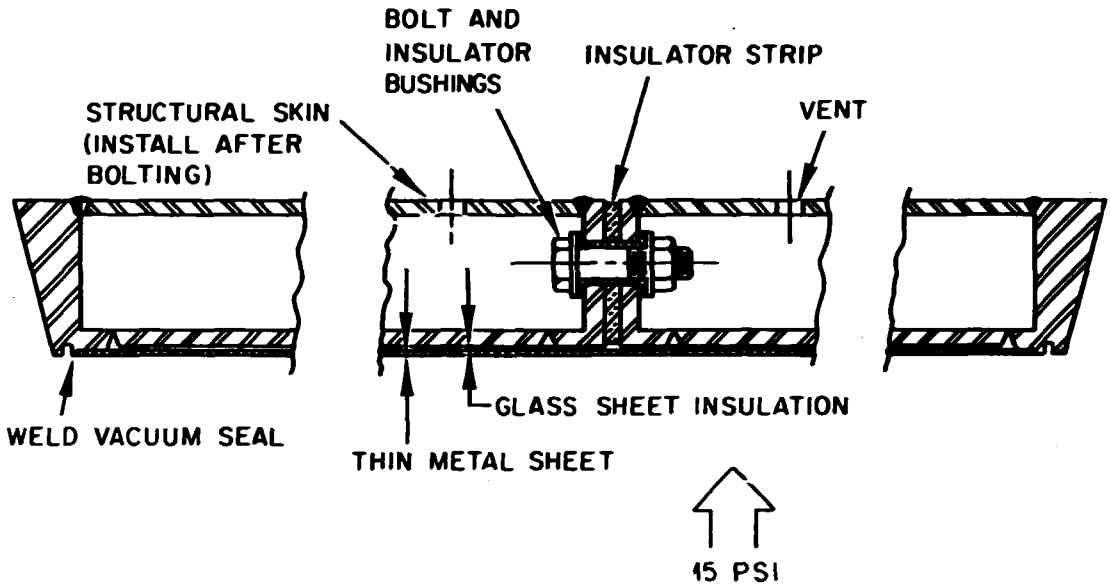

Fig. 4-27. Dielectric break design option: high resistance thin metal sheet.

ORNL-DWG 82-3816 FED

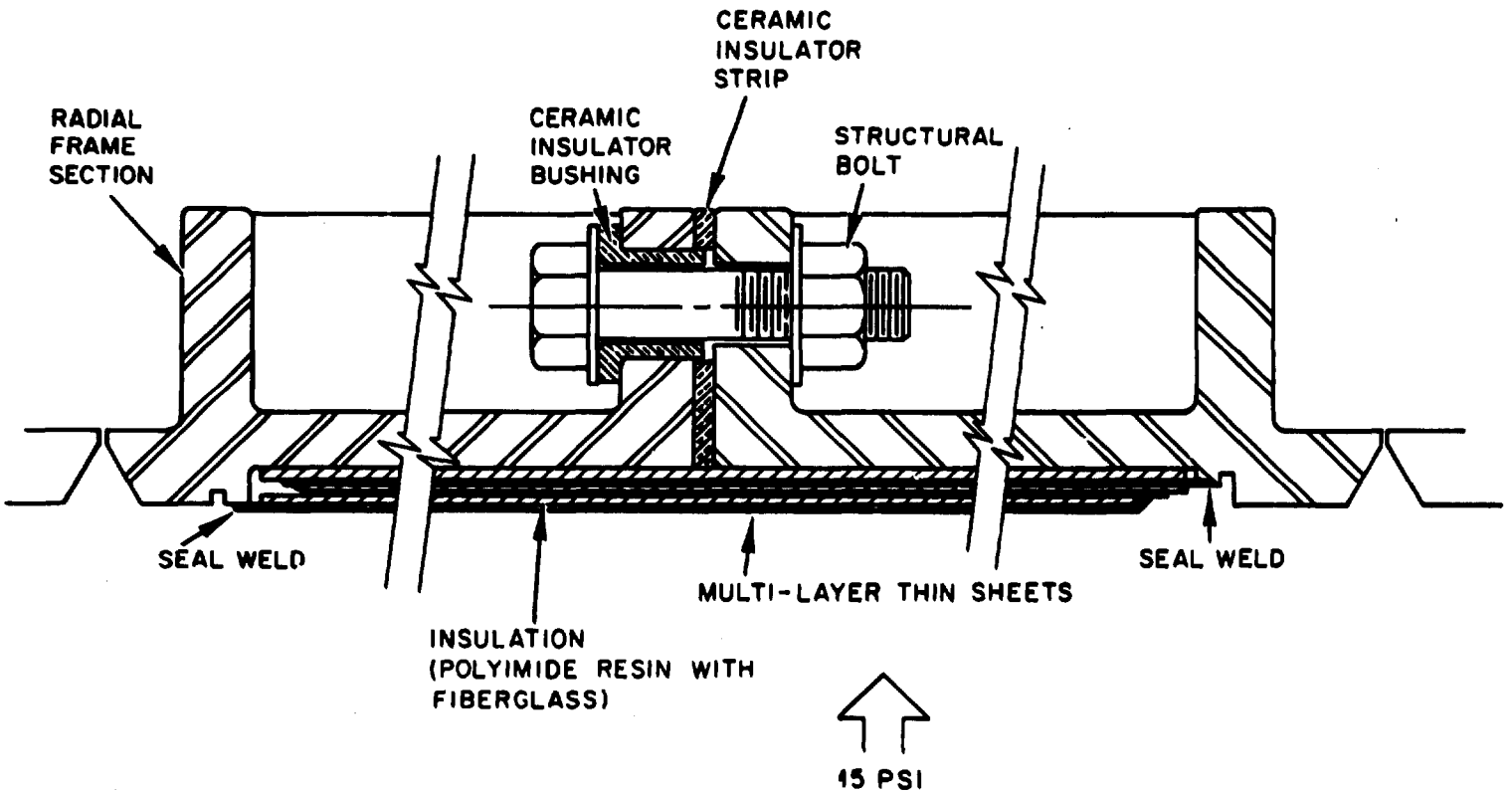

Fig. 4-28. Baseline dielectric break/vacuum seal design multilayer thin sheets used for vacuum seal.

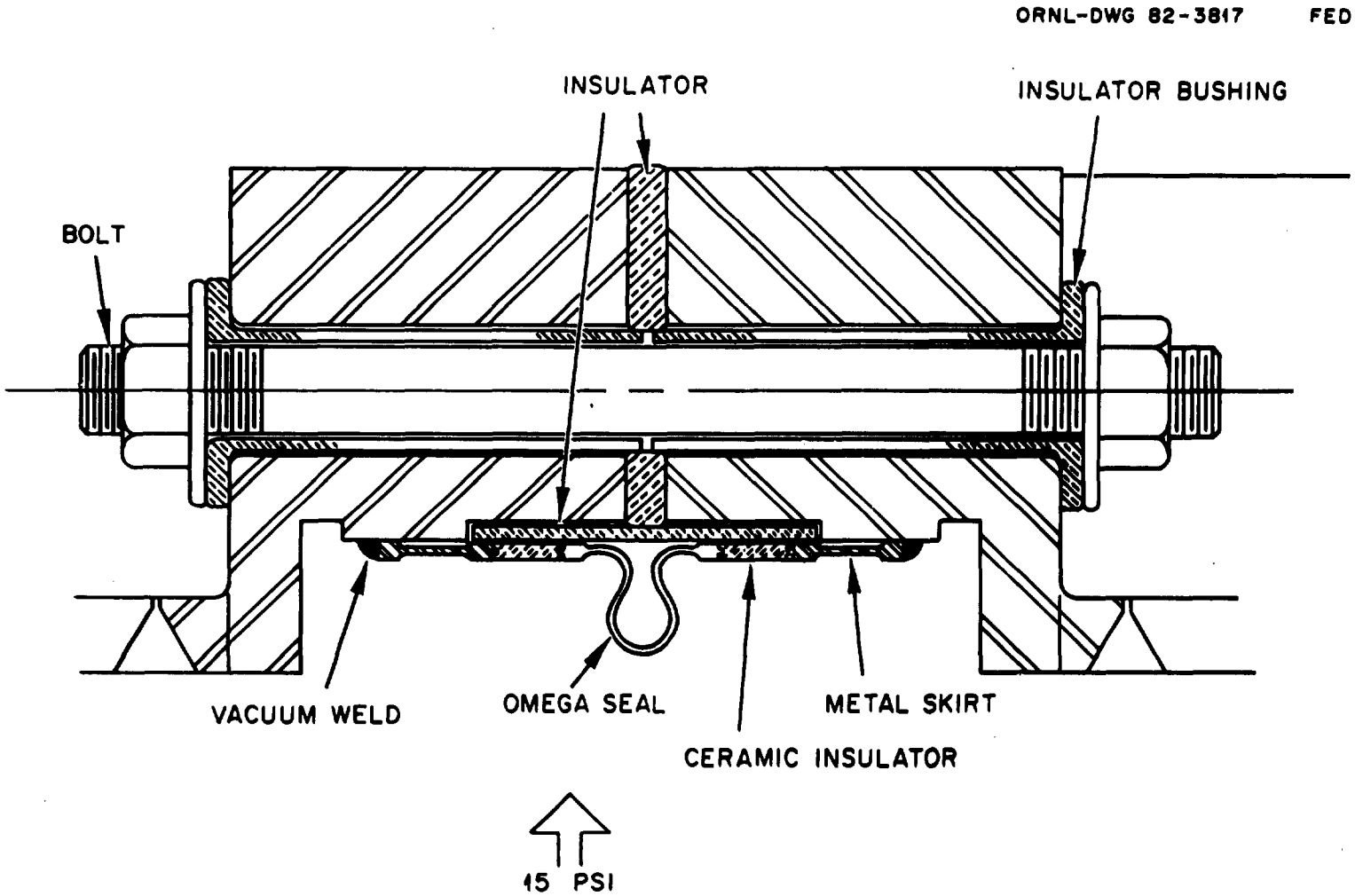

Fig. 4-29. Dielectric break design option: electrically insulated omega seal.

Table 4-6. Design consideration results for the high-resistive break

Design considerations					
Function					
• Current path	Discontinuous	Through the bellows	Through thin metal sheet	Through multilayer thin sheet	Discontinuous
• Vacuum seal	Gasket (dielectric)	Bellows	Thin metal sheet	Multilayer thin sheet	Omega seal
• Structural attach	Bolts in insulator bushings	Bolts in insulator bushings	Bolts in insulator bushings	Bolts in insulator bushings	Bolts in insulator bushings
Evaluation criteria					
• Margin for increase in electrical resistance	Highest possible in absence of arcing	Limited by depth, thickness, and span	Limited by span	Relatively unlimited	Highest possible in absence of arcing
• Susceptibility to vacuum leaks	Relatively high but can be pumped	Subject to fatigue in bellows	Relatively low	Relatively low	Moderate, metal-to-ceramic braze integrity
• Effect on radial build	Small	Large	Small	Small	Small
• Ability to carry loads – atmospheric pressure	Good	Questionable, fatigue limited	Good	Good	Good
– electromagnetic	Good	Questionable, fatigue limited	Undetermined	Undetermined	Undetermined
• Impact on shielding	Small/local	May be large	Small	Small	Small (local)
Fabricability					
• Components	Relatively simple	Moderately complex	Simple	Moderately complex	Complex (ceramic-to-metal braze)
• Assembly	Relatively simple but depends on curing requirements	Complex	Complex	Complex	Complex
• Susceptibility to damage	Low	High (could add protection)	Moderate	Moderate	High (could add protection)

The selected concept consists of two sections of the radial frame bolted together with a ceramic insulator between the section and insulated bolts. The ceramic insulator must be of sufficient thickness to prevent current flow between the two frame sections. On the outside of the frame, the vacuum seal is installed. The vacuum seal consists of a welded multilayer thin metal sheet assembly with an insulator material between the sheets. The vacuum seal insulator material is a composite of polyimide resin and fiberglass. The number of thin metal sheets can vary (must be an odd number) to achieve the desired electrical resistance. The vacuum seal assembly does not carry any structural loads. All structural loads will be reacted by the insulated bolts. The radial frame assembly is to be shop fabricated and tested prior to shipment to the facility.

At the present time, all polyimide fiberglass composite applications are small in size compared with the proposed design. Furthermore, the irradiation data base for the polyimides is very limited, and the compatibility between the polyimides and tritium is not well-defined. Therefore, additional R&D will be required for the dielectric break concept.

4.4.4 Evaluation of Concepts

The resistance properties of the high-resistance structure approach are illustrated in Fig. 4-23. It is clear that a stainless steel structure is not capable of meeting the resistance requirement ($\sim$400 $\mu\Omega$). Inconel 625, on the other hand, may provide as much as eight times the inner shield resistance level for a door vacuum seal thickness of 0.25 cm (0.10 in.). The titanium material (6Aℓ-4V), while providing much more resistance, is also much more expensive and requires a higher degree of complexity where transitions are made between titanium and 316 SS. Titanium is also more expensive to fabricate. Hence, it was eliminated from further consideration.

The stainless steel structure may be augmented with high-resistance breaks of the types described in Sect. 4.4.3. For instance, a single membrane panel with a thickness of 0.005 cm (0.002 in.) has a resistance

of 160 μΩ. If two breaks are provided to the stainless steel, a total resistance of about 430 μΩ is achievable or about 11 times the resistance of a copper strap connected inner shield surface.

Hence, the trade-off is between the Inconel 625 spool with no breaks and the 316 SS spool with two or more breaks. Cost was perceived to be an important factor. A cost comparison was made as follows.

The cost of the Inconel 625 spool without breaks is summarized in Table 4-7. In terms of generic manufacturing, there are two types of components in the spool. These are:

1. Panels which employ sheet metal fabrication for the most part (except for closure frames) and
2. Radial frames whose dominant manufacturing procedure is machining.

The unit cost of the Inconel 625 panels and radial frames is obtained by using stainless steel cost data and applying the appropriate multipliers to account for the differences of fabricating, welding, or machining Inconel. The Inconel 625 panel unit costs were estimated by multiplying the 316 SS sheet cost of $18.00/lb by a factor of 3.5, which accounts for welding and forming Inconel. The unit cost of the Inconel radial frames was obtained by multiplying the machined 316 SS cost of $12.00/lb by five to account for the increased difficulty in machining Inconel. The total cost of an Inconel 625 spool is estimated to be $37.9 million.

The costs of a 316 SS spool with two dielectric breaks are summarized in Table 4-8. As discussed in the previous paragraph, the unit cost for the 316 SS sheet metal panels is $18.00/lb. The eight 316 SS machined radial frames without dielectric breaks were costed at a unit cost of $12.00/lb. The two radial frames with dielectric breaks were costed by applying the following multipliers to the unit cost of the frames without breaks:

- Multiplier for cost increase in basic frame (two pieces instead of one) = 2.0
- Multiplier for assembly of frame and break = 2.0
- Multiplier for build-up of thin multilayer stainless steel sheets and fiberglass insulation that makes up the break panel = 1.5

Table 4-7. Cost of Inconel torus spool with no breaks

Component	Volume per sector (m^3)	Material	Weight per sector (lb.)	Unit cost ($/lb.)	Cost per sector ($ × 10^6)	Number of sectors	Total cost ($ × 10^6)
Panels	1.16	625	21,692	63.00	1.367	10	13.670
Radial frames	2.16	625	40,392	60.00	2.424	10	24.240
							37.910

Table 4-8. Cost of stainless steel torus spool with high-resistance breaks

Component	Material	Volume per sector (m^3)	Weight per sector (lb.)	Unit cost ($/lb.)	Cost per sector ($ × 10^6)	Number of sectors	Total cost ($ × 10^6)
Panels	316 SS	1.16	20,111	18.00	.362	10	3.620
Radial frames w/o break	316 SS	2.16	36,580	12.00	.439	8	3.512
Radial frames w/break	316 SS	2.16	36,580	72.00	2.634	2	5.268
Total							12.40

Hence, the frames with the breaks cost 6.0 times that of the frames without the break. The total cost is $12.4 million, or less than one-third of the Inconel spool.

The reliability is higher, of course, without the breaks and difficult to evaluate without a specific reliability development program. The flexibility in meeting an uncertain resistance goal is much higher with the 316 SS concept with the breaks.

As a result of the lower cost and higher resistance margin, it is recommended that the 316 SS spool with breaks be pursued as the baseline approach.

4.5 TEST MODULE SHIELDING

Two of the ten torus sectors are dedicated exclusively for test module installation. A third sector shares testing with diagnostics, instrumentation, and control functions. Test modules are installed in each test sector outboard wall in a 2 x 3 array, as shown in Fig. 4-30. Two types of test module installation are anticipated and are shown in Fig. 4-31. For tests not requiring direct view or exposure to the plasma, Type (a) installations will be used. For direct view or exposure tests, a Type (b) installation which incorporates the vacuum seal at the outboard end of the test module will be used. Each test module has separate cooling, electrical, and instrumentation connections installed such that adjacent test installations are not disrupted by removal of any module.

When the test modules are not installed, the sector cavities are occupied by shield plug modules. With test modules installed, additional external shielding is required. The external, removable shield is capable of being installed and removed with all six test modules, pumped limiter, vacuum duct, ECRH, and various cooling water connections installed and operable. The concept for the shield installation is shown in Fig. 4-32, with more detailed views of test modules and external shield shown in Fig. 4-33.

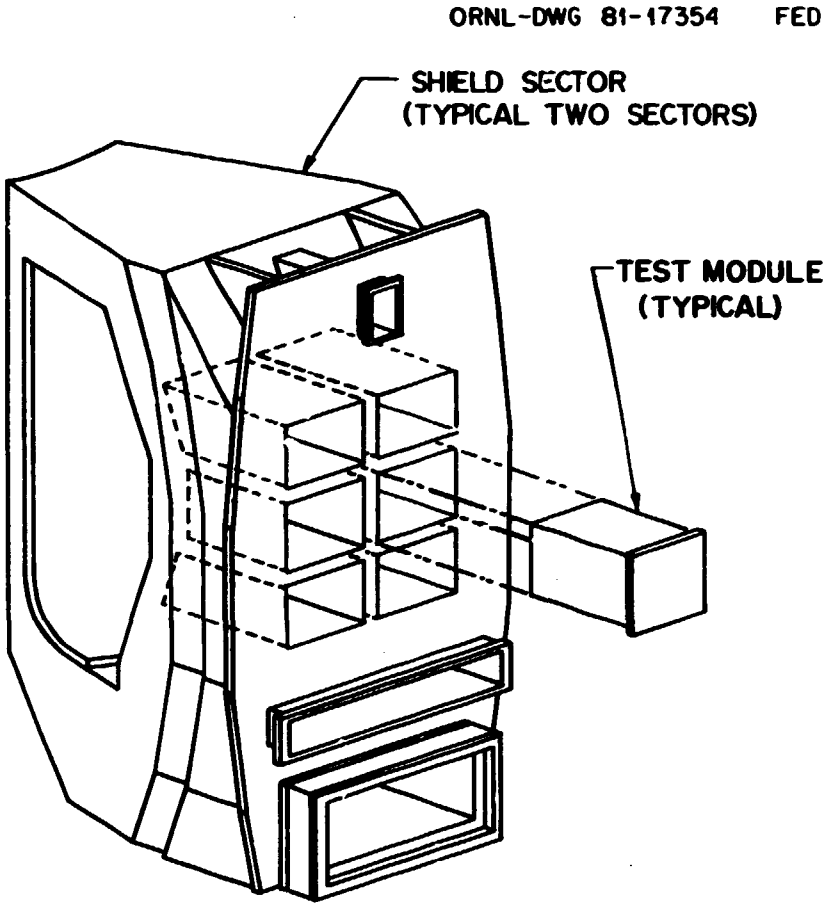

Fig. 4-30. Test module installation in outboard shield.

ORNL-DWG 82-3818 FED

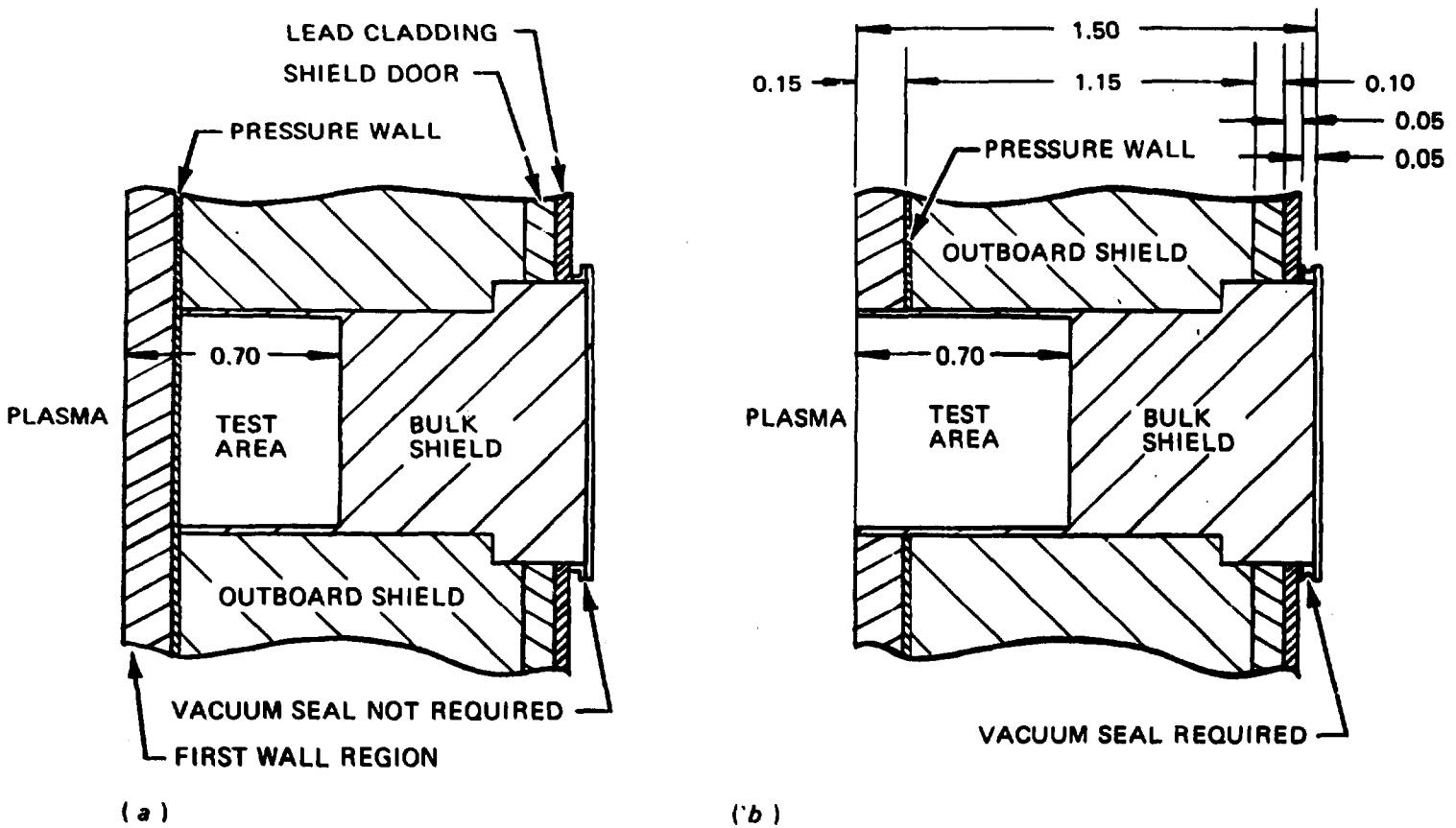

Fig. 4-31. Two types of test module installation.

ORNL-DWG 82-3819 FED

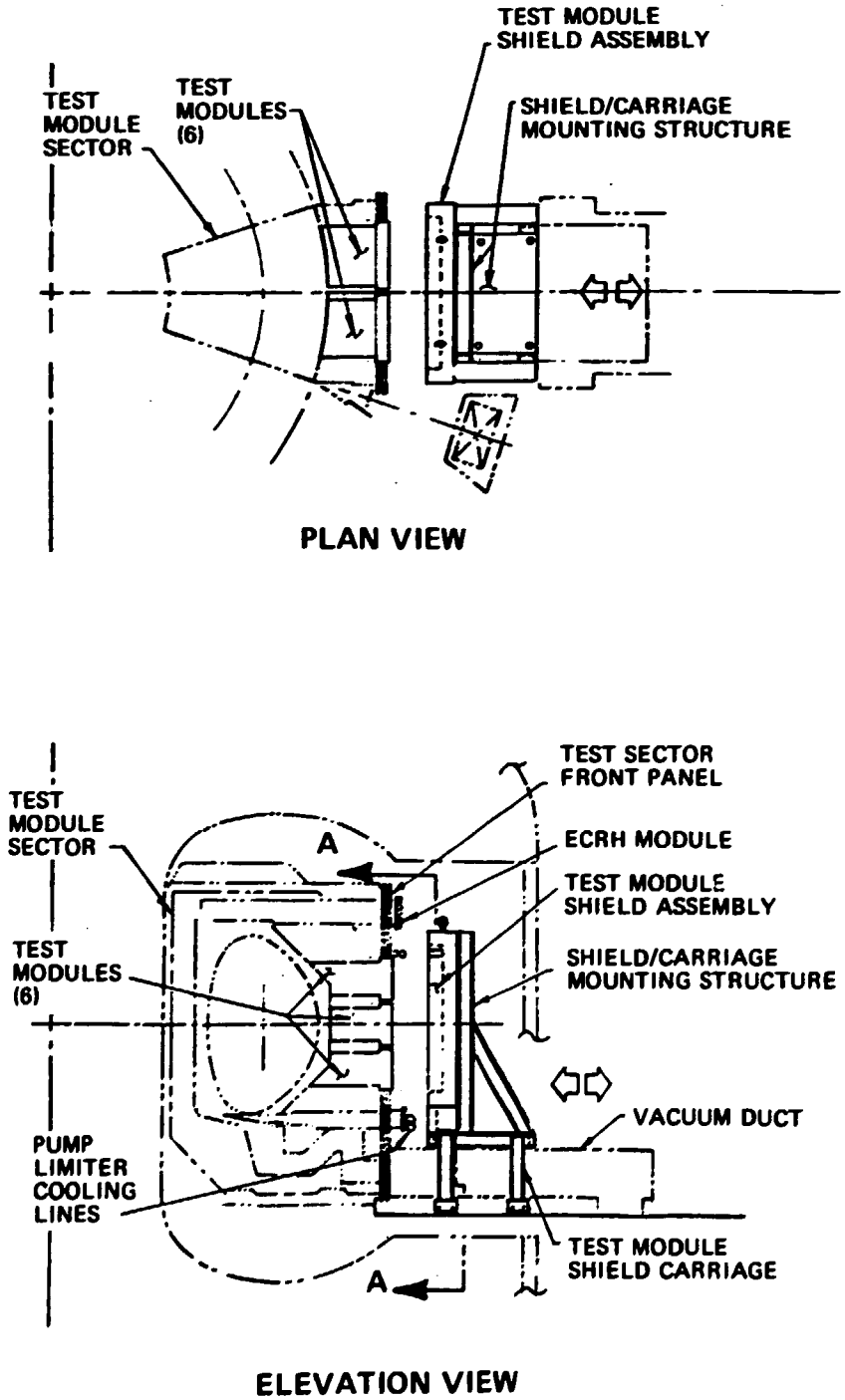

Fig. 4-32. Concept for external test module shield installation.

ORNL-DWG 82-3820 FED

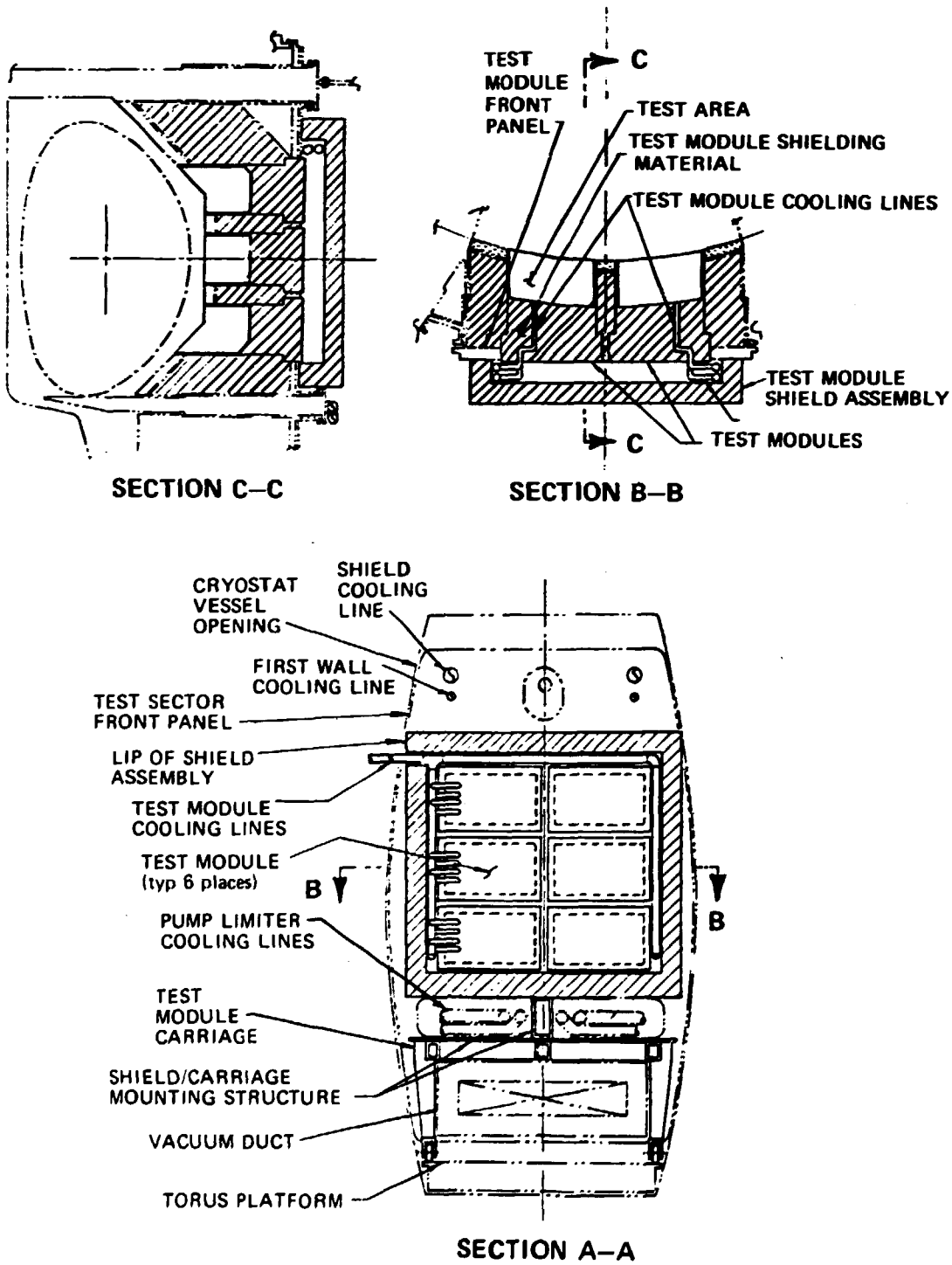

Fig. 4-33. Detail views of test modules and external shield.

4.5.1 Test Module Configuration

Studies of module configuration were aimed at achieving the largest size module which could be effectively shielded, separated from adjacent modules, handled by remote equipment, and installed in the front panel with other components such as the pumped limiter, ECRH, and vacuum duct installed and operable. Previous studies indicated that test modules with a frontal area of approximately 1 m^2 should be adequate to limit the "cross-talk" with adjacent structures and provide the required data. Accordingly, the module size was determined to be 1.33 m wide by 0.75 m high by 1.50 m deep (see Fig. 4-31). A 10-cm offset was configured on the outboard end of the test module to prevent neutron streaming. This offset expands the size of each module at the front panel to 1.53 m wide by 0.95 m high. The module protrudes 5 cm from the front panel to allow vacuum seal welds, if required.

A review of foreseeable tests (Ref. 4) indicates that the first 70 cm of the inboard end of the test module provide sufficient test area. The remaining 80 cm are, therefore, shield material comprised of Nitronic 33 stainless steel and water, with the first 40 cm being 95% steel and 5% water and the outboard 40 cm being 75% steel and 25% water. The shield material contains penetrations for service lines and instrumentation. The shielding effectiveness contributed by the test region of the test modules is assumed to eliminate the full penetration of the neutrons scattered through the module side walls. Each module would weigh approximately 6 metric tons, including shield.

The size and configuration of test modules permits a 30-cm grid of structural and shielding material horizontally and vertically between the test modules. Tests anticipated for each test module most consider the possible influence of adjacent test modules from a neutronics standpoint with the 30 cm of shielding between modules.

4.5.2 Test Module Shielding Effectiveness

The approach taken for determining the shielding requirements for the test modules was to provide a thickness of shielding materials

approximately equivalent to the outboard shield, which is 1.15 m thick. The test module shielding provided includes 80 cm in the outboard end of each test module and 30 cm in the external shield assembly, which also contains 5 cm of lead shielding on the outside surfaces. Additionally, a small shielding allowance could be assumed for materials in the test area of each test module. Therefore, the sum total of 1.15 m of shielding materials provided for the test module shielding should provide a shielding effectiveness equivalent to the outboard shield.

4.5.3 Service Connections

Separate cooling water lines for the test module shielding and test area are provided from inlet and outlet manifolds which penetrate the external shield at a local cutout. Manifolds are attached to the test sector front panel. Local shielding in the cutout region is also required. Penetration of the test module for test area cooling lines is routed with a 90° offset to prevent neutron streaming. The center of each test module is reserved for test instrumentation connections if required.

4.5.4 External Shield Assembly Concept

The external shield is mounted on a structure which is attached to a carriage. The shield is installed and removed by rolling the carriage in place on tracks leading to the test sector. When in place, the shield is to be secured to the test sector door. The carriage straddles the vacuum duct, and pumped limiter cooling lines are routed out of the carriage path.

The shield assembly measures approximately 4.1 m wide by 3.95 m high by 0.30 m thick. Thickness at the lip area around the periphery is 0.65 m. The assembly is made of layered plates of Nitronic 33 stainless steel (25%) and water (75%). An additional 5 cm of lead shielding is provided on the external surface of the shield assembly. The weight of the shield is approximately 34 metric tons.

4.6 SEISMIC RESPONSE

A simplified NASA Structural Analysis (NASTRAN) finite element model of the FED Baseline was developed and used in modal and response analyses. Mode shapes and resonant frequencies were calculated, and deflections and accelerations due to a seismic input were predicted. Results indicate that the maximum lateral deflection of a toroidal support spool and shield sector's cg is 0.86 cm, with a lateral constraint of the torus support ring incorporated at the bottom of the spool. Without the constraint, this predicted deflection is six times larger.

The finite element model used in the initial dynamic response evaluation consisted of the ten 450-ton shield sectors mounted on a support ring which is, supported by ten equally spaced columns, as indicated in Fig. 4-34. Two cases were analyzed, (1) without lateral constraint and (2) with five beams equally spaced around the support ring to reduce the lateral motion of the system with respect to ground. This system was modeled using bars and rigid body elements (Fig. 4-35). The rigid body elements are represented as large triangles with their cg's at the triangles' apexes.

Modal analyses were performed to evaluate the adequacy of the model and define the modes in the frequency range below 33 Hz, which is considered to be the highest frequency significantly affected by the spectrum defined in NRC 1.60. A response spectrum analysis used all 30 of the modes below 33 Hz and defined maximum responses (displacements and accelerations) in all six degrees of freedoms at each grid point. The forcing function representing the seismic event is based on the seismic response spectra for Risk Zone 2 (damping = .02 $C/_{Cc}$, as defined in NRC 1.60).

The maximum lateral responses are listed in Table 4-9. Values at the sector cg are the square roots of the sums of the squares of the values calculated for the points showing the largest response. Values at the tops of the sectors include the effect of rotations about the cg's. Vertical responses are approximately 10% of the smallest lateral response.

ORNL–DWG 82-3875 FED

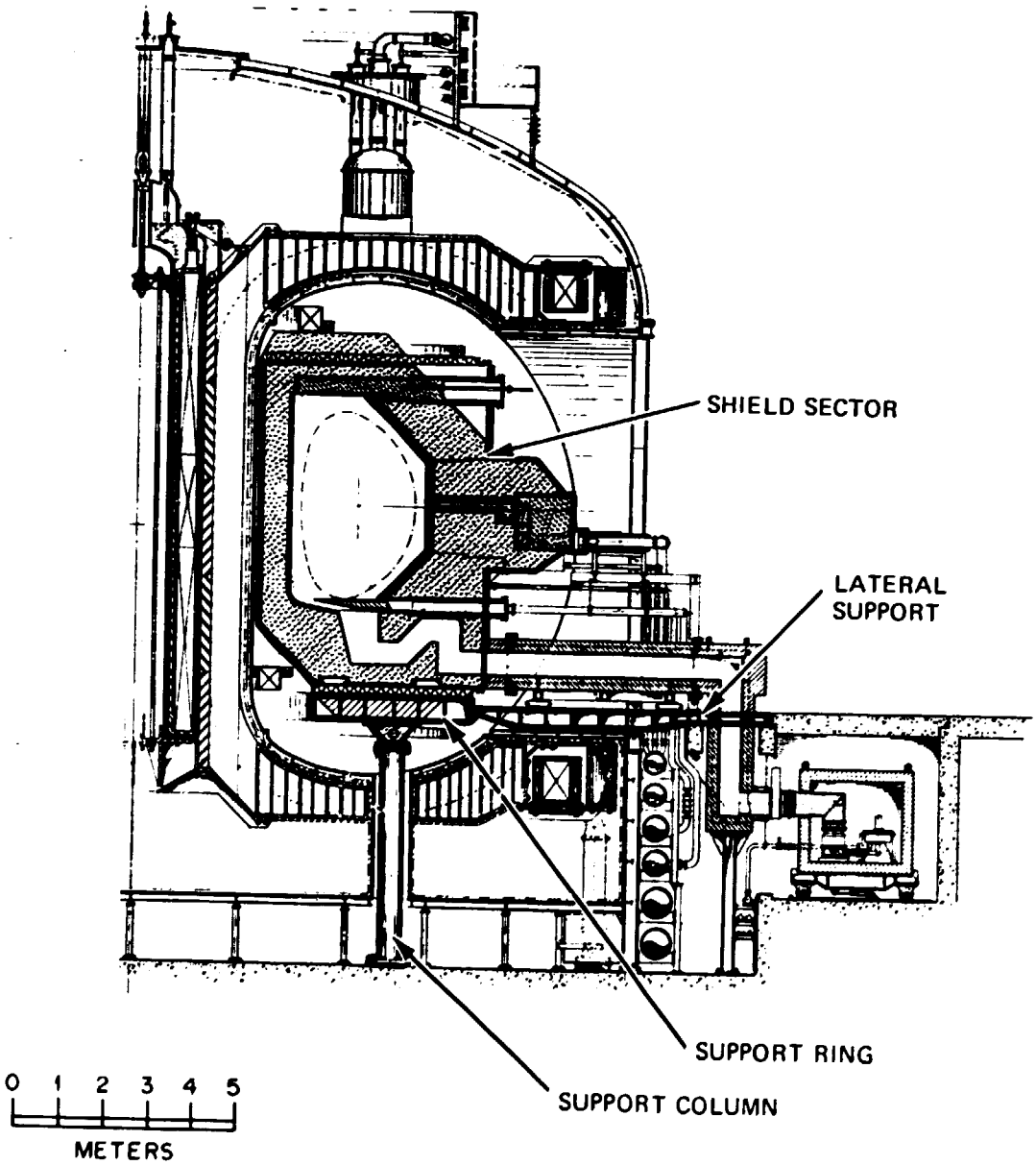

Fig. 4-34. Components for seismic analysis.

ORNL-DWG 82-3821 FED

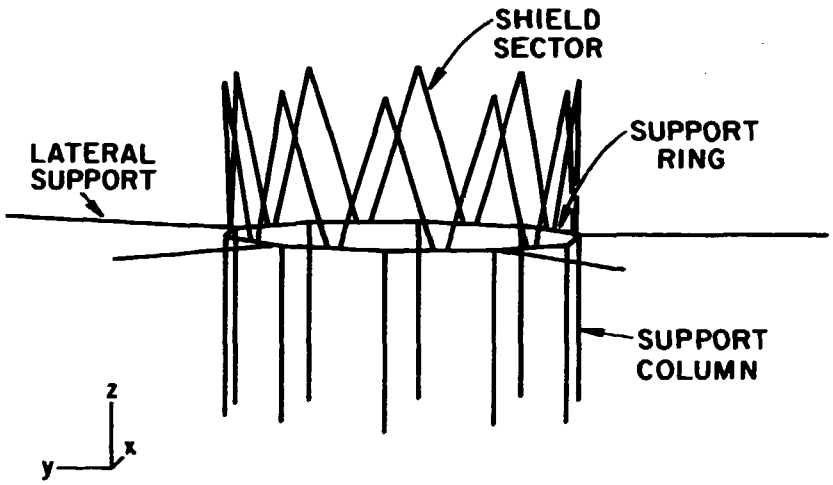

Fig. 4-35. Components and elements used in FED seismic analysis.

Table 4-9. Impact of lateral support on lateral response

	With lateral support	Without lateral support
Lateral acceleration at Sector cg (g)	0.78	0.71
Lateral deflection at Sector cg (cm)	0.86	5.20
Lateral deflection at top of sector (cm)	1.55	7.29

Representative mode shapes are shown in Fig. 4-36. Shown are a torsional mode (toroidal movement of the support ring) and a sector tipping mode. Both of these are at very low frequencies of 1.28 and 2.60 Hz.

4.7 TEMPERATURE VARIATIONS OF THE FIRST WALL

The FED first wall system consists of: (1) graphite armor tiles which cover the inboard surface, top surface, and regions near the limiter where charge-exchange (C-X) neutrals impinge, (2) stainless steel panels covering the outboard surfaces, and (3) a pumped limiter with graphite tiles brazed to a copper substrate in the bottom of the plasma chamber. Previous analyses with decoupled one-dimensional thermal models of inboard tiles and outboard panels (Ref. 1) demonstrated that the tiles and panels operate in desired temperature ranges. However, these analyses did not account for poloidal temperature variations (2-D effects).

The purpose of this analysis was to determine the poloidal variation of first wall temperatures and to evaluate the impact of these variations on first wall performance. Several causes for poloidal variation of first wall temperatures are:

- Different first wall materials (graphite on the inboard and top surfaces, stainless steel on the outboard)
- Different geometric radiation view factors between first wall surfaces
- Nonuniform poloidal heating distribution

Only the first of these causes, different first wall materials, was included in detail for the previous analysis (Ref. 1). Another objective of these studies was to examine the sensitivity of first wall temperatures to changes in assumptions or conditions dealing with plasma edge conditions as well as material properties. The assumptions and scope of the sensitivity studies are discussed in the following section.

ORNL-DWG 82-3822 FED

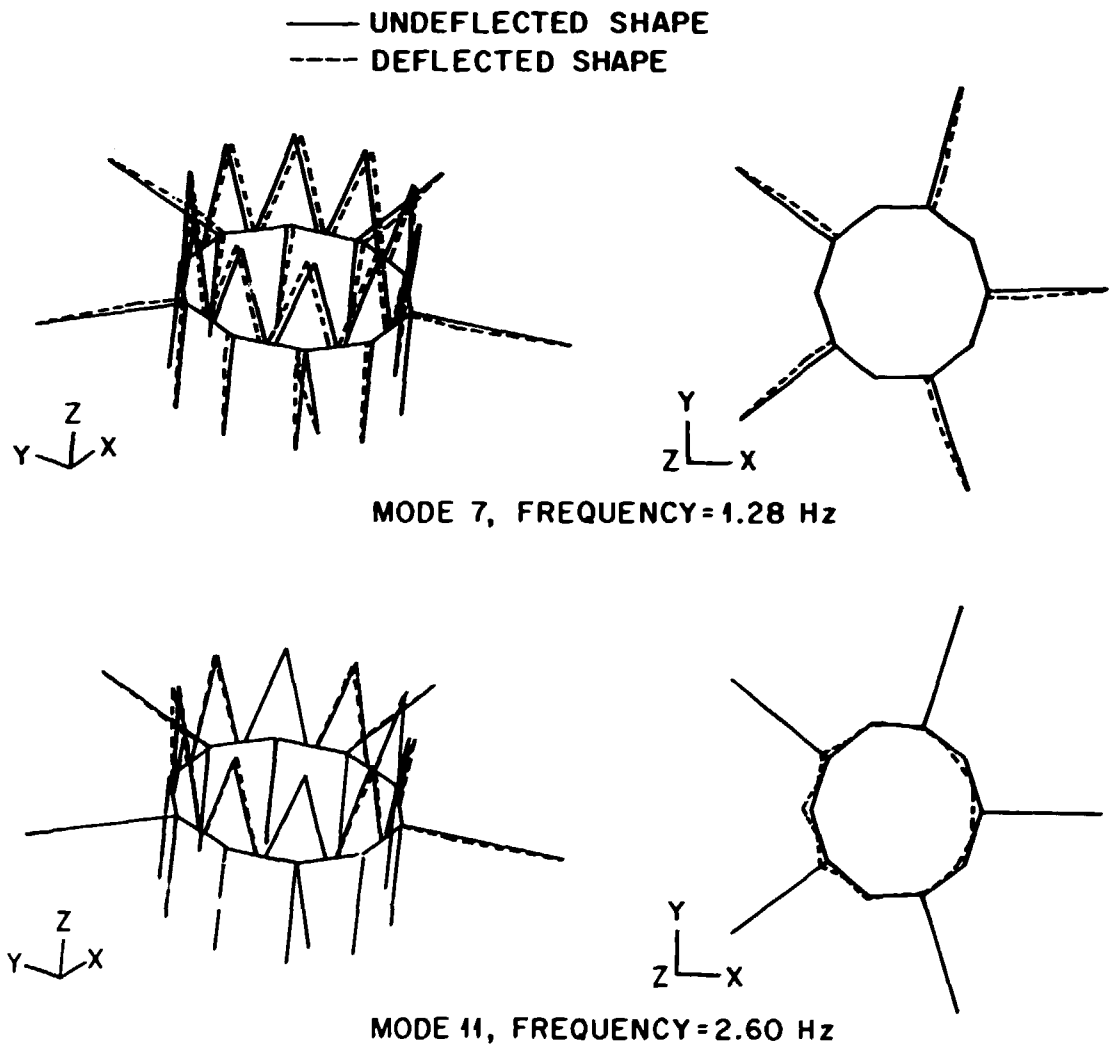

Fig. 4-36. Representative mode shapes under seismic load.

4.7.1 Approach

A two-dimensional transient finite difference thermal model of all first wall components was constructed. Assumptions and conditions used for these analyses are listed in Table 4-10. The reference case conditions are shown, along with conditions used for sensitivity studies. The reference case conditions represent operation at a magnetic field of 10 T, with worst case (from a heating viewpoint) plasma edge conditions.

Parameters varied for the sensitivity studies included: magnetic field (from 10 T to 8 T), plasma edge conditions (from 84 MW to the first wall for "worst case" conditions to 20 MW for the "best case"), poloidal heating distribution (from uniform to a variation similar to the variation of neutron flux for INTOR, presented in Ref. 4), stainless steel emittance (from 0.8 to 0.2), graphite thermal conductivity (from the value representing the unirradiated condition to the value after irradiation), and contact conductance between graphite armor tiles and shield (from no contact to a contact conductance representing an upper limit for a mechanical attachment).

4.7.2 Results

Maximum temperatures for all first wall surface nodes after 15 consecutive burn cycles are shown in Fig. 4-37. All graphite tiles pass through the methane generation range from 400°C to 800°C during the initial burn cycles, operating in this range for less than 300 s. The C-X neutral armor located on the outboard surface operates near 1520°C. The top surface operates at 1400°C, and the inboard surface reaches 1300°C. The maximum stainless steel panel temperature is 330°C and occurs at the outlet end of the upper 45° facet. This is judged to be an acceptable operating temperature for the panels.

Erosion of the graphite tiles at these elevated temperatures by sublimation is insignificant. Chemical erosion by formation of methane is avoided by maintaining the surface temperatures above the methane generation range of 400°C to 800°C. However, recent experimental studies (Ref. 5) have demonstrated that sputtering erosion of Papyex

Table 4-10. Key assumptions and analysis conditions

Condition	Description: Reference case	Description: Sensitivity studies
Peak magnetic field	10 T	8 T
On/off time per burn cycle	50 s on/52 s off	100 s on/52 s off
Plasma edge condition (see Ref 1 for details)	Case D, 74 MW radiation from plasma, 10 MW C-X neutral power	Case A, 10 MW radiation from plasma, 10 MW C-X neutral power
Poloidal heating distribution		
Radiation from plasma	Uniform	Same as INTOR variation of neutron flux
Neutronic heating	Uniform	Same as INTOR variation of neutron flux
Stainless steel emittance	0.8 (coated with graphite redeposited from other first wall surfaces)	0.5 (bare stainless steel)
Graphite conductivity	30 W/m·K (irradiated condition)	60 W/m·K (unirradiated)
Coolant inlet temp./pressure		
First wall panels	60°C/0.7 MPa	---
Shield	60°C/0.7 MPa	---
Limiter	60°C/1.0 MPa	---
Contact conductance (C) between armor tiles and shield	0	$0 < C < 0.3$ W/cm^2·K

ORNL-DWG 82-3823 FED

- REFERENCE CASE
- TEMPERATURES AFTER 15 CONSECUTIVE BURN CYCLES

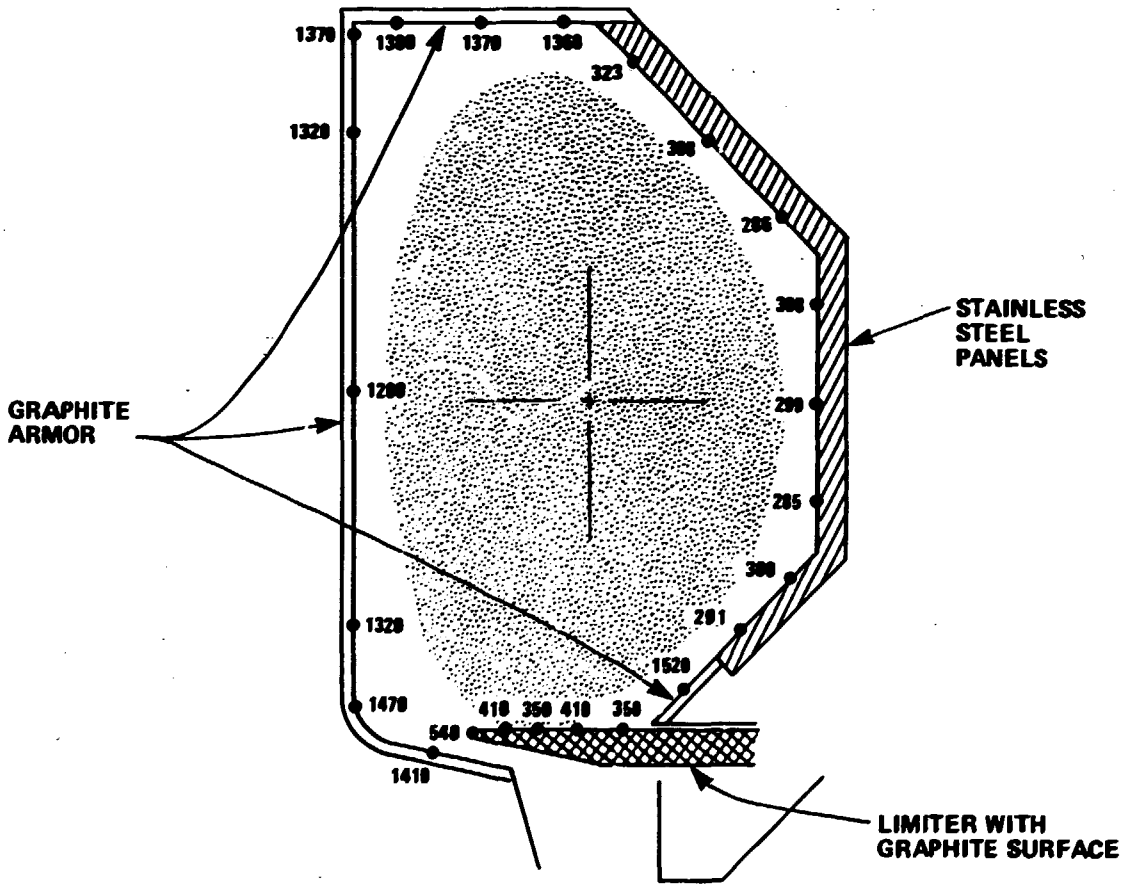

Fig. 4-37. Maximum surface temperatures.

graphite at temperatures above 1000°C is significantly higher than physical sputtering erosion at temperatures less than 400°C. Since this increased erosion occurs with helium as well as hydrogen, the mechanism cannot be chemical erosion. Further experimental studies are required to investigate whether this enhanced erosion mechanism exists for other types of graphite and to what extent this mechanism can be reduced by surface conditioning.

Using the enhanced sputtering erosion yield data from Ref. 5 and including disruption-induced erosion by sublimation, the total erosion of the C-X neutral armor is estimated to be 12.4 cm over the total FED lifetime. Since 3 cm out of a total tile thickness of 5 cm is allowed for erosion, the C-X neutral armor tiles would need to be replaced four times during the FED lifetime if the enhanced sputtering erosion occurs.

Since the flux of energetic particles on the inboard surface (away from the C-X neutral impingement region) and top surface is negligible, sputtering erosion is insignificant in these regions. Therefore, these tiles are expected to last the entire ten-year FED lifetime, regardless of whether enhanced sputtering occurs at temperatures above 1000°C.

Sensitivity studies

Sensitivity study results are summarized in Table 4-11. The impact of each parameter variation on the maximum temperature of the graphite tiles and stainless steel panels is indicated in the table. For example, operating with a peak magnetic field of 8 T, instead of the reference value of 10 T, results in a 100°C reduction in the graphite armor temperatures and a 50°C reduction in the maximum stainless steel temperature.

4.7.3 Conclusions

The stainless steel panels which form the outboard first wall surface operate at acceptable temperature levels (below 340°C) for all conditions examined. The 5-cm-thick graphite armor tiles designed for FED operate between 800°C and 1600°C, depending on poloidal location,

Table 4-11. Results of first wall temperature sensitivity analysis

Parameter varied	Reference value	Range of variation in parameter	Temperature increase above reference value* due to parameter variation, °C	
			Graphite tiles	316 SS panels
Magnetic field	10 T	10 T to 8 T	-100	-50
Plasma edge condition	74 MW plasma radiation	74-10 MW plasma radiation	-300	-150
Stainless steel emittance	0.8	0.8 to 0.2	+350	-30
Graphite thermal conductivity	30 W/m·K (irradiated condition)	30-60 W/m·K	-50	-20
Contact conductance between tile & substrate	0. (radiation only)	0-30 W/m·K	-200	-80
Poloidal variation of heating	Uniform	Uniform vs INTOR-type neutron flux variation	±50	±15
Cyclic variation during burn cycle	End of burn	Start of burn to end of burn	-200	-200

*Temperatures at reference conditions:
- o Graphite armor
  - o Inboard Surface → 1300°C
  - o Top Surface → 1400°C
  - o C-X Neutral Surface → 1520°C
- o Stainless Steel Panels → 330°C

plasma edge conditions, and material properties. This is above the methane generation range of 400°C to 800°C and at low enough temperatures to avoid significant erosion by sublimation. Recent experimental evidence suggests that enhanced sputtering erosion can occur at temperatures above 100°C. This should not cause any problems for inboard and top armor surfaces not exposed to energetic particle impingement. However, erosion of the C-X neutral armor tiles located near the pumped limiter could be significantly impacted. It this erosion mechanism cannot be avoided, four replacements of the C-X neutral armor tiles would be required during the FED lifetime.

REFERENCES

1. ORNL/TM-7948 (see Ref. 1, Chapt. 1).
2. C. W. Kimblin, "Erosion and Ionization in the Cathode Spot Region of Vacuum Arcs," *J. of Appl. Physics*, Vol. 44, No. 7, July 1973, pp. 3074-3081.
3. W. S. Miller, editor, "Nonferrous Metals," *Machine Design*, Vol. 52, No. 8, April 17, 1980, pp. 73-92.
4. Report No. US INTOR/81-1, The U.S. Contribution to the International Tokamak Reactor Phase-1 Workshop, Conceptual Design, Chapter XIV, June 1981.
5. J. Roth, J. Bohdansky, and K. L. Wilson, *Proc. 5th Int. Conf. on Plasma-Surface Interactions, May 3-5, 1982, Gatlinburg, Tennessee.*

5. MAGNET SYSTEMS

5.1 INTRODUCTION

The emphasis of this year's study of the magnet systems was to reevaluate various systems with the objective of reducing the device cost, to develop component details, and to consider new design approaches. Several concepts were identified with potential for cost reduction. For example, designs of the TF coil and intercoil structures were developed to reduce the weight and eddy current losses, and both of these lead to lower cost of the machine. A design to increase the ohmic heating solenoid peak field to 8 T (from 7 T in the Baseline) was also developed. This increased field capability can be utilized for reducing the cost of the machine or for obtaining longer burn time.

Alternate winding concepts were considered for both TF and PF coils. Application of a superfluid helium-cooled conductor was considered for the TF coils. The conclusion was that this winding approach can be accommodated into the specified FED baseline "TF coil cavity," provided the conductor support structure is made similar to that proposed for the GA 12-T conductor concept. Likewise, ohmic heating solenoid and ring coil concepts were developed on the basis of forced-cooled NbTi conductors. The forced-cooled concept offers a more compact winding design and eliminates the need for a non-conducting helium vessel that is required for the pool-boiling winding.

Considerable analytical work was done to confirm the feasibility of the proposed concepts. A few examples of this work are:

1. fracture mechanics methodology was used for the purpose of selecting allowable stresses for designing the magnet structures;
2. candidate insulating materials were identified for application in future designs where lifetime radiation dose is expected to approach 10^{12} rads;
3. pool-boiling winding concepts were employed in the ohmic heating solenoid and the ring coils. They were evaluated to ensure that no helium entrainment occurs during the pulsed operation. The coil designs were found satisfactory in this respect;

4. computer codes were updated to study the stability of the forced cooled windings; and
5. a fault analysis was performed to identify potential problems such as over-currents in shorted coils or over-voltage in various PF coils during normal pulsed operation or following a plasma disruption.

All coils, except one, were found to be trouble-free. Overcurrent is expected in the coil that is "sandwiched" between the two end modules of the ohmic heating solenoid. In the event of an unintentional shutdown, it would be necessary to discharge the ohmic heating coil over a time period much longer than the normal shutdown time of 10 s.

This year's activities have provided an opportunity to perform a critical evaluation of various subsystems, and several improvements in the design approach were identified.

5.2 TOROIDAL FIELD COILS

5.2.1 Superfluid Helium Cooled Coil Design

The FED Baseline TF coil winding cavity is sized[1] to accommodate all cooling options (pool-boiled, forced-flow, and superfluid bath-cooled) for fields up to 10 T. This section describes the superfluid helium-cooled 10-T TF coils. This cooling approach has a better heat transfer characteristic at operating temperatures ($\sim$1.8 K) below the lambda point transition temperature of 2.18 K, as compared to pool-boiling systems. The thermal conductivity of the superfluid is $\sim 10^4$ W/cm-K for this operating temperature range. As a result, the heat transport is so rapid that no appreciable temperature gradients can be sustained. The entire bath volume is, therefore, available to absorb thermal energy (up to the lambda point). This thermal conduction is augmented by the near-zero viscosity of the superfluid helium.

A major uncertainty associated with superfluid helium cooling is that no large scale magnet systems have yet been built using this option. Other disadvantages are the increased refrigeration power required

at lower temperatures and the poor dielectric strength of saturated vapor at 1.8 K and 0.016 atm, which limits the maximum allowable discharge voltages for the winding.

A TF coil winding design is described that employs a modified General Atomic 12-T Program[2] conductor. It is concluded that the above conductor can be accommodated in the assigned cavity, with minor modification of the conductor.

5.2.1.1 Conductor design

The cable type of conductor[2] proposed by GA is shown in Fig. 5-1, along with the stainless steel support strips to be co-wound with the conductor. Its relevant parameters are given in Table 5-1. The conductor consists of a three-level insulated, unsoldered, NbTi cable to reduce ac losses due to the pulsed poloidal fields and under plasma disruption. It offers ease of coil winding due to its flexibility and can be manufactured at reasonable cost with conventional fabrication methods. It also provides the required cryogenic stability margin ($\sim$180 mJ/cm^3) due to high effective surface-to-area cooling characteristics. The main disadvantage of the unsoldered cabled conductor is that it cannot carry any loads. Therefore, most of the loads must be borne by the stainless steel supporting strips. These strips have openings for helium, as shown schematically in Fig. 5-1(a). The turn-to-turn and pancake-to-pancake insulation is provided by G-10 sheets 0.3 mm thick and 5 mm thick, respectively.

The conductor is designed to carry 15,000 amperes at 10 T and is cooled by saturated superfluid helium at 1.8 K. The temperature dependence[3] of the critical current for this conductor is shown in Fig. 5-2. The operating conductor current has been chosen to provide adequate stability margin.

The winding current density of roughly 1500 A/cm^2 can be achieved with the above conductor configuration for an operating current of 15 kA. However, the winding cannot be accommodated in the available FED Baseline cavity with this low winding current density. Consequently, the supporting structure for the conductor is modified to accommodate

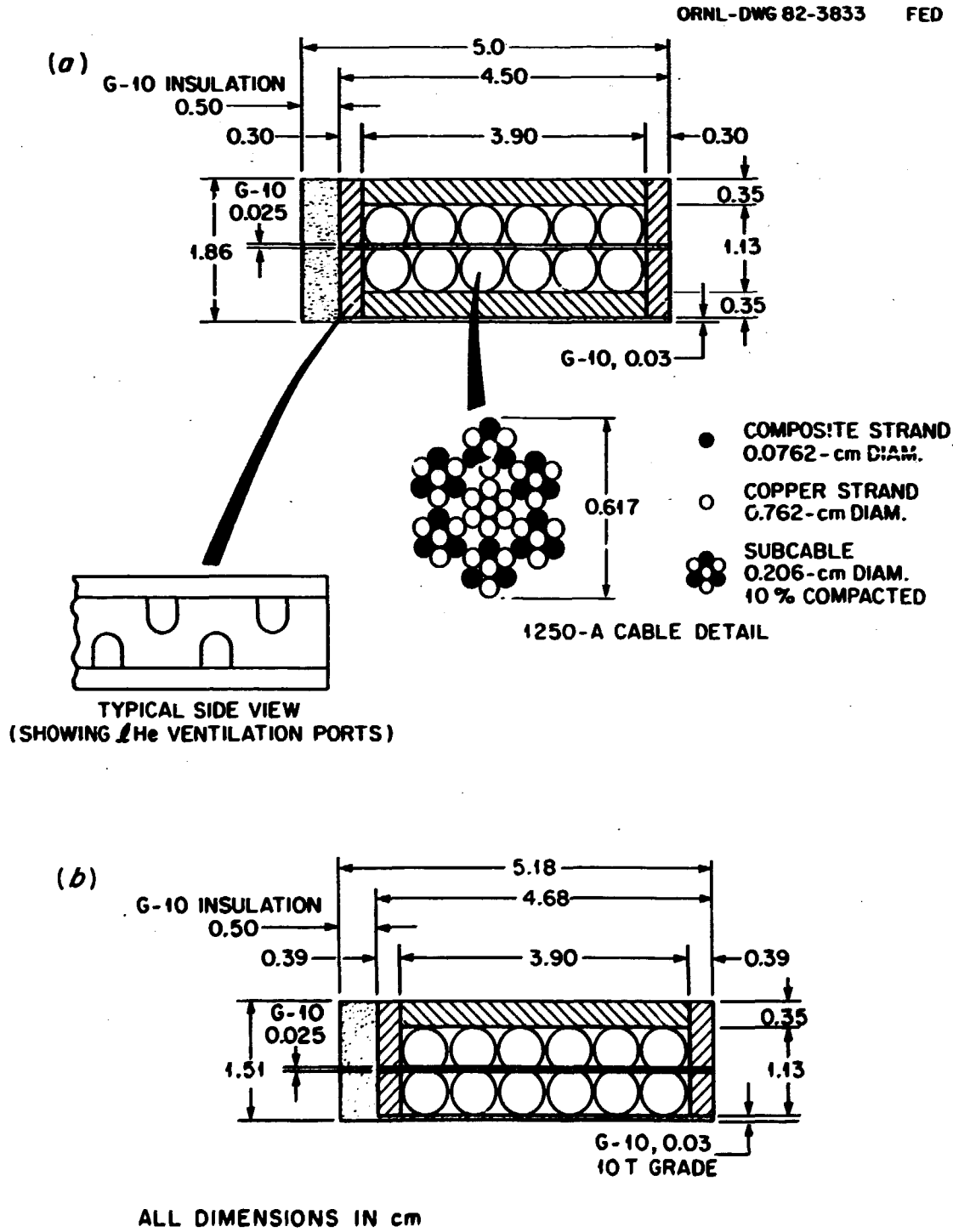

Fig. 5-1. Configurations and dimensions for 10 T grade conductor, (a) GA conductor (b) modified conductor.

Table 5-1. Parameters of conductors for superfluid option (10 tesla operation)

Parameter	GA conductor 10 T grade	Modified conductor 10 T grade
Operating current at 10.0 T and 1.8 K (kA)	15.0	15.0
Critical current at 10.0 T and 1.8 K (kA)	22.5	22.5
Conductor current density including insulation (A/cm^2)	1600	1920
Overall dimensions including insulation	50 mm x 18.6 mm	51.8 mm x 15.1 mm
Total area (mm^2)	930	782
SS area (mm^2)	383	252
Insulation area (mm^2)	106	90
Helium area (mm^2)	164	164
NbTi area (mm^2)	19	19
Copper area (mm^2)	250	250
Supporting strip G-10 area (mm^2)	7.5	7.5
Void fraction in cable space	0.37	0.37
Cu/Sc ratio in S.C. strand	4.25:1	4.25:1
Overall Cu/SC ratio	13.3:1	13.3:1
Strand diameter (mm)	0.762	0.762
Subcable diameter (mm)	2.06	2.06
Cable diameter (mm)	6.17	6.17
Filament diameter (μm)	10	10
Number of filaments in S.C. strands	1108	1108
Strand twist pitch (mm)	~7	~7
Thermal capacity ΔH at 10 T and 1.8 K (mJ/cc)	180	180

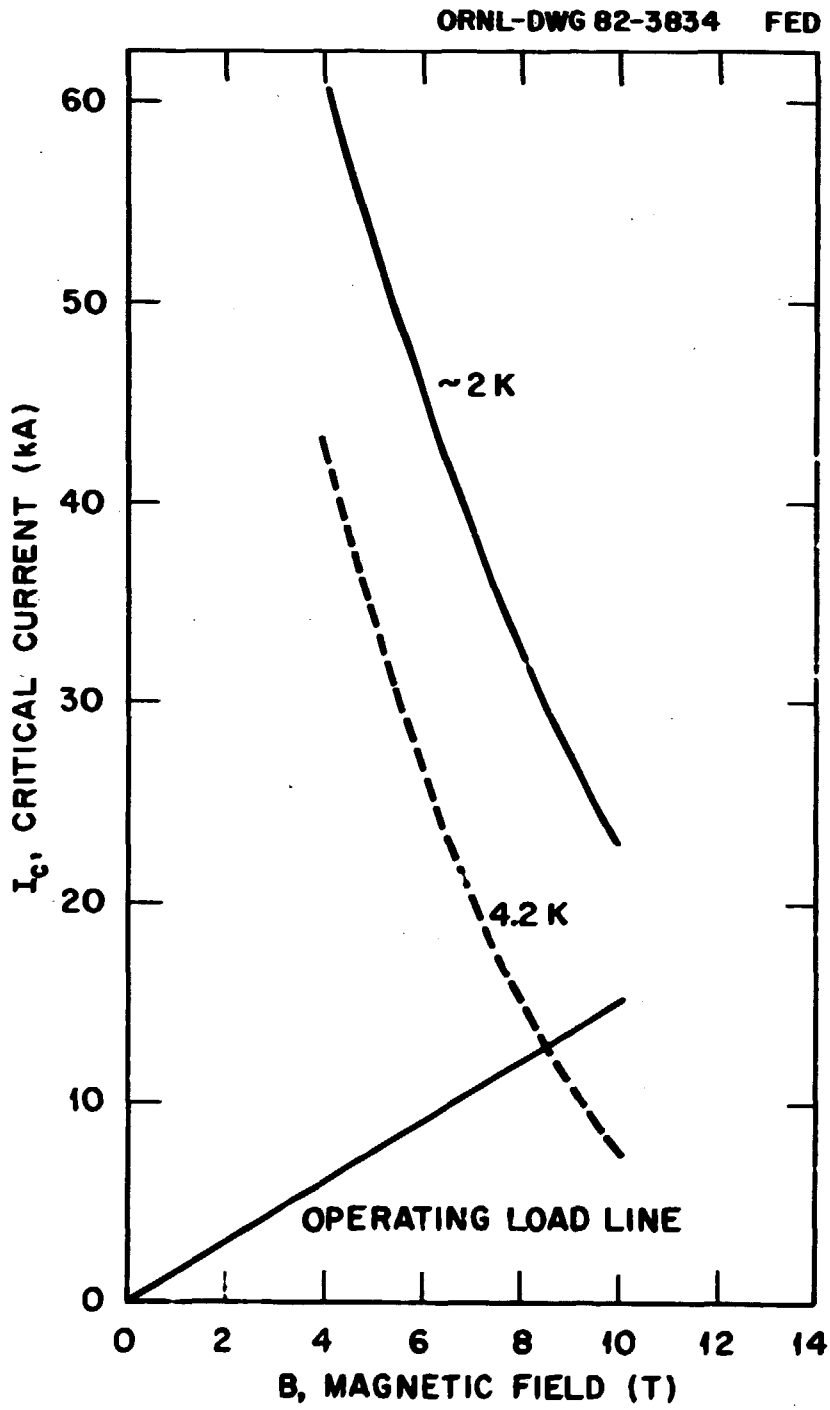

Fig. 5-2. Critical current I_c as a function of field and temperature. Load line for 10 T operation at 2 K for 10 T grade conductor.

the winding in the FED Baseline cavity. The modified conductor is shown in Fig. 5-1(b). The NbTi cable space (metal + helium cross section) in the 10-T grade is the same as in the original conductor. The supporting stainless steel strips (forming a U-channel) on the three sides have been sized for the magnetic loads of FED and are discussed later in this section. The TF coil design with the modified conductor is described in the following section.

5.2.1.2 TF coil design description

The TF coil winding schematic using superfluid helium is shown in Fig. 5-3. The coils are pancake wound and employ two grades (10 T and 5 T) of the modified conductor. Table 5-2 lists the relevant parameters of the winding.

In developing these layouts of the winding, the magnetic loads are assumed to be the same as in the 10-T Baseline design. The coil case heat loads are removed by cooling channels (~1 cm x 1 cm) incorporated between the helium vessel and the coil case. The heat loads in the thin helium vessel (thickness ~0.5 cm) are removed by the helium in the winding. The ground insulation thickness is 0.5 cm. With the required coil case thickness (5.4 cm on sides and 8 cm on inner and outer side of the coil), the total thickness on the sides is 7.4 cm and at the inner and outer sides of the coil is 10 cm (Fig. 5-3).

5.2.1.3 Conductor support structure

In the GA conductor design, the cabled strands are placed around a G-10 sheet and two stainless steel channels are co-wound in the form of a box, completely surrounding the strands (Fig. 5-1). To increase the winding current density, a single U-channel approach (similar to General Electric 12-T conductor[4] design) is suggested for the support of the conductor. The cable and helium cross section is the same as in the original GA 10-T grade conductor. The U-channel has been sized according to the structural design criteria used[5] at FEDC, on the basis of the magnetic loads for the FED Baseline reference design. The overall width

ORNL-DWG 82-3835 FED

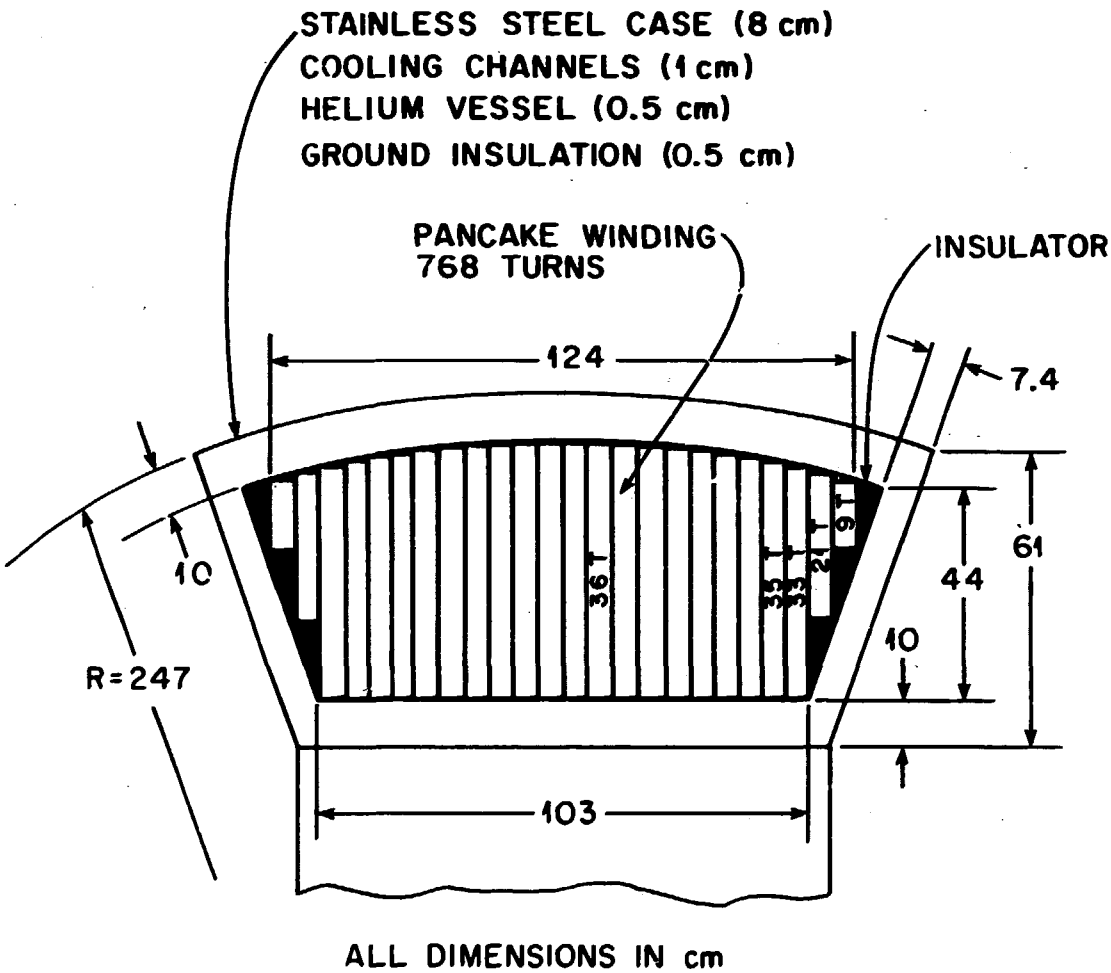

Fig. 5-3. TF winding cross section (inboard region) for superfluid shown with modified conducter (U channel).

Table 5-2. FED TF coil design parameters for superfluid option (10 T operation)

Parameter	Baseline (forced flow option)	With GA conductor (superfluid option)	With modified conductor (superfluid option)
Field on plasma axis (T)	4.6	4.6	4.6
Nominal peak field at the winding (T)	10	10	10
Ampere turns/coil (MAT)	11.5	11.5	11.5
Operating current (kA)	25.5	15	15
Winding current density (A/cm^2)	2100	1600	1920
Number of turns	144	768	768
Number of full pancakes	28	20	20
Number of partial pancakes	4	6	4
Ratio of operating/critical current	0.521	0.667	0.667
Operating temperature (K)	3.1	1.8	1.8
Major radius due to winding buildup (M)	5.0	5.13	5.0
Major radius for same burn time (M)	5.0	5.3	5.0
Change in major radius for same burn time (M)	0	0.3	0

of the conductor for the two grades (10 T and 5 T) is identical, although not necessarily in agreement with the corresponding GA conductor dimensions. The dimensions of U channel and the conductor are shown in Fig. 5-1. The overall cross sectional area for the low field grade and high field grade conductors is reduced by roughly 20% and 16%, respectively, resulting in higher winding current density ($\sim$2000 A/cm^2). The allowable stresses are consistent with the structural design criteria given in Table 5-3 of Ref. 5. The winding stresses are less than, or equal to, allowable stresses. Thus, the U-channel approach for supporting the conductors appears feasible.

5.2.2 Redesign of Coil Case

The FED Baseline design described in Refs. 1 and 5 uses a TF coil case having a zoned wall thickness. The region of maximum thickness is the outboard "window" region, where a 12-cm case wall thickness is used. Although such thicknesses are within present-day fabrication capabilities, a study was performed which showed that a thinner walled case reinforced with stiffening ribs at intervals results in reduced overall case weight and fabrication expense. Furthermore, the case design using the thinner material results in a large reduction in coil case eddy current losses, which constitute about one-third the heat load on the cryogenic system. The reduction in losses permits use of a smaller refrigeration system and also affords a reduction in the refrigeration system power consumption throughout the life of the plant.

Figure 5-4 compares typical longitudinal segments of the TF coil case using the thick-wall concept (t = 12 cm) and the built-up section concept (t = 5 cm). The 5-cm plate stock thickness used in the latter concept for both the case wall and the stiffening ribs was selected somewhat arbitrarily but is considered easily weldable and is representative of the case thickness in other toroidal field coils such as LCP.

The coil case wall is loaded by a distributed pressure load resulting from the Lorentz forces developed in the winding, both in the plane of the coil and normal to the plane of the coil. The spacing and depth of the reinforcing ribs are determined by limiting the resulting plate

ORNL-DWG 82-3745A FED

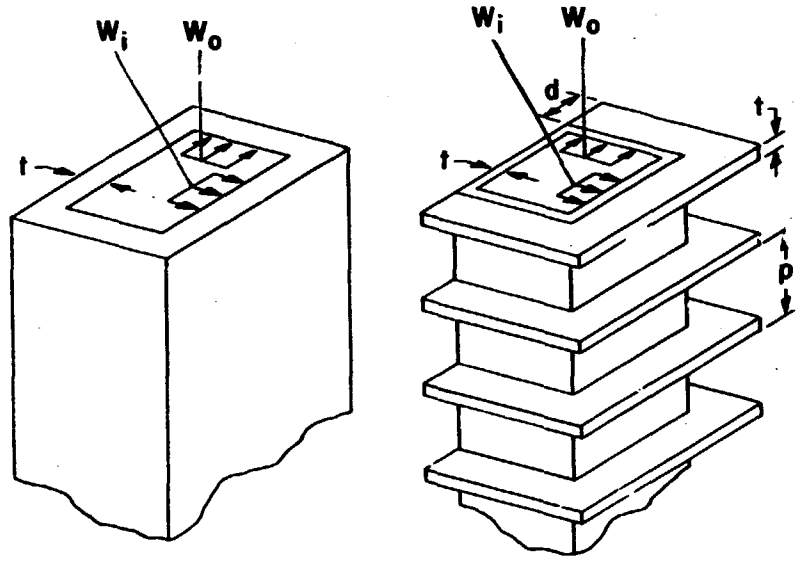

(*a*) THICK-WALL DESIGN (*b*) BUILT-UP DESIGN

t = WALL THICKNESS, RIB THICKNESS
p = RIB SPACING
d = RIB DEPTH
W_o = OUT-OF-PLANE LOAD (pulsed)
W_i = IN-PLANE LOAD (steady)

Fig. 5-4. Comparison of TF coil case concepts.

bending stresses to the allowable, namely (31 ksi) 215 MPa for the pulsed out-of-plane load and (74 ksi) 513 MPa for the steady in-plane load. The result is a rib spacing of 25 cm and a rib depth varying from 7 to 20 cm, as shown in Fig. 5-5.

The costs of material and welding for the two coil case concepts were compared. It was found that for equal lengths of the two case designs, the cost of structural material and welding (including weld prep, deposition of weld metal, and dye-penetrant testing) is about 40% less for the built-up section. The cost is $6.25 per pound for both concepts, the lower cost of the built-up design being reflected in the lower weight of equal length segments. The cost of material and welding is about half the total cost of fabricated case structure (usually assumed to be $12 per pound). If the other costs (e.g., engineering design, machining, structure handling, shipping, overhead, etc.) are assumed the same for both concepts, the overall reduction in coil case fabrication expenses is about 20%, or $5 M for FED.

The principal cost saving associated with use of the built-up coil case concept results from the reduced eddy current losses. The TF coil case losses in the built-up design are 15 kW, compared to 32 kW in the thick-wall design. The 17-kW reduction in the heat load on the cryogenic system leads to a savings of $3.2 M in refrigeration system capital costs. In addition, there is a savings over the ten-year life of the plant of $21.4 M in demand charges and power consumption charges, attributable to the 17 kW reduction in AC losses.

The overall savings associated with using the built-up TF coil case concept is $30 M.

5.2.3 Redesign of Intercoil Support Structure

The FED Baseline design described in Refs. 1 and 5 uses an intercoil support structure (ISS) consisting of box-like modules containing inner and outer metallic shells (5 cm thick), separated by circumferential stiffening ribs. This structure effectively reacts the overturning loads but has eddy current losses of about 46 kW, accounting for about half the heat load on the cryogenic system. To prevent this heat from

ORNL-DWG 82-3836 FEC

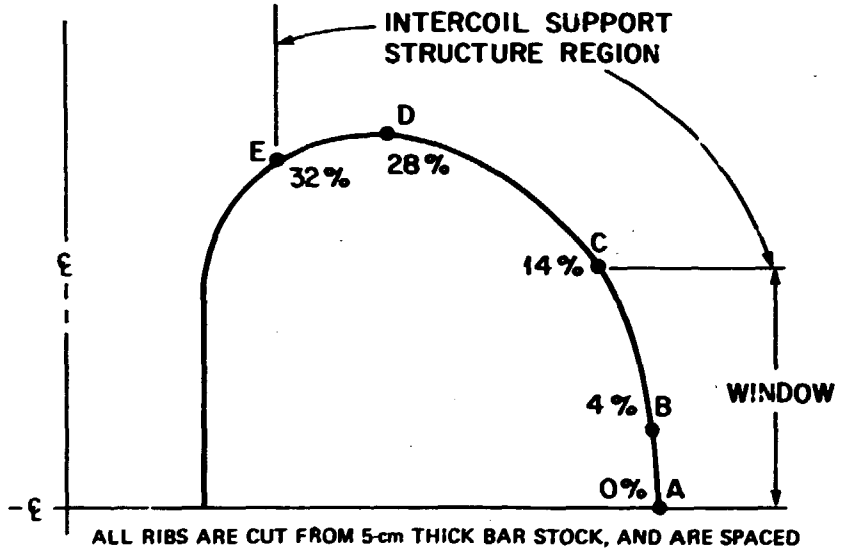

ALL RIBS ARE CUT FROM 5-cm THICK BAR STOCK, AND ARE SPACED 25 cm, CENTER-TO-CENTER

SPAN	SIDEWALL (cm)	OUTER WALL (cm)
A–B	7	17
B–C	7 at B, 16 at C (linear variation)	17
C–D	21	17
D–E	15	17

Fig. 5-5. TF coil rib dimensions.

reaching the TF coil winding, coolant lines are included in the ISS modules near the juncture with the TF coil case sidewall.

An alternate ISS concept was developed which reduces the weight of the structure and virtually eliminates the AC losses. The near-total elimination of ISS losses permits elimination of the ISS coolant lines, simplifying the refrigeration system. The principal feature of the new concept is the elimination of the 5-cm-thick metallic shells, which caused high eddy current losses in the present Baseline design. The metallic shells are replaced by non-conducting G-10 shells. The circumferential stiffening ribs are steel beams which are electrically isolated from the TF coil case and from each other, thereby eliminating most of the eddy current paths. The beams are sized to react the full overturning moment on the TF coils and are built up from plate stock ranging from 5 to 8 cm in thickness. Figure 5-6 shows a cross sectional view of the ISS construction.

The I-beams and box-beams are bolted onto the sidewall of the TF coil case in the manner depicted in Fig. 5-7. A faceplate is welded to each end of the beam. A G-10 insert is placed between the faceplate and the coil case sidewall; the G-10 insert electrically isolates the beam from the coil case and also provides a means of shimming between beam and sidewall in the event of imprecise match. Electrically insulated bolts pass through the faceplate and G-10 insulating panel into the case.

The inner and outer G-10 shells are bolted to the beam flanges. The G-10 shell provides shear rigidity to the ISS module but keeps the ISS beams electrically isolated from each other.

By eliminating most of the losses in the ISS, there is a large decrease in refrigeration costs. The capacity of the cryogenic plant can be substantially reduced, which results in a savings in capital cost of about $3.4 M. Furthermore, the lower heat load affords a reduction in refrigeration system power consumption charges and demand charges over the ten-year life of the plant of about $23.3 M. In addition, the elimination of the 5-cm-thick metallic shells reduces the weight of the ISS modules by about 15%, which is estimated to save about $5.5 M in

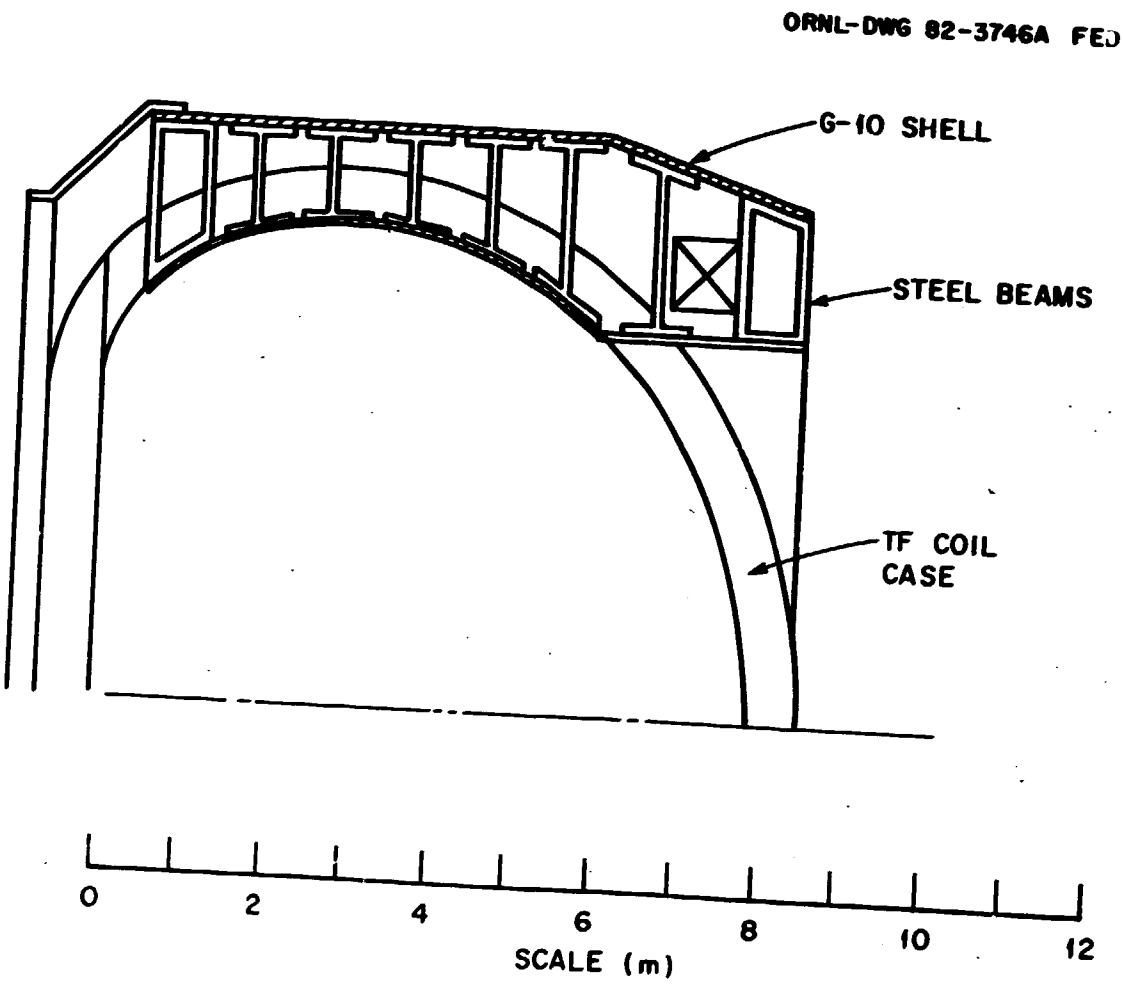

Fig. 5-6. Intercoil support structure concept.

ORNL-DWG 82-3837 FED

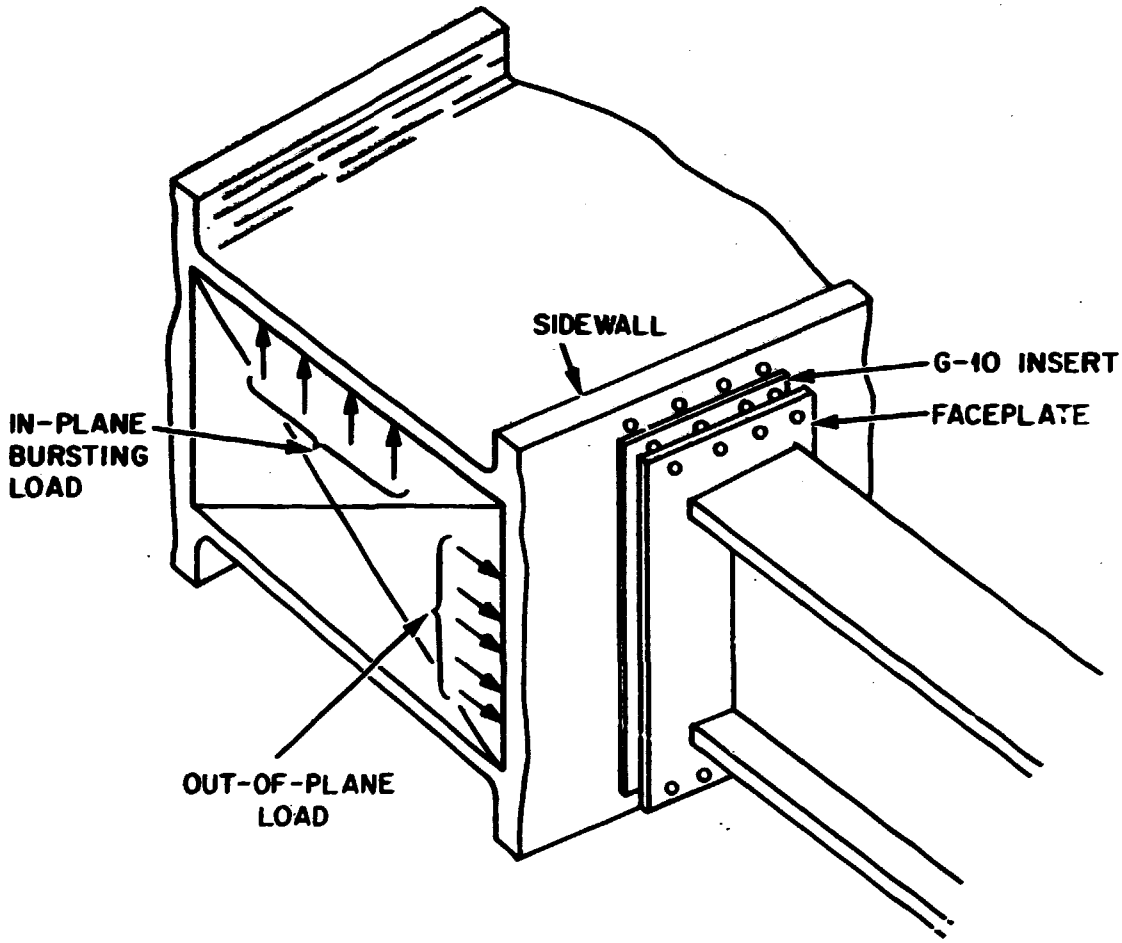

Fig. 5-7. Attachment of ISS beams to TF coil case.

fabrication cost. The combined cost savings associated with the new ISS concept is $32 M.

5.2.4 Fracture Mechanics Methodology

The structural design criteria used in the analysis of all magnet system components for which FEDC has design responsibility include a limit on peak tensile stress. This limit is based on the assumed existence of a structural flaw which can grow under the action of a cyclic stress, with the potential for eventual fracture. The size of the assumed flaw is taken as the maximum size defect which can escape detection during ultrasonic testing.

A fundamental fracture mechanics equation is used to relate the defect size, the stress acting normal to the plane of the defect, and the stress intensity factor in the vicinity of the defect tip. Growth of the assumed initial flaw is determined using the Paris equation, which is a well-known and commonly used empirical crack growth law containing two temperature- and material-dependent parameters which are determined by testing. The two equations are combined to define an allowable stress level which is below the critical failure stress by a factor S_s (safety factor on stress) following S_N design lives (S_N = safety factor on cycles).

Because of the large number of pulses for which FED is to be designed, the above criterion leads to a design allowable stress for cyclically loaded components which is only a small fraction of the material yield strength. In FED, this structural criterion is more restrictive than companion criteria which limit primary membrane and bending stresses to fractions of yield and ultimate strength. Consequently, the section thickness of several key structural components, such as TF and PF coil cases and TF coil intercoil support structure, is dictated by fatigue considerations and is much greater than if the same loads were acting as steady loads. The number of pulses in FED would have to be lowered by roughly two orders of magnitude before fatigue would cease to be a design limiter.

Because this structural criterion is design-limiting in FED, a review of the fracture mechanics methodology was conducted with the objectives of eliminating any undue conservatism and finding areas in which a refinement of the analytical procedure could lead to higher allowable stresses. The main results and conclusions are as follows:

1. For initial flaw sizes and cyclic stress levels typical of FED applications, the Paris crack growth law is conservative in that it overpredicts the rate of crack growth during the early stages of device operation. Measurements of crack growth rate vs stress intensity factor range, which are the basis for determining the parameters in the Paris equation, typically do not go down to low enough values of stress intensity factor range to include conditions representative of FED beginning-of-life operation. In the absence of better information, the Paris equation is extrapolated, which is a conservative assumption.

   It has been demonstrated that if the range of testing were extended downward to eliminate the need to extrapolate the Paris equation, significantly higher allowable stresses could be justified. Although the necessary data do not exist for the austenitic stainless steels which would be candidate structural materials for FED, such data do exist for A286. Using the A286 crack growth data, the Paris equation was replaced by a two-branch equation which reflects decreased crack growth at low values of stress intensity factor range. Use of this improved approximation led to about a 50% increase in design allowable stress. Provided data are available to properly define the parameters of such a two-branch fit, this crack growth law can be incorporated into the fracture mechanics methodology with little or no increase in effort or complexity.

   The weight of structural components which carry primarily membrane loads varies inversely as the allowable stress, whereas the weight of components which carry mostly bending loads varies inversely as the square root of the allowable stress. It is apparent that a sizable increase in design allowable stress would lead to savings

in structural fabrication that would more than offset the cost of the additional materials testing needed to justify the higher design allowable stresses.

2. The design allowable stress is taken as the more limiting solution corresponding to the previously defined safety factors 3 on stress and 1 on cycles or 2 on stress and 2 on cycles. Prior to this review, the allowable stress had been the more limiting solution corresponding to 2 on stress and 1 on cycles or 1 on stress and 4 on cycles. The new safety factors are consistent with the safety factors embodied in the companion ASME-type primary stress limits and in typical FED applications result in about a 20% increase in allowable stress.

Figure 5-8 shows the allowable stress as a function of the required number of pulses, for selected initial flaw sizes. These curves reflect the new design factors on stress and cycles.

5.2.5 Permissible Radiation Dose for Candidate Insulators

A survey of the existing test data was made to select a recommended maximum radiation dose for insulators for use in the superconducting magnets. This is important because the radiation effects in the insulators of the superconducting TF coils, or of other superconducting magnets, may determine the useful lifetime of the magnet. Requiring an acceptable lifetime in turn will determine the shielding required to protect the magnet insulator. The use of radiation-resistant insulators thus reduces one constraint on shield requirements and may allow thinner shielding and reduced reactor size.

Candidate insulators mainly fall into three categories. The preferred insulation, due to cost, availability, and experience is a glass-fabric-filled epoxy, such as G-10 or G-11. Greater irradiation resistance at higher material cost is offered by glass-fabric-filled polyimide. A much less likely group of materials is the inorganic insulators, including ceramic or glass-ceramic materials. Use of these inorganics would involve much higher costs and could require much more space than the glass-reinforced organics.

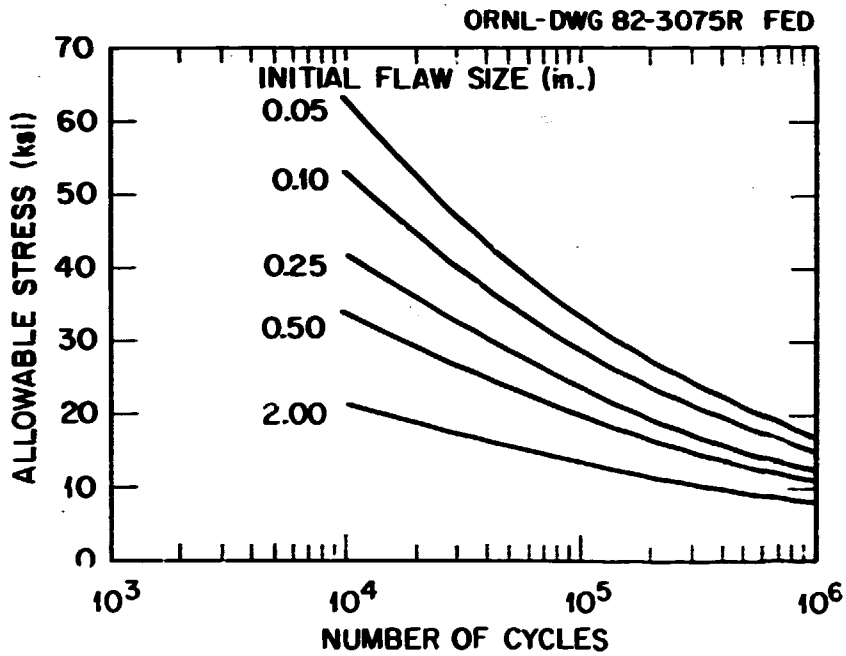

FOR A GIVEN FLAW SIZE,

$$\left(\frac{\sigma_1}{\sigma_2}\right) \cong \left(\frac{N_1}{N_2}\right)^{-1/n}$$

, n = CRACK GROWTH EXPONENT (3.26 FOR 316 LN)

Fig. 5-8. Allowable stress vs number of cycles for selected initial flaw sizes (316 LN material).

As functional components of the reactor, the insulation must withstand voltages between conductors, both turn-to-turn and layer-to-layer, and between the conductor and the magnet support structures or the case. This is not a very demanding requirement, with voltages typically quite low. A more taxing function of the insulation is to carry the mechanical loads from the conductor through to the support structure. Degradation during service of the ability to fill these functions can signal the end of useful life of the magnet.

Irradiation of solids at low temperatures can produce structural changes that are reflected in changes in physical and mechanical properties. Electronic processes (ionization and bond breaking), atom displacement, and atom transmutations result from irradiation. The electronic processes are of no importance in metals but are very important in such materials as organic solids where the breaking and healing of bonds can produce new molecules, either to be contained in the solid or to be released. Displaced atoms can rearrange to create structural defects, and transmutation can result in elements that may not be present in the original material. The irradiation field at a fusion superconducting magnet will be composed of both neutrons and gamma rays. The neutrons can produce all three of the processes mentioned, but the gammas can only produce ionization events.

Anticipated irradiation fields can produce changes in the conductivity, in dielectric strength, and in the strength properties of the insulators. Changes in the strength properties are judged to be the most likely limitation on the insulators, and there is a small amount of data on these changes. There is far less data on changes in other properties.

The data base on which to judge the performance limits of insulators for superconducting magnets is severely restricted. In addition to the scarcity of data, the applicability of the data is not always clear. Several problems compound the issue:

1. it is not clear what properties, and property levels, will be required of insulators for successful magnet operation;

2. there is little standarization of materials, so that results cannot be directly compared between different experiments;
3. ranges of test methods are used, again preventing comparison between experiments;
4. irradiation and test conditions, especially temperatures, are often not the same as the projected application temperature; few, if any, tests have been done at 4 K, without warmup between irradiation and testing; and
5. the limitations on experimental insulator irradiation programs have not allowed work to determine the mechanisms of irradiation effects. Without this understanding, extrapolation of results to more relevant properties or more relevant irradiation conditions is not possible.

Within these restrictions discussed, the available data can be examined to suggest approximate radiation limits on each class of insulator and to provide a relative ranking of the insulator classes.

The glass-fabric-filled epoxy insulations G-10 and G-11 have been irradiated and tested under several conditions. Coltman and Klabunde[6] irradiated both materials in a predominantly gamma flux. The samples were irradiated at 5 K, warmed up to 307 K, and then cooled to 77 K for testing. Flexure and compression loading showed a 25% decrease in strength resulting for irradiation doses of 2.1 to 3.7 $\times 10^8$ rads. The G-11 was superior to the G-10 within these tests. Limited examination by optical microscopy suggests that debonding between the glass and the resin is the cause of the strength loss. Part of the strength loss may be due to the warmup, however, perhaps due to the migration of gas atoms released during irradiation to the glass fiber-matrix interface. Indirect support for this assumption can be drawn from a comparison of Coltman and Klabunde's results with results obtained by Takamura and Kato.[7] The latter experimenters found strength decreases of 15% or less in the fiber reinforced epoxies irradiated to 1.1 $\times 10^9$ rad at 5 K, and then tested at 5 K or at 77 K, without any warming beyond the test temperature. These results, if confirmed, will require that reactor warming cycles be adequately simulated in test programs. The fusion magnets are expected to be warmed during their lifetime for annealing radiation-induced resistivity increases of the copper.

Similar materials were irradiated by MIT and INEL in the ATR reactor. The irradiations were at 320 K to a fluence of $\sim 10^{20}$ n/cm^2 and 3.8×10^{11} rads of gamma irradiation. Compression fatigue tests at room temperature and at 77 K indicated only modest effects of irradiation on the fatigue strength.[8,9] While these results are quoted as showing greater irradiation resistance than shown by Coltman and Klabunde, conditions of irradiation and testing are too different for comparison of the results. It would be risky to discard fluence (dose) limits based on 4-K irradiation in favor of limits set by irradiation at 320 K, when projected service is at 4 K. The long history of irradiation effects in solids shows that extrapolation in temperature is only possible when mechanisms are fully understood and must be supported even then by at least enough experimental data to confirm trends.

Coltman and Klabunde[10] tested glass-fabric-reinforced polyimide insulation under conditions similar to the tests on the G-10 insulation. Their results showed a 5- to 10-fold improvement of the polyimide over the epoxy material, with an approximate 25% loss of strength requiring a irradiation dose of 2 to 4×10^9 rad. Schultz[8] quotes results from the Rutherford High Energy Laboratory confirming the approximately one order of magnitude of superiority of the irradiation resistance of polyimides over epoxies. The quoted dose limits were 2×10^{10} and 5×10^9 rad for the two materials at an unspecified temperature, based on a loss of flexure strength.

While ceramic insulators will likely not be used in superconducting magnets for FED, they are limited by cost and space requirements, not by irradiation performance. Al_2O_3, MgO, $MgAl_2O_4$, and other ceramics have shown resistance to neutron fluences in the range 10^{21} to 10^{22} n/cm^2 at elevated temperatures but have been little studied at cryogenic temperatures. Because MgO and $MgAl_2O_4$ have cubic crystal structures and because they are relatively immune to ionization damage, their prospects for high fluence service at cryogenic temperatures are good. Tests would only be justified if the more easily used insulations prove inadequate.

Until more detailed analyses and more complete experimental data become available, the irradiation limits for magnet insulators should be

taken as 2×10^8 rad for glass-reinforced epoxy and 1×10^9 rad for glass-reinforced polyimides. The scanty experimental data suggest these values may be conservative, and experimental programs in progress should refine limits within a few years. The additional experimental work is urgently needed.

5.2.6 Thermal Analysis of Internally Cooled Conductors

To be cryostable, a superconducting magnet must have enough reserve cooling available locally from the helium coolant that the magnet will recover from a short heat pulse that drives a portion of the conductor from the superconducting state into the normal state. This reserve cooling capacity is typically much larger than the combined capacity required to remove the heat that is generated during regular operation of the magnet (e.g., for a TF coil, heat from nuclear radiation and from eddy current losses due to operation in the pulsed field of the PF coils).

Internally cooled cable superconductors (ICCS) appear much more favorable for use in large cryostable superconducting magnets after it was found[11,12] that such conductors are highly stable against short heat pulses even when the coolant, at steady state, is moving at low velocity or is stagnant. The increased transient cooling is attributed to the transient flow of helium following local heating and pressure rise.

A computer code has been developed by the National Bureau of Standards for the stability of ICCS.[13] This code is based upon one-dimensional energy, mass, and momentum balance considerations within the helium and predicts the high velocity, high pressure helium flows which are not predicted by simpler models.

This code has been modified and combined with the TASS (Thermal Analyses for Safety and Stability) code[14] to form the code SSICC (Safety and Stability of Internally Cooled Conductor). The analysis described below has been carried out with the SSICC code.

Studies of heat transfer to supercritical helium and other fluids in turbulent flow support the correlation

$$Nu \propto (Re)^{4/5} \quad (1)$$

where the Nusselt number Nu is the non-dimensional heat transfer coefficient and the Reynolds number Re is the non-dimensional flow parameter. However, the stability data from experiments at ORNL with ICCS[15] were better approximated by

$$Nu \propto (Re)^{4/15} \quad (2)$$

In the analyses described below, both correlations were used, with the proportionality constant chosen so that Eqs. (1) and (2) give the same value for Nu at Re $\sim 10^4$.

5.2.6.1 The model

A single channel of FED TF coil conductor, 173 m in length, was modeled. A heat pulse of 200 mJ/cm^3 was applied to the metal of the central 6 m of conductor in 10 ms. Steady-state conditions were first determined; the inlet temperature, pressure, and velocity were specified; and the outlet temperature and pressure and the mass flow rate were determined. Because the variation of superconductor properties with temperature is better known at 8 T than at 10 T, the 8-T, 20-kA, 4.2-K operation was modelled. Other input constants are given in Table 5-3.

5.2.6.2 Results

The steady-state results appear in Table 5-4, for background (nuclear plus eddy current) heating rates of 6 W, 7 W, and 9 W per channel. The outlet temperature is less than the current sharing temperature of 4.98 K, and thus there is no Joule heating in the conductor near the outlet.

In every case considered, the 200 mJ/cm^3 heat pulse resulted in a quench, for heat transfer coefficients governed by either Eq. (1) or (2). In the following, only the 6-W/channel cases are considered, as the others are unstable even without a heat pulse. In each case, the

Table 5-3. Parameters for stability study of ICC for FED TF coil

Parameter value	
Cross section of Nb Ti	0.588 cm^2
Cross section of copper	0.643 cm^2
Cross section of helium	2.154 cm^2
Cooled perimeter	203 cm
Hydraulic diameter	0.0406 cm
Current	20 kA
Magnetic field	8.0 T
Length of conductor	173 m
Heated length	6.0 m
Heating time	10 ms
Heat input	200 mJ/cm^3 of metal
Inlet temperature	4.0 K
Inlet pressure	5.0 atm
Inlet velocity	9.29 cm/s
Background heating	6 W, 7 W, 8 W, 9 W

Table 5-4. Computed steady-state parameters

Parameter	Units	FED coil design	6 W/channel	7 W/channel	8 W/channel	9 W/channel
Mass flow rate	g/s	3.7	3.06	3.06	3.06	3.06
Outlet pressure	atm	4.3	4.510	4.506	4.502	4.498
Outlet temperature	K	4.5	4.624	4.689	4.753	4.811

temperature and pressure rise during the 10-ms heat pulse, fall to a minimum (pressure is minimum at 15 ms, temperature is minimum at 20 to 25 ms), and then rise steadily thereafter. With the heat transfer coefficient given by Eq. (1), the minimum temperature (5.90 K) is greater than the critical temperature (5.78 K); with Eq. (2), the minimum temperature (6.43 K) lies below the critical temperature but well above the current-sharing temperature (4.655 K). Temperature and pressure are shown in Figs. 5-9 and 5-10.

5.2.6.3 Discussion

These results should be viewed as suggestive rather than definitive. The SSICC code has been applied to the experiments of Lue and Miller[15] and, with Eq. (2), gave good general agreement on current and stability margin for a 1-cm heated region of triplex conductor at 7 T but did not reproduce the multiple stability regions observed in those experiments. Moreover, the extrapolation to a different conductor, different heated length, and much different overall length conductor, plus the superposition of a background heating and an overall flow velocity, inevitably leads to uncertainties in the analysis. Additional work is needed to develop better correlation between theory and experiment.

5.3 POLOIDAL FIELD COILS

A considerable amount of new work has been done on the designing and analysis of PF coils. Alternate coil concepts have been developed using both pool boiling and forced flow cooling concepts.

A 7-T central solenoid design using pool-boiling cooling for FED has been described previously.[1] An 8-T solenoid design was developed by using a modified pool-boiling cooled conductor. The conceptual design of the 8-T solenoid is described in this section. The major problem of helium bubble clearance and removal (due to large ~10 M height of the solenoid) was studied in detail. It is shown that through a careful design of the structural support components the helium bubble clearance and removal does not affect the performance of the solenoid.

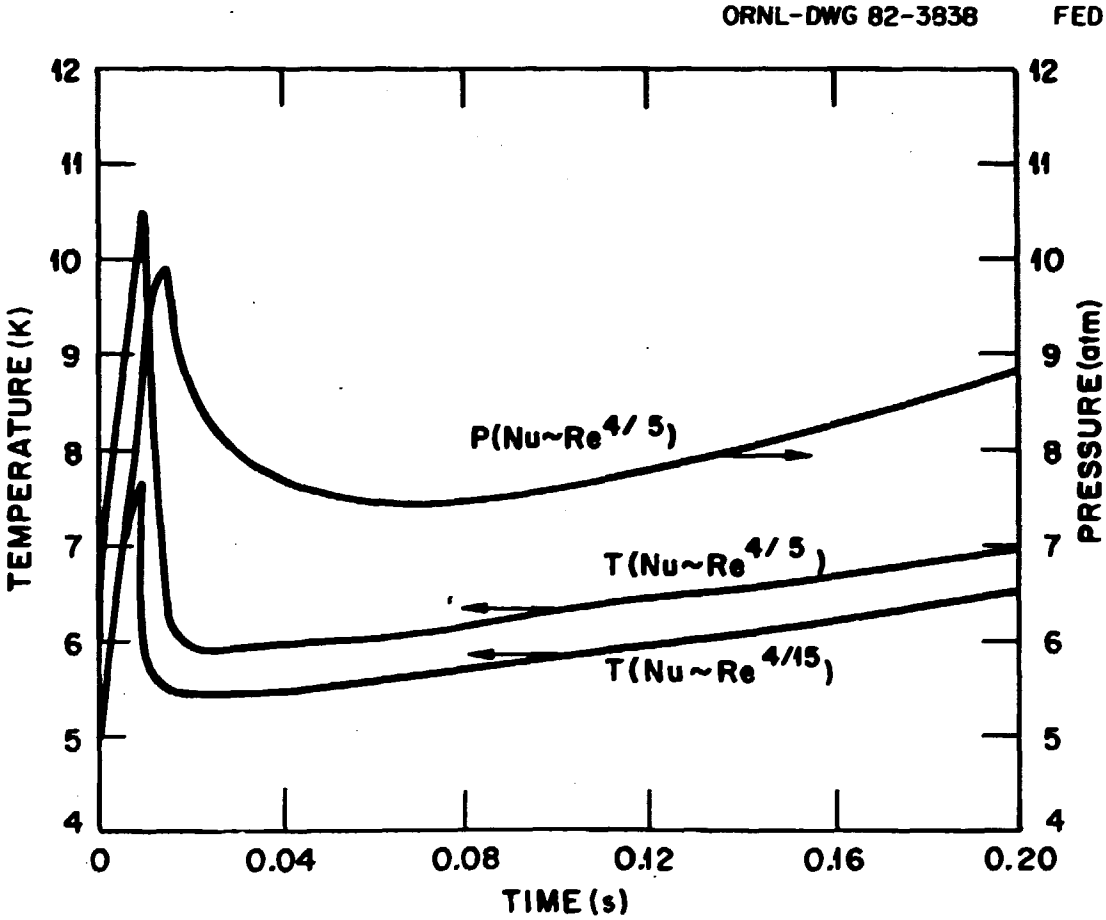

Fig. 5-9. Pressure and temperature variation in first 0.2 second.

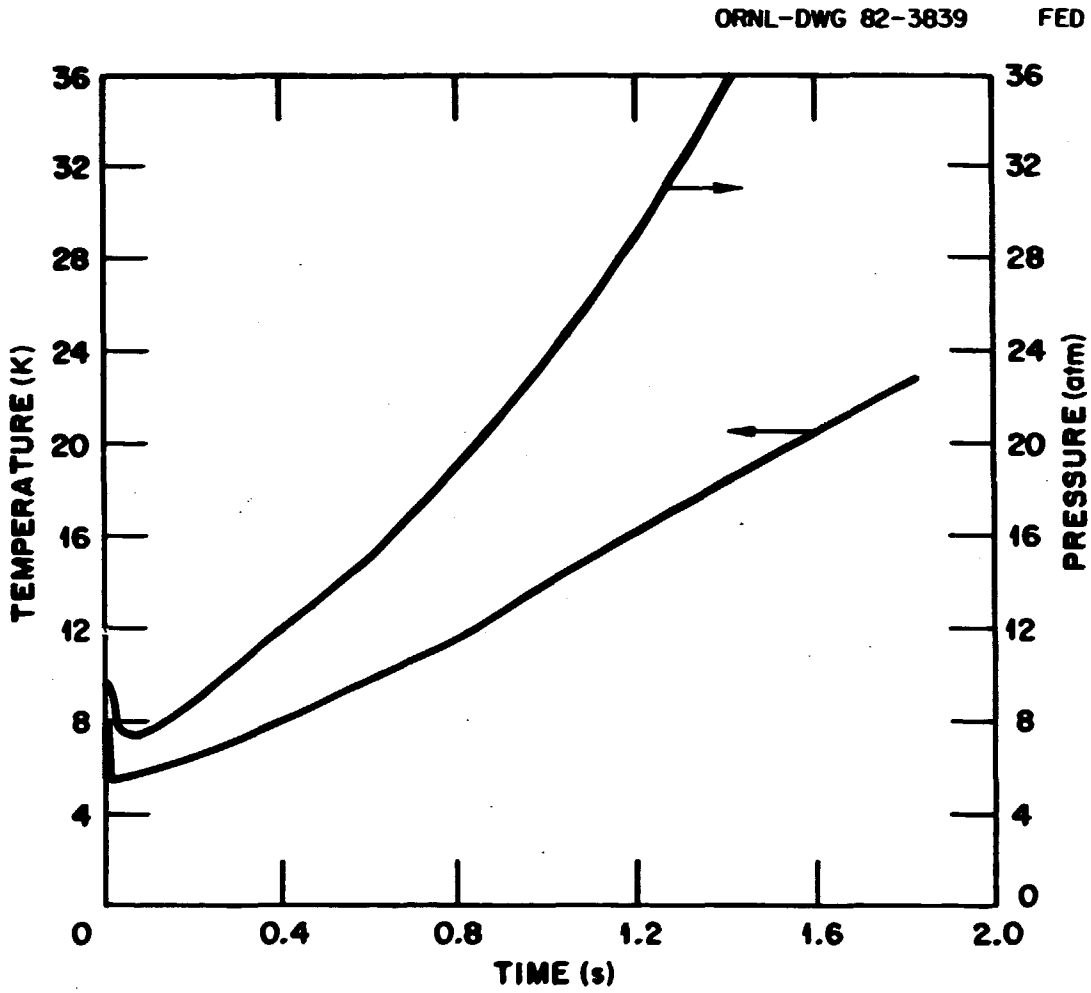

Fig. 5-10. Pressure and temperature variation of first 1.8 seconds ($Nu \sim Re^{4/15}$).

Solenoid and ring coils were also designed with forced-cooled conductor. A solenoid design for 8-T peak field was developed. Both design approaches have some critical problem which needs to be resolved for a credible coil design. For example, the pool-boiled cooled concept requires a fiberglass epoxy[1] helium vessel (difficult to manufacture), which is not needed for the forced-cooled concept. The ICCS concept, however, requires extensive helium manifolding, and there is a concern for heat removal following a thermal quench. The proposed design of ohmic heating solenoid and ring coils is discussed below using the two types of conductors.

5.3.1 8-T Solenoid Design Using Pool-Boiling-Cooled Conductor (PBCC)

The longer startup periods (6-12 s vs 1-2 s) being considered for the FED tokamaks substantially reduce the energy losses in the superconducting coils. Loss, stability, and quench recovery calculations indicate that the operating field for a PBCC central solenoid with NbTi superconductor can be as high as 8 T.

The 50-kA pool-boiling cooled conductor (PBCC) originally designed for the Los Alamos 20-MJ-scaled prototype ohmic heating was adopted as a model for analyzing poloidal field (PF) coils. Design modifications were made to that conductor to maintain stability with heat flux capability of 0.26 W/cm^2 ($I_{op}/I_{stability}$ = 0.77, measured experimentally), the number of subcables chosen to match the appropriate PF coil maximum field and provide the necessary heat transfer area, and the NbTi quantity in each strand selected to provide $I_{op}/I_c \leq 0.71$ and Cu/NbTi = 4.38. No other efforts were made to optimize the basic strand design, although a reduced NbTi filament diameter would clearly be effective for reducing the dominant hysteresis losses. The 50-kA conductor used as a model should be regarded as a generic representation of PBCC subject to specific optimization. Detailed PBCC and 8-T central solenoid dimensions are given in Table 5-5 and correspond to Figs. 5-11 and 5-12.

Table 5-5. 8-T central solenoid and 50-kA PBCC dimensions

Field, T (max)	8
Number subcables	38
Dimensions	
A, cm	13.13
B, cm	1.84
C, cm	0.56[a]
D, cm	11.86
E, cm	47.8
F, cm	3.7
G, m	0.73
H, m	1.34
J, height, m	10.93[b]
N turns per pancake coil	24
Number pancake coils	60
Current density, A/cm^2	1080[c]

[a]Central solenoid 50-kA conductor uses two strips of 0.282-cm-thick Nitronic 40 for mandrel.

[b]The height is based upon dimension A plus 0.15-cm (0.060-in.) clearance.

[c]Current density includes all G-10 CR structure indicated in Fig. 5-11.

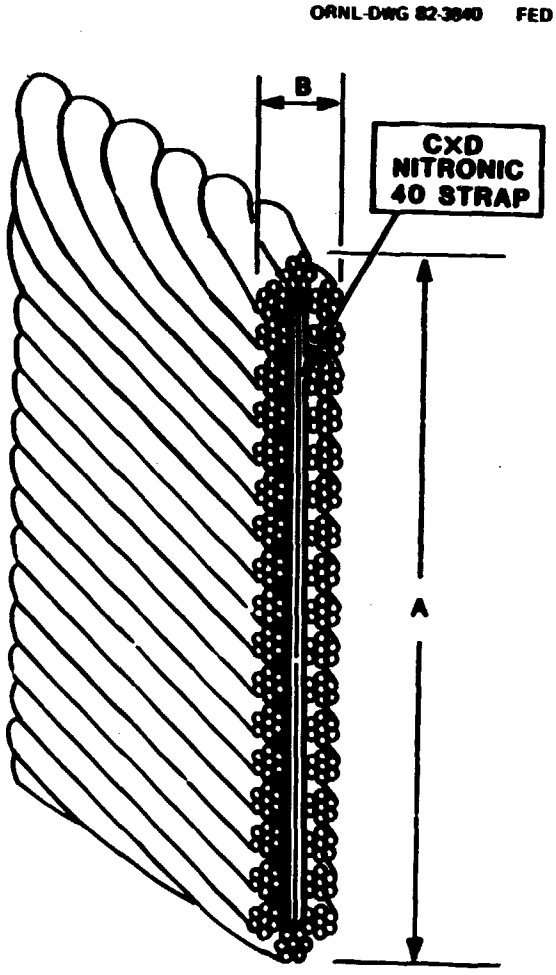

Fig. 5-11. 50 kA PF coil conductor.

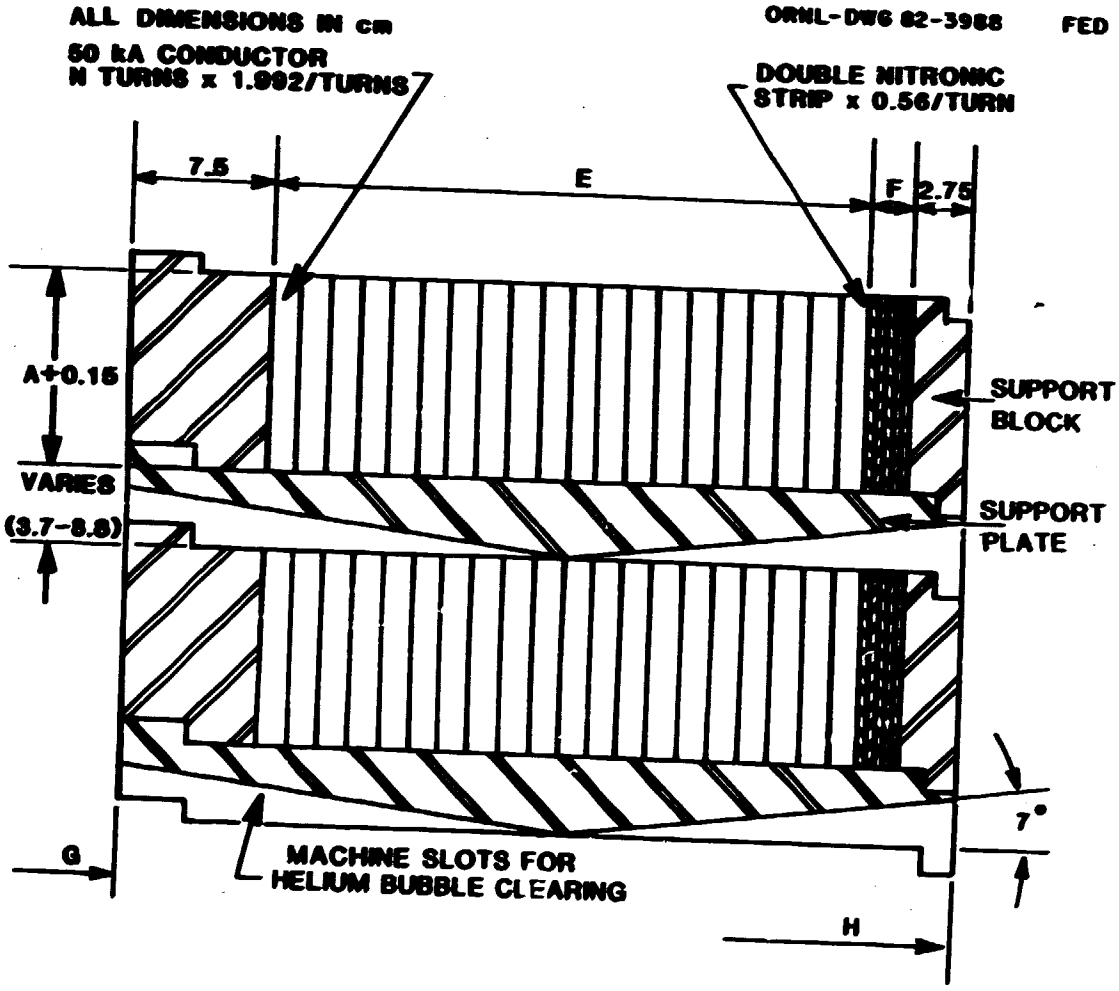

Fig. 5-12. Typical solenoid double pancake.

5.3.1.1 Losses and vapor dynamics

Losses for the 8-T PBCC central solenoid were calculated for current variations of the FED reference design (Ref. 1) modified for 6, 10, and 15-s startup. The results for the entire central solenoid for the total current variation cycles of 152, 156, and 161 s are given in Table 5-6. The vapor velocities in this and the next table (Table 5-7) are not true values but were calculated as if the vapor escapes through the flow channels between the vertical interturn spacers (Ref. 1) at the rate the gas is generated. These velocities were averaged over the entire coil and exceed, by the factors of the last row of the table, the real terminal bubble rise velocity, 0.039 m/s (Ref. 16), which is the maximum rate that helium vapor will actually move through the coil. Because these values are larger than 1, a more detailed analysis is required.

Table 5-7 gives the results of the detailed examination for losses in the innermost 8.2% high field region of the entire coil length during startup when almost all the vapor is generated. The number of pancake coils per section (0.47 and 0.91, for 6- and 10-s startup periods, respectively) in the second to last row was obtained by having divided the 60 pancake coils by the vapor to bubble velocity. Thus, fractional pancake coils, an impractical condition, are indicated as being necessary to reduce the actual vapor to bubble velocity to one. A more detailed examination of the bubble dynamics leads to an acceptable condition. In reality, during the 6 s bubbles travel 0.234 m or nearly twice the height of the conductor (13.13 cm), based on a terminal bubble rise velocity of 0.039 m/s. Thus, although some bubbles generated at the start of the cycle will still be in the vapor removal slots of the structural separator (they travel along the 7° inclined slots at 0.046 m/s or the somewhat higher unrestricted bubble rise velocity), the momentary vapor accumulation in the conductor region at the end of the 6 s is in the range from that corresponding to the instantaneous vapor generation rate at the bottom edge to 15% of the helium volume at the top edge of the conductor. This is an acceptable accumulation, and a structural vapor separator for each pancake coil is adequate. Reduction of the NbTi filament diameter to 10 μm from 22 μm, as used in the assumed

Table 5-6. FED 8-T central solenoid OH1-OH2-EF5 losses
($h < 0.26$ W/cm^2 and $I_{op}/I_c < 0.71$ at 4.5 K, 1 atm)
(basis modified 20-MJ TPFS prototype coil 50-kA conductor, entire coil)

Field, T		8	
Number subcables		38	
NbTi/strand, mm^2		0.561	
Startup, s	6	10	15
Total time, s	152	156	161
Losses overall, kJ			
Hysteresis	286	286	286
Coupling	66	45	36
Eddy	45	32	25
Total	397	363	347
Vapor generated, m^3	128	1.17	1.12
Vapor/helium space,[a] %	14	13	12.5
Velocity vapor for total coil height, 10^{-3} m/s	105	94	87
Vapor/bubble velocity for entire coil height	2.69	2.41	2.23

[a]The actual vapor/helium space percent values are less because no vapor escape from the winding is considered.

Table 5-7. FED 8-T central solenoid OH1-OH2-EF5 losses
($h < 0.26$ W/cm^2 and $I_{op}/I_c < 0.71$ at 4.5 K, 1 atm)
(basis modified 20-MJ TPFS prototype coil 50-kA conductor high heat generation region for startup times only, innermost 8.2%)

Field, T		8	
Number subcables		38	
NbTi/strand, mm^2		0.561	
Startup, s	6	10	15
Losses, kJ			
Hysteresis	35.1	35.1	35.1
Coupling	15.1	10.4	8.2
Eddy	10.1	7.1	5.5
Total	60.3	52.6	48.8
Vapor generated, m^3	0.195	0.170	0.158
Vapor/helium space,[a] %	27	23	21
Velocity vapor for total coil height, m/s	4.95	2.59	1.60
Vapor/bubble velocity	127	66	41
Number pancake coils/section	0.47	0.91	0.46
(actual)	1	1	1

[a]These vapor/helium space percent values in the conductor winding are high because the assumption is that no vapor escapes from the winding during the current cycle. Accounting for vapor escape reduces these values.

superconducting strand, would decrease the hysteresis losses by a factor of 0.45; however, as desirable as it is to reduce the losses by optimization, not generally undertaken here, a structural vapor separator is still required with this simple change.

Measurements made on the 0.54-MJ superconducting coil, developed for the Los Alamos METS Program, verify the correctness of the calculated helium bubble terminal rise velocity of this report.

Entrainment of liquid helium from pool bath cooled poloidal field coils was analyzed by the application of empirical correlations combined with theoretical expressions for entrainment. The correlations are based upon 152 data sets for perforated distillation column plates covering a wide range of velocities, spacings, and entrainment ratios for seven widely different vapor-liquid systems with considerably different physical properties. The study used here was originally developed for application to entrainment in kettle reboilers (Ref. 17).

The entrainment calculated from this analysis for the central solenoid, OH1-OH2-EF5, is E = 0.00138 kg ℓHe/kg He vapor or 0.0083 kg/s, which is negligible. Because the entrainment is essentially zero, the helium vent lines from the dewar carry only single phase vapor helium at 4.5 K.

5.3.1.2 Quench recovery and thermal margin

The recovery of the conductor after a normalcy was studied with the computer code QUENCH (Ref. 18) and by simple power balance considerations which equate the Joule losses to the heat transferred to the helium bath. The QUENCH code uses the temperature dependence of the resistivity, heat capacity, and heat transfer to the helium bath but does not directly consider thermal conductivity along the wire in its energy balance. The normalcy in the conductor is accomplished by instantaneously raising a length of conductor to some given temperature, an event which might be caused by conductor motion. Because there is no thermal conduction along the wire, the calculations are conservative and can be considered to be made on a unit length basis.

For the calculations the current was held constant during the recovery or runaway, and values of 50, 60, and 70 kA were used. Reduction

of current as an intentional protective discharge will hasten recovery and make total coil discharge unnecessary. The matrix ratio for the conductor was taken to be Cu:CuNi:NbTi = 9.8:1:2.2, and the residual resistance ratio is about 75. The total cross-sectional area of the unit cell used in the quench recovery calculation is 31.3 cm^2, with the conductor occupying 24% of the area and liquid helium occupying another 25%. The remaining space is occupied by stainless steel strap and epoxy fiberglass, which was omitted from the heat capacity calculations because of its low thermal conductivity. The geometrical perimeter of the sum of all the strands of the cable is 140.5 cm, but only 2/3 of this perimeter of 93.7 cm was used as the wetted perimeter available for heat transfer. This assumption is consistent with observations made during stability experiments on the conductor. Some of the calculations varied the value of the wetted perimeter to investigate the sensitivity of the thermal runaway temperature to this parameter.

Two different curves were used to calculate heat transfer from the conductor to the helium bath. The first is an extrapolation beyond 10 K and modification of a curve calculated for the 20-MJ prototype coil (Ref. 19). The second curve is a slight modification of the heat transfer from flat metal surfaces to liquid helium. For comparison, the first heat transfer curve is roughly 75% higher than the second for temperature differences greater than 10 K. Table 5-8 gives the parameters for the heat transfer curves.

Calculations considered the helium to be continuously replenished and investigated the recovery of superconductivity for different initial temperatures and conductor currents. For these conditions, recovery times as a function of initial temperatures are given in Table 5-9 for the 50-kA PBCC. Figure 5-13 gives the runaway temperatures for several currents in the PBCC as a function of wetted perimeter.

The thermal response during startup of the FED central solenoid was studied under the same basic power considerations as the recovery calculation. The temperature response of a strand follows the equation

$$\lambda A\, c_p \frac{dT}{d\theta} = (q_m + q_j)\, A - Up\, (T - T_b)$$

Table 5-8. Heat transfer coefficients

Curve 1	$0 < \Delta T < 3$ K	$h = 0.233\ \Delta T$ W/cm^2
	$3 < \Delta T < 7.5$	$h = 0.28$
	$7.5 < \Delta T$	$h = 0.01 + 0.036\ \Delta T$
Curve 2	$0 < \Delta T < 0.8$	$h = 1.2\ \Delta T$
	$0.8 < \Delta T < 3.7$	$h = 0.075$
	$3.7 < \Delta T$	$h = 0.001 + 0.02\ \Delta T$

Table 5-9. 50-kA PBCC recovery time for initial temperatures

$T_{initial}$, K	Curve 1	Time, s (heat transfer)	Curve 2
50	<1		3
100	5		21
150	9		72
200	12		

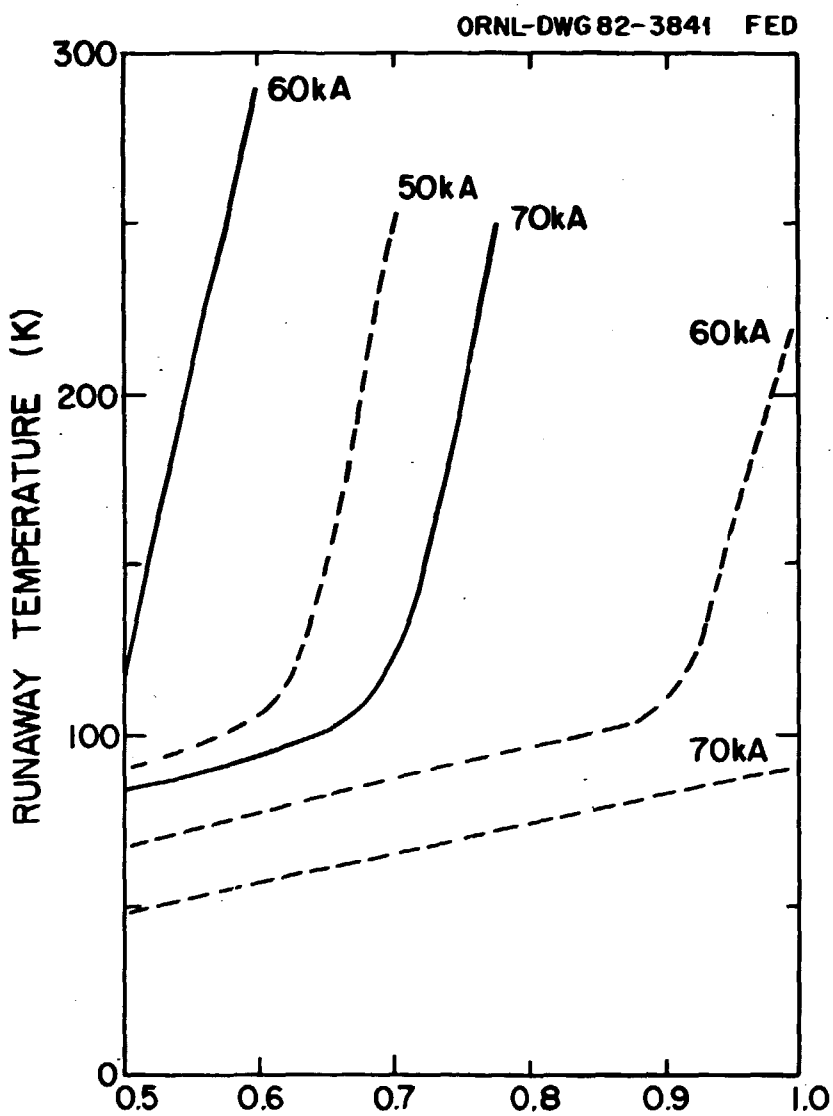

Fig. 5-13. Runaway temperature as a function of the fraction of geometrical perimeter available for cooling. Solid and dashed lines are based on curve 1 and curve 2, respectively, of Table 5-8.

where

λ is the density of the strand, g/cm^3,

A is the area of the strand, cm^2,

c_p is the specific heat of the strand, J/g-K,

T is the strand temperature, K,

θ is the time,

q_m is the volumetric heat generation during discharge, W/cm^3,

q_j is the volumetric heat generation by Joule heating, W/cm^3, and

U is the effective conductance between the strands and the helium, W/cm^2K,

p is the wetted perimeter, cm, and

T_b is the helium bath temperature, K.

The hysteretic and dynamic losses during the field swing determine q_m. This calculation assumes an initial strand temperature of 4.5 K, the same as the bath temperature. Results of numerical integration of the equation for a maximum field of 7 T and a linear field reversal in 6 s are shown in Fig. 5-14 for a wetted perimeter equal to two-thirds of the strand circumference (0.854 cm). The design is conservative, the maximum temperature excursion is only 0.02 K, and the conductor is well removed from the current sharing regime. The significance of Fig. 5-14 and the small temperature rise of only 0.02 K is that the conductor is heat-transfer-area dominated for stability and the 0.02-K temperature rise is hardly discernible. For an 8-T bipolar field swing in 6 s, the temperature rise will be 0.026 K, which is also quite small.

The pool-bath-cooled conductors are stable and will recover from reasonable excursions, such as conductor motion, that would drive portions into the normal conducting state. The thermal margin for conventional programmed current and field variation is quite adequate.

5.3.1.3 Central solenoid helium vessel

The helium vessel for the central solenoid in the FED reference design was specified as being made of epoxy fiberglass (Ref. 1). There

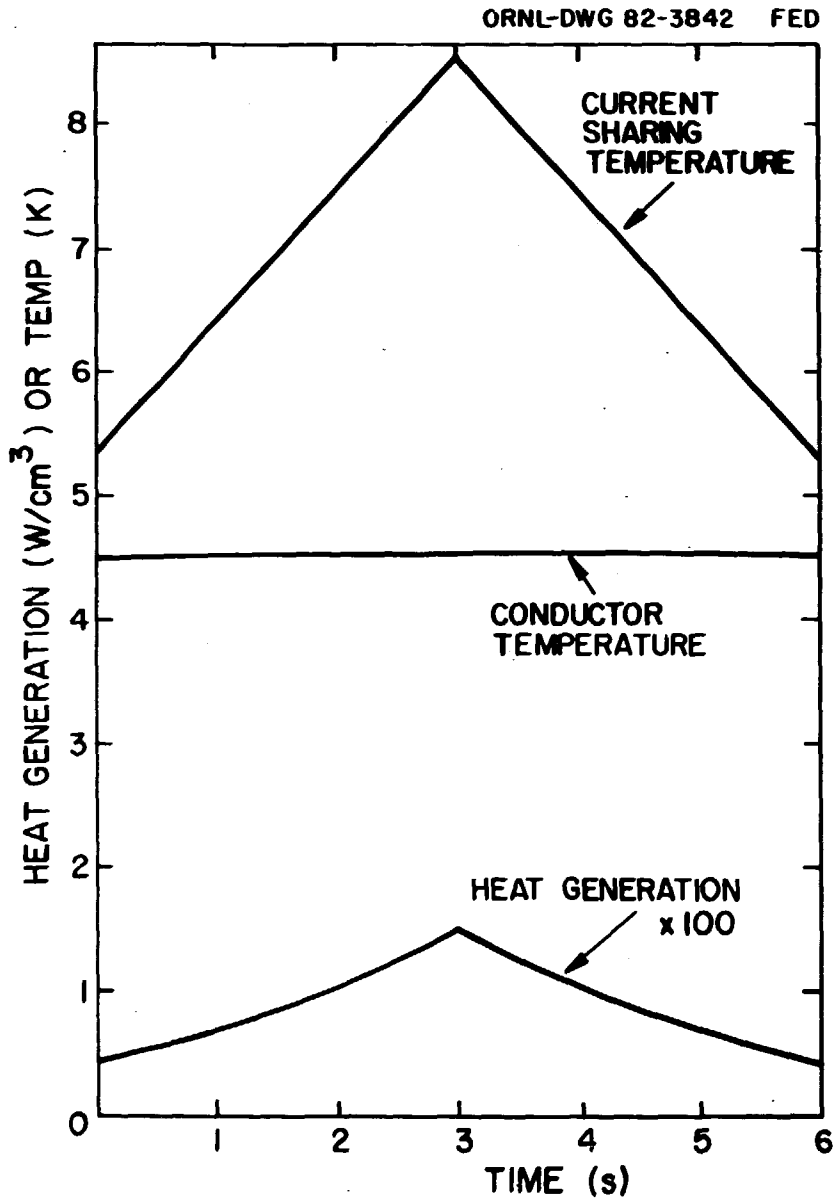

Fig. 5-14. Thermal response of 50 kA conductor in a pool bath cooled system to a 6 s total current reversal with 7 T maximum field.

are some difficulties in making large, leak-tight, all-epoxy-fiberglass vessels. An alternative to an all-plastic vessel that should be considered is the use of a composite in which epoxy-fiberglass forms the main structural support and a thin metal liner provides the seal between the helium pool and the vacuum. The welding in the metal liner must be helium leak tight, but the total weld length is small. Thin walled vessels were successfully developed as part of the early Atlas rocket program in the U.S.; and vessels of 0.25-0.50 mm thickness, integrated into an epoxy-fiberglass vessel wall for support, are reasonable to consider. The central solenoid dewar is annular shaped to minimize the volume of liquid helium required and would require a metal liner on both walls of the annulus. Table 5-10 lists losses for a composite central solenoid dewar for several alloys (Ref. 20) as candidate thin walled liners. The losses can be made reasonably low.

5.3.2 Ring Coil Design Using Pool-Boiling-Cooled Conductor (PBCC)

Ring coil designs presented in the FED baseline[1] were based on the LANL 50-kA conductor that was developed for the 7.5 T, 20 MJ pulsed coils. However, the ring coils have much lower field, and rate of change of current during startup is also low. These requirements considerably relax the design of the conductor of the ring coils. Thus, a more realistic design of these coils is presented in this section. The conductor for the PBCC central solenoid PF coil was modified with changes only in amount of NbTi to maintain $I_{op}/I_c < 0.71$ and number of subcables with heat flux <0.26 W/cm^2 for stability. Table 5-11 gives the number of subcables, $I_{op}/I_{stability}$, Cu/NbTi ratio, and NbTi cross sectional area per superconducting strand as a function of field. The basic strand diameter of 2.040 mm and NbTi filament diameter of 22 μm were retained for the design; however, for a final conductor optimization these could be changed and losses decreased, but the general results would be the same.

Dimensions for EF2 and EF3 with the modified conductor are listed in Table 5-12 for Figs. 5-15 and 5-16, which depict EF2. EF3 differs by having five pancake coils.

Table 5-10. Thin metal liner (0.25 mm) composite dewar eddy current losses

Material	4-K resistivity,* mL-m	6-s startup losses, kJ
304 L	0.50	340
316	0.55	309
Inconel 718	1.19	143
Inconel X	1.21	141
Ti-13Va-11Cr-3Al	1.57	108
Ti-5Al-2.5Sn	1.36	125

*Reference 20.

Table 5-11. 50-kA cable for poloidal field coils based on 20-MJ coil conductor

Field, T	3	4	5[a]	6	7	7.5[b]	8	8	8[c]
Number of subcables	27	29	31	33	35	36	36	37	38
I_{op}/I_{stab}	0.68	0.69	0.70	0.72	0.75	0.78	0.81	0.79	0.77
Cu/NbTi	12.9	10.0	8.5	7.2	5.8	5.16	4.15	4.27	4.38
NbTi area/strand, mm^2	0.191	0.247	0.289	0.343	0.424	0.476	0.592	0.576	0.561

[a]Used for EF2.

[b]7.5 T, 20 MJ TPFS coil.

[c]Used for the 8-T central solenoid, OH1-OH2-EF5.

Table 5-12. Poloidal field ring coils and 50-kA conductor dimensions

Coil	EF2	EF3
Field, T (max)	4.7	5.4
Field change, T	4.0	4.8
Number subcables	31	32
Mean radius, m	9.5	9.5
Dimensions		
A, cm	10.85	11.17
B, cm	1.532	1.532
C, cm	0.256	0.256
D, cm	9.58	9.90
E, cm	52.1	62.2
J, height, m	0.714[a]	0.894[a]
N turns per pancake coil	31	37
Number pancake coils	4	5
Current density,[b] A/cm^2	1298	1343

[a]The total height in these cases is based upon the vertical height per pancake of dimension A plus 0.15 cm (0.060 in.) clearance.

[b]Current density includes all G-10 structure indicated in Figs. 5-11 and 5-15.

ORNL-DWG 82-3989 FED

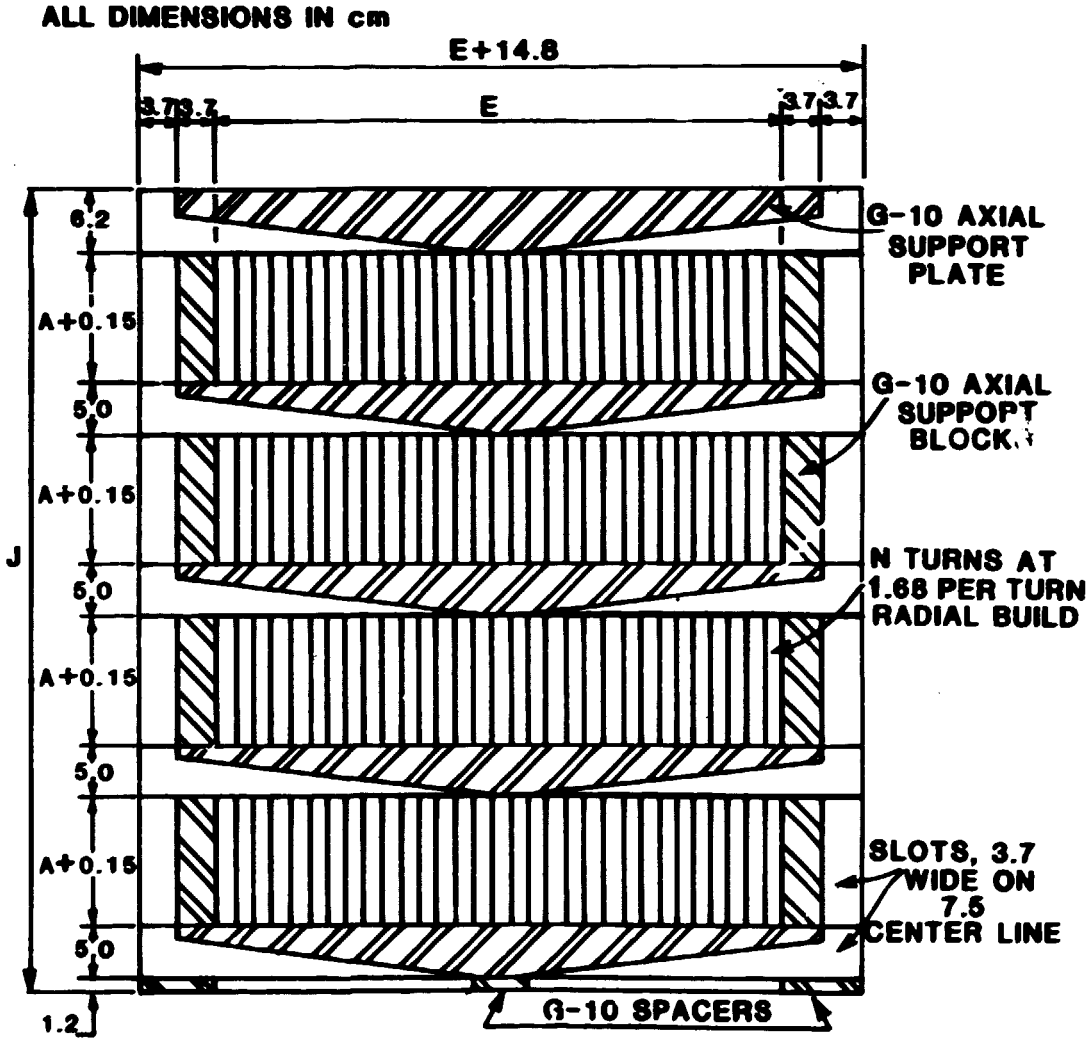

Fig. 5-15. Coils EF2 and EF3 winding pack layout. The figure shows four pancake coils for EF2. EF3 has five pancake coils.

ORNL-DWG 82-3843 FED

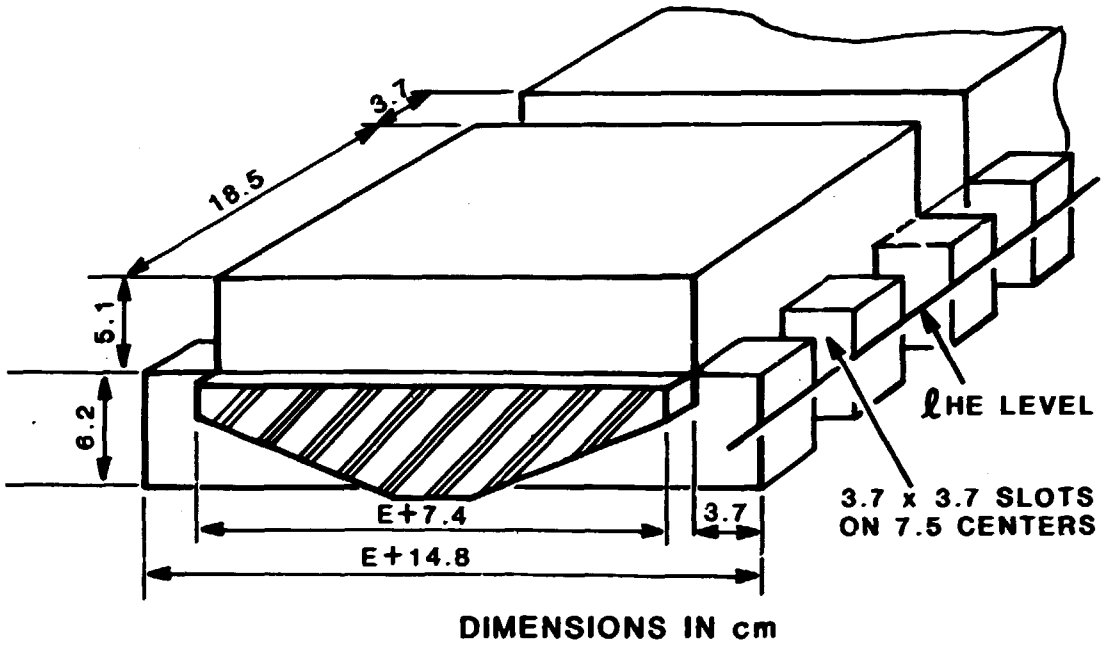

Fig. 5-16. Top structural support block for coils EF2 and EF3 to provide deentrainment and vapor removal channels.

5.3.2.1 Losses and vapor dynamics

The FED baseline design outer ring coils, EF2 and EF3, were analyzed for losses and vapor dynamics. These coils are typical of other ring coils being considered, and major diameter variations and even somewhat increased height or number of pancake coils in a given ring coil will not lead to any major changes in conclusions reached. Nearly identical results were obtained from a similar analysis performed on ring coil 11 of the INTOR design.[21]

The design analysis performed for the ring coils was the same as described in detail for the 8-T PBCC central solenoid of Sect. 5.3.1. The results are given in Tables 5-13 and 5-14. The first tabulates data for ring coils EF2 and EF3 for losses for the entire coil for the total current variation cycle periods of 152, 156, and 161 s with respective startup times of 6, 10, and 15 s. The maximum fields listed include the toroidal field (TF) coil fringing fields and all other PF coils energized without the plasma. Table 5-14 is more significant for vapor dynamics. Tabulated values are for the high field innermost 10% of the coil for startup times only when the heat generation rate is maximum. The vapor velocities are actually based upon the vapor generation rate and are fictitious values to determine whether the real vapor velocity, the terminal bubble rise velocity of 0.039 m/s, will be sufficient to remove the vapor from the winding as it is generated. The vapor (generation rate) velocities/bubble velocities are less than or close to one, and the vapor will not accumulate in the winding. Thus, interpancake coil bubble divertors are not needed for EF2 and EF3 for 4 and 5 pancake coils, respectively. In both tables the percents of coolant space occupied by vapor are low and assure that the heat transfer will not be reduced by excessive vapor adjacent to the conductor. These values are conservative because they are calculated as if no vapor escapes from the winding during the time intervals considered. The elimination of the thick structural vapor divertors in EF2 and EF3 with the use of co-wound steel to take axial loads is to be evaluated to determine if a current density increase can be achieved.

Table 5-13. FED PF ring coil losses and vapor dynamics data for entire winding

Coil		EF2			EF3	
Field, T (max)		4.7			5.4	
Field change, T		4.0			4.8	
Number subcables		31			32	
NbTi/strand, mm^2		0.289			0.310	
Startup, s	6	10	15	6	10	15
Total time, s	152	156	161	152	156	161
Losses overall, kJ						
Hysteresis	45.5	45.5	45.5	104.4	104.4	104.4
Coupling	12.6	9.0	7.3	24.8	14.9	9.9
Eddy	5.5	3.8	3.2	11.2	6.7	4.5
Total	63.6	58.3	56.0	140.4	126.0	118.8
Vapor generated, m^3	0.21	0.19	0.18	0.45	0.41	0.34
Vapor/helium space, %	3.6	3.2	3.1	5.2	4.7	4.0

Table 5-14. FED PF coil loss study and vapor dynamics data for high field region during startup period

Coil	EF2			EF3		
Field, T (max)		4.7			5.4	
Field change, T		4.0			4.8	
Region	----------innermost 10%----------					
Number subcables		31			32	
Startup, s	6	10	15	6	10	15
Losses, kJ						
Hysteresis	2.44	2.44	2.44	4.77	4.77	4.77
Coupling	1.71	1.03	0.68	3.40	2.04	1.36
Eddy	0.73	0.44	0.29	1.50	0.91	0.60
Total	4.88	3.91	3.41	9.67	7.72	6.73
Vapor generated, m^3	0.016	0.013	0.011	0.031	0.025	0.022
Vapor/helium space, %	2.8	2.2	1.9	3.5	2.9	2.5
Velocity vapor for total coil height, m/s	0.028	0.0134	0.007	0.0464	0.0222	0.0148
Vapor/bubble velocity	0.72	0.34	0.20	1.19	0.57	0.38
Number pancake coils/section		4		4.2	5	
Vapor/bubble velocity/section	0.72	0.34	0.20	1.19	0.57	0.38

From an entrainment and vapor clearing analysis made on the PF ring coils, EF2 and EF3, the FED baseline design horizontal plane projection of coolant channel areas exceed those needed for vapor escape without entrainment. This holds whether structural vapor divertors (Fig. 5-15) are used or the vapor flows upwards from each pancake coil through all the other coils in the absence of divertors. Figure 5-16 shows an alternative top structural support block for the ring coils EF2 and EF3 with dimensions. This piece increases the coil height, J, in Table 5-12 by only 5.1 cm and provides adequate flow area for vapor escape without entrainment and for vapor collection and removal. The helium liquid level, by appropriate inlet line valving, is metered as determined by redundant level sensors in the vertical 3.7 x 3.7 cm slots on the perimeters to be maintained near the mid-height of the 6.2-cm dimension to ±1.5 cm. Such control is easy to accomplish. The horizontal plane projection of the vertical 3.7 x 3.7 cm slots located on both perimeters of the support block is 2.2 m^2, which exceeds the required bubble escape areas, without entrainment, of 0.94 m^2 and 1.12 m^2 for EF2 and EF3, respectively. Maximum vapor flow velocity in the two 5.1 x 3.7 cm perimeter flow channels at the top of the support block is less than 0.7 m/s for EF3 and smaller still for EF2, based upon equal vapor flow in each perimeter slot and vapor removal from the EF ring coil dewar cases at each TF coil. The corresponding maximum pressure drop is about 0.02 in. of water or $7.2(10)^{-4}$ psi. Clearly, for such a low pressure drop fewer than 10, one per TF coil, vapor removal lines might be used. To maintain the 2(5.1 x 3.7) = 37.8 cm^2 cross sectional area of two perimeter flow channels, for compatible structural ruggedness with the EF coil dewar case, and for flow balance, ten 9 cm (3.5 in.) diameter vapor removal lines, one at or near each TF coil, are recommended. Lines as small as 5 cm (2 in.) diameter can be used with no adverse affect. These lines are to penetrate the EF dewar coil cases from the top side just above either the inner or outer perimeter flow channels. The 3.7 x 3.7 cm crossover flow channels on 18.5 + 3.7 = 22.2 cm centers between the perimeter flow channels are more than adequate to allow vapor to flow from one perimeter channel to the other.

The G-10 CR epoxy fiberglass structural support pieces, as shown in Figs. 5-15 and 5-16 dedicate about half the underside horizontal surface area to vapor clearing with 7° inclined upper surfaces in the slots. This area is more than ample for vapor bubble escape from the windings. For helium bubbles, the velocity along the slots at the 7° angle will be essentially the same as the vertical terminal rise velocity in an open bath without any small channel effect or 0.046 m/s.[16] Because each cable bears individually on a structural support piece and no axial force accumulation occurs directly through the conductor winding, vertical loading on the conductor is not significant.

5.3.3 8-T Central Solenoid and Ring Coil Design Using Forced Cooled Conductors

Poloidal field (PF) coil design employing force cooled conductors were considered because these coils are more compact and have better performance than the pool bath cooled designs.

The conceptual electromagnetic design of the central solenoid and ring coils employing internally cooled cable superconductor (ICCS) is described. The ICCS was sized to withstand the electromagnetic loads and to provide cryostable operation of the PF coils. An innovative helium manifolding concept is described which minimizes the space requirement. These coils do not require a leak-tight helium vessel. The insulating joints[1] in the coil cases, required to interrupt the eddy currents, are not required to contain liquid helium.

The various PF coils are shown in Fig. 5-17. The design of the central solenoid, EF_2 and EF_3 coils using an ICCS is feasible. The forced cooled windings have the advantages of higher current density, monolithic integral winding, and higher charge/discharge voltages. The main drawbacks of the forced cooled concept are extensive helium manifolding requirements and a concern for heat removal following a thermal quench. The winding and conductor designs are described in the following sections.

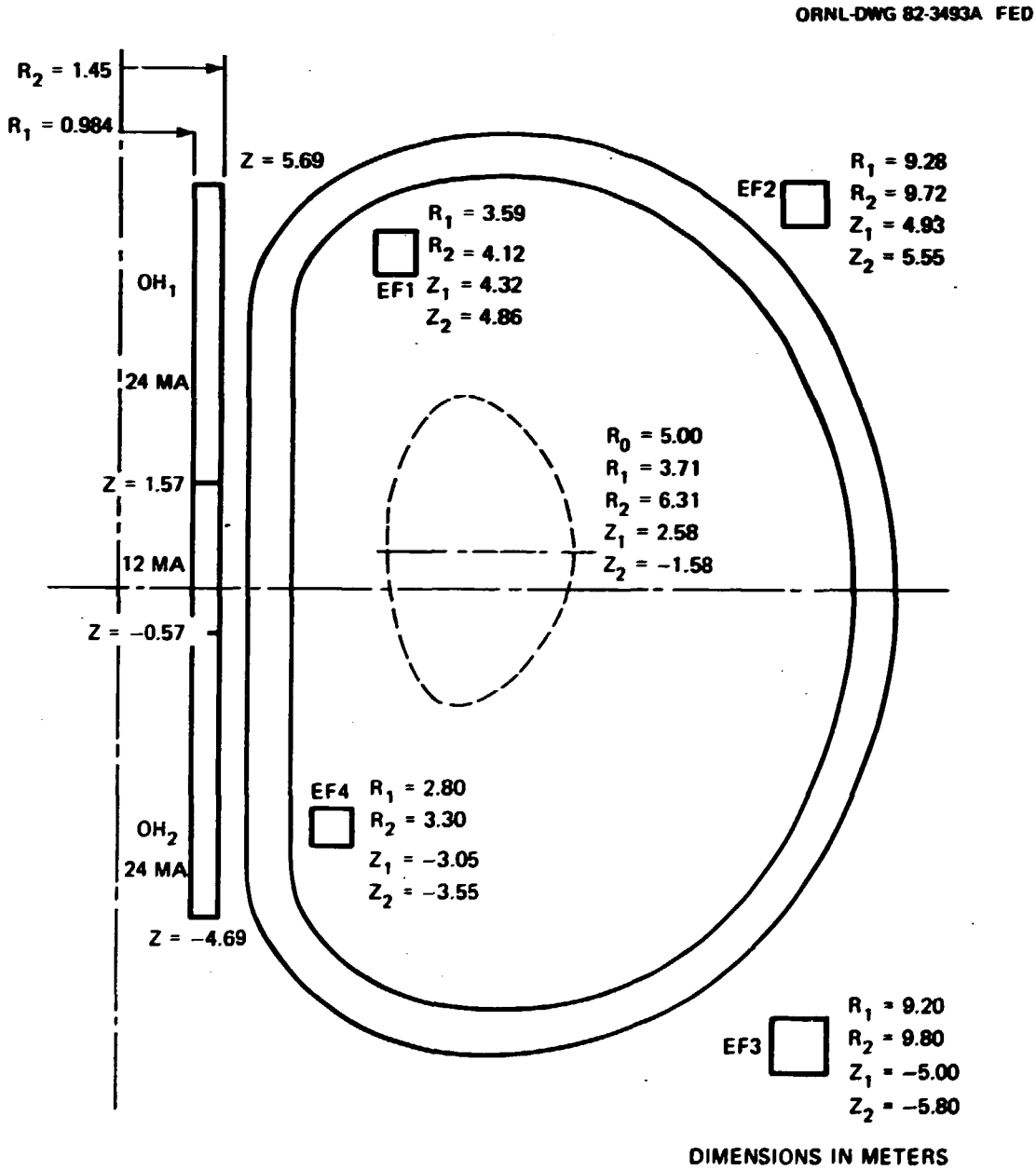

Fig. 5-17. FED 8T/10T magnetic system with forced cooled PF coils.

5.3.3.1 Central solenoid design

The major design parameters of the central solenoid (modules OH_1, OH_2, and EF_5) are summarized in Table 5-15, and the winding cross section is shown in Fig. 5-18. The operating current for the solenoid is 21,300 A, which is 60% of the critical current at 8 T. Each solenoid module is powered with a separate pair of leads. The leads are located in the central bore region.

The OH_1 and EF_5 modules are layer wound with transition joints (splices) made at the top of the winding. The splices for the layer wound OH_2 are located at the bottom of the winding. The solenoid details are shown in Fig. 5-19. The splices are made between the terminations from adjoining layers by bending the conductor out of the plane of the winding. Helium inlet connections are made at the splice, and the metallic tubing from this connection is brought to the manifold located in the central bore region. An insulating tubing (G10) is employed for electrically isolating the helium port at the conductor splice from the common helium manifold. At the bottom of the modules OH_1 and EF_5, the helium outlet connections are made by attaching metallic tubing to the conductor conduit. No conductor-to-conductor splice is made on this end. The helium manifolds and splices can be accommodated within a 20-cm axial gap between adjacent modules. The solenoidal modules OH_1 and OH_2 are layer wound with two conductors in hand to limit the helium pressure drop to less than 3 atm in the cooling path length of roughly 360 m. The EF_5 coil is wound with a single conductor in hand. The layer winding approach for these coils has the advantage of reducing the number of splices and the helium manifolding as compared to the pancake winding approach. All windings are epoxy impregnated. These windings are cooled with supercritical helium (T_{inlet} = 4.0 K, P_{inlet} = 5 atm, T_{out} = 4.5 K, P_{out} ~ 2.0 atm). These inlet and outlet conditions for the helium are chosen to provide adequate heat removal capability under normal pulsed operation and plasma disruption.

Table 5-15. Design parameters of central solenoidal modules OH_1, OH_2, and EF_5

	Reference bath-cooled design	Forced cooled design
Geometric		
Winding dimensions		
Inside radius (m)	0.939	0.984
Outside radius (m)	1.339	1.450
Height (m)	10.45	10.39
Electromagnetic		
Maximum field at winding (T)	7.0	8.0
Ampere turns (MA)	60	60
Operating current (kA)	50	21.3
Number of turns	1200	2820
Number of pancakes or layers	60	12
Winding current density (A/cm^2)	1435	1292
Maximum discharge voltage (kV)	4.0	10.0
Cryogenic		
Helium inlet temperature (K)	4.5	4.0
Helium outlet temperature (K)	4.5	4.5
Helium inlet pressure (atm)	∿1.0	5.0
Helium outlet pressure (atm)	∿1.0	2.0
Total helium mass flow rate (g/s)	Pool boiled	990
Maximum quench pressure (atm)	---	190
Cooling path length (m)	---	364
Performance		
Maximum rate of change of field (T/s)	2.3	2.7
Discharge time (s)	6	6
Maximum stored energy (mJ)	1000	1010

ORNL-DWG 82-3496R FED

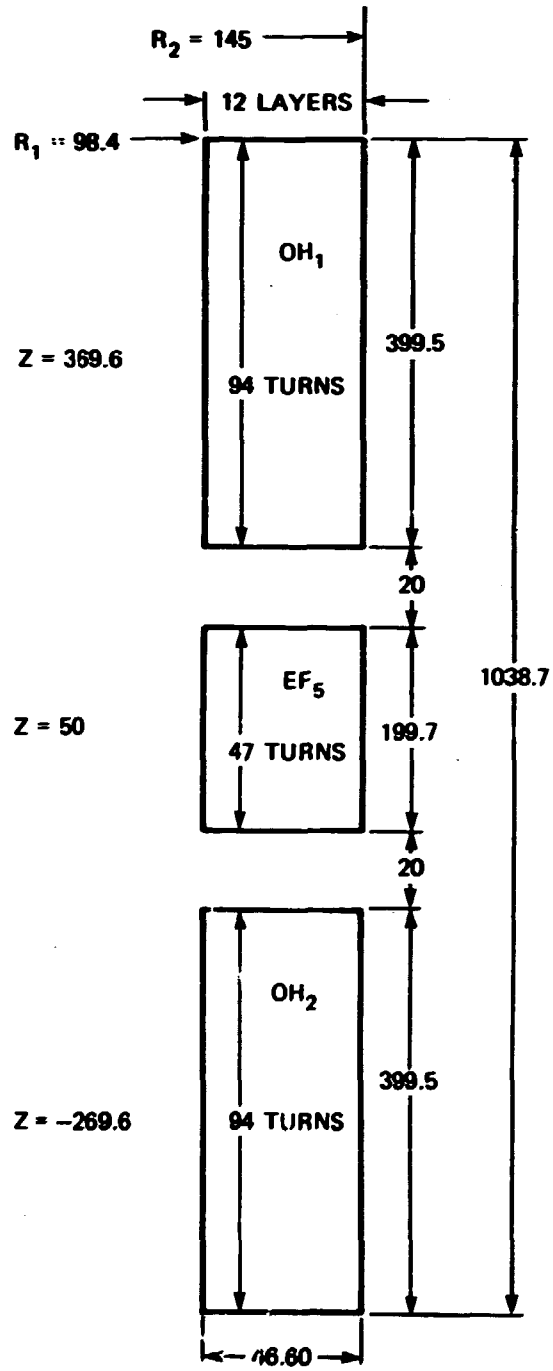

ALL DIMENSIONS IN cm

Fig. 5-18. Schematic of central solenoid cross section with ICCS.

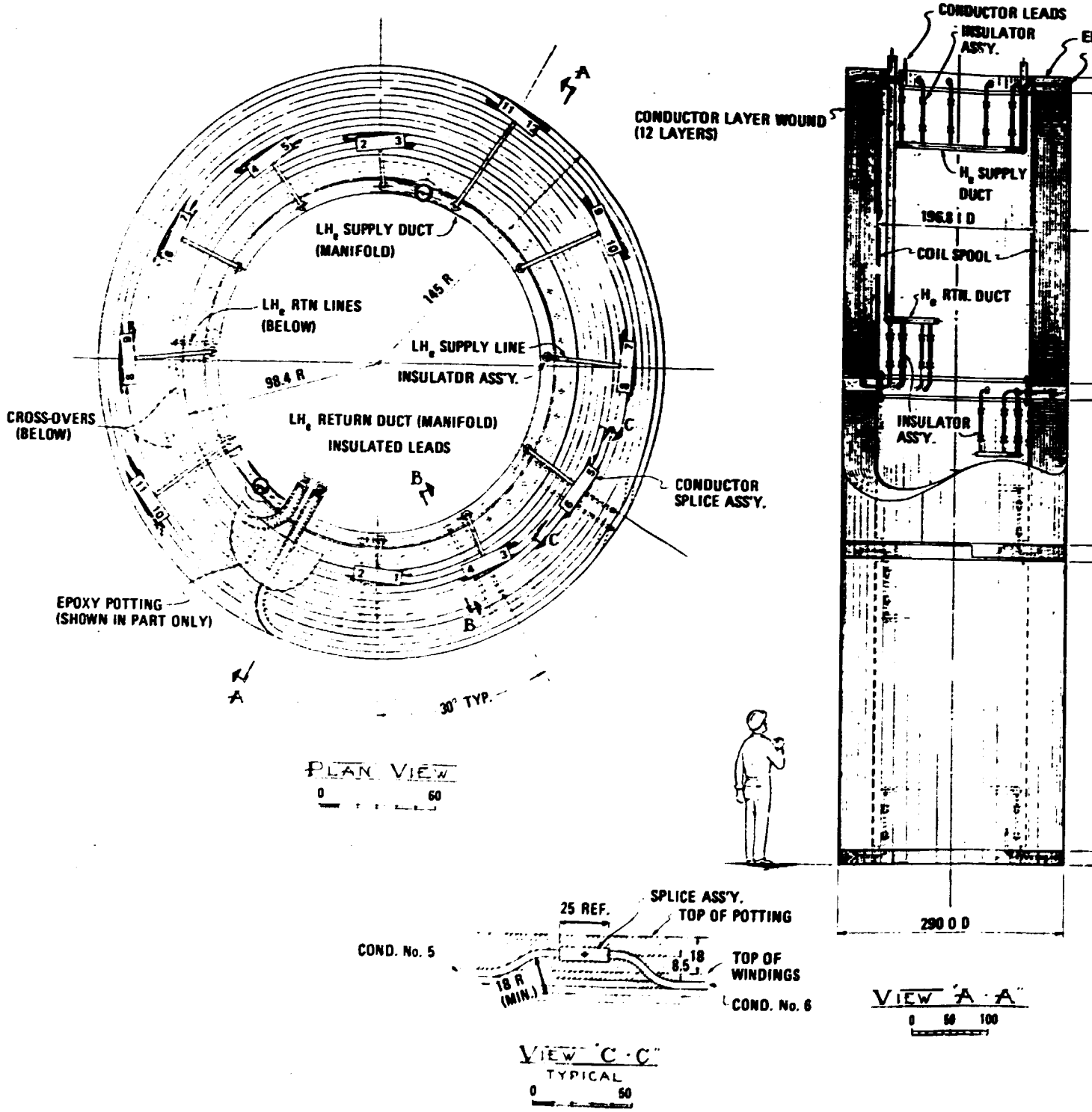

Fig. 5-19. Central solenoid, layout, splices, and manifoldi

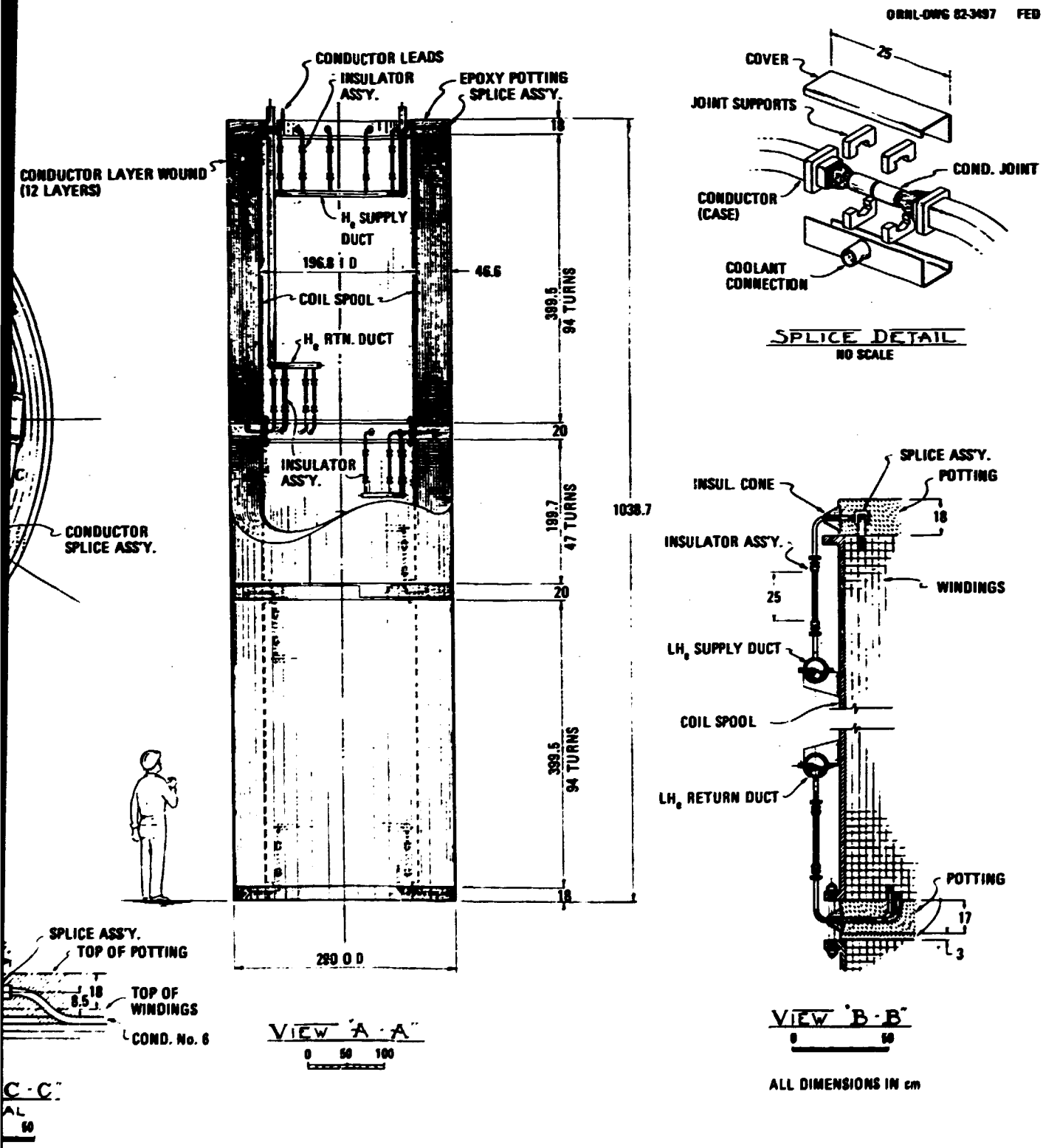

al solenoid, layout, splices, and manifolding details.

5.3.3.2 Ring coil design

The major design parameters of the ring coils (EF_2 and EF_3) are presented in Table 5-16, and the schematic cross section of the windings with ICCS conductor is shown in Figs. 5-20 and 5-21. The C-channel thickness for EF_2 and EF_3 conductors are 8.2 mm and 7.6 mm, respectively (Table 5-17). The operating currents for EF_2 and EF_3 coils are 50,830 A and 41,300 A, respectively. These operating currents are 60% of the critical current of the conductor.

The coils are layer wound with splices and helium inlet manifolding located on the top of the winding. The helium outlet manifolding is located at the bottom of the winding. Both EF_2 and EF_3 coils are layer wound with four conductors in hand for limiting the cooling path lengths to roughly 240 meters and 180 meters for coils EF_3 and EF_2, respectively. The coil cases, shown schematically in Figs. 5-20 and 5-21, are based on the structural analysis described in Sect 5.3.4.

5.3.3.3 Conductor design

The ICCS conductor used for PF coils is shown in Fig. 5-22, and its relevant parameters are listed in Table 5-17. It is similar to the conductor used for the TF coils, but it is modified to meet the requirements of the PF coils. The superconducting filament diameter has been reduced, and a cupro-nickel barrier is provided between adjacent filaments for reducing the hysteresis and coupling losses. Individual strands are insulated with a (5-μm thick) layer of copper oxide for reducing the interstrand eddy current losses. The conduit thickness (3 mm) was chosen to assure leak-free closure welds from manufacturing consideration. The conductor can withstand a maximum quench pressure of 285 atmospheres. The stainless steel C-shaped channel is co-wound with the conductor to provide a direct load path to the coil case for the accumulated magnetic loads in the winding that would otherwise crush the conductor conduit. Without the C-channel, the magnetic loads would have to be transmitted through successive conduits in the bending action (because of the

Table 5-16. Design parameters of ring coils

Parameter	Coil EF_2			
	Forced-cooled design	Pool-bath-cooled Ref. des.	Forced-cooled design	Pool-boil Ref. des.
Geometric				
Winding dimensions				
Inside radius (m)	9.28	8.86	9.20	8.61
Outside radius (m)	9.72	10.13	9.80	10.40
Mean radius (m)	9.5	9.50	9.50	9.50
Mean height (m)	5.24	5.24	-5.4	-5.40
Radial build (m)	0.43	0.71	0.59	0.82
Axial build (m)	0.62	0.78	0.80	0.96
Electromagnetic				
Maximum field at winding (T)	5.7	4.7	6.4	5.4
Operating current (kA)	50.8	50	41.3	50
Ampere turn (MA)	6.1	6.2	9.25	9.25
Total number of turns	120	124	224	185
Number of pancakes or layers	10	4	14	5
Winding current density (A/cm^2)	2280	1300	1940	1340
Maximum discharge voltage	10	2.5	10	2.5
Cryogenic				
Helium inlet temperature (K)	4.0	~4.5	4.0	~4.5
Helium outlet temperature (K)	4.5	4.5	4.5	~4.5
Helium inlet pressure (atm)	5.0	~1	5.0	~1
Helium outlet pressure (atm)	4.0	~1	4.0	~1
Total helium mass flow rate (g/s)	112		185	
Cooling path length (m)	180		240	
Maximum quench pressure (A/m)	250		264	
Performance				
Maximum rate of change of field (T/s)	0.95	0.78	1.1	0.9
Charge time (s)	6	6	6	6
Maximum stored energy (MJ)	875	900	2000	2000

ORNL-DWG 82-3498R FED

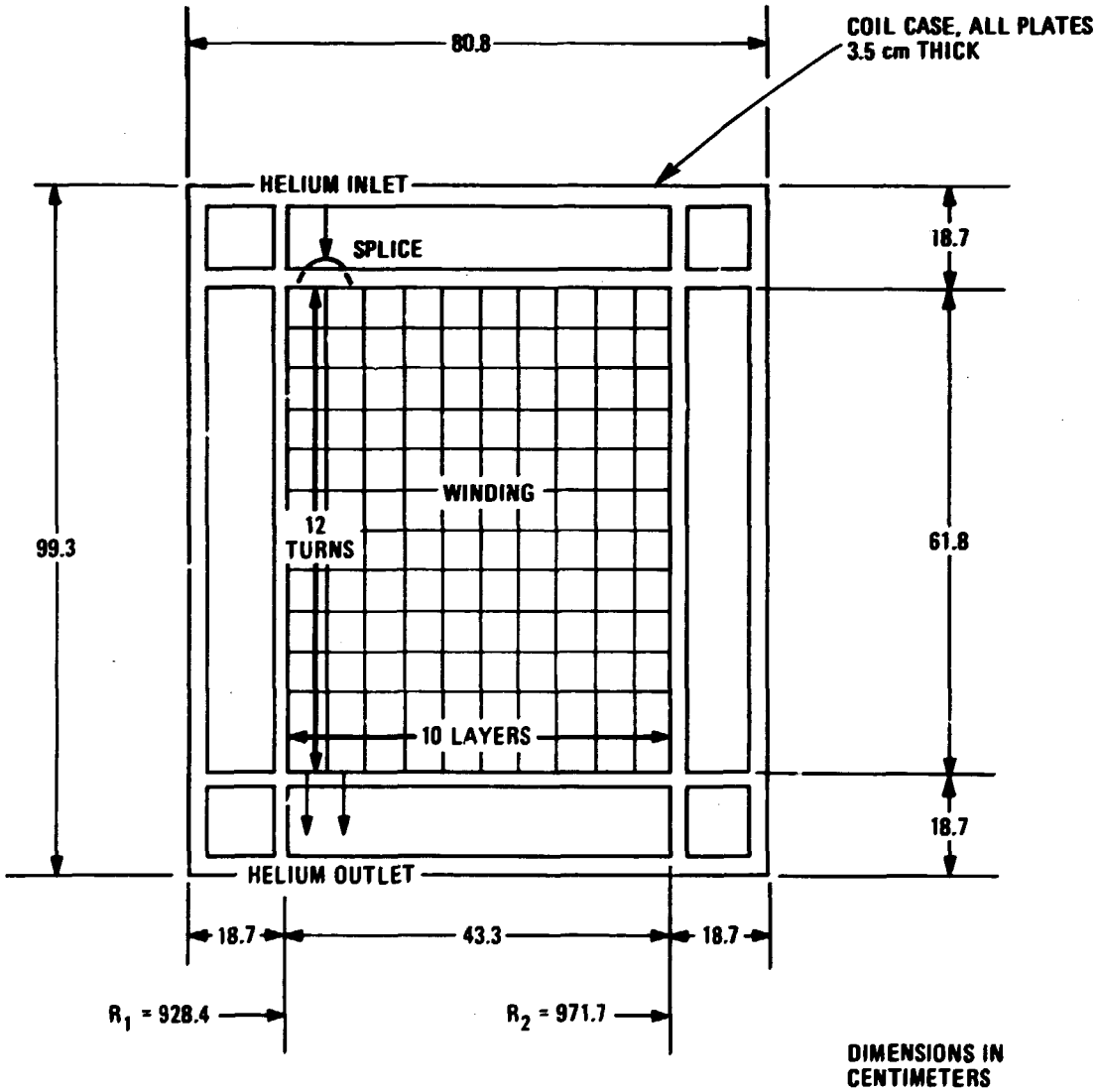

Fig. 5-20. EF_2 winding and coil case schematic with ICCS.

ORNL-DWG 82-3989 FED

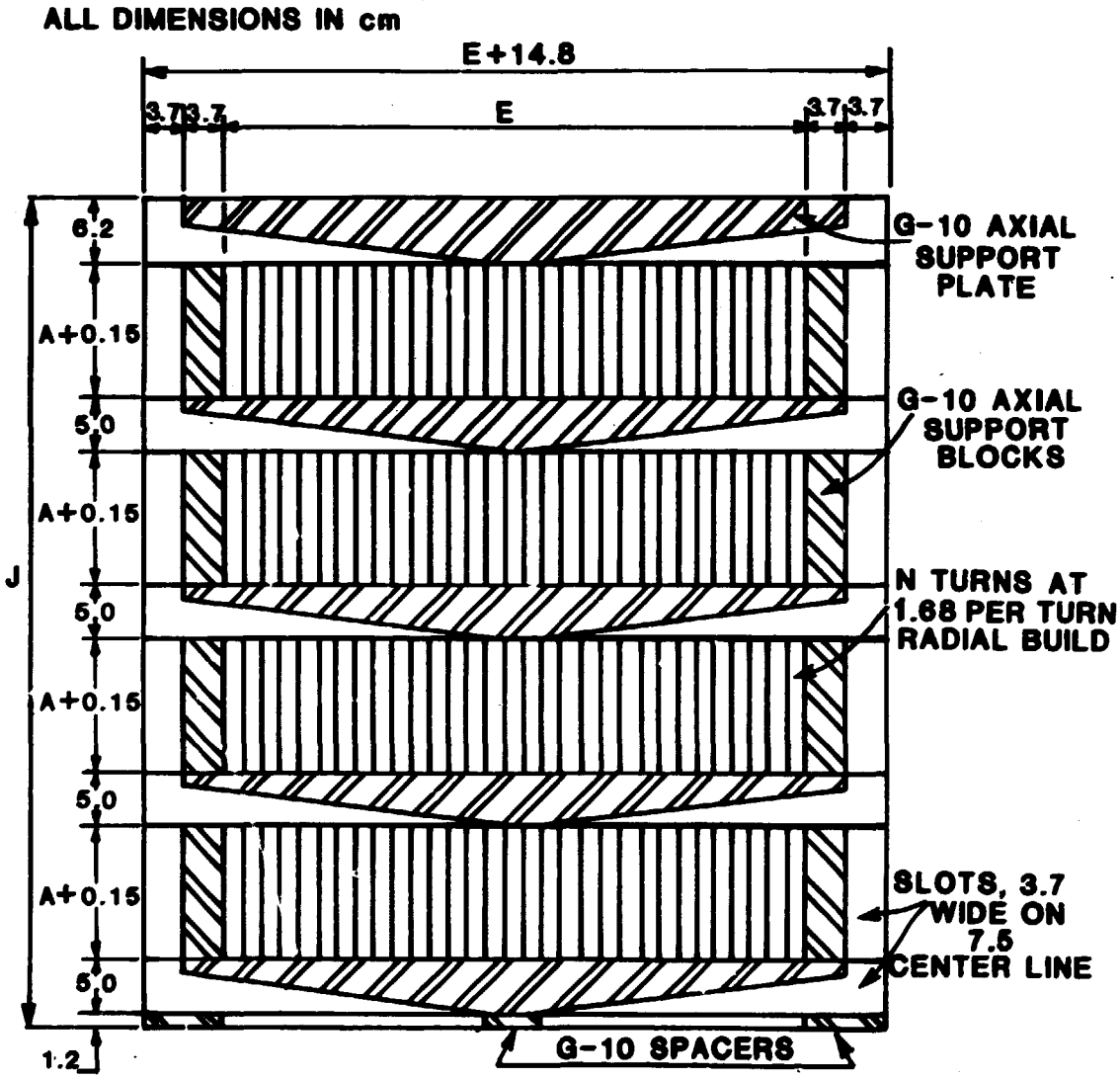

Fig. 5-21. EF_3 winding schematic with ICCS.

Table 5-17. Parameters of ICCS conductor of PF coils

Parameter	Value
Operating current at 8.0 T (kA)	21.3
Conductor current density including insulation (A/mm^2)	12.92
Critical current at 8 T (kA)	36.0
Limiting current (kA)	55.0
Overall dimensions including insulation (central solenoid)	42.5 mm × 38.8 mm
Total area (mm^2)	1649
S.S. area with insulation (mm^2)	887
Helium area (mm^2)	304
NbTi area (mm^2)	59
Copper area (mm^2)	264
Cu/Sc ratio	4.5
CuNi area (mm^2)	120
Strand insulation area (mm^2)	15
Void fraction	0.4
NbTi filament diameter (μm)	5.0
Strand diameter with insulation (mm)	0.631
Number of filaments per strand	2050
Number of strands	$6 \times 3^5 = 1458$
CuNi barrier thickness (μm)	1
Strand surface insulation copper oxide thickness (μm)	5
Filament twist pitch (mm)	15
Strand twist pitch (mm)	3.9
Thermal capacity ΔH at 8.0 T and 4.5 K (mJ/cc)	180
Max. quench pressure withstanding capability limit (atm)	285
C channel thickness for EF_2 (mm)	8.2
C channel thickness for EF_3 (mm)	7.6
Overall dimensions including insulation (EF_2)	51.5 mm × 43.3 mm
Overall dimensions including insulation (EF_3)	50.3 mm × 42.3 mm

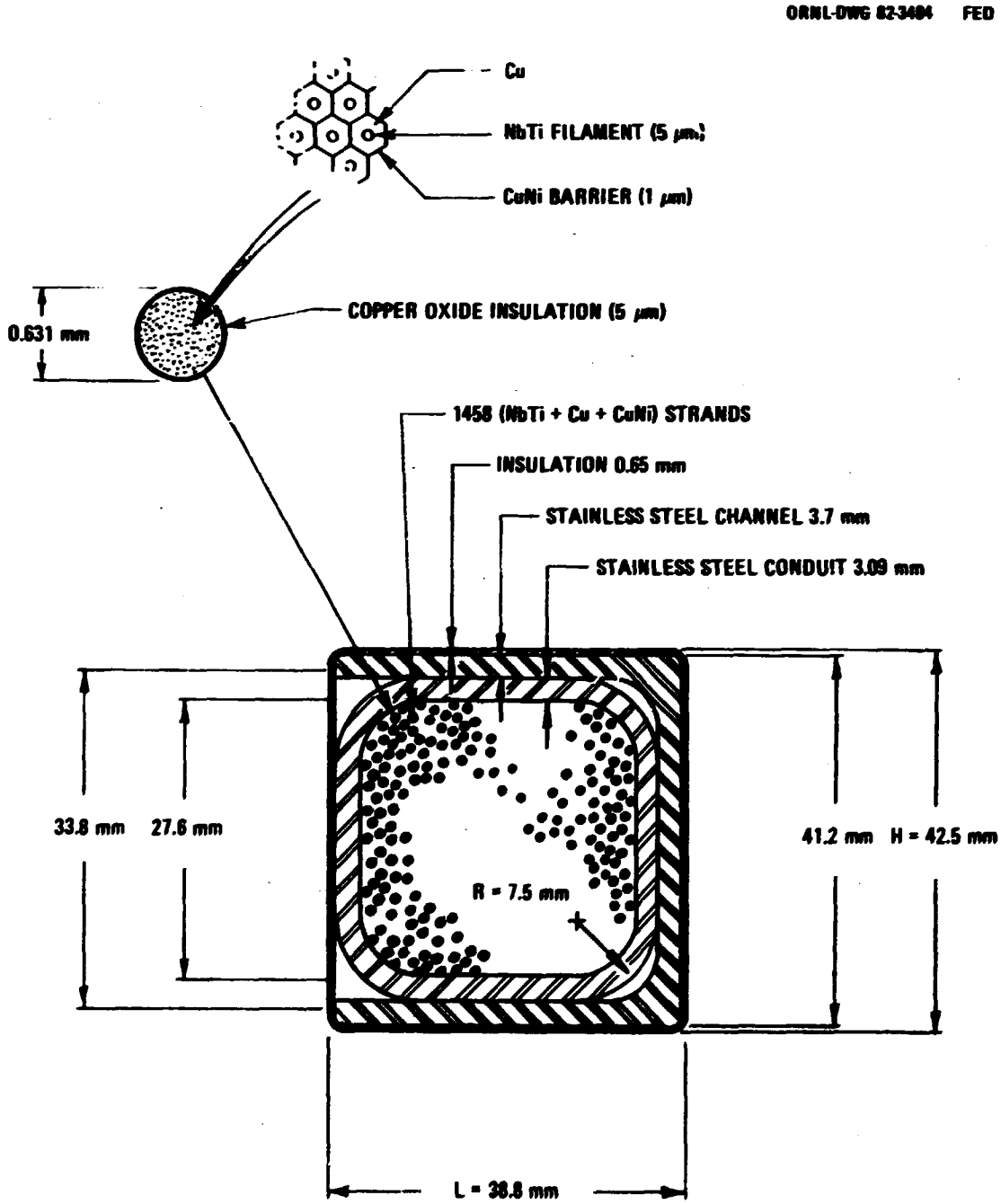

Fig. 5-22. ICCS conductor dimensions and configuration for use in the central solenoid and PF coils of FED.

rounded conduit corners) which would result in an unacceptable conduit wall thickness. The conductors for the ring coils (EF_2 and EF_3) have the same configuration (conduit and cable space) as for the central solenoid, except the C-channel thickness, which is larger for these coils (Table 5-17). The conductor and channel are prewrapped with Kapton and fiberglass tape insulation before winding. A similar ICCS[22] has been proposed for the PF coils of the Japanese Fusion Engineering Reactor (FER).

The conductor is designed to carry 21,300 amperes at 8.0 T and is cooled by supercritical helium at 4.5 K. The critical current at 4.5 K as a function of field is shown in Fig. 5-23. The operating conductor current for the central solenoid and coils EF_2 and EF_3 are chosen to provide adequate stability margin.[23]

5.3.3.4 AC losses

The winding ac losses of central solenoid coils EF_2 and EF_3 were calculated using analysis of Ref. 24. The losses were minimized by using insulated strands and optimizing the filament diameter to 5 μm in the conductor. Each filament is surrounded by a copper and cupro-nickel matrix for reducing the coupling losses in the conductor. The losses in the windings are listed in Table 5-18. The ring coil windings are subjected to relatively large axial (B_z) and radial (B_R) field components as compared to the tangential field (B_T) component. The tangential component (B_T), however, does not cause any ac losses as it is due to the steady TF coil fields. The hysteresis and coupling losses are the dominant components. The eddy current losses in the stainless steel conduit and the support channel are the most dominant component for the central solenoid due to large pulsed fields. All the losses occur during the startup period (6 s) and shutdown period (10 s) and are time averaged over the pulse cycle period of 152 s. The losses must be removed as they occur during the startup and shutdown periods without causing the conductor to lose its cryostability. The conductor losses are removed by flow of supercritical helium through the conductor to keep the coils operating in the cryostable mode, as discussed in the following section.

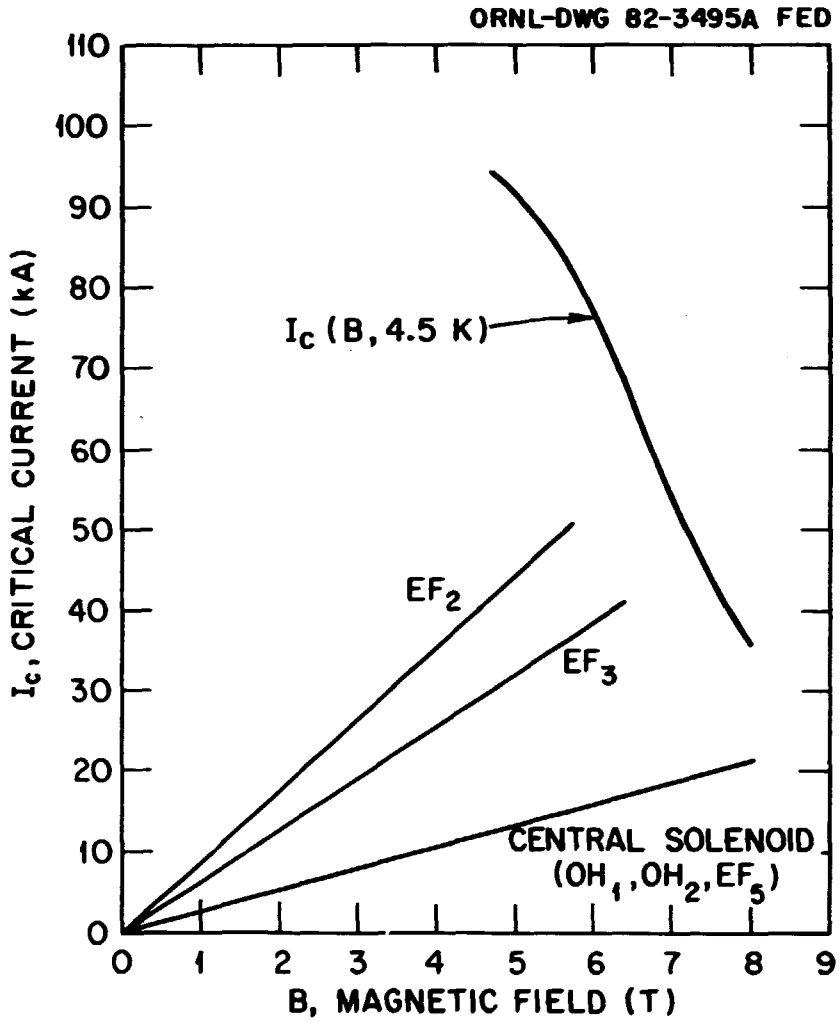

Fig. 5-23. Critical current I_c and load lines for central solenoid, EF_2 and EF_3.

Table 5-18. Summary of AC losses in central solenoid, EF_2, and EF_3 coils with ICCS conductor

(Time averaged over the cycles period of 152 s)

Coil	Losses				Total (forced-cooled design) (W)	Losses for pool-boil ref. design (W)
	B_Z (W)	B_R (W)	Splices (W)	Conduit C channel (W)		
Central solenoid	230	95	30	460	815	530
EF_2 winding	30	30	24	45	130	270
EF_3 winding	60	50	45	85	240	395

5.3.3.5 Cooling requirements

As mentioned earlier, the windings are cooled by the flow of supercritical helium (T_{in} = 4.0 K, P_{in} = 5 atm and T_{out} = 4.5 K, P_{out} ≅ 2.0 atm). It is necessary to divide the windings for the cooling purpose into sections so that the pressure drop in each cooling path is limited to ∿3 atm. The mass flow rate of helium, pressure drop, and cooling path length for the central solenoid and EF_2, EF_3 coil are given in Tables 5-15 and 5-16. The pressure ΔP along the channel length L was calculated[25] from

$$\Delta P = \frac{\dot{m}^2 P_{cool} L f}{2\rho A_{He}^3} \tag{1}$$

where $\dot{m}$ is the mass flow rate of the helium, P_{cool} is the cooled perimeter of the conductor, and ρ and A_{He} are the density and flow cross-sectional area for helium. The cooling path length was chosen to limit the pressure drop to about 3 atm. The friction factor (f) was evaluated[25] using Reynold's number (Re) given by

$$Re = \frac{4\dot{m}}{\eta P_{cool}} \tag{2}$$

where η is the dynamic viscosity of helium (a function of both temperature and pressure). The friction factor (f) has been measured as a function of Reynold's number for conductors[25] with superconducting strands. The friction factor for the conductor was calculated from these experimental measurements[25] for turbulent helium flow.

Once the pressure drop was established to a reasonable level (∿3.0 atm), the coolant mass flow rate $\dot{m}$ was calculated from the enthalpy change $\Delta h = h_o - h_i$ and the steady-state heat load q for the inlet (4.0 K, 5 atm) and outlet (4.5 K, ∿2.0 atm) conditions of the helium flow by

$$q = \dot{m}\,\Delta h \tag{3}$$

The heat transfer coefficient[26] from the conductor strands to the helium fluid was calculated from the following equations

$$h = \frac{NuKP_{cool}}{4A_{He}} \tag{4}$$

$$\text{Nusselt number (Nu)} = 0.023(Re)^{0.85}Pr^{0.4} \tag{5}$$

$$\text{Prandtl number (Pr)} = \frac{\eta C_p}{K} \tag{6}$$

where K and C_p are the thermal conductivity and specific heat for the bulk coolant conditions in the conductor. The value of h obtained using the above relationships is roughly 0.07 W/cm^2 K, which provides sufficient heat transfer capability even for a temperature difference ΔT of 0.1 K between the strands and bulk helium. The peak heat flux at the conductor strands is only 0.05 mW/cm^2; thus, the heat removal capacity per unit area is much higher than the heat generation rate. This results in maintaining the temperature of the coil winding at ~4.5 K and, therefore, keeps the winding operating in cryostable mode.

5.3.3.6 Stability considerations

All PF coils are required to remain operating in cryostable mode for the normal pulse operation and following plasma disruption. To meet this requirement, adequate helium flow must be maintained in the windings to effectively remove steady-state heat loads and to ensure recovery to the cryostable mode from localized heat inputs (due to strand or conductor movements, localized ac losses, etc.).

The winding stability for the central solenoid, EF_2, and EF_3 coils is evaluated. A summary of peak heat loads is given in Table 5-19. The ac losses in the winding were calculated[24] using the peak pulsed

Table 5-19. Peak heat loads and winding stability data for central solenoid, EF_2, and EF_3 coils

Winding	Normal pulse operation: Instantaneous heat load (W/m of conductor)	Integrated heat load (6 s) (J/m of conductor)	Load density (mJ/cc)
Central solenoid	1.1	6.6	15.0
EF_2	0.57	3.4	8.0
EF_3	0.68	4.1	9.3

	Plasma disruption – 0.10-s decay time constant at PF coils: Integrated heat load (0.10 s) (J/m of conductor)	Load density (mJ/cc)
Central solenoid	24	54
EF_2	12.5	28
EF_3	15	34

poloidal components during the startup period and during plasma disruption. The heat lead from the coil case (for EF_2 and EF_3) to the winding was neglected. This heat load, if large, can be removed by employing separate cooling channels[27] in the coil case. The maximum integrated heat load density for 0.1 s (under plasma disruption) in the conductor is 54 mJ/cc, which is less than the thermal capacity (∿180 mJ/cc) available in the helium within the winding. The basis and detailed calculations for the thermal capacity of ∿180 mJ/cc is described in Refs. 28. Thus, the winding is expected to remain cryostable during normal pulse operation and under plasma disruption.

Poloidal field coil designs employing forced cooled conductor appear attractive because they are compact and a need for non-metallic helium vessel has been eliminated. However, additional analysis is needed[28] for demonstrating that the force cooled windings provide adequate performance during normal pulsed operation and during and following a fault.

5.3.4 Structural Evaluation of Internally Cooled Cable Superconductor (ICCS) for PF Central Solenoid and Ring Coils

5.3.4.1 Design loads and material limits

The structure of the ICCS must be designed to resist several types of loadings. The conductor conduit or sheath must withstand a large internal pressure arising from a possible magnetic quench. Fabrication capability limits the conduit thickness to 3 mm and thus determines the pressure that in turn limits the length of ICCS. The conductor conduit cannot support the magnetic loads and must be co-wound with stainless channels for turn-to-turn support both radially and axially. These C-shaped channels transmit the individual conduit loads into the total load path where they become cumulative.

For the ring coils, EF2 and EF3, of the FED reference design,[1] there is the additional problem that the loadings are not axisymmetric, and large bending loads from the TF fringe fields must be carried by an external coil case or structure. Thus, to size individual turns of these ring coils to be free standing is impractical, and the loads are

allowed to accumulate from turn to turn to be transmitted to an external stiffened structural case to carry the radial dilational and radial and axial bending loads. In contrast, the ICCS and co-wound channel at the smaller diameter of the central solenoid, OH1-OH2-EF5, require no additional structure for load support.

Forces for the individual ICCSs were obtained from fields calculated from a version of BARC-13 and integrated in the plane of the cross section where the magnetic fields are maximum, or they were used as local loads in a finite element structural model code, ADINA, to determine stresses at various locations in the coils to ascertain worst-case conditions. Both the channel and ICCS conduit were considered as supporting the forces. No credit was taken for the strength of the epoxy impregnant or the superconducting cable.

The allowable design stresses are given in Table 5-20 with their governing criteria.[29-31] All structural material considered is taken to be 316 LN stainless steel with a yield stress S_y = 965 MPa (140 ksi) and an ultimate strength S_u = 1.6 GPa (225 ksi) for thin sections at low temperature. The criterion for increased design stress for operation at 10 T is an allowance for a reduced number of combined cycles.

5.3.4.2 ICCS conduit and channel design

The design equation for the conduit wall thickness is given as[32]

$$\frac{p_o L}{t}\left(0.707 + 6\, C_5 \frac{L}{t}\right) = S_D$$

where

p_o = internal quench pressure,

L = dimension of conduit = 3.061 cm (1.087 in. + 0.118 in.),

t = wall thickness of conduit, 3 mm

C_5 = bending moment coefficient dependent upon r/t for curved corner = 0.031.

Table 5-20. Allowable design stresses for structural components

Component	Design stress — S_C MPa (ksi)	Governing criteria
Conductor conduit	776. (112.5)	1. Quench pressure (noncylic loading) 2. Membrane and bending factor of 3/2 3. Ultimate stress design factor of 1/3 4. $S_D = (3/2)(1/3)S_u$
Ring coil structural channels	274. (39.7)	1. Cyclic stress limit based on flaw propagation limit S_c 2. 350,000 cycles at 8 T operation 3. Upgrade to 10 T by $(10/8)^2$ factor, $S_D = (10/8)^2 S_c$
Central solenoid structural channels	212. (30.8)	1. Cyclic stress limit based on flaw propagation limits S_c 2. 700,000 cycles at 8 T operation 3. Upgrade to 10 T by $(10/8)^2$ factor, $S_D = (10/8)^2 S_c$

Figure 5-24 shows a cross section of the conductor conduit that defines the variables pictorially. Application of this equation with S_D = 776 MPa (112.5 ksi) and the tabulated dimensions lead to a value for p_o = 285 atm. The ICCS conductor with a co-wound channel is shown in Fig. 5-25.

Figure 5-26 shows a general free body diagram indicating some of the possible load conditions. Note, however, that the purpose of the channel is to transfer the conductor forces into the overall load path. Therefore, different design models are used to size the channels under the assumptions: 1) for the non-self-standing PF ring coils, EF2 and EF3, that require external structural support, the channel can be sized as a plane strain frame; 2) for the self-standing central solenoid, OH1-OH2-EF5, an axisymmetric structural model of a radial cross section should be examined.

From the first assumption, two models can be developed. The free body diagram shown in Fig. 5-27 can be used to size the member thicknesses for a channel located at the top or bottom of the conductor array where the maximum radial field and, consequently, where the maximum axial force on a single turn occur. The lower channel member is assumed to carry one-half the vertical component of the supported conductor loading (f_z) as a cantilever frame member, and the immediately adjacent conductor frame carries the other half of the cantilever load. The design equation of this model is

$$S_D = \frac{6M_{max}}{t^2} = \frac{3f_z L}{2t^2} . \qquad (1)$$

Note that the calculated stress is not the maximum stress but is only the bending stress in the leg of the channel. The maximum stress is not used because the maximum stress is compressive (the accumulation of radial load produces compressive membrane stress in the legs of the channel) and compressive stresses do not grow cracks. Use of the bending stress for the maximum tensile stress may be somewhat conservative in that the membrane stress (compressive) tends to offset the tensile

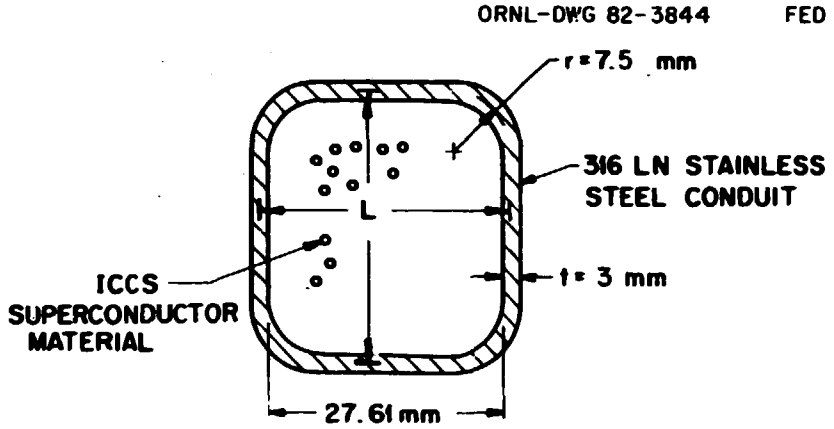

Fig. 5-24. Cross section of conduit and superconductor in the ICCS.

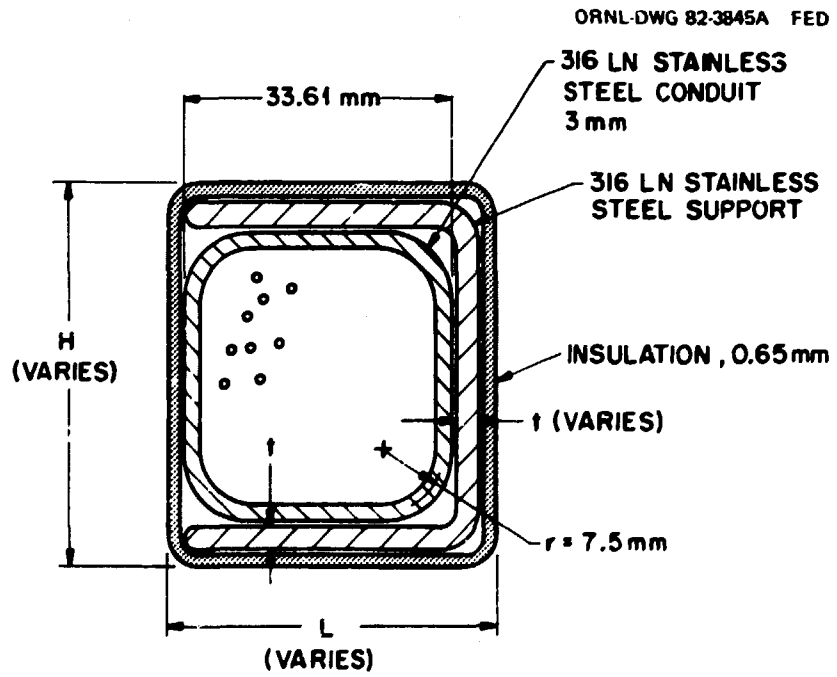

Fig. 5.25. ICCS conductor configuration.

ORNL-DWG 82-3846 FED

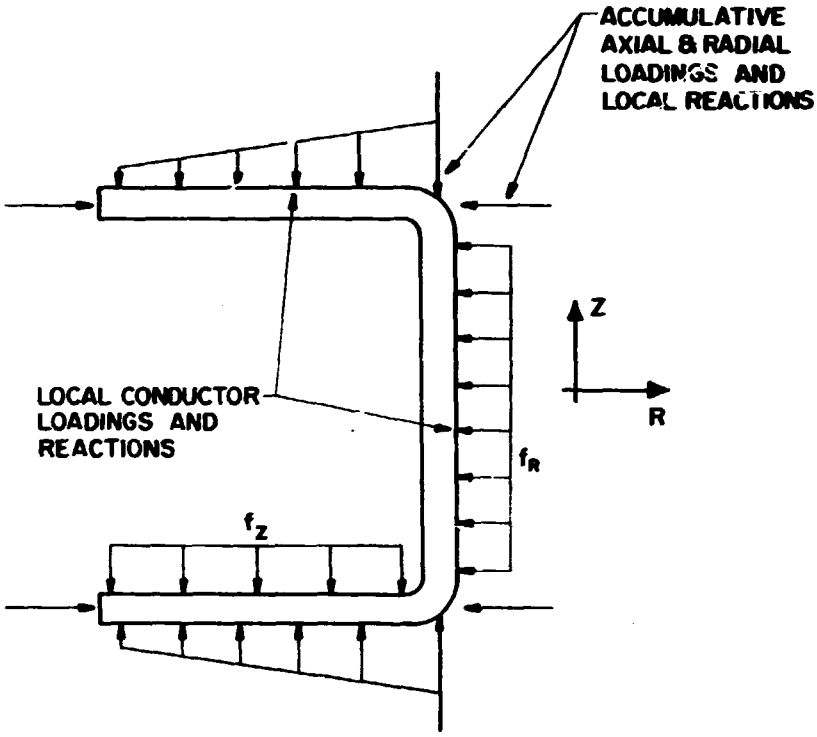

Fig. 5-26. General free body diagram of support channel.

ORNL-DWG 82-3847 FED

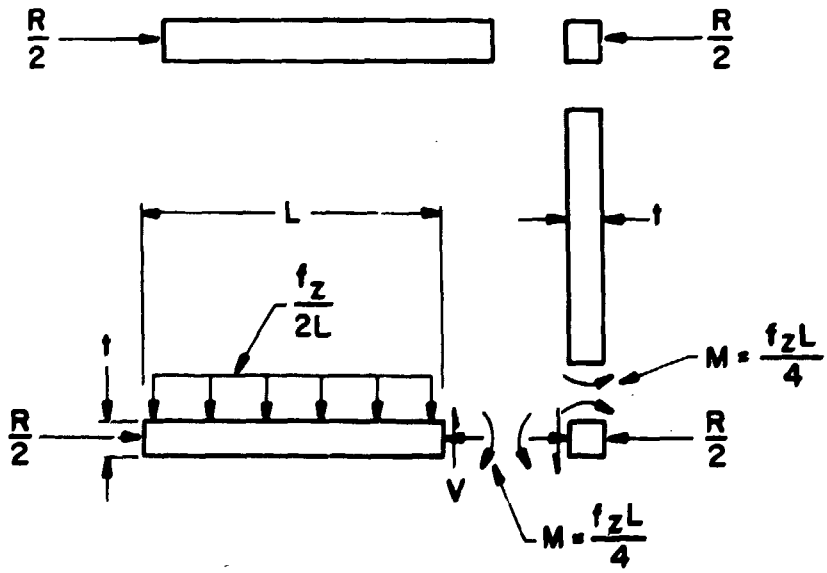

Fig. 5-27. Idealized free body diagram of a channel located on the top (or bottom) of a coil design model 1.

bending. On the other hand it is considered imprudent to depend upon the uniform accumulation of load from turn to turn to offset the tensile bending stress. In any event, the conservatism introduced by neglecting the compressive membrane stress is small.

Equation (1) can be solved for t. Note that if this model governs the design, a uniform wall thickness is implied, because approximately the same maximum moment occurs in the vertical frame member as in the horizontal member. The small ring resistance supplied by their intersection is neglected.

Another possible model that should be examined is for the inner portion of the coil where the axial force from the radial field is maximum. The design equation for the vertical member of this model is

$$S_D = \frac{6M_{max}}{t^2} = \frac{3f_R L}{4t^2} . \qquad (2)$$

As in Eq. (1) the compressive membrane stress is not included. If this model governs, the thickness of the bottom channel member is determined from Eq. (1). Note that this model only applies to the ring coils where external structural support is used to equilibrate the loads, which accumulate from turn to turn.

For self-standing coils, such as the central solenoid, the problem is not statically determinate and a radial structural model (Model 3) of the coil cross section must be used. The finite element structural code, ADINA,[34] is suitable for modeling the cross section with local radial and axial forces determined as indicated above. Figure 5-28 shows the idealized model of an axisymmetric portion of the central solenoid.

Table 5-21 includes the results of this ICCS design model. The final dimensions of all conductors can be calculated by using this table. The dimensions L and H of Fig. 5-25 are summarized in this table.

For coil EF5, the design model (Model 1) indicates the channel thickness of 2.2 mm (0.092 in.) will allow the stresses in the conductor

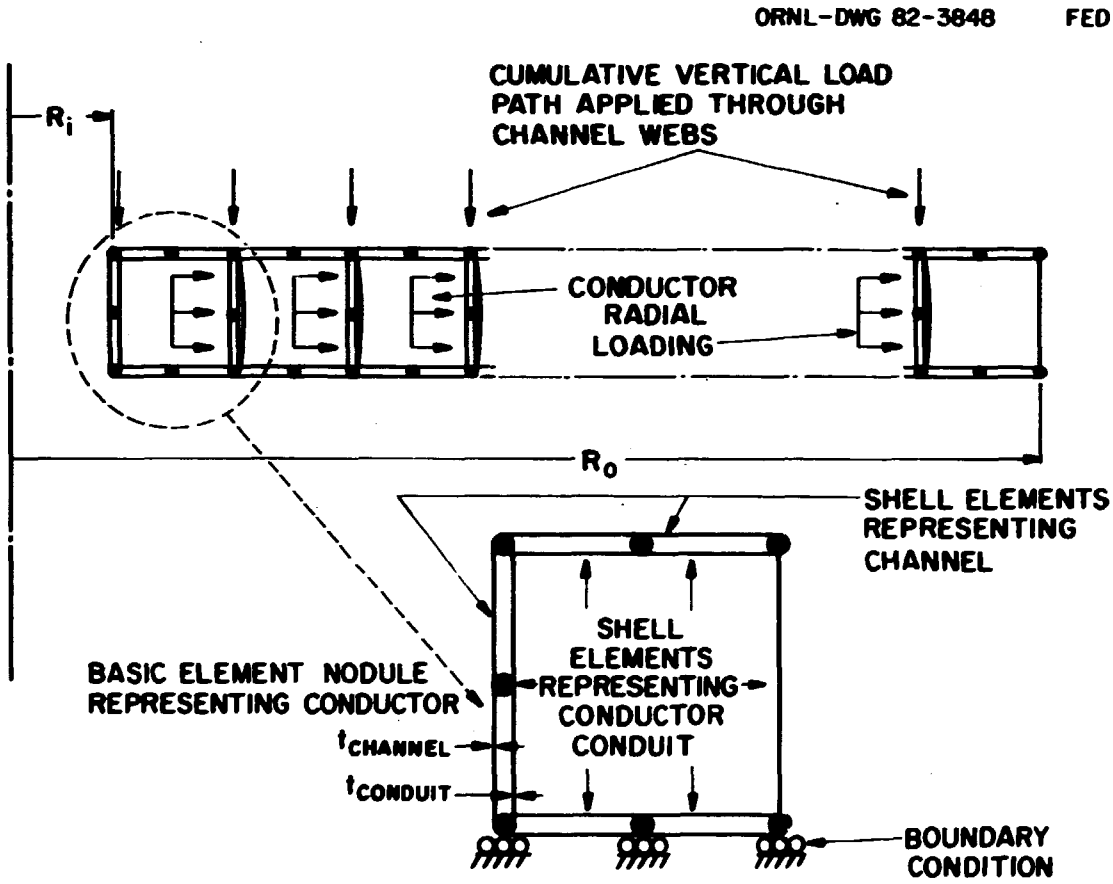

Fig. 5-28. ADINA finite element structural model of a coil cross section.

Table 5-21. Summary of ICCS support channel design

	EF_2	EF_3	EF_5	OH_1, OH_2
Model 1 Axial Loads (MN/m)	0.270	0.240	0.0174	0.072
Calculated thickness Eq. (1), mm	7.04*	6.65*	2.20	3.66*
Model 2 radial loads (MN/m)	0.252	0.235	NA	NA
Calculated thickness Eq. (2), mm	4.81	4.67	NA	NA
Model 3 calculated thickness, mm	NA	NA	1.34	1.1
Max. radial bearing stress (MPa)	57	71	very small	very small
Max. axial bearing stress (MPa)	146	152	365*[a]	346
Des. thickness, mm (summary)	7.04	6.65	3.40[b]	3.66
L (Fig. 5-25), mm	41.95	41.56	38.5	38.8
H (Fig. 5-25), mm	38.99	48.21	41.9	42.5

*Controlling criterion.

[a]Maximum allowable bearing stress on insulation.

[b]Determined by bearing stress.

conduit and channel to approach the design stress. However, if the vertical load transfer path from channel to channel is assumed to be distributed uniformly across the vertical web thickness of the channel member, then maximum bearing stresses for the insulation will be exceeded. Therefore, the channel thickness is set at 3.4 mm based on a maximum bearing stress criterion. At this thickness, the maximum hoop stress in any conductor wall is about 76 MPa (11 ksi).

Winding tensile stresses and cooldown stresses have not been included in the design. Both effects contribute principally to the hoop stresses. As seen in Table 5-24, in no case do the hoop stresses govern the design. The design is governed principally by load paths and load transfer for the vertical loadings through bending and bearing.

5.3.4.3 Ring coil case design

Coil cases were designed[32] to provide the strength needed to support the winding for the bending loads. A comparison of coil dimensions and weights (with minor revision of the values reported in Ref. 32 to reflect review comments from LANL) is given in Table 5-22.

5.3.4.4 Construction methods and forces

The purpose of this section is to anticipate problems that could affect the construction of these coils. For this discussion, winding concepts for the central solenoid are examined with relatively simple models. The central solenoid is chosen because the conductor must be wound to a tighter radius than that of the ring coils and in winding will exceed the elastic limit. Winding tension, drum or winding table torque, and other forces required during construction affect the fabricability.

The winding tension required to prevent springback and the torque required on the winding drum are estimated. The tendency to spring back after being wound around a coil form is a result of the elastic unloading moment. Because the unloading curve is elastic, the stress can be related to the elastic unloading moment through the flexure formula

Table 5-22. Comparison of forced-flow and bath-cooled ring coil designs

	Coil EF_2		Coil EF_3	
	Forced flow	Bath cooled	Forced flow	Bath cooled
Winding dimensions, in.				
Radial build	16.51	28.07	22.90	32.34
Axial build	23.14	30.88	30.37	37.85
Coil case dimensions, in.				
Radial build	31.26	50.07	37.65	60.34
Axial build	37.89	36.88	45.12	44.85
Current density, A/cm^2				
Winding	2475	1090	2060	1170
Overall	798	510	840	530
Weight, tons				
Winding	104	104	188	153
Structure	138	165	167	257
Total	242	269	355	410

Coil EF_2 — 9.5-m radius, 6.1 MAT

Coil EF_3 — 9.5-m radius, 9.25 MAT

$$S = \frac{My}{I} \tag{3}$$

where

S = the normal fiber stress at y,

y = perpendicular distance from the neutral bending axis to the fiber,

I = bending axis area moment of inertia.

The strain in the outer fibers of the channel is given by C/R, where C is the maximum value of y and R is the curvature, and is about 2.4% for the inner turn of the channel. This strain corresponds to a stress of about 303 MPa (44 ksi). The elastic unloading moment for the channel can, thus, be calculated through Eq. (3). A free body diagram shows that this unloading moment can be resisted during winding by an equivalent torque of 2RT, where R is the radius from the winding axis to the member neutral axis for bending and T is the winding tension. The product RT is the minimum required drum torque. Thus, the winding tension can be computed for each coil turn and each member. Table 5-23 shows the results of these calculations for the inner and outer turns of coil EF5. Because a two-in-hand winding technique is used for this portion of the central solenoid, the largest winding forces will be encountered during this coil construction. Obviously, these coils must be clamped to prevent relative motion of the ends while maintaining this tension or unwinding will occur.

An alternative to applying tension during winding is to overbend the conductor and allow springback to the proper radius. This method is employed in practice when a coil form is not used as applied for the Westinghouse coil for the Large Coil Program. Such a scheme might be effected for the central solenoid by overbending the ICCS on a small radius lead spool immediately adjacent to the coil as it is wound.

Another scheme which needs investigation is to overstrain the conductor to minimize the required clamping structure with additional applied tension above that of Table 5-23. The amount of tension required

Table 5-23. Construction forces calculated for winding OH1

Member	Winding tension N (lb)		Required drum torque N-m (ft-lb)	
	Inner turn	Outer turn	Inner turn	Outer turn
Conductor conduit	493 (111)	291 (66)	485 (364)	414 (310)
Channel support	1459 (328)	970 (218)	1453 (1077)	1325 (982)
Two-in-hand conductor	3904 (878)	2522 (568)	3876 (2882)	3480 (2584)

to minimize the springback can be calculated by an elastic-plastic beam analysis.

At least one additional set of forces needs to be considered for construction. When members such as channels are bent to small radii, they will tend to flatten. The web in this member also is subject to buckling. Dies or flanged wheels for preventing such actions are a normal part of the manufacturing process. Forces involved should be estimated.

5.3.4.5 Summary

This study has revealed several advantages for the ICCS concept vs the pool boiling cooled concept. Winding current density is higher in the ICCS approach, which for the solenoid has a direct effect on machine radial build. An advantage of the ICCS conductor in ring coil applications is the relative ease of providing insulating breaks in the case. Both concepts require insulating breaks in the structural cases to interrupt eddy currents; in the ICCS concept, the breaks in coil case need not be leak-tight and therefore they would be easier to design.

5.3.5 Impact of Poloidal Field Coil Faults on Coil Design and Operations

Forces, fields, and currents very different from those for regular operation of a tokamak may occur in the PF coil system under fault conditions. Unbalanced currents among TF coils, though highly unlikely, will result in high out-of-plane magnetic loading on the PF coils. The current decay time in the toroidal field coils during a dump is around 60 s, while the current decay time in the poloidal field coils during a protective current discharge is less than 10 s.[1] As a result, current can be removed from the poloidal field coils in many fault conditions before any substantial current imbalance could occur in the TF coils. For this reason, conditions arising from TF coil faults that might affect the PF coil set were excluded from consideration. A variety of PF fault mode conditions can be postulated. Only the ones thought to be most severe or unique were analyzed in detail.

Two different fault situations were evaluated. The first is the unique major disruption in which the plasma current disappears in 0.1 s. The main concern is the magnitude of the induced currents in the PF coil system. The second relates to discharge of the PF system on detection of some fault such as a normalcy in one of the PF coils. The areas of concern are the relative sizes of dump resistors for the various PF coils, the magnitude of the maximum discharge voltage, and the effect of the occurrence of a simultaneous short across any one of the PF coils during the discharge.

5.3.5.1 Modeling of fault conditions

The plasma disruption is represented by a linear ramp of the plasma current from 6.5 MA, corresponding to the 10-T toroidal field option, to zero current in 0.1 s. The long decay time constant is a characteristic of current induced in the vacuum vessel and other structures by the termination of the actual plasma current. When the plasma current reaches zero, an emergency discharge of the PF system is assumed to occur. This discharge of the PF system is produced by phasing the power supply voltages back to zero and switching appropriately sized dump resistors into the circuits. The size of each dump resistor is set by the maximum safe voltage which can be placed across an individual coil. Peak voltage values of 3 to 10 kV were considered as the credible range for coils OH1 and OH2, and cases were calculated for these extreme values. Coil EF5 has half the number of turns of either OH1 or OH2 but is closely coupled to both of them. During startup, coil EF5 requires half the voltage of either OH1 or OH2 to keep its current in phase with OH1 and OH2 current. Maximum voltage on EF5 was therefore taken to be half of the maximum voltage across OH1 or OH2. This prevents transferring current inductively between EF5 and OH1 or OH2.

The normal coils EF1 and EF4 run at much higher currents and lower voltages than the superconducting coils. Their peak current is around 120 kA and the resistive drop at this current is 140 V. The inductive voltage needed to build up current in these coils is in the range of 100

to 150 V and is mostly provided by coupling from the other TF coils. These coils can be designed to withstand the above voltages.

Each of the large diameter ring coils is poorly coupled to the other PF coils, so only self-inductance effects are important. The maximum voltage permitted on each coil depends on whether the bath-cooled or forced-flow options are used. For forced-flow cooling two cases, 3 kV and 10 kV, are used for the maximum discharge voltage just as in the case of the OH1 and OH2 coils. There has been some concern about the maximum voltage which can be applied to the bath-cooled coils without electrical breakdown to the grounded coil cases. Both the EF2 and EF3 coils have all metal cases as a support against the magnetic forces. In the FED baseline design, the maximum voltage referenced to ground for the EF2 coil was limited to 3 kV by center tapping the coil and applying +3 kV to one lead and -3 kV to the other. Coil EF3 was subdivided into three subcoils with a maximum potential difference of 3 kV across each subcoil. In the cases investigated here, peak voltages of 3 and 10 kV, as labeled on the figures, were allowed <u>across each subcoil</u> during an emergency discharge. This is equivalent to putting 6 and 20 kV across EF2 and 9 and 30 kV across EF3, if they were single coils. With this technique for energizing EF2 and EF3, the power supplies and dump circuits must be interlocked to ensure that current is the same in all subsections of the coil. The subsections are so well coupled that if two sections of EF3 were brought to zero current, the third section could have its current almost tripled through inductive coupling.

5.3.5.2 Results

The effects of a disruption and an emergency discharge of the PF system were calculated in one time sequence. The sequence begins 12 s after the start of the tokamak heating cycle when currents in the plasma and all coils are close to their maximum values (Ref. 1). The plasma current is brought to zero over a period of 0.1 s with all coils shorted. After the plasma current is brought to zero, it is assumed that it remains zero for the rest of the sequence. As soon as the

plasma current reaches zero, an emergency discharge of the PF coil system is begun. In addition to a conventional discharge of the PF system, the cases in which one of the superconducting coils shorts at its terminals at the beginning of the discharge were investigated. Currents in the coils are displayed in Figs. 5-29 through 5-32, with zero time assigned to the start of the disruption. The "forced flow" and "bath cooled" terms in the figure titles are necessary because the coils for these two options operate at different currents and have different numbers of turns. For reference, Table 5-24 gives the parameters of the internally cooled cable superconductor (ICCS) or forced flow PF coils. The plasma has also been represented by a coil of rectangular cross section. Table 5-25 gives the number of turns and peak currents for the pool bath cooled conductor (PBCC) coils; the other parameters are very similar to those of the ICCS coils.

Inspection of the figures shows that a disruption has only a minor effect on the PF field system because of poor coupling. Current actually decreases in the superconducting coils because of the opposite current direction of the plasma. The effect of shorting an EF coil during the emergency discharge is also relatively small, except for coil EF5. Because the effect on all the PF coils, each considered to be shorted in turn during a discharge, is small, only the large effect on coil EF5 is shown in Figs. 5-30 and 5-32. Note that the current in coils EF1 and EF4 and the plasma current were scaled to fit on the graphs. The difference between 3 and 10 kV peak discharge voltages is what would be expected; it takes three times longer to bring the current down to any given level with 3 kV across the coil than it does with 10 kV. The discharge times are comparable to the time required for plasma startup because the voltages are comparable. Table 5-26 gives the change in current, starting after the plasma disruption, for each of the superconducting coils as the result of shorting only that coil during an emergency discharge. The current changes listed are small, as already indicated, except for coil EF5, which is closely coupled to OH1 and OH2, and should be compared with the normal operating currents listed in Tables 5-24 and 5-25.

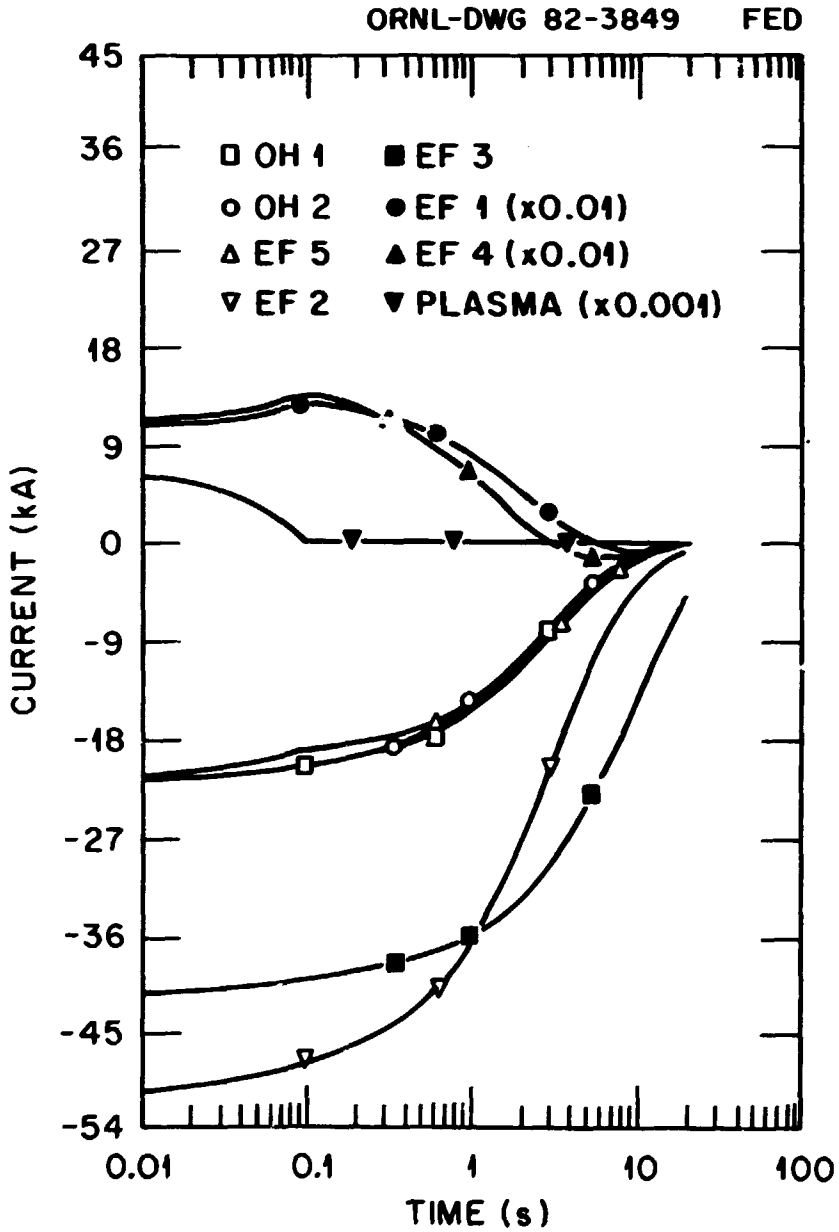

Fig. 5-29. Forced flow, ICCS 10 kV discharge voltage with no coil shorted.

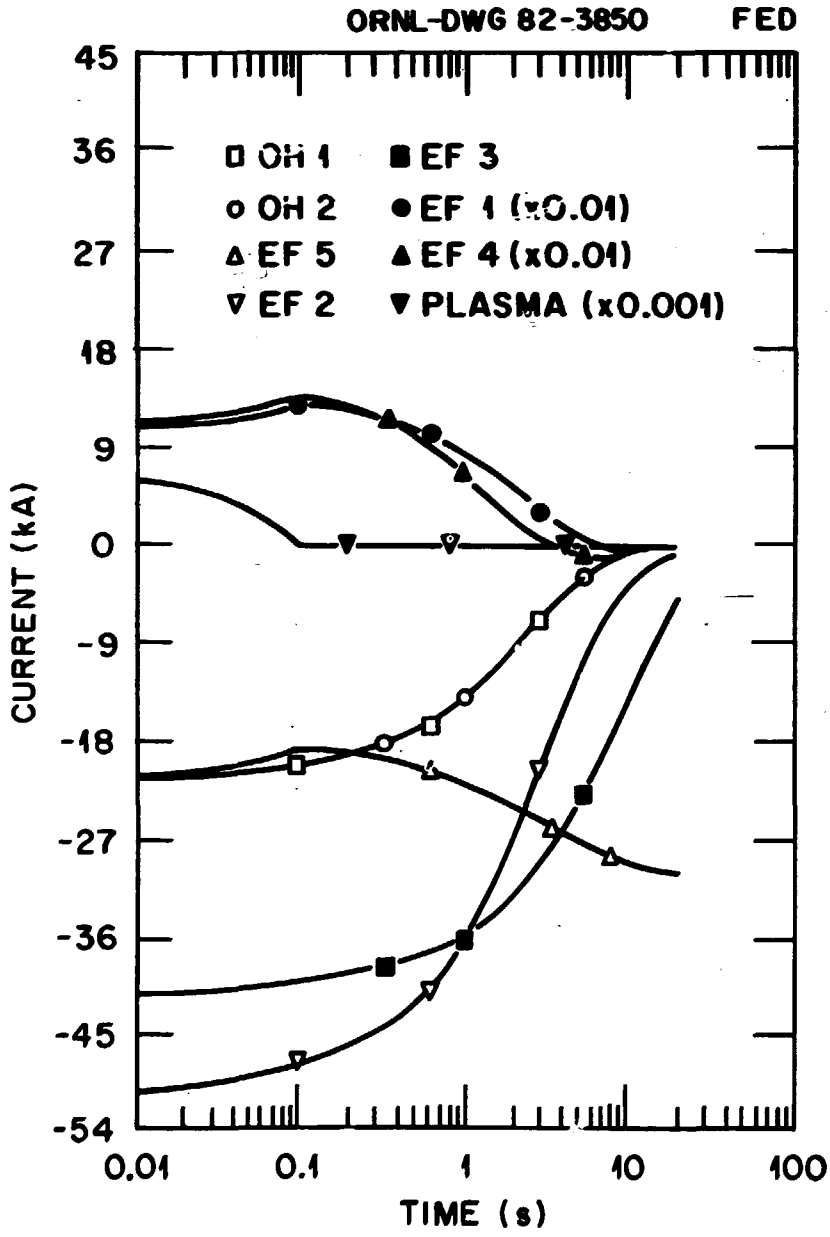

Fig. 5-30. Forced flow, ICCS 10 kV discharge voltage with coil EF5 shorted.

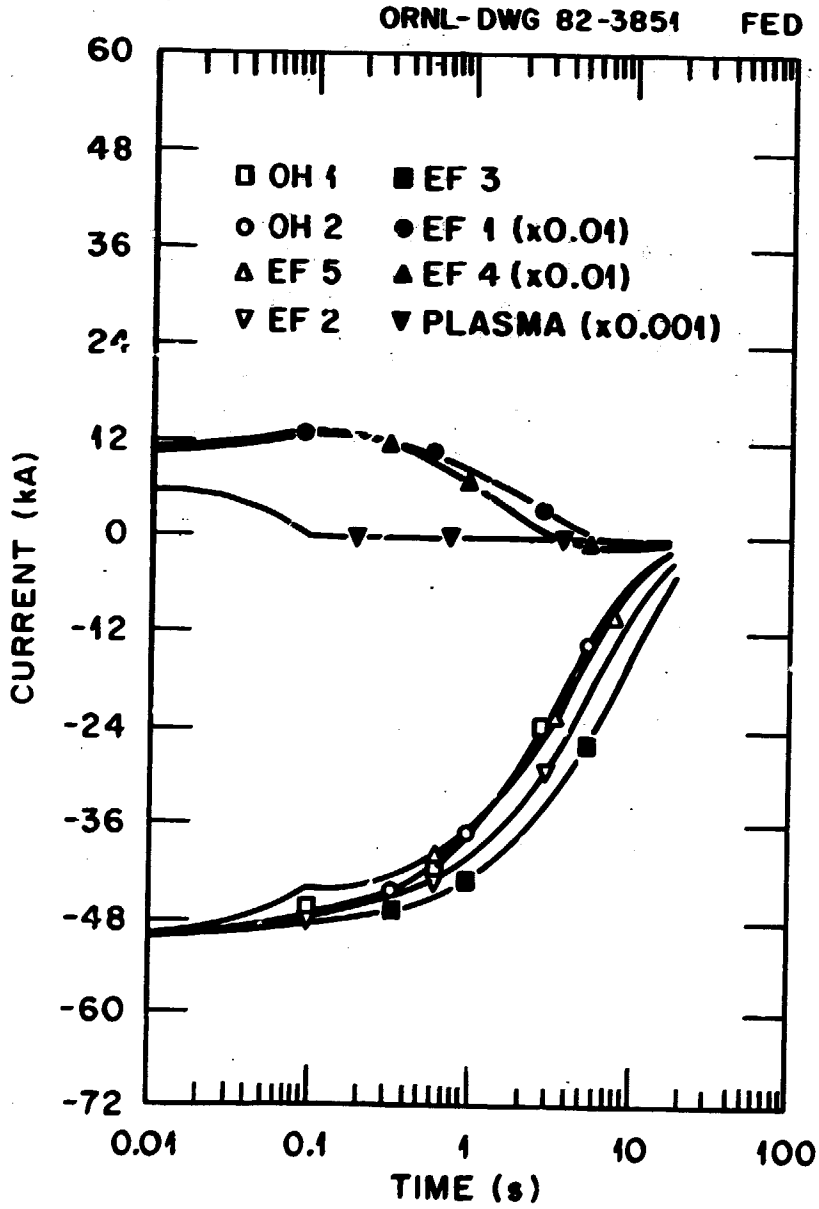

Fig. 5-31. Bath cooled, PBCC 3 kV discharge voltage with no coil shorted.

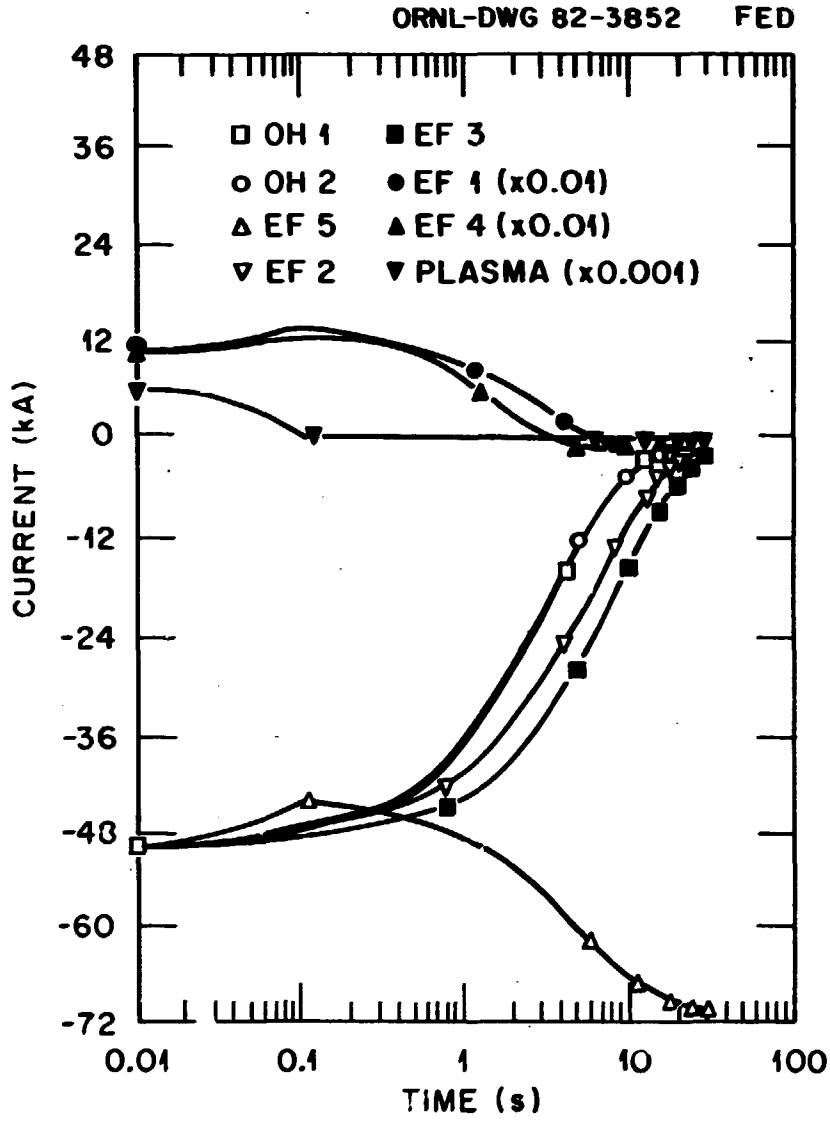

Fig. 5-32. Bath cooled, PBCC 3 kV discharge voltage with coil EF5 shorted.

Table 5-24. Parameters of ICCS poloidal field coils

Coil	Median plane (m)	Turns	Mean radius (m)	Axial length (m)	Radial bulk (m)	Maximum current (kA)
OH1	3.37	1128	1.23	3.56	0.44	-21.3
OH2	-2.37	1128	1.23	3.56	0.44	-21.3
EF5	0.50	564	1.23	1.78	0.44	-21.3
EF2	5.24	120	9.5	0.45	0.36	-50.8
EF3	-5.40	224	9.5	0.61	0.51	-41.3
EF1	4.59	36	3.85	0.53	0.53	119
EF4	-3.30	30	3.05	0.49	0.49	123
Plasma	0.50	1	5.01	4.16	2.60	6500

Table 5-25. Maximum current and turns for the PBCC coils

Coil	Turns	Maximum current (kA)
OH1	480	-50
OH2	480	-50
EF5	240	-50
EF2	124	-50
EF3	185	-50
EF1	36	119
EF4	30	123
Plasma	1	6500

Table 5-26. Current change in shorted superconducting coils as a result of an emergency discharge

Shorted coil	ΔI, ICCS (kA)	ΔI, PBCC (kA)
OH1	-2.0	-5.1
EF5	-11.3	-26.9
EF2	-4.8	-4.9
EF3	-2.2	-2.6

5.3.5.3 Conclusion

The effect of a plasma disruption on the PF coil system current level is small. A short circuit across the terminals of one of the PF coils is a dangerous situation which could result in extensive coil damage. However, only in the case of coil EF5 is there some possibility of coupling large amounts of energy from the PF coil system into the shorted coil. Thus, only coil EF5 would experience substantial current overdriving if shorted, and the other closely coupled PF coils to EF5, especially OH1 and OH2, would require programming at a slower discharge rate. No unusual structural design for the PF coils is anticipated except possibly for EF5. The consequence to design for the excessive induced current in EF5 would result in a large current density reduction. The apparent best way to cope with a short in EF5 is to program the OH1 and OH2 discharge slowly. Slow discharge of OH1 and OH2 coils does not have any significant effect on the TF coils.

If the ring coils are divided into separate subcoils to reduce the maximum voltage on the coil, as assumed for the treatment of the PBCC coils herein, the power supplies and dump circuits for these coils must be interlocked to keep the currents identical in all subcoils.

5.3.6 50-kA Vapor Cooled PF Coil Current Leads

Helium vapor-cooled leads (Fig. 5-33) to operate at 50 kA and 2 kV were designed based upon 25 kA, 60 kV leads designed and operated at the Los Alamos National Laboratory. These leads carry a 50-kA continuous current from the ambient temperature bus to the superconducting coil conductor at 4.5 K. The liquid helium consumption is 150-175 ℓ/h with 50 kA current, 60-70 ℓ/h with no current, and about 30 ℓ/h if a liquid nitrogen cooling station is added near the warm end. Such a station is not advised for the FED leads, because they have a high duty factor. The leads can operate without damage for about 15 minutes with full current and no helium vapor flow. They are designed to withstand 15 kV fault or cyclic voltage.

Each lead is built from a 127-mm (5-in.) nominal diameter copper pipe filled with roughly 1100, 3.175 mm (1/8 in.) diameter, phosphorous

ORNL-DWG 82-3853 FED

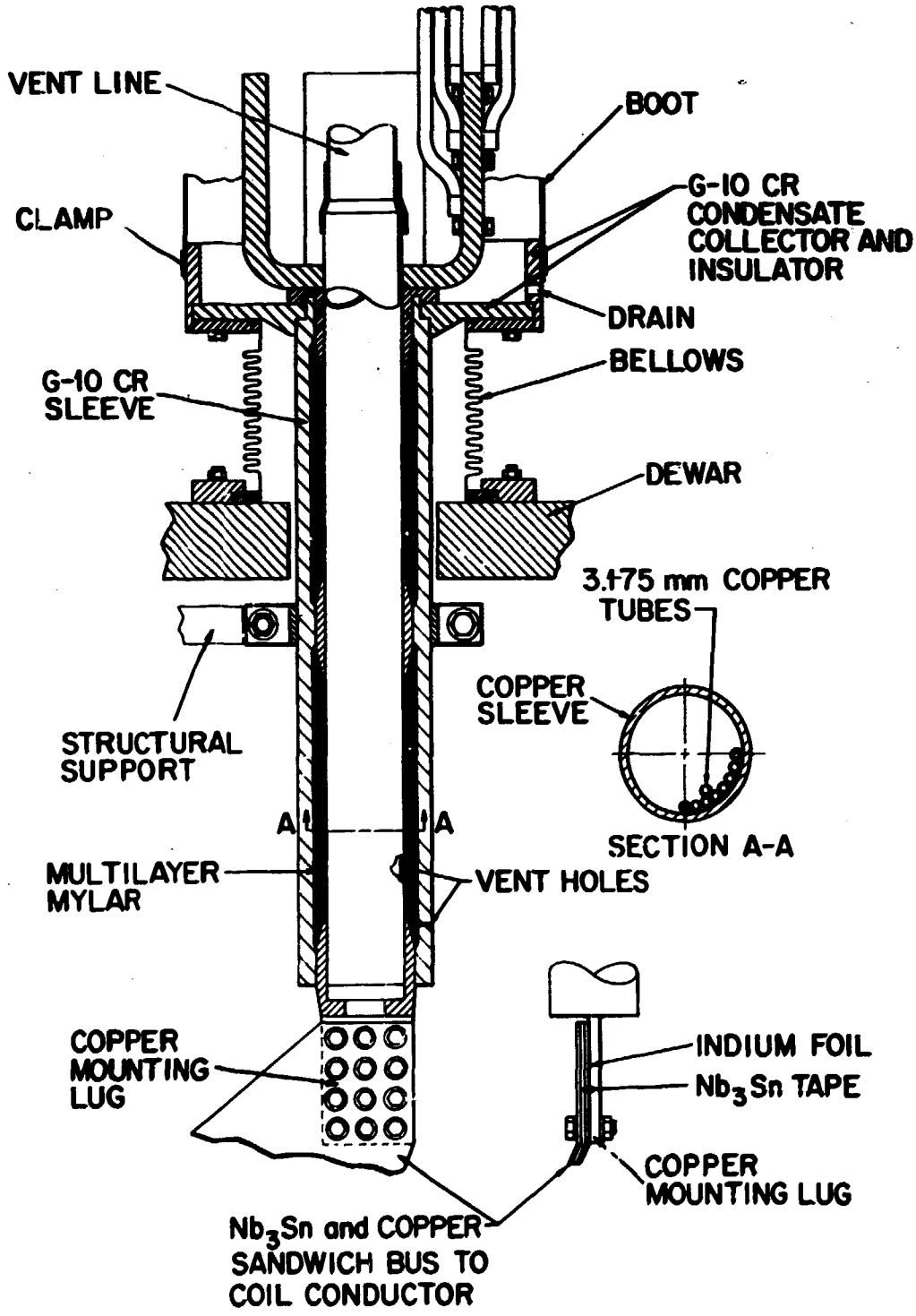

Fig. 5-33. 50 kA vapor cooled lead.

deoxidized copper refrigeration tubes. The gas flows through the bore of the tubes that are soldered to each other and the pipe jacket at the ends. This section is 1 m long. The ends are finished with copper lugs to match coil and bus connections.

The leads are designed to avoid flashover along the insulation surface outside the dewar in air, flashover along the insulation surface inside the dewar in warm helium, and breakdown across warm helium inside the dewar. The following design guidelines were adopted:

1. In air, the electric stress limit on the outside surface of insulation, including the dewar, is 394 V/cm.
2. In warm helium at one atmosphere, the electric stress limit along the surface of the insulation is 80 V/cm.
3. In warm helium at one atmosphere, the electric stress across the gas space is limited to 500 V/cm.

To increase the creepage path between the two leads inside the dewar, a 229-mm (9-in.) diameter G-10 CR tube is placed around each current lead. To decrease the electrical stress across the helium space, the current leads are wrapped with multilayered Mylar (DuPont trademark) internal to the G-10 CR tube. The top of the G-10 CR tube is finished in a G-10 plate and a skirt that acts as a condensation collector and provides additional electrical insulation. For lower voltage withstand requirements, the thickness of the G-10 CR sleeve and number of layers of Mylar can be reduced.

Because of the operational nature of the PF coils and to eliminate unusual cyclic loads on the 50-kA coil superconducting cable, the vapor cooled leads are rigidly attached to a fixed conductor terminal on the coil with a structural copper-Nb_3Sn tape sandwich bus. This superconducting bus attaches to the bottom end lug of the lead with a bolted indium foil pressure contact. The top end of the lead is free to move to account for differential thermal motion and relative coil motion arising from cyclic operation. This arrangement locates the cyclically loaded components with large deflections at ambient temperature and requires a structural support near the warm end of the lead that allows axial motion and takes the lateral Lorentz force load arising from

fringing fields. The superconducting structural bus is oriented to minimize eddy currents from varying fringe fields. The top end lug is devised to attach to a flexible connector, a number of fine wire copper cables, that in turn attaches to a 50-kA bus. These flexible connectors, the top end lug, and the attachment to the 50-kA bus, all are surrounded with a rubber boot.

Table 5-27 gives detailed data for such a 50-kA vapor-cooled lead. Thermal criteria for the leads are to:

1. be free of thermally induced coolant flow instabilities,
2. operate for minutes with no coolant flow,
3. operate successfully with a few blocked coolant passages,
4. have a low pressure drop,
5. have a low top end temperature,
6. have low losses from circulating currents induced by changing magnetic fields, and
7. have low losses at bolted connections.

Resistivity and top end temperature have little effect on the equilibrium boiloff rate; hence, the choice of these parameters is open. Choosing high resistivity copper and a low warm end temperature results in a large cross section, low current density, and cold lead. Such a lead has a high heat capacity with a low power generation; hence, a long time to failure if coolant flow is stopped and the current flow continues. The lead temperature does not fluctuate wildly as a result of instability or accidental loss of flow, giving sensors and control systems time to react. The top end temperature of these leads is designed to be 110-140 K, and 15 to 60 min to reach 300 K in the event of an accident. The top end temperature can be raised by reduced vapor flow; however, the lead must be monitored for stability. Low conductivity copper is used where eddy or circulating currents are present in the lead, bottom end lug, and superconducting bus. Table 5-28 illustrates the temperature rise in copper blocks of various thicknesses and resistivity ratio, cooled by liquid helium, and subject to a ramp field reversal. High resistivity copper clearly has a much lower temperature rise. This is accompanied by higher Joule losses when conducting current and the best design required a compromise between eddy currents and Joule losses.

Table 5-27. 50-kA vapor-cooled lead characteristics

Current, kA	50
Voltage, steady state, kV	2
Voltage, cyclic or fault, kV	15
Boiloff rate at 50 kA, ℓ/h	150-175
Boiloff rate at no current, ℓ/h	75
Number tubes	1100-1270
Current carrying area, cm^2	79.9-89.5
Length, cm	117
Iℓ/A, kA/cm	73.4-65.4
Top end temperature, K	140-110
Current density, A/cm^2	627-559
Time to raise top temperature from 100-300 K with no coolant, min	15-60
150 ℓ/hr stability parameter $L_o^{0.5}\ I/(\dot{m}C_p)_{He}$ (unstable)	1.16
174 ℓ/hr stability parameter $L_o^{0.5}\ I/(\dot{m}/C_p)_{He}$	1.00
ΔT at 300 K (ga to tube), K	3.6
Reynolds number at 300 K	246
Reynolds number at 4.5 K	3770
NTU, $[hA/(pC_p)_{min}]$	163
Pressure drop, MPa	4.8×10^{-5}
Temperature rise, one blocked tube, K	3.4
Joule loss, bottom bolted connection, W	1.17
Bolting pressure, MPa	15
Bolt stress, MPa	185
Copper resistivity ratio (300 K/4.5 K)	7-10

Table 5-28. Circulating current loss in copper blocks

Thickness cm	ΔB^a T	Resisitivity ratio	ΔT K
5.0	3	500	6.86
2.5	3	5	0.35
2.5	3	2	0.14

[a]Change of field from +1.5 to -1.5 T in 1 s.

Figure 5-33 shows a version of the vapor-cooled lead that has its last interface made at the bottom end superconducting bus before final dewar closure at a location other than at the lead attachment to the dewar. If the last step is to make the dewar closure at the lead top end, then a variation on the top end design is needed. This lead can be scaled in cross section for lower current applications as required for ICCS conductor. The lead must be increased in length as much as 30% without major redesign, but it should not be shortened substantially. It is capable of being interfaced on the bottom end with an appropriate superconducting bus to either PBCC or ICCS. For the latter, the transition from the ICCS to the vapor cooled lead will require an intermediate bath (approximately 1 atm, 4.5 k) as being used on the Large Coil Project (LCP) at the Oak Ridge National Laboratory (ORNL). A direct accommodation to an ICCS conductor can be made with a change in the bottom end lug configuration and a surrounding manifold with split flow returning most of the cold supercritical pressure helium directly to the refrigerator and directing a portion through the lead for cooling. Exhaust gas from the lead feeds through a length of electrically insulating pipe to a metering valve that controls the gas flow.

5.4 CRYOSTAT DESIGN WITHOUT LIQUID NITROGEN SHIELD

The purpose of this design study was to assess the effect of eliminating the liquid nitrogen cold wall between the 300 K magnet system vacuum vessel and the 4.5 K coil helium vessels.

A description of the cryostat in the FED Baseline is contained in Sect. 4.3 of Ref. 1. The baseline cryostat concept (Fig. 5-34) consists of a single vacuum vessel enclosing all of the superconducting magnets; individual helium vessels for each of the magnets (the magnet stainless steel structural cases also serve as the helium vessel for toroidal field coils and superconducting poloidal field coils, while the solenoid is enclosed in a glass epoxy helium vessel); and a liquid nitrogen cold wall affixed to the inside surface of the vacuum vessel whose purpose is to reduce the radiation heat leak to the liquid helium vessels. This concept is an adaptation of the LCP concept, was adopted

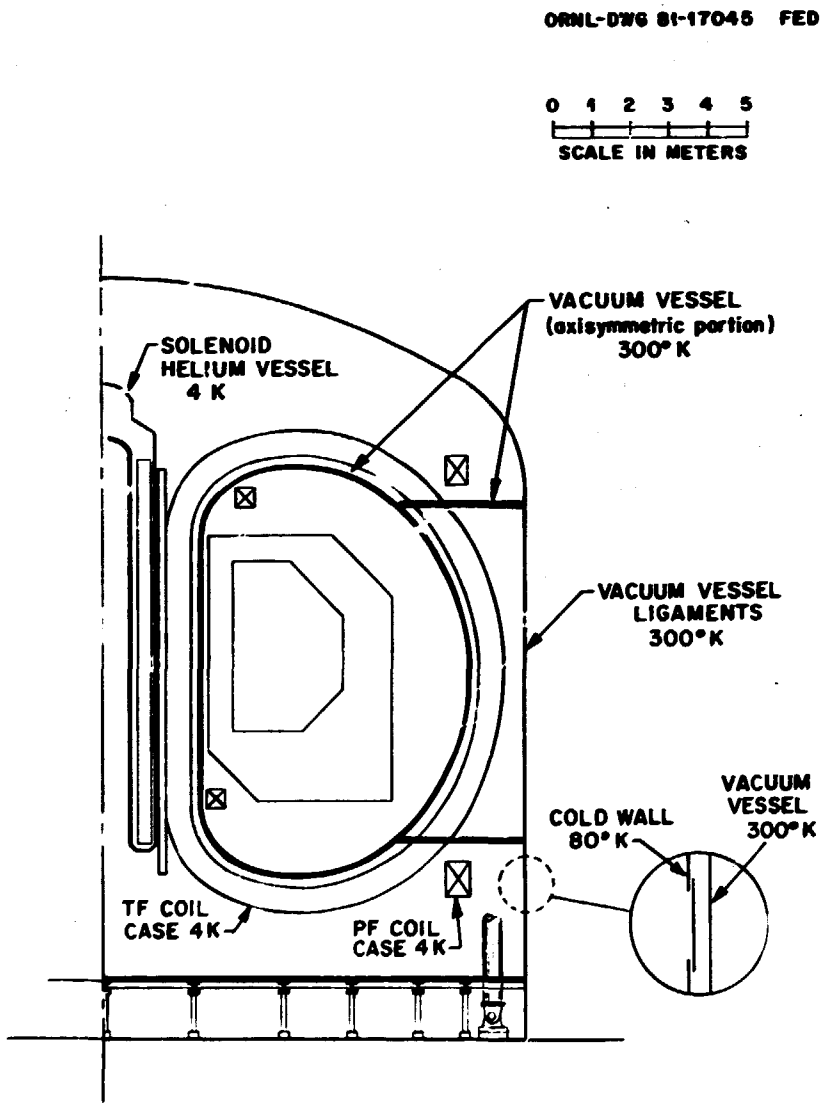

Fig. 5-34. Cryostat concept.

early in the ETF Program, and has persisted through ETF, INTOR, and FED studies with no alternate concepts ever seriously considered.

This design study was initiated as a potential cost saving. Because the space occupied by the cold shield in the inboard region of the toroidal field coils contributes directly to the machine major radius, this study was initiated to determine if the capital cost saving associated with deleting the cold wall would be greater or less than the resulting increase in operating cost due to the added heat leak. The space potentially saved by elimination of the cold shield is required for providing radiation shielding in the gap between the coil case and the vacuum vessel, and, therefore, there is no net reduction in the machine size.

Elimination of the cold wall results in cost increase in some respects and cost reduction in others. The following were found to be the major cost contributors:

1. Capital cost reduction on the order of $6 M due to deletion of cold wall itself.
2. Operating lifetime cost increase by $3.7 M because of higher heat load on the liquid helium cooled components.
3. Capital cost increase of $0.6 M for providing the greater cryogenic capability to dissipate the greater heat load.

Item 1 is estimated to be $5.68 M based on an estimated 2815 m^2 area and a unit cost of $2018/$m^2$; the unit cost is derived from cost data for a similar cold wall on LCTF which, for a 372 m^2 wall, costs about $0.75 M, including material cost, installation, and testing, but excluding the cost of multi-layer insulation which, if there were no cold wall, would be installed on the helium vessels instead. Item 2 is estimated to be $3.72 M, based on an increased heat load of 2.4 kW at 4 K, a cryoplant power factor of 600 watts electrical/watt at 4 K, an electrical cost of $21.54/month (2.2¢/kW hr usage charge plus a demand charge of $5.70/kW/month), and a design life of 120 months. Item 3 is estimated to be $0.61 M, which is the incremental cost of supplying an additional 2.4 kW of 4 K capacity in a cryoplant which is already designed for 90 kW at 4 K.

The net cost reduction is Item 1 saving minus the Items 2 and 3 cost increases, or $1.35 M.

It is concluded that the LN_2 cold wall should be eliminated from FED baseline cryostat conceptual design. The life cycle cost savings has been estimated to be $1.35 M over the ten-year life of the machine. This saving in the context of a $1,000-M machine is not by itself a strong argument either for or against eliminating the cold wall. A more significant advantage, difficult to quantify but nevertheless real, is the resulting simplicity. This simplicity will undoubtedly result in cost savings during construction as well as operational savings due to enhanced reliability. Eliminating the need to install, leak check, and operationally test the cold wall will be particularly beneficial in the toroidal field coil nose region where this activity would be directly in series with the limiting construction path, i.e., landing of magnets, erection of vacuum vessel, and landing of torus segments. Leaks that might develop during operation would interrupt testing until they are isolated and repaired. As mentioned above, it is difficult to assign a cost to construction and operational delays; in this context, however, it is noted that a 15% capital charge on a $1,000-M investment is $411 K per day.

REFERENCES

1. ORNL/TM-7948/V1, Fusion Engineering Device Design Description Volume 1, December 1981.
2. GA Staff, "ETF Toroidal Field Coil Concept Employing NbTi Alloy Superconductor and Saturated Superfluid LHe Bath Cooling," General Atomic Company, prepared for MIT, Francis Bitter National Magnet Laboratory, Report No. GA-A15818, San Diego, CA (March 1980).
3. David C. Larbalestier, "Superconducting Materials — A Review of Recent Advances and Current Problems in Practical Materials," Fusion Engineering Programs, Nuclear Engineering Dept., University of Wisconsin, Madison, Wisconsin, Report UWFDM-417 (March 1981).
4. GE 12-Tesla Toroidal Field Coils Engineering Test Facility (ETF), Part 1 Final Report — Scoping Study of a 12 T ETF TF Coil, General Electric Company (November 2, 1979).
5. DOE/TIC-11600, "The Fusion Engineering Device, Volume II Design Description" (October 1981).
6. R. R. Coltman, Jr. and C. E. Klabunde, "The Strength of G-10CR and G-11CR Epoxies after Irradiation at 5 K by Gamma Rays," paper submitted to J. Nucl. Mater., May 1982.
7. S. Takamura and T. Kato, "Effect of Low Temperature Irradiation on Insulators and other Materials for Superconducting Magnets," J. Nucl. Mater., 103 and 104 (1981) 729-734.
8. J. H. Schultz, "Design Practice and Operational Experience of Highly Irradiated, High Performance Magnets," draft report, August, 1982.
9. MIT FED-R Report, draft, July 15, 1982.
10. R. R. Coltman, Jr. and C. E. Klabunde, "Mechanical Strength of Low-Temperature-Irradiated Polyimides: A Five-to-Tenfold Improvement in Dose-Resistance over Epoxies," J. Nucl. Mater., 103 and 104 (1981), 717-722.
11. Y. Twasa, M. O. Boenig, and D. B. Montgomery, "Cryostability of a Small Superconducting Coil Wound with Cabled Hollow Conductor," IEEE Trans. Magn. MAG-13 (1977), pp. 678-681.

12. J. W. Lue, J. R. Miller, and L. Dresner, "Vapor Locking as a Limitation to the Stability of Composite Conductors Cooled by Boiling Helium," Adv. Cryog. Eng. 23 (1978), pp. 226-234.

13. Vincent D. Arp, "Stability and Thermal Quenches in Force-Cooled Superconducting Cables," 1980 Superconducting MHD Magnet Design Conference (MIT, 1980), pp. 142-157.

14. L. R. Turner, "Safety of Superconducting Magnets for Fusion: Thermal Analysis of Large Cryostable Magnets," IEEE Trans. Magn. MAG-17 (1981), pp. 463-466.

15. J. W. Lue and J. R. Miller, "Heated Length Dependence of the Stability of an Internally Cooled Superconductor," 9th Symposium on Engineering Problems of Fusion Research (Chicago, 1981), pp. 652-659.

16. G. B. Wallis, *One Dimensional Two Phase Flow*, McGraw Hill, New York (1969), pp. 286, 287.

17. Communication from Harwell by way of Walter Kirchner, Los Alamos National Laboratory.

18. W. Hassenzahl, "Quench-Modifications and Documentation," Centre-d'Etudes Nucleaires De Saclay report SUPRA/78-61 CEN (October 1978).

19. "20 MJ Superconducting Pulsed Energy Storage Coil, Phase 1 Final Report," Westinghouse Electric Corporation, Large Rotating Apparatus Division, East Pittsburgh, PA, April 1980 (limited distribution).

20. A. F. Clar, G. E. Childs, and G. H. Wallace, "Electrical Resistivity of Some Engineering Alloys at Low Temperatures," Cryogenics, p. 295, August 1970.

21. "International Tokamak Reactor: Phase One," IAEA, Vienna, 1982; STI/PUB/619, ISBN 92-0-131082-X.

22. M. Tsujj, L. Dresner et al., "Large-Current Conductor Development for Superconducting Poloidal Coils," Proc. 9th Symp. Eng. Prob. Fus. Res. Oct. 26-29, 1981, Chicago, IL (1982).

23. J. R. Miller, "The Development of Forced Cooled Superconductors For Use in Large Magnets," Proc. 9th Cryogenic Eng. Conference, San Diego, CA, to be published (1982).

24. M. S. Walker et al., "Superconductor Design and Loss Analysis for a 20 MJ Induction Heating Coil," IEEE Trans. MAG-17 908 (1981).

25. J. W. Lue, J. R. Miller, and J. C. Lotin, "Pressure Drop Measurements on Forced Flow Cable Conductor," IEEE Trans., MAG-15 53 (1979).

26. G. Claudet, "Cooling Modes for Superconducting Magnets," IEEE Trans., MAG-17, 1749 (1981).

27. V. C. Svivastava, "Enhanced Cooling with Helium Channels in the TF Coils Casing for FED," Proc. 9th Symp. Eng. Prob. Fus. Res. p. 358 (1981).

28. V. C. Svivastava, "FED Poloidal Field Coil Design Concept Employing an Internally Cooled Cable Superconductor (ICCS)," FEDC ORNL/TM-8474, to be published.

29. Hunter to Distribution, "ETF Magnet Structural Limits," memo ETF-M-80-MS-070, September 18, 1980.

30. Hooper to Kalsi, "Review of FED Fracture Mechanics Procedures," memo FEDC-M-81-MS-120, November 30, 1981.

31. Hunter to Distribution, "FED-Design Criteria for Insulating Materials," memo FEDC-M-81-MS-070, June 19, 1981.

32. B. L. Hunter to S. S. Kalsi, "FED-Application of Forced Flow Conductor to Superconducting Ring Coils," Fusion Engineering Design Center Memo FEDC-M-82-E/M-066, April 19, 1982.

33. K. J. Bathe, "ADINA, A Finite Element Program for Automatic Dynamic Incremental Nonlinear Analysis," MIT Dept. of Mech. Eng. report 82448-1, September 1975, Revised December 1, 1978.

6. ELECTROMAGNETIC STUDIES

6.1 INTRODUCTION

The electromagnetic studies consist of calculations of current, energy, voltages, and forces on conductors and structures as the result of transient conditions such as startup, shutdown, disruption, and minor plasma fluctuations.

Because of the interrelationships and conflicting requirements on the structures associated with electromagnetics, there is no one simple, best arrangement. The importance or significance of the electromagnetic design features are not generally understood because the philosophy for the design of the present generation of machines is not appropriate for FED Baseline. The designs of toruses must change from a high-resistance structure with low induced currents to one of low resistance to allow large induced currents.

The criteria used in determining the torus electromagnetic features must change, for the following reasons:

1. The present torus designs must provide for neutron shielding.
2. Disruption energies are more than two orders of magnitude larger and, hence, a more dominant factor in the design.

The large neutron loading has many effects on the electromagnetic design features. In FED, the neutron loading results in structure changes in the first wall steel. The larger volumes and active cooling for reactors require heavy structures. The requirement for neutron shielding of the coils and adjacent components requires the thickness of the torus to be more than a meter. If eddy currents are allowed to flow radially through this meter thick structure, they will react with the 8 to 10 T toroidal fields to produce very high forces (in the order of 3 million lbs per meter of thickness). The neutron flux levels result in the location of field windings relatively remote from the plasma. This will require larger control systems or better self-stabilization (passive circuits).

The major driving factor in the electromagnetic design for FED Baseline is providing for a major disruption. The structure must be designed to safely accommodate a disruption of the thermal quench energy, and the torus must be designed to maintain the current decay phase of the disruption long enough to transfer the magnetic energy to I^2R heat. The external torus structure should be a high-resistive structure with a time constant at least five times that of the inner conductors.

6.2 DISRUPTIONS

The good conducting shell near the plasma can possibly reduce the number of disruptions, but its primary design feature is to conduct disruption-induced currents approaching 6 million amperes. By allowing induced eddy currents to flow in this low-resistance structure, the plasma can be held away from the inner wall during the current decay phase of a disruption. If the disruption current decay time is long enough, the plasma magnetic stored energy transfers to I^2R heating in the structure with little or no damage. A high-resistance structure which allows the plasma to quickly move to the wall results in dissipating a large percentage of this energy in thermal heating of the structure in contact with the plasma. This can produce very high temperatures in the structure in contact with the edge of the plasma, with the possibility of severe damage.

The initial disruption specification for FED Baseline provided times for thermal quench and current quench and provided information as to where the energy would be deposited.

The thermal quench is the fast transient time in which the hot core of the plasma loses its good confinement and transfers the major part of the thermal energy to the limiter and wall surfaces.

The current quench time is much longer than the thermal quench time. In this phase of the disruption, the plasma circuit reacts to the small change in current due to the thermal quench. In a major disruption, the plasma equilibrium is lost. The plasma is then driven into the wall or limiters. If the conducting wall or passive conductors are not of

sufficient capacity, the self-inductive magnetic energy is transferred to ohmically heating the plasma remaining in the torus. This energy is then primarily deposited on the limiters or walls which are in contact with the plasma. This transfer of magnetic energy to thermal energy results in melt layers on stainless steel surfaces and has led to the use of armor surfaces inside of the torus.

By providing a low impedance first wall, which is toroidally continuous, the large eddy currents flow can be maintained toroidally, but not radially. These currents react only with the poloidal fields and not the toroidal field, and the forces per unit length are reduced by an order-of-magnitude. With this type of design, the disruption forces on the torus can be limited to less than the equivalence of one atmosphere.

The good conducting toroidal circuit near the plasma allows the high eddy currents to produce self-stabilization, and it prevents high induced voltages. By maintaining the voltages across segment gaps, to values less than 20 volts, arc erosion will not occur; and the induced transient voltages in the PF coils will be negligible. This good conducting structure also absorbs most of the disruption energy and thus shields the superconducting structures. Therefore, it reduces the refrigeration loading and the possibility of a superconductor going normal due to a disruption.

Making the structure surface near the plasma a conductor equivalent to 4 or 5 cm of stainless steel, the disruption current decay time can be made longer than 25 miliseconds, and very little plasma magnetic energy will be transferred to surface heating of the structure contacting the plasma. There will be no arc erosion during a disruption, and a control field system of less than 30 megawatts will be sufficient for normal position control.

The startup energy loss will be about 25 megajoules, and the startup blip coils will be approximately 3 MAT capacity, with a peak voltage of 30 volts per turn.

As the understanding and calculations improve, the specification for the current quench phase of disruption have become outdated. The

recent calculations do not assume that the plasma current decay and deposit of thermal energy are independent of the eddy currents and structures. They allow the plasma to move freely to its equilibrium position, whereas the initial estimates were based on the plasma remaining fixed in the center of the torus.

The recent engineering calculations for disruption current decay were based on a simple plasma of uniform current (Ref. 1). It was assumed that the plasma moves to its equilibrium position, and it is scraped off by the wall and limiter. The calculations were based on conservation of energy. The results of the calculation for the worst disruption case are summarized below:

1. The FED current decay time is 25 miliseconds rather than the 10 specified in Ref. 2.
2. The magnetic energy transferred to thermal energy during the current decay phase of disruption is only 2% of the 144 megajoules instead of the 21% now specified.
3. The current decay may be adequately represented by a linear approximation (Fig. 6-1).

Additional work on characterizing the current decay phase of disruption using improved plasma modeling is being developed by PPPI and ORNL.

The values given in Ref. 2 for the FED Baseline are, on the average, higher than would be obtained with updated calculations. Having the plasma decay time longer would reduce the numbers by a factor of 2.5, but allowing the plasma to move away from the center of the torus will result in an increase in the forces on the inside torus wall. Thus, the force of the inside torus wall may not change appreciably from the 0.2 MPa originally calculated.

6.3 STARTUP VOLTAGE AND ENERGY

With the advent of rf-assisted startup, a high voltage around the plasma loop is not required. This allows the design of the torus to change from a high-resistance structure to a low-resistance structure at the inner surface. The advantages of the low-resistance structure near

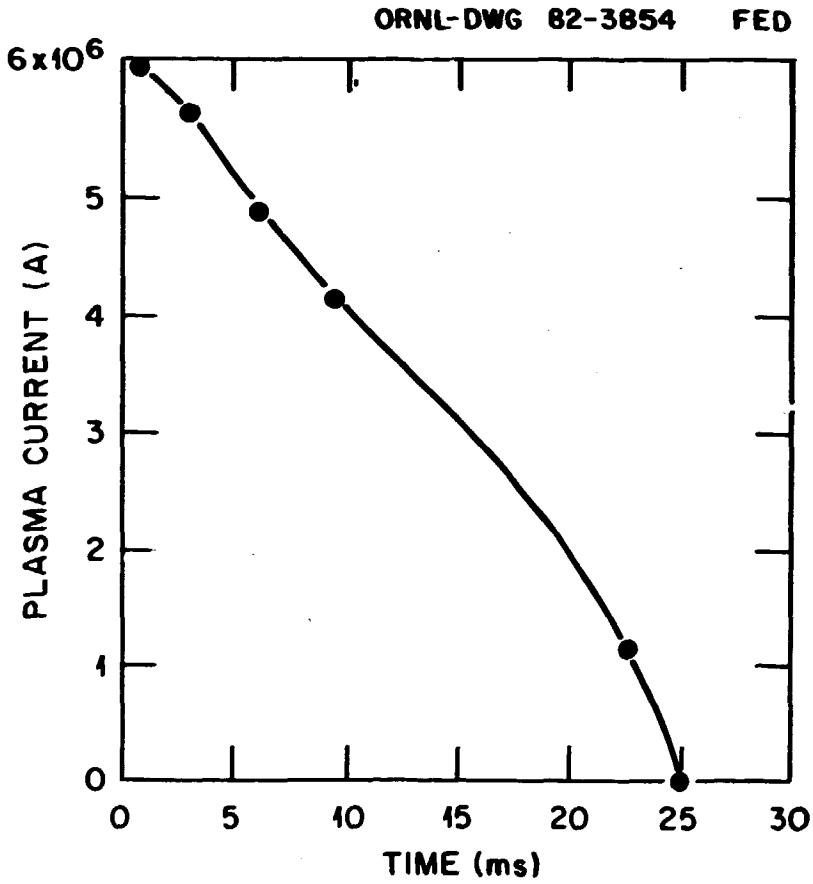

Fig. 6-1. Plasma current decay.

the plasma for disruption control are outlined above. For lower power and low loss startup, a high-resistance vessel is desired. Our studies to date show that the major torus electromagnetic design factor should be based on the disruption control, the startup requirements being a second-level consideration.

The rf-assisted startup occurs as three different functions:

1. breakdown of gas
2. providing the energy to heat the plasma above the point where radiation losses are negligible (above 50 ev)
3. reducing the resistive losses in the plasma by supplementing heating during the current rise (before bulk heating is applied).

By reducing the required startup plasma voltage from 250 volts to about 10 volts, a reasonable startup coil (previously called a blip coil) can be provided. This startup coil must drive the field through the torus spool structure (outer shell) and the good conductive circuit near the plasma (inner shell). It is also coupled to the external structures such as the cryostat and, hence, it supplies this energy loss. In the design of startup coils, it is advantageous to provide a high forcing voltage to quickly raise the voltage around the plasma loop to 10 volts. However, the high startup voltage also induces surge voltages on the PF coils. Thus, there is a compromise in the maximum magnitude of the startup peak voltage.

The basic torus design approach for the startup electromagnetics is as follows:

1. Design the inner structure near the plasma to prevent disruption damage.
2. Design the outer structure to the highest practical resistivity. The general rules of thumb are: (a) the external shell and structure toroidal field time constant should be less than 1/5 of the value for the inner shell and (b) the resistivity of the outer wall of the vacuum vessel should have a toroidal resistance of approximately ten times that of the inner shell.
3. Place the startup coils as close to the plasma as practical, with as poor a coupling to the external toroidal electrical circuits and

structures as possible. Locating these coils inside of the torus vacuum system, between the torus and the cryostat, provides the best electromagnetic characteristics; but the radiation is high and accessibility is low. If they are installed in the cryostat external to the TF coils, there will be higher energy loss, larger heat dissipation in the superconducting region, as well as high induced voltages within the PF coils. The best location for the coils must be determined by a tradeoff study.

The startup coil design is considered to be a second-level design factor; hence, the location, size, and design functions will be determined at a later date. In the baseline design (Ref. 2), the EF1 and EF2 poloidal field coils were used in conjunction with smaller coils located on the outer corners of the vacuum vessel to produce a 25-volt plasma loop voltage. The four small control coils produce a field null inside of the torus at the position where the plasma is initiated. The results from the work described in Section 4 indicate that the outer vacuum system will require high-resistance bellows or insulating breaks.

6.4 CONTROL

The position control of plasma is basically a third-order design consideration. With the advant of a low-voltage startup and a good passive conductor near the plasma, the control becomes comparatively easier than that obtained on existing machines. The required power and frequency responses are reduced, but the effects associated with large external structures, such as the outer shell and the cryostat, increase the power requirements.

The basic electromagnetic configuration from a control consideration is a good conducting shell near the plasma to provide passive control. It may be desirable from a simple position control consideration to provide a configuration with toroidal breaks in the shells to allow horizontal and vertical fields to penetrate easily. However, these same breaks would allow plasma instability to proceed at a faster rate. Toroidal gaps impede the flow of helical eddy currents and, thus, they may result in an increase in the probability of a disruption. The

specific gains would require detailed analysis and would complicate the design of the shells. For the present, the possible gains with toroidal breaks do not outweigh the difficulties encountered and the problems associated with toroidal gaps.

The major control requirement may be to prevent the plasma current decay after a major thermal quench disruption. If this does not become a control design driver, then the initial studies reported in Ref. 3 show that four small coils in the corners of the vacuum vessel will be satisfactory.

REFERENCES

1. J. G. Murray and G. Bronner, Disruption Model PPPL 1909, July 1982.
2. Fusion Engineering Device Design Description, ORNL/TM-7948, VII.
3. J. G. Murray, "FED Control Power," IEEE Pub. No. 81CH17115-2-NPS, 1302.

7. MAINTENANCE STUDIES

7.1 INTRODUCTION

Earlier maintenance studies at the Design Center concentrated on component disassembly and handling and were very influential in the development of the overall device configuration. The most noteworthy example of this influence is the torus sector arrangement and the concept of sector removal between fixed toroidal field coils. This approach was used to develop disassembly scenarios[1] for major components and to make relative estimates of downtime. It did not identify in specific detail what the maintenance and handling equipment requirements were, what these machines looked like, or what their cost might be. The answers to these questions were the basis for the maintenance-related work described herein.

The maintenance studies accomplished at the Design Center during this past year focussed on developing maintenance equipment concepts and costs. This work was also an extension of the Maintenance Equipment Workshop[2] held at the FEDC in January and March 1981.

The workshop identified the basic equipment needs and categorized them as either general purpose or special purpose items. In order to go beyond this first level of detail within the limits of our effort, it was decided to focus on one major component replacement, that of a torus sector. This approach had the following strategy:

- develop the detailed steps for sector replacement,
- use these detailed steps to identify the equipment needed and the functional and operational specifications for this equipment,
- develop equipment conceptual designs based on these specifications, and
- estimate the equipment costs based on these designs.

The detailed sector replacement scenario was developed at the Design Center, along with a listing of preliminary specifications. This information was used by two design groups outside the Design Center as the basis for developing the conceptual designs and the cost

estimates. The Sector Handling Machine and the Movable Manipulator System were developed by EG&G at INEL; an In-Vessel Manipulator System was developed jointly by the Fuel Recycle Division (FRD) and UCC-ND Engineering at ORNL.

7.2 SECTOR REPLACEMENT

Figure 7-1 shows a torus sector removed from its position in the plasma chamber. In developing this scenario as the basis for the maintenance equipment study,[3] several assumptions are noteworthy:

- the maintenance operations of interest are generally those which require remote handling,
- contact maintenance is preferred wherever it is practical to do so, and
- peripheral components (pumped limiter, ICRH, and ECRH) are assumed to remain installed in the sector during its removal.

For simplicity, sector replacement can be viewed as a two-part scenario: sector removal (Table 7-1) and sector replacement (Table 7-2). In addition, each of these has three stages of operation.

7.2.1 Sector Removal

General device shutdown is the first stage and consists of deenergizing the coils, draining and storing the torus coolant, a bakeout of the torus for detritiation, and the preparation of maintenance equipment. Based on the present understanding of these procedures, 64 hours is required, which is greater than the 24-hour shutdown period necessary for personnel access to the device. Therefore, contact maintenance is permitted to assist in the setup of remote equipment and to accomplish tasks which are more efficiently done hands-on.

Disassembly of the sector interfaces is accomplished in Stage 2. It consists of removing structural attachments between the sector and the support spool/frame, cutting the vacuum flange, uncoupling coolant and electrical connections and removing pipe assemblies, decontaminating

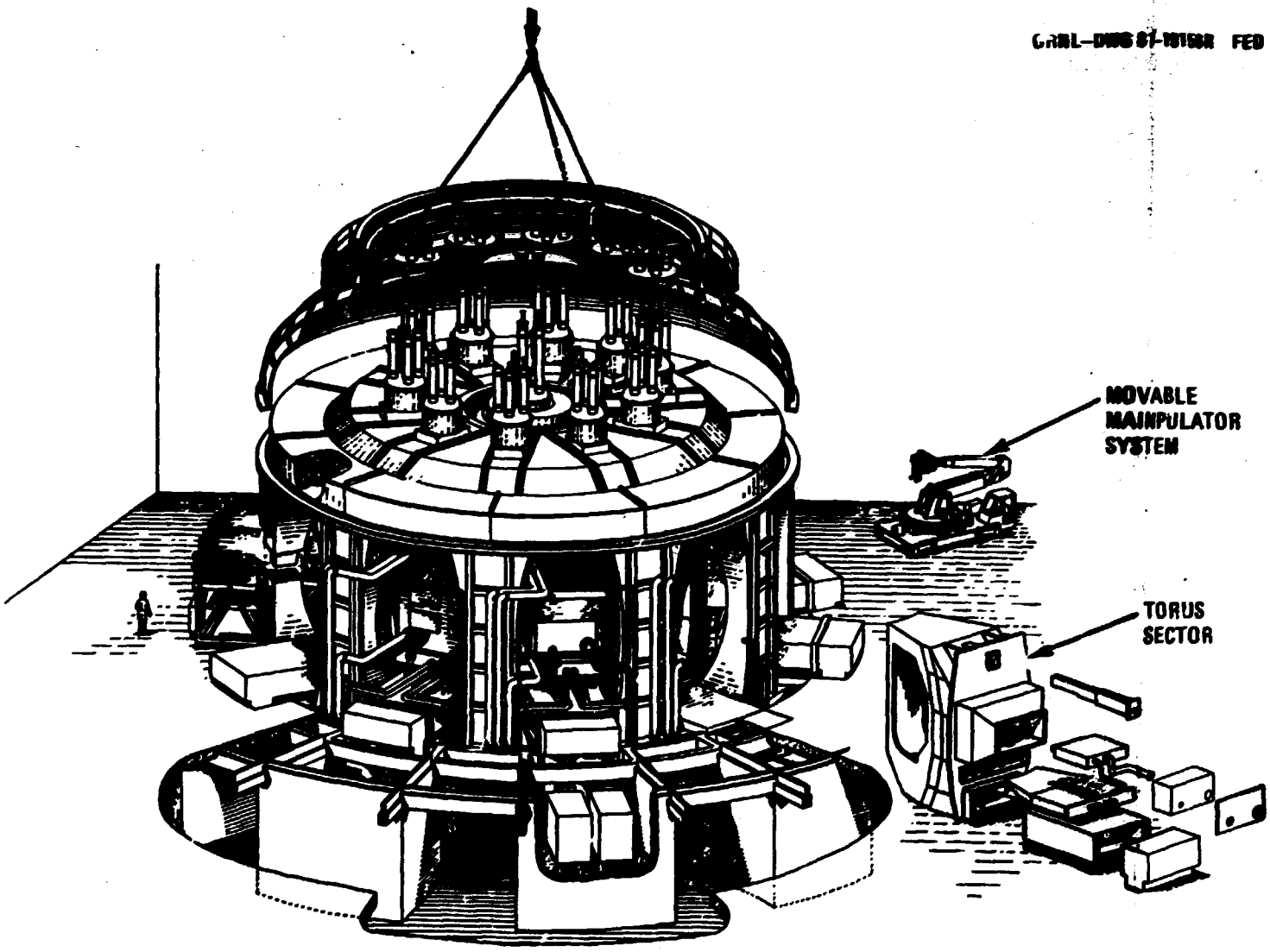

Fig. 7-1. FED sector replacement.

Table 7-1. Sector Removal Procedures and Equip

1 General Device Shutdown		2 Disassemble Sector Interfaces
• De-energize coils • Drain & store torus coolant water	3 h	• Remove struct. bolts (44-2 1/2 cm) • Cut vac. flange (22 m) • Uncouple coolant lines
• Bakeout torus using hi-temp N_2 gas	18.5/24 h	
• Lower torus temperature	18.5 h	
• Prepare maintenance equipment		
	64 h	

Lines	Connects	Diam (cm)
2	4	30
1	2	20
6	12	8
1	2	10
4	8	15

- Uncouple waveguide

1	2	3

- Uncouple coax (combination electrical & coolant)

1	2	20

- Remove lines in window area
- Cut vac. flange of duct elbow
- Remove elbow to storage
- Install floor cover plate over open
- Cut vac. flange of duct
- Roll back duct; remove to storage

Equipment - Stage 1

- General device shutdown does not require the use of maintenance equipment; the procedures listed are automated and executed from the control room
- Preparation of maintenance equipment consists of removing equipment fro storage and placing it in reactor cell during the 18.5-h cooldown phase

Equipment - Stage 2

- General purpose mobile manipulator
- Debolting tool (2-1/2 cm bolts)
- Track-mounted cutter
- Nut runner for "Grayloc" type couplir
- Lifting slings for pipe sections
- O/H crane(s)

*Sector handling device has provisions for containing contaminated debris.

7-1. Sector Removal Procedures and Equipment

2

Disassemble Sector Interfaces

- Remove struct. bolts (44-2 1/2 cm)
- Cut vac. flange (22 m)
- 24 h Uncouple coolant lines

Lines	Connect's	Diam (cm)
2	4	30
1	2	20
6	12	8
1	2	10
4	8	15

- Uncouple waveguide

1	2	3

- Uncouple coax (combination electrical & coolant)

1	2	20

- Remove lines in window area
- Cut vac. flange of duct elbow
- Remove elbow to storage
- Install floor cover plate over open duct
- Cut vac. flange of duct
- Roll back duct; remove to storage

Equipment - Stage 2

- General purpose mobile manipulator
- Debolting tool (2-1/2 cm bolts)
- Track-mounted cutter
- Nut runner for "Grayloc" type couplings
- Lifting slings for pipe sections
- O/H crane(s)

3

Sector Removal

- Install sector handling device* and lock into position
- Engage extraction mechanism to sector
- Pull sector onto handling device
- Extract handling device and sector
- Attach contaminant collector to sector
- Lift sector and transport to hot cell air lock

Equipment - Stage 3

- General purpose manipulator
- O/H crane(s)
- Sector handling device

ntaining contaminated debris.

Table 7-2. Sector Replacement Procedures and Equipment

4 Sector Replacement

- Visually inspect floor area and open bay for particulate matter
- Decontaminate open bay and floor area
- Transport repaired sector to handling device
- Engage extraction mechanism to sector
- *Roll handling device and sector into window area
- Lock handling device into position
- Push sector into its final position in torus
- Inspect vacuum flanges and bolt holes for alignment
- Remove sector handling device
- Install structural bolts (44-2 1/2 cm)
- **Weld vacuum seal (22 m)
- Inspect floor area; decontaminate as required

5 Assemble Sector Interfaces

- Install shielded duct; weld vacuum flange (8 m)
- Remove floor cover plate
- Install duct elbow; weld flanges (8 m, 8 m)
- Leak check all welded flanges (22 m, 8 m, 8 m, 8
- †Position lines, connect couplings

Lines	Connections	Diam (cm)
2	4	30
1	2	20
6	12	8
1	2	10
4	8	15

- Same for waveguide

1	2	3

- Same for ICRH coax assembly

1	2	20

- Leak check each coupling by pressurizing systems with tracer gas
- Check work area around sector for contaminated debris; cleanup as required

Equipment - Stage 4

- CCTV (general purpose mobile manip.)
- Decon vacuuming device
- Radiation monitoring device
- General purpose mobile manipulator
- O/H crane crane
- Sector handling device
- Bolting tool
- Track-mounted welder

Equipment - Stage 5

- O/H crane
- Portable remote viewing
- Track-mounted welder
- ††Leak detection equipment
- General purpose mobile manipulator
- Decontamination equipment

*Sector alignment onto handling device is provided by guidelines; final alignment is provided
**Vacuum seal flange on sector is prepared in hot cell.
†Lines are preassembled into holding fixture.
††Pump down torus to base pressure; use tracer gas analyzer at sector pump system for vacuum te

ctor Replacement Procedures and Equipment

5

Assemble Sector Interfaces

11 shielded duct; weld vacuum flange (8 m)
e floor cover plate
11 duct elbow; weld flanges (8 m, 8 m)
check all welded flanges (22 m, 8 m, 8 m, 8 m)
ion lines, connect couplings

Lines	Connections	Diam (cm)
2	4	30
1	2	20
6	12	8
1	2	10
4	8	15
for waveguide		
1	2	3
for ICRH coax assembly		
1	2	20

check each coupling by pressurizing
ms with tracer gas
work area around sector for contaminated
s; cleanup as required

Equipment - Stage 5

crane
ble remote viewing
-mounted welder
detection equipment
ral purpose mobile manipulator
ntamination equipment

6

General Device Startup

- Final inspection by maintenance personnel
- Remove maintenance equipment to storage
- Circulate coolant in sector
- Activate torus pump system
- Recondition plasma chamber using bakeout, discharge cleaning, etc.
- Energize coils
- Begin reactor operations

Equipment - Stage 6

- O/H crane

d by guidelines; final alignment is provided by guide tracks which support the handling device.
cell.

analyzer at sector pump system for vacuum test; use tracer gas analyzer at coolant couplings.

the duct and the sector, removing the pump duct, and installing shield plugs over duct openings.

Removal of eroded particulate matter from the first wall surfaces of the sector prior to its removal is a measure which will minimize the potential contamination resulting from debris falling out of the sector during its extraction. This operation, as well as the installation of shield plugs, will enhance recovery back to contact operations before the sector is removed. Section 10 contains a discussion of the control of activated particulate matter.

Removing the sector is accomplished in the third stage. This consists of installing the sector handling machine, engaging the mechanisms of that device, attaching the contaminant collector to the sector, extracting the sector through the window area, and transporting the sector to the hot cell using the overhead crane.

Also shown in Table 7-1 is a listing of the major equipment needed in each of the three stages.

7.2.2 Sector Replacement

Sector replacement is Stage 4 of the complete scenario. It consists of inspection and decontamination of the open torus and the adjacent floor area, transporting the repaired sector from the hot cell to the sector handling machine, positioning the sector into the torus, inspecting vacuum flanges and bolt holes for alignment, removing the sector handling machine, installing structural attachments, welding the sector seal, and inspecting the floor area and decontaminating as required. If a shield plug is installed into the sector at the duct opening, personnel access to the sector is possible.

Stage 5 is the reassembly of all of the sector interfaces and final vacuum testing. It consists of installing the shielded duct and welding the flange joint, installing the duct elbow and welding its two flange joints, leak checking all three joints, installing all of the pipe assemblies and connecting couplings, leak testing the couplings, general inspection, and radiation check and cleanup as required. Many of the operations during this stage can be assisted by personnel. Continuous

radiation monitoring will be required before and during these manned operations.

General device startup is the sixth and final stage. It consists of a final inspection by maintenance personnel, removal of all maintenance equipment to storage, circulating coolant in the sector, starting up the torus pump system, reconditioning the plasma chamber, energizing the coils, and finally reactor plasma startup.

Table 7-2 includes a listing of the major equipment needed during each stage. It is the same equipment shown in Table 7-1, with the addition of leak detection equipment.

Table 7-3 is a listing of the major equipment identified from the sector removal and replacement scenarios, along with relevant comments. It is worth noting here that for the replacement of a single sector, there is no requirement for more than one unit of any equipment listed. The consideration of multiple sector replacement may require duplicating some of the equipment. The desirability of this approach could be determined by doing a cost-benefit analysis which assesses machine downtime saved versus the capital cost of the additional equipment required.

7.3 EQUIPMENT SPECIFICATIONS

The equipment specifications listed below reflect the functional and operational requirements of the maintenance equipment needed for sector removal and replacement. They were used as a starting point in developing the conceptual designs and in some cases were modified and expanded by the design teams where it was appropriate to do so. The use of magnetic materials is a case in point. The original specification mandated the use of nonmagnetic materials throughout the designs. Both design teams pointed out the unnecessary cost penalty which this requirement would impose; therefore, the original material specification was amended.

Also included below are the specifications for the In-Vessel Manipulator System (IVMS). Although this equipment is not actually required for sector replacement it was deemed important enough to be

Table 7-3. Manintenance equipment for the removal and replacement of one sector

Item	Comments
Movable manipulator system	• Used in all six stages of sector replacement • It interfaces directly with the equipment having an asterisk (*)
*Bolt removing tool	• Pneumatically driven
*Nut-runner	• For coolant couplings
Cutter/welder system	• Track mounted
*Lifting slings	• For lifting pipe assemblies
Overhead cranes	• 50-tonne capacity and 500-tonne capacity
Sector handling device	• Provisions for containment of contaminated debris
*Portable CCTV	• General viewing and inspection
*Leak detection equipment	• Inspection of flanges and couplings
*Decontamination equipment	• Portable vacuuming system

included in the equipment inventory. Its purpose and function are discussed below (Sect. 7.5). Its specifications are listed here for completeness in this section.

7.3.1 General Requirements for Equipment Design

7.3.1.1 Materials

- In general, nonmagnetic materials are preferred and should be considered where they do not have a significant impact on the cost of the equipment design. Nonmagnetic materials are a requirement for small tools (e.g., wrenches) used in the reactor building.
- All materials should exhibit resistance to degradation from gamma radiation. This is especially true for the use of organic substances.
- Impermeability to tritium should be a key factor in the selection of materials.
- External materials should be resistant to chemicals used for cleaning and decontamination.

7.3.1.2 Surfaces and finishes

- All equipment surfaces must be smooth, having at least a mill-quality finish. Magnetic materials may require coatings to protect their surfaces from corrosion and oxidation.
- Inaccessible equipment surfaces are to be avoided to ease cleaning and inspection.
- Penetrations into the maintenance equipment for moving parts, modular interfaces, and umbilicals must be sealed.

7.3.1.3 Equipment assembly

- Components which make up the maintenance equipment should be modular. Full access to the modular components is a requirement for maintenance of the equipment.
- Small equipment assembles or their modular components should be capable of glovebox repair when hands-on repairs are not possible.

7.3.2 Movable Manipulator System Requirements

7.3.2.1 Functional requirements

1. Steerable, wheel-mounted vehicle (tracked capability may be desirable).
2. Capability for lifting by O/H crane.
3. Independent (electric) drive to each wheel.
4. Mechanical tie-down capability at discrete locations around the tokamak.
5. Hydraulically actuated crane with two pivot joints (a telescoping boom may be desirable).
6. Lifting hook at end of boom.
7. Pair of force-reflecting arms with six DOF.
8. Remote viewing and audio systems.
9. Over-ride capability of tie-down mechanism for failure recovery.
10. Built-in tool storage.
11. Capability for unassisted tool changeout.
12. Crane base rotation: ±180° CW and CCW.

7.3.2.2 Operating requirements

1. Radiation environment of 100 rad/h.
2. Several tons of lift capacity at full reach of hook.
3. 10-meter reach at end-effector.

7.3.3 Sector Handling Machine Requirements

7.3.3.1 Functional requirements

1. Capability for lifting by O/H crane.
2. Track-mounted vehicle.
3. Mechanical tie-down to torus spool structure.
4. May incorporate one or more manipulator arms (force-reflecting or articulated) to assist sector removal task.
5. One or more viewing systems.
6. Over-ride capability of locking mechanism for failure recovery.

7.3.3.2 Operating requirements

1. Radiation environment of 1000 rads/h.
2. Extraction, retraction, and transport of a 375-tonne sector, 7 x 5 x 4 m.

7.3.4 In-Vessel Manipulator Systems Requirements

7.3.4.1 Functional requirements

1. Capability for lifting by O/H crane.
2. Track-mounted base.
3. Mechanical tie-down to torus shield or platform support.
4. Bilateral, force-reflecting manipulator system, mounted on a telescoping boom.
5. Viewing and audio systems.
6. Over-ride capability of locking mechanism and boom extension mechanism for failure recovery.
7. Storage and handling capacity for 100 armor tiles.
8. Tool storage.
9. Unassisted tool changeout.

7.3.4.2 Operating requirements

1. Radiation environment of 10^5 rads/h.
2. Boom base rotatable 90° CC and CCW in horizontal plane.
3. Boom up 24° and down 26° from the horizontal plane.
4. Full boom extension of 9 m with 500-lb lift capacity.
5. Static and dynamic compliance of a magnitude which does not hinder operations.
6. All-electric drive mechanisms.
7. Preprogrammed positioning of boom/manipulator.
8. Capability to decontaminate vessel surfaces.

7.4 TORUS SECTOR MAINTENANCE EQUIPMENT STUDIES

The sector replacement procedures and equipment specifications discussed in Sections 7.2 and 7.3 were used as a starting point for developing conceptual designs for two major pieces of equipment: the Sector Handling Machines (SHM) and the Movable Manipulator System (MMS). Two additional handling machines were also studied: a sub-component Handling Machine (SCHM), primarily used for replacing test modules, and a Limiter Blade Handling Machine (LBHM). Although these are not directly related to the sector replacement scenario, they are nevertheless of interest. A more detailed treatment of these four equipment designs as well as the trade studies which led to their development can be found in Reference 4.

7.4.1 Sector Handling Machine

Six methods of removal and replacement for the torus sector were investigated along with several different handling machine concepts.

1. Radial and vertical movement provided by a cantilevered machine.
2. Radial movement via straight radial tracks with redesigned radial seal.
3. Radial movement via straight radial tracks with a removable flat seal (EG&G's previous design).
4. Air bearing system with removable flat.
5. Moving chain to move the sector radially and support its weight.
6. Vertically moving track that rises up behind the sector seal flange.

Several of the above methods require that the seal be reconfigured from that shown in the FED baseline design description document.[1] The reconfiguration may use a radial seal (relative to the torus centerline) or the flat seal configuration developed by EG&G in the remote cutter/welder study.[5] Several of the concepts also require a rearrangement of the vacuum ducting to provide room for the seal. Approach 5 was determined to be the preferred method.

7.4.1.1 General arrangement

The sector handling machine assembly consists of two components: the machine itself and the machine handling frame. The handling machine is basically a 7 m x 6 m x 4 m stainless steel containment box designed to remove, replace, and house an FED torus sector. The machine contains a sealable door that allows for contamination control and entry and exit of the sector to and from the machine. The floor of the machine is a structural steel framework that provides radial tracks for the sector to roll on. It also provides for mounting a two chain pulling system to pull and push the sector into and out of the torus sector. Figure 7-2 shows the floor of the machine; Fig. 7-3 shows the chain system. A lifting frame could not be included in the design of the machine because it would increase the machine envelope to the point where it would not pass between the toroidal field coils. Accordingly, a conceptual design was developed for a detachable lifting fixture (Fig. 7-4).

7.4.1.2 Containment box

When the sector is removed from the torus, it may have a significant amount of radioactive contamination on its inside surfaces. This contamination could possibly become airborne and spread within the reactor building. To prevent this possibility, the sector will be cleaned prior to removal. Further, the sector handling machine will include a steel containment box to preclude contamination spread during handling of the sector. The contaminent will face seal to the torus frame at the sector seal weld flange. The seal is an inflatable elastomer that is mounted to the front face of the containment box. The seal will be inflated after the handling machine is in place and ready to remove a sector. Figure 7-5 shows the containment box and the seal configuration.

The containment box sides, top, and back are constructed of thin steel sheet. The walls are kept thin to reduce the overall machine weight. Stiffeners are welded to the walls to attain the necessary wall rigidity. Figure 7-5 also shows the stiffeners located at approximately 1-m centers and on the outside of the box. They were placed on the

ORNL-DWG 82-3866 FED

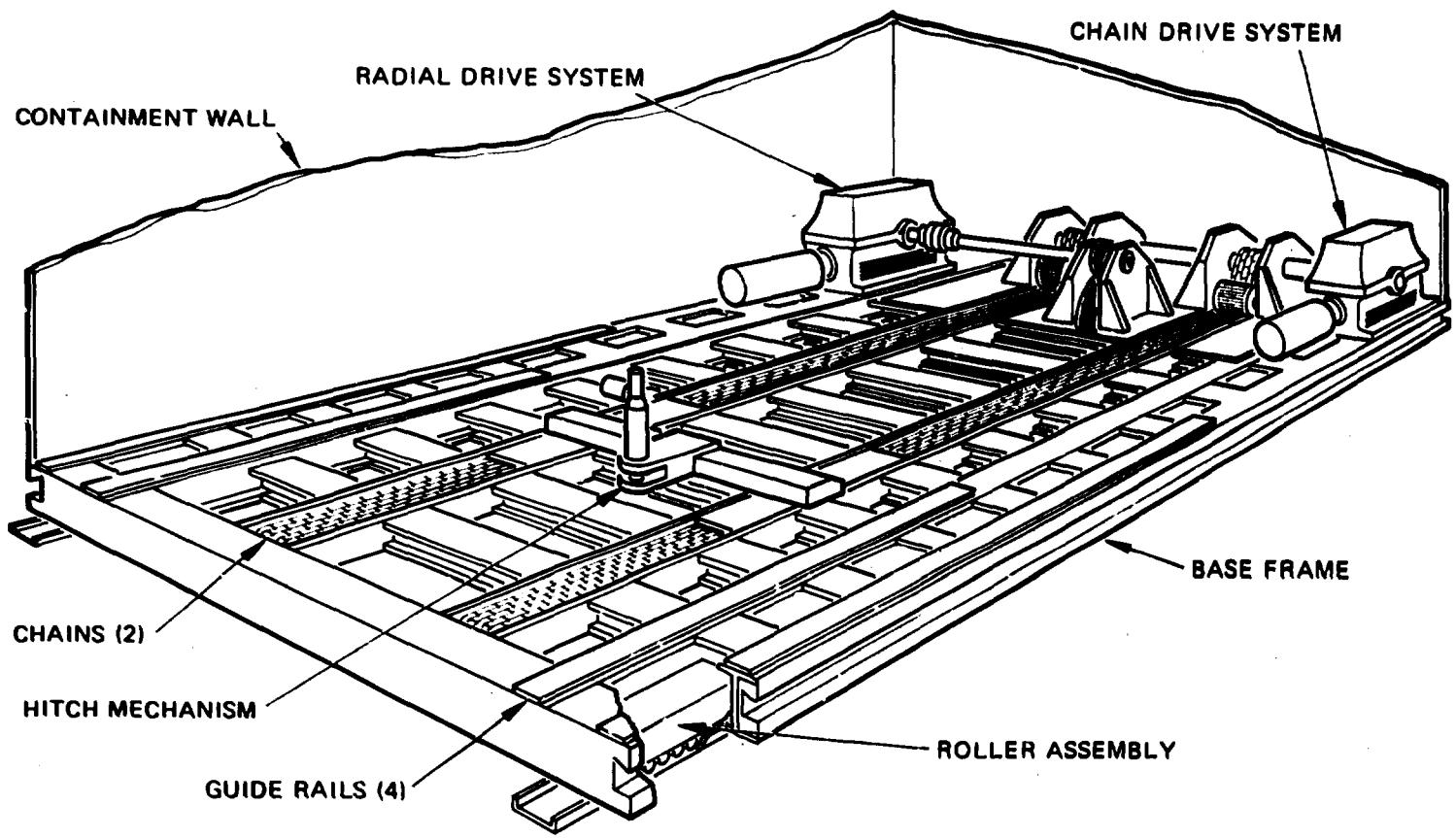

Fig. 7-2. Floor assembly of the sector handling machine.

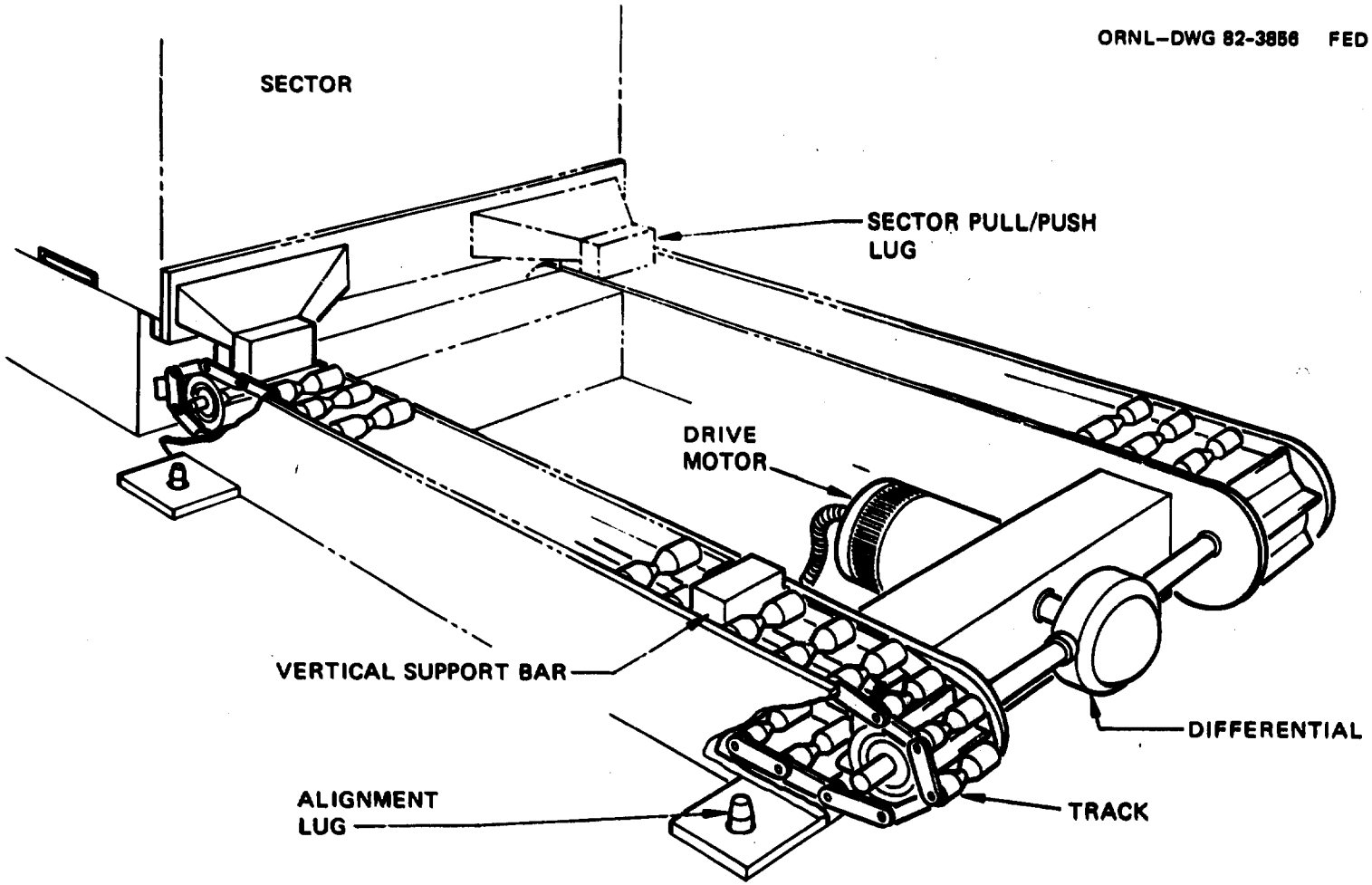

Fig. 7-3. Push/pull chain system for sector movement.

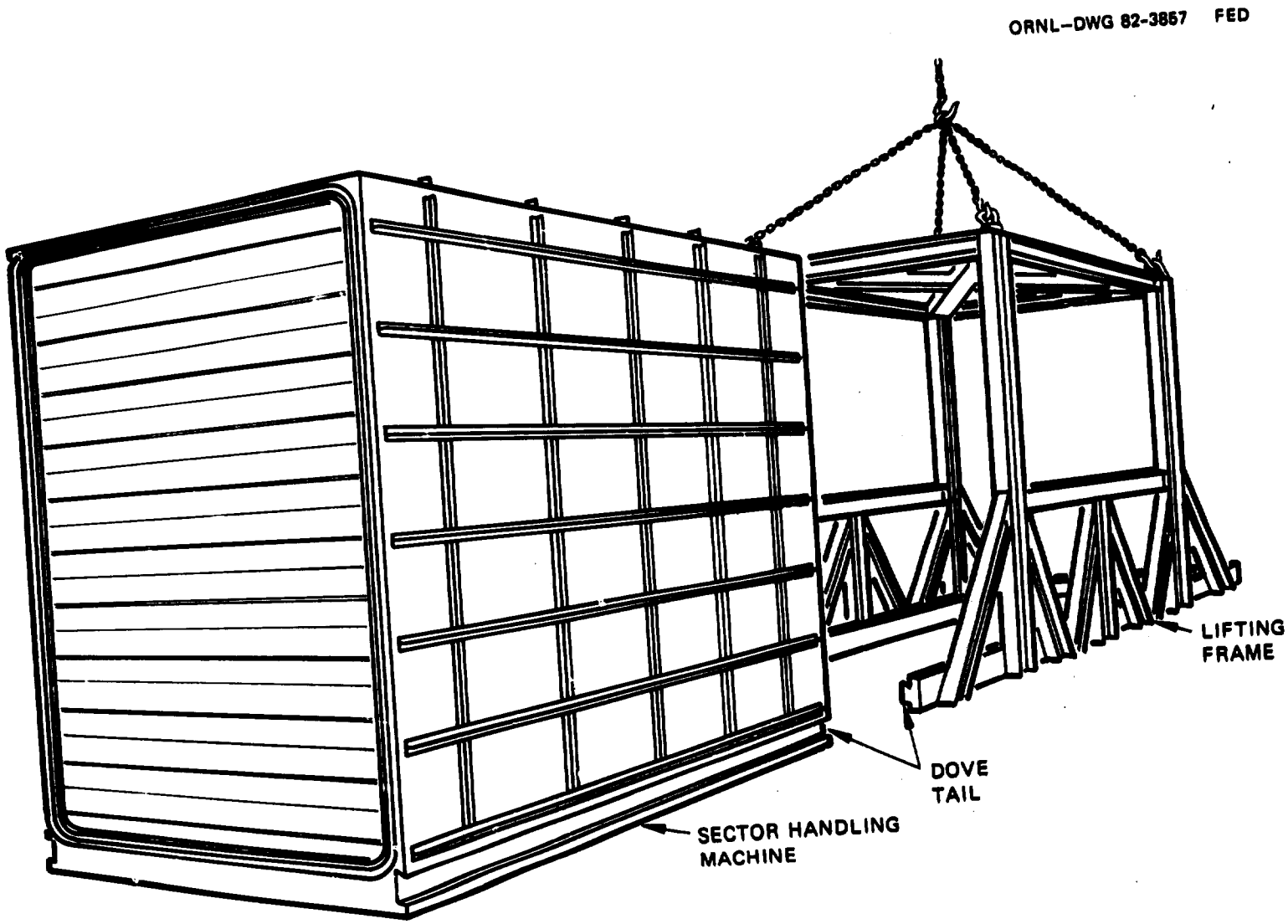

Fig. 7-4. Detachable lifting fixture.

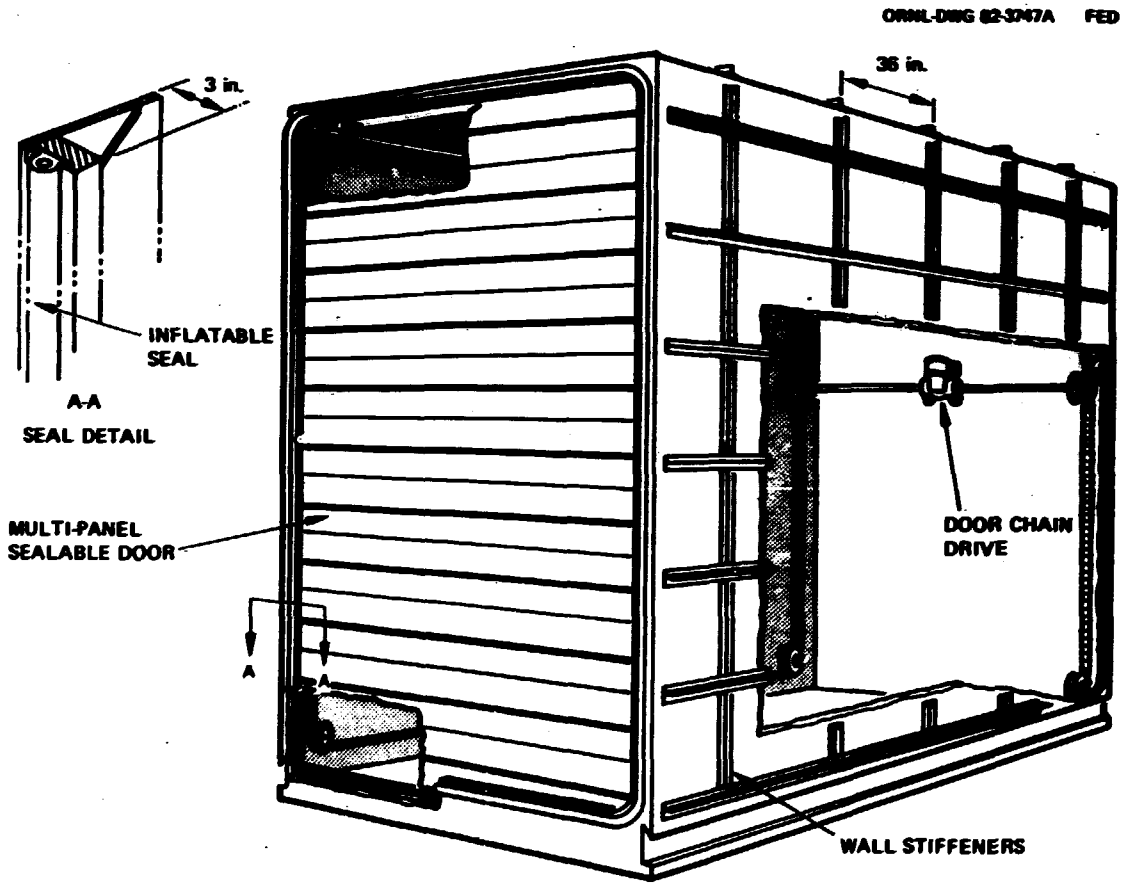

Fig. 7-5. Containment box and seal configuration.

outside to reduce decontamination concerns. If these stiffeners cause the containment box to be too wide to fit between the TF magnets, they could be moved to the inside of the box where they could occupy the same relative area as the door chains. This may, however, make contamination control and decontamination of the box more difficult.

7.4.1.3 Door assembly

The door assembly consists of the door, the door drive system, and the door tracks. The door design is patterned after large multipanel garage-type doors that are presently being installed in new fire stations and other similar facilities. These doors are made of a polyurethane core which is covered with steel coated with baked-on enamel finish. The doors incorporate inflatable seals between panels and at the top, bottom, and sides of the door. The thermal seals should act as excellent means of preventing the spread of contamination. The door as well as all other surfaces is painted with decontaminable paint, which is easy to clean up using a freon base system.

The door wheels travel in standard heavy duty garage door type tracks. These tracks are mounted to the sides (internal) of the containment box. They extend from the bottom front of the box, over the top, then down approximately 1/4 of the height of the back wall.

The door chains are continuous roller chains that attach to the top and bottom door panels. This attachment method should allow the door to always be pulled rather than pushed and pulled as in a single attachment method. A chain sprocket is located at each corner of the containment box. Thus, use of several idler sprockets is anticipated.

Both chains are driven by a common motor and gearbox. The gearbox has a shaft coming from each end that rotates the drive sprockets. The motor includes an encoder so that the position of the door can be continuously monitored. Microswitches are also included to establish door stopping points and provide some position redundancy.

7.4.1.4 Machine base

The base of the sector handling machine is constructed of structural steel shapes that have been welded together. The base provides four flat-plate-type guide rails that are used to support the weight of the sector and to guide and align it to the torus and to the handling machine. The flat tracks interface with heavy duty equipment chain rollers which are attached to the bottom of the sector. Figure 7-2 shows that the guide rails are of two different lengths. The shorter rails interface with the inner (radially) sector chain rollers and the longer with the outer ones.

The outer edge of the frame has a dove tail feature that allows for attachment of the lift fixture. The base structure is very rigid to prevent bending when the sector handling machine is lifted from the outside edges. The lifting frame is not attached to the sector handling machine because it would interfere with the toroidal field coils, as previously mentioned.

The base frame provides the guides for the sector pulling chains. It is also used for mounting the chain sprockets, the chain drive system, and the sector handling machine radial (reactor reference) drive assembly. Heavy duty equipment chain rollers are mounted to the bottom of the frame to provide for radial movement of the machine.

7.4.1.5 Chain drive assembly

The chain drive shown in Figs. 7-2 and 7-3 provides for pulling and pushing the sector out of and into the torus frame opening. The chains are driven via an electric motor driving a right angle gearbox which drives both pulling/pushing chains. The average tensile strength of the chains is approximately 200,000 lbs. The chain drive sprocket has one idler located in front and below it and one idler sprocket located directly below it. The idler sprockets are needed because of the height of the gearbox.

The chains attach to each end of the hitch mechanism which is an "H-shaped" structure. The legs of the "H" are guided by rollers that

interface with the base frame. These rollers are contained in slots that prevent the hitch from overturning while pulling or pushing. The body of the "H" is a structural steel member which attaches to its legs. A linear actuator is mounted to a tab which is located on the sector side of the body of the hitch. The actuator drives a pin between two plates on the hitch. The pin interfaces with a tongue which is permanently attached to the sector. The sector handling machine requires accurate alignment to the sector so that the hitch interfaces properly.

7.4.1.6 Radial drive

Since the reactor cryostat interferes with overhead lifting space, a rack and gear system is provided to move the sector handling machine radially toward the center of the torus. A gear rack is mounted in the floor of the reactor building. The drive gear is mounted to the base frame and is driven by a right angle gearbox, which is driven by an electric motor. Figure 7-3 does not show a cover over the drive train although one is included to prevent contamination spread out the bottom of the handling machine frame. It is a requirement to cover all the drive trains within the containment to improve the decontaminability of the machine.

7.4.2 Movable Manipulator System

7.4.2.1 General arrangement

The movable manipulator system (Fig. 7-6) consists of a dolly with motor-driven, power-turn drive wheels at each corner, an articulated boom-arm assembly mounted on a trunnion which is basemounted to the dolly, and a boom-arm tip section with an integral tool interface block. Two bilateral force-reflecting manipulators are mounted on either side of the boom-arm assembly near the tip section. All motive power devices are electric on the mobile manipulator. A control console for remote control of the machine is provided.

ORNL-DWG 82-3858 FED

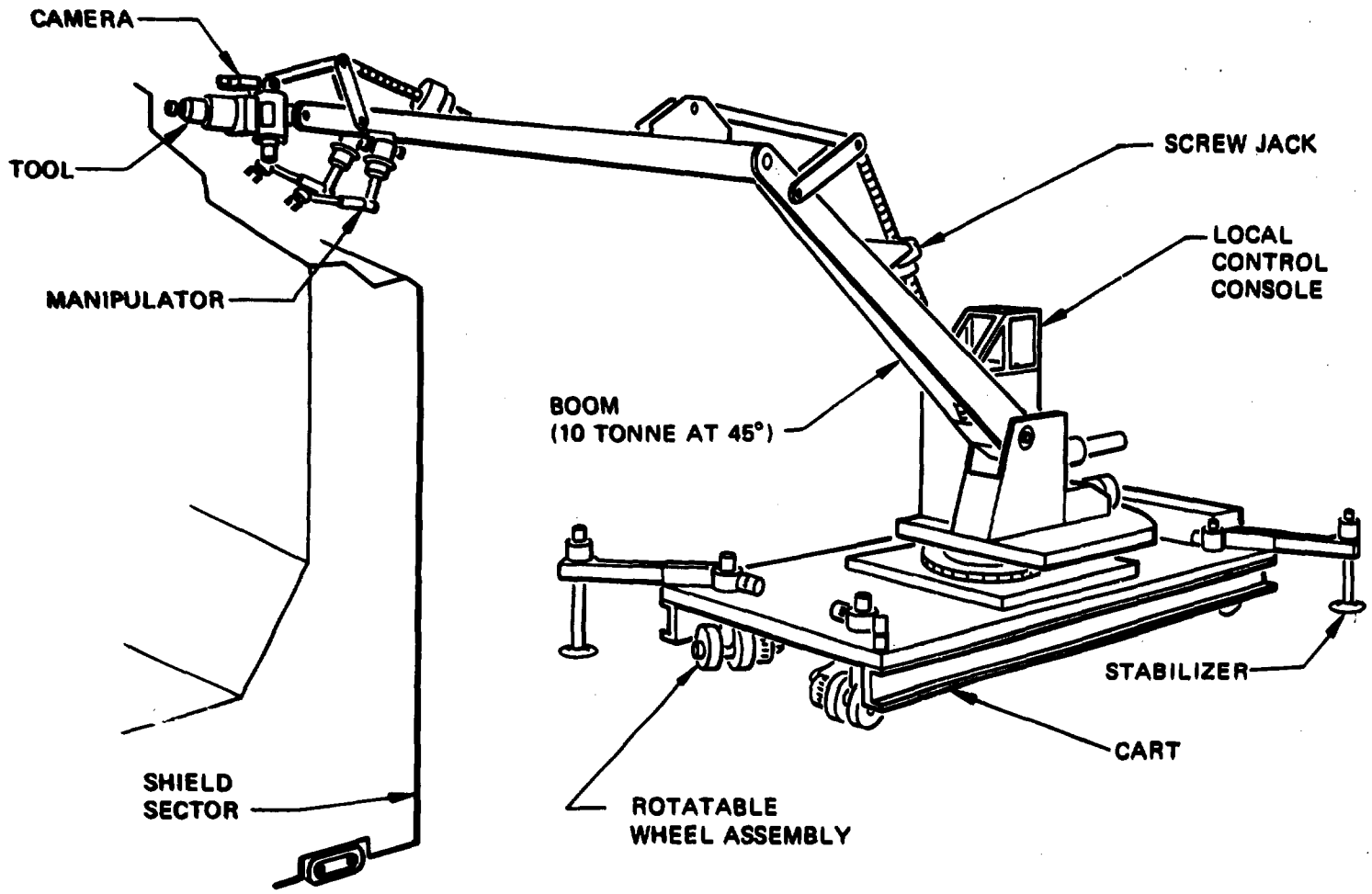

Fig. 7-6. Movable manipulator system.

7.4.2.2 Dolly

The mobile manipulator dolly is sized to provide a stable work platform for the boom-arm assembly when extended and loaded within the 10-m, 45°, 10-tonne design limit. The dolly footprint, with the stabilizers extended, is about 6 m on a side. The dolly framework is made up of structural steel shapes and plates as shown in Fig. 7-7. Mobility of the machine is provided by 4 drive wheels, one at each corner of the dolly.

The drive wheel assemblies each consist of 3 polyurethane-rimmed caster-type wheels, the center one of which is driven, with the 2 outer wheels free-wheeling to permit easy pivot motion. These 3 wheels share a common shaft. An electric motor gearbox combination connected to the shaft provides dolly translation capability, and a steering spindle connects the caster frame to a steering gear reducer which is mounted on the dolly top surface. These steering gear reducers are connected to a steering motor gear reducer combination by means of shafting and two electric clutches. The MMS can drive in any direction or can rotate about its own central axis by means of clutching either of the two pairs of casters.

Each corner of the dolly is fitted with stabilizer beams which are supported to the dolly framework by means of roller bearings. Also supporting the stabilizer beams are rack and pinion combinations which are electric gear motor-driven for beam extension and retraction. A commercial jactuator on the beam outer end drives support columns to the facility floor.

The dolly is fitted with a tool storage rack for remote tool change-out and with one or more combination power and control wiring umbilical cables for connecting to electric receptacles which must be located at proper intervals on the walls or floor of the reactor room. Provision is also made for attachment of slings to the dolly for lifting and transporting the entire MMS using the main overhead crane.

An alternate "floor-mounted" design of the wheel-mounted dolly would incorporate pins on each corner of the dolly structure. These pins would fit floor pockets installed at selected locations near each

ORNL-DWG 82-3859 FED

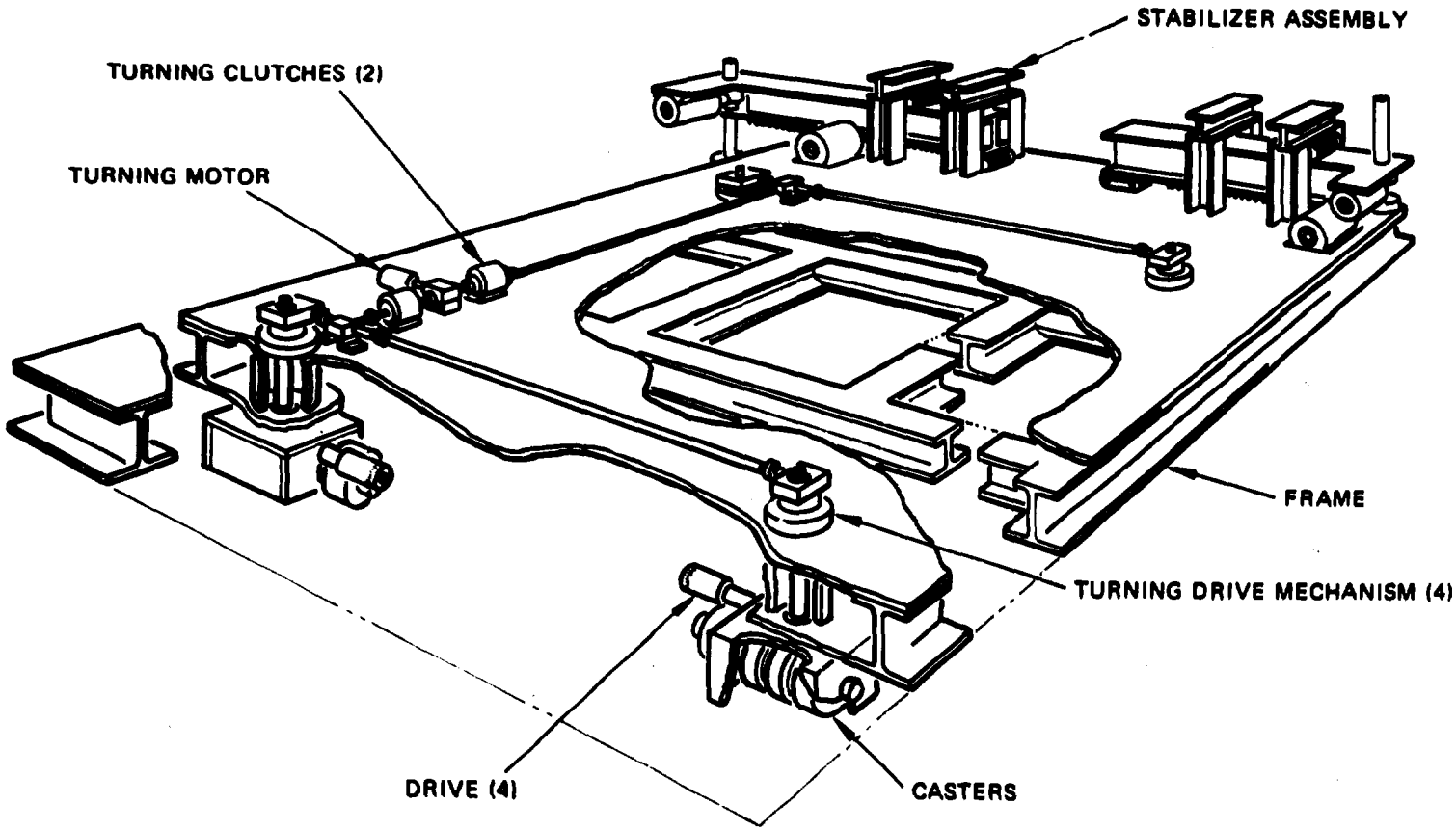

Fig. 7-7. Undercarriage for the MMS.

torus sector. The locations would provide 360° coverage of the reactor face. The movable manipulator system would also be positioned using the overhead crane in this version.

7.4.2.3 Boom-arm assembly

The MMS boom-arm assembly is trunnion-mounted through a base to the center of the dolly. The trunnion assembly consists of the base plate, a large combination ring gear and bearing assembly for trunnion rotation, an electric gear motor with the rotation drive pinion, structural plates with the boom pivot bearings, the boom jactuator-type actuators, and the operator cab. Lead counterweights totaling 11,000 kg are mounted on the trunnion structural plate just above the main rotational bearing.

The boom is built from welded steel plates which have a tapered rectangular tube configuration. An electric-motor-driven actuator mounted near the boom end controls the arm position. The actuator location on the top of the boom provides a clean lower boom surface to allow closest proximity to the reactor face for maximum vertical reach capability.

The arm assembly is similar in construction to the boom and incorporates an actuator at its end to control the tip vertical/rotational position. Two force-sensing, electrically driven, slave manipulators are mounted on each side of the arm tip. These are envisioned to be capable of handling larger loads than the commercial manipulators now available but can be based on the same structural and control systems designs.

7.4.2.4 Tip

The boom-arm tip section performs the primary lifting function of the MMS. It also incorporates a plate which is the interface to a wide variety of specialty tools which are individually mounted to it. The specialty tools include impact wrenches, lift hooks, welding heads, etc. Figures 7-8 and 7-9 are two different views of this component.

The interface plate performs pitch, yaw, and roll motions, similar to a human wrist. A CCTV camera is mounted on the tip just behind the

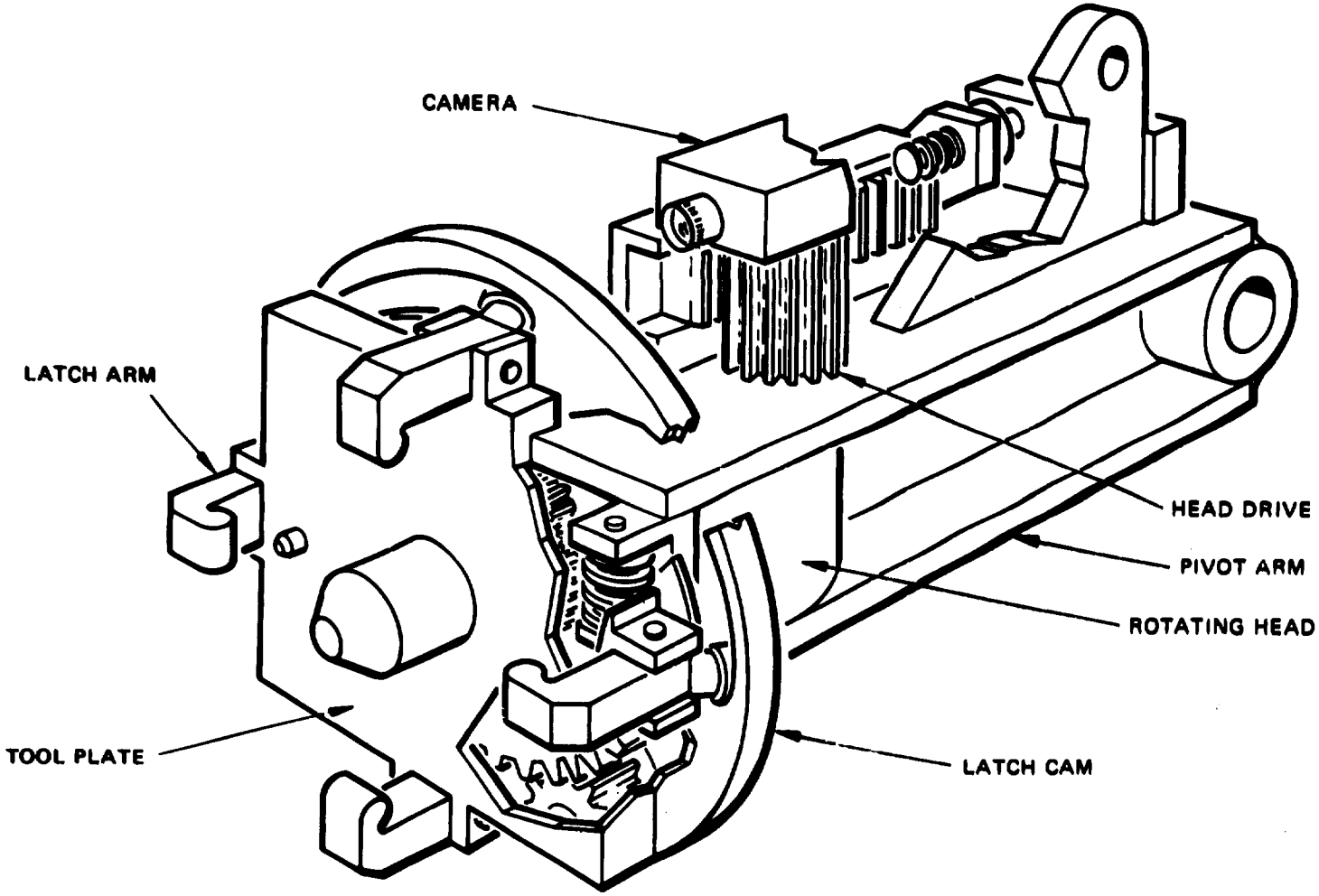

Fig. 7-8. MMS tip end.

ORNL-DWG 82-3861 FED

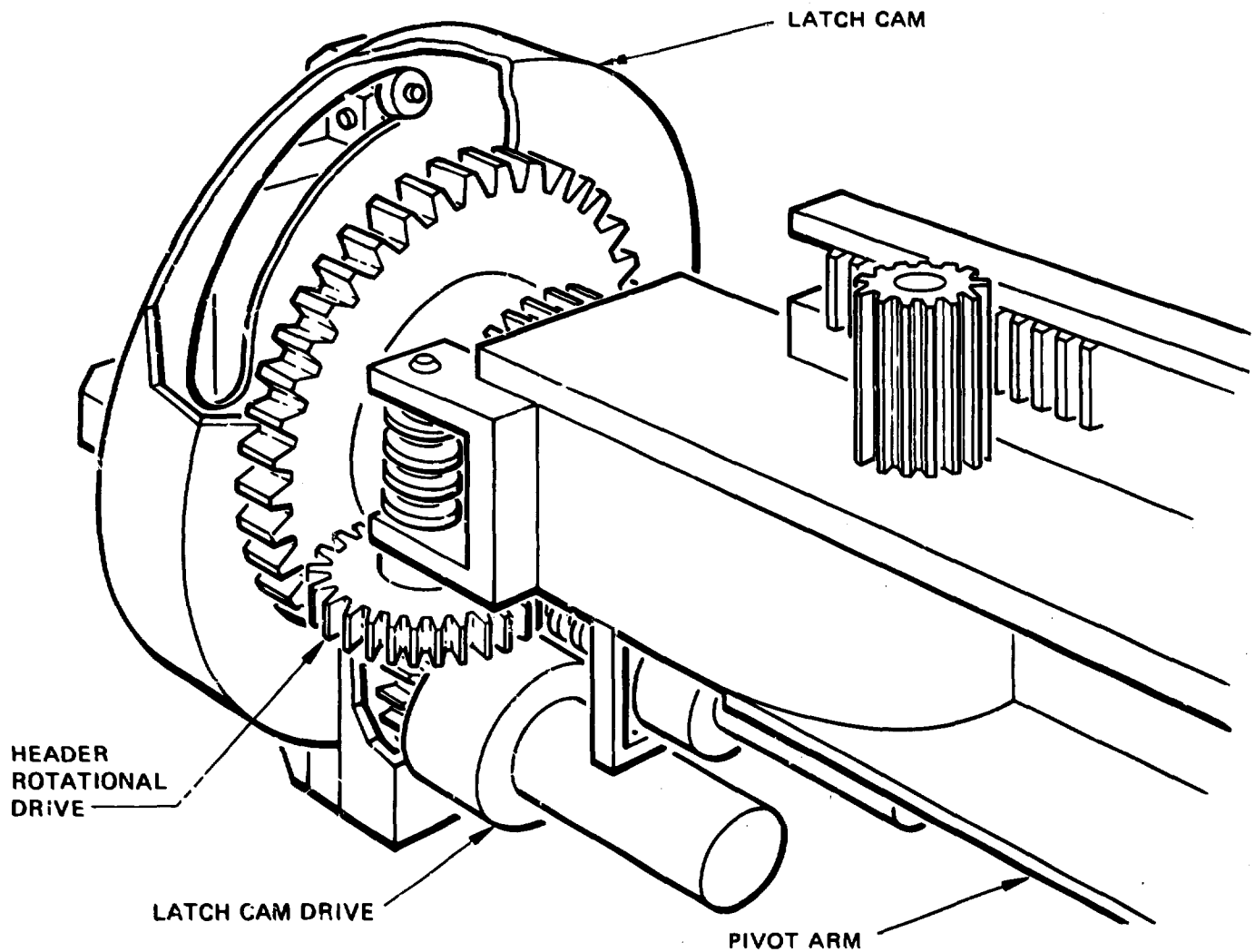

Fig. 7-9. MMS tip end.

plate and allows viewing the actions performed both by the tooling and by the slave manipulators. Radiation monitors can also be mounted on the tip for general and specific informational purposes.

The design of the tip area of the boom arm includes provisions for frequent decontamination by a variety of means. This requires that the materials of fabrication should be highly resistant to radiation and corrosion. Bearings are double sealed and the avoidance of crevices is incorporated into the design to avoid trapping contaminated material.

7.4.2.5 Control console

Control of the MMS is accomplished with a console positioned outside the reactor room. The control room may have a shielding window allowing the operator to observe gross manipulator movements. The control console has TV monitoring for viewing tip tool actions recorded by the remote camera at the arm tip. Additional viewing of the mobile manipulator system is by means of the CCTV systems located throughout the reactor room.

The control console contains primarily four functional areas. Figure 7-10 shows the arrangement of controls, displays, and annunciators. The first functional area is for basic manual manipulator control. The dolly has switches for power on and off, travel forward and reverse, left and right turn, and stabilizers extend up and down. The base section has controls for power on and off, boom dip up and down, boom swing right and left, and arm swing up and down. The tip section has tool locked and free, tip plate rotate clockwise and counterclockwise, tip swing right and left, and tip dip up and down. Four switches are provided for tool function control.

The second control console area includes digital readouts for numerical indication of the various manual operations. These include boom swing, boom dip, arm dip, tip dip, tip swing, tip rotate, and radiation levels. The numerical indications could include readings of boom-arm element angle, three-dimensional coordinate readings, and even force inputs from load cells built into the MMS at a variety of locations. Excessive movements or forces could be visually indicated by lights

ORNL-DWG 82-3862 FED

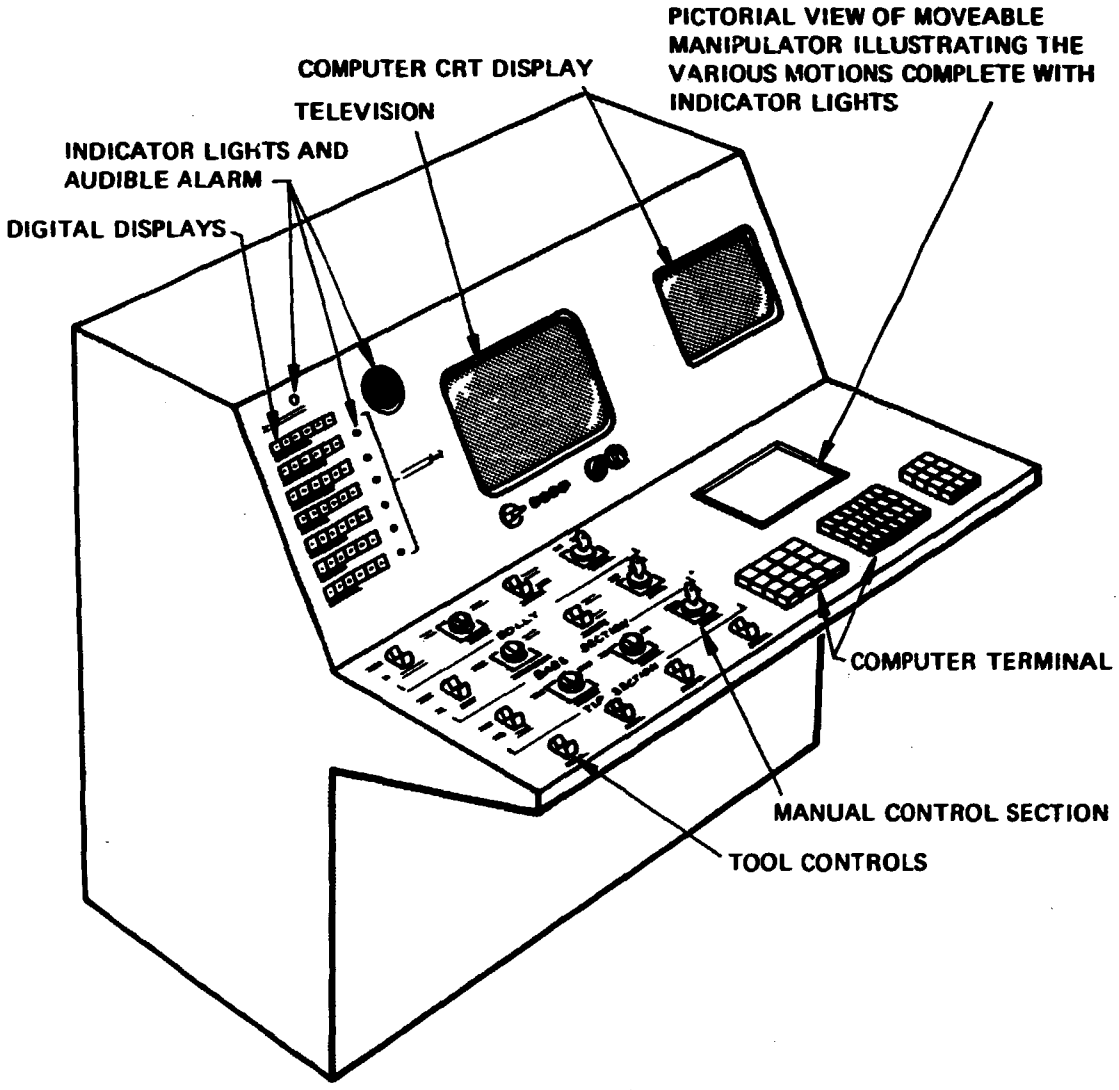

Fig. 7-10. MMS control console arrangement.

adjacent to each digital display, and an audible alarm is also provided to call operator attention to an improper situation.

The third area is the CCTV screen which monitors cameras located on the manipulator itself and those located elsewhere in the reactor room.

The fourth area represents a control methodology not included above, which is programmed control of the boom, arm, and tip by microprocessor. It is believed to be desirable to have certain system functions preprogrammed. These functions would be repetitious in nature and would require "zeroing" the manipulator elements in relation to the article on the reactor face prior to performing the functions. They may include, for example, unscrewing a series of captive bolts. Preprogrammed operations are expected to greatly reduce the time needed to relocate the tool tip and to perform the operation at that location. The computer CRT displays the procedural step being performed and can also be used in programming new operations into the microprocessor system. An example is a computer-drawn picture of the mobile manipulator taking information from encoders located at various positions on the mobile manipulator. This feature may be useful in determining the correct interfacing of the manipulator tooling with elements on the reactor structure.

It is a requirement that the movable manipulator system be capable of manual operation. Therefore, the control console in the cab essentially duplicates the control areas described above except for the fourth area, which is not required.

7.4.3 Sub-Component Handling Machine

During the development of the conceptual design of the Sector Handling Machine and the movable manipulator system it was recognized that a machine was required to handle sector subcomponents. Examples of these subcomponents are:

- plasma heating systems,
- shield plugs, and
- test modules.

The heaviest of these items could weight as much as 65 tonnes.

In addition, it was felt that to design a movable manipulator system for a capacity of up to 65 tonnes would result in a machine design that would be excessively large and expensive, and the manipulator would be much too cumbersome to do routine tasks around the reactor. It was recognized that a manipulator system of this type could not accurately position and retrieve large components without a significant potential for alignment problems and equipment damage.

A detailed set of conceptual design requirements has not been developed for the subcomponent handling machine. However, the general requirements are for the device to (a) handle components weighing up to 65 tonnes (i.e., ICRH shielding plug), (b) provide insertion and removal of subcomponents with x-y-z positioning accuracy to 0.5 cm, and (c) provide a common tooling interface for fixtures used to handle various subcomponents.

7.4.3.1 General arrangement

Figure 7-11 shows the general arrangement of the Sub-Component Handling Machine (SCHM). The machine is basically a right-angle structural steel frame which has two travel frames, one for horizontal motion of the tooling plate and one for vertical motion. This provides x and y motion of the tooling plate to line up with subcomponents for insertion and removal.

7.4.3.2 Frame

The right angle frame is made of structural steel I-beams that form the base and the vertical riser. The base has corner-to-corner gussets to provide rigidity. Vertical stability of the risers is provided by two I-beam gussets that are welded to the risers and the frame. A 40-tonne counter-weight is mounted to the back of the base to prevent tipping while lifting and moving large components. Lead would make an ideal counter-weight material and would result in a reasonably sized structure.

Travel rollers are provided at each corner of the frame to provide for z-motion of the tooling plate and the entire machine. The cart is

ORNL-DWG 82-3863 FED

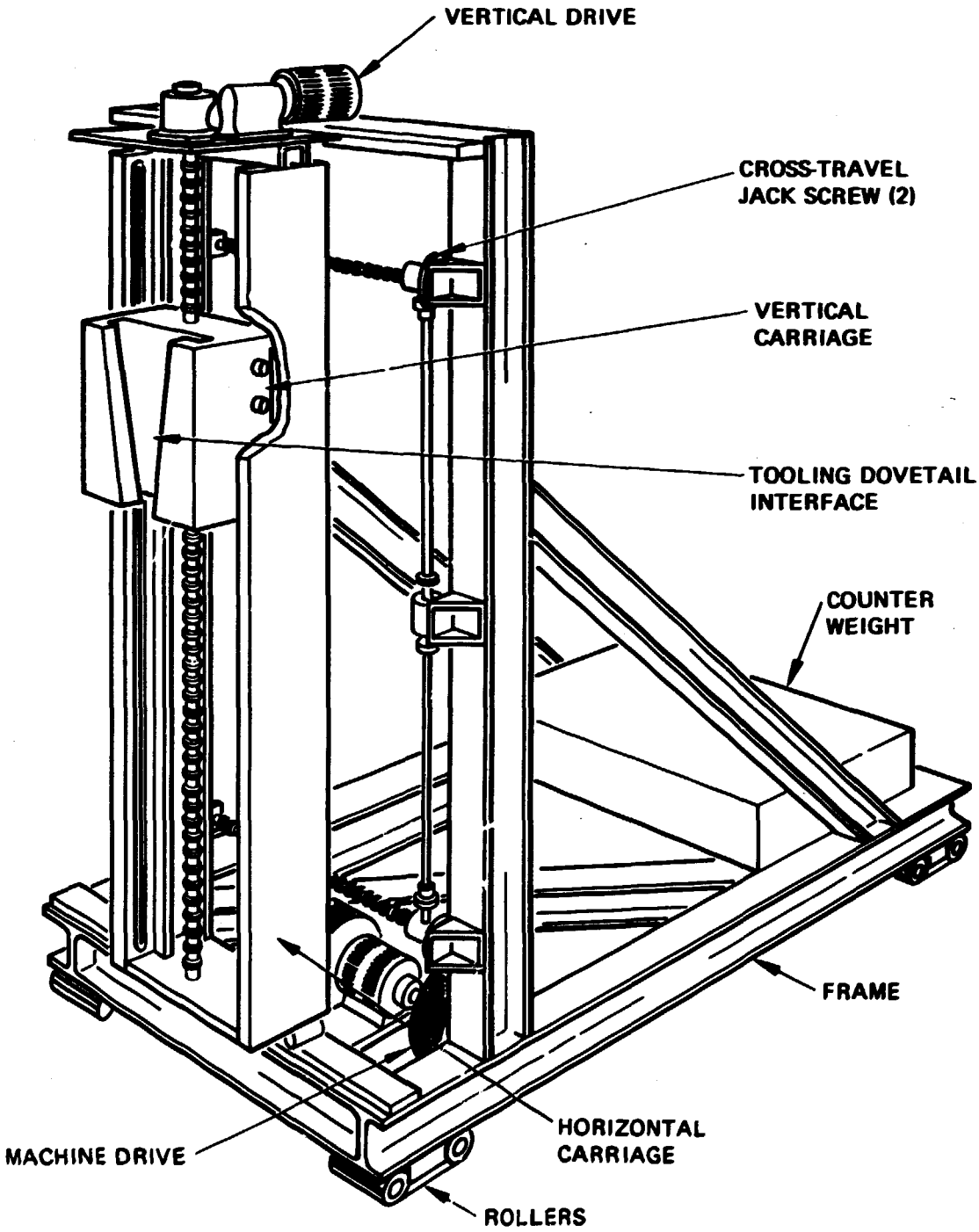

Fig. 7-11. Sub-component handling machine.

driven by an electric motor which attaches to two-friction drive wheels which contact the floor. A rack drive similar to that shown for the SHM may prove to be more desirable. Sizing of the drive motor depends on gearbox size and ratio and the desired pulling and pushing force.

7.4.3.3 Vertical travel frame

The vertical travel frame provides for the horizontal movement of the tooling plate and the mounting for the mechanisms that accomplish the vertical movement of the tooling plate. The frame is constructed of two structural steel I-beams on the sides. The sides are tied together at the top and bottom using plates and beams. Rollers are mounted to the bottom plate to carry the weight of the vertical travel frame and the component being lifted. These rollers interface with the top of the right angle frame. Cam rollers at the top of the vertical travel frame interface with a guide track on the right angle frame and prevent overturning of the vertical travel frame when it is loaded. The frame is moved horizontally by two jactuators, one located near the top and one near the bottom of the frame. The jactuators, motor, gearboxes, and bearings are mounted on the base frame vertical risers.

7.4.3.5 Tooling plate

The tooling plate is mounted to the vertical travel frame via cam rollers mounted in grooves in the sides of the frame. These cam rollers prevent overturning of the tooling plate. The vertical travel of the plate is provided by a jactuator screw which is routed through the back of the tooling plate structure. The jactuator motor and gearbox are mounted on the top of the vertical travel frame. The interface between tools and the tooling plate is a simple V-guide arrangement. A more sophisticated interface may be desirable in future designs and after tooling designs are established.

7.4.4 Limiter Blade Handling Machine

A handling device for the replacement of limiter blades generally has all of the maintenance equipment requirements previously discussed. The additional requirement of holding the plasma chamber at vacuum during this operation is desirable because it appears to minimize the impact to availability. Thus, a concept was developed to depict a method for limiter blade removal and replacement without significantly affecting the torus vacuum (Fig. 7-12).

7.4.4.1 Operating scenario

The limiter blade is mechanically fastened and sealed to the torus sector. Removal of this component begins by inflating a seal between the blade mounting flange outer circumference and a similar concentric flange (inside circumference) that is attached to the sector. After the seal is inflated, the limiter blade fasteners can be removed using a hands-on operation. The Limiter Blade Handling Machine (LBHM) is then moved into place so that its front flange interfaces with the outside circumference of the sector flange mentioned above. A second inflatable seal is then expanded between the sector flange and the limiter blade handling flange. The internal volume of the LBHM is then evacuated in preparation for pulling the blade radially out of the torus sector.

The handling machine lower chain drive system assembly is then elevated so that the chain lugs interface with a pulling lug on the divertor blade. The inner inflatable seal is then deflated and the chain drive is actuated in order to pull the blade from the sector. The roller chain supports the limiter weight. When the blade is fully retracted, the chain drive assemblies are then lowered until the replacement blade which is located on the upper chain drive assembly is in line with the sector opening. The upper chain drive assembly is now actuated and the new divertor blade is installed into the sector.

After the replacement blade is installed, the inner inflatable seal is expanded so that the divertor blade is sealed to the sector. The LBHM internal volume is then let up to air, the outer inflatable seal

ORNL-DWG 82-3884 FED

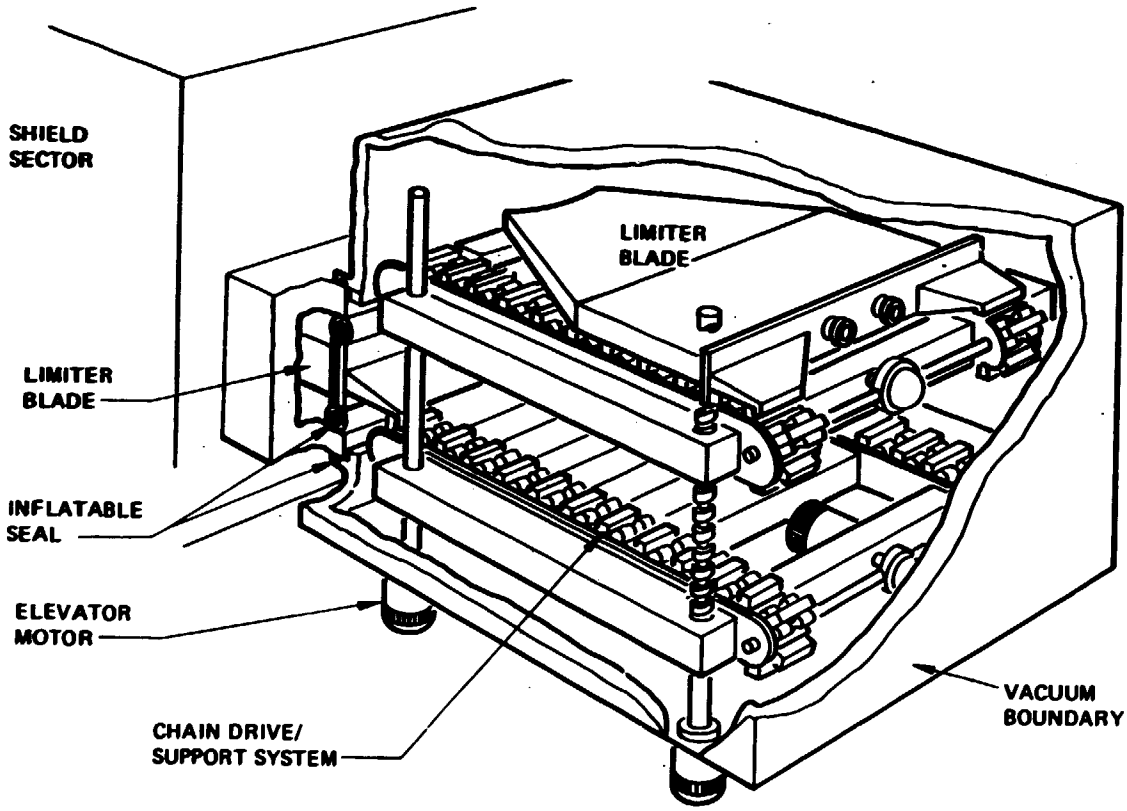

Fig. 7-12. Limiter blade handling machine.

is deflated, and the machine is moved radially away from the torus. The limiter blade can be fastened in place and the inner inflatable seal can be deflated.

7.4.4.2 Design description

The Limiter Blade Handling Machine was configured to remove and replace blades from the torus sector while maintaining the vacuum integrity of the plasma chamber. The machine consists of a rectangular vacuum vessel, two elevatable chain tables, an inflatable seal, drive components for the chains and tables, and the control system. It was assumed that there will be tracks in the floor to support and align the machine to the sector/limiter blade. It was also assumed that there is adequate vertical space to allow the machine to be moved into position. This is actually not the case for the FED baseline design because the vacuum duct interferes with the machine's lower surfaces. However, it is likely that the vacuum ducting will be relocated in future FED designs.

The vacuum boundary of the LBHM is intended to be capable of withstanding a differential pressure of ≅15 psi. Because the surface area is very large, the boundary will have to be honeycombed or gusseted to handle this pressure. The lower plate of the vacuum boundary will also have to be heavily reinforced to support the elevator drive system, the floors, and the limiter blade. The front face of the vacuum boundary includes a flange which houses an inflatable elastomer seal. This seal interfaces with a flange on the sector and establishes the enclosed volume of the limiter blade handling machine.

Vertical movement of the chain tables is accomplished by four jactuators located at the corners of the tables. The base of the jactuator is mounted to and sealed to the vacuum boundary wall. The jactuator screws are routed through nuts located in the side structure of the chain tables. The jactuator motors include encoders so that the rotation of each screw can be synchronized to the others, to assure level movement. Limit switches control the limits of movement and the stopping positions for the chain tables to allow insertion and removal of the divertor blade.

Each chain table has a drive system which rotates the two chains simultaneously. The drive system consists of an electric motor, encoders, a gear box, and a differential. The continuous roller chains are routed over gears located at each end of the table and are located in guides to prevent side movement. The lower portion of the chain passes through a channel to prevent sagging. Riser bars are welded to the chain links so that the limiter blade does not rest on the chain rollers. The bars are designed to engage pulling lugs on the divertor blade so that it can be removed and replaced by the chain movement.

Vacuum grade electrical feedthroughs and connectors are provided on the outside of the containment for easy hookup of the control system. The control panel includes lights indicating microswitch position, four digital counters to indicate table/jactuator positions, and digital counters to indicate position of the chain. Controls for a mechanical vacuum pump and a TC vacuum gauge are included. These are contained in a small portable electrical rack.

7.4.5 Equipment Costs

The conceptual designs discussed in Sects. 7.4.1 through 7.4.4 were developed in sufficient detail to determine if present equipment technology is adequate for these machine requirements and to determine what these equipment costs would be. Table 7-4 is a summary of the direct and indirect capital costs for the major handling equipment envisioned for sector and sector-mounted component replacement operations.

7.5 IN-VESSEL MANIPULATOR SYSTEM

7.5.1 In-Vessel Maintenance Operations

Maintenance operations using in-vessel procedures are required to maximize availability. A study was undertaken to identify potential in-vessel operations, assess the requirements of these operations, and determine what benefits exist.

Table 7-4. Summary of equipment costs*

Capital costs ($ K)	Sector handling machine	Movable manipulator system	Sub-component handling machine	Limit blade handling machine
Direct (procurement and fabrication)	479	1,037	383	494
Indirect (engineering, design, and testing)	451	1,472	418	869
Subtotal	930	2,509	801	1,363
Contingency (30%)	279	753	240	409
Total	1,209 K	3,262 K	1,041 K	1,772 K

*Reference 4 contains a detailed description of the cost breakdown.

The primary maintenance scenario which was considered is the replacement of first wall armor tiles using an in-vessel manipulator system (IVMS) in conjunction with other maintenance equipment. Entry into the plasma chamber is through three torus penetrations, namely, the fueling bay and two of the heating bays. Modular removal of the fueling system or the ICRH heating system along with their respective shield plugs provides the required opening into the plasma chamber. The locations of the entry ports are not necessarily optimized for in-vessel operations in the present configuration. They were located according to the FED baseline and are shown in Fig. 7-13.

It was found that a minimum reduction of 10% in downtime is realized when comparing in-vessel operations to hot cell operations. In addition, in-vessel procedures are also a maintenance option which provides flexibility to handle the unexpected – a feature which is consistent with the experimental nature of the FED mission.

7.5.1.1 Discussion

Disassembly of the plasma chamber has had a major influence on the configuration development of FED. It has impacted the size of the TF coils, the location of intercoil structure, and the positioning of the EF coils. As a result, individual shield sector modules are readily replaceable through individual window openings should there be a need for torus maintenance. Several examples of primary failure modes which could require its replacement/repair are (1) first wall panel or bulk shield coolant leaks into the plasma chamber; (2) diagnostic or instrument failures; and (3) armor tile damage. All of these represent unscheduled events in view of the fact that the torus is designed as a lifetime component with the potential to remain undisturbed throughout the FED operations. Of the failures listed above, the first two require hot cell operations; i.e., replacement of a F/W panel in its current design does not appear to be a viable in-vessel operation. Replacement of armor tiles, however, depending on the number involved, may require less time using in-situ operations. The following discussion is an assessment of armor tile replacement comparing in-vessel operations to

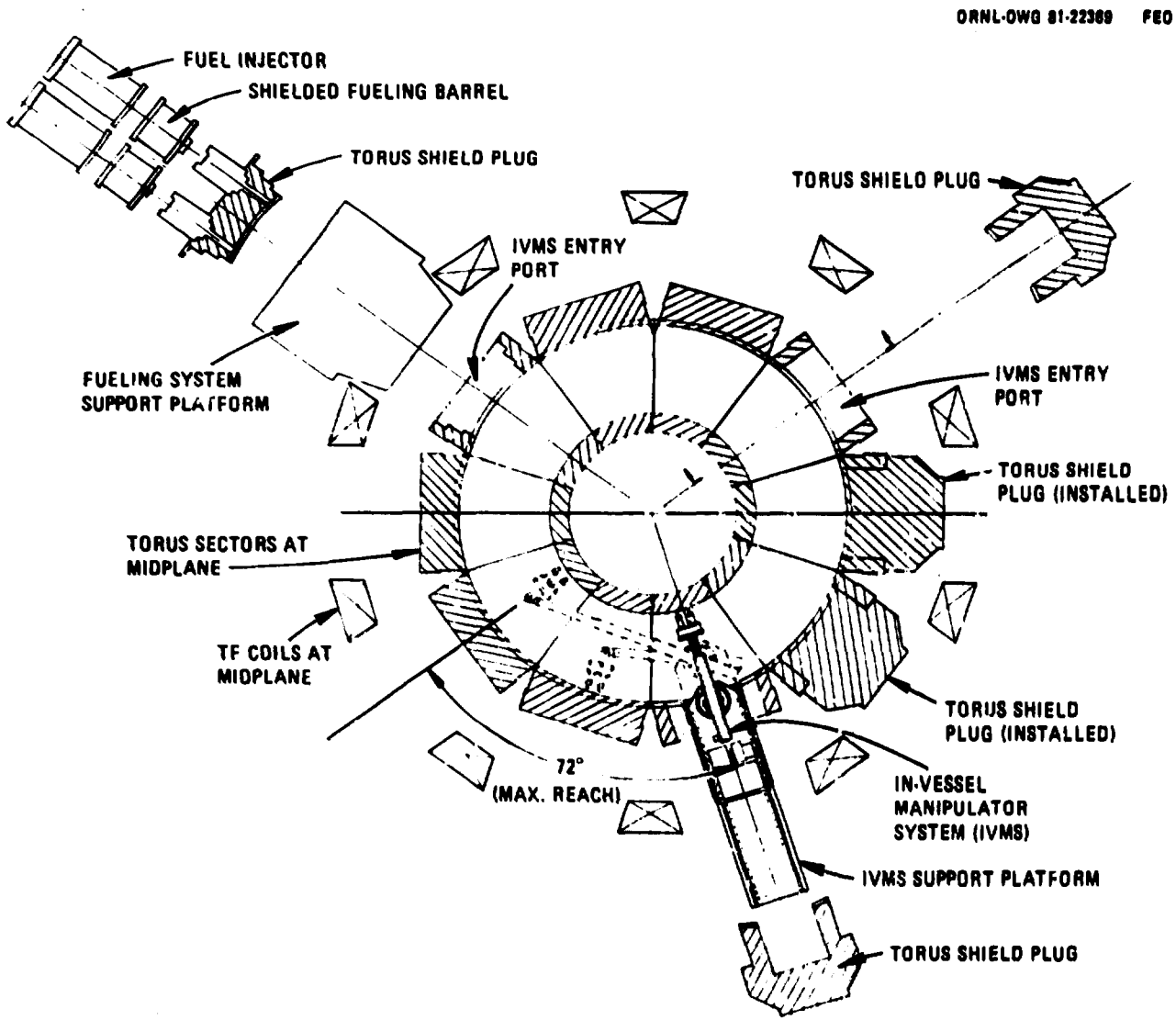

Fig. 7-13. MMS entry ports.

removing a sector to the hot cell. The operation which has the smaller downtime for the device will be the preferred choice if it is shown to be cost-effective. Also, if this proves to be beneficial, other internal operations can be postulated.

In developing the in-situ details for making this assessment, the following were considered:

- the failure scenario,
- location and size of entry ports for an in-vessel manipulator system (IVMS),
- design requirements for the IVMS (Sect. 7.3.3),
- other maintenance equipment requirements,
- a time and motion evaluation,
- cost of in-vessel operations, and
- other in-vessel operations which may be possible.

7.5.1.2 Failure scenario

A failure scenario was assumed in order to establish the need for tile replacement. It is that a large piece of a tile (or tiles) has broken off and comes to rest on the limiter blade surface. The resulting unprotected F/W surface will probably not require immediate attention, but the graphite mass on the limiter may impede plasma operations depending upon its location on the blade. It is further assumed that the graphite piece has a high probability of ending up where the plasma scrape-off meets the limiter. (Small tile fragments on the limiter or pieces that have fallen into the limiter duct are assumed to pose no immediate problem.)

For this failure scenario, it may also be assumed that the damage is first assessed by some means of in-vessel inspection and that the unprotected wall surfaces can be visually located to individual sectors; therefore, the locations of broken tiles in the plasma chamber can be mapped. The importance of in-vessel inspection is recognized within the context of overall device maintenance even though it could not be included in this assessment. It is being planned for inclusion in next year's work.

7.5.1.3 Entry ports

In the design description report for FY 81[1] in-vessel operations are briefly mentioned in Sects. 3 and 8, and the possible location of entry ports was shown in Fig. 3-21. These four locations were chosen to provide symmetry and to minimize the "reach" of an IVMS. As it turns out, they are not ideally located when considering the FED plan view and the arrangement of component systems. There are two basic requirements for the ports: (1) they must provide a sufficient opening for the manipulator system and (2) they must be readily accessible. The component bays which qualify for these requirements are those for the fuel injector and the ICRH heating. The remaining bays are occupied by I&C and testing modules, and, unlike the fueling and heating bays, they have numerous small penetrations (<1 m^2) with many electrical and coolant connections. Figure 7-13 shows the relative position of the currently proposed openings. The longest reach required is 72° between the injector shield plugs. The figure also shows the modular breakaway of the pellet injector components and the ICRH launcher components.

In order to minimize the total downtime, disassembly and reassembly of the components must be accomplished by handling the largest modules possible. In the case of the fueling system, two injectors and their adjunct service connections are first removed, followed by two shielded tubes and the torus shield plug. The opening into the torus after removing this shield plug is 2.5 m wide by 2.0 m high.

For the case of the heating system, the coax assembly is first removed along with the service connections to the launcher, followed by the shield plug which includes the launcher in an undisturbed state. The opening into the torus is 2.5 m wide by 2.9 m high. For both of these cases, the relatively undisturbed modules are stored in the reactor cell until their reassembly is required. At that time, testing and final checkout should be limited to their modular interfaces and their service connections (i.e., electrical, coolant, and vacuum).

The entry port accessed by removing an ICRH launcher is considered in this study because it appears to be more difficult than removing the

pellet injector system for several reasons. The launcher shield plug module is considerably heavier than the largest fueling module (145 tonnes vs 60 tonnes); it does not have overhead access; and its removal requires special maintenance and handling equipment. Therefore, it is assumed that the results of the time and motion evaluation using the ICRH launcher port will always be worse than the results of the evaluation for the pellet injector port.

7.5.1.4 Time and motion evaluation

The time and motion evaluation of these in-vessel operations is one element in the determinination of whether a cost benefit exists (the other is cost). If it can be shown that in-vessel operations on one sector are less time-consuming than the same operations for a sector removed to the hot cell, a potential benefit will be established. For this study, the time comparison is between reaching the damaged tiles in situ versus removing a sector to the hot cell; all other procedures are assumed to be equal. Furthermore, if the in situ operations are required on more than one sector, a significant advantage may then be demonstrated over hot cell operations.

Figure 7-14 shows the logic of the operations needed for in situ replacement of tiles, and Table 7-5 is the itemized listing of the required steps and their estimated time.

The time required to move the same sector to the hot cell for identical repairs is 105 hours, as reported in Sect. 3.2. This number has been adjusted from that shown in Ref. 1 to account for an additional 48 hours of detritiation and five hours for plasma chamber venting. The gain in availability resulting from in-situ operations for tile replacement is ~10%. In considering the merit of this gain, three areas were looked at.

1. Worth of availability — a reduction in device downtime may be considered a reduction in "nonproductive" operating costs. A number such as $7000/h can be postulated by assuming that 200 staff people are still charging the program during this period of nontesting. Using this rate, the following data were developed:

ORNL-DWG 82-3865 FED

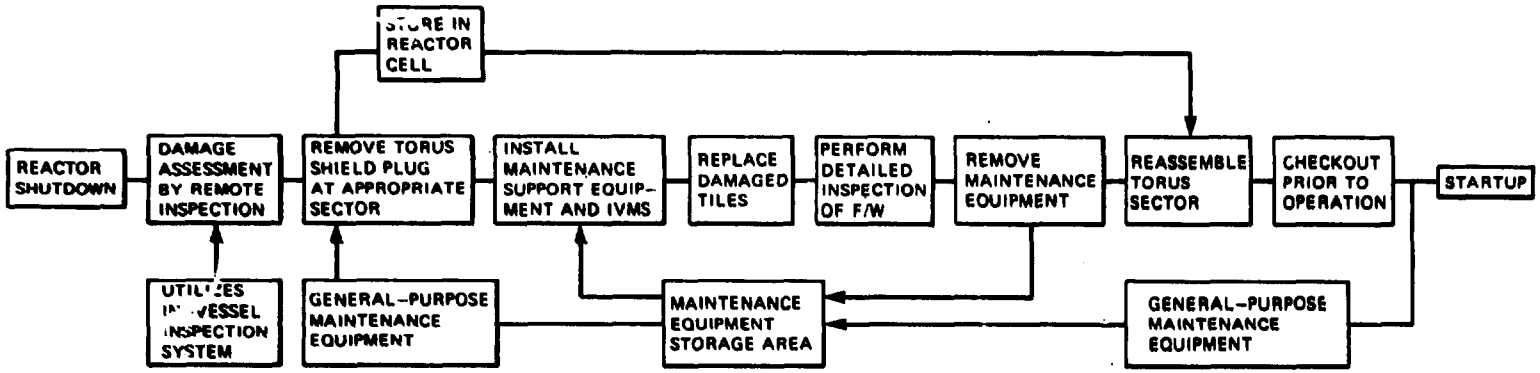

Fig. 7-14. Task logic for the in-vessel replacement of F/W armor tiles.

Table 7-5. Time and motion evaluation to reach F/W armor tiles in situ

Operation	Mode	Duration (h)
1. Device Shutdown		
• Close off appropriate valves; drain sector	A	
• Elevate temperature of torus to 250°C	A	
• De-energize magnets (time required for personnel entry)	A	24 24
• Hold elevated temperature for detritiation	-	24
• Lower torus temperature to ambient	A	
• Assemble maintenance equipment to reactor cell	C/R	24
2. Removal of ICRH Launcher Shield Module		
• Let plasma chamber up to atmospheric pressure	A	5
• Uncouple electrical and coolant lines	C	4
• Uncouple collar shield and flange attachments of coax assembly	C	1
• Install lifting cable	C	
• Remove coax; store in reactor cell	C/R	1
• Install shield plug in coax opening	R	
• Remove coax support stand	C	1
• Install temporary support stand	C/R	
• Position balance-beam on support stand	C/R	1
• Move crane hook to center fitting	C	
• Attach free end of beam to module	C	1
• Set up vacuum cutting equipment	C	1
• Cut welded seal; remove structural attachments	A/C	1
• Extract shield module; store in reactor cell	R	1

Table 7-5 (continued)

Operation	Mode	Duration (h)
3. Install platform	R	1
4. Install IVMS		
• Position on platform using overhead crane	R	
• Connect umbilicals using a general-purpose reactor cell manipulator	R	
• Check out and operate manipulator subsystems	R	
• Position manipulator base in locking channels	R	1
• Extend telescoping boom to desired sector and verify previous in-vessel inspection of damaged tiles	R	1
Time elapse before starting repairs		92 h

Cost Rate	$7000/h					
Operating Time (h)[a]	184 (in-vessel)			210 (hot cell)		
Number of occurrences	5	10	15	5	10	15
Nonproductive cost ($ x 10^6)	6.4	12.8	19.2	7.4	14.7	22.1
Cost reduction ($ x 10^6)	1.0	1.9	2.9			

[a]For the sake of simplicity, the total time from Table 6-3 is doubled to account for the removal of the IVMS, the maintenance equipment, and reassembly of the torus.

Plotted as a graph, Fig. 7-15, data of this type can be used to trade off the cost of an IVMS against reduced cost as a function of estimated usage. Assuming the direct capital cost estimated for the IVMS to be $1.1 M, then using Fig. 7-15, the system must be used seven times for the cost reduction to equal the investment in equipment. Similarly, if total capital cost (at $2.3 M) is used, the breakeven point occurs after 11 usages.

2. Multiple repairs — if two or more adjacent sectors require armor repairs, in-vessel operations appear to be advantageous. Consider the case of two sectors: the time required to reach the failed tiles is still 92 hours in situ, but the time to remove two sectors to the hot cell may be >200 h. For this case a downtime reduction of ∿100 h may be realized. The maximum number of sectors which can be reached by the IVMS through one port is 4. It includes the open sector and 1-1/2 adjacent sectors on each side.
3. Flexibility — considering the experimental nature of the FED mission and the uncertainty in the area of failures, it seems prudent to have an operating range (i.e., some options) for maintenance in the same way we have an operating range of performance. The capability for in-vessel operations in addition to sector removal may provide a way to correct unforeseen problems. As long as any design flexibility does not become a major cost burden for FED, it should be pursued.

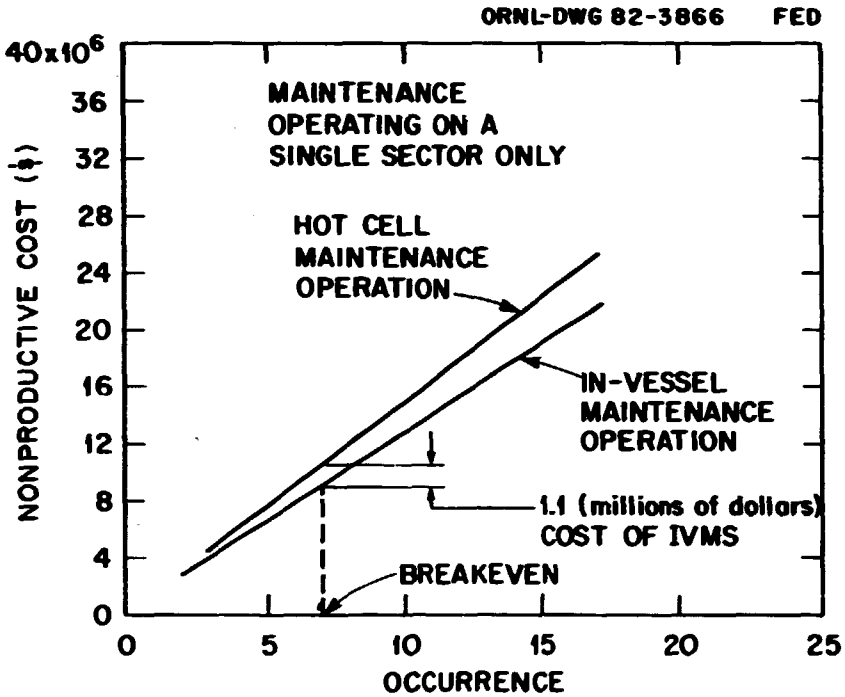

Fig. 7-15. Downtime cost vs occurrence.

7.5.1.5 Other in-vessel operations

There are several other maintenance operations which could be accomplished using in-vessel procedures. First wall panel replacements are probably the most ambitious but not necessarily the most difficult. For this procedure, the panels must be structurally accessible from inside the torus and be of a size and weight which are compatible with the IVMS. Repairs to the F/W for coolant leaks are another possibility. Patch-type repairs to the plasma side of a panel appear straightforward, and repairs to the backside could be accomplished if the panels were designed to tip out. These F/W repairs are very dependent on prior in-situ inspection, as are repairs to the electrical connectors across the sector-to-sector interface.

7.5.2 In-Vessel Manipulator System

Using the material discussed in the previous section as a starting point, an IVMS conceptual design was developed.

7.5.2.1 Machine design

The intended use of an IVMS is to provide the capability to repair equipment inside the reactor vessel. Of particular importance is the inspection and replacement of the graphite armor tiles on the chamber walls. As previously mentioned, access is provided by existing ports in three of the ten reactor sectors. Because of the location of these ports, the IVMS must be capable of reaching essentially two sectors away from the port sector opening. This worst case reach is required in only one location, but results in a 9-m, fully extended boom length. The boom positions and orients the tip-mounted servomanipulator to replace any tile on the wall, ceiling, or floor. Because of the wide variety of motions that are possible within such a small volume, position control probably has to be computer enhanced with collision avoidance.

The present concept for the IVMS is shown on Figs. 7-16 through 7-18. The assembly items list is shown on Fig. 7-16 and the installation views are Figs. 7-17 and 7-18. Commercial equipment has been used

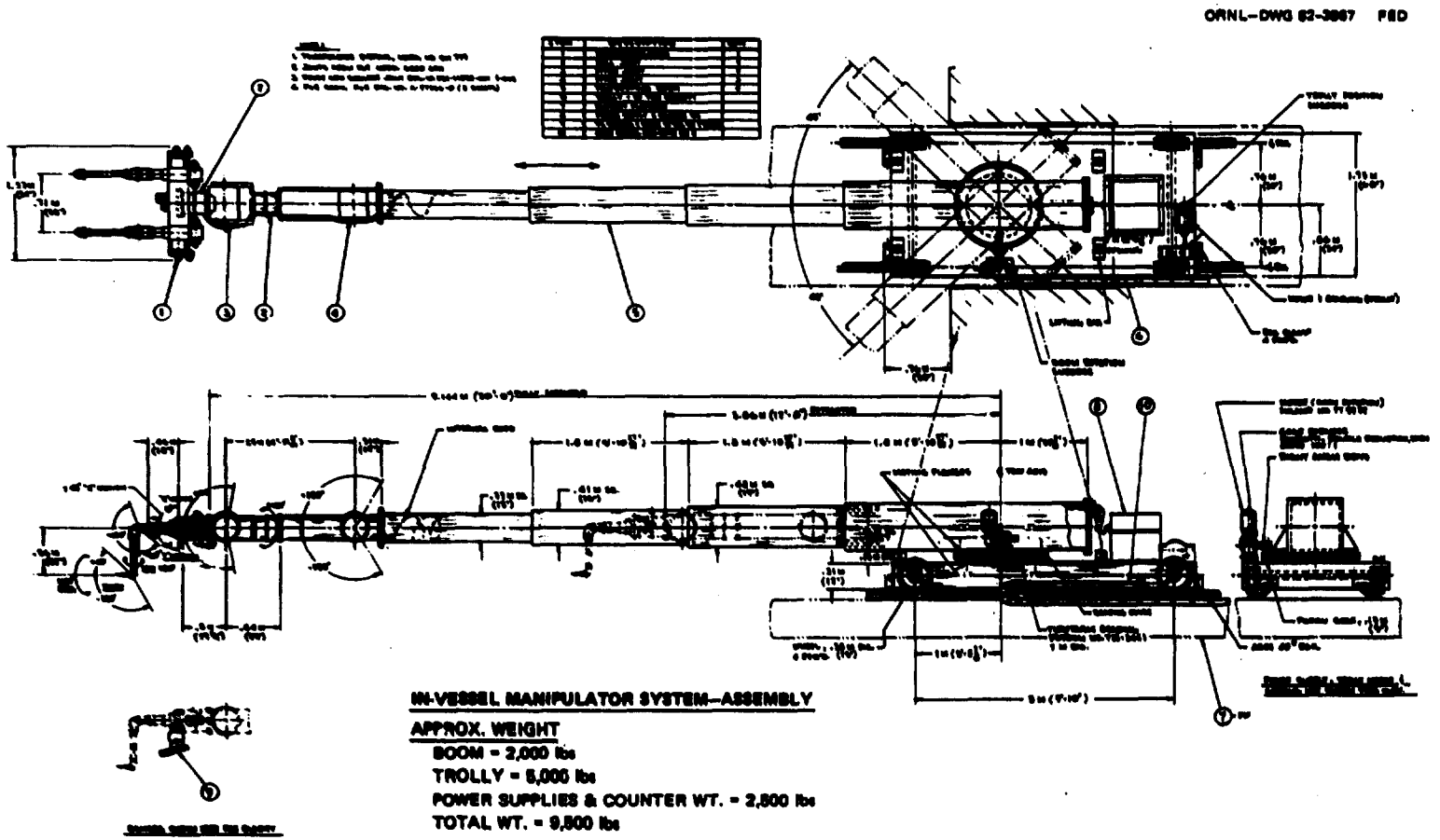

Fig. 7-16. In-vessel manipulation system — assembly.

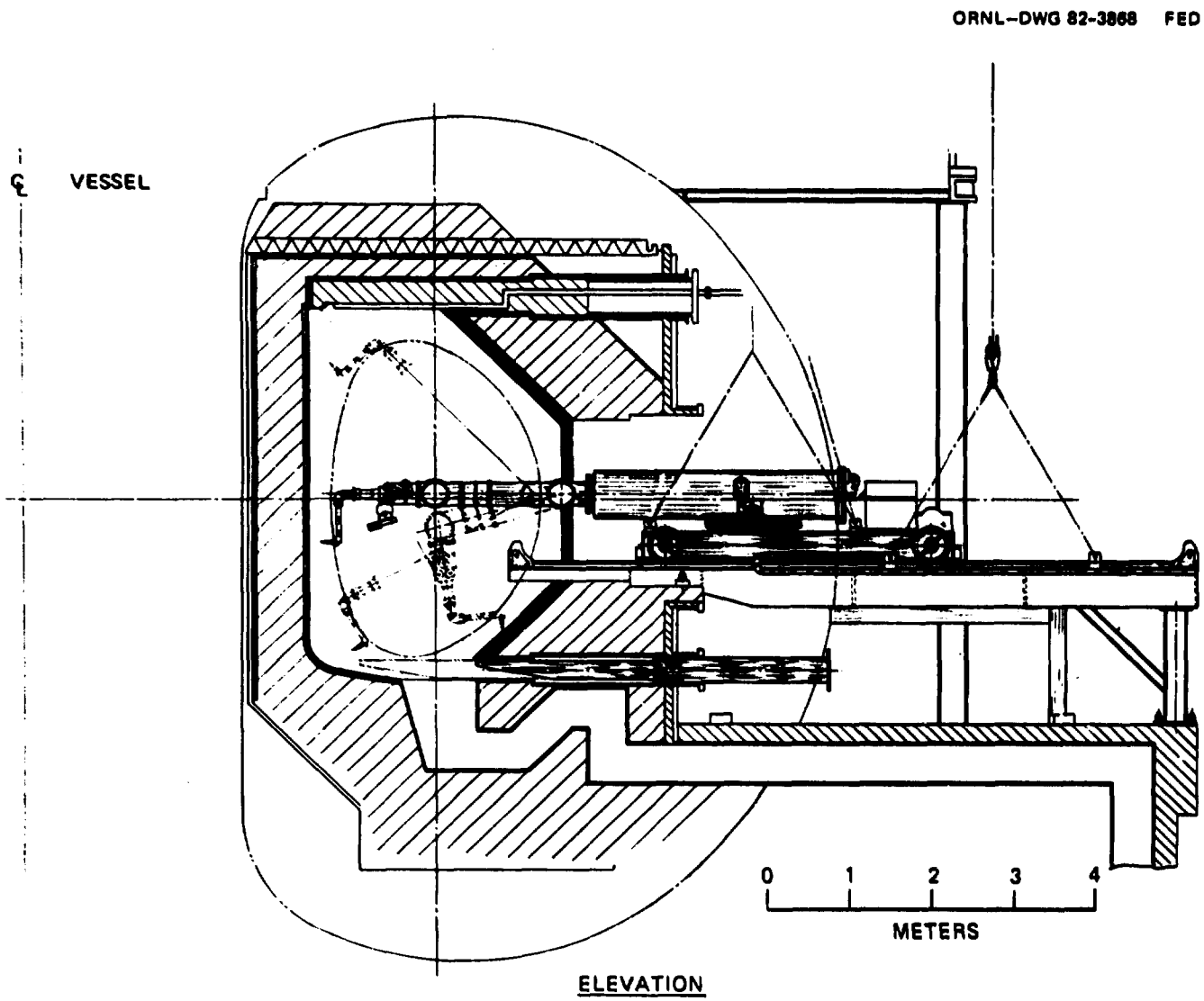

Fig. 7-17. In-vessel manipulation system — elevation.

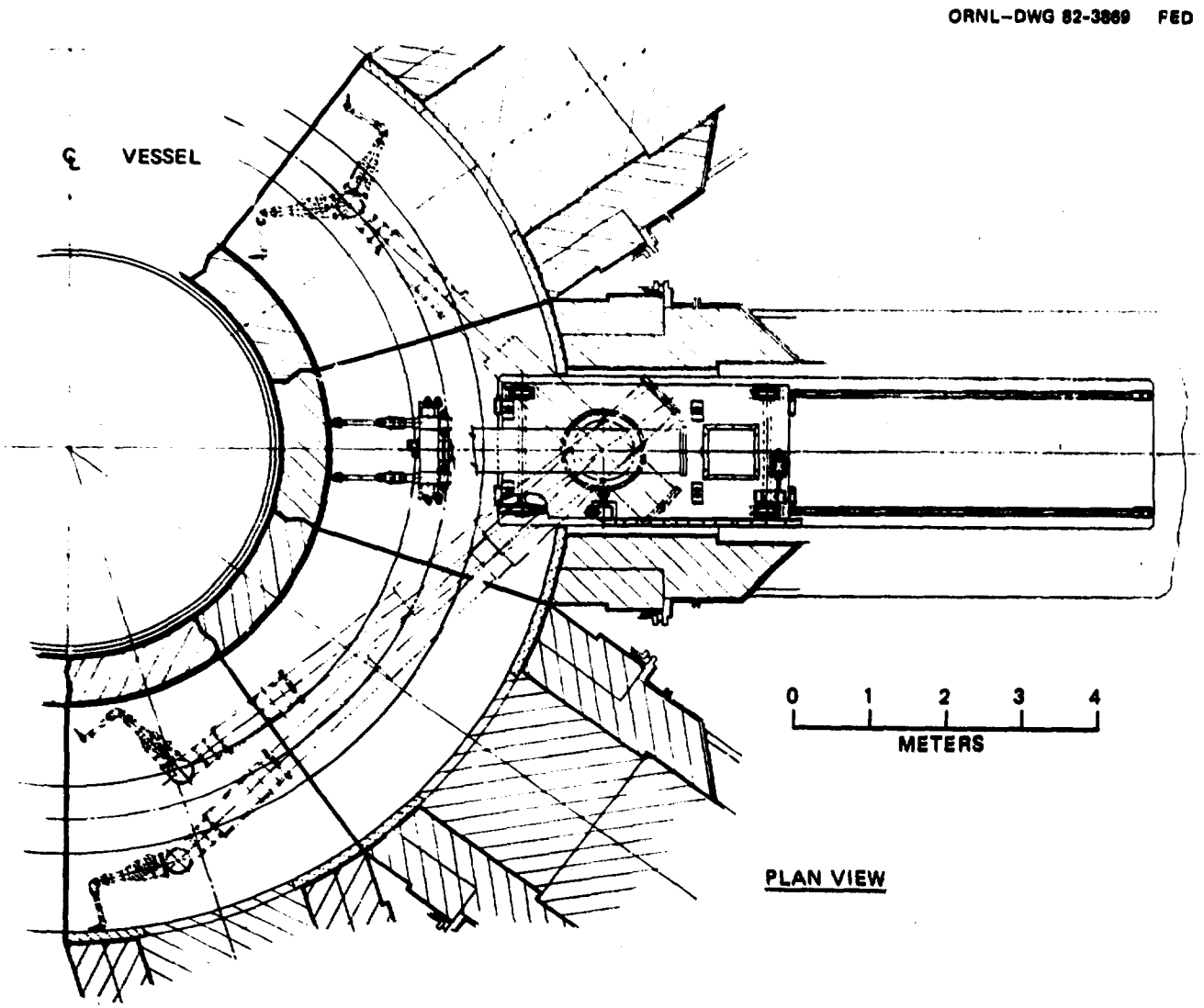

Fig. 7-18. In-vessel manipulation system — plan.

whenever possible in order to support the cost estimate. All of the items on the trolley and boom were sized to accommodate the port opening and the prescribed installation requirements. The pair of servomanipulator arms (Item 1) is made commercially by TeleOperator Systems, Model SM 229. These arms each have a 10-kg capacity and are thought to be the best presently available for this application. The arms are guided to the work site with the boom-mounted TV and lights (additional surveillance cameras can always be added). This viewing system (Item 9) contains standard components that provide pan, tilt, and zoom, with a high resolution black and white format.

The arms are supported and positioned by the multidegree of freedom, articulated boom (Item 5). This boom is essentially the same as an 11-m boom already existing in the Remote Operation and Maintenance Demonstration Facility (ROMD) at the Fuel Recycle Division (FRD) at ORNL and is manufactured by P&R Systems Division of the GCA Corporation. The P&R engineers provided the assurance that the cable drive (pull only for vertical operation) can be replaced in this design with a rack and pinion drive for push/pull. They also noted that the decrease in extended length (11 m to 9 m) will allow the boom capacity to be increased to 225 kg. P&R can also provide the roll-pitch-roll (RPR) joints (Items 2 and 3) at the end of the boom, which are utilized in their Model 6000 power arm. The RPR combination is required from the kinematic analysis with the vessel geometry. This basically allows the servomanipulators to be located in any possible orientiation, for any given position. However, the second pitch joint (Item 4), which provides elevation, is not commercially available. Because of the large torques required at this joint (approximately 5500 N-m), a special design is necessary. Such a joint has already been designed, fabricated, and proof-tested by FRD as part of their power arm development program.

The boom is mounted to a 10,000-kg capacity hoist trolley (Item 6) through a rotating turret. The turret is commercially available from several sources, this one being selected from Kaydon Division of Keene Corporation. It is rated at 638,000 N-m, with a calculated maximum load of 135,000 N-m. This turret provides the yaw motion necessary to reach

adjacent sectors. A pitch joint is not required at the turret location because the elevation is provided by the second pitch joint (Item 4). The pitch joint at the turret was avoided because of the significant torque that would have to be reacted at this location (approximately 135,000 N-m). This would require a completely new joint design. In addition, torques of this magnitude are normally achieved with hydraulic power, an alternative that is not allowed in the torus.

The trolley is mounted on the support platform (Item 7) described in Sect. 7.5.3. The trolley is provided with clamps to lock to the rails located on the support platform.

7.5.2.2 Uncertainties

Before a full conceptual design can be completed, several areas need to be addressed and resolved. Most important is the determination of the overall tile maintenance scheme, including tile failure detection and location, the alignment and fastening, tile handling, and installation inspection. All this must be done with specific regard to the maintenance equipment that is available. The special tooling, tool rack, and tile bin also must be included in the overall scheme to assure proper reaches, clearances, and viewing. Failure recovery also requires some detailed consideration. Although this general philosophy was maintained during the development of this concept, a detailed component by component failure recovery analysis is mandatory for equipment of this nature. The effects of the grahpite dust in the vessel must also be evaluated. Booting of the slave arms and telescoping tubes is probably necessary to avoid contamination and mechanical failures.

The deflection of the telescoping boom is of similar concern. The three available ports in a ten-sector arrangement require the IVMS to reach that tenth sector from two sectors away. This is a large penalty in cost and capacity, since a 9-m reach is required instead of the 6-m reach to adjacent sectors, resulting in over three times the deflection. An arrangement which has four ports is desirable. The best reference point available for deflection of such tubes is the existing tube in the ROMD. At a maximum reach of 11 m, this tube deflects 30 cm with a

180-kg load. This is primarily due to the tube section interface, rather than tube deflection itself, so eliminating a section (as could be done with a 6-m reach) greatly reduces deflection. This would improve overall operation efficiency and maintenance as well as reducing the cost of the system.

7.5.3 IVMS Cost*

A cost estimate was prepared based on the conceptual design described above. In fourth-quarter FY-1982 dollars, the total is $2,300,000. This includes approximately $1,100,000 procured and fabricated items, $500,000 for design costs, and a $700,000 contingency. (A contingency of 45% was assumed because of the preliminary nature of this design study. The contingency would be reduced upon completion of a conceptual design.)

7.5.4 Supporting Equipment for In-Vessel Operations

Other maintenance equipment is required in addition to the IVMS for entry through either the fueling shield plug or the heating shield plug ports. Because of ample overhead access and the relatively low weight of the fueling system modules, the basic equipment required is the movable manipulator system (MMS) shown in Fig. 7-19 and an overhead crane. The support platform for the fueling system remains in place for use by the IVMS. The heating module removal requires the MMS, the overhead crane, and additional equipment: a temporary work stand, a lifting beam, a counterweight, and a support platform for the IVMS. A description of this equipment and its requirements are discussed below; Table 7-6 lists the weights of the components to be handled.

---

*The direct and indirect capital costs shown above were prepared by the ORNL design group which developed the details of the IVMS concept. Their numbers for indirect costs may differ slightly from those presented in Sect. 11.

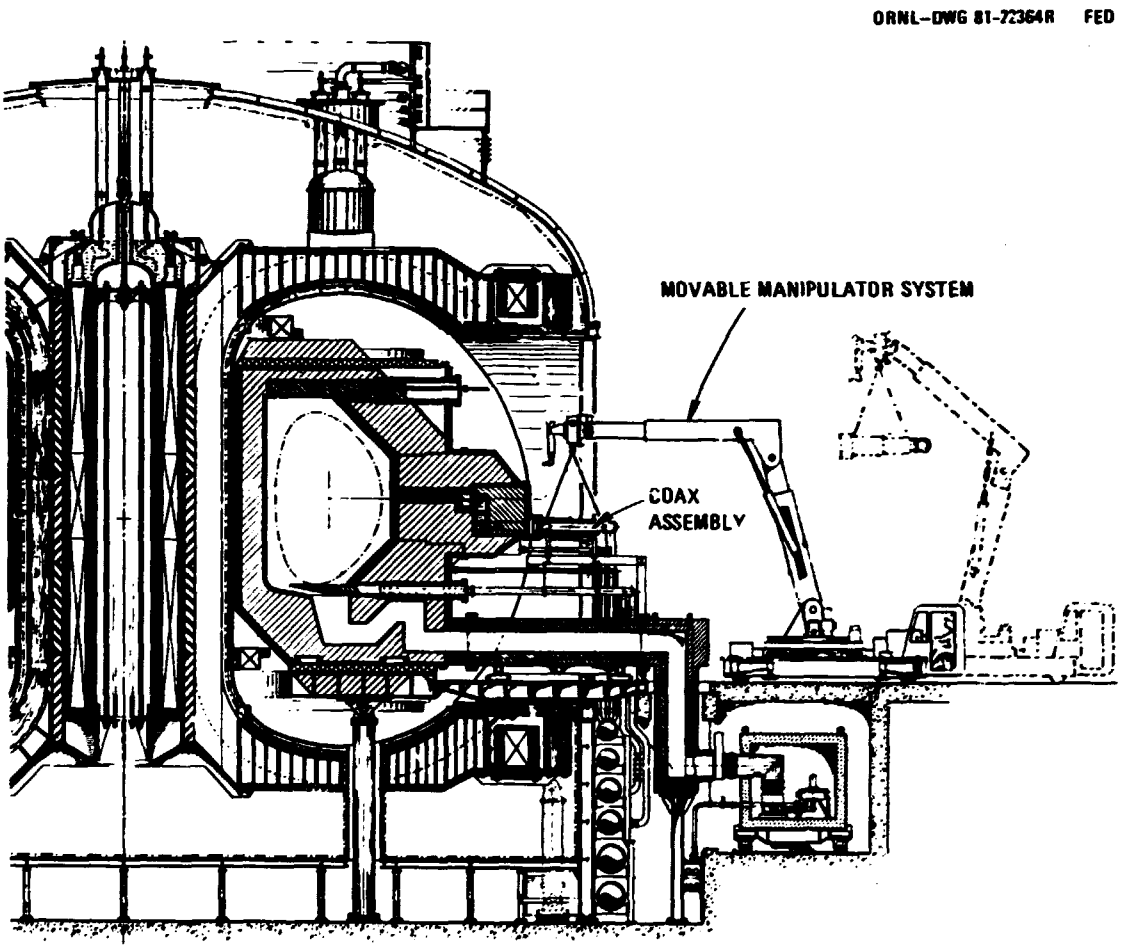

Fig. 7-19. Movable manipulator system.

Table 7-6. Component weights to be handled for in-vessel maintenance operations

Entry port component	Weight (tonnes)	Quantity
Fueling		
Fuel injector	30	2
Shielded tube	22	2
Torus shield plug	60	1
Heating		
Coax assembly	<1	1
Work stand	<5	1
Beam & counterweight	147	1
Torus shield plug	145	1
Platform	<5	1
IVMS	<10	1

7.5.4.1 Movable manipulator system

Figure 7-19 shows the movable manipulator system. It is a hydraulically actuated crane with a telescoping boom. The boom has a lifting capacity of 10 tonnes and also incorporates a single articulated arm; the boom has a maximum reach of 10 m. This equipment is classified as general purpose and can be used as a manned vehicle. It can be used to lift most of the components in Table 7-6, particularly those which require horizontal access such as the coax assembly.

7.5.4.2 Overhead cranes

The 50-tonne overhead crane (identified at the Cost Workshop under reactor cell equipment) can handle most of the components in the above table, and it can also be used to complement the MMS above (i.e., it may allow parallel handling operations to take place). Installation of the beam/counterweight requires the 500-tonne crane, as does the combination of the beam/counterweight/shield plug which weighs 292 tonnes. Figure 7-20 shows this operation.

7.5.4.3 Lifting beam

The lifting beam shown in Fig. 7-21 can be fabricated from carbon steel using a standard structural shape, 33 WF 220. The length of the beam is 7 m, and it has two hoist fitting attachments. One is located at the centerline for lifting out the shield plug, while the other is positioned just to the left of the center of the counterweight, at the c.g. of the combined beam and counterweight. The beam does not require an adjustable position for the main hoist fitting. It is assumed that this calibration was done when the shield plug was first installed, and that any minor c.g. adjustments which may be required can be accomplished by adding or subtracting weight in small increments from the counterweight.

ORNL-DWG 81-22370R FED

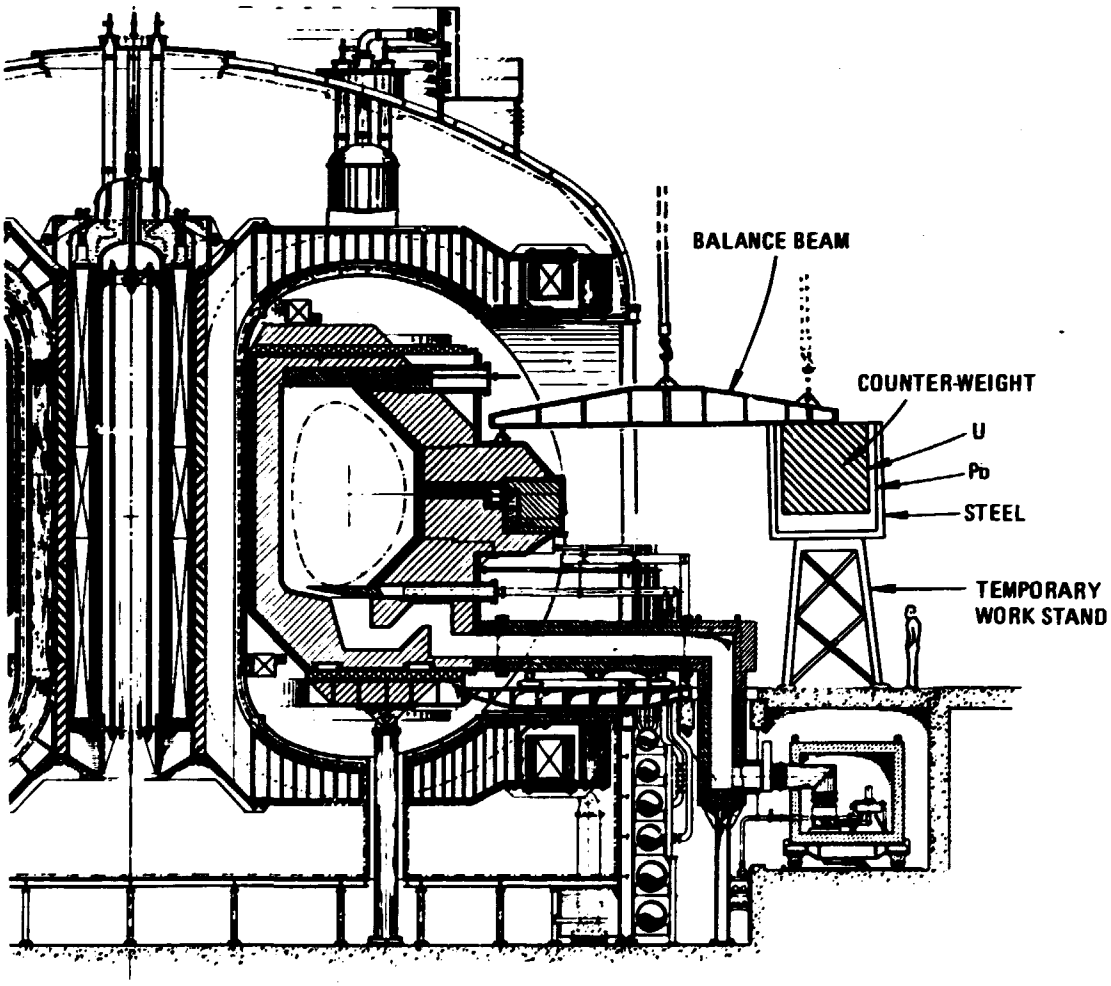

Fig. 7-20. Equipment setup for removal of the ICRH shield module plug.

ORNL-DWG 81-22365 FEO

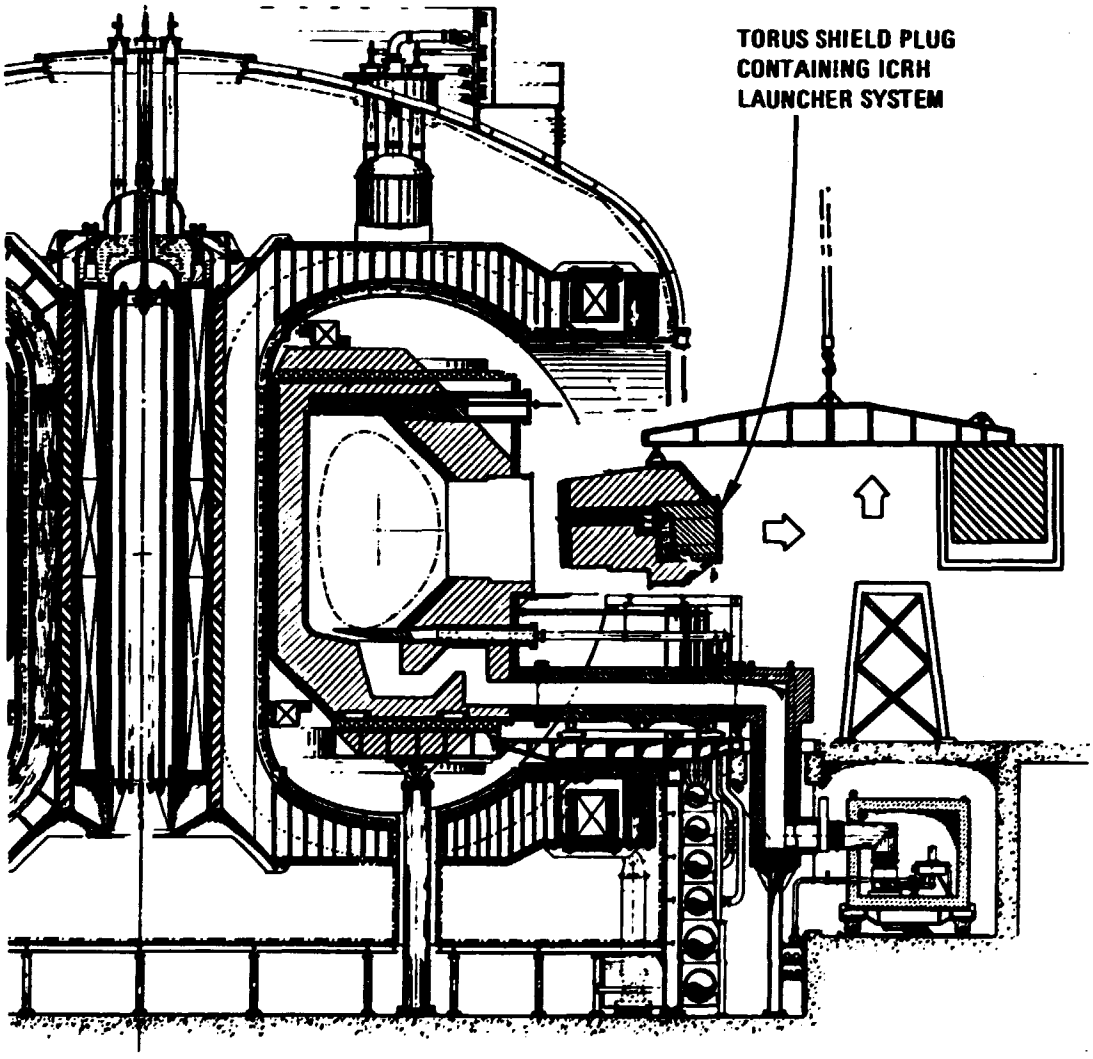

Fig. 7-21. Removal of torus shield plug.

7.5.4.4 Counterweight

The counterweight is the 145-tonne balance to the weight of the torus shield plug. It is shown in Fig. 7-21 in three different volumetric sizes as a function of material. Table 7-7 indicates the volume required for each cubic configuration. From the table, it is obvious that the depleted uranium cube would require the smallest space in the tool storage area. However, because of the potential for secondary fissioning in a neutron environment, it requires storage outside the reactor cell or behind a shielded area with the cell. Further study is required to determine the best material for this application.

7.5.4.5 Work stand

The work stand is a temporary piece of equipment which acts as a holding fixture for the combined lifting beam and counterweight. It has an adjustable height and is fabricated from carbon steel. The exact positioning of the stand is by means of index points located on the reactor cell floor. During in-vessel maintenance operations, the work stand shown in Fig. 7-21 plus a second stand adjusted to a different height could be used to store the entire beam assembly in the reactor cell.

7.5.4.6 Support platform

The support platform is fabricated from carbon steel. Its primary structure is a pair of 14 WF 87 beams connected by a flat plate. It has a width of 2 m and an overall length of 7.6 m. The installation of the platform is a remote operation; hence, lifting and positioning are designed to be simple. The front of the platform has two tapered locating pins which are matched to a pair of guide holes in the torus shield. Positioning and alignment are aided by the CCTV camera mounted under the cryostat dome. Figure 7-22 shows the platform being hoisted into position; detail A shows the engaged guide pins and the torus support fitting under the WF beams.

Table 7-7. The volume of the counterweight is significantly impacted by the choice of material

Material	Cubic dimension (cm)	Volume (m^3)
Steel	260	17.6
Lead	230	12.2
Depleted uranium metal	190	7.3

ORNL-DWG 81-22366 FED

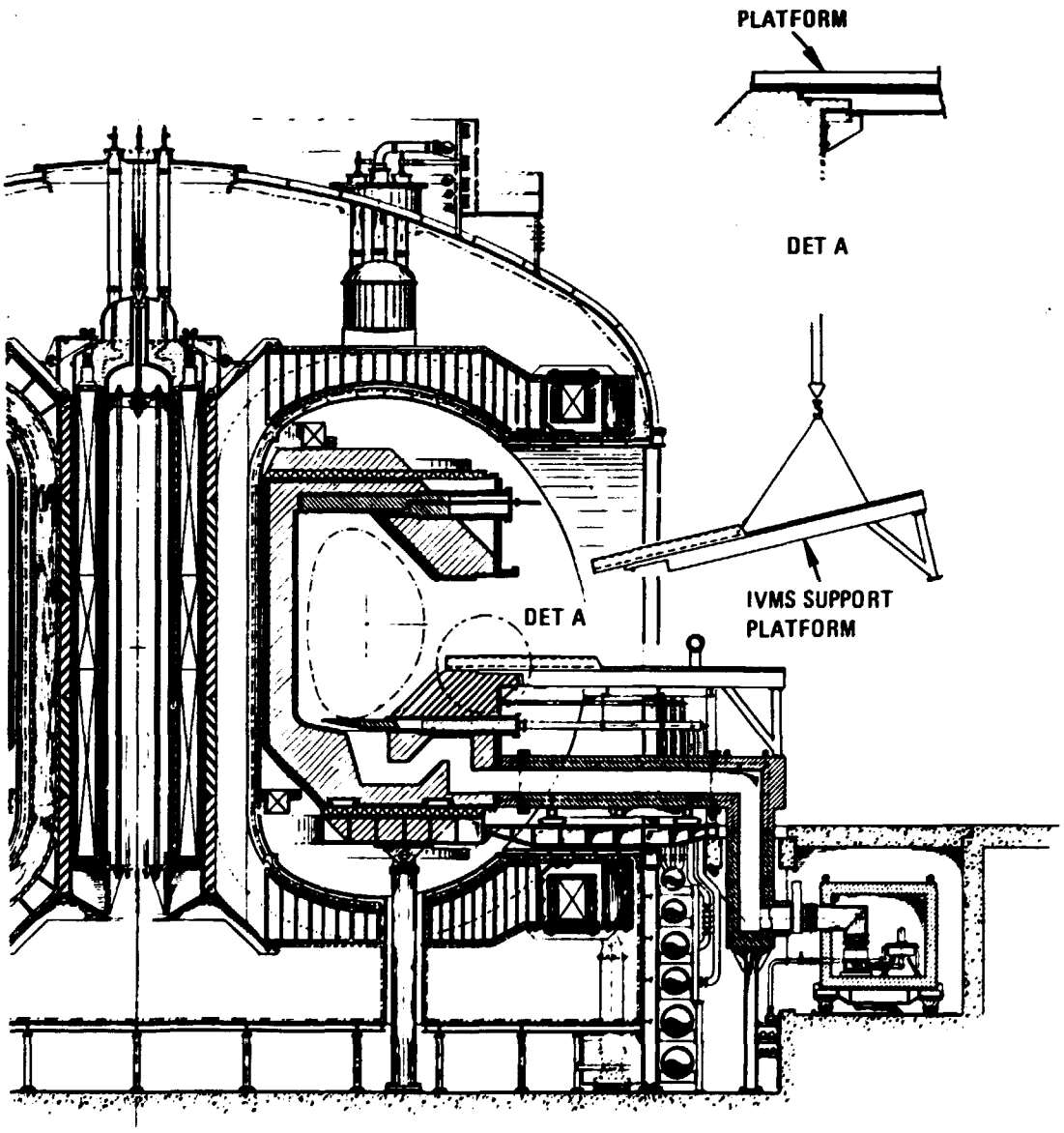

Fig. 7-22. Support platform for IVMS.

Stability for the manipulator system is provided by a pair of channel locks at the front end of the platform. Section A-A in Fig. 7-23 shows the side rollers of the manipulator base engaged in the channels.

7.6 TF COIL REPLACEMENT

7.6.1 Objective

The objective of this study was to establish the tasks and special equipment required to remove and replace a toroidal field coil from the FED baseline configuration, to identify critical design features which might require improvement to facilitate maintenance procedures, and to assure that TF coil removal and replacement is a credible and viable option. A more detailed discussion of this task can be found in Ref. 6.

7.6.2 Approach

The approach employed was to establish the major tasks (or steps) required and to arrange them in a sequential order. Each major task was subjected to engineering scrutiny of sufficient depth to gain a thorough understanding of the substeps involved, to identify the prerequisites to each step, to identify the special equipment which may be required, and to recognize problem areas and their possible solution.

During this process, data, such as the size and quantity of fasteners to be removed or installed, the linear feet of cutting and welding required, and so forth, were accumulated. The detail baseline design of each component was assessed from a maintenance viewpoint. Working conditions (headroom, access opening sizes), the weight and bulk of needed maintenance equipment, and the character of the FED components to be removed and replaced were noted. The need for such mundane and obvious items as scaffolding, auxiliary ventilation and lighting, and safety precautions was not overlooked so that the scope and degree of difficulty of each task could be assessed.

The removal and replacement of a TF coil require extensive cutting and welding operations. Therefore, a review of various cutting and welding techniques was conducted and a number of recommendations were made.

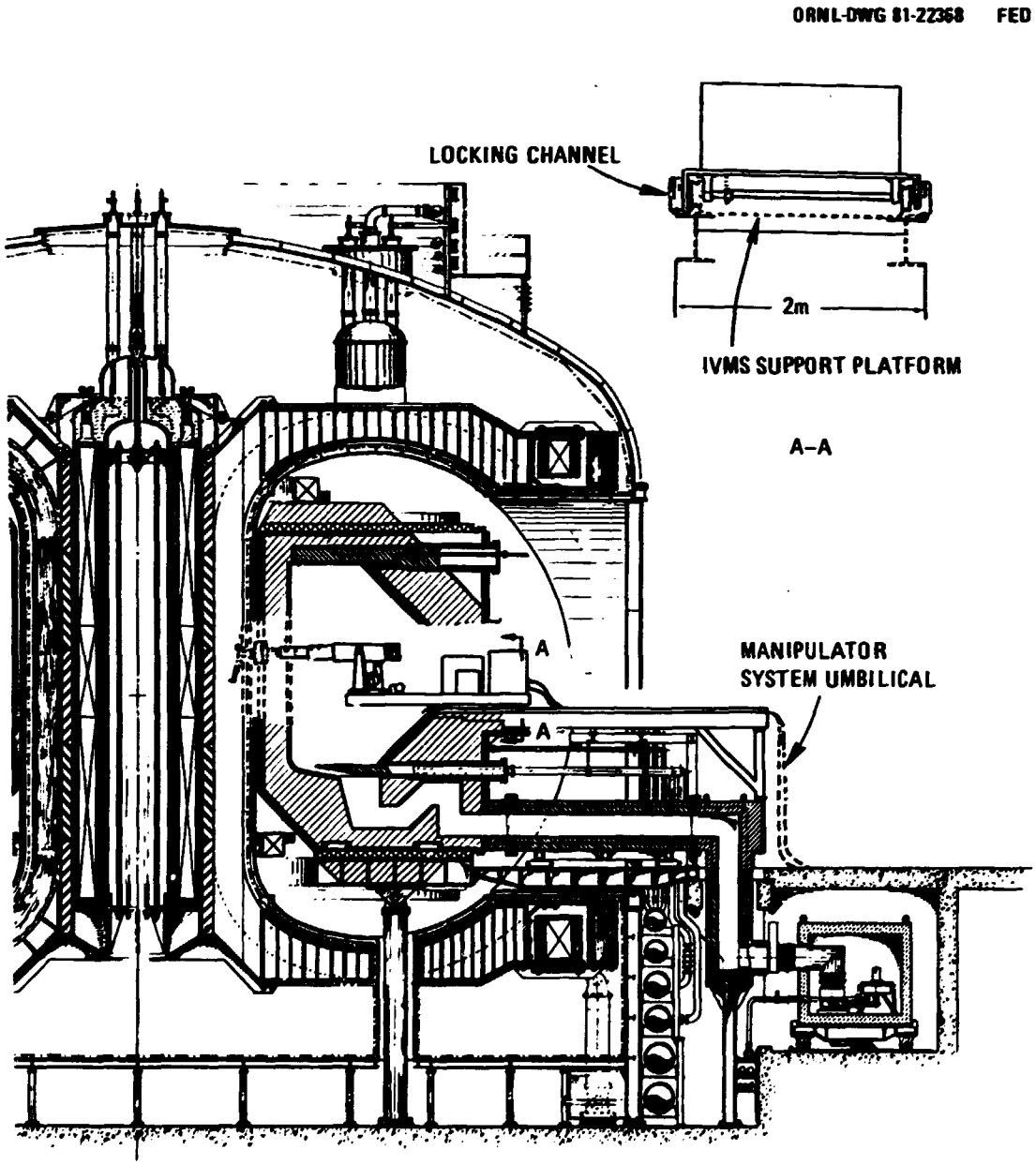

Fig. 7-23. IVMS installation.

7.6.3 Stepwise Removal

The replacement of a toroidal field coil is perhaps the most difficult and most lengthy maintenance procedure required for the FED device. Table 7-8 lists nineteen major tasks that must be accomplished prior to actual removal of the TF coil; each major task is composed of numerous subtasks.

The TF coil replacement procedure involves disassembly and removal (either totally or partially) of four major components of the FED device: the poloidal field coils, the cryostat system, the torus vacuum vessel, and the vessel support structure. These components can be seen in Fig. 1-1.

7.6.4 Major Problem Areas

The nineteen steps required prior to the removal of a TF coil are all considered to be quite difficult to accomplish and will require a significant downtime. Four areas, however, deserve special discussion because of their outstanding degree of difficulty. They are (in order of increasing difficulty):

1. removal and replacement of control coils #1-4,
2. removal and replacement of EF coils #1 and #4,
3. removal and replacement of the cryostat structure adjacent to the defective TF coil, and
4. remote removal and remote replacement of two spool panel assemblies and one spool radial frame.

7.6.4.1 Poloidal field coils

Of the total of eight PF coils, six are located within the bore of the TF coils as shown in Fig. 7-24. All six are "normal" conducting water cooled copper conductors. They are each initially assembled in two 180° segments which are bolted together. Brazed "jumper" tubes provide continuity of the water coolant passages. Figure 7-25 illustrates the normal coil joint design.

Table 7-8. FED TF coil maintenance: major tasks

1. Remove 2 limiter ducts; plug openings with temporary shielding.
2. Remove cryostat vessel dome.
3. Remove EF coil #2.
4. Cut control coils #1 in 10 pieces and #2 in 20 pieces and remove.
5. Cut EF coil #1 in approximately 10 pieces and remove.
6. Cut and remove upper dished cryostat panels above 2 sectors and 2 associated lintel cryostat panels.
7. Remove 2 sections of the upper intercoil structure.
8. Remove lower cryostat wall (locally) and limiter duct "floor" structure (locally) for access to lower cryostat.
9. Cut control coil #3 in approximately 20 pieces and remove.
10. Cut and remove the lower dished cryostat panels located beneath 2 sectors and 2 associated threshold cryostat panels.
11. Remove 2 sections of the lower intercoil structure.
12. Lower control coil #4 and EF coil #4 to a position suitable for cutting.
13. Cut control coil #4 and EF coil #4 to approximately 10 pieces and remove.
14. Remove a section of the torus support platform located beneath 2 sectors.
15. Install mobile jacks (20) and lower EF coil #3.
16. Remove 2 sectors.
17. Remotely cut and remove 2 spool panel assemblies and 1 spool radial frame.
18. Cut and remove cryostat inboard wall segment.
19. Unfasten bucking cylinder interface.
20. Remove defective TF coil.
21. Reverse sequence (welding operations replace cutting operations).

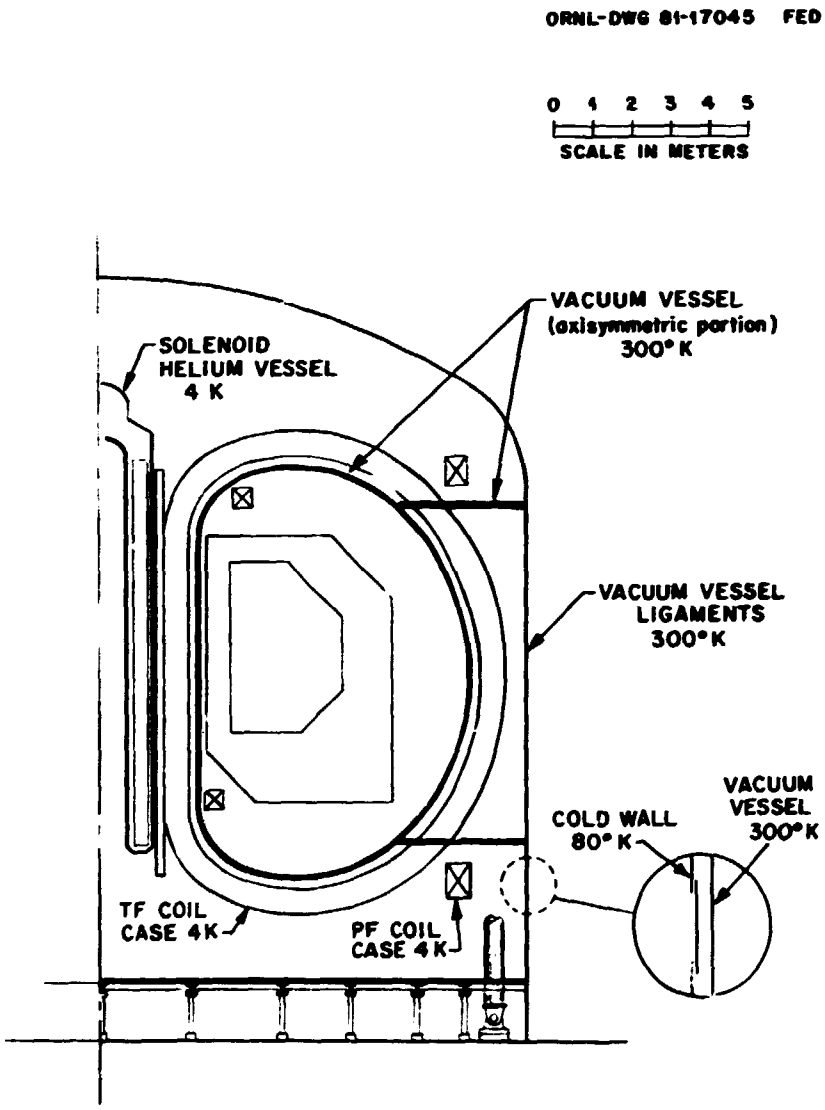

Fig. 7-24. FED magnetic system arrangement.

ORNL-DWG 81-16981 FED

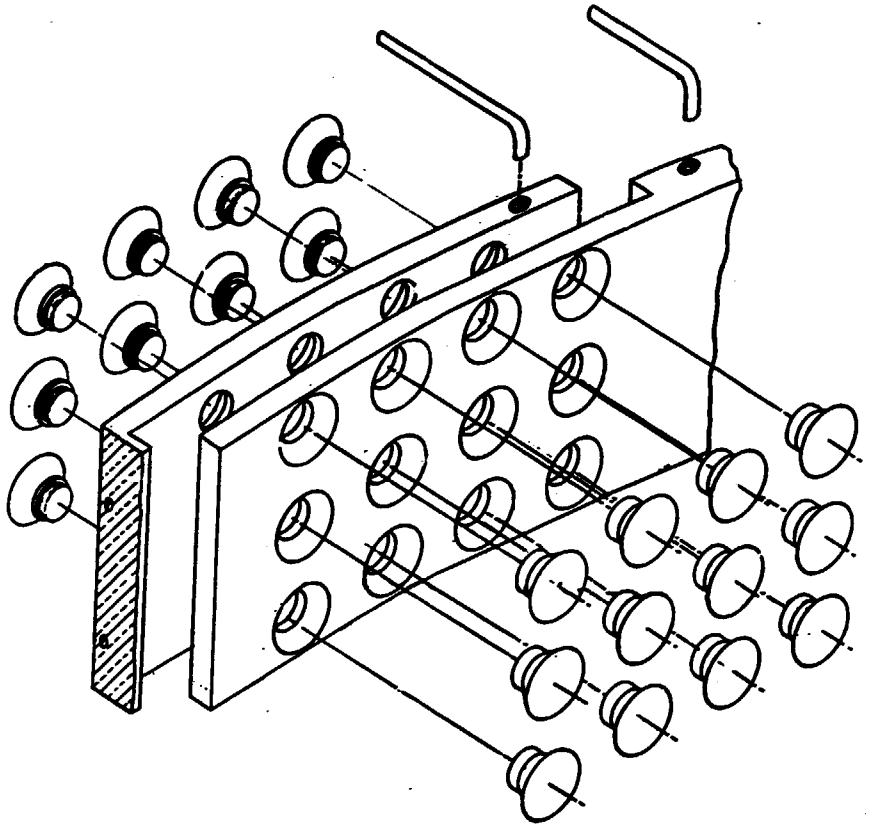

Fig. 7-25. Resistive coil joint design.

At the time of initial assembly, the upper and lower cryostat panels and the intercoil support structure (which bridges the distance between TF coils) are not in place and sufficient access exists for the insertion of the two 180° coil segments. These structures, however, are in place at the time of maintenance operations. It will be necessary, therefore, to cut the six "internal" PF coils into pieces approximately eight or nine feet long and to create a "removal window" by removing the upper and lower cryostat panels and the upper and lower intercoil structures on both sides of the defective TF coil. (These components must be removed in any event.) The upper dished cryostat is identified in Fig. 7-26; Figs. 7-27, 7-28, and 7-29 illustrate the intercoil support structure which must be removed to create a removal window for the cut PF coil pieces.

As shown in Section A-A of Fig. 7-26, fasteners (for structural requirements) are located at both the inside and outside cross-sectional surfaces of the intercoil structure. Removal of the inside fasteners cannot be accomplished until the removal of the dished cryostat panels is accomplished. The proximity of EF coil #1 and control coils #1 and #3 prohibit the insertion of a cutting device to sever the dished cryostat panels, and hence two sections of each of these coils must be cut and temporarily moved out of the way prior to the removal of the cryostat panels.

It is proposed that all six PF coils be scrapped. The only possible replacement procedure is the in situ assembly of many conductor segments bolted together as illustrated in Fig. 7-25. The difficulty of this operation is exemplifed by the extremely difficult working conditions (average headroom is 1 m), the limited access for men and equipment — particularly the access to the lower PF coils, and the need to design and fabricate special maintenance equipment.

7.6.4.2 Control coil removal and replacement

Table 7-9 presents in outline form some of the more prominent difficulties of control coil removal.

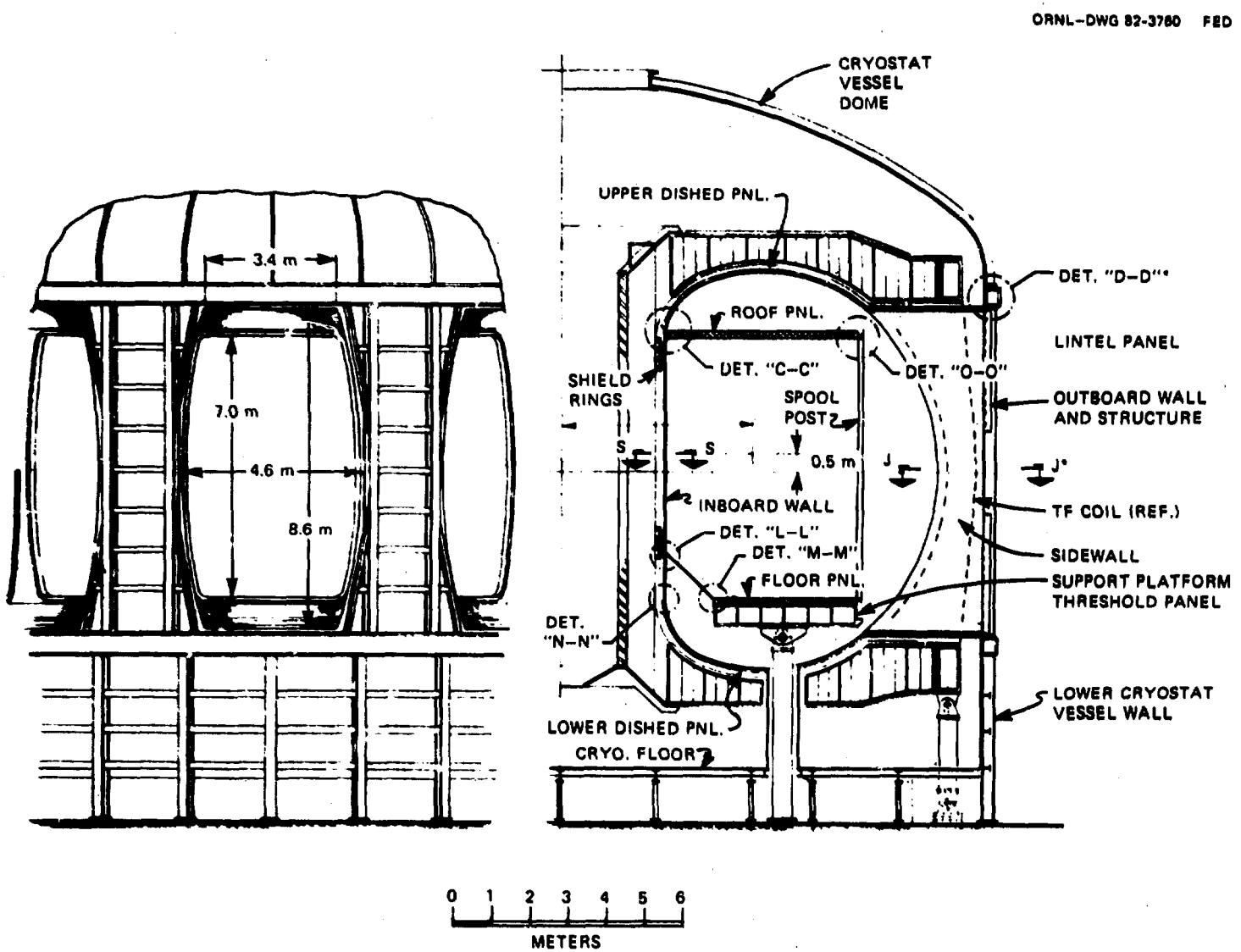

Fig. 7-26. Cryostat structure.

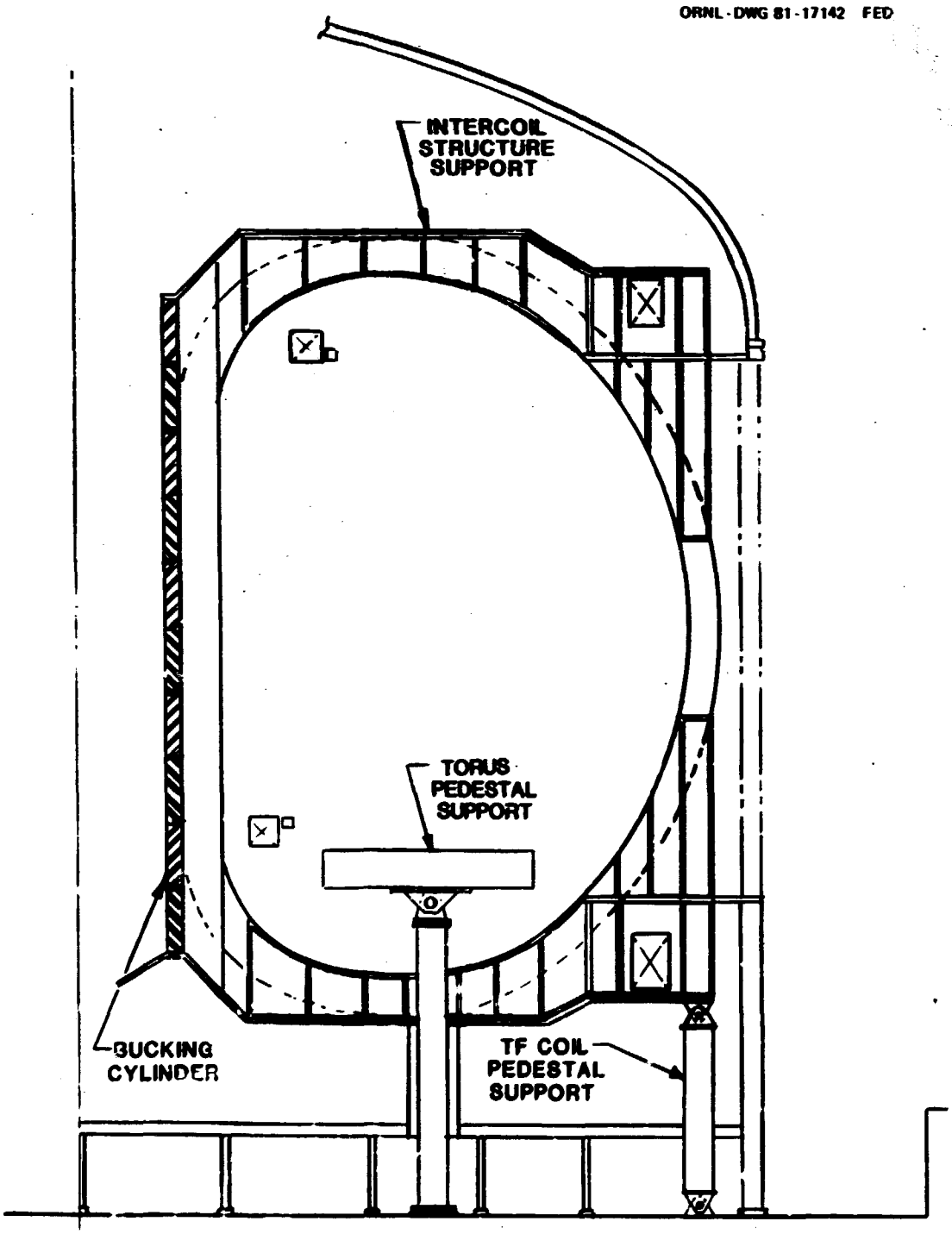

Fig. 7-27. FED TF coil and surrounding support structure.

ORNL-DWG 81-17143 FED

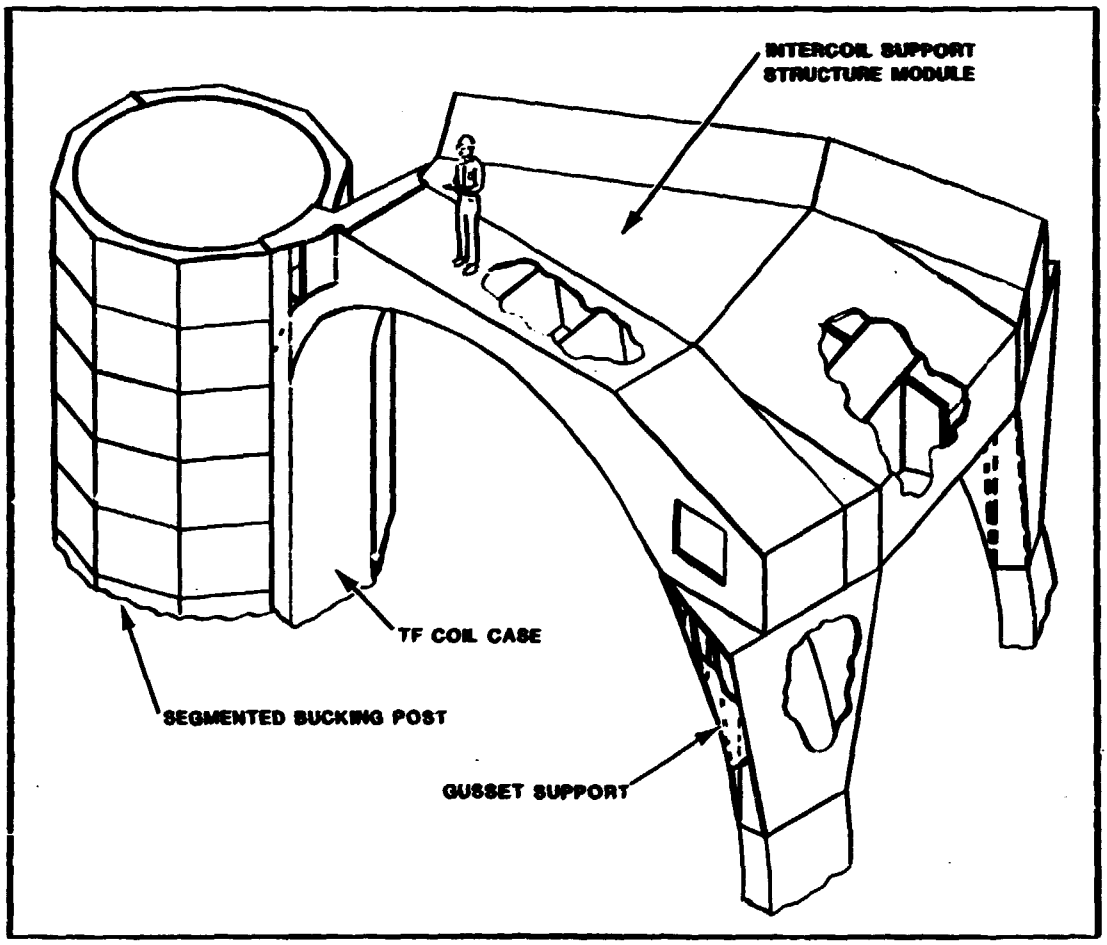

Fig. 7-28. Cutaway view of TF coil and its support structure.

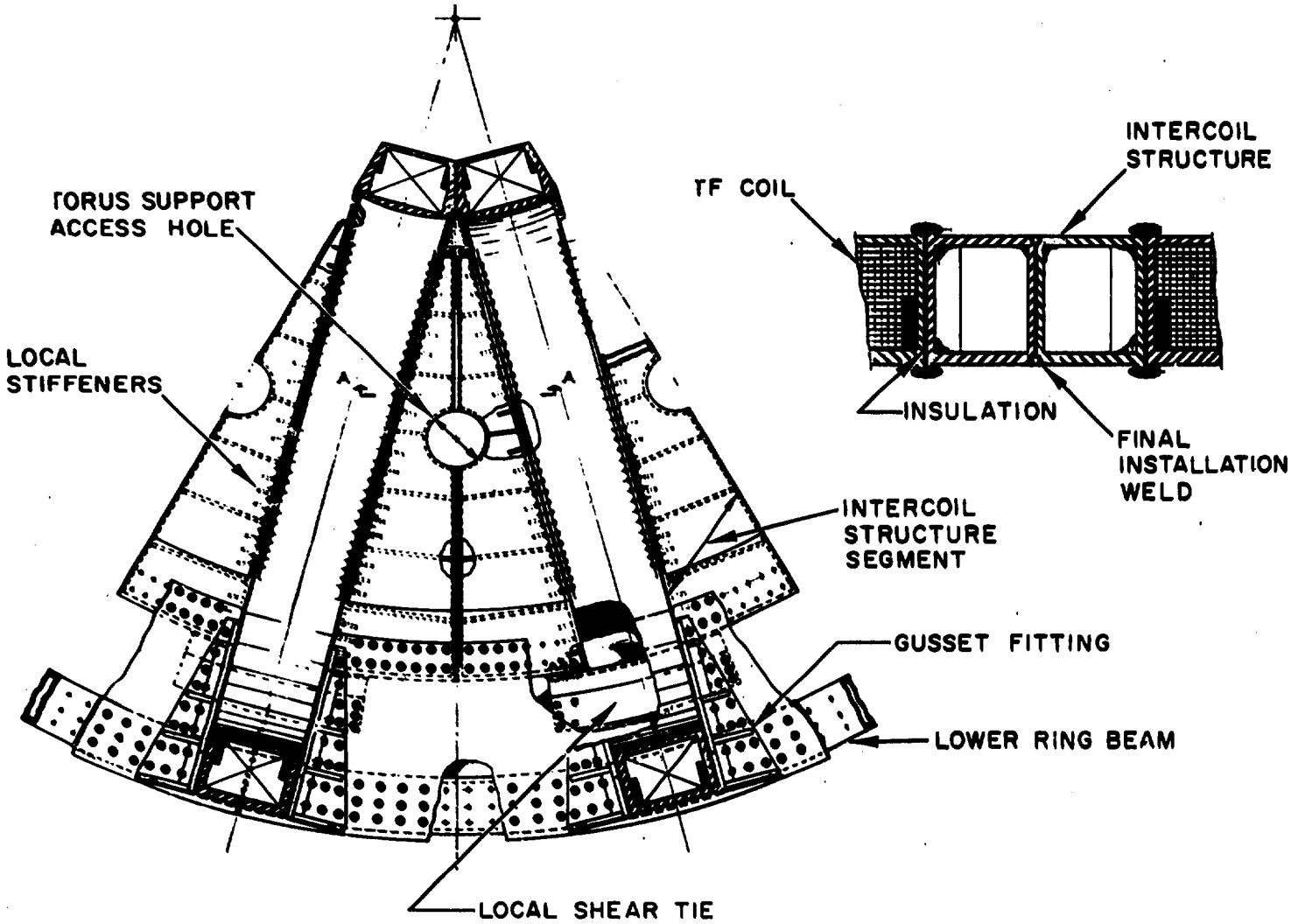

Fig. 7-29. Plan view of TF intercoil structure.

Table 7-9. Characteristics of control coil removal

A. Control Coil No. 1

1. Hands and knees working conditions (average working headroom: 1 meter)
2. Minimum of 10 cuts required through a 20 × 20 cm (8 × 8 in.) copper cross section
3. Length of each cut piece 2.65 m (8.7 ft)
4. Weight of each cut piece 4000 lbs.
5. Required development of special reciprocating saw cutting machine
6. Cutting operations to be accomplished "dry" (without cutting lubricants)
7. Requires chip/debris containment and removal
8. Close proximity to EF coil No. 1 and limited space difficulties
9. Requires special device to transport cut sections to a removal "window"
10. In-situ construction of the replacement coil is required. Estimate 52 joints, 6 bolts per joint.

B. Control Coil No. 2

1. Minimum of 20 cuts, 104 joints required

C. Control Coil No. 3

1. More difficult location
2. Minimum of 20 cuts, 104 joints required

D. Control Coil No. 4

1. Requires lowering to more suitable position for removal/replacement operations

E. Totals for All Coils

1.	Number of cuts	60
2.	Number of construction joints	312
3.	Number of fasteners	1,872

7.6.4.3 EF coil removal and replacement

EF coil removal and replacement are essentially the same procedure as control coil maintenance. The scope of procedure is made more difficult, however, because of the larger coil size and weight. Table 7-10 itemizes the difficulties associated with EF coil removal.

7.6.4.4 Special PF coil equipment

A specially designed cutting device will be required. A reciprocating saw device capable of being directly attached to the coil appears to be a logical choice. Replaceable "heads" could be employed so that the device can be used to sever control coils and EF coils. The device must be compatible with the access limitations to the coil areas and must incorporate a chip containment and removal system. The cutting tool must be capable of cutting the copper sections without lubrication.

The cut sections of control coil will weigh approximately 4000 pounds and those of the EF coils will approach 23,000 pounds. It will therefore be necessary to design a special device to temporarily support a cut section and to transport it to the "removal window". Its envelope must meet the access requirements of the coil area. An alternative to this is cutting and removing each conductor winding in approximately 10 segments. This would reduce weight of pieces to be handled but may significantly add to the downtime.

The in-situ assembly of the PF coils will require the development of a device to transport, position, and at least assist in the installation of the conductor segments. One concept of such a device is shown in Fig. 7-30.[1] Although this device was configured for a remote operation, it is indicative of the complexity of disassembly operations for the coils.

7.6.4.5 Cryostat structure

The cryostat structures (Fig. 7-26) that must be removed are two lintel panels, two threshold panels, three upper and three lower dished panels, and one inboard wall panel. It is believed that the four panels

Table 7-10. Characteristics of EF coil removal

A. EF Coil No. 1

1. Manual hands and knees operation (average working headroom 1 m)
2. Requires minimum of 10 separate cuts through a 50 × 50 cm (20 × 20 in.) copper cross section
3. Requires development of special reciprocative saw cutting machine
4. Cutting operations to be accomplished "dry" (i.e., without cutting lubricants)
5. Chip/debris containment and removal required; close proximity to control coil No. 1 and limited space difficulties
6. Length of each cut piece 2.42 m (7.94 ft)
7. Weight of each cut piece 10,300 Kg (22,712 lbs)
8. Requires special devices to transport cut sections to a removal "window"
9. "In-situ construction of replacement coil is required:
   - 288 to 360 joints, 12 bolts per joint
   - brazing of coolant tube jumpers at each joint

B. EF Coil No. 4

1. Requires partial removal of lower cryostat wall for access by men and equipment: (cutting of wall and subsequent rewelding)
2. Coil must be lowered to a more suitable position for cutting
3. Working headroom, space limitations and access are significantly more severe than for EF coil No. 1

C. Totals for Both Coils

1. Number of cuts required 20
2. Number of construction joints 576 to 720
3. Number of fasteners = 6,912 to 8,640
4. Number of conductor sections = 528 to 660

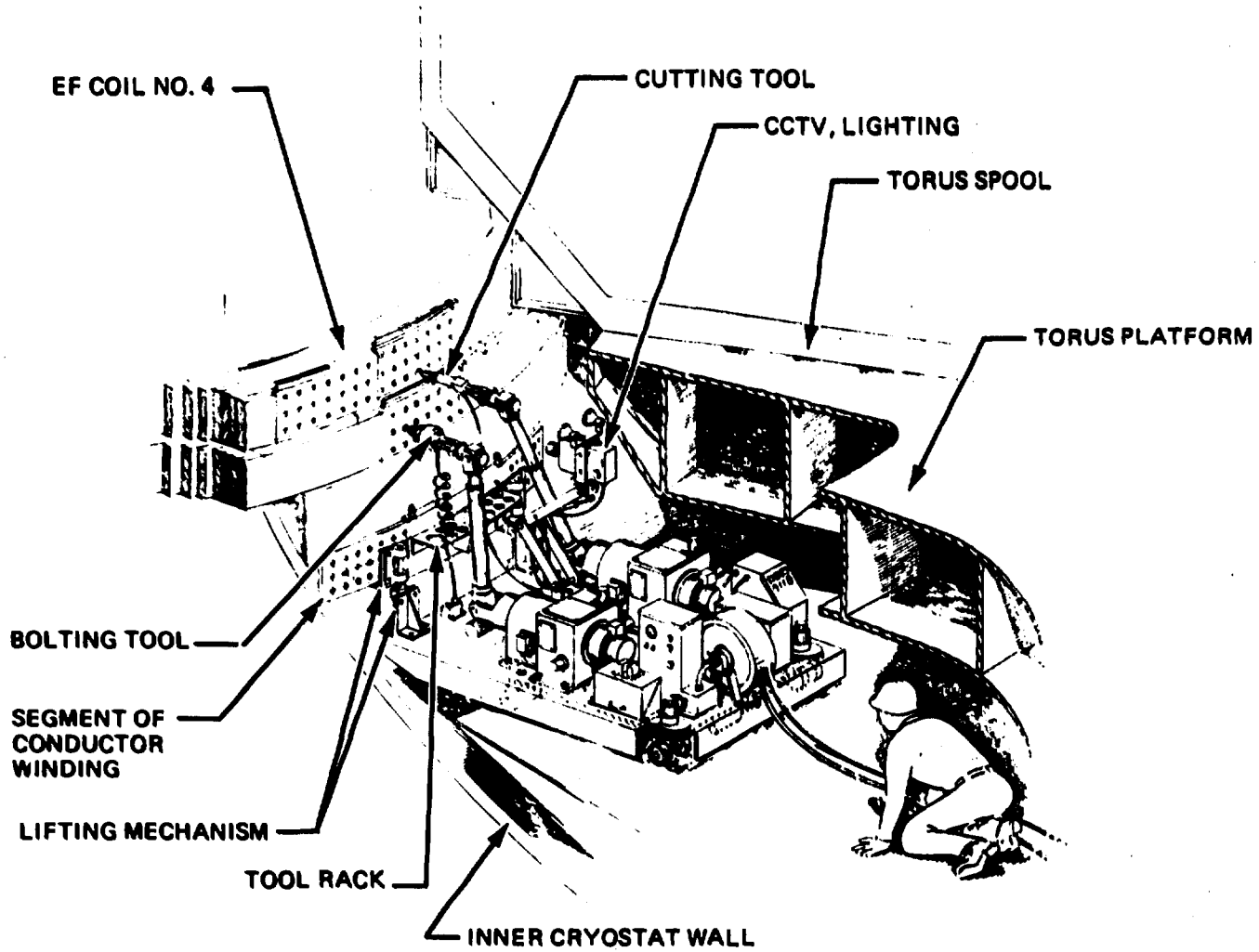

Fig. 7-30. Complex disassembly of EF coil #4.

forming the cryostat column surrounding the outboard leg of the TF coil can be left essentially intact and removed as an entity with the TF coil.

As presently designed, the cryostat panels are approximately one-half inch thick stainless steel. The panels are structurally welded together to form the cryostat vacuum chamber. To sever them for removal, a cutting machine must travel a total linear distance of approximately 133 m at least two times. At least one cut is required to prepare a channel for the "filler passes" of the subsequent rewelding process when the panels are reinstalled, and one cut is required to sever the material and form a "land" for the "root" pass of the subsequent rewelding process. Experience with cutting stainless steel panels of similar and thinner thickness strongly indicates that it is not feasible to make both cuts simultaneously.

Built-in structures must be provided for the accurate guidance and rigid attachment of the cutting machine.

During reassembly, the panels must be temporarily supported and very accurately positioned and aligned so that the "root" pass of the rewelding operation can be properly performed. The reassembly of the cryostat panels will be considerably more difficult than the initial assembly due to the restricted working space and the difficulties of dealing with reworked material.

7.6.4.6 Special cryostat maintenance equipment

The development of an automatic cutting machine is required. The machine must meet the following requirements:

- capacity to make a weld preparation cut,
- cut 304 SS without the use of cutting lubricants,
- possess variable speed forward drive and cutter RPM,
- be compatible with the space limitations of the cryostat area,
- incorporate a chip containment and removal system, and
- incorporate provisions for automatic cutter downfeed.

A device of this type may have a direct capital cost on the order of $750 K.

7.6.5 Cutting and Welding

The preferred method of assuring vacuum integrity for the tokamak device is to join the vessel segments by welding. Unfortunately, welded segments must be severed by some kind of cutting device which most often must be developed for the particular application. A review of various cutting techniques was conducted to determine which were most suitable for TF coil removal procedures. The techniques studied included laser cutting, flame cutting, abrasive (grinding) methods, shearing and nibbling, reciprocating saw cutting, milling, electrical discharge, and fly cutting.

It is recommended that for FED use, shearing and nibbling techniques be given first consideration for the removal of "seal" welds, with end milling and possibly laser cutting as alternates. For structural thicknesses of material, milling is the most feasible technique to make a weld preparation cut. End milling is preferable to side milling because of lower power requirements. A reciprocating saw device is the best method for cutting the "normal" conducting PF coils. However, electrical discharge techniques, in spite of the need for a liquid bath surrounding the electrode, hold sufficient promise to warrant further study.

Laser cutting is suitable for relatively thin sections but the cut edges must be dressed prior to rewelding. Power requirements (and hence costs) increase dramatically as section thickness increases. Flame cutting is unsuitable for TF coil replacement. The cut edges require considerable machining to remove "burned" material and shielding must be installed to intercept "blow out" deposits which otherwise weld themselves to neighboring structure. Abrasive and grinding techniques were also rejected because they are relatively slow cutting processes, which generate large quantities of powder and dust. In addition, the binders used in abrasive wheels are undesirable plasma contaminants.

7.6.6 Key Issues for Baseline Revisions

The accumulation of all the major and minor operations required to replace a TF coil creates a formidable maintenance task. It is the four major problem areas, however, that tend to concentrate the difficulties. These appear to make TF coil removal and replacement with regard to the FED reference configuration the most difficult of maintenance tasks. To improve this situation, design reconsideration must be given to the baseline design.

Examination of the four major problem areas reveals that two are caused by the location of PF coils within the bore of the TF coils, one is caused by the need to provide weld preparation cuts and subsequent structural welding operations in very large, heavy gauge stainless steel panels, and the last is a result of the need to have some major operations fully remote.

Relocation of the PF coils external to the TF coils should be considered. The extremely difficult working conditions, the limited access for men and equipment, the large number of difficult cutting operations required, the special equipment needed and, most of all, the in situ piece-by-piece assembly of replacement coils combine to make internal PF coils undesirable from the maintenance viewpoint.

Alteration of the design of the cryostat structure may greatly alleviate the difficulties of the third major problem area. The employment of fasteners (to take the structural loads) and seal welds (to provide vacuum integrity) rather than structural welds will greatly reduce (although hardly eliminate) the degree of difficulty and increase the reliability of the weldments. The number of traverses of cutting machinery would be reduced from two or three to one. Nibbling or shearing techniques could be used rather than milling. The number of weld passes could be reduced from five to one and the equipment complexity reduced.

The disassembly and removal of two spool panel assemblies and one spool radial frame assembly, shown in Figs. 7-31 and 7-32, requires fully remote removal of approximately 210 bolts of 1 to 1-1/2 in. diameter and the full remote cutting and subsequent remote welding of at least 66 m of linear length of vacuum seal.

ORNL-DWG 81-17356 FED

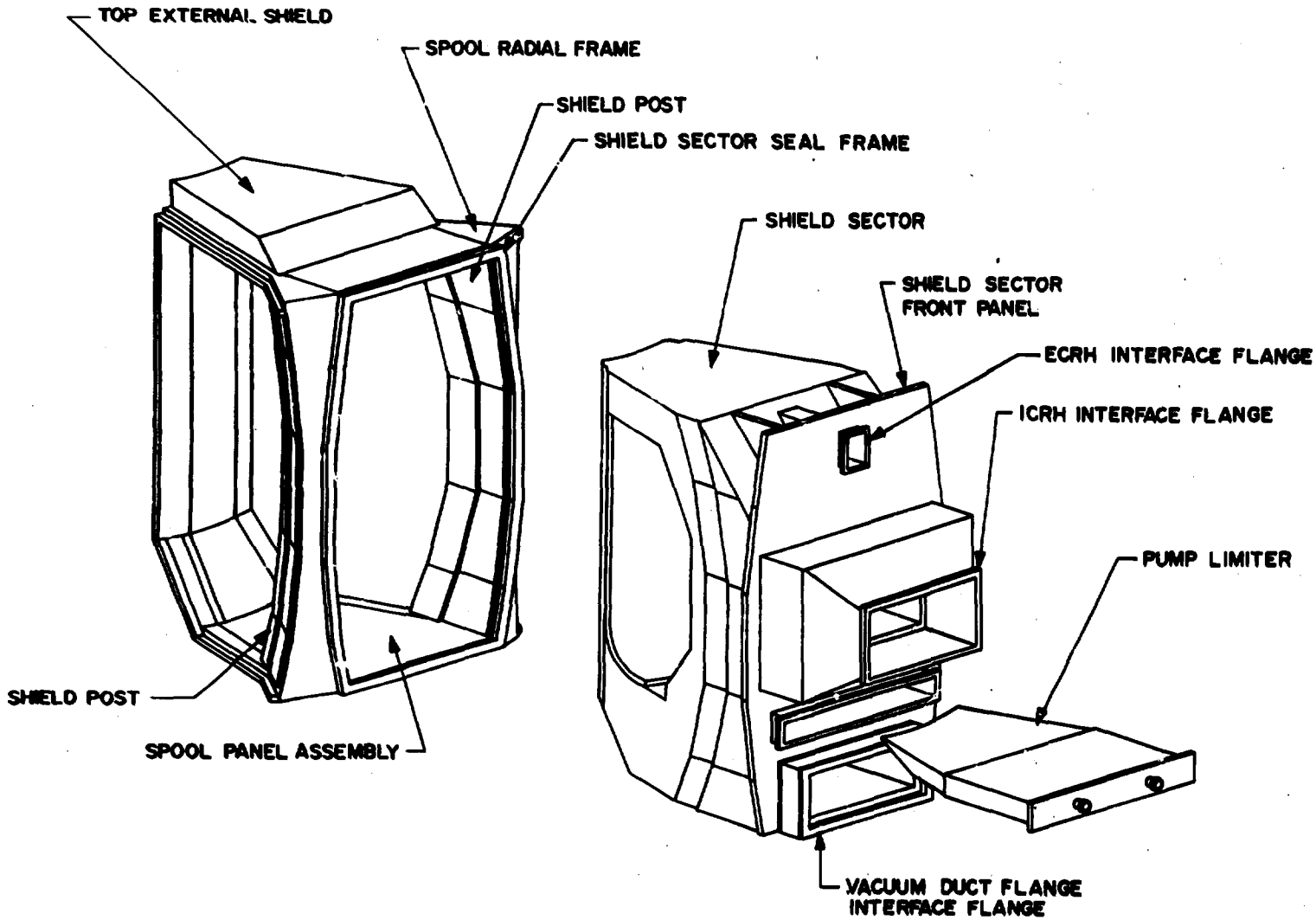

Fig. 7-31. The spool arrangement and the torus sector.

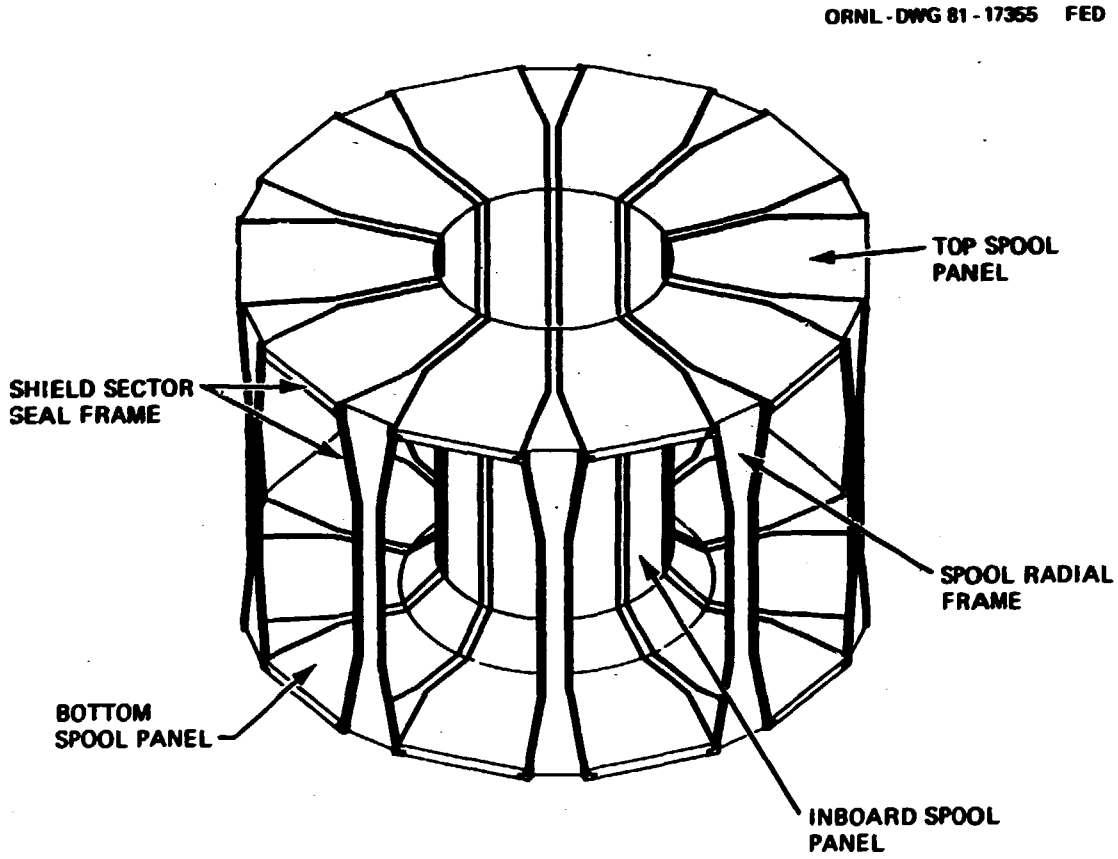

Fig. 7-32. Torus spool.

The need for fully remote operations to remove a portion of the spool assembly probably cannot be circumvented. However, even here, considerable reduction of the level of difficulty can be achieved. The reference configuration employs recessed, 0.36-cm-thick straps which are welded on both edges to the neighboring structures to join the individual spool assemblies and to provide vacuum integrity. A flanged joint design which could be cut by shearing or nibbling would considerably reduce cutting difficulties, would eliminate the need to install (remotely) new straps, would reduce the number of weld passes from two to one, and would increase weld reliability.

REFERENCES

1. C. A. Flanagan, D. Steiner, G. E. Smith, FEDC Staff, "Fusion Engineering Device Design Description," ORNL/TM-7948, Oak Ridge National Laboratory Report, Oak Ridge, Tennessee (December 1981), Section 3.2.
2. P. H. Sager et al., "Proceedings of FED Remote Maintenance Equipment Workshop," ORNL/TM-7769, Oak Ridge National Laboratory Report, Oak Oak Ridge, Tennessee (November 1981).
3. P. T. Spampinato, "Remote Maintenance Equipment for the Fusion Engineering Device," Proceedings of the ANS/RSTD Annual Meeting, Los Angeles, California (June 1982).
4. L. S. Masson, K. D. Watts, W. C. Aldrich, R. J. M. McPhearson, "Fusion Engineering Device Torus Sector Remote Maintenance Special Purpose Equipment Conceptual Design Report," EGG-FT-6008, Idaho National Engineering Laboratory Report, Idaho Falls, Idaho (September 1982).
5. L. S. Masson et al., "Preconceptual Design Requirements and System Description for FED Frame Seal Welder Cutter," EGG-FT-5786, Idaho National Engineering Laboratory Report, Idaho Falls, Idaho (March 1981).
6. L. P. Dietz, "TF Coil Replacement Considerations for the FED Baseline Configuration," ES82-235, Grumman Aerospace Corp., Bethpage, New York (October 1982).

8. FACILITY DESIGN STUDIES

8.1 INTRODUCTION

A facility design study was carried out which culminated in a major redesign of the Hot Cell Facility (HCF). This study was undertaken to improve the understanding of HCF design with the hope of improving the cost estimate. The HCF redesign resulted in some modification of the reactor building design which, in turn, led to rearrangement of other buildings on the site plan. In addition to the HCF study, more details were developed for equipment sizes and arrangements in the tritium processing building which resulted in a smaller building.

In this section, the design aspects of the FED facility studies are addressed. Cost-related facility studies and associated results are reported in Section 11.4.

8.2 HOT CELL FACILITY

The hot cell facility (HCF) supports the maintenance of the FED. Major components are removed from the device and taken into the HCF for repair and adjustment. A description of the HCF was included with the FED Design Description (Ref. 1). A review of the HCF design shows that it is one of two major buildings of the FED facilities. Since the HCF contributed substantially to overall facility cost, an investigation of the basis and cost of the HCF was undertaken with the hope of improving the design and reducing the cost. This study resulted in substantial revision to the detailed HCF design.

The HCF investigation consisted principally of visiting existing hot cell facilities and interviewing hot cell design and operating personnel. The hot cell facilities are at the Oak Ridge National Laboratory (ORNL), Idaho National Engineering Laboratory (INEL), and Hanford Engineering Development Laboratory (HEDL). There are, of course, many different methods and techniques to accomplish similar tasks, and each application requires its own unique solution. Nevertheless, several areas of consistency were noted in the discussions and tours.

This base of operating and design experience was adapted to the FED requirements to yield an improved HCF description.

8.2.1 Hot Cell Requirements

A review of the basic HCF requirements concluded that the requirements summarized in Ref. 1 continue to be applicable. However, the size, shape, and design of the HCF for meeting the basic requirements have been substantially altered. The major equipment for hot cell maintenance remains the same as identified in Table 9-4 of Ref. 1. An anechoic chamber is still required to test and adjust RF components. The decontamination area has increased in importance due to the study.

8.2.2 Hot Cell Design Issues and Options

All of the HCF design issues and options are closely interrelated. The biggest issues are caused by contamination control within the facility and into and out of the facility. The contamination control issues affect component and tool movements, ventilation, and HCF maintenance activities and eventually impact the size, shape, and general features of the HCF.

Decontamination of components and equipment was almost universally noted as a difficult problem which must be carefully and thoroughly addressed. It was stressed by a number of experienced people that contamination control can only be accomplished when designers and operators pay close attention to details.

Decontamination cell

All movements into and out of the hot cell area should pass through a contamination control station where each item can be checked for contamination and cleaned if necessary. This contamination checking and decontamination applies to all items (e.g., waste containers, tools, and components) whether they are going into or coming out of the hot cell area and whether they are going into or coming out of the reactor building. The purpose of this activity is to prevent contamination from

passing between areas and to the outside. The decontamination area needs to provide several means of cleaning contaminated items. A spray chamber is most useful to the cleaning operations. Often high pressure water is adequate to remove loose contamination. However, capabilities must be included to use other cleaning fluids as well; detergent solutions, acetone, alcohol, and freon have all been mentioned as possible cleaning fluids. Even uncontaminated items must be cleaned before entering the contaminated areas. Grease and films from manufacturing and shipping would collect and transport contamination within the hot cell and/or reactor building and make later decontamination more difficult. The FED designs have additional cleanliness requirements due to the high vacuum requirements. The vacuum requirements are likely to require grease and oil removal to very low levels and will probably limit the types of cleaning fluids and chemicals that can be used within the HCF and reactor building.

Hot cell maintenance

The method to e used to maintain the hot cell facility is also influenced by contamination control considerations. Two approaches can be taken to maintain the work stations in the hot cell area. The approach used for the HCF in Ref. 1 was to provide several individual cells which would allow personnel entry for hands-on or bubble suit maintenance. The individual cells were shielded and isolated from each other so that radioactive component maintenance could continue in the adjacent cells while cell maintenance was being performed. The cell to be maintained would have to be decontaminated before personnel entry. The most desirable feature of this approach was the use of hands-on (or bubble suit) maintenance, which was faster and more efficient.

The alternative approach is to have all the work stations in one large area and perform all the cell maintenance operations remotely. Tools and equipment could be removed, decontaminated, and repaired in a separate glove-box type of area; no personnel entry is allowed into the hot cell area. The advantages of this approach are that the work

stations do not have to be decontaminated for maintenance operations, and the reduced shielding requirements may reduce the cost and complexity of the facility.

The first approach was attacked vigorously by several people with hot cell design and operating experience. Decontamination of hot cells for personnel entry is very difficult and time-consuming. Thus, the advantage of personnel entry is largely negated. Movement of cranes and components through contaminated areas after decontamination would likely lead to recontamination of the component and the work stations, even though they are isolated most of the time. On the other hand, totally remote maintenance of hot cells has been demonstrated in a number of facilities. Thus, while it is not easy, the non-entry cell is at least feasible. Unfortunately, the size of the HCF and the components to be repaired for FED are substantially larger than most current experience with totally remote hot cell maintenance. Thus, the HCF for FED represents a significant extrapolation of current technology.

One particular area of concern is the maintenance of the overhead crane. The 400- to 500-ton capacity crane needed for FED is probably a factor of 20 larger than any crane currently designed for totally remote maintenance. The crane maintenance is likely to be a major difficulty for any totally remote design. It is possible that the crane will be high enough above the sources of contamination to allow glove-box type maintenance of the components.

Ventilation systems

The ventilation system plays a key role in the control of contamination in existing hot cells. The most successful flow pattern appears to be where the clean air enters near the top of the cell and flows out through gratings in the floor. Each work station has a section of the outlet within its boundary. This flow pattern tends to pin the contamination to the floor and sweep it to the filters beneath the floor without contaminating other areas of the hot cell. This pattern has been very successful in reducing contamination in the upper areas of the hot cells. Smaller vacuum hoods and enclosures with special purpose filters

should be used for operations that produce dust or fumes. Contamination from some fairly dirty machining, cutting, and welding operations has been successfully controlled with these ventilation techniques.

Component transport

The movement of components, materials, and tools into and out of contaminated areas is one of the most difficult problems of contamination control. The need for decontamination has already been discussed, but the problem of the spread of contamination by the transport device has been a source of continuing concern at existing hot cells. Crane cables and hooks pick up contamination and spread it from one area to another. Wheels and bearing grease on carts and trolleys also become heavily contaminated and spread the contamination to other areas. Thus, the use of airlocks by themselves has not been very successful in controlling contamination. As a result, almost every one of the hot cells which were visited has developed some version of what can be called the down-over-and-up movement pattern for moving material into and out of hot cells. This pattern describes the technique of lowering the item to be moved through a hatch onto a cart in a separate compartment. The cart is then moved under the hot cell floor where the hot cell crane lifts the item into the hot cell through a hatch in the floor. The compartment and hatch arrangement serve as an airlock between the two areas. The cart generally has an enclosure or tank which is covered during transfer to reduce the contamination spread to the compartment. Each part of the transport system stays in its own space without traveling from one space to another. Thus, the amount of contamination spread from one area to the other is more effectively controlled. The transfer compartment stays clean or can be decontaminated to levels that allow personnel entry for cart transport system maintenance. The hatch covers can provide good sealing characteristics because no loads go over the sealing surfaces; of course, contamination travels with the item during transport, but this is the contamination that is to be handled by the decontamination area. Techniques must be provided for decontaminating the interior of the enclosure or tank on the cart.

Hot cell atmosphere

The use of an inert gas atmosphere for the hot cell area has been suggested by some experienced personnel. The normal advantages of an inert gas atmosphere are that fire hazards are greatly reduced and the formation of ozone is prevented. Ozone is formed from the oxygen in the air by high levels of radiation. Ozone is highly corrosive to metals and attacks many of the plastics which are desirable for use in hot cells. Additional advantages for the FED situation include the possibility of performing cutting and welding operations without special inert gas sources and the possibility of easier removal of any tritium that gets released to the hot cell atmosphere. The weight of these advantages tends to offset the disadvantages of additional cost and complexity of maintaining an inert gas atmosphere. However, as long as a non-entry hot cell area is used, the use of an inert gas has little influence on the HCF design, and the impact on overall cost is negligible.

8.2.3 Hot Cell Investigations and Studies

The main thrust of the hot cell investigation was to apply as much hot cell-related design and operation experience as possible in the time available to the FED hot cell design. To accomplish this, hot cell designers and operators were interviewed and hot cell facilities were toured at three national laboratories: ORNL, INEL, and HEDL. The facilities which were discussed and toured are summarized in Table 8-1. Most of these discussions provided the personnel with an opportunity to comment on the design of the HCF for FED.

The process of gathering information for hot cell design was progressive in that more and better questions were possible as more information was gathered. After each discussion, design ideas were altered and the altered set formed the basis for the next discussion.

After all the discussions and tours, the information was distilled and applied to the FED situation. This was not an analytical process, and a great deal of judgement and interpretation was necessary to translate the information into the HCF design. Several iterations were

Table 8-1. Summary of hot cell facility tours and discussions

Location	Design/operation discussions	Facilities visited
INEL	Hot Fuel Examination Facility/North and South (HFEF)	Toured both facilities
	Test Area/North (TAN)	Toured facilities
	New Waste Calcining Facility (NWCF)	Toured workup area and facility which was not yet in operation
HEDL	Fusion Materials Irradiation Test (FMIT)	
	Fuel and Materials Examination Facility (FMEF)	Mockup area
	Engine Maintenance Assembly and Disassembly (EMAD)	(Pictures only)
	Material and Fuel Examination Hot Cells and Reprocessing Experimental Hot Cells	Toured sets of facilities
ORNL	ORNL Hot Cell Facilities at X-10	Three complexes of hot cells at X-10
	Hot Experimental Facility (HEF)	HEF mockup and testing area

made as the layout of the HCF was prepared. The overriding goal was to provide an HCF design with the key features perceived as necessary for FED and to provide an improved basis for estimating HCF costs.

8.2.4 Hot Cell Design Description

The HCF that resulted from this investigation is shown in Fig. 8-1, and the major characteristics are given in Table 8-2. The major areas include a decontamination cell with spray chamber, the main hot cell with an area for assembly and disassembly of major device components, a separate area with a number of work stations for working on smaller components and working with necessary machine tools, and a tool maintenance area above the decontamination cell for repair of tools, equipment, and low radioactive components. The transportation of components and equipment uses a combination of overhead cranes and an underground rail shuttle. Storage areas, anechoic chamber, and some ventilation system details are also included.

The rail shuttle system, in combination with the decontamination cell, is the first line of defense against the spread of contamination between the reactor building and the HCF and release of contamination to outside areas. The rail system uses double-wide railroad cars to handle the weight and bulk of the major device components. Each car is mounted with a large cylindrical tank to completely enclose the component during movement. A typical movement would start with positioning the shuttle car beneath the appropriate hatch. The sealing mechanism of the hatch is used to establish a seal between the hatch and the cylindrical tank. The hatch cover is then released and removed with its own driving mechanism. The tank cover is then removed with the overhead crane and placed in its parking area. The component is lifted into place in the tank with the overhead crane, the tank cover replaced, the hatch cover repositioned, and the sealing mechanism retracted. The shuttle car is repositioned with its driving mechanism, also located in the transfer chamber, beneath the appropriate hatch for component removal, and the process is then repeated. Because of the radioactive nature of the

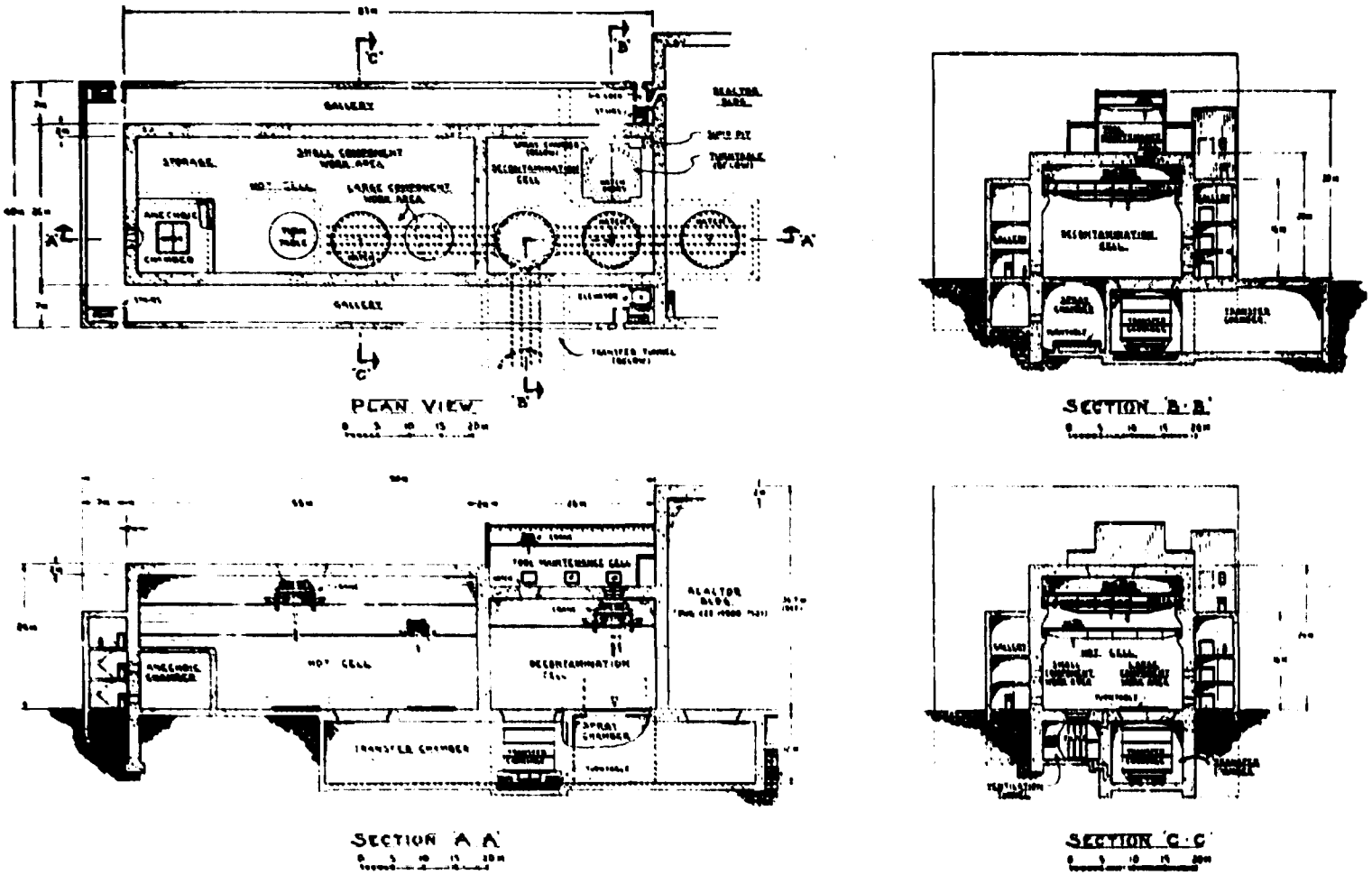

Fig. 8-1. Hot cell facility layout.

Table 8-2. Hot cell facility characteristics

Construction type =	controlled ventilation resistant to natural phenomena and missiles
Shape =	Irregular rectangular
Size (overall dimensions):	length ≅ 90 m width ≅ 40 m height ≅ 36 m volume = 96,500 m^3
Basic hot cell and decontamination cell walls and roof constructed with up to meters of concrete for shielding	

major device components, the entire transportation proc st be accomplished by totally remote control. Full-capacity cranes must be provided in the reactor building, the decontamination cell, and the hot cell area.

The decontamination cell is centrally positioned so that all movements of contaminated components must pass through the cell for inspection and cleaning. Movements directly between the reactor building and hot cell area are blocked both mechanically and administratively. The decontamination cell is equipped to measure radioactivity and contamination, and a variety of decontamination methods is available to clean and decontaminate any component or piece of equipment. The spray chamber is provided for the most difficult cases. Spray nozzles in the chamber are capable of using different cleanup fluids such as demineralized water, detergent, solvent, and possibly freon. The component to be cleaned is placed on the turntable and rotated to direct the spray. A pump is provided as part of the control system for the cleaning fluids. The turntable also serves the important function of establishing the appropriate orientation of the large components before they are moved into the reactor building.

All the surfaces of the decontamination cell and many of the surfaces of the hot cell facility require steel liners to protect the concrete structure, prevent concrete dust formation, and allow decontamination. Other surfaces must be coated with high-quality paint to allow washdown and decontamination.

Tool and manipulator maintenance is provided in the tool maintenance region above the decontamination cell. Tools are first removed from the hot cell, decontaminated, and then lifted into the tool maintenance area through a hatch in the decontamination chamber ceiling. Depending on residual contamination levels, the maintenance of these tools and manipulators may be done with either direct contact procedures or glove-box arrangements. Many smaller device components that are not directly exposed to neutron activation can also be maintained in this area.

The main areas of the HCF are completely isolated from the rest of the facility by the transportation and ventilation systems. No personnel entry will be allowed after the cell becomes contaminated. This means that all the maintenance operations in the main hot cell areas must be performed with totally remote control. All components enter the hot cell areas through the transfer chamber. Large components are placed on one of two large turntables where servomanipulators and power arms will be used to further disassemble the components and perform other maintenance operations. Small components, which are either brought in through the transfer chamber or removed from the larger components, are moved to the small component work area by the lower of the two overhead crane systems.

The operations are performed in the small component work area with through-the-wall manipulators and wall or overhead-mounted power arms. The actual operations are expected to include mechanical assembly and disassembly, welding, cutting, machining, grinding, lathe turning, milling, and other related machine shop activities.

Since no personnel entry is allowed in the main hot cell area, the possibility of providing an inert atmosphere such as argon gas for this area can be considered without substantially hampering maintenance activities. The advantages of the inert atmosphere include greatly reducing fire hazards, eliminating ozone production with its potential for corrosion and plastic degradation, allowing more flexible arrangements for cutting and welding, and reducing oxidation and corrosion caused by air. The fire hazard might be particularly significant if breeding blankets containing lithium and lithium compounds are to be handled in the hot cell.

8.3 REACTOR BUILDING

The reactor building has received some design attention because modifications of the HCF have impacted the reactor building design. The basic reactor building design has remained the same, with the PF coil laydown area modified to allow removal of the magnet coils through the side of the building instead of into the HCF.

8.3.1 Reactor Building Issues and Options

The only major requirement to be changed by the HCF studies was the location of the area for removing the PF and TF magnets from the building. The FED Baseline design in Ref. 1 provided for removal of the magnets through a removable wall section into the hot cell area. This technique used a lot of space just for magnet handling and was not compatible with the restructured HCF requirements for contamination control.

Several reactor building configurations were considered to eliminate the need for removing the magnets without passing through the HCF. Most of the options were differences in arrangement of the PF coil laydown area. The most important difference was the method of controlling contamination. One method is to design a separate room just for the PF coil laydown area which can be isolated from the rest of the reactor building. This leads to a large volume which is not very useful except for those rare occasions when one of the magnets fails and needs to be removed. The second option is to provide the space for the PF coil laydown area and an enclosing structure but to expect to erect the structure only if and when it is needed. In this way, the PF coil laydown area can be used for other maintenance activities, and the cost of the additional temporary structure can be substantially less than that of a permanent structure.

8.3.2 Reactor Building Design

The reactor building studies consisted of making several layout sketches and determining which configuration best met the requirements and other constraints. The revised reactor building configuration is shown in Fig. 8-2, and the characteristics are summarized in Table 8-3. This configuration is very similar to that shown in Ref. 1, but the dimensions have been altered slightly to reflect the exact FED configuration shown in the earlier report. The PF coil laydown area has remained the same, but the positions of the temporary structure for contamination control are shown for information. The removal of the

ORNL-DWG 82-3870 FED

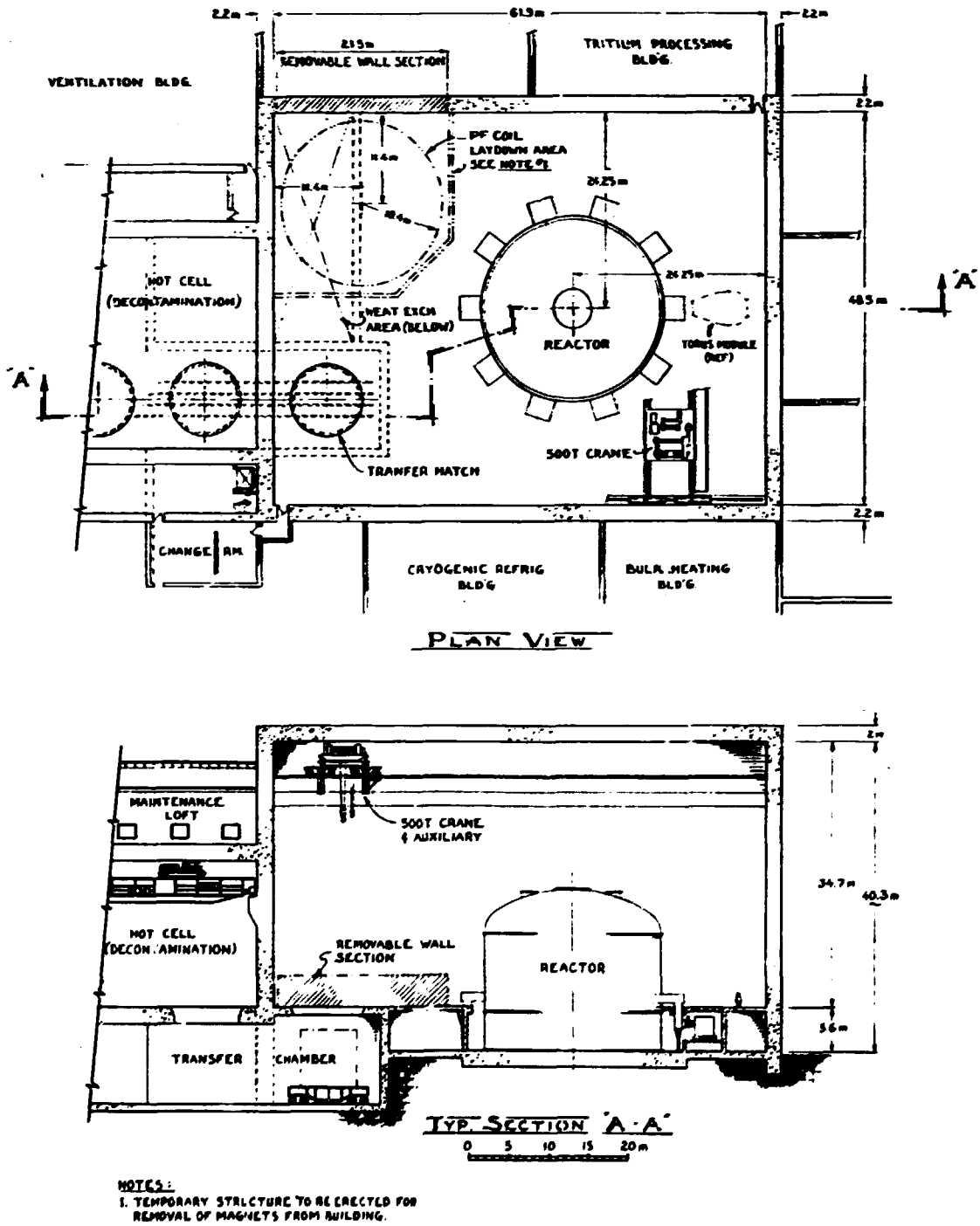

Fig. 8-2. Reactor building layout.

Table 8-3. Tokamak building characteristics

Construction type =	confinement, low leakage (∿1 bldg. volume/day) resistant to natural phenomena and missiles
Size: length	≅ 66 m
width	≅ 53 m
height	≅ 45 m
volume	≅ 157,000 m^3
Walls and roof constructed with 2 meters of concrete for shielding	

magnets is now planned for the side wall instead of the wall between the HCF and reactor building.

8.4 FACILITY PLOT PLAN

The site plan was changed to reflect the revision of the HCF and reactor building, as well as a revised tritium process building size. The revised site arrangement is shown in Fig. 8-3. Some buildings were rearranged to accommodate the removal of magnets through the side of the reactor building. The rearrangement will have no impact on cost estimates. The reduction of the tritium building size was the result of more detailed equipment sizing and arrangement. The decrease in tritium building size is reflected in a corresponding decrease in tritium building cost.

ORNL-DWG 82-3871 FED

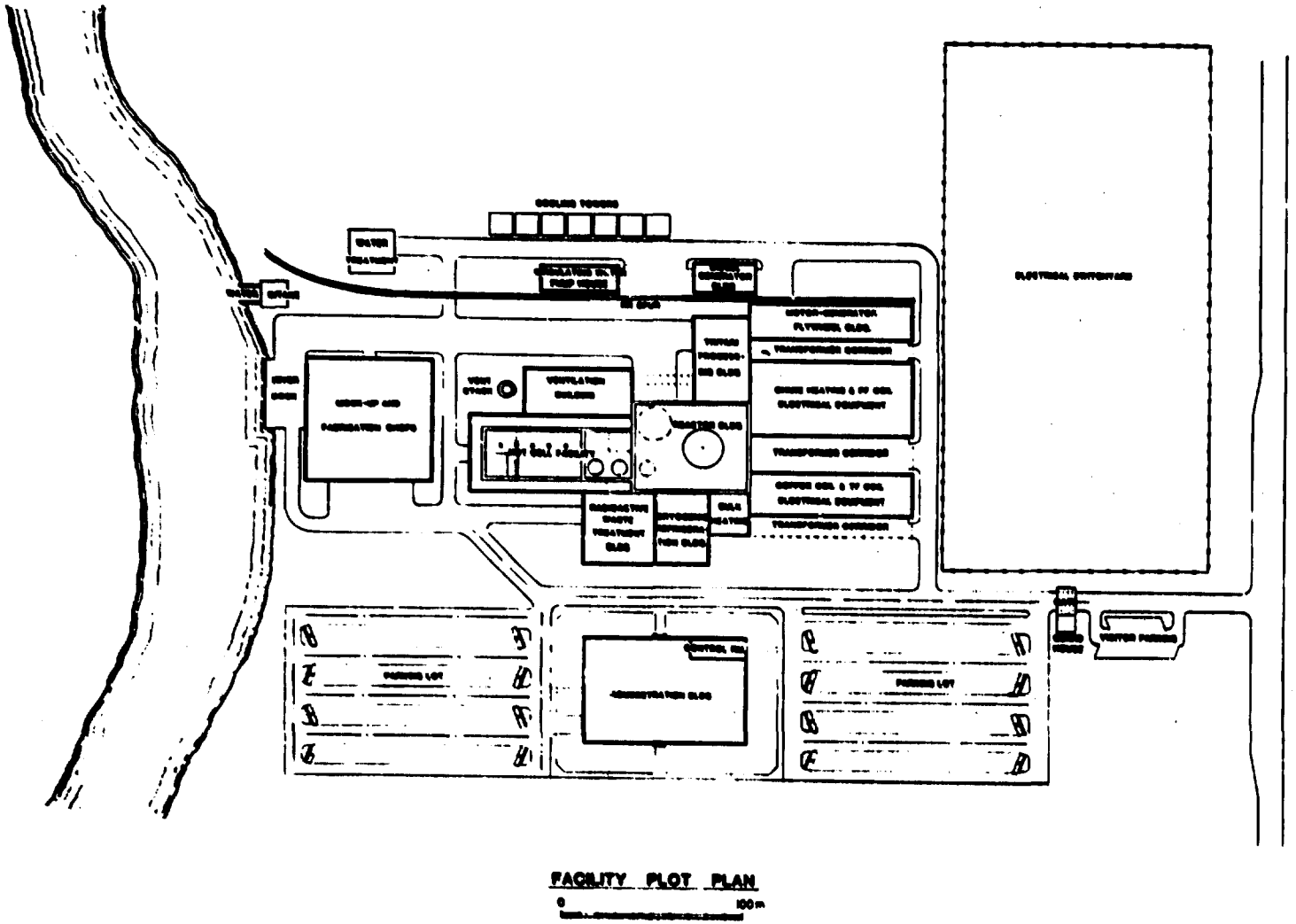

Fig. 8-3. Facility plot plan.

REFERENCE

1. Fusion Engineering Device Design Description, ORNL/TM-7948/V2, Oak Ridge National Laboratory, December 1981.

9. RAM REQUIREMENTS

9.1 INTRODUCTION

In order to satisfy its mission objectives in a timely manner, FED must satisfy certain RAM (reliability, availability, and maintainability) requirements. These requirements must be specified early in the design development in order to ensure that the design concepts adopted are consistent with the RAM requirements. In the following sections, overall device requirements will be discussed. System and component specifications consistent with meeting overall device requirements are then presented.

9.2 OVERALL DEVICE REQUIREMENTS

A fundamental consideration in the design of FED is that the availability* which FED is capable of achieving be commensurate with the availability required by the plan of operations. The availability which FED is capable of achieving is determined by the reliability, maintainability, and supportability characteristics of the design and by scheduled maintenance requirements.

A plan which integrates FED testing requirements into sequenced phases of operation and establishes guidelines for operation in each phase was developed. Table 9-1 summarizes the phases of operation, operating guidelines, and the estimated number of cycles associated with each phase. The availability shown is that associated with accomplishing the indicated number of cycles in the time allotted.

The lower level of availability requirements shown in earlier phases is consistent with the operational constraints which are expected to impact initial FED operation. These operational constraints include:

---

*Availability is defined by the ratio of operating time to operating time plus downtime. For the purpose of this analysis, all nonoperating periods were assumed to be downtime periods wherein maintenance could be accomplished.

Table 9-1. Proposed FED operation plan

Phase	Duration (years)	Description	Operating guidelines	Number of cycles[a]	$\frac{SOT}{CT}$[b]	$\frac{OT}{SOT}$[c]	Availability[d]
I	1	Integrated system checkout	2 shifts/day 5 days/week 2 weeks/4 weeks[e]	15,000 (≤8 T)	0.20	0.35	0.07
II	2	Hydrogen (deuterium) operation	2 shifts/day 5 days/week 4 weeks/6 weeks	50,000 (≤8 T)	0.32	0.38	0.12
III	1	8-T, DT operation	2 shifts/day 4 days/week 5 weeks/8 weeks	25,000 (8 T)	0.30	0.40	0.12
IV	1	10-T, DT operation	2 shifts/day 5 days/week 5 weeks/8 weeks	25,000 (10 T)	0.30	0.27	0.08
V	5	DT engineering testing	2 shifts/day 5 days/week 9 weeks/12 weeks	200,000 (8 T)	0.36	0.54	0.19

[a]Cycle times of 152 s for ≤8-T operation and 102 s for 10-T operation were assumed.

[b]Scheduled operating time/calendar time.

[c]Operating time/scheduled operating time.

[d]Operating time/calendar time.

[e]Two weeks out of four weeks.

- Hardware checkout and software debugging
- "Infant mortality" failures due to deficiencies in initial design, fabrication, and assembly
- Initial unfamiliarity with maintenance procedures
- Incorporation of design upgrades for improved performance

Phase IV is a period of 10-T DT operation for which a year has been allotted. The lower availability requirement during 10-T operation reflects the judgement that, due to higher stress levels, FED should not be expected to achieve the same availability during 10-T operation that it is capable of achieving during operation at 8 T. Also, since FED is currently designed for a relatively limited number of cycles during 10-T operation, there may be a tendency to conserve the number of cycles initiated.

Phase V operation includes 65% of FED operating time, has the highest availability requirement, and, hence, is considered most critical with respect to availability. Phase V operation has been estimated to involve approximately 200,000 cycles at 8 T in a five-year period. Assuming a cycle length of 152 s, FED would have to achieve an availability greater than 19% in order to complete the indicated number of cycles in the time allotted. Nominal operation* will be two (eight-hour) operating shifts per day, five days per week. (Maintenance crews were assumed available around-the-clock, seven days per week.) A three-week period every third month has been identified for scheduled maintenance and reconfiguration activities. FED would have to operate 54% of the scheduled operating time in order to achieve an availability of 19%.

In addition to the availability requirements which have been discussed, FED must satisfy reliability requirements dictated by the FED test program. The FED test program features several tests, e.g., tritium recovery tests and thermal-hydraulic and thermomechanical response tests, which require long periods ($>10^3$ cycles) of continuous operation.

---

*The nominal operation described represents a typical mode of operation. It is recognized that specific tests may dictate more (or less) intense modes of operation for the duration of such tests.

While these tests do not involve a major fraction of the total number of cycles in the life of FED, it is desirable to have a reasonable probability (>0.5) of successfully completing a test once it is initiated. Consistent with this premise, a mean-time-between-failure (MTBF) of 72 hours will be taken as an overall reliability requirment.

9.3 DEVELOPING SYSTEM AND COMPONENT REQUIREMENTS

By considering the FED plan of operations and test program, a picture of the overall availability and reliability requirements emerged. The task remained, however, of translating these overall requirements into specific system and component requirements. An infinite number of permutations of system and component requirements exist which satisfy the overall requirements. However, only one permutation is optimal from a cost standpoint. The purpose of this effort was to establish an initial set of system and component requirements which satisfies the overall requirements and which, hopefully, is not too different from the optimum set. It is expected that the set of requirements generated in this document will be periodically revised to allow more optimal sets of requirements to be put in place.

The overall availability requirement changes from one phase of operation to another because of different operational constraints and operating requirements. The most stringent availability requirement (19%) is associated with the longest phase of operation, Phase V. For this analysis, it was assumed that a set of system/component requirements which has a high probability ($\sim$0.9) of satisfying the overall availability requirement for Phase V operation would be adequate for other phases of operation as well.

In developing system and component requirements, it is important to recognize global maintenance constraints, including the following:

1. A 24-hour cooldown time is required prior to manned access to the reactor cell.
2. Sixty-four hours are required for detritiation prior to letting the plasma vacuum chamber up to air.

3. One hundred sixty-eight hours are required for reconditioning the plasma vacuum chamber once it has been let up to air.
4. For maintenance requiring warming superconducting coils to room temperature, two weeks are required for warmup and four weeks for subsequent cooldown.

Some of the above constraints such as Items (1) and (2) may be conducted in parallel.

The operating guidelines for Phase V operation (Table 9-1) thus allow scheduled manned access to the reactor cell for four shifts per week. Scheduled maintenance requiring letting the plasma vacuum chamber up to air (e.g., for changing unpocketed test modules, diagnostics, and limiter blades) must be accomplished in a coordinated fashion during two-week windows which occur at three-month intervals. It is implicit in the operating guidelines that there is no scheduled maintenance requiring warm-up of the superconducting coils. All FED scheduled maintenance must be accomplished within the operating guidelines established for Phase V operation, as shown in Table 9-1.

During Phase V, the device is only scheduled to operate 36% of the total calendar time. In order to satisfy the 19% availability requirement, FED must operate >54% of the time scheduled for operation. The unscheduled maintenance parameters of FED systems/components, i.e., failure rate (λ) and mean time to repair (MTTR), must be commensurate with allowing FED to operate >54% of the time scheduled for operation. In order to ensure that this requirement is met, it is sufficient to specify that the downtime ratio, ρ, where

$$\rho = (\lambda)\ (\text{MTTR})\ \text{downtime hours/operating hours},$$

is less than a maximum acceptable value for each system/component.

Specifying the downtime ratio for each system/component, however, is not sufficient to ensure that the overall MTBF requirement of 72 hours will be met. Thus, it is also necessary to specify a failure rate for each system and component. Figure 9-1 shows the acceptable combinations of λ and MTTR which satisfy the requirements of $\lambda < \lambda_{max}$ and $\rho < \rho_{max}$.

ORNL-DWG 82-3872 FED

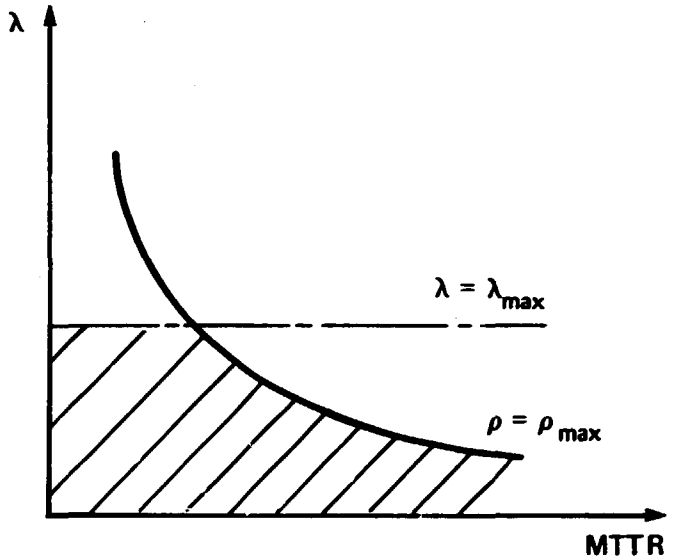

Fig. 9-1. Acceptable combinations of λ and MTTR.

Two "words of warning" should be given when considering λ and MTTR:

1. λ is the system/component failure rate when the device is being operated. Some systems/components will exhibit a significant "offline" failure rate. In generating system/component requirements, this phenomenon has been taken into account. The specified λ thus has units of failures per operating hour.
2. MTTR is the time required to restore the reactor to operating condition from the time of failure. It includes cooldown time, reconditioning time, time awaiting parts, etc., as well as active repair time.

9.4 SYSTEM REQUIREMENTS

For each FED system, failure rate (λ) and downtime ratio (ρ) requirements were generated and are listed in Table 9-2. With these system requirements, FED will operate an average of 63% of the time scheduled for operation, with a standard deviation of about 8%. The probability of completing Phase V operation within the time allotted, i.e., demonstrating an operating time/scheduled operating time >54%, would be ~90%. The MTBF characteristic of FED operation would be 72 hours.

It may be seen in Table 9-2 that the availability drivers (systems with the highest ρ) are expected to be the TF, PF, and power absorption (first wall/limiter) systems. It may also be seen that the main reliability driver is the INFACS (Information and Control) system. Reference 1 provides a discussion of reliability, maintainability, and supportability features for each FED system.

9.5 SELECT COMPONENT REQUIREMENTS

Failure rate (λ) and downtime ratio (ρ) component requirements consistent with the system requirements presented in Sect. 9.4 were generated for select FED components and are listed in Table 9-3. An earlier discussion of reliability, maintainability, and supportability features for FED components may be found in Ref. 1.

Table 9.2. FED system failure rate (λ) and downtime ratio (ρ) requirements

System	λ_{max}	ρ_{max}
Coil Systems		
TF system	3.6-4[a]	1.9-1
PF system	1.1-3	3.0-1
Coil vacuum system	3.4-5	7.2-3
Coil support structure	5.0-7	7.5-3
Torus Systems		
Shield structure	2.3-4	3.7-2
Power absorption	1.2-3	3.9-1
Electrical contacts	4.7-5	1.0-2
Spool structure	5.1-6	3.4-3
Torus vacuum system	2.5-4	8.7-3
Torus support structure	2.7-5	1.9-3
Fuel Systems		
Fuel processing	1.0-4	6.0-3
Fuel storage and delivery	6.4-4	1.9-2
RF Systems		
ECRH	1.3-4	1.8-2
ICRH	1.2-3	9.0-2
Heat Transport Systems		
Main heat transport	5.5-4	3.3-2
Cryogenic systems	8.0-4	4.8-2
AC Power Systems		
Control diagnostics	5.1-4	8.6-2
Information and Control Systems	6.0-3	1.2-2
Experimental Systems	3.0-4	7.0-2
Facilities Systems	2.0-4	6.4-3

[a]Read as 3.6×10^{-4} failures per operating hour.

Table 9-3. Failure rate (λ) and downtime ratio (ρ) requirements for select FED components

Component	λ_{max}	ρ_{max}	Comments
TF coil winding	2.1-6[a]	1.2-2	Assume spare
EF2 coil winding	9.4-6	5.5-2	Assume no spare
EF3 coil winding	1.6-5	1.6-1	Assume no spare
OH/EF solenoid	1.4-5	1.9-2	Assume spare pancake
S/C coil power lead	2.0-6	2.4-3	Assume spares
TF PWR CONV/PROTECT	2.5-4	2.0-3	
PF PWR CONV/PROTECT	1.0-3	8.0-3	
S/C coil vacuum vessel	4.2-6	1.0-3	
Bucking post	1.0-7	6.0-3	
ICSS	2.0-7	5.8-4	
Sector module	7.2-6	3.0-3	
Shield post	3.6-7	1.8-4	
Armor tile	5.0-8	1.7-5	5 cm x 5 cm tile
First wall panel	7.5-6	3.2-3	Assume spare
Pump limiter module	2.5-5	8.4-3	Assume spare
Bellows contact	6.7-8	2.8-5	
Spool structure	5.1-6	3.4-3	
Pellet injector	2.0-3	9.6-2	1 of 2 required
ECRH launch window	5.0-6	1.3-3	
ICRH launch window	2.0-5	5.1-3	
ICRH ridge loaded waveguide launcher	5.0-5	1.3-2	

[a]Read as 2.1×10^{-6} failures per operating hour.

10. SAFETY STUDIES

10.1 INTRODUCTION

A number of safety-related studies were initiated as a result of questions raised by other design studies. These studies involve the application of safety criteria and guidelines to specific design problems. The safety and environmental criteria and guidelines reported in Ref. 1 have not been changed during the current period. All the current safety applications involve the control of radioactivity or radioactive material. Potential activation of the reactor building walls and structure, contamination of the reactor building, tritium absorption on building surfaces, and possible tritium leakage all impact the design of the facilities for the protection of the maintenance staff. The impact of cryogen blowdown on radioactive material release and possible production of carbon-14 both affect the design for protection of the general public and the environment.

All of the safety studies performed can be characterized as scoping studies. In each study, efforts were made to identify the severity of the impact and to identify possible design solutions. The information and design details in all of these areas are sparse. Thus, these scoping studies must be updated as more information becomes available, and some issues still require resolution.

10.2 ACTIVATION OF BUILDING WALLS AND STRUCTURES

The potential activation of the reactor building walls and structures by neutrons leaving the FED during operation could impact the dose rate to maintenance staff. Any significant dose would add to the expected dose coming directly from the reactor and make it more difficult to meet the guideline of 2.5 mR/hr dose rate after 24 hours of shutdown. The 24-hour shutdown dose rate on the inside surface of the concrete wall has been estimated in the range of 1 to 20 mR/hr. This dose rate would significantly impact maintenance operation within the reactor building. A large portion of this estimated range does not meet the current FED

guideline for contact maintenance. Any maintenance work in levels of radiation above the criteria would have to be more strictly limited and would require additional maintenance personnel.

The addition of 1 w/o (one percent by weight) boron to the first foot of concrete would substantially reduce the concrete activation. The estimated cost of adding boron in the form of boron frits to the building concrete was estimated to be in the range of $7 million to $14 million.

Another option is to carefully specify the concrete aggregate to reduce those elements that contribute most to the activation. The specification and availability of special aggregates need to be investigated further. The cost of special aggregates will be highly site-dependent. Handling special aggregates on a major construction site also leads to additional quality assurance requirements and increased costs. Due to the uncertainties in availability, specification, and site dependency, no estimate can be made for the cost of special aggregate at this time. However, it is anticipated to be less expensive than adding boron frits to the concrete.

10.3 CONTAMINATION IN THE REACTOR BUILDING

The most important potential source of contamination in the reactor building is the radioactive dust and debris released from the plasma vacuum chamber during maintenance operations. The activated steel dust with its cobalt isotopes is the most potent of these radioactive materials. This debris has the possibility of contaminating reactor building surfaces and becoming airborne; either of these possibilities would adversely affect contact maintenance operations.

As a result of scoping studies, maintenance procedures have been modified to provide vacuum cleaning of the plasma chamber before the torus sector is removed and to provide maintenance equipment to enclose torus shield sectors during removal and transport within the reactor building. In addition, floors and structural members near the device are expected to be lined with steel to make decontamination activities possible. Ventilation systems will be expected to handle radioactive

dust. The costs associated with these contamination control techniques have not been estimated, but their costs are considered small compared to the total building and facilities costs.

10.3.1 Stainless Steel Debris

Most of the activated steel dust comes from the 316 SS outboard first wall panels during startup. The amount of erosion of the first wall during actual operation is almost nonexistent. During startup, however, the erosion from charge-exchange neutrals amounts to 150 kg of material in the life of the reactor and is composed to a significant degree of Co-60 and Co-58.

Because of the complexities and uncertainties inherent in particle transport and plasma conditions, detailed analyses of erosion product transport during startup were not performed. However, based on prior analyses of the pumped limiter, a significant number of the sputtered stainless steel atoms may be redeposited near their initial positions. If most sputtered atoms redeposit and become attached to interior torus surfaces such as the first wall, limiter, pump ducts, and ICRH ducts, the amount of activated erosion products available to escape from the torus after opening the vacuum chamber to the reactor building environment will be significantly reduced. Nevertheless, by making several conservative assumptions as to the distribution and fraction of steel dust which may fall out of the sector during sector removal, as much as 200 g of steel dust was estimated to fall from a single sector during removal. This dust would contain 12 Ci of Co-60 and 120 Ci of Co-58. If this activity were spread on the floor it would significantly hamper and probably preclude contact maintenance operations in the building until it was thoroughly cleaned and decontaminated. The results of this scoping study indicate that control of stainless steel dust will be essential to continued contact maintenance activities in the reactor building.

10.3.2 Carbon Debris

The calculations for graphite erosion from the limiter and first wall tiles assumed that 50% of the eroded graphite is converted to methane. Therefore, accumulation rates per pulse for solid carbon are 30 g/pulse for 8-T operation and 25 g/pulse for 10-T operation. Disruptions contribute <1% to the total accumulation of graphite debris. The volumetric increase of eroded carbon was taken to be 4, or approximately the same density as carbon black. The maximum volume of material which potentially accumulates during the lifetime of the machine is about 21 m^3 (724 ft^3). If this material were allowed to accumulate and were distributed uniformly around the torus in the duct chamber, the debris would be 44.2 cm (17.4 in.) deep, roughly as shown in Fig. 10-1. Each sector would have 1/10, or 7.55×10^5 g, of activated carbon debris. If 10% of the material is available to fall out upon sector removal, about 7.55×10^4 g (166 lb) is the potential contaminant to the reactor building. Calculations indicate there will be about 4.0×10^{-3} μCi of carbon-14 per gram of carbon dust. This carbon-14 activity is not expected to cause a significant direct radiation hazard to maintenance personnel. However, the carbon dust will probably cause a problem if it gets into the reactor building. Carbon dust on wall and floor surfaces will make decontamination efforts much more difficult.

The ventilation system in the building can be designed to maintain the dust particle concentration at 10 μg/m^3. Therefore, airborne solid carbon will be in concentrations <10 μg/m^3. This results in about 40×10^{-15} μCi/cm^3 of carbon-14 activity in the reactor building atmosphere. Since maximum permissible concentration (MPC) for carbon-14 is 4×10^{-6} μCi/cm^3, the expected carbon-14 activity is not expected to cause a significant hazard to maintenance personnel.

10.3.3 Cleanup and Control of Radioactive Debris

As a means of preventing the buildup of carbon and stainless steel matter, an in-vessel cleanup will be required as part of the periodic limiter blade changeout. This can be accomplished either through the

ORNL-DWG 82-3873 FED

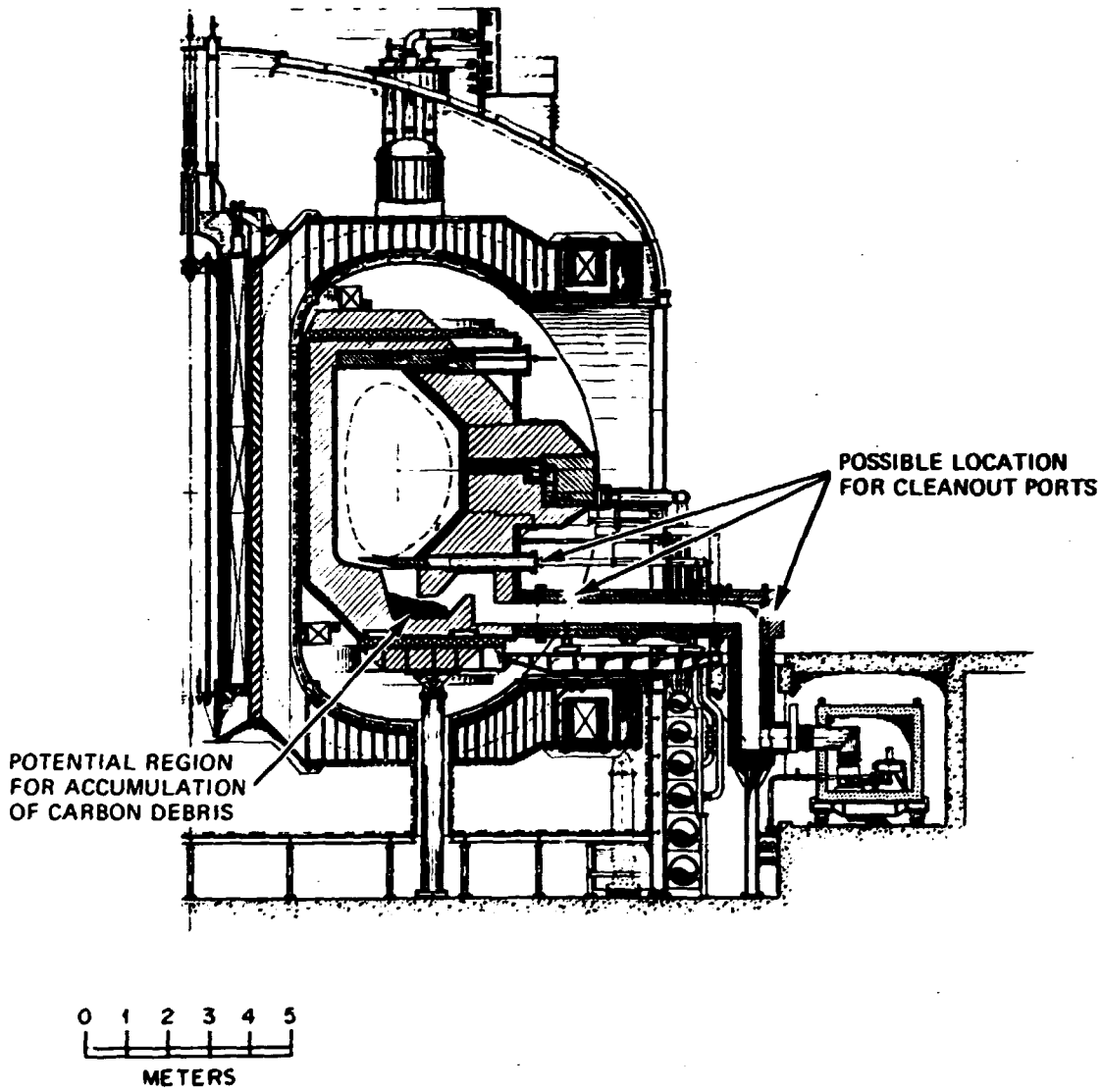

Fig. 10-1. Access for the removal of eroded particulate matter.

open limiter port or through an opening provided in the vacuum duct. The operation will be designed for remote handling. Figure 10-1 shows several possible cleanout port locations.

A similar cleanup will be required prior to removing a sector. As an added measure of contamination control, the sector handling device will be capable of containing particulate matter during sector removal as well as during transport to the hot cell. A possible design of the sector handling device is discussed in Section 7.

In addition, building floor and wall surfaces will be designed to allow high levels of cleanup and decontamination. The floors will be lined with steel plates, and the walls will be coated with high-quality paint and possibly steel plates in some areas.

10.3.4 Conclusions

Based on given erosion rates for the vacuum vessel armor, a significant amount of debris will accumulate unless in-situ cleaning is accomplished on a periodic basis. A means of in-situ cleaning must, therefore, be provided on a scheduled basis.

Residual debris will likely be present after in-situ cleaning operations are completed. Provisions must, therefore, be made for containment of residue during any maintenance operations which involve opening of the vacuum vessel (i.e., sector removal, limiter blade removal, etc.) and for cleanup and decontamination of any spills. The amount of activated airborne dust will be maintained well below the maximum permissible concentration (MPC) in the reactor cell by the ventilation system. However, the activated stainless steel dust represents a potential radioactive hazard to maintenance workers and warrants careful control techniques.

10.4 TRITIUM ISSUES

10.4.1 Liners and Coatings

Studies have shown that tritium which is accidentally released to the reactor building will be absorbed by bare concrete surfaces. Then, when atmospheric tritium cleanup is performed, the release of tritium from the bare concrete is slow enough to substantially delay the reductions of tritium levels in the building to the levels required by contact maintenance. Coatings or liners on the concrete greatly reduce the tritium absorption and make it possible to remove the tritium from the reactor building quicker. The cost of metal liners is quite high compared with painting the surfaces with high-quality epoxy paint. Therefore, epoxy paint has been selected for the FED Baseline. Additional testing is planned at TSTA to confirm that the tritium absorption properties of epoxy paint are acceptable for this application.

10.4.2 Tritium Leakage Sources

Scoping studies of potential tritium sources for leakage to the reactor building atmosphere, performed specifically for the FED Baseline, show that the major source of tritium leakage is the leakage of primary coolant. Leakage directly from the plasma vacuum chamber and other sources has been shown to be negligible. This conclusion should be further considered as the details and designs of the primary coolant system are developed. Pumps, valves, and process equipment should be enclosed within their own enclosures or cubicles to allow more careful control and monitoring of any tritium leakage and to prevent tritium from mixing with the total reactor building atmosphere. Tritium cleanup should then be significantly faster and have less impact on maintenance. The cost of providing enclosures and cells is considered small in comparison with the total cost of the reactor building and is currently considered to be a part of the estimated unit cost.

10.5 CRYOGENIC BLOWDOWN

The rate at which cryogens could be released from the magnet systems during postulated accidents affects the types of tritium control systems that may be used and, hence, potentially impacts the reactor building design. Studies have been initiated to scope the magnitude of possible magnet blowdown accidents. Early results are encouraging because the time necessary for cryogenic blowdown appears to be long compared with normal ventilation times. Thus, only manageable overpressures will be developed in the building during the postulated event, and the blowdown effluent can be vented through normal ventilation systems. This result helps confirm that a rectangular reactor building with 3 to 5 psi overpressure capability is adequate for FED Baseline. The more detailed results of this study are also expected to form the basis of sizing ventilation and tritium atmospheric cleanup systems.

10.6 CARBON-14 PRODUCTION

In the initial investigation of carbon-14 production, only the possible activation of the nitrogen in the reactor building air was considered as a source of C-14. After considering the thickness of the outboard shield, this C-14 production was estimated to be negligible. Another possible source is the activation of the carbon in the graphite armor within the plasma chamber. The magnitude of this source was also estimated and is considered negligible. A third possible source is the activation of the nitrogen in the liquid nitrogen systems. If liquid nitrogen is used in the cold shield inside the cryostat vacuum vessel boundary, as much as 40 Ci/yr of C-14 may be produced. This amount is not sufficient to constitute a serious hazard but is sufficient to require controls to prevent its release to the environment. Thus, the liquid nitrogen system would probably have to be treated as a radioactive system, a processing system devised to remove carbon, and a means implemented to dispose of the carbon as solid radioactive waste. No cost estimates for these systems have been developed.

10.7 CONCLUSIONS

The safety studies carried out in support of FED Baseline design activities are affecting the baseline design. Possible activation of building walls and structures is leading to specification of concrete type. Possible contamination of the reactor building by radioactive debris from the plasma chamber is affecting maintenance procedures and equipment. Possible tritium absorption by bare concrete results in specifying epoxy paint or metal liners for concrete surfaces in the reactor building. Possible tritium leakage from the primary coolant systems is expected to lead to the use of enclosures and cubicles for primary coolant system components. Possible cryogenic blowdown accidents will provide the basis for sizing ventilation systems and confirming the reactor building type and shape. Possible C-14 production has led to the consideration of the liquid nitrogen system as a potentially radioactive system. None of the studies has uncovered any safety-related impacts which would threaten the feasibility of the baseline design. Few of the impacts have reliable cost estimates at this time, but it does not appear that any of them will result in substantial additional cost.

REFERENCE

1. C. A. Flanagan, G. E. Smith, D. Steiner, FEDC Staff; *Fusion Engineering Device Design Report*, ORNL/TM-7948, Oak Ridge National Laboratory, Oak Ridge, Tennessee, December 1981.

11. COST PROJECTIONS

11.1 INTRODUCTION

The original cost projection for the FED Baseline configuration was developed during FY 1981 and documented in Ref. 1. The direct FED capital cost projections contained in the aforementioned report were generated in large part through the use of unit costs, costing algorithms, and other pertinent costing relationships which, in part, were based upon experience gained from other large experimental fusion programs.

During the period following publication of Ref. 1, a number of projected modifications and revisions having an impact on FED costs have taken place. One such item is escalation of FED costs to 1982 dollars. Additional changes in cost could result from the adoption of proposed designs changes identified in the studies which were carried out using the FED Baseline configuration as a point of departure.

Costing studies were also undertaken in the facility area, with primary emphasis directed toward potential cost reductions in the Hot Cell Facility (HCF) and reactor building. An additional cost study was undertaken to explore the possible cost payoff associated with incorporation of tritium breeding in the FED configuration.

A major product of these studies was the development of revised design approaches which result in potential decreases in projected FED Baseline costs. In contrast, some of the investigative studies yielded increases in cost as a consequence of the more detailed information gained from the study effort.

In this section of the report, we will first show the effect of escalation on the original baseline cost estimate. The remainder of the section will be devoted to a summarization of those FED Baseline studies which have an impact on cost. The results of each study are briefly described, and the potential plus or minus cost increments are identified.

These cost increments have not as yet been incorporated in the FED Baseline cost projection. They serve, however, as an indication of the cost decreases or increases which may be anticipated in any further effort to improve and otherwise update the FED Baseline.

Prior to starting the discussion on escalation and study results, a brief recapitulation of the costing methodology employed in development of FED Baseline costs is presented in Sect. 11.2.

11.2 COSTING METHODOLOGY

The costing methodology applied to the original FED Baseline cost projection consists of three major elements: the assumptions which guided the costing effort; the approach to establishing the direct capital cost; and the method employed for determination of the indirect capital cost. These topics are addressed briefly in the following three subsections.

11.2.1 Costing Assumptions

Five primary assumptions were observed in establishing the original FED Baseline cost projection. With the exception of inserting 1982 dollars for 1981 dollars, it is envisioned that the assumptions enumerated below would also be applied to future updates of the FED Baseline.

- All costs were based on 1981 dollars.
- Direct capital costs included all costs associated with component procurement and fabrication, including shipping to the construction site.
- The indirect capital costs included engineering design and project management, as well as all equipment assembly and installation at the construction site.
- A 30% contingency was included in the total cost (i.e., 30% of the total direct cost plus engineering, management, and installation costs).
- The cost projection covered only the FED construction project and did not include any operating or maintenance costs, spare parts, fuel, associated research and development, transmission lines, or decommissioning.

11.2.2 Direct Capital Cost

The FED Baseline direct capital cost projection was determined through the use of unit costs, cost algorithms, and other costing data obtained from major fusion projects including TFTR, TSTA, LCP, and JET. These costing relationships are resident in the FEDC systems code and are listed in accordance with the standard cost accounts defined in Ref. 2.

In order to develop a broad base for the FED capital cost projection within the framework of the current design status, a special cost workshop, involving ten cognizant organizations in the fusion community, was held in the early summer of 1981. As described in Ref. 1, the participating organizations developed independent cost estimates of the FED system. Although there was considerable scatter among the results, the average of ten major cost accounts showed reasonable agreement with the results obtained from the FEDC systems code.

11.2.3 Indirect Capital Cost

As noted under "Costing Assumptions" (Sect. 11.2.1), the indirect capital costs include engineering design, project management, and equipment assembly and installation at the construction site. Engineering and project management were taken to be 45% of the total direct capital cost, where the 45% figure is based upon TFTR and ORNL data. Similarly, the assembly and installation cost was taken to be 15% of the direct capital cost. As previously mentioned, a 30% contingency was applied to the total of the direct capital cost, the engineering/management cost, and the assembly/installation cost. The 30% cost contingency figure is used by ORNL for projects which are in an early stage of conceptual design.

11.3 ESCALATED BASELINE COST PROJECTION

Table 11-1 contains the escalated capital cost projection for the FED Baseline configuration. The 10% escalation factor reflects the effect of general inflation. As shown in the table, the escalated

Table 11-1. Cost escalation summary

	1981 $M	1982 $M
Magnet system	312.2	343.4
Torus	161.9	178.1
Cooling systems	38.5	42.4
Tritium and fuel handling	54.0	59.4
RF	89.0	97.9
Electrical systems	99.1	109.0
Vacuum pumping system	24.0	26.4
I&C	67.0	73.7
Maintenance equipment	60.4	66.4
Facilities	138.6	152.5
TOTAL DIRECT COST	1,044.7	1,149.2
Indirect costs		
Engineering & management (45%)	470.1	517.1
Installation (15%)	156.7	172.4
TOTAL (direct + indirect)	1,671.5	1,838.7
Contingency (30%)	500.5	550.6
TOTAL COST	2,172.0	2,389.2

direct 1982 capital cost and the total (direct plus indirect) capital costs are $1149 M and $2389 M, respectively. Also shown, for purposes of comparison, are the unescalated 1981 costs.

11.4 POTENTIAL COST IMPACT OF BASELINE ENGINEERING STUDIES

A number of technical studies were undertaken during FY 1982, using the FED Baseline as a point of departure. These studies are described in detail elsewhere in this report. Included are configuration level studies described in Sect. 3, subsystem studies and analyses described in Sects. 4 and 5, maintenance studies described in Sect. 7, and facility studies described in Sect. 8. In this section, those studies which could result in a cost impact to the FED Baseline are briefly recapitulated. A summary description of each study is provided and the potential cost impact identified.

11.4.1 Modified Reactor Configurations

This study was undertaken to determine the impact of varied TF coil shapes, PF coil locations, and vacuum boundaries on cost. The configurations which were investigated comprised: (a) the FED Baseline, (b) the FED Baseline with a combined vacuum boundary at the TF coil inner leg, (c) the FED Baseline with ten reduced-size TF coils of arbitrary shape (i.e., non-constant tension), separate vacuum boundaries, and all-exterior PF coils, and (d) a minimum-size machine with 12 TF coils of arbitrary shape, a combined vacuum boundary, and all-exterior PF coils. With comparable machine performance (i.e., same burn time and wall loading), it was found that:

- Use of the partially combined vacuum boundary with constant tension TF coils results in a direct capital cost saving of 6% over the FED Baseline.
- A reduced-size TF coil of arbitrary shape, coupled with an all-exterior PF system, results in a direct capital cost decrease of 4%.
- The minimum-sized machine with a combined vacuum boundary, 12 non-constant tension TF coils, and an all-external PF system results in a

cost saving over the FED Baseline of approximately 17.4%. This corresponds to a direct capital cost saving of $182 M, when referred to the FED Baseline total direct cost of $1044.7 M.

A significant portion of the cost reduction afforded by the minimum size machine is attributable to a reduction in machine major radius, a reduction in TF coil size, reduced requirements on the PF system, and associated reductions in power supply costs. Also, the smaller TF coils have smaller overturning moments and, hence, impose lighter loads on the intercoil support structure (ISS). As a consequence of the lighter loads and the smaller machine size, ISS weight decreases with a consequent further reduction in cost.

11.4.2 ISS Design for Reduced AC Losses

The present FED Baseline all-steel ISS exhibits high eddy current heat losses which account for approximately 50% of the heat load on the cryogenic plant. Substitution of a non-conducting G-10 inner and outer shell structure for the FED Baseline stainless steel ISS shell results in a significant weight saving and also electrically isolates the ISS beams from one another, thus obviating the high AC losses due to eddy currents. The ISS weight is reduced by 15%, which results in a cost reduction of approximately $5.5 M in fabrication cost. The reduction in eddy current losses is estimated to result in a $3.4 M savings in refrigeration system capital expense, for a total capital cost savings of $8.9 M. An additional savings of approximately $23.3 M would accrue from the savings in refrigeration power consumption over the ten-year life of the device.

11.4.3 Facility Costing Studies

In June and July of 1981, the FEDC held a two-part workshop for the purpose of obtaining FED cost estimates from independent sources. Preparation of facility costs was a part of the workshop task and in fact the results of this effort formed the basis for the initial facility costs documented in Ref. 1. Since publication of Ref. 1, a continuing

effort has been directed toward further definition of facility design and the associated impact upon facility costs. Particular emphasis has been placed on investigation of the Hot Cell Facility (HCF) and the reactor building, which together account for over 50% of the total facility direct cost.

The following paragraphs include: (a) a brief account of further investigations pertaining to HCF and reactor building design and cost and (b) a comparison of presently recommended costs versus initial baseline costs for all the buildings making up the FED facility complex.

HCF and reactor building costs

During the recent FED HCF study, discussions with hot cell operators and designers indicated that the baseline HCF unit cost projection was too low. As the HCF study progressed, three sets of information which supported this contention became available. The first input consisted of cost estimates for the Hot Experimental Facility (HEF) being designed at ORNL (Ref. 4), which placed the process building unit costs at about $\$385/m^3$. The second input was actual cost information for the New Waste Calcining Facility (NWCF), which is about to commence operation at INEL. This information indicated a unit cost of approximately $\$400/m^3$ for the process building. The third item of information was a set of cost algorithms developed by Bechtel for fusion power reactor studies which also indicated unit costs above originally predicted values.

Two applicable Bechtel algorithms plus the HEF, NWCF, facility workshop, and STARFIRE[3] unit cost data are depicted on Fig. 11-1, which is a plot of unit cost in $\$/m^3$ vs building volume in cubic meters. No clear-cut conclusions can be drawn from the plot with respect to the relationship between unit cost and building volume. For example, the NWCF and the HEF have approximately the same unit cost, $\$400/m^3$, but their volumes are quite different, 58,000 m^3 and 866,000 m^3, respectively. This inconsistency is probably attributable to the fact that the HEF and NWCF were designed to satisfy different requirements. Similarly, the scatter in the workshop cost data reflects the range of differing

experience of the participants with respect to the generation of building designs and costs.

Nevertheless, the data shown in Fig. 11-1 seem to confirm the impression of personnel experienced with hot cell design and operations that the FED Baseline cost estimates for the HCF and reactor building (based on unit costs of approximately $260/m^3$ to $270/m^3$) are too low. A unit cost of $400/m^3$ appears to be more consistent with the most current data and algorithms. Therefore, the value of $400/m^3$ is recommended for use as the unit building cost for the HCF and the reactor building.

The $400/m^3$ reflects total direct construction cost including building structure; piping; electrical work; normal heating, ventilating, and air conditioning equipment; normal lighting; and standard building services. Engineering, installation, and contingency costs are not covered in the $400/m^3$ figure. As indicated in the costing methodology section, these indirect costs are obtained for the overall machine and its facilities by taking appropriate percentages of the total direct capital costs of the machine and its facilities.

Other facility costs

A detailed review of the June/July 1981 Cost Workshop showed that the scatter in the individual cost estimates was much wider than could be deduced from inspection of the total estimates. Nevertheless, the estimates for each building were reviewed and unit costs recommended for use in determination of FED cost projections. The results of this activity are shown in Table 11-2, which lists: the buildings making up the FED Baseline facility; the building volumes; the recommended building unit costs in dollars per cubic meter; and the recommended FED cost projections. The recommended cost projection is obtained by multiplication of the values for building volume and unit cost. Shown for comparison (in the right-hand column) are the cost projections which were developed for the FED Baseline and which are documented in Ref. 1. It should be noted that differences between the recommended and original baseline cost projections are primarily due to changes in unit cost

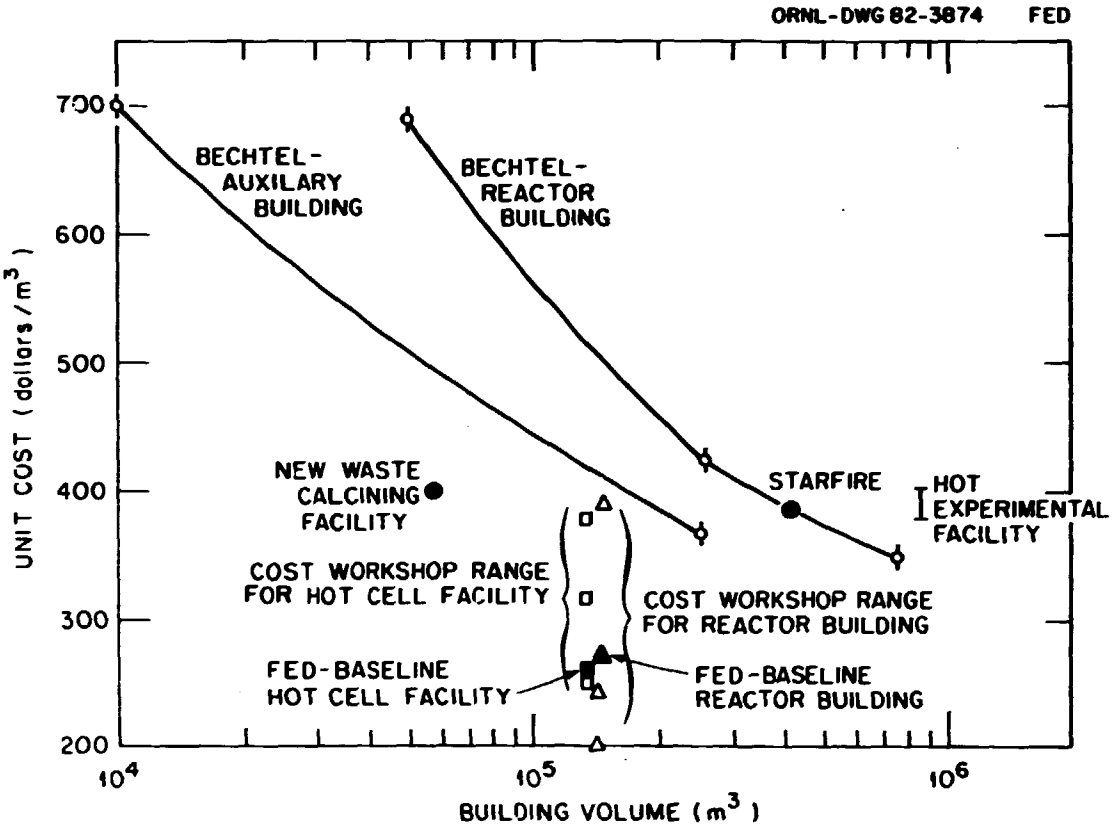

Fig. 11-1. Unit cost vs building volume.

Table 11-2. Recommended structures and site cost estimates

Work breakdown structure	Description	Volume (m^3)	Recommended unit cost ($\$/m^3$)	Recommended cost ($\$ \times 10^6$)	FED Baseline ($\$ \times 10^6$)
13	Structures and site facilities				
13.1	Site improvements and facilities			12.3	0.0
13.2	Reactor building and hot cell facility			101.4	74.2
13.2.1	Reactor building	157,000	400	62.8	39.1
13.2.2	Hot cell facility	96,500	400	38.6	35.1
13.3	Cooling system structures			2.6	1.1
13.3.1	Intake structures	1,350	220	0.3	0.1
13.3.2	Discharge structures				
13.3.3	Water treatment building	6,250	220	1.4	0.5
13.3.4	Recirculating structures	6,750	140	0.9	0.5
13.3.5	Cooling tower systems				
13.3.5.1	Cooling towers				
13.3.5.2	Recirculating water system				
13.4	Power supply & energy storage bldgs.			12.7	7.6
13.4.1	Copper and TF coil elect. eqpt. bldg.	21,120	150	3.2	1.7
13.4.2	OH and PF elect. eqpt. bldg.	37,840	120	4.5	3.0
13.4.3	Bulk heating elect. eqpt. bldg.	4,160	120	0.5	0.3
13.4.4	Motor generator flywheel bldg.	32,000	140	4.5	2.6
13.5	Miscellaneous bldgs.				
13.5.1	Auxiliary bldgs.			23.4	26.7
13.5.1.1	Cryogenic refrigeration bldg.	12,000	120	1.4	1.0
13.5.1.2	Tritium processing bldg.	52,200	230	12.0	14.0
13.5.1.3	Ventilation bldg.	43,500	230	10.0	11.7
13.5.2	Radioactive waste bldg.	16,000	230	3.7	4.3
13.5.3	Control room bldg.	(4,500)[a]			
13.5.4	Diesel generator bldg.	5,120	200	1.0	0.4
13.5.5	Administration bldg.	54,000	120	6.5	4.3
13.5.6	Service bldg.				
13.5.6.1	Mockup and shop bldg.	196,000	80	15.7	15.7
13.5.7	Miscellaneous structures & bldg. work				
13.5.7.1	Control room tunnel				
13.6	Ventilation stack			2.0	2.0
	TOTAL			181.3	136.3

[a]Control room included in the Administration Bldg.

values; building volumes have remained substantially the same, except in the cases of HCF and reactor buildings.

As a consequence of the facility design effort addressed in Sect. 8 of this report, the HCF building volume has been reduced from the 130,000 m^3 reported in Ref. 1 to 96,500 m^3 for the revised HCF design. This reflects a volume reduction of approximately 26%, which partially offsets the previously mentioned unit cost increase.

The reactor building, on the other hand, has undergone an 8.3% increase in volume, from 145,000 m^3 to 157,000 m^3. The bulk of this increase is due to the dimensional changes required to better accommodate the FED configuration described in Ref. 1. In addition to the HCF and reactor buildings, the cost projections of several other buildings have been changed substantially in the recommended estimates as a consequence of closer scrutiny of building requirements. Included in this category are the cooling system structures, which more than doubled; the power supply and energy storage buildings, which increased by more than 50%; the diesel generator building, which increased by a factor of 2.5; and the administration building, which increased by 50%. A further major change in the projected costs is the addition of $12.3 M for site improvements. This item was not included in previous FED cost estimates; the Cost Workshop pointed out the need for its inclusion. Partially counteracting these increases is a decrease of 12% in auxiliary building costs.

The recommended total updated structure and site facility cost projection is $185.9 M as opposed to $136.3 M for the FED Baseline. These figures reflect an overall increase in facility cost of $49.6 M, or 36%.

11.4.4 Maintenance Equipment Design and Costing Study

The maintenance equipment cost reported for FED in FY 1981 (Ref. 1) was $60.4 M. This direct capital cost reflected the estimate of equipment needed in both the reactor building and the HCF building. The primary basis for this costing was the Hot Experimental Facility (HEF) Conceptual Design Report (Ref. 4). HEF is a totally remotely operated

facility which has maintenance equipment requirements similar in a number of areas to those of the FED. In the absence of specific fusion-related maintenance equipment details, the HEF costs were extrapolated to FED where appropriate.

A review of the list of maintenance equipment included in the baseline cost of $60.4 M indicates that approximately 75% is available as off-the-shelf equipment. The remaining items require some level of engineering development in order to determine feasible concepts and high-confidence cost projections. In recognition of this, a major part of the maintenance-related work this year focussed on equipment concept development leading to more accurate cost estimates. This is a part of the continuous effort to provide more detailed definition of major FED components and, hence, better costs. The details of the maintenance concept development work are discussed in Sect. 7 of this report, "Maintenance Studies." The recommended revisions to the cost of major maintenance equipment which resulted from this work are summarized in Table 11-3. Also shown is the comparison with the costs used in the FY 1981 baseline cost projection (Ref. 1). The table shows a $2.23 M decrease in maintenance equipment direct cost over that of the FED Baseline for these major components. A factor in the cost decrease is the additional level of detail which was established as a result of the design study activity. This led to better design definition and, in this case, a slightly lower direct cost than reflected by the original estimates.

11.4.5 TF Coil Case Construction

A quantitative analysis was carried out to compare the cost of fabricating the TF coil case from rib-stiffened, thin (5-cm) plate stock vs the cost of using thick (up to 12-cm) plate stock. The study was based upon a loading condition and an allowable stress which were representative of the FED Baseline design.

It was concluded from the study that use of the built-up approach results in a 40% savings in material and welding costs. Approximately half of the total cost of the TF magnet structure is attributable to

Table 11-3. Major maintenance equipment cost update

Equipment	Function/comments	Recommended direct costs ($ M)	Baseline direct costs ($ M)[a]
Movable manipulator system	General purpose reactor cell handling	1.04	0.88
Sector handling device	Special purpose torus sector handling	0.48	2.2
Test module handling device	May be adopted for handling ICRH, ECRH	0.38	0.44
Limiter module handling device	Required to maintain plasma chamber vacuum integrity	0.49	Not estimated
In-vessel manipulator system	General purpose operations in plasma chamber	1.1	2.2
TOTAL		3.49	5.72
Net decrease		2.23	

[a]Baseline direct cost has been increased by 10% to permit direct comparison with recommended costs, which are in FY 1982 dollars.

materials and welding. If the remaining costs (other fabrication expenses, structure handling costs, shipping, engineering design, etc.) are assumed to be the same for both approaches, the overall saving in TF coil case costs is approximately 20%, or $5.2 M ($20.7 M for the built-up section vs $25.9 M for the heavy wall design). Use of the built-up section also results in reduced eddy current losses in the coil case, with an attendant reduction in refrigeration capital cost of approximately $3.2 M. The total capital cost savings is therefore $8.4 M. An additional saving of $21.4 M in operational cost accrues over the ten-year life of the machine.

11.4.6 Elimination of FED Cold Shields

The purpose of this study was to determine the possible cost saving resulting from deletion of the 80°K liquid nitrogen cold shield which follows the inner surface of the magnet vacuum vessel. The primary area of interest was the inboard leg of the TF coils, where removal of the nitrogen cold shield afforded the possibility of a reduction in machine major radius with a consequent significant reduction in overall machine cost. The study was aimed at determining whether the capital cost savings associated with removing the cold wall would be greater than the increase in operating cost due to the added heat leak.

As a result of a parallel study of gap streaming problems in the center solenoid area, it was concluded that the anticipated reduction in machine major radius could not be exploited. This resulted from the need to provide radiation shielding in the gap between the vacuum vessel and the TF coil case, which effectively prevented any decrease in machine major radius.

Under these conditions, the study showed: a capital cost saving (due to deletion of the cold wall) of $5.68 M; a capital cost increase (for additional refrigeration capability) of $0.61 M; and an operational cost increase (due to higher refrigeration power over the ten-year life of the device) of $3.72 M. Based on the above, the net savings in capital cost is $5.07 M, and the net overall cost savings is $1.35 M.

In addition to the cost savings, the simplicity of the revised design makes deletion of the nitrogen cold shield highly desirable.

11.4.7 Tritium Breeding Economics

An economic evaluation of tritium breeding options was performed to determine whether it would be cost-effective to incorporate tritium breeding blankets on FED. Two options were considered: partial (top and outboard wall) blanket coverage and full (inboard, top, and outboard wall) blanket coverage.

For the partial coverage option, it was assumed that a blanket similar to the INTOR blanket would be adopted. The blanket would cover the top and outboard wall regions to a depth of 0.5 m and be backed by a 1.0-m-thick SS/H_2O shield. The local tritium breeding ratio of the blanket was taken to be 1.1. The volumetric cost of the combined blanket and shield was assumed to be comparable to a 75 v/o SS, 25 v/o H_2O shield, i.e., $\sim\$0.15/cm^3$.

With partial blanket coverage, the outboard shield thickness of 1.15 m on the FED Baseline design increases to 1.50 m to accommodate the blanket and shield. The increase in thickness would not require a change in plasma dimensions or TF coil size. The incremental cost of the blanket and shield was estimated using the FEDC systems code to be $62 M. An additional $4 M increment was allotted for increased tritium systems capital costs, bringing the total incremental capital cost of this option to $66 M.

With partial blanket coverage, approximately 240 m^2 (the surface area of the top wall and 90% of the outboard wall) could be covered with breeding blankets. This accounts for 59% of the total plasma chamber area. With a local tritium breeding ratio of 1.1, the net tritium breeding ratio would be in the neighborhood of 0.65. In the course of DT operation, approximately 8.4 kg of tritium will be burned. With a net tritium breeding ratio of 0.65, the maximum potential savings would be 5.5 kg or $55 M (assuming a tritium cost of $10 K/g), which is less than the capital investment required. Table 11-4 provides a more

Table 11-4. Partial tritium breeding cost evaluation

Period	Construction								Tritium-free operations			
Year	1	2	3	4	5	6	7	8	9	10	11	12
Tritium usage (g)												
ΔFusion												0
ΔBlanket inventory buildup[a]												52
ΔDecay												14
ΔBreeding												-53
ΔPurchase												0
ΔOperating cost ($M)	--	--	--	--	--	--	--	--	--	--	--	0
ΔCapital cost ($M)[b]	8.30	8.30	8.30	8.30	8.30	8.30	8.30	8.30	--	--	--	--
ΔO&C costs ($M)[c]	8.30	8.30	8.30	8.30	8.30	8.30	8.30	8.30	0	0	0	0
Discount factor[d]	.952	.907	.864	.823	.784	.746	.711	.677	.645	.614	.585	.5
ΔPresent value cost ($M)	7.90	7.53	7.17	6.83	6.50	6.19	5.90	5.62	0	0	0	0
Cumulative P.V. costs ($M)	7.90	15.4	22.6	29.4	35.9	42.1	48.0	53.6	53.6	53.6	53.6	53.

[a] A blanket inventory of 750 g was assumed.

[b] Incremental capital costs were assumed to be uniformly distributed over the period of construction.

[c] Incremental operating and capital costs are expressed in constant dollars.

[d] The discount factor relates a constant dollar cost at t = n years to a present value cost at t = 0 where d is the discount rate (assumed to be 5%).

11-4. Partial tritium breeding cost evaluation

				Tritium-free operations			D-T operations						
	6	7	8	9	10	11	12	13	14	15	16	17	18
							0	0	0	0	0	0	0
							522	228	0	0	0	0	0
							14	40	41	41	41	41	41
							-536	-679	-858	-858	-858	-858	-858
							0	-411	-817	-817	-817	-817	-817
	--	--	--	--	--	--	0	-4.1	-8.2	-8.2	-8.2	-8.2	-8.2
0	8.30	8.30	8.30	--	--	--	--	--	--	--	--	--	--
0	8.30	8.30	8.30	0	0	0	0	-4.1	-8.2	-8.2	-8.2	-8.2	-8.2
4	.746	.711	.677	.645	.614	.585	.557	.530	.505	.431	.458	.436	.416
0	6.19	5.90	5.62	0	0	0	0	-2.17	-4.14	-3.94	-3.76	-3.58	-3.41
9	42.1	48.0	53.6	53.6	53.6	53.6	53.6	51.5	47.3	43.4	39.6	36.1	32.6

formly distributed over the period of construction.

essed in constant dollars.

st at t = n years to a present value cost at t = 0 and is equal to $\left(\frac{1}{1 + d}\right)^n$,

detailed breakdown of tritium consumption and costs. It may be seen from the table that the life cycle cost of this option would be approximately $33 M.

For the full coverage option, an additional blanket is required on the inboard wall. The inboard wall blanket was taken to be 0.3 m thick, backed by a 0.45-m SS/H_2O shield. The local tritium breeding ratio and volumetric costs for the inboard wall blanket were assumed to be the same as for the outboard wall blanket.

With full blanket coverage, the inboard shield thickness of 0.60 m on the FED Baseline design increases to 0.75 m to accommodate the blanket and shield. Changes in outboard shield dimensions are the same as for the partial coverage option. In order to maintain the same wall loading and burn time as the FED Baseline design, increases in minor radius from 1.30 m to 1.37 m and in major radius from 5.00 m to 5.34 m were required. The fusion power increased from 185 MW to 195 MW at 8 T and from 450 to 475 MW at 10 T. The capital cost impact of this option was estimated using the FEDC systems code to be $191 M. Approximately 45% of the cost impact was in the cost of blankets and shielding, the remainder being primarily in magnetics and power supplies. An additional $5 M increment was allotted for increased tritium systems capital costs, bringing the total capital cost of this option to $196 M.

With full blanket coverage, approximately 380 m^2 could be covered with breeding blankets, accounting for 83% of the total plasma chamber area. With a local tritium breeding ratio of 1.1, the net tritium breeding ratio would be 0.92. In the course of DT operation, approximately 9.0 kg of tritium will be burned. With a net tritium breeding ratio of 0.92, the amount of tritium to be purchased would be greater than 0.7 kg. Since on the smaller FED Baseline design only 8.4 kg of tritium would be burned, the maximum potential savings would be 7.7 kg or $77 M, which is far less than the capital investment required. Table 11-5 provides a more detailed breakdown of tritium consumption and costs. It may be seen from the table that the life cycle cost of this option would be ~$129 M.

Table 11-5. Full tritium breeding cost evaluation

Period	Construction							Tritium-free operations			
Year	1	2	3	4	5	6	7	8	9	10	11
Tritium usage (g)											
ΔFusion											
ΔBlanket inventory buildup[a]											
ΔDecay											
ΔBreeding											
ΔPurchase											
ΔOperating cost ($M)											
ΔCapital cost ($M)[b]	24.5	24.5	24.5	24.5	24.5	24.5	24.5	24.5			
ΔO&C costs ($M)[c]	24.5	24.5	24.5	24.5	24.5	24.5	24.5	24.5	0	0	0
Discount factor[d]	.952	.907	.864	.823	.984	.746	.711	.677	.645	.614	.585
Present value - O&C costs ($M)	23.3	22.2	21.2	20.2	19.2	18.3	17.4	16.6	0	0	0
Cumulative P.V. costs ($M)	23.3	45.5	66.7	86.9	106	124	142	158	158	158	158

[a] A blanket inventory of 1060 g was assumed.

[b] Incremental capital costs were assumed to be uniformly distributed over the period of constructi

[c] Incremental operating and capital costs are expressed in constant dollars.

[d] The discount factor relates a constant dollar cost at t = n years to a present value cost at t = where d is the discount rate (assumed to be 5%).

Full tritium breeding cost evaluation

Tritium-free operations						D-T operations						
6	7	8	9	10	11	12	13	14	15	16	17	18
						50	63	80	80	80	90	80
						783	277	0	0	0	0	0
						22	53	58	58	58	58	58
						-805	-1024	-1288	-1288	-1288	-1288	-1288
						50	-631	-1150	-1150	-1150	-1150	-1150
						0.5	-6.3	-11.5	-11.5	-11.5	-11.5	-11.5
24.5	24.5	24.5										
24.5	24.5	24.5	0	0	0	0.5	-6.3	-11.5	-11.5	-11.5	-11.5	-11.5
.746	.711	.677	.645	.614	.585	.557	.530	.505	.481	.458	.436	.416
18.3	17.4	16.6	0	0	0	0.3	-3.3	-5.8	-5.5	-5.3	-5.0	-4.8
124	142	158	158	158	158	159.	155	150	144	139	134	129

rmly distributed over the period of construction.

sed in constant dollars.

at t = n years to a present value cost at t = 0 and is equal to $\left(\frac{1}{1 + d}\right)^n$,

It does not appear cost-effective to incorporate either the partial blanket coverage option or the full blanket coverage option on FED. With partial blanket coverage (TBR = 0.65), the incremental capital cost of breeding would have to be reduced from $66 M to $26 M for breakeven to occur. Similarly, with full blanket coverage (TBR = 0.92), the incremental capital cost would have to be reduced from $196 M to $36 M for breakeven to occur. Improvements in local tritium breeding ratios or reductions in tritium blanket inventories over the values assumed might allow breakeven incremental capital costs to increase. However, it is not clear that even the most optimistic assumptions would favor tritium breeding on FED since it is essentially a low fluence device.

11.4.8 Impact of an 8-T Forced Flow Solenoid

The purpose of this study was to determine the effect of utilizing a forced flow 8-T solenoid instead of the pool-boiling, 7-T solenoid used in the FED Baseline. Three possible approaches were investigated:

1. The first alternative used an 8-T forced flow solenoid with plasma performance the same as the FED Baseline. This approach yielded an increase in burn time of 135 seconds, due to the larger, higher field solenoid. Cost for the longer burn time was approximately $1 M.
2. The second approach employed the FED Baseline plasma minor radius but reduced the aspect ratio (and, consequently, the major radius) until the FED Baseline burn time was reached. This case showed a cost savings of approximately $30 M. Neutron wall loading, however, is reduced from the FED Baseline value of 1.05 MW/m^2 to 0.99 MW/m^2.
3. The third approach maintained the same neutron wall loading and burn time as the FED Baseline. This was achieved by increasing the plasma minor radius from the FED Baseline value of 1.30 to 1.33 and simultaneously reducing the aspect ratio from 3.85 to 3.65. The cost reduction in this case, which has the same performance goals as the FED Baseline, is $9 M.

The large potential cost savings reflected for Case 2 clearly indicate that the wall loading is an important parameter which should be re-examined in the light of its high sensitivity. The burn time requirements should also be examined, since a major extension can be achieved for a modest investment. If it is decided that the wall loading and burn time should be maintained at the baseline design conditions, adopting the 8-T solenoid should still be considered as a substantial cost savings.

11.4.9 Torus Support Spool Candidate Concepts

The torus support spool structure serves as the plasma chamber vacuum boundary and is designed to take the applied atmospheric pressure load, the shield dead weight, and the electromagnetic loads due to disruptions and pulsing of the equilibrium field coils. In addition to its structural design requirements, the torus support spool is required to provide a high toroidal electrical resistance in order to inhibit the development of eddy currents during startup.

Three spool designs were considered. The FED Baseline design (Ref. 1) featured a double-wall corrugated structure using Inconel as the structural material to provide the necessary electrical resistance. A second design, developed since the baseline, utilizes a stainless steel single stiffened skin structure which incorporates two dielectric breaks to inhibit eddy currents. The third design also employs a single skin stiffened structure but is electrically continuous and uses Inconel to provide the necessary resistance. The direct capital costs of these three deisgns are $22 M, $10.8 M, and $37.9 M, respectively. It can be seen that adoption of the stainless steel design with dielectric breaks yields a capital cost saving (with respect to the baseline) of $11.2 M. The stainless steel approach also exhibits a clear cost advanatage over the third design, reflecting a cost difference of $27.1 M.

11.5 OVERALL COST IMPACT

The potential capital cost changes which have been discussed in this section are summarized in Table 11-6. The table indicates the decreases or increases in capital cost which would be anticipated if the potential changes were implemented.

As shown in the table, the largest potential contribution to direct capital cost reduction ($182 M) would be obtained by implementation of the minimum-sized device featuring 12 reduced-size TF coils, a combined vacuum boundary, and an all-external PF coil system.

The total cost reduction shown in Table 11-6 amounts to $227 M. This sum is partially offset by cost increases totaling $45 M, which leaves a net reduction of $182 M.

All the potential changes listed in the table are applicable to the FED Baseline; while none are mutually exclusive, each design study and cost projection was generated independently using the FED Baseline machine as the reference design. Although not yet confirmed, it is anticipated that most of these changes will be equally applicable to the minimum-sized machine discussed in Sect. 11.4.1.

Also worth noting is a potential additional saving in life cycle operating cost of $41 M (23.3 + 21.4 - 3.7). Finally, study results show that incorporation of tritium breeding in FED is clearly not a desirable step for either of the two cases considered.

Table 11-6. Summary of potential cost reductions/increases — FED Baseline

Cost element	Potential cap. cost change from baseline: Increase	Decrease	Comments
1. Modified reactor configuration (minimum size)		$182 M	o Delta costs are based on total direct capital costs resident in the system code
2. Intercoil support structure (ISS) design for reduced AC losses		$8.9 M	o Add'l. $23.3 M in op'l. cost saving accrues from reduced refrigeration power
3. Facility size and costing studies	$45 M		o Net change - reduced bldg. volume but higher $\$/m^3$ unit cost
4. Maintenance equip. design and costing study		$2.23 M	o Difference in direct capital cost
5. TF coil case construction		$8.4 M	o Add'l. $21.4 M op'l. cost savings due to reduced refrig. pwr. (reduced eddy currents)
6. Elimination of FED cold shields		$5.1 M	o Net capital cost decrease o Operating cost increases by $3.72 M
7. Tritium breeding economics			o $33 M or $129 M add'l. life cycle costs for partial or full blanket coverage, respectively; not recommended
8. Impact of an 8-T forced flow solenoid		$9 M ($30 M)	o Provides same wall loading and burn time as baseline o Requires wall loading decrease
9. Torus support spool candidate concepts		$11.2 M	o Cost decrease of SS spool with 2 dielectric breaks vs baseline
Total cost increase/decrease	$45 M	$226.8 M	
Net cost decrease		$181.8	

REFERENCES

1. Fusion Engineering Design Center Staff (C. A. Flanagan, D. Steiner, and G. E. Smith, eds.), *Fusion Engineering Device Design Description*, ORNL/TM-7928, December 1981.
2. S. C. Shulte, T. L. Willse, J. R. Young, *Fusion Reactor Design Studies — Standard Accounts for Cost Estimates*, Battelle Memorial Institute, PNL-2648/UC20, May 1978.
3. C. C. Baker, M. A. Abdou et al., *STARFIRE — A Commercial Tokamak Fusion Power Plant Study*, Argonne National Laboratory, ANL/FPP-80-1, September 1980.
4. "Conceptual Design Report, Hot Experimental Facility," Oak Ridge, Tennessee, Bechtel National Inc. and Union Carbide Coporation — Nuclear Division, ORNL/CFRP-81/4, June 1981.
5. "International Tokamak Reactor, Phase One," Tokamak Reactor Workshop, International Atomic Energy Agency, Vienna 1982.

ORNL/FEDC-82/2
Dist. Category UC-20

INTERNAL DISTRIBUTION

1. R. J. Barrett
2. S. K. Borowski
3. T. G. Brown
4. R. D. Burris
5. G. Bussell
6. R. E. Clausing
7. T. B. Cook
8. B. A. Cramer
9. H. O. Eason
10. B. A. Engholm
11. C. A. Flanagan
12. G. M. Fuller
13. S. K. Ghose
14. H. H. Haselton
15. P. N. Haubenreich
16. L. M. Hively
17. S. S. Kalsi
18. R. R. Kindsfather
19. P. King
20. J. Kirchner
21. V. D. Lee
22. J. F. Lyon
23. D. H. Metzler
24. J. G. Murray
25. W. D. Nelson
26. J. A. O'Toole
27. Y-K. M. Peng
28. R. L. Reid
29. W. T. Reierson
30. J. A. Rome
31-35. P. H. Sager
36. M. J. Saltmarsh
37. T. E. Shannon
38. J. Sheffield
39. P. T. Spampinato
40. V. C. Srivastava
41. P. Stevens
42. D. J. Strickler
43. N. Uckan
44. T. Uckan
45. F. W. Wiffen
46. K. F. Wu
47-48. Laboratory Records Department
49. Laboratory Records, ORNL-RC
50. Document Reference Section
51. Central Research Library
52. Fusion Energy Division Library
53. Fusion Energy Division Reports Office
54. ORNL Patent Office

EXTERNAL DISTRIBUTION

55. M. A. Abdou, Associate Director, FPP/207, Argonne National Laboratory, 9700 South Cass Avenue, Argonne, IL 60439
56. N. A. Amherd, Fusion Power Program, Advanced Systems Department, Electric Power Research Institute, P.O. Box 10412, Palo Alto, CA 94304
57. J. L. Anderson, CMB-3, Mail Stop 348, Los Alamos National Laboratory, P.O. Box 1663, Los Alamos, NM 87545
58. D. J. Anthony, Advanced Power Program, Advanced Energy Programs Department, Building 2, Room 551, General Electric Company, Schenectady, NY 12345
59. C. C. Baker, FPP/208, Argonne National Laboratory, 9700 South Cass Avenue, Argonne, IL 60439
60. T. H. Batzer, L-536, Lawrence Livermore National Laboratory, P.O. Box 808, Livermore, CA 94550
61. J. F. Baur, GA Technologies, Inc., P.O. Box 85608, San Diego, CA 92138

62. D. S. Beard, Office of Fusion Energy, Office of Energy Research, Mail Stop G-256, U.S. Department of Energy, Washington, DC 20545
63. R. J. Beeley, ETEC, Rockwell International, P.O. Box 1449, Canoga Park, CA 91304
64. D. C. Berkey, Vice President & General Manager, Energy System and Technology Division, General Electric Company, P.O. Box 7600, Stamford, CT 06904
65. R. F. Beuligmann, General Dynamics, Convair Division, P.O. Box 80847, San Diego, CA 92138
66. K. L. Black, Department E452, McDonnell Douglas Astronautics Company, P.O. Box 516, St. Louis, MO 63166
67. R. R. Borchers, Lawrence Livermore National Laboratory, P.O. Box 5511 (L-640), Livermore, CA 94550
68. R. Botwin, C47-05, Grumman Aerospace Corporation, P.O. Box 31, Bethpage, NY 11714
69. W. B. Briggs, McDonnell Douglas Astronautics Company, P.O. Box 516, St. Louis, MO 63166
70. G. Bronner, Princeton Plasma Physics Laboratory, P.O. Box 451, Princeton, NJ 08540
71. J. N. Brooks, FPP/207, Argonne National Laboratory, 9700 South Cass Avenue, Argonne, IL 60439
72. R. D. Brooks, Advanced Energy Programs Department, General Electric Company, Building 2, Room 433, Schenectady, NY 12345
73. S. C. Burnett, GA Technologies, Inc., P.O. Box 85608, San Diego, CA 92138
74. J. D. Callen, Department of Nuclear Engineering, University of Wisconsin, Madison, WI 53706
75. J. F. Clarke, Office of Fusion Energy, Office of Energy Research, Department of Energy, MS G-256, Washington, DC 20545
76. R. G. Clemmer, Fusion Power Program, Argonne National Laboratory, 9700 South Cass Avenue, Argonne, IL 60439
77. D. R. Cohn, MIT Plasma Fusion Center, 167 Albany Street, Cambridge, MA 02139
78. R. W. Conn, School of Chemical, Nuclear, and Thermal Engineering, Boelter Hall, University of California, Los Angeles, CA 90024
79. J. G. Crocker, EG&G Idaho, P.O. Box 1625, Idaho Falls, ID 83401
80. J. E. Cummings, Electric Power Research Institute, P.O. Box 10412, Palo Alto, CA 94303
81. A. E. Dabiri, Energy Systems and Conservation Division, Science Applications, Inc., P.O. Box 2351, La Jolla, CA 92038
82. R. C. Davidson, Massachusetts Institute of Technology, 77 Massachusetts Avenue, Cambridge, MA 02139
83. N. A. Davies, Office of Fusion Energy, Office of Energy Research, Mail Station G-256, U.S. Department of Energy, Washington, DC 20545
84. J. W. Davis, McDonnell Douglas Astronautics Company, E457, Building 81/1/B7, P.O. Box 516, St. Louis, MO 63166
85. S. O. Dean, Director, Fusion Energy Development, Science Applications, Inc., 2 Professional Drive, Suite 249, Gaithersburg, MD 20760
86. D. DeFreece, E451, Building 81/1/B7, McDonnell Douglas Astronautics Company, P.O. Box 516, St. Louis, MO 63166

87. R. A. DeLuca, P.O. Box 2325, Boston, MA 02107
88. D. A. Dingee, Program Manager, Fusion Technology, Pacific Northwest Laboratories, Battelle Boulevard, Richland, WA 99352
89. J. N. Doggett, L-441, Lawrence Livermore National Laboratory, P.O. Box 808, Livermore, CA 94550
90. H. Dreicer, Division Leader, CRT, Los Alamos National Laboratory, P.O. Box 1663, Los Alamos, NM 87544
91. H. P. Eubank, Princeton Plasma Physics Laboratory, P.O. Box 451, Princeton, NJ 08540
92. F. Farfaletti-Casali, Engineering Division, Joint Research Center, Ispra Establishment, 21020 Ispra (Varese), Italy
93. A. Favale, Grumman Aerospace Corporation, Mail Stop A01-26, Bethpage, NY 17714
94. P. A. Finn, Fusion Power Program, Argonne National Laboratory, 9700 South Cass Avenue, Argonne, IL 60439
95. H. K. Forsen, Bechtel Group, Inc., Research & Engineering, P.O. Box 3965, San Francisco, CA 94119
96. J. S. Foster, Jr., Building R4-2004, TRW Defense and Space Systems, 1 Space Park, Redondo Beach, CA 90278
97. T. K. Fowler, Associate Director for MFE, L-436, Lawrence Livermore National Laboratory, P.O. Box 808, Livermore, CA 94550
98. J. W. French, EBASCO Services, Inc., Forrestal Campus, CN-59, Princeton University, Princeton, NJ 08540
99. J. G. Gavin, Jr., President, A01-11, Grumman Aerospace Corporation, P.O. Box 31, Bethpage, NY 11714
100. G. Gibson, Westinghouse Electric Corporation, Fusion Power Systems Department, P.O. Box 10864, Pittsburgh, PA 15236
101. J. R. Gilleland, Manager, Fusion Project, GA Technologies, Inc., P.O. Box 85608, San Diego, CA 92138
102. J. Glancy, Science Applications, Inc., 1200 Prospect Street, La Jolla, CA 92038
103. R. W. Gould, Department of Applied Physics, California Institute of Technology, Pasadena, CA 91109
104. M. W. Griffin, Department E236, McDonnell Douglas Astronautics Company, P.O. Box 516, St. Louis, MO 63166
105. C. D. Henning, Mirror Program Office, L-644, Lawrence Livermore National Laboratory, P.O. Box 5511, Livermore, CA 94550
106. T. Hiraoka, JT-60 Project Office I, Japan Atomic Energy Research Institute, Tokai Research Establishment, Tokai-mura, Ibaraki-ken, Japan
107. J. C. Hosea, Princeton Plasma Physics Laboratory, P.O. Box 451, Princeton, NJ 08540
108. D. Hwang, Princeton Plasma Physics Laboratory, P.O. Box 451, Princeton, NJ 08540
109. C. J. Inukai, Department E231, McDonnell Douglas Astronautics Company, P.O. Box 516, St. Louis, MO 63166
110. Institute of Physics, Academia Sinica, Peking, Peoples Republic of China
111. D. L. Jassby, Princeton Plasma Physics Laboratory, P.O. Box 451, Princeton, NJ 08540
112. B. B. Kadomtsev, I. V. Kurchatov Institute of Atomic Energy, 46 Ulitsa Kurchatova, P.O. Box 3402, Moscow, U.S.S.R.

113. R. A. Krakowski, CTR-12, Mail Stop 641, Los Alamos National Laboratory, P.O. Box 1663, Los Alamos, NM 87545
114. G. L. Kulcinski, University of Wisconsin, Department of Nuclear Engineering, Engineering Research Building, Room 439, 1500 Johnson Drive, Madison, WI 53706
115. D. L. Kummer, McDonnell Douglas Astronautics Company, 969 Executive Parkway, Bellerive Office Center, Creve Coeur, MO 63141
116. L. M. Lidsky, MIT Plasma Fusion Center, 167 Albany Street, Cambridge, MA 02139
117. B. G. Logan, Lawrence Livermore National Laboratory, P.O. Box 808, Livermore, CA 94550
118. J. A. Maniscalco, TRW Energy Development Group, One Space Park, Redondo Beach, CA 90278
119. R. F. Mattas, Fusion Power Program, Argonne National Laboratory, 9700 South Cass Avenue, Argonne, IL 60439
120. R. McGrath, Fusion Power Program, Argonne National Laboratory, 9700 South Cass Avenue, Argonne, IL 60439
121. V. A. Maroni, CEN/205, Argonne National Laboratory, 9700 South Cass Avenue, Argonne, IL 60439
122. W. Marton, Office of Fusion Energy, Office of Energy Research, Mail Station G-256, U.S. Department of Energy, Washington, DC 20545
123. L. G. Masson, EG&G Idaho, Idaho National Engineering Laboratory, P.O. Box 1625, Idaho Falls, ID 83401
124. D. G. McAlees, Exxon Nuclear Company, Inc., 777 106th Avenue, NE, Bellevue, WA 98009
125. D. M. Meade, Princeton Plasma Physics Laboratory, P.O. Box 451, Princeton, NJ 08540
126. A. T. Mense, Building 107, Post B2, McDonnell Douglas Astronautics Company, P.O. Box 516, St. Louis, MO 63166
127. L. Michaels, Princeton Plasma Physics Laboratory, P.O. Box 451, Princeton, NJ 08540
128. D. Mikkelsen, Princeton Plasma Physics Laboratory, P.O. Box 451, Princeton, NJ 08540
129. G. H. Miley, University of Illinois, 214 NEL, 103 S. Goodwin, Urbana, IL 61801
130. R. L. Miller, GA Technologies, Inc., P.O. Box 85608, San Diego, CA 92138
131. J. T. D. Mitchell, Culham Laboratory, Abingdon, Oxon OX14 3DB United Kingdom
132. P. W. Moir, Lawrence Livermore National Laboratory, P.O. Box 808, Livermore, CA 94550
133. D. B. Montgomery, MIT Plasma Fusion Center, 170 Albany Street, Cambridge, MA 02139
134. A. E. Munier, Grumman Aerospace Company, P.O. Box 31, Bethpage, NY 11714
135. P. Murray, Westinghouse Electric Corporation, 1801 K Street, NW, Washington, DC 20006
136. R. E. Nygren, FPP/207, Argonne National Laboratory, 9700 South Cass Avenue, Argonne, IL 60439
137. T. Ohkawa, GA Technologies, Inc., P.O. Box 85608, San Diego, CA 92138

138. M. Okabayashi, Princeton Plasma Physics Laboratory, P.O. Box 451, Princeton, NJ 08540
139. A. Opdenaker, Office of Fusion Energy, Department of Energy, Mail Stop G-256, Washington, DC 20545
140. D. Overskei, GA Technologies, Inc., P.O. Box 85608, San Diego, CA 92138
141. R. R. Parker, Francis Bitter National Magnet Laboratory, 170 Albany Street, Cambridge, MA 02139
142. M. Petravic, Princeton Plasma Physics Laboratory, P.O. Box 451, Princeton, NJ 08540
143. D. E. Post, Princeton Plasma Physics Laboratory, P.O. Box 451, Princeton, NJ 08540
144. L. K. Price, Department of Energy, Oak Ridge Operations, P.O. Box E, Oak Ridge, TN 37830
145. R. E. Price, Office of Fusion Energy, Office of Energy Research, Mail Station G-256, Washington, DC 20545
146. F. A. Puhn, GA Technologies, Inc., P.O. Box 85608, San Diego, CA 92138
147. J. Purcell, GA Technologies, Inc., P.O. Box 85608, San Diego, CA 92138
148. R. V. Pyle, University of California, Lawrence Berkeley Laboratory, Berkeley, CA 94720
149. M. Rabinowitz, Lebedev Institute of Physics, Academy of Sciences of the U.S.S.R., Leninsky Proespect 53, Moscow, U.S.S.R.
150. J. M. Rawls, GA Technologies, Inc., P.O. Box 85608, San Diego, CA 92138
151. P. J. Reardon, Princeton Plasma Physics Laboratory, P.O. Box 451, Princeton, NJ 08540
152. J. D. Rogers, Los Alamos National Laboratory, P.O. Box 1663, Los Alamos, NM 87545
153. M. L. Rogers, Monsanto Research Corporation, Mound Laboratory Facility, P.O. Box 32, Miamisburg, OH 45342
154. M. N. Rosenbluth, RLM 11.218, Institute for Fusion Studies, University of Texas, Austin, TX 78712
155. P. H. Rutherford, Princeton Plasma Physics Laboratory, P.O. Box 451, Princeton, NJ 08540
156. M. M. Sabado, EBASCO Services, Inc., A Site, Building 1-A, Forrestal Campus, Princeton, NJ 08540
157. J. A. Schmidt, Princeton Plasma Physics Laboratory, P.O. Box 451, Princeton, NJ 08540
158. K. R. Schultz, GA Technologies, Inc., P.O. Box 85608, San Diego, CA 92138
159. F. R. Scott, Electric Power Research Institute, P.O. Box 10412, Palo Alto, CA 94304
160. G. Sheffield, Princeton Plasma Physics Laboratory, P.O. Box 451, Princeton, NJ 08540
161. T. J. M. Sluyters, Accelerator Department, Brookhaven National Laboratory, Upton, NY 11973
162. D. Smith, Materials Science Division, Argonne National Laboratory, 9700 South Cass Avenue, Argonne, IL 60439
163. L. Southworth, GA Technologies, Inc., P.O. Box 85608, San Diego, CA 92138

164. W. M. Stacey, Jr., Georgia Institute of Technology, School of Nuclear Engineering, Atlanta, GA 30332
165. D. Steiner, Nuclear Engineering Department, Rensselaer Polytechnic Institute, NES Building, Tibbits Avenue, Troy, NY 12181
166. E. Stern, Grumman Aerospace Corporation, CN-59, Forrestal Campus, Princeton, NJ 08540
167. L. D. Stewart, Princeton Plasma Physics Laboratory, P.O. Box 451, Princeton, NJ 08540
168. W. Stodiek, Princeton Plasma Physics Laboratory, P.O. Box 451, Princeton, NJ 08540
169. P. M. Stone, Office of Fusion Energy, Office of Energy Research, Mail Station G-256, Washington, DC 20545
170. E. W. Sucov, Westinghouse Electric Corporation, Advanced Reactors Division, P.O. Box 158, Madison, PA 15663
171. I. N. Sviatoslavsky, Room 33, Engineering Research Building, 1500 Johnson Drive, University of Wisconsin, Madison, WI 53706
172. T. Tamano, GA Technologies, Inc., P.O. Box 85608, San Diego, CA 92138
173. R. E. Tatro, Manager, Energy Systems, M.Z. 16-1070, General Dynamics-Convair Division, P.O. Box 80847, San Diego, CA 92138
174. F. Tenney, Princeton Plasma Physics Laboratory, P.O. Box 451, Princeton, NJ 08540
175. F. Thomas, B-20-5, Grumman Aerospace Corporation, Bethpage, NY 11714
176. K. I. Thomassen, Lawrence Livermore National Laboratory, P.O. Box 808, Livermore, CA 94550
177. R. J. Thome, Francis Bitter National Magnet Laboratory, 170 Albany Street, Cambridge, MA 02139
178. B. J. Thorpe, General Manager, Advanced Energy Programs Department, P.O. Box 527, 501 Allendale Road, King of Prussia, PA 19406
179. M. Tigner, Laboratory for Nuclear Studies, Cornell University, Ithaca, NY 14853
180. C. Trachsel, McDonnell Douglas Astronautics Company, P.O. Box 516, St. Louis, MO 63166
181. J. R. Treglio, General Dynamics-Convair Division, P.O. Box 80847, San Diego, CA 92138
182. V. I. Tolok, Physical-Technical Institute of the Ukrainian S.S.R., Academy of Sciences, 310108, Kharkov, U.S.S.R.
183. L. R. Turner, Fusion Power Program, Argonne National Laboratory, 9700 South Cass Avenue, Argonne, IL 60439
184. M. A. Ulrickson, Princeton Plasma Physics Laboratory, P.O. Box 451, Princeton, NJ 08540
185. K. Uo, Plasma Physics Laboratory, Kyoto University, Grokasho Uji, Kyoto, Japan
186. F. Verdaguer, Division of Fusion, Junta de Energia Nuclear, Madrid 3, Spain
187. H. F. Vogel, Los Alamos National Laboratory, P.O. Box 1663, Los Alamos, NM 87545
188. K. E. Wakefield, Princeton Plasma Physics Laboratory, P.O. Box 451, Princeton, NJ 08540
189. D. Weldon, Los Alamos National Laboratory, P.O. Box 1663, Los Alamos, NM 87545

190. J. C. Wesley, GA Technologies, Inc., P.O. Box 85608, San Diego, CA 92138
191. W. R. Wilkes, Monsanto Research Corporation, Mound Laboratory Facility, P.O. Box 32, Miamisburg, OH 45342
192. J. E. Wilkins, EG&G Idaho, Idaho National Engineering Laboratory, P.O. Box 1625, Idaho Falls, ID 83401
193. H. Willenberg, Mathematical Sciences Northwest, Inc., P.O. Box 1887, Bellevue, WA 98009
194. J. E. C. Williams, MIT Francis Bitter National Magnet Laboratory, Albany Street, Cambridge, MA 02139
195. H. H. Yoshikawa, W/A-62, Hanford Engineering Development Laboratory, P.O. Box 1970, Richland, WA 99352
196. K. M. Young, Princeton Plasma Physics Laboratory, P.O. Box 451, Princeton, NJ 08540
197. N. E. Young, EBASCO Services, Inc., Princeton Plasma Physics Laboratory, P.O. Box 451, Princeton, NJ 08540
198. Bibliothek, Institut fur Plasmaphysik, D-8046 Garching bei Munchen, Federal Republic of Germany
199. Bibliotheque, Service du Confinement des Plasmas, CEA, B.P. No. 6, 92 Fontenay-aux-Roses (Seine), France
200. Documentation S.I.G.N., Department de la Physique du Plasma et de la Fusion Controlee, Association EURATOM-CEA, Centre d'Etudes Nucleaires, B.P. 85, Centre du Tri, 38041 Grenoble, Cedex, France
201. Library, Centre de Recherches en Physique des Plasmas, 21 Avenue des Bains, 1007 Lausanne, Switzerland
202. Library, Culham Laboratory, UKAEA, Abingdon, Oxon, OX14 3DB, England
203. Library, FOM Institute voor Plasma-Fysica, Rijnhuizen, Jutphaas, Netherlands
204. Library, Institute for Plasma Physics, Nagoya University, Nagoya 464, Japan
205. Library, International Centre for Theoretical Physics, Trieste, Italy
206. Library, JET Joint Undertaking, Abingdon, Oxfordshire, OX14, DB, England
207. Library, Laboratoria Gas Ionizzati, Frascati, Italy
208. Plasma Research Laboratory, Australian National University, P.O. Box 4, Canberra, ACT 2600, Australia
209. Thermonuclear Library, Japan Atomic Energy Research Institute, Tokai, Naka, Ibaraki, Japan
210. Library, Plasma Physics Laboratory, Kyoto University, Gokasho Uji, Kyoto, Japan
211. R. Varma, Physical Research Laboratory, Navangpura, Ahmedabad, India Institute of Physics, Academia Sinica, Peking, Peoples Republic of China
212. Office of the Assistant Manager for Energy Research and Development, Department of Energy, Oak Ridge Operations, Oak Ridge, TN 37830

213-320. Given distribution as shown in TID-4500, Magnetic Fusion Energy (Distribution Category UC-20)

☆ U.S. GOVERNMENT PRINTING OFFICE 1983-646-066/336

Printed in the United States of America. Available from
National Technical Information Service
U.S. Department of Commerce
5285 Port Royal Road, Springfield, Virginia 22161
NTIS price codes—Printed Copy: A20 Microfiche A01

This report was prepared as an account of work sponsored by an agency of the United States Government. Neither the United States Government nor any agency thereof, nor any of their employees, makes any warranty, express or implied, or assumes any legal liability or responsibility for the accuracy, completeness, or usefulness of any information, apparatus, product, or process disclosed, or represents that its use would not infringe privately owned rights. Reference herein to any specific commercial product, process, or service by trade name, trademark, manufacturer, or otherwise, does not necessarily constitute or imply its endorsement, recommendation, or favoring by the United States Government or any agency thereof. The views and opinions of authors expressed herein do not necessarily state or reflect those of the United States Government or any agency thereof.